Advanced Structured Materials 7

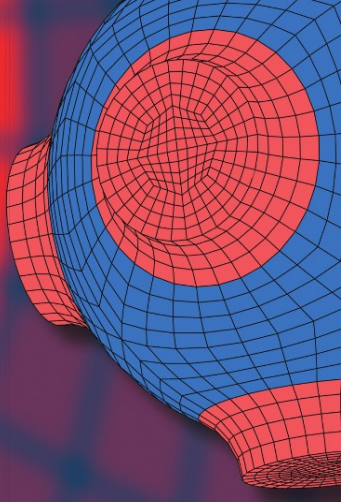

Holm Altenbach
Gérard A. Maugin
Vladimir Erofeev *Editors*

Mechanics of Generalized Continua

Springer

Advanced Structured Materials

Volume 7

For further volumes:
http://www.springer.com/series/8611

Holm Altenbach · Gérard A. Maugin
Vladimir Erofeev
Editors

Mechanics of Generalized Continua

Springer

Editors
Holm Altenbach
Zentrum für Ingenieurwissenschaften
Martin-Luther-Universität
Halle-Wittenberg
Kurt-Mothe-Str. 1
06099 Halle (Saale)
Germany
e-mail: holm.altenbach@iw.uni-halle.de

Gérard A. Maugin
Institut Jean Le Rond d'Alembert
UPMC
Tour 55, Place Jussieu 4
75252 Paris
France

Vladimir Erofeev
IMASH, RAN
Belinskogo str. 85
603024 Nizhny Novgorod
Russia

ISSN 1869-8433 e-ISSN 1869-8441

ISBN 978-3-642-19218-0 e-ISBN 978-3-642-19219-7

DOI 10.1007/978-3-642-19219-7

Springer Heidelberg Dordrecht London New York

Cover design: WMXDesign GmbH, Heidelberg

Printed on acid-free paper

Springer is part of Springer Science+Business Media (www.springer.com)

Preface

Generalized Continua are in the focus of scientists from the end of the 19th century. A first summary was given in 1909 by the Cosserat brothers[1] and some previous works of such famous scientists like Lord Kelvin. All these contributions were focussed on the fact that in a continuum one has to define translations and rotations independently (or in other words, one has to establish force and moment actions as it was done by Euler).

After World War II a true renaissance in this field occurred with a publication of Ericksen & Truesdell in 1958. Further developments were connected with the fundamental contributions of, among others, Kröner (Germany), Aero and Palmov (Soviet Union), Nowacki (Poland), Eringen (USA), and Maugin (France). The reason for the revival was that some effects of the mechanical behavior of solids and fluids could not be explained by the available classical models. Examples of this are the turbulence of a fluid or the behavior of solids with a significant and very complex microstructure. The enthusiasm in this field was so great that the International Union of Theoretical and Applied Mechanics (IUTAM) in the mid 1960s decided to organize a special IUTAM-Symposium in 1967 in Stuttgart-Freudenstadt (Coordinator E. Kröner). The state of the art was then summarized and published by Springer[2].

Since the suggested models fulfill all requirements from Continuum Thermomechanics (the balance laws were formulated and the general representations of the constitutive equations were suggested) the scientific community was satisfied for a while but missed real applicative developments. Indeed, for practical applications the proposed models were not useful. The reason for this was a gap between the formulated constitutive equations and the possibilities to identify the material parameters. As often the case one had much more parameters compared to classical models. In addition, computational progress and available machines in these times

[1] E. et F. Cosserat: Cosserat, F.: Théorie des Corps Déformables, Hermann Editeurs, Paris, 1909 (Reprint, Gabay, Paris, 2008)

[2] E. Kröner (Ed.): Mechanics of Generalized Continua (Proceedings of the IUTAM-Symposium on the Continuum Theory of Dislocations with Applications, Freudenstadt and Stuttgart, Germany, 1967), Springer, Berlin/Heidelberg/New York, 1968

were limited. So from the end of the 1960s until the 1990s, there were only a few members of the scientific and engineering communities working in the field of Generalized Continua.

During the last ten years the situation has drastically changed. More and more researches emerged, being kindled by the partly forgotten models since now one has available much more computational possibilities and very complex problems can be simulated numerically. In addition, with the increased attention paid to a large number of materials with complex microstructure and a deeper understanding of the meaning of the material parameters (scale effects) the identification becomes much more well founded. We have thus contributions describing the micro- and macro-behavior, new existence and uniqueness theorems, the formulation of multi-scale problems, etc., and now it is time to ponder again the state of matter and to discuss new trends and applications. Strong interest in the field was checked and kindled by the two colloquia held in Paris in 2009 and celebrating the centennial of the Cosserats' book. The results of the first symposium were published again by Springer[3].

The present publication is a collection of papers of French, German and Russian scientists in field of *Generalized Continua*. France, Germany and Russia have a long tradition in the above mentioned research area. Under the leadership of Gérard Maugin new research directions were established within this topic. In Germany the research in this field was stimulated by Kröner, Lippmann, Besdo, and Rothert among others. Actual applications are directed to the modeling and simulation of continua with complex microstructure like foams or porous media. In Russia, starting with the pioneering works of Aero et al. and Palmov many new models for structural mechanics applications (rods, plates, and shells) were presented.

During the last years there were established a small number of common projects of these scientists (for example, Altenbach & Eremeyev worked out new models for plates made of foams based on the micro-polar elasticity and the Cosserat plate theory, Maugin & Porubov worked on nonlinear waves in micro-structured bodies; Maugin & Lazar worked on defects in generalized continua, Forest & Sievert worked on anelasticity in generalized continua). New research directions will be presented from the point of view of modeling and simulation, experimental identification, and numerical methods. The basics were discussed at the First trilateral French-German-Russian seminar held in Lutherstadt Wittenberg (Germany) August 9–11, 2010. The contributions to the present publication are focussed on the most recent research items, i.e.,

- new models,
- application of well-known models to new problems,
- micro-macro aspects,
- computational effort,
- possibilities to identify the constitutive equations, and

[3] G.A. Maugin, A.V. Metrikine (Eds): Mechanics of Generalized Continua: One Hundred Years After the Cosserats, Advances in Mathematics and Mechanics Vol. 21, Springer, Berlin, 2010

- old problems with incorrect or non-satisfying solutions based on the classical continua assumptions

During the Wittenberg seminar the following lectures were presented

- Gérard Maugin: An historical perspective of generalized continuum mechanics
- Patricio Neff: Subgrid interaction and micro-randomness. Novel invariance requirements in infinitesimal gradient elasticity
- Jean-François Ganghoffer: Construction of micropolar continua from the discrete homogenization of repetitive beam lattices
- Alexey Porubov: Nonlinear dynamic processes in media with internal structure
- Evgeny Lomakin: Constitutive models of mechanical behavior of media with stress state dependent material properties
- Anton Krivtsov: Modeling of media with microstructure at different scale levels using particles
- Wolfgang Ehlers: Coupling of discrete media and continuum mechanics: a computational approach towards micropolar continua
- Paul Fischer: Cahn-Hilliard generalized diffusion modeling using the C^1 natural element method
- Igor Shardakov: Couple stress effects in elastic materials (analytical and numerical solutions, experiments)
- Lalaonirina R. Rakotomanana: Some remarks on the invariance of Lagrangean function of higher gradient continuum
- Albrecht Bertram & Samuel Forest: An axiomatic framework for gradient materials
- Victor Eremeyev: On the application of generalized continua models to structural mechanics problems
- Elena Ivanova: On one model of generalized continuum and its thermodynamical interpretation
- Rasa Kazakevičiūtė-Makovska: Micromechanical basis of superelastic behavior of certain biopolymers
- Dmitry Indeitsev: Kinetics of chemical reactions in deformable solids with dynamic loading
- Stéphane Berbenni: Internal length scale effects on the local and overall behaviors of polycrystals
- Mikhail Karyakin: Theory of isolated and continuously distributed disclinations and dislocations in micropolar media
- Denis Sheydakov: Buckling of elastic composite rod of micropolar material subject to combined loads
- Céline Chesnais: Generalized media and structural dynamics
- Vladimir Erofeev: Nonlinear waves in the Cosserat Continuum with restricted rotation
- Rainer Glüge: Elastic modeling of deformation twinning
- Daniel Scharding: Parameter identification for extended continua
- Arthur Lebée: A full bending gradient theory for periodic plates homogenization

- Thomas Michelitsch: Wave propagation in quasi-continuous linear chains with self-similar harmonic interactions - towards a fractal mechanics
- Qi-Chang He: Symmetry classes of flexoelectricity
- Sergey Gerasimov: Visualization at studying hydrodynamic instability in strong media

Contributions in this book provide in print a large selection from these lectures.

Such a publication can be realized only with generous support of different people and organizations. So we have to acknowledge:

- Dipl.-Ing. Andreas Kutschke and Prof. Victor A. Eremeyev for fulfilling the organizational duties during the Trilateral seminar,
- Mrs. Dipl.-Ing. Barbara Renner, Mrs. MSc Oksana Ozhoga-Maslovskaja, MSc Adili Maimaiti, MSc Ivan Lvov, Dipl.-Ing. Andreas Kutschke and Prof. Victor A. Eremeyev for the assistance in the manuscript preparation,
- Dr. Christoph Baumann from Springer for supporting the project and solving a lot of difficulties, and last but not least
- the Leucorea administration for organizing the hosting in Wittenberg.

Finally, it should be noted that the Deutsche Forschungsgemeinschaft, the Russian Foundation of Basic Research and the French partner organization CNRS gave financial support for the realization of the project.

Halle, *Holm Altenbach*
Nizhny Novgorod, *Vladimir I. Erofeev*
Paris, *Gérard A. Maugin*
December 2010

Contents

Part VI Further Applications

List of Contributors

Eron L. Aero
Institute of Problems in Mechanical Engineering,
Bol'shoy pr. 61, V.O., 199178 St. Petersburg, Russia,
e-mail: 16aero@mail.ru

Holm Altenbach
Martin-Luther-Universität Halle-Wittenberg,
Kurt-Mothes-Str. 1, 06120 Halle (Saale), Germany,
e-mail: holm.altenbach@iw.uni-halle.de

Boris R. Andrievsky
Institute of Problems in Mechanical Engineering,
Bol'shoy pr. 61, V.O., 199178 St. Petersburg, Russia,
e-mail: bandri@yandex.ru

Stéphane Berbenni
LPMM, CNRS, Arts et Métiers ParisTech, Technopole,
4, rue Augustin Fresnel, 57078 Metz Cedex 03, France,
e-mail: stephane.berbenni@ensam.eu

Albrecht Bertram
Institut für Mechanik, Otto-von-Guericke-Universität,
Universitätsplatz 2, 39106 Magdeburg, Germany,
e-mail: albrecht.bertram@ovgu.de

Claude Boutin
DGCB, FRE CNRS 3237, École Nationale des Travaux Publics de l'État,
Université de Lyon, France,
e-mail: claude.boutin@entpe.fr

Vladimir M. Catson
Saratov State Technical University,
Politekhnicheskaja St. 77, 410054 Saratov, Russia,
e-mail: bobah311@yandex.ru

Céline Chesnais
Laboratoire Central des Ponts et Chaussées,
Université Paris-Est, Paris, France,
e-mail: celine.chesnais@lcpc.fr

Shahram Derogar
Department of Civil and Structural Engineering,
University of Sheffield, United Kingdom,
e-mail: derogar2002@yahoo.com

Victor A. Eremeyev
Martin-Luther-Universität Halle-Wittenberg,
Kurt-Mothes-Str. 1, 06120 Halle (Saale), Germany,
South Scientific Center of RASci & South Federal University,
Milchakova St. 8a, 344090 Rostov on Don, Russia,
e-mail: eremeyev.victor@gmail.com,
e-mail: victor.eremeyev@iw.uni-halle.de

Vladimir I. Erofeev
Nizhny Novgorod Branch of Blagonravov Mechanical Engineering Research Institute RAS,
Belinskogo St. 85, 603024 Nizhny Novgorod , Russia,
e-mail: erf04@sinn.ru

Paul Fischer
Chair of Applied Mechanics, University of Erlangen-Nuremberg,
Egerlandstrasse 5, 91058 Erlangen,Germany,
e-mail: paul.fischer@ltm.uni-erlangen.de

Samuel Forest
Mines ParisTech CNRS Centre des Matériaux UMR 7633, BP87,
91003 Evry, France,
e-mail: samuel.forest@ensmp.fr

Jean-François Ganghoffer
LEMTA, ENSEM,
2, Avenue de la Forêt de Haye, BP 160, 54504 Vandoeuvre Cedex, France,
e-mail: jean-francois.ganghoffer@ensem.inpl-nancy.fr

Stéphane Hans
DGCB, FRE CNRS 3237, École Nationale des Travaux Publics de l'État,
Université de Lyon, France,
e-mail: stephane.hans@entpe.fr

Elena A. Ivanova
Institute for Problems in Mechanical Engineering of the Russian Academy of Sciences,
Bol'shoy pr. 61, V.O., 199178, St. Petersburg, Russia,
e-mail: elenaivanova239@post.ru

Mikhail I. Karyakin
Southern Federal University,
Milchakova 8a, 344090 Rostov on Don, Russia,
e-mail: karyakin@math.sfedu.ru

Rasa Kazakevičiūtė-Makovska
Mechanics-Continuum Mechanics, Ruhr-University Bochum,
D-44780 Bochum, Germany,
e-mail: Rasa.Kazakeviciute-Makovska@rub.de

Ellen Kuhl
Departments of Mechanical Engineering, Bioengineering and Cardiothoracic Surgery,
Stanford, CA 94305, USA,
e-mail: ekuhl@stanford.edu

Leonid P. Lebedev
Universidad Nacional de Colombia,
Cr. 45, # 2685, Bogotá D.C., Colombia,
e-mail: llebedev@unal.edu.co

Arthur Lebée
Université Paris-Est, Laboratoire Navier (ENPC/LCPC/CNRS), École des Ponts ParisTech,
6 et 8 avenue Blaise Pascal, 77455 Marne-la-Vallée, France,
e-mail: arthur.lebee@enpc.fr

Evgeny V. Lomakin
Faculty of Mechanics and Mathematics, Moscow State Lomonosov University,
119992 Moscow, Russia,
e-mail: lomakin@mech.math.msu.su

Gérard A. Maugin
Université Pierre et Marie Curie – Paris 6, Institut Jean Le Rond d'Alembert, UMR CNRS 7190,
4 place Jussieu, 75252 Paris Cedex 05 France,
e-mail: gerard.maugin@upmc.fr

Thomas M. Michelitsch
Université Pierre et Marie Curie – Paris 6, Institut Jean Le Rond d'Alembert, UMR CNRS 7190,
4 place Jussieu, 75252 Paris Cedex 05 France,
e-mail: michel@lmm.jussieu.fr

Franck C.G.A. Nicolleau
Department of Mechanical Engineering, University of Sheffield, United Kingdom,
e-mail: f.nicolleau@shefield.ac.uk

Andrzej F. Nowakowski
Department of Mechanical Engineering, University of Sheffield, United Kingdom,
e-mail: a.f.nowakowski@shefield.ac.uk

Alexey V. Porubov
Institute of Problems in Mechanical Engineering,
Bol'shoy pr. 61, V.O., 199178 St. Petersburg, Russia,
e-mail: porubov.math@mail.ioffe.ru

Amirtham Rajagopal
Chair of Applied Mechanics, University of Erlangen-Nuremberg,
Egerlandstrasse 5, 91058 Erlangen, Germany,
e-mail: kalya@gmail.com

Lalaonirina R. Rakotomanana
IRMAR - UMR 6625 CNRS, Université de Rennes 1,
35042 Rennes Cedex, France,
e-mail:lalaonirina.rakotomanana-ravelonarivo@univ-rennes1.fr

Francisco Dos Reis
LEMTA, ENSEM, 2, Avenue de la Forêt de Haye, BP 160,
54504 Vandoeuvre Cedex, France,
e-mail: francisco.dos-reis@ac-strasbourg.fr

Karam Sab
Université Paris-Est, Laboratoire Navier (ENPC/LCPC/CNRS). École des Ponts ParisTech,
6 et 8 avenue Blaise Pascal, 77455 Marne-la-Vallée, France,
e-mail: karam.sab@enpc.fr

Denis Sheydakov
South Scientific Center of Russian Academy of Scienes,
Chekhova Ave. 41, 344006 Rostov on Don, Russia,
e-mail: sheidakov@mail.ru

Sergey F. Sheshenin
Nizhny Novgorod Branch of Blagonravov Mechanical Engineering Research Institute RAS,
Belinskogo St. 85, 603024 Nizhny Novgorod , Russia,
e-mail: shesheninsf@nnov.transneft.ru

Holger Steeb
Mechanics-Continuum Mechanics, Ruhr-University Bochum,
D-44780 Bochum, Germany,
e-mail: Holger.Steeb@rub.de

Paul Steinmann
Chair of Applied Mechanics, University of Erlangen-Nuremberg,
Egerlandstrasse 5, 91058 Erlangen, Germany,
e-mail: steinmann@ltm.uni-erlangen.de

Nirmal Antonio Tamarasselvame
IRMAR - UMR 6625 CNRS, Université de Rennes 1,
35042 Rennes Cedex, France,
e-mail: nirmal.antonio-tamarasselvame@univ-rennes1.fr

Aleksandr I. Zemlyanukhin
Saratov State Technical University,
Politekhnicheskaja St. 77, 410054 Saratov, Russia,
e-mail: zemlyanukhinai@sstu.ru, e-mail: bobah311@yandex.ru

Leonid M. Zubov
Southern Federal University,
Milchakova 8a, 344090 Rostov on Don, Russia,
e-mail: zubov@math.sfedu.ru

Part I
Historical Background and Future Trends

Chapter 1
A Historical Perspective of Generalized Continuum Mechanics

Gérard A. Maugin

Abstract In a period of forty years the author has had the opportunity to work, or to entertain friendly connections, with many actors of the scene of generalized continuum mechanics (GCM). This training and knowledge here is used to the benefit of the readers as an overview of this scene with the aim to delineate further avenues of development within the framework of the trilateral seminar held in Wittenberg (2010). Starting essentially with Pierre Duhem and the Cosserat brothers, this specialized, albeit vast, field of continuum mechanics has developed by successive abandonments of the working hypotheses at the basis of standard continuum mechanics, that mechanics masterly devised by Euler and Cauchy and some of their successors in the 19th century (Piola, Kirchhoff, *etc.*). In the present survey we briefly analyze successive steps such as the introduction of nonsymmetric stresses, couple stresses, internal degrees of freedom and microstructure, the introduction of strain gradient theories, and material inhomogeneities with a length scale, nonlocality of the weak and strong types, the loss of Euclidean geometry to describe the material manifold, and finally the loss of classical differentiability of basic operations as can occur in a deformable fractal material object.

Key words: Generalized continua. Nonsymmetric stress. Couple stress. Micromorphic bodies. Micropolar materials. Nonlocality. Strain-gradient materials. Non-Euclidean manifold.

1.1 Introduction

At a recent colloquium [73] we have given a historical view of the development of so-called "generalized continuum mechanics". The thesis presented was that gener-

Gérard A. Maugin
Université Pierre et Marie Curie – Paris 6, Institut Jean Le Rond d'Alembert, UMR CNRS 7190, 4 place Jussieu, 75252 Paris Cedex 05 France
e-mail: gerard.maugin@upmc.fr

H. Altenbach et al. (eds.), *Mechanics of Generalized Continua,*
Advanced Structured Materials, 7, DOI: 10.1007/978-3-642-19219-7_1,

alization occurs through the successive abandonment of the basic working hypotheses of standard continuum mechanics of Cauchy: that is, introduction of a rigidly rotating microstructure and *couple stresses* (Cosserat continua or *micropolar* bodies, nonsymmetric stresses), introduction of a truly deformable microstructure (*micromorphic* bodies), "weak" *nonlocalization* with *gradient theories* and the notion of *hyperstresses*, and the introduction of characteristic lengths, "strong nonlocalization" with space functional constitutive equations and the loss of the Cauchy notion of stress, and finally giving up the Euclidean and even Riemannian material background.

This evolution is paved by landmark papers and timely scientific gatherings (*e.g.*, Freudenstadt in 1967, Udine in 1970, Warsaw in 1977) to which the Paris colloquium of 2009 must now be added (Maugin and Metrikine, editors [76]). This will be examined in some detail in the following sections. Here we simply note that the publication of the book of the Cosserat brothers in 1909 [10] was a true initial landmark, although at the time noticed by very few people – among them Élie Cartan and Ernst Hellinger [44]. In passing we also emphasize that this was one of the first attempts to exploit some group theoretical argument (so-called Euclidean action) in the general formulation of continuum mechanics. Thus a real "generalized continuum mechanics" developed first slowly and rather episodically and then with a real acceleration in the 1960s. Accordingly, a new era was born in the field of continuum mechanics.

1.2 From Cauchy and the 19th Century

Here we consider as a classical standard the basic model considered by engineers in solid mechanics and the theory of structures. This essentially is the theory of continua set forth by A.L. Cauchy in the early 19th century for isotropic homogeneous elastic solids in small strains. The theory of continua respecting Cauchy's axioms and simple working hypotheses is such that the following holds true:

1. **Cauchy's postulate**: The traction $\mathbf{T}^d$ on a facet cut in the solid depends on the geometry of that facet only at the *first order* (the local unit normal of components n_j); it will be linear in that normal. From this follows the notion of *stress tensor* $\boldsymbol{\sigma} = \{\sigma_{ji}; i, j = 1,2,3\}$, the so-called stress being the only "internal force" in the theory. That is, using a classical Cartesian tensor notation:

$$T_i^d = n_j \sigma_{ji}. \tag{1.1}$$

2. **It being understood** that both physical space (of Newton) and material manifold (the set of material particles constituting the body) are Euclidean and connected, hence the notion of displacement $\mathbf{u} = \{u_i\}$ is well defined.
3. **Working hypotheses**

   (i) There are no applied couples in both volume and surface.

(ii) There exists no "microstructure" described by additional internal degrees of freedom.

According to items 3 (i) and (ii) the Cauchy stress tensor is symmetric:

$$\boldsymbol{\sigma} = \boldsymbol{\sigma}^T \quad i.e. \quad \sigma_{ji} = \sigma_{ij}. \tag{1.2}$$

This results from the application of the balance of angular momentum. Isotropy, homogeneity, and small strains are further hypotheses but they are not so central to our argument.

Then generalizations of various degrees consist in relaxing more or less these different items above, hence the notion of *generalized continuum*. This notion of generalization depends also on the culture and physical insight of the scientists. For instance the following generalizations are "weak" ones:

- "Generalized" Hooke's law (linear, homogeneous, but *anisotropic* medium);
- Hooke–Duhamel law in thermoelasticity;
- Linear homogeneous piezoelectricity in obviously anisotropic media (no center of symmetry)

These are "weak" generalizations because they do not alter the main mathematical properties of the system. Of course, thermoelasticity and linear piezoelectricity require adding new independent variables (*e.g.*, temperature θ or scalar electric potential ϕ). In some sense, the problem becomes four-dimensional for the basic field (elastic displacement and temperature in one case, elastic displacement and electric potential in the other). The latter holds in this mere simplicity under the hypothesis of weak electric fields, from which there follows the neglect of the so-called ponderomotive forces and couples, *e.g.*, the couple

$$(\mathbf{P} \times \mathbf{E})_i = \varepsilon_{ijk} P_j E_k \tag{1.3}$$

with ε_{ijk} as the permutation symbol in Cartesian tensor index notation, and this will yield (square brackets denote anti-symmetrization)

$$\sigma_{[ji]} = C_{ji}, \quad e.g., \quad C_{ji} = P_{[j} E_{i]}, \tag{1.4}$$

when electric field $\mathbf{E}$ and electric polarization $\mathbf{P}$ are not necessarily aligned; see Eringen and Maugin [30]. Such theories, just like standard elasticity, do not involve a *length scale*. But classical linear *inhomogeneous* elasticity presents a higher degree of generalization because a characteristic length intervenes necessarily, the characteristic length over which the material properties vary in the absence of loading.

1.3 True Generalizations

From here on we envisage three true (in our view) generalizations. The first of these is that the Cauchy stress tensor becomes nonsymmetric. The second one is that the

validity of the Cauchy postulate can be lost. And last but not least that the Euclidean nature of the material manifold can be lost. In what follows all three items will be discussed in detail.

1.3.1 Various Reasons of the Nonsymmetry of the Cauchy Stress Tensor

The nonsymmetry may be due to

(i) the existence of body couples (*e.g.*, just as above in electromagnetism:

$$\mathbf{P}\times\mathbf{E} \quad \text{or/and} \quad \mathbf{M}\times\mathbf{H}$$

if $\mathbf{M}$ and $\mathbf{H}$ denote volume magnetization and magnetic field; case of intense electromagnetic fields or linearization about intense bias fields);

(ii) the existence of surface couples (introduction of "internal forces" of a new type: so-called *couple stresses*); the medium possesses internal degrees of freedom that modify the balance of angular momentum;

(iii) the existence of internal degrees of freedom (of a nonmechanical nature in origin, *e.g.*, polarization inertia in ferroelectrics, intrinsic spin in ferromagnetics (see [67]);

(iv) the existence of internal degrees of freedom of "mechanical" nature.

This is where the Cosserats' model comes into the picture. The first example in this class pertains to a *rigid microstructure* (three additional degrees of freedom corresponding to an additional rotation at each material point, independently of the vorticity). Examples of media of this type go back to the early search for a continuum having the capability to transmit transverse waves (as compared to acoustics in a pure fluid), *i.e.*, in relation to optics. The works of McCullagh [77] and Lord Kelvin must be singled out (*cf.* Whittaker [106]). Pierre Duhem [15] proposes to introduce a triad of three rigidly connected directors (unit vectors) to represent this rotation. In modern physics there are other tools for this including Euler's angles (not very convenient), quaternions and spinors. It is indeed the Cosserats, among other studies in elasticity, who really introduced internal degrees of freedom of the rotational type (these are *micropolar continua* in the sense of Eringen [26, 27]) and the dual concept of *couple stress*. Hellinger, in a brilliant essay [44], recognized at once the new potentialities offered by this generalization but did not elaborate on these.

A modern rebirth of the field had to await works in France by crystallographs (Laval [53, 54, 55]; Le Corre [59]), in Russia by Aero and Kuvshinskii [1], and Palmov [87], in Germany by Schaefer [94], Günther [43], Neuber [82], and in Italy by Grioli [42] and Capriz – see his book [7]. But the best formulations are those obtained by considering a field of orthogonal transformations (rotations) and not the directors themselves: Eringen [23], Kafadar and Eringen [45], Nowacki [86],

although we note some obvious success of the "director" representation, *e.g.*, in *liquid crystals* (Ericksen [21]; Leslie [62], Stokes [98]) and the kinematics of the deformation of slender bodies (works by Ericksen, Truesdell, Naghdi).

But in the mid 1960s a complete revival of continuum mechanics took place which, by paying more attention to the basics, favored the simultaneous formulation of many more or less equivalent theories of generalized continua in the line of thought of the Cosserats (works by Mindlin [78], Mindlin and Tiersten [81], Mindlin and Eshel [80], Green and Rivlin [41], Green and Naghdi [40], Toupin [100, 101], Truesdell and Toupin [103], Truesdell and Noll [102], and Eringen and Suhubi [31, 32], *etc.*).

More precisely, in the case of a *deformable microstructure* at each material point, the vector triad of directors of Duhem-Cosserats becomes deformable and the additional degree of freedom at each point, or micro-deformation, is akin to a general linear transformation (nine degrees of freedom). These are **micromorphic continua** in Eringen's classification [26, 27]. A particular case is that of **continua with microstretch** [24]. A truly new notion here is that of the existence of a conservation law of *micro-inertia* (Eringen [2]). We illustrate these various generalizations by giving the relevant form of the local equation of moment of momentum in quasi-statics:

- **Micromorphic bodies** (Eringen [2, 31, 32], Mindlin [78, 80, 81]; Years 1962-1966) [Notation: μ_{kji} is the hyperstress tensor, s_{ji} is the so-called symmetric micro-stress, and ℓ_{ij} is the body-moment tensor of which the skew part represents a body couple $C_{ji} = -C_{ij}$]:

$$\begin{array}{ll} \mu_{kij,k} + \sigma_{ji} - s_{ji} + \ell_{ij} = 0, & \sigma_{ji} = \sigma_{(ji)} + \sigma_{[ji]}, \\ s_{[ji]} = 0, & \ell_{ji} = C_{ji} + \ell_{(ji)}. \end{array} \tag{1.5}$$

- **Micropolar bodies** (Cosserat brothers [10], *etc.*) [Notation: $\mu_{k[ji]}$ is the couple-stress tensor; C_i is the axial vector uniquely associated with C_{ji} while m_{ji} is associated in the same way with $\mu_{k[ji]}$]:

$$\mu_{k[ji],k} + \sigma_{[ji]} + C_{ij} = 0 \quad \text{or} \quad m_{ji,j} + \varepsilon_{ikj}\,\sigma_{kj} + C_i = 0. \tag{1.6}$$

- **Bodies with microstretch** (Eringen [24]) [Notation: m_k denotes the intrinsic dilatational stress or microstretch vector; ℓ is the body microstretch force such that $\ell_{ij} = (\ell/3)\,\delta_{ij}$, and σ and s are intrinsic and micro scalar forces]:

$$\mu_{klm} = \frac{1}{3} m_k\,\delta_{lm} - \frac{1}{2}\varepsilon_{lmr}\,m_{kr} \tag{1.7}$$

so that

$$m_{kl,k} + \varepsilon_{lmn}\,\sigma_{mn} + C_l = 0, \quad m_{k,k} + \sigma - s + \ell = 0. \tag{1.8}$$

- **Dilatational elasticity** (Cowin and Nunziato [11]) [only the second of Eqs (1.8) is relevant]:

$$m_{k,k} + \sigma - s + \ell = 0. \tag{1.9}$$

In these equations given in Cartesian components in order to avoid any misunderstanding (note that the divergence is always taken on the first index of the tensorial object to which it applies), μ_{kij} is a new internal force having the nature of a third-order tensor. It has no specific symmetry in Eqs (1.5) and it may be referred to as a *hyperstress*. In the case of Eqs (1.6) this quantity is skewsymmetric in its last two indices and a second order tensor – called a *couple stress* – of components m_{ji} can be introduced having *axial* nature with respect to its second index. The fields s_{ji} and ℓ_{ij} are, respectively, a symmetric second order tensor and a general second order tensor. The former is an *intrinsic interaction stress*, while the latter refers to an external source of *both* stress and couple according to the last of Eqs (1.5). Only the skew part of the later remains in the special case of micropolar materials (Eqs (1.6) in which C_i represents the components of an *applied couple*, an axial vector associated with the skewsymmetric C_{ji}). The latter can be of electromagnetic origin, and more rarely of pure mechanical origin. Equations (1.7) and (1.8) represent a kind of intermediate case between micromorphic and micropolar materials. The case of dilatational elasticity in Eq. (1.9) appears as a further reduction of that in Eqs (1.8). This will be useful in describing the mechanical behavior of media exhibiting a distribution of holes or cavities in evolution.

Concerning the micromorphic case, a striking example is due to Drouot and Maugin [14] while dealing with fluid solutions of macromolecules, while Pouget and Maugin [89] have provided a fine example of truly micromorphic solids with the case of piezoelectric powders treated as continua.

Remark 1.1. Historical moments in the development of this avenue of generalization have been the IUTAM symposium organized by E. Kröner in Freudenstadt in 1967 (see Kröner [49]) and the CISM Udine summer course of 1970 (were present: Mindlin [79], Eringen [25], Nowacki [85], Stojanovic [97], Sokolowski, Maugin, Jaric, Micunovic, *etc.*).

Remark 1.2. Strong scientific initial motivations for the studies of generalized media at the time (1960s-1970s) were (i) the expected elimination of field singularities in many problems with standard continuum mechanics, (ii) the continuum description of *real* existing materials such as granular materials, suspensions, blood flow, *etc.* But further progress was hindered by a notorious lack of knowledge of new (and too numerous) material coefficients despite trials at estimates of such coefficients *e.g.*, by Gauthier and Jashman [37] at the Colorado School of Mines by building artificially microstructured solids.

Remark 1.3. The intervening of a rotating microstructure allows for the introduction of wave modes of rotation of the "optical" type with an obvious application to many solid crystals (*e.g.*, crystals equipped with a polar group such as $NaNO_2$; *cf.* Pouget and Maugin [89, 90]).

Remark 1.4. In some physical theories (micromagnetism, *cf.* Maugin [64]), an equation such as the first of Eqs (1.6) can be obtained in full dynamics:

$$m_{kij,k} + \sigma_{[ji]} + C_{ij} = \dot{S}_{ij}, \tag{1.10}$$

where m_{kij} (Heisenberg exchange-force tensor that is skewsymmetric in its last two indices), C_{ij} (interaction couple between material and electronic-spin continua) and S_{ij} (magnetic spin) all have a magnetic origin.

1.3.2 Loss of Validity of the Cauchy Postulate

Then the geometry of a cut intervenes at a higher order than one (variation of the normal unit, role of the curvature, edges, apices and thus capillarity effects). We may consider two different cases referred to as the *weakly nonlocal theory* and the *strongly nonlocal theory* (distinction introduced by the author at the Warsaw meeting of 1977; *cf.* Maugin [65]). Only the first type does correspond to the exact definition concerning a cut and the geometry of the cut surface. This is better referred to as *gradient theories of the n-th order*, it being understood that the standard Cauchy theory in fact is a *theory of the first gradient* (meaning by this first gradient of the displacement or theory involving just the strain and no gradient of it in the constitutive equations).

1.3.2.1 Gradient Theories

Now, as a matter of fact, gradient theories abound in physics, starting practically with all continuum theories in the 19$^{\text{th}}$ century. Thus, Maxwell's electromagnetism is a first-gradient theory (of the electromagnetic potentials); the Korteweg theory of fluids [47] is a theory of the first gradient of density (equivalent to a second-gradient theory of displacement in elasticity); Einstein's theory of gravitation (general relativity [16, 17]) is a second-gradient theory of the metric of curved space-time, and Le Roux [60, 61] seems to be the first public exhibition of a second-gradient theory of (displacement) elasticity in small strains (using a variational formulation). There was a renewal of such theories in the 1960s with the works of Casal [8] on capillarity, and of Toupin [100], Mindlin and Tiersten [81], Mindlin and Eshel [80], and Grioli [42] in elasticity.

However, it is with a neat formulation basing on the *principle of virtual power* that some order was imposed in these formulations with an unambiguous deduction of the (sometimes tedious) boundary conditions and a clear introduction of the notion of *internal forces* of higher order, *i.e.*, *hyperstresses* of various orders (see, Germain [38, 39]; Maugin [66]). Phenomenological theories involving gradients of other physical fields than displacement or density, coupled to deformation, were envisaged consistently by the author in his Princeton doctoral thesis [64] dealing with typical ferroïc electromagnetic materials. This is justified by a microscopic approach, *i.e.*, the continuum approximation of a crystal lattice with medium-range interactions; with distributed magnetic spins or permanent electric dipoles. This also applies to the pure mechanical case (see, for instance, the Boussinesq paradigm in

Christov *et al.* [9, 75]). The following are examples of such theories illustrated by the dependence of the potential energy W per unit volume for small strains:

- **Le Roux** [60, 61]:
$$W = W(u_{i,j}, u_{i,jk}, \ldots), \tag{1.11}$$
where $u_{i,j}$ denotes the displacement gradient, and $u_{i,jk}$ is the second gradient of the displacement.
- **Modern form** (Mindlin [78, 80, 81], Toupin [100, 101], Sedov [95], Germain [38], *etc.*; in the period 1962–1972):
$$W = W(e_{ij}, e_{ij,k}). \tag{1.12}$$
In the last case, *the symmetric first-order stress* $\bar{\sigma}_{ji}$ and the second-order stress or *hyperstress* m_{kji} (symmetric in its last two indices) are given by
$$\bar{\sigma}_{ji} = \frac{\partial W}{\partial e_{ij}} = \bar{\sigma}_{ij}, \quad m_{kji} = \frac{\partial W}{\partial e_{ij,k}} = m_{kij}, \tag{1.13}$$
where e_{ij} is the symmetric small strain, and $e_{ij,k}$ denotes its first gradient. Then the symmetric Cauchy stress reads
$$\sigma_{ji} = \bar{\sigma}_{ji} - m_{kji,k} = \frac{\delta W}{\delta e_{ij}} = \sigma_{ij}. \tag{1.14}$$
This is the functional derivative of the energy W.

Very interesting features of these models are:

F1. Inevitable introduction of characteristic lengths;
F2. Appearance of so-called capillarity effects (surface tension) due to the explicit intervening of curvature of surfaces;
F3. Correlative boundary layers effects,
F4. Dispersion of waves with a possible competition and balance between nonlinearity and dispersion, and the existence of solitonic structures (see Maugin [70]);
F5. Intimate relationship with the Ginzburg–Landau theory of phase transitions [12, 93] and, for fluids, van der Waals' theory [4, 104].

Indeed, a typical characteristic length ℓ is introduced by the ratio
$$\ell = \frac{|m_{kji}|}{|\bar{\sigma}_{ji}|}, \tag{1.15}$$
and this is obviously supposed to be much smaller than a typical macroscopic length L, *i.e.*, $\ell \ll L$.

Features F2 and F3 above are typically illustrated by the following set of boundary conditions [38, 99] ($\Omega = -D_j n_j/2$ is the mean curvature)

$$n_j \sigma_{ji} + (n_j D_p n_p - D_j)(n_k m_{kji}) = T_i^d \quad \text{at } \partial B - \Gamma\uparrow, \tag{1.16}$$

$$n_k m_{kji} n_j = R_i \quad \text{at } \partial B - \Gamma\uparrow, \tag{1.17}$$

$$\varepsilon_{ipq}\tau_p [n_k m_{kjq} n_j] = E_i \quad \text{along } \Gamma\uparrow, \tag{1.18}$$

where $\Gamma\uparrow$ is an oriented edge, τ_p denotes its unit tangent, and D indicates a tangential gradient. Here T_i^d, R_i and E_i are, respectively, an applied surface traction, a prescribed double-normal force, and a linear force density.

Remark 1.5. The principle of virtual power here is an interesting tool to obtain the set (1.16)–(1.18) unambiguously. But it also shows in agreement with Eq. (1.14) that the power of internal forces can be written either as

$$p_{(\text{int})}(\sigma) = -\sigma : \nabla\dot{\mathbf{u}}, \tag{1.19}$$

or as

$$p_{(\text{int})}(\bar{\sigma}, \mathbf{m}) = -(\bar{\sigma} : \nabla\dot{\mathbf{u}} + \mathbf{m} : \mathbb{W}\ \dot{\mathbf{u}}), \tag{1.20}$$

so that

$$p_{(\text{int})}(\sigma) = p_{(\text{int})}(\bar{\sigma}, \mathbf{m}) + \nabla\cdot(\mathbf{m} : \nabla\dot{\mathbf{u}}). \tag{1.21}$$

Here we used the convention that

$$\bar{\sigma} : \nabla\dot{\mathbf{u}} = \sigma_{ji}\dot{u}_{i,j}, \quad \mathbf{m} : \mathbb{W}\ \dot{\mathbf{u}} = m_{kji}\dot{u}_{i,jk}.$$

Repeated use of the divergence theorem will then directly lead to the set (1.16)–(1.18).

Truly sophisticated examples of the application of these gradient theories are found in

(i) the coupling of a gradient theory (of the carrier fluid) and consideration of a microstructure in the study of the inhomogeneous diffusion of microstructures in polymeric solutions (Drouot and Maugin [14]).
(ii) the elimination of singularities in the study of structural defects (dislocations, disclinations) in elasticity combining higher-order gradients and polar microstructure (*cf.* Lazar and Maugin [58]).

Most recent works consider the application of the notion of gradient theory in elastoplasticity for nonuniform plastic strain fields (works by Aifantis [2, 3, 107], Fleck & Hutchinson [33, 34, 35], and many others) – but see the thermodynamically admissible formulation in Maugin [68].

In so far as general mathematical principles at the basis of the notion of gradient theory are concerned, we note the fundamental works of Noll and Virga [84] and dell'Isola and Seppecher [13], the latter with a remarkable economy of thought.

1.3.2.2 Strongly Nonlocal Theory (Spatial Functionals)

Initial concepts in this framework were etablished by Kröner and Datta [50], Kunin [51, 52], Rogula [92], Eringen and Edelen [29]. As a matter of fact, the Cauchy con-

struct does *not* apply anymore. In principle, only the case of **infinite bodies** should be considered as any cut would destroy the prevailing long-range ordering. Constitutive equations become integral expressions over space, perhaps with a more or less rapid attenuation with distance of the spatial kernel. This, of course, inherits from the action-at-a-distance dear to the Newtonians, while adapting the disguise of a continuous framework. This view is justified by the approximation of an infinite crystal lattice: the relevant kernels can be justified through this discrete approach. Of course this raises the matter of solving integro-differential equations instead of partial-differential equations. What about boundary conditions that are in essence foreign to this representation of matter-matter interaction? There remains a possibility of the existence of a "weak-nonlocal" limit by the approximation by gradient models. Typically one would consider in the linear elastic case a stress constitutive equation in the form

$$\sigma_{ji}(\mathbf{x}) = \int_{\text{all space}} C_{jikl}\left(|\mathbf{x}-\mathbf{x}'|\right) e_{kl}(\mathbf{x}')\,\mathrm{d}^3\mathbf{x}', \tag{1.22}$$

where the constitutive functions C_{jikl} decreases markedly with the distance between material points $\mathbf{x}'$ and $\mathbf{x}$. In space of one dimension, an inverse to Eq. (1.22) may be of the form

$$\sigma - K\nabla^2\sigma = E\,e \tag{1.23}$$

with coefficients K and E, a model that we call "Helmholtz's" one because of the presence of the Laplacian ∇^2 that reflects the equivalence of interactions to the "right" and the "left". It is this kind of relation that allows one to compare the effects of "weakly" and "strongly" nonlocal theories in so far as the degree of singularity of some quantities is concerned (*cf.* Lazar and Maugin [58]).

The historical moment in the recognition of the usefulness of strongly nonlocal theories was the EUROMECH colloquium on nonlocality organized by D. Rogula in Warsaw in 1977 (*cf.* Maugin [65]). A now standard reference is Eringen's book [28]. A recent much publicized application of the concept of nonlocality is that to *damage* by Pijaudier-Cabot and Bažant [88].

Note in conclusion to this point that any field theory can be generalized to a nonlocal one while saving the notions of linearity and anisotropy; but loosing the usual notion of flux. Also, it is of interest to pay attention to the works of Lazar and Maugin [56, 57] for a comparison of field singularities in the neighborhood of structural defects in different "generalized" theories of elasticity (micropolar, gradient-like, strongly non local or combining these).

1.3.3 Loss of the Euclidean Nature of the Material Manifold

Indeed the basic relevant problem emerges as follows. How can we represent **geometrically** the fields of structural defects (such as **dislocations** associated with a

loss of continuity of the elastic displacement, or **disclinations** associated with such a loss for rotations)? A similar question is raised for **vacancies and point** defects. One possible answer stems from the consideration of a non-Euclidean material manifold, *e.g.*, a manifold without curvature but with affine connection, or an Einstein-Cartan space with **both** torsion and curvature, *etc.* With this one enters a true "geometrization" of continuum mechanics of which conceptual difficulties compare favorably with those met in modern theories of gravitation. Pioneers in the field in the years 1950-70 were K. Kondo [46] in Japan, E. Kröner [48] in Germany, Bilby [5] in the UK, Stojanovic [96] in what was then Yugoslavia, W. Noll [83] and C.C. Wang [105] in the USA. Modern developments are due to, among others, M. Epstein and the author [18, 19], M. Elzanowski and S. Preston (see the theory of material inhomogeneities by Maugin, [69]). Main properties of this type of approach are

(i) the relationship to the multiple decomposition of finite strains (Bilby, Kröner, Lee) and
(ii) the generalization of theories such as the theory of volumetric growth (Epstein and Maugin [20]) or the theory of phase transitions within the general **theory of local structural rearrangements** (local evolution of reference; see Maugin [72], examining Kröner's inheritance and also the fact that true **material inhomogeneities** (dependence of material properties on the material point) are then seen as **pseudo-plastic effects** [71]).

All local structural rearrangements and other physical effects (*e.g.*, related to the diffusion of a dissipative process) are reciprocally seen as pseudo material inhomogeneities [72]. Many of these advances are first-hand critically expanded in a recent book [74]. An original geometric solution is presented in the book of Rakotomanana [91] which offers a representation of a material manifold that is everywhere dislocated. Introduction of the notion of fractal sets opens new horizons (*cf.* Li and Ostoja–Starzewski, [63]). An antiquated forerunner work of all this may be guessed in Burton [6], but only with obvious good will by a perspicacious reader.

1.4 Conclusions

Since the seminal work of the Cosserats, three more or less successful paths have been taken towards the generalization of continuum mechanics. These were recalled above. An essential difference between the bygone times of the pioneers and now is that artificial materials can be man-made that are indeed generalized continua. In addition, mathematical methods have been developed (homogenization techniques) that allow one to show that generalized continua are deduced as macroscopic continuum limits of some structured materials. This is illustrated by the book of Forest [36].

In conclusion, we can answer three basic questions that are clearly posed:

(1) Do we need GCM at all?
(2) Do we find the necessary tools in what exists nowadays?

(3) What is the relationship between discrete and continuous descriptions if there must exist a consistent relationship between the two?

The first two questions are positively answered in view of the above described developments. The third question is of a different nature because, in principle, continuum theories can be developed independently of any precise microscopic vision, being judged essentially on their inherent logical structure, the possibility to have access through appropriate experiments to the material constants they introduce, and finally their efficiency in solving problems. However, in contrast to those hard-line continuum theoreticians, we personally believe that any relationship that can be established with a sub-level degree of physical description is an asset that no true physicist can discard.

References

[1] Aero, E.L., Kuvshinskii, E.V.: Fundamental equations of the theory of elastic media with rotationally interacting particles. Engl. Transl. Soviet Physics Solid State **2**, 1272–1281 (1961) (in Russian, 1960)

[2] Aifantis, E.C.: On the microscopic origin of certain inelastic models. Tran ASME J. Engng Mat. Technol.**106**, 326–330 (1984)

[3] Aifantis, E.C.: On the role of gradients in the localization of deformation and fracture. Int. J. Engng Sci. **30**, 1279–1299 (1992)

[4] Baidakov, V.G., Boltachev, G.Sh., Potsenko, S.P., Chernykh, G.C.: The van der Waals theory of capillarity and computer simulation. Colloid J. (transl. from Russ.) **64**, 6, 661–670 (2002)

[5] Bilby, B.A.: Geometry and continuum mechanics. In: *Mechanics of generalized continua (Proc. IUTAM Symp. Freudenstadt, 1967)*, ed. E. Kröner, pp.180–199, Springer-Verlag, Berlin (1968)

[6] Burton, C.V.: Theory concerning the constitution of matter. Phil. Mag., **33**, No. 201, 191–204 (1891)

[7] Capriz, G.: *Continua with microstructure*. Springer-Verlag, New York (1989)

[8] Casal, P.: Capillarité interne en mécanique. C.R. Acad. Sci. Paris, **256**, 3820–3822 (1963)

[9] Christov, C.I., Maugin, G.A., Porubov, A.S.: On Boussinesq's paradigm on nonlinear wave propagation, C.R. Mécanique (Acad. Sci. Paris, Special Issue on Boussinesq) **335**(9-10), 521–535 (2007)

[10] Cosserat, E., Cosserat, F.: *Théorie des Corps Déformables*. Hermann Editeurs, Paris (1909) (Reprint, Gabay, Paris, 2008)

[11] Cowin, S.C., Nunziato, J.W.: Linear elastic materials with voids. J. Elasticity **13**, 125–147 (1983)

[12] Cyrot, M.: Ginzburg-Landau theory for superconductors. Report Progress in Physics, 36/2, 103–158 (1973)

[13] Dell'Isola, F., Seppecher, P.: The relationship between edge contact forces, double forces and intersticial working allowed by the principle of virtual power. C.R. Acad. Sci. Paris IIb, **321**, 303–308 (1995)
[14] Drouot, R., Maugin, G.A.: Phenomenological theory for polymer diffusion in non-homogeneous velocity gradient flows. Rheologica Acta **22**(4), 336–347 (1983)
[15] Duhem, P.: Le potentiel thermodynamique et la pression hydrostatique. Ann. Ecol. Norm., **10**, 187–230 (1893)
[16] Einstein, A.: Die Grundlage der allgemeinen Relativitätstheorie. Ann. der Phy. **49**, 769–822 (1916)
[17] Einstein, A.: *The Meaning of relativity*. Princeton University Press, Princeton (1956)
[18] Epstein, M., Maugin, G.A.: The energy-momentum tensor and material uniformity in finite elasticity. Acta Mechanica **83**(3-4), 127–133 (1990)
[19] Epstein, M., Maugin, G.A.: Notions of material uniformity and homogeneity (Opening Lecture of MS1, ICTAM, Kyoto, 1996). in: *Theoretical and Applied Mechanics*, eds. T. Tatsumi, E. Watanabe, and T. Kambe, 201–215, Elsevier, Amsterdam (1997)
[20] Epstein, M., Maugin, G.A.: Thermomechanics of volumetric growth in uniform bodies. Int. J. Plasticity **16**(7-8), 951–978 (2000)
[21] Ericksen, J.L.: Anisotropic fluids. Arch. Rat. Mech. Anal. **4**, 231–237 (1960)
[22] Eringen, A.C.: Theory of micropolar fluids. J. Math. Mech. **16**, 1–18 (1966)
[23] Eringen, A.C.: Theory of micropolar elasticity. in: *Fracture: A treatise*, ed. H. Liebowitz, Vol. II, 621–729, Academic Press, New York (1968)
[24] Eringen, A.C.: Micropolar fluids with stretch. Int. J. Engng.Sci. **7**, 115–127 (1969)
[25] Eringen, A.C.: Formulation of micropolar thermoelasticity. CISM Courses and Lectures No. 23, Udine, Springer, Vienna (1970)
[26] Eringen, A.C.: *Microcontinuum field theories, I- Foundations and solids*. Springer, New York (1999)
[27] Eringen, A.C.: *Microcontinuum field theories, II- Fluent media*. Springer, New York (2001)
[28] Eringen, A.C.: *Nonlocal continuum field theories*. Springer, New York (2002)
[29] Eringen, A.C., Edelen, D.G.B.: On nonlocal elasticity. Int. J. Egng. Sci. **10**(3), 233–248 (1972)
[30] Eringen, A.C., Maugin, G.A.: *Electrodynamics of continua*. 2 vol. Springer-Verlag, New York (1990)
[31] Eringen, A.C., Suhubi, E.S.: Nonlinear theory of simple microelastic solids I. Int. J. Engng. Sci. **2**(2), 189–203 (1964)
[32] Eringen, A.C., Suhubi, E.S.: Nonlinear theory of simple microelastic solids II. Int. J. Engng. Sci. **2**(4), 389–404 (1964)
[33] Fleck, N.A., Hutchinson, J.W.: A phenomenological theory of strain-gradient effects in plasticity. J. Mech. Phys. Solids, **41**, 1825–1857 (1993)
[34] Fleck, N.A., Hutchinson, J.W.: Strain gradient plasticity. In: Advances in Applied Mechanics, ed. J.W. Hutchinson, Vol. 33, pp. 296–361 (1997)

[35] Fleck, N.A., Muller, G.M., Ashby, M.F., and Hutchinson, J.W.: Strain-gradient plasticity: Theory and Experiment. Acta Metallurgica et Materialia **42**, 475–487 (1994)
[36] Forest, S.: *Milieux continus généralisés et matériaux hétérogènes*. Presses de l'Ecole des Mines, Paris (2006)
[37] Gauthier, R.D., Jashman, W.E.: A quest for micropolar elastic constants. J. Appl. Mech., Trans. ASME Ser E., **42**(2), 369–374 (1975)
[38] Germain, P.: La méthode des puissances virtuelles en mécanique des milieux continus, Première partie: théorie du second gradient. J. de Mécanique (Paris), **12**, 235–274 (1973)
[39] Germain, P.: The method of virtual power in continuum mechanics-II: Microstructure. SIAM J. Appl. Math., **25**(3), 556–575 (1973)
[40] Green, A.E., Naghdi, P.M.: Micropolar and director theories of plates. Quart. J. Mech. Appl. Math., **20**, 183–199 (1967)
[41] Green, A.E., Rivlin, R.S.: Multipolar continuum mechanics. Arch. Rat. Mech. Anal. **17**, 113–147 (1964)
[42] Grioli, G.: Elasticità asimmetrica. Ann. Mat. Pura ed Applicata, Ser. IV, **50**, 389–417 (1960)
[43] Günther, W.: Zur Statik und Kinematik des Cosseratschen Kontinuums. Abh. Braunschweig. Wiss. Ges., **10**, 195 (1958)
[44] Hellinger, E.: Die allgemeinen Ansätze der Mechanik der Kontinua. in: *Enz. Math. Wiss.*, Vol. **4**, 602–694, eds. F. Klein and K. Wagner, Springer, Berlin (1914)
[45] Kafadar, C.B., Eringen, A.C.: Micropolar media -I- The classical theory. Int. J. Engng. Sci. **9**(3), 271–308 (1971)
[46] Kondo, K.: Non-Riemannian geometry of imperfect crystals from a macroscopic viewpoint. in: *RAAG Memoirs of the unifying study of basic problems in engineering and physical sciences by means of geometry*, Vol. **1**, 459–480, ed. K. Kondo, Gakujutsu Bunken Fukyukai, Tokyo (1955)
[47] Korteweg, D.J.: Sur la forme que prennent les équations du mouvement des fluides si l'on tient compte des forces capillaires causées par des variations de densité considérables mais continues et sur la théorie de la capillarité dans l'hypothèse d'une variation de la densité. Arch. Néer. Sci. Exactes et Nat., Série II, **6**, 1–24 (1901)
[48] Kröner, E.: *Kontinuumstheorie der Versetzungen und Eigenspannungen*, Springer-Verlag, Berlin (1958)
[49] Kröner, E. (Editor): *Generalized Continua*. Proc. IUTAM Symp. Freudenstadt, Springer-Verlag, Berlin (1968)
[50] Kröner, E., Datta, B.K.: Nichtlokal Elastostatik: Ableitung aus der Gittertheorie. Z. Phys. **196**(3), 203–211 (1966)
[51] Kunin, I.A.: Model of elastic medium with simple structure and space dispersion. Prikl. Mat. Mekh. **30**, 542–550 (1966)
[52] Kunin, I.A.: *Elastic media with microstructure I & II*. Springer-Verlag, Berlin (1982) (translated from the 1975 Russian edition)

[53] Laval, J.: L'élasticité du milieu cristallin -I: J. Phys. Radium **18**(4), 247–259 (1957)
[54] Laval, J.: L'élasticité du milieu cristallin -II: J. Phys. Radium **18**(5), 289–296 (1957)
[55] Laval, J.: L'élasticité du milieu cristallin -III: J. Phys. Radium **18**(6), 369–379 (1957)
[56] Lazar, M., Maugin, G.A.: Defects in Gradient Micropolar Elasticity. I - Screw Dislocation. J. Mech. Phys. Solids **52**, 2263–2284 (2004)
[57] Lazar, M., Maugin, G.A.: Defects in Gradient Micropolar Elasticity. II - Edge dislocation and disclinations. J. Mech. Phys. Solids **52**, 2285–2307 (2004)
[58] Lazar, M., Maugin, G.A.: On microcontinuum field theories: The Eshelby stress tensor and incompatibility conditions. Phil. Mag. **87**, 3853–3870 (2007)
[59] Le Corre, Y.: La dissymétrie du tenseur des efforts et ses conséquences. J. Phys. Radium **17**(11), 934–939 (1956)
[60] Le Roux, J.: Etude géométrique de la torsion et de la flexion, dans les déformations infinitésimales d'un milieu continu. Ann. Ecole Norm. Sup., **28**, 523–579 (1911)
[61] Le Roux, J.: Recherches sur la géométrie des déformations finies. Ann. Ecole Norm. Sup. **30**, 193–245 (1913).
[62] Leslie, F.M.: Constitutive equations for liquid crystals. Arch. Rat. Mech. Anal., **28**, 265–283 (1968)
[63] Li, J., Ostoja–Starjeswki, M.: Fractals, product measures and continuum mechanics. In: *Mechanics of Generalized Continua: One hundred years after the Cosserats*. Eds. Maugin, G.A., Metrikine, A.V., pp. 315–323, Springer, New York (2010).
[64] Maugin, G.A.: Micromagnetism and polar media. Ph. D. thesis, Princeton University (1971)
[65] Maugin, G.A.: Nonlocal theories or gradient-type theories: A matter of convenience? Arch. Mechanics (PL, Proc. Euromech Coll. on Nonlocal Theories, Warsaw, 1977), **31**(1), 15–26 (1979)
[66] Maugin, G.A.: Method of virtual power in continuum-mechanics: Application to coupled fields. Acta Mechanica **35**(1-2), 1–70 (1980)
[67] Maugin, G.A.: *Continuum mechanics of electromagnetic solids*. North-Holland, Amsterdam (1988)
[68] Maugin, G.A.: Internal variables and dissipative structures. J. Non-Equilibrium Thermodynamics **15**(2), 173–192 (1990)
[69] Maugin, G.A.: *Material inhomogeneities in elasticity*. Chapman & Hall, London (1993)
[70] Maugin, G.A.: *Nonlinear waves in elastic crystals*. Oxford University Press, Oxford (1999)
[71] Maugin, G.A.: Pseudo-plasticity and pseudo-inhomogeneity effects in materials mechanics. J. Elasticity **71**(1-3), 81–103 (2003)

[72] Maugin, G.A.: Geometry and thermomechanics of structural rearrangements: Ekkehart Kroener's Legacy (GAMM'2002, Kröener's Lecture, Augsburg, 2002). Z. Angew. Math. Mech. **83**(2), 75–84 (2003)
[73] Maugin, G.A.: Generalized continuum mechanics: What do we understand by that? In: *Mechanics of Generalized Continua: One hundred years after the Cosserats*, eds G.A. Maugin & A.V. Metrikine, pp. 3–13, Springer, New York (2010)
[74] Maugin, G.A.: *Configurational forces: Thermomechanics, Mathematics, Physics, Numerics*. CRC/Chapman & Hall/Taylor and Francis, Boca Raton, FL, USA (2010)
[75] Maugin G.A., Christov C.I.: Nonlinear waves and conservation laws (Nonlinear duality between elastic waves and quasi-particles). In: *Topics in Nonlinear Wave Mechanics*, eds. C.I. Christov & A. Guran, pp. 117–160, Birkhäuser, Boston (2002)
[76] Maugin, G.A., Metrikine, A.V. (Eds): *Mechanics of Generalized Continua: One hundred years after the Cosserats*. Springer, New York (2010)
[77] McCullagh, J.: An essay towards a dynamical theory of crystalline reflexion and refraction. Trans. Roy. Irish Acad. Sci. **21**, 17–50 (1839)
[78] Mindlin, R.D.: Microstructure in linear elasticity. Arch. Rat. Mech. Anal. **16**, 51–78 (1964)
[79] Mindlin, R.D.: *Polarization gradient in elastic dielectric*. CISM Courses and Lectures No. 24, Udine, Springer, Vienna (1970)
[80] Mindlin, R.D., Eshel, N.N.: On first strain-gradient theories in linear elasticity. Int. J. Solids Structures **4**(1), 109–124 (1968)
[81] Mindlin, R.D., Tiersten, H.F.: Effects of couple stresses in linear elasticity. Arch. Rat. Mech. Anal. **11**, 415-448 (1962)
[82] Neuber, H.: On the general solution of linear elastic problems in isotropic and anisotropic Cosserat continua. In: *Proc. 11th International Conference of Applied Mechanics* (München, 1964), ed. H. Görtler, pp. 153–158, Springer-Verlag, Berlin (1964)
[83] Noll, W.: Materially uniform simple bodies with inhomogeneities. Arch. Rat. Mech. Anal., **27**, 1–32 (1967)
[84] Noll, W., Virga, E.G.: On edge interactions and surface tension. Arch. Rat. Mech. Anal., **111**, 1–31 (1990)
[85] Nowacki, W.: *Theory of micropolar elasticity*. CISM Courses and Lectures No. 25, Udine, Springer, Vienna (1970)
[86] Nowacki, W.: *Theory of asymmetric elasticity*. Pergamon Press, Oxford, U.K. (1986)
[87] Palmov, A.: Fundamental equations of the theory of asymmetric elasticity. Prikl. Mat. Mekh. **28**, 401–408 (1964)
[88] Pijaudier–Cabot, G., Bazant, Z.P.: Nonlocal damage theory. J. Eng. Mech. ASCE, **113**(10), 1512–1533 (1987)
[89] Pouget, J., Maugin, G.A.: Non-linear electroacoustic equations for piezoelectric powders. J. Acoust. Soc. Amer. **74**(3), 925–940 (1983)

[90] Pouget, J., Maugin, G.A.: Nonlinear dynamics of oriented elastic solids -I- Basic equations. J. Elasticity, **22**(2–3), 135–155 (1989)
[91] Rakotomanana, L.R.: *A geometric approach to thermomechanics of dissipating continua*. Birkhäuser, Boston (2003)
[92] Rogula, D.: Influence of spatial acoustic dispersion on dynamical properties of dislocations. Bull. Acad. Pol. Sci., Sér. Si. Tecchn., **13**, 337–385 (1965)
[93] Rosenbum, P., Li, D.: Ginzburg-Landau theory of type II superconductors in magnetic field. Rev. Modern Physics **82**, 1, 109–168 (2010)
[94] Schaefer, H.: Das Cosserat-Kontinuum. Z. Angew. Math. Mech. **47**, 34 (1967)
[95] Sedov, L.I.: Some problems of designing new models of continuum mechanics. In: *Proc. 11*th *International Congress of Applied Mechanics* (Munich, 1964), ed. H. Görtler, pp. 23–41, Springer, Berlin (1966)
[96] Stojanovic, R.: *Mechanics of polar continua*. CISM, Udine Italy (1969)
[97] Stojanovic, R.: *Recent developments in the theory of polar continua*. CISM Courses and Lectures No. 27, Udine, Springer, Vienna (1970)
[98] Stokes, V.K.: *Theories of fluids with microstructure*. Springer-Verlag, Berlin (1984)
[99] Tiersten, H.F.: Surface couplings in magnetoelastic insulators. In: *Surface Mechanics*, 126–143, ASME, N.Y. (1969)
[100] Toupin, R.A.: Elastic materials with couple stress. Arch. Rat. Mech. Anal. **11**, 395–414 (1962)
[101] Toupin, R.A.: Theories of elasticity with couple-stress. Arch. Rat. Mech. Anal. **17**, 85–112 (1964)
[102] Truesdell, C.A., Noll, W.: Nonlinear field theories of mechanics. In: *Handbuch der Physik*, Bd. III/3, ed. S. Flügge, Springer-Verlag, Berlin (1965)
[103] Truesdell, C.A., Toupin, R.A.: The classical theory of fields. In: *Handbuch der Physik*, Bd. III/1, ed. S. Flügge, Springer-Verlag, Berlin (1960)
[104] van der Waals, J.D.: The thermodynamic theory of capillarity under the hypotheses of a continous variation of density. Z. f. phys. Chemie **13**, (1894)
[105] Wang, C.C.: On the geometric structure of simple bodies, a mathematical foundation for the theory of continuous distributions of dislocations. Arch. Rat. Mech. Anal. **27**, 33–94 (1967)
[106] Whittaker, E.T.: *A history of the theories of aether and elasticity*. Vol.1 & 2, Thomas Nelson, New York (1951). Reprint in one volume. Dover, New York (1953)
[107] Zbib, H., Aifantis, E.C.: On the gradient-dependent theory of plasticity and shear banding. Acta Mechanica **92**, 209–225 (1992)

Part II
Beams, Plates, and Shells

Chapter 2
Micropolar Shells as Two-dimensional Generalized Continua Models

Holm Altenbach, Victor A. Eremeyev, and Leonid P. Lebedev

Abstract Using the direct approach the basic relations of the nonlinear micropolar shell theory are considered. Within the framework of this theory the shell can be considered as a deformable surface with attached three unit orthogonal vectors, so-called directors. In other words the micropolar shell is a two-dimensional (2D) Cosserat continuum or micropolar continuum. Each point of the micropolar shell has three translational and three rotational degrees of freedom as in the rigid body dynamics. In this theory the rotations are kinematically independent on translations. The interaction between of any two parts of the shell is described by the forces and moments only. So at the shell boundary six boundary conditions have to be given. In contrast to Kirchhoff-Love or Reissner's models of shells the drilling moment acting on the shell surface can be taken into account.

In the paper we derive the equilibrium equations of the shell theory using the principle of virtual work. The strain measures are introduced on the base of the principle of frame indifference. The boundary-value static and dynamic problems are formulated in Lagrangian and Eulerian coordinates. In addition, some variational principles are presented. For the general constitutive equations we formulate some constitutive restrictions, for example, the Coleman-Noll inequality, the Hadamard inequality, etc. Finally, we discuss the equilibrium of shells made of materials un-

Holm Altenbach
Martin-Luther-Universität Halle-Wittenberg, Kurt-Mothes-Str. 1, 06099 Halle (Saale), Germany
e-mail: holm.altenbach@iw.uni-halle.de

Victor A. Eremeyev
Martin-Luther-Universität Halle-Wittenberg, Kurt-Mothes-Str. 1, 06099 Halle (Saale), Germany; South Scientific Center of RASci & South Federal University, Milchakova St. 8a, 344090 Rostov on Don, Russia
e-mail: eremeyev.victor@gmail.com;victor.eremeyev@iw.uni-halle.de

Leonid P. Lebedev
Universidad Nacional de Colombia, Cr. 45, # 2685, Bogotá D.C., Colombia
e-mail: llebedev@unal.edu.co

H. Altenbach et al. (eds.), *Mechanics of Generalized Continua,*
Advanced Structured Materials, 7, DOI: 10.1007/978-3-642-19219-7_2,

dergoing phase transformations, such as martensitic transformations, and formulate the compatibility conditions on the phase interface.

Key words: Micropolar shells. 6-parametric theory of shells. Variational principles. Constitutive inequalities. Coleman-Noll inequality. Hadamard inequality. Phase transformations.

2.1 Introduction

The Mechanics of Generalized Continua has long history of development. Since the centurial book of Cosserat brothers [13] in the literature there are known various generalizations of the classical or Cauchy continuum which are summarized in many books and papers, see, for example, the books by Eringen [25, 26], Nowacki [47], and the recent proceedings [45], see also the historical review by Maugin [44] in this book. Using the direct approach, Ericksen and Truesdell [24] extended the Cosserat model to construction of the nonlinear mechanics of rods and shells, i.e. to one-dimensional and two-dimensional media. Since [24] the generalized models of shells and plates are extensively discussed in the literature, see the recent review [5].

Below we consider the model of a micropolar shell as the example of the generalized 2D continuum. Indeed, a micropolar shell is a two-dimensional analogue of the three-dimensional (3D) micropolar continuum, i.e. a micropolar shell is a deformable directed surface each particle of which has six degrees of freedom as rigid bodies. The kinematics of the micropolar shell is described by two fields. The first field is the position vector of the base surface of the shell while the second one is the proper orthogonal tensor describing the rotation of the shell cross-section. In contrast to Kirchhoff-Love and Mindlin-Reissner type theories of plates and shells the boundary-value problem of a micropolar shell consists of 6 scalar equations and 6 boundary conditions. Within the micropolar shell theory the so-called drilling moment can be taken into account.

Let us note that the basic equations of the micropolar shell models presented in [16, 22, 23, 60] using the direct approach coincide with the general nonlinear theory of shells initiated by Reissner [55] and presented by Libai and Simmonds [38, 39], Pietraszkiewicz [51], and Chróścielewski et al. [10], which is also named 6-parametric theory of shells.

The paper is organized as follows. In Sect. 2.2 we recall the basic equations. We derive the equilibrium equations from the principle of virtual work. Various statements of the nonlinear boundary-value problem are given and few variational principles are formulated. The case of small deformations is also considered. Following [22] in Sect. 2.3 we present in details some inequalities such as the Coleman-Noll inequality, the Hadamard inequality, strong and ordinary ellipticity conditions, etc. These inequalities can be regarded as the constitutive restrictions, i.e. the restrictions for the constitutive equations of an elastic shell. In Sect. 2.4 we discuss the compatibility conditions on the phase interface in shells.

Further we use the direct tensorial notations, see for example [36, 42]. Vectors are denoted by semibold normal font like **A**. Tensors are denoted by semibold sans serif upright font like A. Functionals are denoted by calligraphic letters like $\mathcal{A}$. Greek indices take values 1 and 2, while Latin indices are arbitrary.

2.2 Basic Relations of Micropolar Shell Theory

In this section we use the so-called direct approach to the formulation of the basic equations of micropolar shell theory. The advantage of the latter approach is discussed in many papers, see for example [24]. Within framework of the direct approach, an elastic micropolar shell is a two-dimensional analogue of the Cosserat continuum, i.e. a micropolar shell is a material surface each particle of which has six degrees of freedom of the rigid body. Further we will use the notations [16, 22, 23].

2.2.1 Kinematics of a Micropolar Shell

Let σ be a base surface of the micropolar shell in the reference configuration (for example, in an undeformed state), q^α $(\alpha = 1,2)$ be Gaussian coordinates on σ, and $\mathbf{r}(q^1,q^2)$ be a position vector of σ, see Fig. 2.1. In the actual (deformed) configuration the surface is denoted by Σ, and the position of its material points (infinitesimal point-bodies) is given by the vector $\mathbf{R}(q^1,q^2)$. The orientation of the point-bodies is described by the so-called *microrotation tensor* (or turn-tensor) $\mathbf{Q}(q^1,q^2)$, which is the proper orthogonal tensor. If we introduce three orthonormal vectors $\mathbf{d}_k$ $(k = 1,2,3)$, which describe the orientation in the reference configuration, and three

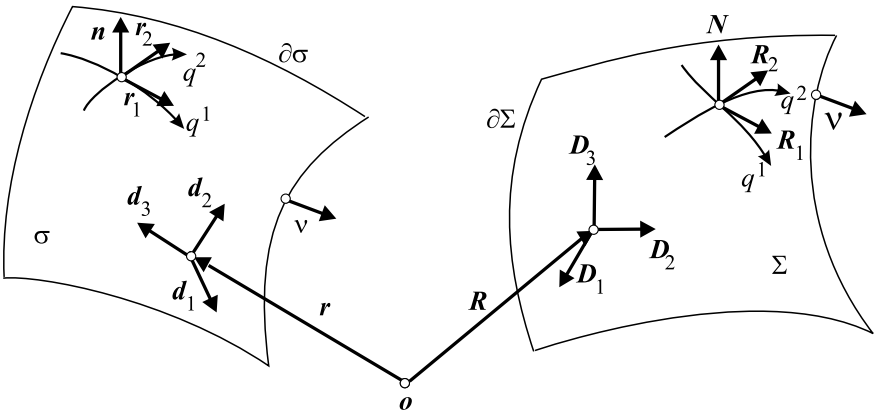

Fig. 2.1 Kinematics of a micropolar shell, reference configuration (on the left) and actual one (on the right)

orthonormal vectors $\mathbf{D}_k$, which determine the orientation in the actual configuration, then the tensor $\mathbf{Q}$ is given by $\mathbf{Q} = \mathbf{d}_k \otimes \mathbf{D}_k$. Thus, the micropolar shell is described by two kinematically independent fields

$$\mathbf{R} = \mathbf{R}(q^\alpha), \quad \mathbf{Q} = \mathbf{Q}(q^\alpha). \tag{2.1}$$

For the micropolar shell made of an elastic material there should exist a strain energy density W. By using the principle of local action [57, 58] the constitutive equation for the function W is given by the formula [16, 22, 23]

$$W = W(\mathbf{R}, \nabla\mathbf{R}, \mathbf{Q}, \nabla\mathbf{Q}),$$

where

$$\nabla\boldsymbol{\Psi} \triangleq \mathbf{r}^\alpha \otimes \frac{\partial \boldsymbol{\Psi}}{\partial q^\alpha}, \quad \mathbf{r}^\alpha \cdot \mathbf{r}_\beta = \delta^\alpha_\beta, \quad \mathbf{r}^\alpha \cdot \mathbf{n} = 0, \quad \mathbf{r}_\beta = \frac{\partial \mathbf{r}}{\partial q^\beta}.$$

Here the vectors $\mathbf{r}_\beta$ and $\mathbf{r}^\alpha$ denote the natural and reciprocal bases on σ, $\mathbf{n}$ is the unit normal to σ, δ^α_β is the Kronecker symbol, ∇ is the surface nabla operator on σ, and $\boldsymbol{\Psi}$ is an arbitrary differentiable tensor field given on σ.

From the principle of material frame-indifference we can find that W depends on two *Cosserat-type strain measures* $\mathbf{E}$ and $\mathbf{K}$ only

$$W = W(\mathbf{E}, \mathbf{K}),$$

$$\mathbf{E} = \mathbf{F}\cdot\mathbf{Q}^T, \quad \mathbf{K} = \frac{1}{2}\mathbf{r}^\alpha \otimes \left(\frac{\partial \mathbf{Q}}{\partial q^\alpha}\cdot\mathbf{Q}^T\right)_\times, \tag{2.2}$$

where $\mathbf{F} = \nabla\mathbf{R}$ is the surface deformation gradient, $\mathbf{T}_\times$ is the vectorial invariant of a second-order tensor $\mathbf{T}$ defined by

$$\mathbf{T}_\times = (T^{mn}\mathbf{R}_m \otimes \mathbf{R}_n)_\times = T^{mn}\mathbf{R}_m \times \mathbf{R}_n$$

for any base $\mathbf{R}_m$, see e.g. [36], $\times$ is the vector product.

A proper orthogonal tensor describes rotation about an arbitrary axis. It can be represented by Gibbs' formula

$$\mathbf{H} = (\mathbf{I} - \mathbf{e}\otimes\mathbf{e})\cos\chi + \mathbf{e}\otimes\mathbf{e} - \mathbf{e}\times\mathbf{I}\sin\chi, \tag{2.3}$$

where χ and $\mathbf{e}$ are the angle of rotation about the axis with the unit vector $\mathbf{e}$, and $\mathbf{I}$ is the 3D unit tensor, respectively. Introducing the vector $\boldsymbol{\theta} = 2\mathbf{e}\tan\chi/2$ and using the formulae

$$\cos\chi = \frac{1-\tan^2\chi/2}{1+\tan^2\chi/2}, \quad \sin\chi = \frac{2\tan\chi/2}{1+\tan^2\chi/2}$$

we obtain the representation of $\mathbf{Q}$ in the form which does not contain trigonometric functions

$$\mathbf{Q} = \frac{1}{(4+\theta^2)}\left[(4-\theta^2)\mathbf{I} + 2\boldsymbol{\theta}\otimes\boldsymbol{\theta} - 4\mathbf{I}\times\boldsymbol{\theta}\right], \quad \theta^2 = \boldsymbol{\theta}\cdot\boldsymbol{\theta}. \tag{2.4}$$

In the rigid body kinematics the vector $\boldsymbol{\theta}$ is called *Rodrigues' finite rotation vector*, cf. [41]. In the theory of Cosserat-type shells we will call it the *microrotation vector*. Other known vectorial parameterizations of an orthogonal tensor are summarized in [53]. From Eq. (2.4), for a given proper orthogonal tensor $\mathbf{Q}$ we find uniquely the vector $\boldsymbol{\theta}$

$$\boldsymbol{\theta} = 2(1+\operatorname{tr}\mathbf{Q})^{-1}\mathbf{Q}_{\times}. \tag{2.5}$$

Using the finite rotation vector we can express $\mathbf{K}$ as follows

$$\mathbf{K} = \mathbf{r}^{\alpha}\otimes\mathbf{L}_{\alpha} = \frac{4}{4+\theta^2}\nabla\boldsymbol{\theta}\cdot\left(\mathbf{I}+\frac{1}{2}\mathbf{I}\times\boldsymbol{\theta}\right). \tag{2.6}$$

The strain measures $\mathbf{E}$ and $\mathbf{K}$ are the two-dimensional analogues of the strain measures used in 3D Cosserat continuum [52, 53].

2.2.2 Principle of Virtual Work and Boundary-value Problems Statements

The Lagrangian equilibrium equations of the micropolar shell can be derived from *the principle of virtual work*

$$\delta\iint\limits_{\sigma} W\,d\sigma = \delta' A, \tag{2.7}$$

where

$$\delta' A = \iint\limits_{\sigma}\left(\mathbf{f}\cdot\delta\mathbf{R}+\mathbf{c}\cdot\delta'\boldsymbol{\psi}\right)d\sigma + \int\limits_{\omega_2}\boldsymbol{\varphi}\cdot\delta\mathbf{R}\,ds + \int\limits_{\omega_4}\boldsymbol{\gamma}\cdot\delta'\boldsymbol{\psi}\,ds,$$
$$\mathbf{I}\times\delta'\boldsymbol{\psi} = -\mathbf{Q}^{T}\cdot\delta\mathbf{Q}.$$

In Eq. (2.7), δ is the symbol of variation, $\delta'\boldsymbol{\psi}$ is the virtual rotation vector, $\mathbf{f}$ is the surface force density distributed on σ, $\mathbf{c}$ is the surface couple density distributed on σ, $\boldsymbol{\varphi}$ and $\boldsymbol{\gamma}$ are linear densities of forces and couples distributed along corresponding parts of the shell boundary ω, respectively.

Using the formulae [23]

$$\delta W = \frac{\partial W}{\partial\mathbf{E}}\bullet\delta\mathbf{E}+\frac{\partial W}{\partial\mathbf{K}}\bullet\delta\mathbf{K},$$
$$\delta\mathbf{E} = (\nabla\delta\mathbf{R})\cdot\mathbf{Q}^{T}+\mathbf{F}\cdot\delta\mathbf{Q}^{T},\quad \delta\mathbf{K} = (\nabla\delta'\boldsymbol{\psi})\cdot\mathbf{Q}^{T},$$
$$\delta'\boldsymbol{\psi} = \frac{4}{4+\theta^2}\left(\delta\boldsymbol{\theta}+\frac{1}{2}\boldsymbol{\theta}\times\delta\theta\right),$$

where $\mathbf{X} \bullet \mathbf{Y} = \mathbf{X} \cdot\cdot \mathbf{Y}^T$ for any tensors $\mathbf{X}$ and $\mathbf{Y}$ of the second-order, see [36], from Eq. (2.7) we obtain the *Lagrangian shell equations*

$$\nabla \cdot \mathbf{D} + \mathbf{f} = \mathbf{0}, \quad \nabla \cdot \mathbf{G} + \left[\mathbf{F}^T \cdot \mathbf{D}\right]_\times + \mathbf{c} = \mathbf{0}, \tag{2.8}$$

$$\mathbf{D} = \mathbf{P}_1 \cdot \mathbf{Q}, \quad \mathbf{G} = \mathbf{P}_2 \cdot \mathbf{Q}, \qquad \mathbf{P}_1 = \frac{\partial W}{\partial \mathbf{E}}, \quad \mathbf{P}_2 = \frac{\partial W}{\partial \mathbf{K}}, \tag{2.9}$$

$$\begin{aligned} &\omega_1 : \mathbf{R} = \boldsymbol{\rho}(s), \\ &\omega_2 : \boldsymbol{\nu} \cdot \mathbf{D} = \boldsymbol{\varphi}(s), \\ &\omega_3 : \mathbf{Q} = \mathbf{h}(s), \ \mathbf{h} \cdot \mathbf{h}^T = \mathbf{I}, \\ &\omega_4 : \boldsymbol{\nu} \cdot \mathbf{G} = \boldsymbol{\gamma}(s). \end{aligned} \tag{2.10}$$

Here $\boldsymbol{\rho}(s)$, $\mathbf{h}(s)$ are given vector functions, and $\boldsymbol{\nu}$ is the external unit normal to the boundary curve ω ($\boldsymbol{\nu} \cdot \mathbf{n} = 0$). Equations (2.8) are the equilibrium equations for the linear momentum and angular momentum of any shell part. The tensors $\mathbf{D}$ and $\mathbf{G}$ are *the surface stress and couple stress tensors* of the 1st Piola-Kirchhoff type, and the corresponding stress measures $\mathbf{P}_1$ and $\mathbf{P}_2$ in Eqs (2.8) are the referential stress tensors, respectively. The strain measures $\mathbf{E}$ and $\mathbf{K}$ are work-conjugate to the stress measures $\mathbf{D}$ and $\mathbf{G}$. The boundary ω of σ is divided into two parts $\omega = \omega_1 \cup \omega_2 = \omega_3 \cup \omega_4$. The following relations are valid

$$\mathbf{n} \cdot \mathbf{D} = \mathbf{n} \cdot \mathbf{G} = \mathbf{n} \cdot \mathbf{P}_1 = \mathbf{n} \cdot \mathbf{P}_2 = \mathbf{0}. \tag{2.11}$$

The *equilibrium equations* (2.8) may be transformed to the *Eulerian form*

$$\nabla_\Sigma \cdot \mathbf{T} + J^{-1}\mathbf{f} = \mathbf{0}, \quad \nabla_\Sigma \cdot \mathbf{M} + \mathbf{T}_\times + J^{-1}\mathbf{c} = \mathbf{0}, \tag{2.12}$$

where

$$\nabla_\Sigma \cdot \boldsymbol{\Psi} \triangleq \mathbf{R}^\alpha \cdot \frac{\partial \boldsymbol{\Psi}}{\partial q^\alpha}, \quad \mathbf{R}^\alpha \cdot \mathbf{R}_\beta = \delta^\alpha_\beta, \ \mathbf{R}^\alpha \cdot \mathbf{N} = 0, \quad \mathbf{R}_\beta = \frac{\partial \mathbf{R}}{\partial q^\beta},$$

$$\mathbf{T} = J^{-1}\mathbf{F}^T \cdot \mathbf{D}, \quad \mathbf{M} = J^{-1}\mathbf{F}^T \cdot \mathbf{G}, \tag{2.13}$$

$$J = \sqrt{\frac{1}{2}\left\{\left[\mathrm{tr}\left(\mathbf{F}\cdot\mathbf{F}^T\right)\right]^2 - \mathrm{tr}\left[\left(\mathbf{F}\cdot\mathbf{F}^T\right)^2\right]\right\}}.$$

Here $\mathbf{T}$ and $\mathbf{M}$ are the Cauchy-type surface stress and couple stress tensors, ∇_Σ is the surface nabla operator on Σ associated with ∇ by the formula $\nabla = \mathbf{F} \cdot \nabla_\Sigma$.

The *equations of motion* of the micropolar shell are given by the relations (see, for example, [4, 10, 23, 38, 39, 59])

$$\begin{aligned} \nabla \cdot \mathbf{D} + \mathbf{f} &= \rho \frac{\mathrm{d}\mathbf{K}_1}{\mathrm{d}t}, \\ \nabla \cdot \mathbf{G} + \left[\mathbf{F}^T \cdot \mathbf{D}\right]_\times + \mathbf{m} &= \rho\left(\frac{\mathrm{d}\mathbf{K}_2}{\mathrm{d}t} + \mathbf{v} \times \boldsymbol{\Theta}_1^T \cdot \boldsymbol{\omega}\right), \end{aligned} \tag{2.14}$$

with

$$K(\mathbf{v},\boldsymbol{\omega}) = \frac{1}{2}\mathbf{v}\cdot\mathbf{v} + \boldsymbol{\omega}\cdot\boldsymbol{\Theta}_1\cdot\mathbf{v} + \frac{1}{2}\boldsymbol{\omega}\cdot\boldsymbol{\Theta}_2\cdot\boldsymbol{\omega},$$
$$\mathbf{K}_1 \triangleq \frac{\partial K}{\partial \mathbf{v}} = \mathbf{v} + \boldsymbol{\Theta}_1^T\cdot\boldsymbol{\omega}, \quad \mathbf{K}_2 \triangleq \frac{\partial K}{\partial \boldsymbol{\omega}} = \boldsymbol{\Theta}_1\cdot\mathbf{v} + \boldsymbol{\Theta}_2\cdot\boldsymbol{\omega},$$

where

$$\mathbf{v} = \frac{d\mathbf{R}}{dt}, \qquad \boldsymbol{\omega} = \frac{1}{2}\left(\mathbf{H}^T\cdot\frac{d\mathbf{Q}}{dt}\right)_\times$$

are the linear and angular velocities, respectively, ρ is the surface mass density in the reference configuration, ρK is the surface density of the kinetic energy, and $\rho\boldsymbol{\Theta}_1$, $\rho\boldsymbol{\Theta}_2$ are *the rotatory inertia tensors* ($\boldsymbol{\Theta}_2^T = \boldsymbol{\Theta}_2$). For the dynamic problem (2.14), the initial conditions are given by

$$\mathbf{R}\big|_{t=0} = \mathbf{R}^\circ, \quad \mathbf{v}\big|_{t=0} = \mathbf{v}^\circ, \quad \mathbf{Q}\big|_{t=0} = \mathbf{Q}^\circ, \quad \boldsymbol{\omega}\big|_{t=0} = \boldsymbol{\omega}^\circ,$$

where $\mathbf{R}^\circ$, $\mathbf{v}^\circ$, $\mathbf{Q}^\circ$, $\boldsymbol{\omega}^\circ$ are given initial values.

Under some conditions the equilibrium problem of a micropolar shell can be transformed to the system of equations with respect to the strain measures

$$\boldsymbol{\nabla}\cdot\mathbf{P}_1 - \left(\mathbf{P}_1^T\cdot\mathbf{K}\right)_\times + \mathbf{f}^* = \mathbf{0}; \tag{2.15}$$
$$\boldsymbol{\nabla}\cdot\mathbf{P}_2 - \left(\mathbf{P}_2^T\cdot\mathbf{K} + \mathbf{P}_1^T\cdot\mathbf{E}\right)_\times + \mathbf{c}^* = \mathbf{0}, \tag{2.16}$$
$$\omega_2 \ : \ \boldsymbol{\nu}\cdot\mathbf{P}_1 = \boldsymbol{\varphi}^*, \qquad \omega_4 \ : \ \boldsymbol{\nu}\cdot\mathbf{P}_2 = \boldsymbol{\gamma}^*, \tag{2.17}$$
$$\mathbf{f}^* \triangleq \mathbf{f}\cdot\mathbf{Q}^T, \ \mathbf{c}^* \triangleq \mathbf{c}\cdot\mathbf{Q}^T, \quad \boldsymbol{\varphi}^* \triangleq \boldsymbol{\varphi}\cdot\mathbf{Q}^T, \ \boldsymbol{\gamma}^* \triangleq \boldsymbol{\gamma}\cdot\mathbf{Q}^T.$$

Let the vectors $\mathbf{f}^*$, $\mathbf{c}^*$, $\boldsymbol{\varphi}^*$, $\boldsymbol{\gamma}^*$ be given as functions of the coordinates q^1, q^2. From the physical point of view it means that the shell is loaded by tracking forces and couples. Then Eqs (2.15)–(2.17) depend on $\mathbf{E}$, $\mathbf{K}$ as the only independent fields.

2.2.3 On the Constitutive Equations of Micropolar Shells

For an elastic shell the constitutive equations consist of the surface strain energy density as the function of two strain measures. An example of the constitutive equation is the model of *physically linear isotropic shell* [10, 18, 23], the energy of which is given by the quadratic form

$$\begin{aligned} 2W = {} & \alpha_1 \mathrm{tr}^2\mathbf{E}_\| + \alpha_2 \mathrm{tr}\,\mathbf{E}_\|^2 + \alpha_3 \mathrm{tr}\left(\mathbf{E}_\|\cdot\mathbf{E}_\|^T\right) + \alpha_4 \mathbf{n}\cdot\mathbf{E}^T\cdot\mathbf{E}\cdot\mathbf{n} \\ & + \beta_1 \mathrm{tr}^2\mathbf{K}_\| + \beta_2 \mathrm{tr}\,\mathbf{K}_\|^2 + \beta_3 \mathrm{tr}\left(\mathbf{K}_\|\cdot\mathbf{K}_\|^T\right) + \beta_4 \mathbf{n}\cdot\mathbf{K}^T\cdot\mathbf{K}\cdot\mathbf{n}, \\ \mathbf{E}_\| \ & \triangleq \mathbf{E}\cdot\mathbf{A}, \quad \mathbf{K}_\| \triangleq \mathbf{K}\cdot\mathbf{A}. \end{aligned} \tag{2.18}$$

In Eq. (2.18) there are absent the terms that are bilinear in $\mathbf{E}$ and $\mathbf{K}$. It is a consequence of the fact that the bending measure $\mathbf{K}$ is a pseudo-tensor that changes the

sign of the value when we apply the inversion of the space. Note that the constitutive equations contain 8 parameters α_k, β_k ($k = 1,2,3,4$).

In [10] the following relations for the elastic moduli appearing in Eq. (2.18) are used

$$\begin{aligned} &\alpha_1 = C\nu, \quad \alpha_2 = 0, \quad \alpha_3 = C(1-\nu), \quad \alpha_4 = \alpha_s C(1-\nu), \\ &\beta_1 = D\nu, \quad \beta_2 = 0, \quad \beta_3 = D(1-\nu), \quad \beta_4 = \alpha_t D(1-\nu), \\ &C = \frac{Eh}{1-\nu^2}, \quad D = \frac{Eh^3}{12(1-\nu^2)}, \end{aligned} \tag{2.19}$$

where E and ν are the Young's modulus and the Poisson's ratio of the bulk material, respectively, α_s and α_t are dimensionless shear correction factors, while h is the shell thickness. α_s is the shear correction factor introduced in the plate theory by Reissner ($\alpha_s = 5/6$) or Mindlin ($\alpha_s = \pi^2/12$). The parameter α_t plays the same role for the couple stresses. The value $\alpha_t = 0.7$ was proposed by Pietraszkiewicz [48, 49], see also [11]. In [10, 11, 12] the influence of α_s and α_t on the solution is investigated numerically for several boundary-value problems.

2.2.4 Compatibility Conditions

Let us consider how to determine the position vector $\mathbf{R}(q^1,q^2)$ of Σ from the surface strain $\mathbf{E}$ and micro-rotation $\mathbf{Q}$, which are assumed to be given as continuously differentiable functions on σ. By using the equation $\mathbf{F} = \mathbf{E}\cdot\mathbf{Q}$ the problem is reduced to

$$\nabla\mathbf{R} = \mathbf{F}. \tag{2.20}$$

The necessary and sufficient condition for solvability of Eq. (2.20) is given by the relation

$$\boldsymbol{\nabla}\cdot(\mathbf{e}\cdot\mathbf{F}) = \mathbf{0}, \quad \mathbf{e} \triangleq -\mathbf{l}\times\mathbf{n}, \tag{2.21}$$

which we call the compatibility condition for the distortion tensor $\mathbf{F}$. Here $\mathbf{e}$ is the skew-symmetric discriminant tensor on the surface σ. For a simply-connected region σ, if the condition (2.21) is satisfied, the vector field $\mathbf{R}$ may be deduced from Eq. (2.20) only up to an additive vector.

Let us consider a more complex problem of determination of both the translations and rotations of the micropolar shell from the given fields of $\mathbf{E}$ and $\mathbf{K}$. At first, let us deduce the field $\mathbf{Q}(q^1,q^2)$ by using the system of equations following from definition (2.2) of $\mathbf{K}$

$$\frac{\partial\mathbf{Q}}{\partial q^\alpha} = -\mathbf{K}_\alpha\times\mathbf{Q}, \quad \mathbf{K}_\alpha \triangleq \mathbf{r}_\alpha\cdot\mathbf{K}. \tag{2.22}$$

The integrability conditions for the system (2.22) are given by the relation

$$\frac{\partial \mathbf{K}_\alpha}{\partial q^\beta} - \frac{\partial \mathbf{K}_\beta}{\partial q^\alpha} = \mathbf{K}_\alpha \times \mathbf{K}_\beta \quad (\alpha, \beta = 1,2). \tag{2.23}$$

Equations (2.23) are obtained in [38, 49, 50] as the conditions for the existence of the rotation field of the shell. They may be written in the following coordinate-free form

$$\nabla \cdot (\mathbf{e} \cdot \mathbf{K}) + \mathbf{K}^\perp \cdot \mathbf{n} = \mathbf{0}, \tag{2.24}$$

$$\mathbf{K}^\perp \triangleq \frac{1}{2} (\mathbf{K}_\alpha \times \mathbf{K}_\beta) \otimes \left(\mathbf{r}^\alpha \times \mathbf{r}^\beta \right) = \mathbf{K}^2 - \mathbf{K} \mathrm{tr}\, \mathbf{K} + \frac{1}{2} \left(\mathrm{tr}^2 \mathbf{K} - \mathrm{tr}\, \mathbf{K}^2 \right) \mathbf{I}.$$

Using $\mathbf{F} = \mathbf{E} \cdot \mathbf{Q}$ and Eqs (2.2) the compatibility condition (2.21) may be written in the form

$$\nabla \cdot (\mathbf{e} \cdot \mathbf{E}) + \left(\mathbf{E}^T \cdot \mathbf{e} \cdot \mathbf{K} \right)_\times = \mathbf{0}. \tag{2.25}$$

Two coordinate-free vector equations (2.24), (2.25) are the compatibility conditions for the nonlinear micropolar shell. These conditions and the system of equations (2.15)–(2.17) form the complete boundary-value problem for statics of micropolar shells expressed entirely in terms of the surface strain measures $\mathbf{E}$ and $\mathbf{K}$.

2.2.5 Variational Statements

The presented above static and dynamic problems have corresponding variational statements. Two of them for statics and one for dynamics are presented below.

2.2.5.1 Lagrange Principle

Let us assume that the external forces and couples are conservative. In the Lagrange-type variational principle $\delta \mathcal{E}_1 = 0$ the functional $\mathcal{E}_1[\mathbf{R}, \mathbf{Q}]$ is used, where

$$\mathcal{E}_1[\mathbf{R}, \mathbf{Q}] = \iint\limits_\sigma W \mathrm{d}\sigma - \mathcal{A}[\mathbf{R}, \mathbf{Q}], \tag{2.26}$$

and $\mathcal{A}$ is the potential of the external loads.

Here the deformation, i.e. the translations and the rotations, have to satisfy the boundary conditions $(2.10)_1$ and $(2.10)_3$ on ω_1 and ω_3, respectively. The stationarity of $\mathcal{E}_1$ is equivalent to the equilibrium equations (2.8), (2.9) and the boundary conditions $(2.10)_2$ and $(2.10)_4$ on ω_2 and ω_4.

2.2.5.2 Hu-Washizu Principle

For this principle the functional is given by

$$\mathcal{E}_2[\mathbf{R},\mathbf{Q},\mathbf{E},\mathbf{K},\mathbf{D},\mathbf{P}_2] = \iint\limits_{\sigma} [W(\mathbf{E},\mathbf{K}) - \mathbf{D}\bullet(\mathbf{E}\cdot\mathbf{Q}-\nabla\mathbf{R}) \tag{2.27}$$

$$-\mathbf{P}_2\bullet\left(\mathbf{K}-\frac{1}{2}\mathbf{r}^{\alpha}\otimes\left(\frac{\partial\mathbf{Q}}{\partial q^{\alpha}}\cdot\mathbf{Q}^{T}\right)_{\times}\right)\Bigg]\mathrm{d}\sigma - \int\limits_{\omega_1}\boldsymbol{\nu}\cdot\mathbf{D}\cdot(\mathbf{R}-\boldsymbol{\rho})\mathrm{d}s - \mathcal{A}[\mathbf{R},\mathbf{Q}].$$

From the condition $\delta\mathcal{E}_2 = 0$ the equilibrium equations (2.8) and (2.9), the constitutive equations, and the relations (2.2) are deduced. For this principle the natural boundary conditions are given by the relations $(2.10)_1$, $(2.10)_2$ and $(2.10)_4$, respectively.

Several other variational statements are given in [23]. Mixed type variational functionals are constructed in [10]. They are used for the development of a family of finite elements with 6 degrees of freedom in each node. Then a number of nonlinear simulations of complex multifolded shell structures are performed.

2.2.5.3 Hamilton-type Principle

The *kinetic energy of micropolar shells* can be expressed as

$$\mathcal{K} = \iint\limits_{\sigma}\rho K(\mathbf{v},\boldsymbol{\omega})\mathrm{d}\sigma, \quad K(\mathbf{v},\boldsymbol{\omega}) = \frac{1}{2}\mathbf{v}\cdot\mathbf{v} + \boldsymbol{\omega}\cdot\boldsymbol{\Theta}_1\cdot\mathbf{v} + \frac{1}{2}\boldsymbol{\omega}\cdot\boldsymbol{\Theta}_2\cdot\boldsymbol{\omega}, \tag{2.28}$$

where ρK is the surface density of the kinetic energy, $\rho\boldsymbol{\Theta}_1$, $\rho\boldsymbol{\Theta}_2$ are the inertia tensors, $\boldsymbol{\Theta}_2^T = \boldsymbol{\Theta}_2$.

It is obvious that we should assume the kinetic energy to be a positive definite function that imposes some restriction on the form of the inertia tensors. By physical meaning, $\boldsymbol{\Theta}_1$ and $\boldsymbol{\Theta}_2$ have the following properties

$$\boldsymbol{\Theta}_1 = \mathbf{H}^T\cdot\boldsymbol{\Theta}_1^{\circ}\cdot\mathbf{H}, \quad \boldsymbol{\Theta}_2 = \mathbf{H}^T\cdot\boldsymbol{\Theta}_2^{\circ}\cdot\mathbf{H}, \quad \frac{d\boldsymbol{\Theta}_1^{\circ}}{dt} = \frac{d\boldsymbol{\Theta}_2^{\circ}}{dt} = \mathbf{0}. \tag{2.29}$$

The Hamilton principle is a variational principle in dynamics. In real motion, the functional

$$\mathcal{E}_3[\mathbf{R},\mathbf{H}] = \int\limits_{t_0}^{t_1}(\mathcal{K}-\mathcal{E}_1)\,\mathrm{d}t \tag{2.30}$$

takes a stationary value on the set of all possible shell motions that at the range t_0, t_1 take given values of the real motion values and satisfy the kinematic boundary values. In other words, its first variation on a real motion is zero. From condition $\mathcal{E}_3 = 0$ Eqs (2.14) can be established.

2.2.6 Linear Theory of Micropolar Shells

Let us suppose the strains are small. Then we can simplify the equations of the shell theory significantly. In this geometrically linear case we do not differ Eulerian and Lagrangian descriptions. The difference of surfaces σ and Σ is infinitesimal. It is not necessary to distinguish operators ∇ and ∇_Σ as well as earlier different types of stress tensors and couple stress tensors. Let us introduce the *vector of infinitesimal displacements* $\mathbf{u}$ and the *vector of infinitesimal rotation* $\boldsymbol{\vartheta}$ such that there hold

$$\mathbf{R} \approx \mathbf{r} + \mathbf{u}, \quad \mathbf{Q} \approx \mathbf{I} - \mathbf{I} \times \boldsymbol{\vartheta}. \tag{2.31}$$

In Eqs (2.31) the last formula follows from the representation of a proper orthogonal tensor through the finite rotation vector (2.4) if $|\boldsymbol{\theta}| \ll 1$.

Up to the linear addendum, the linear strain measure $\mathbf{E}$ and bending strain tensor can be expressed in terms of the *linear strain tensor* and *linear bending strain tensor* $\mathbf{e}$ and $\boldsymbol{\kappa}$

$$\mathbf{E} \approx \mathbf{I} + \mathbf{e}, \quad \mathbf{K} \approx \boldsymbol{\kappa}, \quad \mathbf{e} = \nabla \mathbf{u} + \mathbf{A} \times \boldsymbol{\vartheta}, \quad \boldsymbol{\kappa} = \nabla \boldsymbol{\vartheta}. \tag{2.32}$$

Here $\mathbf{A} \triangleq \mathbf{I} - \mathbf{n} \otimes \mathbf{n}$. The tensors $\mathbf{e}$ and $\boldsymbol{\kappa}$ are applied in the linear theory of micropolar shells, cf. [59, 60]. Assuming Eq. (2.32) in the linear shell theory the stress tensors $\mathbf{D}$, $\mathbf{P}_1$, $\mathbf{T}$ and the couple tensors $\mathbf{G}$, $\mathbf{P}_2$, $\mathbf{M}$ coincide. In what follows we will denote the stress tensor by $\mathbf{T}$ and the couple stress tensor by $\mathbf{M}$.

The constitutive equations of an elastic shell can be represented through the function of specific strain energy $W = W(\mathbf{e}, \boldsymbol{\kappa})$ as it follows

$$\mathbf{T} = \frac{\partial W}{\partial \mathbf{e}}, \quad \mathbf{M} = \frac{\partial W}{\partial \boldsymbol{\kappa}}. \tag{2.33}$$

In the linear theory the equilibrium equations take the form

$$\boldsymbol{\nabla} \cdot \mathbf{T} + \mathbf{f} = \mathbf{0}, \quad \boldsymbol{\nabla} \cdot \mathbf{M} + \mathbf{T}_\times + \mathbf{c} = \mathbf{0}, \tag{2.34}$$

whereas the boundary conditions are transformed to

$$\begin{aligned} &\omega_1 : \mathbf{u} = \mathbf{u}_0(s), \\ &\omega_2 : \boldsymbol{\nu} \cdot \mathbf{T} = \boldsymbol{\varphi}(s), \\ &\omega_3 : \boldsymbol{\vartheta} = \boldsymbol{\vartheta}_0(s), \\ &\omega_4 : \boldsymbol{\nu} \cdot \mathbf{M} = \boldsymbol{\gamma}(s), \end{aligned} \tag{2.35}$$

where $\mathbf{u}_0(s)$ and $\boldsymbol{\vartheta}_0(s)$ are given functions of the arc length that respectively define the displacements and rotations on a part of the shell contour.

If the strains are small, an example of the constitutive equation is the following quadratic form

$$2W = \alpha_1 \mathrm{tr}^2 \mathbf{e}_\parallel + \alpha_2 \mathrm{tr}\, \mathbf{e}_\parallel^2 + \alpha_3 \mathrm{tr}\left(\mathbf{e}_\parallel \cdot \mathbf{e}_\parallel^T\right) + \alpha_4 \mathbf{n}\cdot\mathbf{e}^T\cdot\mathbf{e}\cdot\mathbf{n} \tag{2.36}$$
$$+\beta_1 \mathrm{tr}^2 \boldsymbol{\kappa}_\parallel + \beta_2 \mathrm{tr}\, \boldsymbol{\kappa}_\parallel^2 + \beta_3 \mathrm{tr}\left(\boldsymbol{\kappa}_\parallel \cdot \boldsymbol{\kappa}_\parallel^T\right) + \beta_4 \mathbf{n}\cdot\boldsymbol{\kappa}^T\cdot\boldsymbol{\kappa}\cdot\mathbf{n}.$$

This form describes *physically linear isotropic shells*. Here α_k and β_k are elastic constants ($k = 1,2,3,4$) and

$$\mathbf{e}_\parallel \triangleq \mathbf{e}\cdot\mathbf{A}, \qquad \boldsymbol{\kappa}_\parallel \triangleq \boldsymbol{\kappa}\cdot\mathbf{A}.$$

Considering Eqs (2.33) and (2.36), the stress tensor and the couple stress tensor are expressed by the formulas

$$\mathbf{T} = \alpha_1 \mathbf{A}\mathrm{tr}\, \mathbf{e}_\parallel + \alpha_2 \mathbf{e}_\parallel^T + \alpha_3 \mathbf{e}_\parallel + \alpha_4 \mathbf{e}\cdot\mathbf{n}\otimes\mathbf{n}, \tag{2.37}$$

$$\mathbf{M} = \beta_1 \mathbf{A}\mathrm{tr}\, \boldsymbol{\kappa}_\parallel + \beta_2 \boldsymbol{\kappa}_\parallel^T + \beta_3 \boldsymbol{\kappa}_\parallel + \beta_4 \boldsymbol{\kappa}\cdot\mathbf{n}\otimes\mathbf{n}. \tag{2.38}$$

Supplemented with Eqs (2.34) and (2.35), the linear constitutive equations (2.37), (2.38) constitute the linear boundary-value problem with respect to the fields of displacements and rotations. It describes the equilibrium of the micropolar shell when strains are infinitesimal.

When the strains are small, the Lagrange variational principle (2.26) is transformed to the following form

$$\mathcal{E}_1[\mathbf{u}, \boldsymbol{\vartheta}] = \iint\limits_\sigma W(\mathbf{e}, \boldsymbol{\kappa})\mathrm{d}\sigma - \mathcal{A}[\mathbf{u}, \boldsymbol{\vartheta}], \tag{2.39}$$

where the potential of the external loads $\mathcal{A}[\mathbf{u}, \boldsymbol{\vartheta}]$ is defined by the equation

$$\mathcal{A}[\mathbf{u}, \boldsymbol{\vartheta}] \triangleq \iint\limits_\sigma (\mathbf{f}\cdot\mathbf{u} + \mathbf{c}\cdot\boldsymbol{\vartheta})\,\mathrm{d}\sigma + \int\limits_{\omega_2} \boldsymbol{\varphi}\cdot\mathbf{u}\mathrm{d}s + \int\limits_{\omega_4} \boldsymbol{\gamma}\cdot\boldsymbol{\vartheta}\mathrm{d}s.$$

Let functional (2.39) be given on the set of twice differentiable fields of displacements and rotations of the surface σ that satisfy the boundary conditions $(2.35)_1$ and $(2.35)_3$ on ω_1 and ω_3, respectively. It is easy to check that the condition of the functional to have a stationary value is equivalent to the equilibrium equations (2.34) and the boundary conditions $(2.35)_2$ and $(2.35)_4$ on ω_2 and ω_4, respectively. Let us note that when the strains are small and the form $W(\mathbf{e}, \boldsymbol{\kappa})$ is positive definite, the Lagrange variational principle is a minimal principle, this means functional (2.39) takes a minimal value on the equilibrium solution.

In the linear theory it is valid a variational principle for free oscillations. By linearity, eigen-solutions are proportional to $e^{i\Omega t}$ ($\mathbf{u} = \mathbf{u}^\circ e^{i\Omega t}$, $\boldsymbol{\vartheta} = \boldsymbol{\vartheta}^\circ e^{i\Omega t}$). Now the variational *Rayleigh principle* can be formulated: the forms of the eigen-oscillations of the shell are stationary points of the strain energy functional

$$\mathcal{E}_4[\mathbf{u}^\circ, \boldsymbol{\vartheta}^\circ] = \iint\limits_\sigma W(\mathbf{e}^\circ, \boldsymbol{\kappa}^\circ)\mathrm{d}\sigma, \tag{2.40}$$

where

$$\mathbf{e}^\circ = \nabla \mathbf{u}^\circ + \mathbf{A} \times \boldsymbol{\vartheta}^\circ, \qquad \boldsymbol{\kappa}^\circ = \nabla \boldsymbol{\vartheta}^\circ,$$

on the set of functions that satisfy the following conditions

$$\omega_1 : \mathbf{u}^\circ = \mathbf{0}, \quad \omega_3 : \boldsymbol{\vartheta}^\circ = \mathbf{0} \tag{2.41}$$

and restriction

$$\iint\limits_\sigma \rho K(\mathbf{u}^\circ, \boldsymbol{\vartheta}^\circ)\,\mathrm{d}\sigma = 1. \tag{2.42}$$

Functions $\mathbf{u}^\circ$, $\boldsymbol{\vartheta}^\circ$ represent the amplitudes of oscillations for the displacements and small rotations.

The Rayleigh variational principle is equivalent to the stationary principle for the *Rayleigh quotient*

$$\mathcal{R}[\mathbf{u}^\circ, \boldsymbol{\vartheta}^\circ] = \frac{\displaystyle\iint\limits_\sigma W(\mathbf{e}^\circ, \boldsymbol{\kappa}^\circ)\mathrm{d}\sigma}{\displaystyle\iint\limits_\sigma \rho K(\mathbf{u}^\circ, \boldsymbol{\vartheta}^\circ)\,\mathrm{d}\sigma}, \tag{2.43}$$

that is defined on kinematically admissible functions $\mathbf{u}^\circ$, $\boldsymbol{\vartheta}^\circ$. Note that the least squared eigenfrequency for the shell corresponds the minimal value of $\mathcal{R}$

$$\Omega^2_{\min} = \inf \mathcal{R}[\mathbf{u}^\circ, \boldsymbol{\vartheta}^\circ]$$

on $\mathbf{u}^\circ$, $\boldsymbol{\vartheta}^\circ$ satisfying (2.41). Using the Courant minimax principle [14] the Rayleigh quotient (2.43) allows us to estimate the values of higher eigenfrequencies. For this we should consider $\mathcal{R}$ on the set of functions that are orthogonal to the previous modes of eigen-oscillations in some sense.

2.2.7 Principle Peculiarities of the Micropolar Shell Theory

Let us summarize principle peculiarities of the shell theory under consideration:

1. The shell equilibrium equation constitute a nonlinear system partial differential equations. In general, the system is elliptic but in some circumstances the ellipticity condition can fail. We will discuss this later.
2. General theorems of existence of equilibrium or dynamic solutions are absent. Moreover, there are examples when under some loads the equilibrium solutions

does not exist. As for other nonlinear systems, a solution of the equilibrium problem can be non-unique, in general.
3. The Lagrange variational principle is not minimal, it is only a stationary variational principle. The only exception is for the linear theory.
4. For the linear theory of micropolar shells it can be demonstrated the theorems of existence and uniqueness of a solution.

Further developments of this version of the shell theory can be produced in the following directions:

1. Development of mathematical theory that should be based on the methods of partial differential equations theory, functional analysis and calculus of variations.
2. Numerical algorithms for solution of the reduced systems of nonlinear equations. For example, it can be done within the framework of the finite element method, see for example the numerical results in [10, 11, 12].
3. Analysis of the restrictions of the nonlinear constitutive equations.
4. Extension of the two-dimensional constitutive equations for the shell made of various materials. In particular, the extension can include viscoelasticity, thermal effects, etc. In particular, the theory of thermoelastic and thermoviscoelastic shells with phase transitions is developed in [19].

Some of the above problems will be considered in later sections.

2.3 Constitutive Restrictions for Micropolar Shells

In nonlinear elasticity there are well known so-called constitutive restrictions. They are the strong ellipticity condition, the Hadamard inequality, the GCN-condition, and some others [56, 57, 58]. Each of them play some role in nonlinear elasticity. They express mathematically precise and physically intuitive restrictions for constitutive equations of elastic bodies. In particular, the GCN condition proposed by Coleman and Noll asserts "that the transformation from deformation gradient to first Piola-Kirchhoff stress tensor shall be monotone with respect to pairs of deformations differing from one another by a pure stretch" (see, [58]).

The aim of this section is to formulate similar constitutive restrictions in the general nonlinear theory of micropolar shells. Here we formulate the generalized Coleman-Noll inequality (GCN-condition), the strong ellipticity condition of equilibrium equations and the Hadamard inequality. The inequalities represent possible restrictions of constitutive equations of elastic shells under finite deformation. We prove that the Coleman-Noll inequality implies strong ellipticity of shell equilibrium equations.

2.3.1 Linear Theory of Micropolar Shells

In the linear shell theory as well as in the case of the three-dimensional elasticity, it is necessary to establish additional restrictions, so-called constitutive inequalities or constitutive restrictions. Again we stipulate the specific strain energy $W(\mathbf{e}, \boldsymbol{\kappa})$ to be positive definite. Now the energy is a quadratic form of both of the linear strain tensor and the linear bending strain tensor. In particular, for an isotropic shell it takes the form (2.36). Positivity of the quadratic form (2.36) for all values of $\mathbf{e}$ and $\boldsymbol{\kappa}$ is equivalent to the following set of inequalities

$$\begin{array}{llll} 2\alpha_1+\alpha_2+\alpha_3>0, & \alpha_2+\alpha_3>0, & \alpha_3-\alpha_2>0, & \alpha_4>0, \\ 2\beta_1+\beta_2+\beta_3>0, & \beta_2+\beta_3>0, & \beta_3-\beta_2>0, & \beta_4>0. \end{array} \tag{2.44}$$

The inequality

$$W(\mathbf{e}, \boldsymbol{\kappa})>0, \quad \forall\, \mathbf{e}, \boldsymbol{\kappa} \neq \mathbf{0}$$

and the following from this the inequalities for the elastic constants of an isotropic material (2.44) are the simplest example of additional inequalities in the shell theory. When they fail it leads to a number of pathological consequences such as non-uniqueness of the solution of boundary value problems of linear shell theory that implies that a solution does not exist for some loads. At second, the propagation of waves in some directions becomes impossible that is not natural from the physical point of view. In the case of finite strains, the positive definiteness of the specific energy $W(\mathbf{E}, \mathbf{K})$ is not a warranty that the desired properties of constitutive equations hold, here must be fulfilled some additional inequalities.

2.3.2 Coleman-Noll Inequality for Elastic Shells

Let us suppose that a certain equilibrium state of a nonlinear elastic shell of the Cosserat type under the action of a given load is known. Further we will call it initial or basic stressed state. This state is defined by the vector field $\mathbf{R}(q^\alpha)$ and the tensor field $\mathbf{Q}(q^\alpha)$. Along with the basic stressed state we consider some perturbed equilibrium state which differs from the basic one. The linear parts of increments of different quantities that characterize the perturbed equilibrium we will denote using dots above, for example

$$\mathbf{D}^{\cdot} = \frac{\mathrm{d}}{\mathrm{d}\tau}\mathbf{D}\left[\nabla\left(\mathbf{R}+\tau\mathbf{u}, \mathbf{Q}-\tau\mathbf{Q}\times\boldsymbol{\theta}, \nabla\left(\mathbf{Q}-\tau\mathbf{Q}\times\boldsymbol{\theta}\right)\right)\right]\Big|_{\tau=0}. \tag{2.45}$$

Here $\mathbf{u}$ is the vector of the additional infinitesimal displacement, while $\boldsymbol{\theta}$ is the vector of the additional infinitesimal rotation characterizing the small rotation with respect to the initial stressed state. The following relations are valid

$$\mathbf{R}^{\cdot} = \mathbf{u}, \quad \mathbf{Q}^{\cdot} = -\mathbf{Q}\times\boldsymbol{\theta}, \quad \mathbf{E}^{\cdot} = \mathbf{F}\cdot\boldsymbol{\varepsilon}\cdot\mathbf{Q}^T, \quad \mathbf{K}^{\cdot} = \mathbf{F}\cdot\boldsymbol{\varkappa}\cdot\mathbf{Q}^T, \tag{2.46}$$

$$\boldsymbol{\varepsilon} = \nabla \mathbf{u} + \mathbf{A} \times \boldsymbol{\theta}, \quad \boldsymbol{\varkappa} = \nabla \boldsymbol{\theta}, \tag{2.47}$$

where $\boldsymbol{\varepsilon}$ is the strain tensor and $\boldsymbol{\varkappa}$ is the bending strain tensor usually used in the linear shell theory of the Cosserat-type [23, 36, 60].

Note that as the reference configuration may be chosen any stressed state of the shell. To avoid awkward expressions and to simplify the calculations let us assume that the reference configuration coincides with the initial (basic) stressed state of the shell. This means that in the reference configuration $\mathbf{F} = \mathbf{E} = \mathbf{I} - \mathbf{n} \otimes \mathbf{n}$, $\mathbf{Q} = \mathbf{I}$, $\mathbf{K} = \mathbf{0}$. Under this choice of the reference configuration and using Eqs (2.9), (2.13), (2.45)–(2.47) we obtain

$$\begin{aligned} \mathbf{D}^{\cdot} &= \frac{\partial^2 W}{\partial \mathbf{E} \partial \mathbf{E}} \bullet \boldsymbol{\varepsilon} + \frac{\partial^2 W}{\partial \mathbf{E} \partial \mathbf{K}} \bullet \boldsymbol{\varkappa} - \mathbf{T} \times \boldsymbol{\theta}, \\ \mathbf{G}^{\cdot} &= \frac{\partial^2 W}{\partial \mathbf{K} \partial \mathbf{E}} \bullet \boldsymbol{\varepsilon} + \frac{\partial^2 W}{\partial \mathbf{K} \partial \mathbf{K}} \bullet \boldsymbol{\varkappa} - \mathbf{M} \times \boldsymbol{\theta}. \end{aligned} \tag{2.48}$$

Here and below we use the operation of a scalar product of tensors given by the formulae

$$\left(C^{kstp}\mathbf{R}_k \otimes \mathbf{R}_s \otimes \mathbf{R}_t \otimes \mathbf{R}_p\right) \bullet \left(U_{mn}\mathbf{R}^m \otimes \mathbf{R}^n\right) \triangleq C^{ksmn}U_{mn}\mathbf{R}_k \otimes \mathbf{R}_s,$$

$$\left(V_{ij}\mathbf{R}^i \otimes \mathbf{R}^j\right) \bullet \left(C^{kstp}\mathbf{R}_k \otimes \mathbf{R}_s \otimes \mathbf{R}_t \otimes \mathbf{R}_p\right) \bullet \left(U_{mn}\mathbf{R}^m \otimes \mathbf{R}^n\right) \triangleq C^{ijmn}V_{ij}U_{mn}.$$

Suppose that the external couples in the initial and perturbed stressed states of the shell vanish $\mathbf{c} = \boldsymbol{\gamma} = \mathbf{0}$, while the external forces are "dead". Then the elastic energy of the shell is given by the relation

$$\Pi \equiv \mathcal{E}_1 = \iint\limits_{\sigma} W \,\mathrm{d}\sigma - \iint\limits_{\sigma} \mathbf{f}\cdot(\mathbf{R} - \mathbf{r})\,\mathrm{d}\sigma - \int\limits_{\omega_2} \boldsymbol{\varphi}\cdot(\mathbf{R} - \mathbf{r})\,\mathrm{d}s.$$

Let us consider the energy increment in the perturbed equilibrium state with respect to the energy in the initial state taking into account terms of order one and two

$$\Pi - \Pi_0 = \tau \left(\frac{\mathrm{d}\Pi}{\mathrm{d}\tau}\right)_{\tau=0} + \frac{1}{2}\tau^2 \left(\frac{\mathrm{d}^2\Pi}{\mathrm{d}\tau^2}\right)_{\tau=0} + \ldots$$

According to the constitutive relations of an elastic shell (2.9) and Eqs (2.46), (2.47) we obtain

$$\begin{aligned} \frac{\mathrm{d}\Pi}{\mathrm{d}\tau} = \iint\limits_{\sigma} \left[\mathrm{tr}\left(\mathbf{D}^T \cdot \nabla \mathbf{u}\right) + \mathrm{tr}\left(\mathbf{D}^T \cdot \mathbf{F} \times \boldsymbol{\theta}\right) + \mathrm{tr}\left(\mathbf{G}^T \cdot \nabla \boldsymbol{\theta}\right)\right] \mathrm{d}\sigma \\ - \iint\limits_{\sigma} \mathbf{f}\cdot\mathbf{u}\,\mathrm{d}\sigma - \int\limits_{\omega_2} \boldsymbol{\varphi}\cdot\mathbf{u}\,\mathrm{d}s. \end{aligned} \tag{2.49}$$

Differentiating Eq. (2.49) with respect to the parameter τ and taking into account that the reference configuration coincides with the basic stressed state and Eqs (2.46) we get

$$\left.\frac{\mathrm{d}^2\Pi}{\mathrm{d}\tau^2}\right|_{\tau=0} = \iint\limits_{\Sigma} \Big[\mathrm{tr}\left(\mathbf{D}^{\cdot T}\cdot\nabla\mathbf{u}\right) + \mathrm{tr}\left(\mathbf{D}^{\cdot T}\times\boldsymbol{\theta}\right) + \mathrm{tr}\left(\mathbf{T}^{T}\cdot(\nabla\mathbf{u})\times\boldsymbol{\theta}\right) + \mathrm{tr}\left(\mathbf{G}^{\cdot T}\cdot\boldsymbol{\varkappa}\right)\Big]\,\mathrm{d}\Sigma.$$

From the equilibrium condition of the basic state and considering Eqs (2.8) and (2.10) it follows that the first variation of the energy

$$\left.\frac{\mathrm{d}\Pi}{\mathrm{d}\tau}\right|_{\tau=0}$$

vanishes, and the second variation due to Eqs (2.47) and (2.48) could be represented as

$$\left.\frac{\mathrm{d}^2\Pi}{\mathrm{d}\tau^2}\right|_{\tau=0} = 2\iint\limits_{\Sigma} w\,\mathrm{d}\Sigma, \quad w = w' + w'', \tag{2.50}$$

$$\begin{aligned} w' &= \frac{1}{2}\boldsymbol{\varepsilon}\bullet\frac{\partial^2 W}{\partial\mathbf{E}\partial\mathbf{E}}\bullet\boldsymbol{\varepsilon} + \boldsymbol{\varepsilon}\bullet\frac{\partial^2 W}{\partial\mathbf{E}\partial\mathbf{K}}\bullet\boldsymbol{\varkappa} + \frac{1}{2}\boldsymbol{\varkappa}\bullet\frac{\partial^2 W}{\partial\mathbf{K}\partial\mathbf{K}}\bullet\boldsymbol{\varkappa}, \\ w'' &= \mathrm{tr}\left(\boldsymbol{\theta}\times\mathbf{T}^{T}\cdot\boldsymbol{\varepsilon}\right) - \frac{1}{2}\mathrm{tr}\left(\boldsymbol{\theta}\times\mathbf{T}^{T}\times\boldsymbol{\theta}\right) + \frac{1}{2}\mathrm{tr}\left(\boldsymbol{\theta}\times\mathbf{M}^{T}\cdot\boldsymbol{\varkappa}\right). \end{aligned} \tag{2.51}$$

The quantity w describes the increment of the elastic energy of the initially prestressed shell under additional infinitesimal deformations. According to Eqs (2.50) and (2.51) this energy may be decomposed into two parts: the energy of pure strains w' and the energy of rotations w''. The coefficients in the quadratic form w'' are expressed in terms of the stress and couple stress tensors of the initial stressed state and do not depend on material properties of the shell. If the basic stressed state of the shell is natural ($\mathbf{T} = \mathbf{M} = \mathbf{0}$), then $w = w'$ and the energy density reduces to the quadratic form of tensors $\boldsymbol{\varepsilon}$ and $\boldsymbol{\varkappa}$. If the decomposition (2.50) and the formulae (2.51) are compared with the similar results on increment of 3D strain energy density [21] of micropolar body one can easily note that they coincide up to notation.

One of the well-known in the nonlinear elasticity [56, 57, 58] constitutive inequalities is the Coleman-Noll inequality. The differential form of the Coleman-Noll inequality (so-called GCN-condition) expresses the property that the elastic energy density under arbitrary infinitesimal non-zero *pure* strains and bending strains for any arbitrary reference configuration should be positive. It is necessary to mention that this inequality does not restrict the constitutive equations with regard to any rotations.

Taking into account the energy decomposition (2.50) we obtain an analogue of the *Coleman-Noll inequality* for elastic shells of the Cosserat type

$$w'(\boldsymbol{\varepsilon},\boldsymbol{\varkappa}) > 0 \quad \forall\,\boldsymbol{\varepsilon}\neq\mathbf{0}, \quad \boldsymbol{\varkappa}\neq\mathbf{0}. \tag{2.52}$$

Using Eqs (2.51) inequality (2.52) can be written in the equivalent form

$$\frac{\mathrm{d}^2}{\mathrm{d}\tau^2} W\left(\mathbf{E}+\tau\boldsymbol{\varepsilon},\mathbf{K}+\tau\boldsymbol{\varkappa}\right)\Big|_{\tau=0} > 0 \quad \forall\, \boldsymbol{\varepsilon}\neq\mathbf{0}, \quad \boldsymbol{\varkappa}\neq\mathbf{0}. \tag{2.53}$$

Condition (2.53) satisfies the principle of material frame-indifference and could serve as a constitutive inequality for elastic shells.

2.3.3 Strong Ellipticity and Hadamard Inequality

The famous constitutive inequalities in the nonlinear elasticity are the strong ellipticity condition and its weak form known as the Hadamard inequality. Following the theory of systems of partial differential equations (PDE) [27, 40] in this section we formulate the strong ellipticity condition of the equilibrium equations (2.8). In the case of dead loading the linearized equilibrium equations have the form

$$\boldsymbol{\nabla}\cdot\dot{\mathbf{D}}=\mathbf{0}, \quad \boldsymbol{\nabla}\cdot\dot{\mathbf{G}}+\left[\mathbf{F}^T\cdot\dot{\mathbf{D}}+(\nabla\mathbf{u})^T\cdot\mathbf{D}\right]_{\times}=\mathbf{0}, \tag{2.54}$$

where $\dot{\mathbf{D}}$ and $\dot{\mathbf{G}}$ are given by formulae similar to Eqs (2.45). Equations (2.54) are the system of linear PDE of second order with respect to $\mathbf{u}$ and $\boldsymbol{\theta}$. If we keep in Eqs (2.54) the differential operators of second order we obtain the relations

$$\boldsymbol{\nabla}\cdot\left\{\left[\frac{\partial^2 W}{\partial\mathbf{E}\partial\mathbf{E}}\bullet\left((\nabla\mathbf{u})\cdot\mathbf{Q}^T\right)+\frac{\partial^2 W}{\partial\mathbf{E}\partial\mathbf{K}}\bullet\left((\nabla\boldsymbol{\theta})\cdot\mathbf{Q}^T\right)\right]\cdot\mathbf{Q}\right\},$$

$$\boldsymbol{\nabla}\cdot\left\{\left[\frac{\partial^2 W}{\partial\mathbf{K}\partial\mathbf{E}}\bullet\left((\nabla\mathbf{u})\cdot\mathbf{Q}^T\right)+\frac{\partial^2 W}{\partial\mathbf{K}\partial\mathbf{K}}\bullet\left((\nabla\boldsymbol{\theta})\cdot\mathbf{Q}^T\right)\right]\cdot\mathbf{Q}\right\},$$

which allow to construct the condition of strong ellipticity of the system (2.54). Using the formal procedure [27, 40] we replace the differential operator ∇ by the unit vector $\boldsymbol{\nu}$ tangential to the surface σ, while the vector fields $\mathbf{u}$ and $\boldsymbol{\theta}$ by the vectors $\mathbf{a}$ and $\mathbf{b}$, respectively. Thus, we have the algebraic expressions

$$\boldsymbol{\nu}\cdot\left\{\left[\frac{\partial^2 W}{\partial\mathbf{E}\partial\mathbf{E}}\bullet\left(\boldsymbol{\nu}\otimes\mathbf{a}\cdot\mathbf{Q}^T\right)+\frac{\partial^2 W}{\partial\mathbf{E}\partial\mathbf{K}}\bullet\left(\boldsymbol{\nu}\otimes\mathbf{b}\cdot\mathbf{Q}^T\right)\right]\cdot\mathbf{Q}\right\},$$

$$\boldsymbol{\nu}\cdot\left\{\left[\frac{\partial^2 W}{\partial\mathbf{K}\partial\mathbf{E}}\bullet\left(\boldsymbol{\nu}\otimes\mathbf{a}\cdot\mathbf{Q}^T\right)+\frac{\partial^2 W}{\partial\mathbf{K}\partial\mathbf{K}}\bullet\left(\boldsymbol{\nu}\otimes\mathbf{b}\cdot\mathbf{Q}^T\right)\right]\cdot\mathbf{H}\right\}.$$

Let us multiply the first equation by the vector $\mathbf{a}$ while the second one by the vector $\mathbf{b}$ and add these expressions. Then we obtain the strong ellipticity condition of Eqs (2.54) in the following form

$$\boldsymbol{\nu}\cdot\left\{\left[\frac{\partial^2 W}{\partial\mathbf{E}\partial\mathbf{E}}\bullet\left(\boldsymbol{\nu}\otimes\mathbf{a}\cdot\mathbf{Q}^T\right)+\frac{\partial^2 W}{\partial\mathbf{E}\partial\mathbf{K}}\bullet\left(\boldsymbol{\nu}\otimes\mathbf{b}\cdot\mathbf{Q}^T\right)\right]\cdot\mathbf{Q}\right\}\cdot\mathbf{a}$$

$$+\boldsymbol{\nu}\cdot\left\{\left[\frac{\partial^2 W}{\partial\mathbf{E}\partial\mathbf{E}}\bullet\left(\boldsymbol{\nu}\otimes\mathbf{a}\cdot\mathbf{Q}^T\right)+\frac{\partial^2 W}{\partial\mathbf{K}\partial\mathbf{K}}\bullet\left(\boldsymbol{\nu}\otimes\mathbf{b}\cdot\mathbf{Q}^T\right)\right]\cdot\mathbf{Q}\right\}\cdot\mathbf{b}>0,$$
$$\forall\,\mathbf{a},\mathbf{b}\neq\mathbf{0}.$$

Using operation $\bullet$ we can transform the latter equations as follows

$$\left(\boldsymbol{\nu}\otimes\mathbf{a}\cdot\mathbf{Q}^T\right)\bullet\frac{\partial^2 W}{\partial\mathbf{E}\partial\mathbf{E}}\bullet\left(\boldsymbol{\nu}\otimes\mathbf{a}\cdot\mathbf{H}^T\right)+2\left(\boldsymbol{\nu}\otimes\mathbf{a}\cdot\mathbf{Q}^T\right)\bullet\frac{\partial^2 W}{\partial\mathbf{E}\partial\mathbf{K}}\bullet\left(\boldsymbol{\nu}\otimes\mathbf{b}\cdot\mathbf{Q}^T\right)$$
$$+\left(\boldsymbol{\nu}\otimes\mathbf{b}\cdot\mathbf{H}^T\right)\bullet\frac{\partial^2 W}{\partial\mathbf{K}\partial\mathbf{E}}\bullet\left(\boldsymbol{\nu}\otimes\mathbf{b}\cdot\mathbf{Q}^T\right)>0,\qquad\forall\,\mathbf{a},\mathbf{b}\neq\mathbf{0}.$$

This inequality can be written in a more compact form using the matrix notation

$$\boldsymbol{\xi}\cdot\mathbb{A}(\boldsymbol{\nu})\cdot\boldsymbol{\xi}>0,\quad\forall\,\boldsymbol{\nu}\in\mathscr{T}_x\sigma,\quad\boldsymbol{\nu}\neq\mathbf{0},\quad\forall\,\boldsymbol{\xi}\in\mathbb{R}^6,\quad\boldsymbol{\xi}\neq\mathbf{0},\tag{2.55}$$

where $\boldsymbol{\xi}=(\mathbf{a}',\mathbf{b}')\in\mathbb{R}^6$, $\mathbf{a}'=\mathbf{a}\cdot\mathbf{Q}^T$, $\mathbf{b}'=\mathbf{b}\cdot\mathbf{Q}^T$, and the matrix $\mathbb{A}(\boldsymbol{\nu})$ is given by

$$\mathbb{A}(\boldsymbol{\nu})\triangleq\begin{bmatrix}\dfrac{\partial^2 W}{\partial\mathbf{E}\partial\mathbf{E}}\{\boldsymbol{\nu}\} & \dfrac{\partial^2 W}{\partial\mathbf{E}\partial\mathbf{K}}\{\boldsymbol{\nu}\}\\[2ex] \dfrac{\partial^2 W}{\partial\mathbf{K}\partial\mathbf{E}}\{\boldsymbol{\nu}\} & \dfrac{\partial^2 W}{\partial\mathbf{K}\partial\mathbf{K}}\{\boldsymbol{\nu}\}\end{bmatrix},$$

where for any fourth-order tensor $\mathbf{K}$ and any vector $\boldsymbol{\nu}$: $\mathbf{K}\{\boldsymbol{\nu}\}\triangleq K_{klmn}\nu_k\nu_m\mathbf{i}_l\otimes\mathbf{i}_n$. The inequality (2.55) is *the strong ellipticity condition* of the equilibrium equations (2.8) of an elastic shells. A weak form of the inequality (2.55) is an analogue of the *Hadamard inequality* for the shell. These inequalities are examples of possible restrictions of the constitutive equations of elastic shells under finite deformations. As in the case of simple materials, a break in inequality the (2.55) means the possibility of existing non-smooth solutions of the equilibrium equations (2.8).

The strong ellipticity condition may be written in the equivalent form

$$\frac{\mathrm{d}^2}{\mathrm{d}\tau^2}W\left(\mathbf{E}+\tau\boldsymbol{\nu}\otimes\mathbf{a}',\mathbf{K}+\tau\boldsymbol{\nu}\otimes\mathbf{b}'\right)\Big|_{\tau=0}>0\quad\forall\,\boldsymbol{\nu},\mathbf{a}',\mathbf{b}'\neq\mathbf{0}.\tag{2.56}$$

Comparing the condition of strong ellipticity (2.56) and the Coleman-Noll inequality (2.53) one can see that the latter implies the former. Indeed, the inequality (2.53) holds for any tensors $\boldsymbol{\varepsilon}$ and $\boldsymbol{\varkappa}$. Note that the tensors $\boldsymbol{\varepsilon}$ and $\boldsymbol{\varkappa}$ may by nonsymmetric, in general. If we substitute in the inequality (2.53) the relations $\boldsymbol{\varepsilon}=\boldsymbol{\nu}\otimes\mathbf{a}'$ and $\boldsymbol{\varkappa}=\boldsymbol{\nu}\otimes\mathbf{b}'$ then we immediately obtain the inequality (2.56). Thus, the strong ellipticity condition is the special case of the Coleman–Noll inequality. This is the essential distinction between the shell theory of the Cosserat type and the theory of simple elastic materials [57, 58] where these two properties completely independent of each other in the sense that neither of them implies the other one. For 3D elastic micropolar media the strong ellipticity and the Hadamard conditions are formulated in [21].

In the shell theory it is widely used the following particular constitutive equation

$$W(\mathbf{E},\mathbf{K}) = W_1(\mathbf{E}) + W_2(\mathbf{K}). \tag{2.57}$$

For example, the constitutive relations (2.18) have the form (2.57).

Now condition (2.55) is equivalent to two more simple inequalities

$$\mathbf{a}\cdot\frac{\partial^2 W_1}{\partial\mathbf{E}\partial\mathbf{E}}\{\boldsymbol{\nu}\}\cdot\mathbf{a} > 0, \quad \mathbf{b}\cdot\frac{\partial^2 W_2}{\partial\mathbf{K}\partial\mathbf{K}}\{\boldsymbol{\nu}\}\cdot\mathbf{b} > 0,$$

$$\forall\,\boldsymbol{\nu}\,, \quad \boldsymbol{\nu}\neq\mathbf{0}, \quad \boldsymbol{\nu}\cdot\mathbf{n} = 0, \quad \forall\,\mathbf{a},\mathbf{b}\in\mathbb{R}^3, \quad \mathbf{a},\mathbf{b}\neq\mathbf{0}.$$

As an example, let us consider when for constitutive equation (2.18) the conditions (2.55) are valid. It can be shown that the second-order tensors

$$\frac{\partial^2 W_1}{\partial\mathbf{E}\partial\mathbf{E}}\{\boldsymbol{\nu}\} \quad \text{and} \quad \frac{\partial^2 W_2}{\partial\mathbf{K}\partial\mathbf{K}}\{\boldsymbol{\nu}\}$$

are given by formulas

$$\begin{aligned}\frac{\partial^2 W_1}{\partial\mathbf{E}\partial\mathbf{E}}\{\boldsymbol{\nu}\} &= \alpha_3\mathbf{A} + (\alpha_1+\alpha_2)\boldsymbol{\nu}\otimes\boldsymbol{\nu} + \alpha_4\mathbf{n}\otimes\mathbf{n},\\ \frac{\partial^2 W_2}{\partial\mathbf{K}\partial\mathbf{K}}\{\boldsymbol{\nu}\} &= \beta_3\mathbf{A} + (\beta_1+\beta_2)\boldsymbol{\nu}\otimes\boldsymbol{\nu} + \beta_4\mathbf{n}\otimes\mathbf{n}.\end{aligned} \tag{2.58}$$

Inequality (2.55) is valid under the following conditions

$$\begin{aligned}&\alpha_3 > 0, \quad \alpha_1+\alpha_2+\alpha_3 > 0, \quad \alpha_4 > 0,\\ &\beta_3 > 0, \quad \beta_1+\beta_2+\beta_3 > 0, \quad \beta_4 > 0.\end{aligned} \tag{2.59}$$

For an linear isotropic shell, the inequalities (2.59) provide strong ellipticity of equilibrium equations (2.34), they are more weak in comparison with the condition of positive definiteness of (2.44). If we consider the constitutive equations of an isotropic micropolar shell (2.18) then the inequality (2.55) reduces to the system of inequalities (2.59).

2.3.4 Strong Ellipticity Condition and Acceleration Waves

Using approach [3, 15, 22], we show that the inequality (2.55) coincides with the conditions for propagation of acceleration waves in a shell. We consider a motion that may be accompanied by a jump in the continuity of kinematic and dynamic quantities on a certain smooth curve $C(t)$, which is called *singular* (Fig. 2.2). We assume that the limit values of these quantities exist on C and that they are generally

different on the opposite sides of C. The jump of an arbitrary quantity $\boldsymbol{\Psi}$ on C is denoted by $[\![\boldsymbol{\Psi}]\!] = \boldsymbol{\Psi}^+ - \boldsymbol{\Psi}^-$.

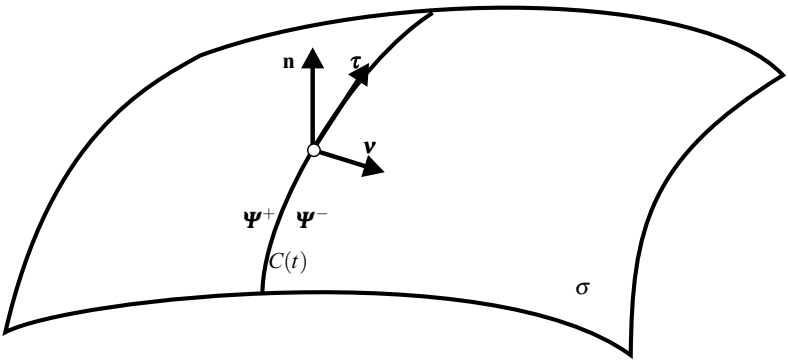

Fig. 2.2 Singular curve

The acceleration wave (weak-discontinuity wave or second-order singular curve) is a moving singular curve C on which the second derivatives (with respect to the spatial coordinates and time) of the radius-vector $\mathbf{R}$ and the microrotation tensor $\mathbf{Q}$ are discontinuous, while the quantities themselves and their first derivatives are continuous, this means

$$[\![\mathbf{F}]\!] = \mathbf{0}, \quad [\![\nabla\mathbf{Q}]\!] = \mathbf{0}, \quad [\![\mathbf{v}]\!] = \mathbf{0}, \quad [\![\boldsymbol{\omega}]\!] = \mathbf{0} \tag{2.60}$$

are valid on C. According to Eqs (2.2), the strain measure $\mathbf{E}$ and the bending strain tensor $\mathbf{K}$ are continuous near C, and, with respect to constitutive equations (2.9), jumps of the tensors $\mathbf{D}$ and $\mathbf{G}$ are absent. The application of the Maxwell theorem [57] to continuous fields of velocities $\mathbf{v}$ and $\boldsymbol{\omega}$, surface stress tensor $\mathbf{D}$, and the surface couple stress tensor $\mathbf{G}$ yields a system of equations that relate the jumps of their derivatives with respect to the spatial coordinates and time

$$\left[\!\left[\frac{d\mathbf{v}}{dt}\right]\!\right] = -V\mathbf{a}, \quad [\![\nabla\mathbf{v}]\!] = \boldsymbol{\nu}\otimes\mathbf{a}, \quad \left[\!\left[\frac{d\boldsymbol{\omega}}{dt}\right]\!\right] = -V\mathbf{b}, \quad [\![\nabla\boldsymbol{\omega}]\!] = \boldsymbol{\nu}\otimes\mathbf{b}, \tag{2.61}$$

$$V\,[\![\boldsymbol{\nabla}\cdot\mathbf{D}]\!] = -\boldsymbol{\nu}\cdot\left[\!\left[\frac{d\mathbf{D}}{dt}\right]\!\right], \quad V\,[\![\boldsymbol{\nabla}\cdot\mathbf{G}]\!] = -\boldsymbol{\nu}\cdot\left[\!\left[\frac{d\mathbf{G}}{dt}\right]\!\right].$$

Here $\mathbf{a}$ and $\mathbf{b}$ are the vector amplitudes for the jumps of the linear and angular accelerations, $\boldsymbol{\nu}$ is the unit normal vector to C such that $\mathbf{n}\cdot\boldsymbol{\nu} = 0$, and V is the velocity of the surface C in the direction $\boldsymbol{\nu}$. If external forces and couples are continuous, the relations

$$[\![\boldsymbol{\nabla}\cdot\mathbf{D}]\!] = \rho\left[\!\left[d\frac{\mathbf{K}_1}{dt}\right]\!\right], \quad [\![\boldsymbol{\nabla}\cdot\mathbf{G}]\!] = \rho\gamma\left[\!\left[\frac{d\mathbf{K}_2}{dt}\right]\!\right]$$

follow immediately from the equations of motion (2.14).

Differentiating constitutive Eqs (2.9) and using equations (2.60) and (2.61), we express latter relations only in terms of the vector amplitudes **a** and **b**

$$\boldsymbol{\nu}\cdot\frac{\partial^2 W}{\partial\mathbf{E}\partial\mathbf{Y}}\bullet\left(\boldsymbol{\nu}\otimes\mathbf{a}\cdot\mathbf{Q}^T\right)+\boldsymbol{\nu}\cdot\frac{\partial^2 W}{\partial\mathbf{E}\partial\mathbf{L}}\bullet\left(\boldsymbol{\nu}\otimes\mathbf{b}\cdot\mathbf{Q}^T\right)=\rho V^2\left[\mathbf{a}\cdot\mathbf{Q}^T\right.$$

$$\left.+\left(\mathbf{Q}\cdot\boldsymbol{\Theta}_1^T\cdot\mathbf{Q}^T\right)\cdot\left(\mathbf{b}\cdot\mathbf{Q}^T\right)\right],$$

$$\boldsymbol{\nu}\cdot\frac{\partial^2 W}{\partial\mathbf{K}\partial\mathbf{E}}\bullet\left(\boldsymbol{\nu}\otimes\mathbf{a}\cdot\mathbf{Q}^T\right)+\boldsymbol{\nu}\cdot\frac{\partial^2 W}{\partial\mathbf{K}\partial\mathbf{L}}\bullet\left(\boldsymbol{\nu}\otimes\mathbf{b}\cdot\mathbf{Q}^T\right)=\rho V^2\left[\left(\mathbf{Q}\cdot\boldsymbol{\Theta}_1\cdot\mathbf{Q}^T\right)\cdot\left(\mathbf{a}\cdot\mathbf{Q}^T\right)\right.$$

$$\left.+\left(\mathbf{Q}\cdot\boldsymbol{\Theta}_2\cdot\mathbf{Q}^T\right)\cdot\left(\mathbf{b}\cdot\mathbf{Q}^T\right)\right].$$

Hence the strong ellipticity condition is valid these relations can be also written in a more compact form

$$\mathbb{A}(\boldsymbol{\nu})\cdot\boldsymbol{\xi}=\rho V^2\mathbb{B}\cdot\boldsymbol{\xi}, \tag{2.62}$$

where the matrix $\mathbb{B}$ is given by

$$\mathbb{B}=\begin{bmatrix}\mathbf{I} & \mathbf{Q}\cdot\boldsymbol{\Theta}_1^T\cdot\mathbf{Q}^T\\ \mathbf{Q}\cdot\boldsymbol{\Theta}_1\cdot\mathbf{Q}^T & \mathbf{Q}\cdot\boldsymbol{\Theta}_2\cdot\mathbf{Q}^T\end{bmatrix}.$$

Thus, the problem of acceleration wave propagation in the shell has been reduced to the spectral problem given by the algebraic equations (2.62). Owing to the existence of the potential-energy function W, $\mathbb{A}(\boldsymbol{\nu})$ is symmetric. Matrix $\mathbb{B}$ is also symmetric and positive definite. This property enables to formulate an analogue of the Fresnel–Hadamard–Duhem theorem for the elastic shell:

Theorem 2.1. *The squares of the velocities of a second order singular curve (acceleration wave) in the elastic shell are real for arbitrary propagation directions specified by the vector* $\boldsymbol{\nu}$.

Note that the positive definiteness of $\mathbb{A}(\boldsymbol{\nu})$, which is necessary and sufficient for the wave velocity V to be real, coincides with the strong ellipticity inequality (2.55).

For a physically linear shell, let us present an example of solution of problem (2.62). Suppose that $\boldsymbol{\Theta}_1$ is zero and $\boldsymbol{\Theta}_2$ is the spherical part of the tensor, that is $\boldsymbol{\Theta}_2=\iota\mathbf{I}$), where ι is the rotatory inertia measure. Let us assume that the inequalities (2.59) are valid. Then solutions of equation (2.62) are

$$U_1 = \sqrt{\frac{\alpha_3}{\rho}}, \quad \boldsymbol{\xi}_1 = (\boldsymbol{\tau}, \mathbf{0}), \quad U_2 = \sqrt{\frac{\alpha_1+\alpha_2+\alpha_3}{\rho}}, \quad \boldsymbol{\xi}_2 = (\boldsymbol{\nu}, \mathbf{0}), \tag{2.63}$$

$$U_3 = \sqrt{\frac{\alpha_4}{\rho}}, \quad \boldsymbol{\xi}_3 = (\mathbf{n}, \mathbf{0}), \quad U_4 = \sqrt{\frac{\beta_3}{\rho\iota}}, \quad \boldsymbol{\xi}_4 = (\mathbf{0}, \boldsymbol{\tau}),$$

$$U_5 = \sqrt{\frac{\beta_1+\beta_2+\beta_3}{\rho\iota}}, \quad \boldsymbol{\xi}_5 = (\mathbf{0}, \boldsymbol{\nu}), \quad U_6 = \sqrt{\frac{\beta_4}{\rho\iota}}, \quad \boldsymbol{\xi}_6 = (\mathbf{0}, \mathbf{n}).$$

Solutions (2.63) describe transversal and longitudinal waves of acceleration and microrotation accelerations.

2.3.5 Ordinary Ellipticity

When equilibrium equations are not elliptic it may result in the break of continuity of solutions. Let us consider this in more detail. We will assume singular time-independent curves of the second order. Suppose on the shell surface σ there exists a curve γ on which a jump in the second derivatives of the position vector $\mathbf{R}$ or microrotation tensor $\mathbf{Q}$ happens. We will call such a jump the *weak discontinuity*. For example, the curvature of Σ is determined through second derivatives of $\mathbf{R}$ so such discontinuity can exhibited in the form of sharp bends of the shell surface.

From the equilibrium equations it follows

$$[\![\nabla \cdot \mathbf{D}]\!] = \mathbf{0}, \quad [\![\nabla \cdot \mathbf{G}]\!] = \mathbf{0}.$$

Repeating transformations of the previous section, we can reduce these to

$$\begin{bmatrix} \dfrac{\partial^2 W}{\partial \mathbf{E} \partial \mathbf{E}}\{\boldsymbol{\nu}\} & \dfrac{\partial^2 W}{\partial \mathbf{E} \partial \mathbf{K}}\{\boldsymbol{\nu}\} \\ \dfrac{\partial^2 W}{\partial \mathbf{K} \partial \mathbf{E}}\{\boldsymbol{\nu}\} & \dfrac{\partial^2 W}{\partial \mathbf{K} \partial \mathbf{L}}\{\boldsymbol{\nu}\} \end{bmatrix} \cdot \begin{bmatrix} \mathbf{a}' \\ \mathbf{b}' \end{bmatrix} = \mathbf{0}$$

We can rewrite this in a more compact form

$$\mathbb{A}(\boldsymbol{\nu}) \cdot \boldsymbol{\xi} = \mathbf{0}, \quad \boldsymbol{\xi} = (\mathbf{a}', \mathbf{b}') \in \mathbb{R}^6. \tag{2.64}$$

The existence of non-trivial solutions of Eq. (2.64) means that weak discontinuities arise. The condition for this is the determinant of matrix $\mathbb{A}(\boldsymbol{\nu})$ should be zero. When there holds

$$\det \mathbb{A}(\boldsymbol{\nu}) \neq 0, \tag{2.65}$$

such discontinuities are impossible.

For the constitutive equation of the form

$$W = W_1(\mathbf{E}) + W_2(\mathbf{K}),$$

condition (2.65) splits into two conditions

$$\det \frac{\partial^2 W_1}{\partial \mathbf{E} \partial \mathbf{E}} \{\boldsymbol{\nu}\} \neq 0, \quad \det \frac{\partial^2 W_1}{\partial \mathbf{K} \partial \mathbf{K}} \{\boldsymbol{\nu}\} \neq 0. \tag{2.66}$$

As an example, we consider the conditions (2.65) for the constitutive equations of a physically linear shell (2.18). With the use of Eqs (2.58) we can show the conditions (2.66) reduce to the inequalities

$$\alpha_3 \neq 0, \quad \alpha_1 + \alpha_2 + \alpha_3 \neq 0, \quad \alpha_4 \neq 0, \quad \beta_3 \neq 0, \quad \beta_1 + \beta_2 + \beta_3 \neq 0, \quad \beta_4 \neq 0.$$

Condition (2.65) is the *ellipticity condition* of the equilibrium equations of shell theory (ellipticity in sense of Petrovsky). The condition follows from the general definition of ellipticity in the theory of partial differential equations. Condition (2.65) is also called the *ordinary ellipticity condition*, which is more weak than the strong ellipticity condition (2.55).

2.4 Phase Equilibrium Conditions in Micropolar Shells

In the shell material can arise structural or phase transitions when it is produced or being in exploitation. For example, such transformations can happen in thin-walled structures made of polymer material or memory shape alloys. Various phase transitions can happen in biology membranes or liquid crystal films. In this chapter, we restrict our consideration by the *frontal phase transitions*, that is the phase transitions with a sharp border between the phases. We consider these transitions that are due to the strain change under constant temperature. Let deformation process to be isothermal or adiabatic. A practically important example of use of thin-walled structures gives us the use of the mono- or polycrystal films of the alloys of the type NiTi, that is NiMnGa, NiTiCu, NiAl, etc., which posses the *shape memory effect*, see e.g. [7, 46]. Such films are used in microelectromechanical systems, MEMS, such as miniature pumps, microengines, etc. One of the first mechanical models of deformations of martensitic films is proposed in [8, 34], see also [7, 46], where, in particular, as a result of a special reduction procedure from a three-dimensional layer to a surface, a model of a directed membrane is elaborated, that is of the shell that does not possesses bending rigidity. Its constitutive equation depends on the displacement field and its derivatives but besides, on the director field that is kinematically independent of the displacement field. Within the nonlinear shell theory, investigation of equilibrium of phases is presented in [17] and extended in [54] to the influence of line tension effects. The quasistatic deformation of two-phase thermoelastic and thermoviscoelastic shells are considered in [19, 20]. Within the framework of the theory of biological membranes the phase transitions in 2D structures are investigated in [2, 9].

2.4.1 Thermodynamic Continuity Conditions

For the sake of simplicity we restrict ourselves by the case of thermodynamic equilibrium. This means that we can use the Gibbs' variational approach [28]. Let us suppose the phase transition happens along the whole shell thickness simultaneously. This allows us to introduce a curve on the shell surface that separates the material phases with different properties. The assumption is based on experimental data for deformation of thin plates and thin-walled tubes with shape memory effect, cf. [31, 32, 33, 37].

For a two-phase shell, surface σ consists of two parts, σ_- and σ_+ (cf. Fig. 2.3), that are separated by a smooth curve γ. Curve γ is unknown in advance, it is a preimage of the phase transition border. In the actual configuration γ is represented by Γ. We should find the shell deformation (2.1) together with γ. Let us note γ is a particular case of the singular curve on which the continuity conditions for some quantities under consideration can be violated.

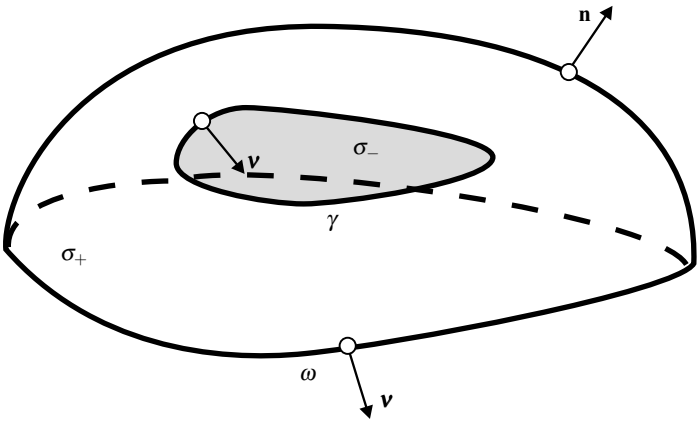

Fig. 2.3 Two-phase shell

Using the Gibbs' variational principle [28], we will find the conditions of thermodynamic equilibrium of the shell in isothermal process. For isothermal or adiabatic processes, the Gibbs' principle reduces to the stationary principle for the total energy over kinematically admissible fields of displacements and microrotations. Here we should suppose the independent position change for the border between the phases. With regard to phase transition, the variational principles of continuum mechanics are developed in [7, 29] among others.

Without the loss of generality, let us suppose that external loads are absent and that $\omega = \omega_1 = \omega_3$, i.e. the displacements and rotations are given at the whole shell contour. Now the strain energy functional takes the form

$$\mathcal{E}_1 = \mathcal{E} \equiv \iint\limits_{\sigma} W \mathrm{d}\sigma. \tag{2.67}$$

To find the first variation of Eq. (2.67), we use the method presented in [14]. Let us consider functional (2.67) on a smooth single-parameter family

$$\mathbf{R} = \mathbf{R}(q^\alpha, \tau), \quad \mathbf{Q} = \mathbf{H}(q^\alpha, \tau), \tag{2.68}$$

each element of which satisfies the border conditions for all τ. Here τ is a small time-like parameter. When $\tau = 0$ deformation (2.68) coincides with (2.1). We accept that in the reference configuration the shell surface as well as the border between the phases depend on τ as well

$$\sigma = \sigma(\tau), \quad \gamma = \gamma(\tau)$$

and $\gamma(\tau)$ lies on $\sigma(\tau)$. In other words, we will study the change of the energy functional in case of variable reference configuration. From the physical point of view, the change of the reference configuration relates to the motion of $\gamma(\tau)$ on σ due to phase transition. We consider the boundary motion to be independent of the strain and rotation fields. This means the surfaces σ and $\sigma(\tau)$ differ one from another only by the partition for different material phases by curves γ and $\gamma(\tau)$, respectively.

Let $\mathbf{r} = \mathbf{r}^*(q^\alpha, \tau)$ be an arbitrary diffeomorphism mapping σ to $\sigma(\tau)$ and such that $\gamma(\tau) = \mathbf{r}^*(\gamma, \tau)$. For sufficiently small τ such a map always exists. We can suppose its support to lie in some small neighborhood of γ. Then

$$\mathcal{E}(\tau) = \iint\limits_{\sigma(\tau)} W(\mathbf{E}(\tau), \mathbf{K}(\tau)) \mathrm{d}\sigma(\tau), \tag{2.69}$$

where $\mathbf{E}(\tau), \mathbf{K}(\tau)$ are the strain measure and the bending strain measure, respectively, that correspond to the family (2.68). We introduce the notations

$$\mathbf{u} = \left.\frac{\partial \mathbf{R}(q^\alpha, \tau)}{\partial \tau}\right|_{\tau=0}, \quad \boldsymbol{\psi} = \frac{1}{2}\left.\left(\frac{\partial \mathbf{H}(q^\alpha, \tau)}{\partial \tau} \cdot \mathbf{H}^T\right)_\times\right|_{\tau=0}, \tag{2.70}$$

$$\mathbf{w} = \left.\frac{\partial \mathbf{r}^*(q^\alpha, \tau)}{\partial \tau}\right|_{\tau=0}.$$

In Eqs (2.70), $\mathbf{u}$, $\boldsymbol{\psi}$, $\mathbf{w}$ are the vectors of small additional displacements, of microrotations and the vector of small perturbations of the reference configuration σ, respectively.

The first variation of $\mathcal{E}$ is the Gâteaux derivative, it can be calculated by the formula

$$\delta\mathcal{E} = \left.\frac{\mathrm{d}\mathcal{E}}{\mathrm{d}\tau}\right|_{\tau=0}.$$

Using integration over σ in Eq. (2.69) and the formula of differentiation of an area element, finally we get

$$\delta\mathcal{E} = \iint\limits_{\sigma} \left\{ \frac{\mathrm{d}W}{\mathrm{d}\tau} + W\boldsymbol{\nabla}\cdot\mathbf{w} \right\} \mathrm{d}\sigma. \tag{2.71}$$

Here and in what follows, in the notation we will omit $\tau = 0$. Vector $\mathbf{w}$ belongs to the tangent plane to σ. Indeed, $\mathbf{n}\cdot\mathbf{w} = 0$ as $\mathbf{w}$ is the infinitesimal velocity vector of curve γ that changes the position on the immovable surface σ. So we derive

$$\delta\mathcal{E} = \iint\limits_{\sigma} \left\{ \frac{\mathrm{d}W}{\mathrm{d}\tau} - \mathbf{w}\cdot\nabla W \right\} \mathrm{d}\sigma + \oint\limits_{\gamma} \boldsymbol{\nu}\cdot[\![W\mathbf{w}]\!]\,\mathrm{d}s,$$

where $\boldsymbol{\nu}$ is the normal vector to γ that is in the tangent plane to σ. The normal direction is from σ_+ to σ_-, see Fig. 2.3. Here in what follows, we denote the jump in quantities on γ with square brackets. For example, $[\![W]\!] = W_+ - W_-$. Where it will be essential, we will use subscripts "+" and "−" of the notation of quantities for different phases. Let us denote expression $\boldsymbol{\nu}\cdot\mathbf{w}$ by $\mathcal{L}_\gamma$. Quantity $\mathcal{L}_\gamma$ is the virtual velocity of the motion of γ in the direction $\boldsymbol{\nu}$; it differs from the velocity V of a singular curve in the previous section in notation only. So we get

$$\frac{\partial\mathbf{E}}{\partial\tau} = (\nabla\mathbf{u})\cdot\mathbf{Q}^T + (\mathbf{F}\times\boldsymbol{\psi})\cdot\mathbf{Q}^T, \quad \frac{\partial\mathbf{K}}{\partial\tau} = (\nabla\boldsymbol{\psi})\cdot\mathbf{Q}^T. \tag{2.72}$$

Calculating the complete derivative with respect to τ, we take into account that the independent variables also depend on τ. Using Eqs (2.72) we can demonstrate that

$$\frac{\mathrm{d}W}{\mathrm{d}\tau} - \mathbf{u}\cdot\nabla W = \frac{\partial W}{\partial\mathbf{E}} \bullet \frac{\partial\mathbf{E}}{\partial\tau} + \frac{\partial W}{\partial\mathbf{K}} \bullet \frac{\partial\mathbf{K}}{\partial\tau} = \mathbf{D}\bullet\nabla\mathbf{u} + \mathbf{G}\bullet\nabla\boldsymbol{\psi} - \left[\mathbf{F}^T\cdot\mathbf{D}\right]_\times\cdot\boldsymbol{\psi}.$$

Thus

$$\delta\mathcal{E} = \iint\limits_{\sigma} \left\{ \mathbf{D}\bullet\nabla\mathbf{u} + \mathbf{G}\bullet\nabla\boldsymbol{\psi} - \left[\mathbf{F}^T\cdot\mathbf{D}\right]_\times\cdot\boldsymbol{\psi} \right\} \mathrm{d}\sigma + \oint\limits_{\gamma} \mathcal{L}_\gamma[\![W]\!]\,\mathrm{d}s, \tag{2.73}$$

and the energy variation does not depend on the choice of diffeomorphism $\mathbf{r}^*$ and Eq. (2.73) includes only the motion of γ.

With regard to Eq. (2.11), we get

$$\delta\mathcal{E} = \delta\mathcal{I}_\sigma + \delta\mathcal{I}_\gamma, \tag{2.74}$$

$$-\delta\mathcal{I}_\sigma = \iint\limits_{\sigma} \left\{ (\boldsymbol{\nabla}\cdot\mathbf{D})\cdot\mathbf{u} + \left[(\boldsymbol{\nabla}\cdot\mathbf{G}) + (\mathbf{F}^T\cdot\mathbf{D})_\times\right]\cdot\boldsymbol{\psi} \right\} \mathrm{d}\sigma,$$

$$\delta\mathcal{I}_\gamma = \oint\limits_{\gamma} \left\{ \boldsymbol{\nu}\cdot[\![\mathbf{D}\cdot\mathbf{u} + \mathbf{G}\cdot\boldsymbol{\psi}]\!] + \mathcal{L}_\gamma[\![W]\!] \right\} \mathrm{d}s.$$

Thus, the condition of stationarity

$$\delta\mathcal{E} = 0$$

splits into two independent equations $\delta\mathcal{I}_\sigma = 0$ and $\delta\mathcal{I}_\gamma = 0$. From the first equation it follows the equilibrium equations (2.2.1) in each of the phase domains. To analyze what happens when the contour integral $\delta\mathcal{I}_\gamma = 0$ takes zero value, we should introduce some assumptions on the nature of variations $\mathbf{u}$ and $\boldsymbol{\psi}$ in a neighborhood of γ. The assumptions follow from the smoothness properties of $\mathbf{R}$ and $\mathbf{Q}$. Vector $\mathbf{R}$ must be continuous on σ, otherwise the shell lacks its continuity. It follows the formula that relates the jump of the additional displacement vector to the jump of the deformation gradient

$$[\![\mathbf{u}]\!] + \mathcal{L}_\gamma \boldsymbol{\nu} \cdot [\![\mathbf{F}]\!] = 0. \tag{2.75}$$

We will differ the *coherent phase interface*, that is when microrotation tensor $\mathbf{Q}$ is continuous, from the *phase interface incoherent in rotations*, that is when its continuity on the border between phases its continuity fails. For coherent phase interface, we obtain the relation for the jumps as it follows

$$[\![\boldsymbol{\psi}]\!] + \mathcal{L}_\gamma \boldsymbol{\nu} \cdot [\![\mathbf{K} \cdot \mathbf{Q}]\!] = 0. \tag{2.76}$$

For the phase transition incoherent in rotations, the variations $\boldsymbol{\psi}_\pm$ are independent and so the last relation is not valid.

Using Eqs (2.75), (2.76) we can transform equation $\delta\mathcal{I}_\gamma = 0$ to the form

$$\oint_\gamma \left\{ \boldsymbol{\nu} \cdot [\![\mathbf{D}]\!] \cdot \mathbf{u}_- + \boldsymbol{\nu} \cdot [\![\mathbf{G}]\!] \cdot \boldsymbol{\psi}_- - \mathcal{L}_\gamma \boldsymbol{\nu} \cdot [\![\boldsymbol{\mu}]\!] \cdot \boldsymbol{\nu} \right\} \mathrm{d}s = 0, \tag{2.77}$$

where $\mathbf{C} = W\mathbf{A} - \mathbf{D} \cdot \mathbf{F}^T - \mathbf{G} \cdot \mathbf{Q}^T \cdot \mathbf{K}^T$ is the *energy-momentum tensor* or *Eshelby tensor* for the shell coherent phase interface [17].

For three-dimensional bodies, the Eshelby tensor describes the energy change when singularity moves inside it [35, 43]. It describes the motion of cracks, phase interfaces, dislocations, shear bands, etc. $\mathbf{C}$ can be also represented in the following form

$$\mathbf{C} = W\mathbf{A} - \frac{\partial W}{\partial \mathbf{E}} \cdot \mathbf{E}^T - \frac{\partial W}{\partial \mathbf{K}} \cdot \mathbf{K}^T.$$

Within the framework of linear theory of plates and shells the properties Eshelby-type tensors are discussed in [35].

As $\mathbf{u}_-$, $\boldsymbol{\psi}_-$ and $\mathcal{L}_\gamma$ in Eq. (2.77) are arbitrary, by Eq. (2.77), the thermodynamic equilibrium conditions of the coherent phase interface take the form

$$\boldsymbol{\nu} \cdot [\![\mathbf{D}]\!] = \mathbf{0}, \qquad \boldsymbol{\nu} \cdot [\![\mathbf{G}]\!] = \mathbf{0}, \qquad \boldsymbol{\nu} \cdot [\![\mathbf{C}]\!] \cdot \boldsymbol{\nu} = 0. \tag{2.78}$$

The first two relations of Eqs (2.78) express the balance conditions for the forces and couples on the singular curve γ in the equilibrium state; the last equation is an additional thermodynamic condition that is necessary for finding the position of the pre-image of γ.

It can be shown that for the phase transition incoherent in rotations, we must change the second equation in Eqs (2.78) to

$$\boldsymbol{\nu}\cdot\mathbf{G}_{\pm}=\mathbf{0}. \tag{2.79}$$

In [17] the phase equilibrium conditions (2.78) and (2.79) are derived in another way. For the geometrically linear shell theory, the phase equilibrium conditions in displacements and rotations are formulated in [23]. Besides, in [23] they are presented in terms of stress functions.

2.4.2 Kinetic Equation

The above results allow us to find the time rate change of the strain energy for the micropolar shell on equilibrium deformation fields that is due to motion of singular curve γ along the shell. It can be found for any physical phenomenon in which γ arises. Namely, there holds

$$\frac{\mathrm{d}\mathcal{E}}{\mathrm{d}t}=\oint_{\gamma}\mathcal{L}_{\gamma}\boldsymbol{\nu}\cdot[\![\mathbf{C}]\!]\cdot\boldsymbol{\nu}\mathrm{d}s. \tag{2.80}$$

In terms of linear irreversible thermodynamics,

$$\boldsymbol{\nu}\cdot[\![\mathbf{C}]\!]\cdot\boldsymbol{\nu}$$

is the *configurational force*, cf. [6, 30, 35]), that is dual to $\mathcal{L}_{\gamma}$. Equation (2.80) allows us to formulate the *kinetic equation* to describe the motion of γ in the surface under small perturbations from thermodynamic equilibrium

$$\mathcal{L}_{\gamma}=-\mathscr{K}\left(\boldsymbol{\nu}\cdot[\![\mathbf{C}]\!]\cdot\boldsymbol{\nu}\right), \tag{2.81}$$

where $\mathscr{K}$ is a positive definite kinetic function. Equation (2.81) is analogous to the kinetic equations of the three-dimensional elasticity of two-phase solids, cf. [1, 6]. Equations (2.80) and (2.81) describe the energy change for the motion of a defect in the micropolar shell. We can generalize Eq. (2.81) with regard for some additional factors such as the energy of γ, that affect its motion, see [19, 54] for details.

After [1, 6, 20], we use the kinetic function $K(\varsigma)$ in the form

$$\mathscr{K}(\varsigma)=\begin{cases}\dfrac{k(\varsigma-\varsigma_0)}{1+\xi(\varsigma-\varsigma_0)} & \varsigma\geq\varsigma_0,\\ 0 & -\varsigma_0<\varsigma<\varsigma_0,\\ \dfrac{k(\varsigma+\varsigma_0)}{1-\xi(\varsigma+\varsigma_0)} & \varsigma\leq-\varsigma_0.\end{cases} \tag{2.82}$$

Here k is a positive kinetic factor, ς_0 describes the effects associated with nucleation of the new phase and action of the surface tension, see [1], and ξ is a parameter describing the limit value of the phase interface velocity [6].

2.5 Conclusions

In this paper the basic relations of the nonlinear micropolar shell theory are reviewed. In Sect. 2.2 the local equilibrium equations and the dynamic boundary conditions of the micropolar shell are derived in terms of the surface stress and couple stress measures using the principle of virtual work. The constitutive equations for elastic shells are defined through the surface strain energy density depending on two surface strain measures by using the frame-indifference principle. Some variational principles are formulated and the nonlinear compatibility conditions for the surface strain measures are presented.

Then in Sec. 2.3 we formulate the differential form of the Coleman-Noll condition which is an analog to the GCN-condition in 3D elasticity. In 3D nonlinear elasticity the so-called constitutive restrictions or constitutive inequalities are presented in [57, 58]. From the physical point of view these restrictions express the our ideas on the physically reasonable behavior of materials. In the linear shell theory, such a restriction is given by the condition of positive definiteness of the shell strain energy. For finite deformation, definite positiveness of the energy is not sufficient. In Sect. 2.3 we also consider the strong ellipticity condition, the Coleman–Noll inequality and the condition of ordinary ellipticity. Then we deduce the linearized equilibrium equations and formulate the strong ellipticity condition (2.55) and the Hadamard inequality. We proved that the Coleman-Noll condition is more general and it implies the strong ellipticity of the equilibrium shell equations. We also show that the strong ellipticity condition is equivalent to the conditions of the existence of accelerations waves in the shell. We establish that the conditions of ordinary ellipticity are more weak. When they fail then there exist non-smooth solutions of the shell equilibrium equations.

In Sect. 2.4 we establish the conditions of thermodynamic equilibrium for shells undergoing phase transitions. In case of small deviation from thermodynamic equilibrium, we formulate a kinetic equation that describe the motion of the phase interface.

Acknowledgements The second author was supported by the DFG grant No. AL 341/33-1 and by the RFBR with the grant No. 09-01-00459.

References

[1] Abeyaratne, R., Knowles, J.K.: *Evolution of Phase Transitions. A Continuum Theory*. Cambridge University Press, Cambridge (2006)

[2] Agrawal, A., Steigmann, D.J.: Coexistent fluid-phase equilibria in biomembranes with bending elasticity. Journal of Elasticity **93**(1), 63–80 (2008)

[3] Altenbach, H., Eremeyev, V.A., Lebedev, L.P., Rendón, L.A.: Acceleration waves and ellipticity in thermoelastic micropolar media. Arch. Appl. Mech. **80**(3), 217–227 (2010)

[4] Altenbach, H., Zhilin, P.A.: A general theory of elastic simple shells (in Russian). Uspekhi Mekhaniki (Advances in Mechanics) **11**(4), 107–148 (1988)
[5] Altenbach, J., Altenbach, H., Eremeyev, V.A.: On generalized Cosserat-type theories of plates and shells. A short review and bibliography. Arch. Appl. Mech. **80**(1), 73–92 (2010)
[6] Berezovski, A., Engelbrecht, J., Maugin, G.A.: *Numerical Simulation of Waves and Fronts in Inhomogeneous Solids*. World Scientific, New Jersey et al. (2008)
[7] Bhattacharya, K.: *Microstructure of Martensite: Why It Forms and How It Gives Rise to the Shape-Memory Effect*. Oxford University Press, Oxford (2003)
[8] Bhattacharya, K., James, R.D.: A theory of thin films of martensitic materials with applications to microactuators. J. Mech. Phys. Solids **36**, 531–576 (1999)
[9] Boulbitch, A.A.: Equations of heterophase equilibrium of a biomembrane. Archive of Applied Mechanics **69**(2), 83–93 (1999)
[10] Chróścielewski, J., Makowski, J., Pietraszkiewicz, W.: *Statics and Dynamics of Multyfolded Shells. Nonlinear Theory and Finite Elelement Method*. Wydawnictwo IPPT PAN, Warszawa (2004)
[11] Chróścielewski, J., Pietraszkiewicz, W., Witkowski, W.: On shear correction factors in the non-linear theory of elastic shells. Int. J. Solids Struct. **47**(25–26), 3537–3545 (2010)
[12] Chróścielewski, J., Witkowski, W.: On some constitutive equations for micropolar plates. ZAMM **90**(1), 53–64 (2010)
[13] Cosserat, E., Cosserat, F.: *Théorie des Corps Déformables*. Hermann Editeurs, Paris (1909) (Reprint, Gabay, Paris, 2008)
[14] Courant, R., Hilbert, D.: *Methods of Mathematical Physics*, Vol. 1. Wiley, New York (1991)
[15] Eremeyev, V.A.: Acceleration waves in micropolar elastic media. Doklady Physics **50**(4), 204–206 (2005)
[16] Eremeyev, V.A.: Nonlinear micropolar shells: theory and applications. In: W. Pietraszkiewicz, C. Szymczak (eds.) Shell Structures: Theory and Applications, pp. 11–18. Taylor & Francis, London (2005)
[17] Eremeyev, V.A., Pietraszkiewicz, W.: The non-linear theory of elastic shells with phase transitions. J. Elasticity **74**(1), 67–86 (2004)
[18] Eremeyev, V.A., Pietraszkiewicz, W.: Local symmetry group in the general theory of elastic shells. J. Elasticity **85**(2), 125–152 (2006)
[19] Eremeyev, V.A., Pietraszkiewicz, W.: Phase transitions in thermoelastic and thermoviscoelastic shells. Arch. Mech. **61**(1), 41–67 (2009)
[20] Eremeyev, V.A., Pietraszkiewicz, W.: On tension of a two-phase elastic tube. In: W. Pietraszkiewicz, I. Kreja (eds.) Shell Structures. Theory and Applications. Vol. 2., pp. 63–66. CRC Press, Boca Raton (2010)
[21] Eremeyev, V.A., Zubov, L.M.: On the stability of elastic bodies with couple stresses (in Russian). Izv. RAN. Mekanika Tvedogo Tela (Mechanics of Solids) (3), 181–190 (1994)

[22] Eremeyev, V.A., Zubov, L.M.: On constitutive inequalities in nonlinear theory of elastic shells. ZAMM **87**(2), 94–101 (2007)
[23] Eremeyev, V.A., Zubov, L.M.: *Mechanics of Elastic Shells (in Russian)*. Nauka, Moscow (2008)
[24] Ericksen, J.L., Truesdell, C.: Exact theory of stress and strain in rods and shells. Arch. Rat. Mech. Analysis **1**(1), 295–323 (1958)
[25] Eringen, A.C.: *Microcontinuum Field Theory. I. Foundations and Solids*. Springer, New York (1999)
[26] Eringen, A.C.: *Microcontinuum Field Theory. II. Fluent Media*. Springer, New York (2001)
[27] Fichera, G.: Existence theorems in elasticity. In: S. Flügge (ed.) Handbuch der Physik, vol. VIa/2, pp. 347–389. Springer, Berlin (1972)
[28] Gibbs, J.W.: On the equilibrium of heterogeneous substances. In: The Collected Works of J. Willard Gibbs, pp. 55–353. Longmans, Green & Co, New York (1928)
[29] Grinfeld, M.: *Thermodynamics Methods in the Theory of Heterogeneous Systems*. Longman, Harlow (1991)
[30] Gurtin, M.E.: *Configurational Forces as Basic Concepts of Continuum Physics*. Springer-Verlag, Berlin (2000)
[31] He, Y.J., Sun, Q.: Scaling relationship on macroscopic helical domains in NiTi tubes. Int. J. Solids Struct. **46**(24), 4242–4251 (2009)
[32] He, Y.J., Sun, Q.: Macroscopic equilibrium domain structure and geometric compatibility in elastic phase transition of thin plates. Int. J. Mech. Sci. **52**(2), 198–211 (2010)
[33] He, Y.J., Sun, Q.: Rate-dependent domain spacing in a stretched NiTi strip. Int. J. Solids Struct. **47**(20), 2775–2783 (2010)
[34] James, R.D., Rizzoni, R.: Pressurized shape memory thin films. J. Elasticity **59**, 399–436 (2000)
[35] Kienzler, R., Herrman, G.: *Mechanics in Material Space with Applications to Defect and Fracure Mechanics*. Springer-Verlag, Berlin (2000)
[36] Lebedev, L.P., Cloud, M.J., Eremeyev, V.A.: *Tensor Analysis with Applications in Mechanics*. World Scientific, New Jersey (2010)
[37] Li, Z.Q., Sun, Q.: The initiation and growth of macroscopic martensite band in nano-grained NiTi microtube under tension. Int. J. Plasticity **18**(11), 1481–1498 (2002)
[38] Libai, A., Simmonds, J.G.: Nonlinear elastic shell theory. Adv. Appl. Mech. **23**, 271–371 (1983)
[39] Libai, A., Simmonds, J.G.: *The Nonlinear Theory of Elastic Shells*, 2nd edn. Cambridge University Press, Cambridge (1998)
[40] Lions, J.L., Magenes, E.: *Problèmes aux limites non homogènes et applications*. Dunod, Paris (1968)
[41] Lurie, A.I.: *Analytical Mechanics*. Foundations of Engineering Mechanics. Springer, Berlin (2001)
[42] Lurie, A.I.: *Theory of Elasticity*. Foundations of Engineering Mechanics. Springer, Berlin (2005)

[43] Maugin, G.A.: *Material Inhomogeneities in Elasticity*. Chapman Hall, London (1993)
[44] Maugin, G.A.: A historical perspective of generalized continuum mechanics. In: H. Altenbach, V.I. Erofeev, G.A. Maugin (eds.) Mechanics of Generalized Continua. From the Micromechanical Basics to Engineering Applications. Springer, Berlin (2011)
[45] Maugin, G.A., Metrikine, A.V. (eds.): Mechanics of Generalized Continua: One hundred years after the Cosserats. Springer, New York (2010)
[46] Miyazaki, S., Fu, Y.Q., Huang, W.M. (eds.): Thin Film Shape Memory Alloys: Fundamentals and Device Applications. Cambridge University Press, Cambridge (2009)
[47] Nowacki, W.: *Theory of Asymmetric Elasticity*. Pergamon-Press, Oxford et al. (1986)
[48] Pietraszkiewicz, W.: Consistent second approximation to the elastic strain energy of a shell. ZAMM **59**, 206–208 (1979)
[49] Pietraszkiewicz, W.: *Finite Rotations and Langrangian Description in the Non-linear Theory of Shells*. Polish Sci. Publ, Warszawa-Poznań (1979)
[50] Pietraszkiewicz, W.: Geometrically nonlinear theories of thin elastic shells. Uspekhi Mechaniki (Advances in Mechanics) **12**(1), 51–130 (1989)
[51] Pietraszkiewicz, W.: Teorie nieliniowe powłok. In: C. Woźniak (ed.) Mechanika sprężystych płyt i powłok, pp. 424–497. PWN, Warszawa (2001)
[52] Pietraszkiewicz, W., Eremeyev, V.A.: On natural strain measures of the non-linear micropolar continuum. Int. J. Solids Struct. **46**, 774–787 (2009)
[53] Pietraszkiewicz, W., Eremeyev, V.A.: On vectorially parameterized natural strain measures of the non-linear Cosserat continuum. Int. J. Solids Struct. **46**(11–12), 2477–2480 (2009)
[54] Pietraszkiewicz, W., Eremeyev, V.A., Konopińska, V.: Extended non-linear relations of elastic shells undergoing phase transitions. ZAMM **87**(2), 150–159 (2007)
[55] Reissner, E.: Linear and nonlinear theory of shells. In: Y.C. Fung, E.E. Sechler (eds.) Thin Shell Structures, pp. 29–44. Prentice-Hall, Englewood Cliffs, NJ (1974)
[56] Truesdell, C.: *Rational Thermodynamics*, 2nd edn. Springer, New York (1984)
[57] Truesdell, C.: *A First Course in Rational Continuum Mechanics*, 2nd edn. Academic Press, New York (1991)
[58] Truesdell, C., Noll, W.: The nonlinear field theories of mechanics. In: S. Flügge (ed.) Handbuch der Physik, Vol. III/3, pp. 1–602. Springer, Berlin (1965)
[59] Zhilin, P.A.: Mechanics of deformable directed surfaces. Int. J. Solids Struct. **12**, 635 – 648 (1976)
[60] Zubov, L.M.: *Nonlinear Theory of Dislocations and Disclinations in Elastic Bodies*. Springer, Berlin (1997)

Chapter 3
Structural Dynamics and Generalized Continua

Céline Chesnais, Claude Boutin, and Stéphane Hans

Abstract This paper deals with the dynamic behavior of reticulated beams made of the periodic repetition of symmetric unbraced frames. Such archetypical cells can present a high contrast between shear and compression deformability, conversely to "massive" media. This opens the possibility of enriched local kinematics involving phenomena of global rotation, inner deformation or inner resonance, according to studied configuration and frequency range. Firstly, the existence of these atypical behaviors is established theoretically through the homogenization method of periodic discrete media. Then, the results are adapted to buildings and confirmed with a numerical example.

Key words: Dynamics. Discrete structure. Periodic homogenization. Local resonance. Atypical modes. Building. Frame. Shear wall.

3.1 Introduction

This paper deals with the macroscopic dynamic behavior of periodic reticulated structures widely encountered in mechanical engineering. Periodic lattices have been studied through various approaches [14] such as transfer matrix, variational approach [11], finite difference operator. Asymptotic methods of homogenization [16] initially developed for periodic media, were extended to multiple parameters and scale changes by [8] and adapted to periodic discrete structures by [4], then [12]. Unbraced frame-type structures have also been considered in structural dynamics.

Céline Chesnais
Laboratoire Central des Ponts et Chaussées, Université Paris-Est, Paris, France
e-mail: celine.chesnais@lcpc.fr

Claude Boutin and Stéphane Hans
DGCB, FRE CNRS 3237, École Nationale des Travaux Publics de l'État, Université de Lyon, France
e-mail: claude.boutin@entpe.fr;stephane.hans@entpe.fr

H. Altenbach et al. (eds.), *Mechanics of Generalized Continua,*
Advanced Structured Materials, 7, DOI: 10.1007/978-3-642-19219-7_3,

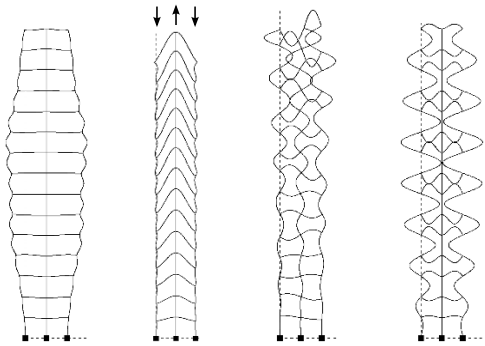

Fig. 3.1 Examples of atypical normal modes of reticulated structures

The first studies focused on an individual bracing element such as a frame or coupled shear walls [1, 17]. Then the models were extended to the whole building [15, 18] and to 3D problems with torsion [13, 15]. All those methods aim to relate the features of the basic cell and the global behavior.

The morphology of reticulated beams is such that the basic cells can present a high contrast between shear and compression deformability (conversely to "massive" beams). This opens the possibility of enriched local kinematics involving phenomena of global rotation, inner deformation or inner resonance, according to studied configuration and frequency range [6, 9]. A numerical illustration of these atypical situations is given in Fig. 3.1 that shows some unusual macroscopic modes.

The present study investigates and summarizes those phenomena by a systematic analysis performed on the archetypical case of symmetric unbraced frame-type cells [2, 5, 9]. Assuming the cell size is small compared to the wavelength, the homogenization method of periodic discrete media leads to the macro-behavior at the leading order.

The paper is organized as follows. Section 3.2 gives an overview of the method and the assumptions. In Sect. 3.3, the studied structures are presented. Section 3.4 summarizes the various generalized beam models which can describe the transverse vibrations according to the properties of the basic cell elements and the frequency range. Section 3.5 is devoted to longitudinal vibrations and the effect of local resonance. Finally Sect. 3.6 explains how the results obtained for this particular class of structures can be generalized to more complex reticulated structures, for instance buildings. It is illustrated by a numerical example.

3.2 Overview of Discrete Homogenization

The analysis of periodic lattices of interconnected beams is performed in two steps [19]: first, the discretization of the balance of the structure under harmonic vibra-

tions; second, the homogenization, leading to a continuous model elaborated from the discrete description. An outline of this method is given hereafter.

Discretization of the Dynamic Balance: Studied structures (Fig. 3.2) are made of plates behaving like Euler-Bernoulli beams in out-of-plane motion, and assembled with rigid connections. The motions of each extremity connected to the same node are identical and define the discrete nodal kinematic variables of the system. The discretization consists in integrating the dynamic balance (in harmonic regime) of the beams, the unknown displacements and rotations at their extremities being taken as boundary conditions. Forces applied by an element on its extremities are then expressed as functions of the nodal variables. The balance of each element being satisfied, it remains to express the balance of forces applied to the nodes. Thus, the balance of the whole structure is rigorously reduced to the balance of the nodes.

Homogenization Method: The key assumption of homogenization is that the cell size in the direction of periodicity ℓ_w is small compared to the characteristic size L of the vibrations of the structure. Thus $\varepsilon = \ell_w/L << 1$. The existence of a macro scale is expressed by means of macroscopic space variable x. The unknowns are continuous functions of x coinciding with the discrete variables at any node, e.g. $U_\varepsilon(x = x_n) = U(node\ n)$. These quantities, assumed to converge when ε tends to zero, are expanded in powers of ε: $U_\varepsilon(x) = U^0(x) + \varepsilon\, U^1(x) + \varepsilon^2\, U^2(x) + \ldots$. Similarly, all other unknowns, including the modal frequency, are expanded in powers of ε. As $\ell_w = \varepsilon\, L$ is a small increment with respect to x, the variations of the variables between neighboring nodes are expressed using Taylor's series; this in turn introduces the macroscopic derivatives.

To account properly for the local physics, the geometrical and mechanical characteristics of the elements are scaled according to the powers of ε. As for the modal frequency, scaling is imposed by the balance of elastic and inertia forces at macro level. This scaling insures that each mechanical effect appears at the same order whatever the ε value is. Therefore, the same physics is kept when $\varepsilon \to 0$, i.e. for the homogenized model. Finally, the expansions in ε powers are introduced in the nodal balances. Those relations, valid for any small ε, lead for each ε-order to balance equations which describe the macroscopic behavior.

Local Quasi-Static State and Local Dynamics: In general the scale separation requires wavelengths of the compression and bending vibrations generated in each local element to be much longer than the element length at the modal frequency of the global system. In that case the nodal forces can be developed in Taylor's series with respect to ε. This situation corresponds to a quasi-static state at the local scale. Nevertheless, in higher frequency range, it may occur that only the compression wavelength is much longer than the length of the elements while local resonance in bending appears. The homogenization remains possible through the expansions of the compression forces and leads to atypical descriptions with inner dynamics. Above this frequency range, the local resonance in both compression and bending makes impossible the homogenization process.

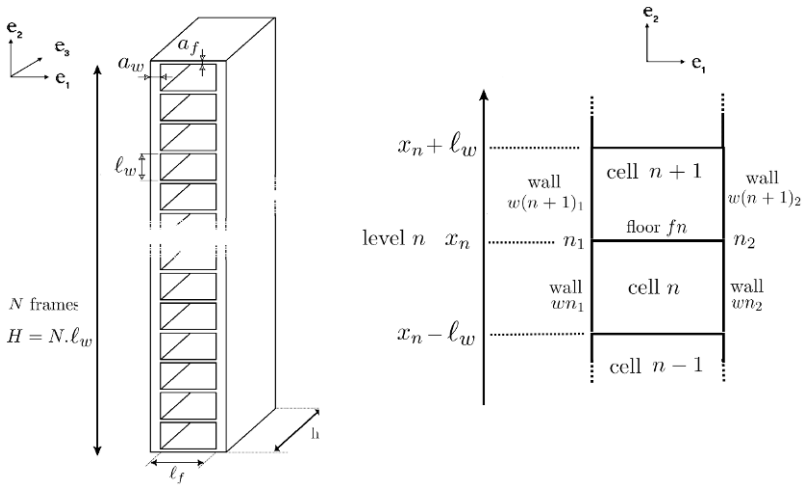

Fig. 3.2 The class of studied structures (left) and the basic frame and notations (right)

3.3 Studied Structures

We study the vibrations of structures of height $H = N \times \ell_w$ constituted by a pile of a large number N of identical unbraced frames called cells and made of a floor supported by two walls (Fig. 3.2). The parameters of floors ($i = f$) and walls ($i = w$) are: length ℓ_i; thickness a_i; cross-section area A_i; second moment of area $I_i = a_i^3 h/12$ in direction $\mathbf{e}_3$; density ρ_i; elastic modulus E_i.

The kinematics is characterized at any level n by the motions of the two nodes in the plane $(\mathbf{e}_1, \mathbf{e}_2)$, i.e., the displacements in the two directions and the rotation (u_1, u_2, θ). These six variables can be replaced by (cf. Fig. 3.3):

- Three variables associated to the rigid body motion of the level n: the mean transverse displacements, $U(n)$ along $\mathbf{e}_1$ and $V(n)$ along $\mathbf{e}_2$, and the global rotation $\alpha(n)$ (differential vertical nodal motion divided by ℓ_f),
- Three variables corresponding to its deformation: the mean and differential rotations of the nodes, $\theta(n)$ and $\Phi(n)$, and the transverse dilatation $\Delta(n)$.

Because of the longitudinal symmetry, the transverse and longitudinal kinematics, respectively governed by (U, α, θ) and (V, Φ, Δ), are uncoupled.

A systematic study enables to identify the family of possible dynamic behaviors by changing gradually the properties of the frame elements and the frequency range.

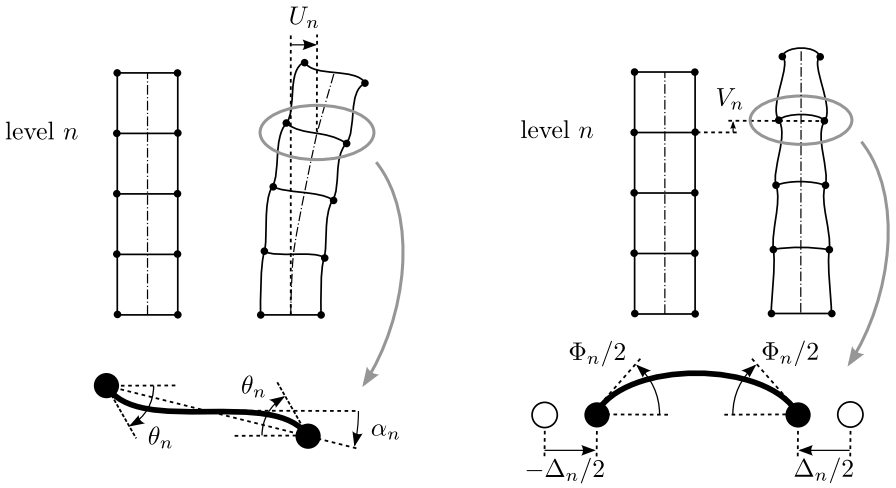

Fig. 3.3 Decoupling of transverse (left) and longitudinal (right) kinematics

3.4 Transverse Vibrations

The transverse vibrations can be classified in two categories according to the nature of the governing dynamic balance. For the first category, the horizontal elastic forces balance the horizontal translation inertia. This corresponds to the "natural" transverse vibration modes presented in Sect. 3.4.1. It can be shown that the associated frequency range is such that the elements behave quasi-statically at the local scale (for lower frequencies, a static description of the structure is obtained). For the second category, the global elastic moment is balanced by the global rotation inertia. This leads to unusual gyration modes investigated in Sect. 3.4.3. This situation occurs at higher frequencies and local dynamics can appear.

3.4.1 "Natural" Transverse Vibrations: Translation Modes

The possible beam-like behaviors were established by varying the properties of the basic frame elements in [9] to which one may refer for a precise analysis. Here below the generic beam model derived from this approach is presented and an example devoted to a given type of cell frame is discussed.

The synthesis of the different macroscopic behaviors shows that only three mechanisms — shear, global bending, inner bending — govern the physics at the macroscale (Fig 3.4). Each of them is associated to a stiffness: in shear K, in global bending $E_w\, I$, and in inner bending $E_w\, \mathscr{I}$. The parameter I is the effective global bending inertia and $\mathscr{I}$ is the effective inner bending inertia. Owing to the quasi-static local state, these parameters are deduced from the elastic properties of ele-

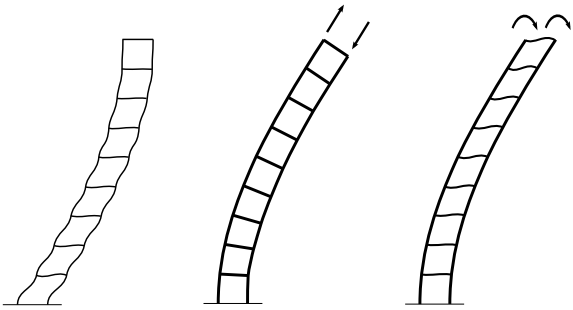

Fig. 3.4 The three transverse mechanisms (left: shear, middle: global bending, right: inner bending)

ments in statics. For structures as in Fig. 3.2, they read (Λ stands for the linear mass):

$$K^{-1} = K_w^{-1} + K_f^{-1} \quad \text{with} \quad K_w = 24\,\frac{E_w\,I_w}{\ell_w^2} \quad \text{and} \quad K_f = 12\,\frac{E_f\,I_f}{\ell_w\,\ell_f} \tag{3.1a}$$

$$I = \frac{A_w\,\ell_f^2}{2} \quad ; \quad \mathscr{I} = 2\,I_w \tag{3.1b}$$

$$\Lambda = \Lambda_w + \Lambda_f \quad \text{with} \quad \Lambda_w = 2\,\rho_w\,A_w \quad \text{and} \quad \Lambda_f = \rho_f\,A_f\,\frac{\ell_f}{\ell_w} \tag{3.1c}$$

A generic beam model is built in order to involve the three mechanisms. It is governed by:

- Three beam constitutive laws relating the kinematic variables to (i) the macroscopic shear force T, (ii) the global bending moment M and (iii) the inner bending moment $\mathscr{M}$:

$$T = -K\left(U' - \alpha\right) \quad ; \quad M = -E_w\,I\,\alpha' \quad ; \quad \mathscr{M} = -E_w\,\mathscr{I}\,U'' \tag{3.2}$$

- The force and moment of momentum balance equations:

$$\begin{cases} (T - \mathscr{M}')' = \Lambda\omega^2\,U \\ M' + T = 0 \end{cases} \tag{3.3}$$

It is worth noticing that the macroscopic behavior depends only on two kinematic variables: U and α which describe the rigid body motion of the cross-section. The third variable associated to the transverse kinematics θ has the status of a "hidden" internal variable which can be derived from the two other "driving" variables. The distinction between "driving" and "hidden" variables enables to generalize models built for the structures as in Fig. 3.2 to more complicated frame-type structures. Indeed, the implementation of the homogenization method of periodic discrete media on structures with three walls shows that the additional kinematic variables are "hidden" variables and that the macroscopic behavior is still described by (3.2) and

(3.3). However expressions (3.1) which give the macroscopic parameters have to be modified. Their calculation in the general case is the subject of Sect. 3.6.2.

The generalized beam description presented above includes the three mechanisms but they do not have necessarily the same importance. The dominating effect(s) that actually drive(s) the effective behavior of a given structure can be identified through a dimensional analysis. In this aim, we introduce the characteristic size of vibration for the first mode $\tilde{L} = 2\,H/\pi$ (for the nth mode of a clamped-free beam the characteristic size is $\tilde{L}_n = 2H/[(2n-1)\pi]$). Moreover, the variables are rewritten as $U = U^r\,U^*$ and $\alpha = \alpha^r\,\alpha^*$ where the superscript ^{r} denotes reference values, and a * denotes the dimensionless terms, $O(1)$ by construction. Introducing the expressions of the beam efforts (3.2) and making the change of variable $\boldsymbol{x} = x/\tilde{L}$, the set (3.3) becomes:

$$\begin{cases} \Omega^2 U^* + U^{*(2)} - C\,\gamma\,U^{*(4)} = (L\,\alpha^r/U^r)\,\alpha^{*\prime} \\ \alpha^* - C\,\alpha^{*(2)} = (U^r/L\,\alpha^r)\,U^{*\prime} \end{cases} \tag{3.4}$$

where superscripts in brackets stand for the order of derivative. The dimensionless numbers C, γ and Ω^2 compare respectively global bending and shear, inner and global bending, translation inertia and shear. They read:

$$C = \frac{E_w\,I}{K\,\tilde{L}^2} \quad ; \quad \gamma = \frac{\mathscr{I}}{I} \quad ; \quad \Omega^2 = \frac{\rho\omega^2\tilde{L}^2}{K} \tag{3.5}$$

Eliminating α^* (or U^*) in (3.4) gives the differential equation governing U^* (or α^*):

$$C\,\gamma\,U^{*(6)} - (1+\gamma)\,U^{*(4)} - \Omega^2\,U^{*(2)} + \frac{\Omega^2}{C}\,U^* = O(\tilde{\varepsilon}) \tag{3.6}$$

The term $O(\tilde{\varepsilon})$ highlights the fact that (3.6) is a zero-order balance and hence is only valid up to the accuracy $\tilde{\varepsilon}$. Consequently, according to the values of C, $C\,\gamma$ and γ compared to $\tilde{\varepsilon}$ powers ($\tilde{\varepsilon} = \ell_w/\tilde{L} = \pi/(2\,N)$), equation (3.6) degenerates into simplified forms. The mapping (Fig. 3.5) gives the validity domain of the seven possible behaviors according to the two parameters x and y defined by $C = \tilde{\varepsilon}^x$ and $\gamma = \tilde{\varepsilon}^y$. Note that, as the validity of the model requires the scale separation i.e. $\ell_w/\tilde{L}_n < 1$, the maximum number of homogenizable modes of a structure of N cells is $n_{max} = N/3$.

3.4.2 An Example: Slender Timoshenko Beam

Consider structures for which $C = O(1)$ and $\gamma \leq O(\tilde{\varepsilon})$. Then the terms related to $C\,\gamma$ and γ are negligible in (3.6) and the generic beam degenerates into a slender Timoshenko beam driven by:

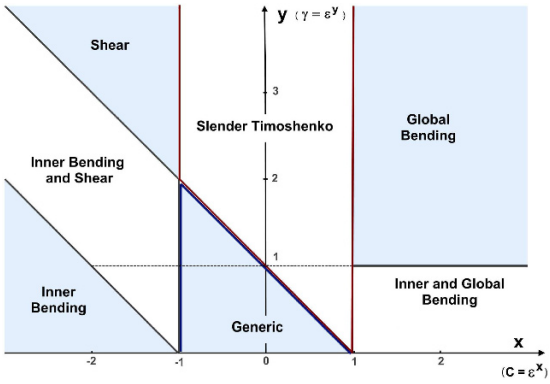

Fig. 3.5 Map of different kinds of transverse "natural" behaviors in function of the parameters $C = \tilde{\varepsilon}^x$ and $\gamma = \tilde{\varepsilon}^y$, [9]

$$U^{*(4)} + \Omega^2\, U^{*(2)} - \frac{\Omega^2}{C}\, U^* = O(\tilde{\varepsilon}) \tag{3.7}$$

To illustrate how to reach (3.7) by homogenization, consider a structure as in Fig. 3.2 with floors thicker than walls:

$$\frac{a_w}{l_w} = O(\varepsilon) \quad ; \quad \frac{a_f}{l_w} = O(\sqrt{\varepsilon}) \quad ; \quad \frac{\ell_w}{\ell_f} = O(1) \quad ; \quad \frac{E_w}{E_f} = O(1) \tag{3.8}$$

so that $\Lambda = O(\Lambda_f)$, $K = O(K_w)$ and, as required:

$$C = \frac{E_w\, I}{K_w\, \tilde{L}^2} = O\left(\frac{\ell_w^2}{a_w^2}\frac{\ell_f^2}{\tilde{L}^2}\right) = O(1) \quad ; \quad \gamma = \frac{2\, I_w}{I} = O\left(\frac{a_w^2}{\ell_f^2}\right) = O(\varepsilon^2) \tag{3.9}$$

The dynamic regime is reached when $\Omega^2/C = O(1)$ i.e., accounting for $C = O(1)$, when the leading order of the circular frequency is:

$$\omega_0 = O(\tilde{L}^{-1}\sqrt{K_w/\Lambda_f}) = O(K_w/\sqrt{E_w\, I\, \Lambda_f})$$

In that case, the leading order equations obtained by homogenization are:

$$-K_w\left(U^{0\prime\prime} - \theta^{0\prime}\right) = \Lambda_f\, \omega_0^2\, U^0 \tag{3.10a}$$

$$K_f\left(\alpha^0 - \theta^0\right) = 0 \tag{3.10b}$$

$$-E_w\, I\, \alpha^{0\prime\prime} - K_w\left(U^{0\prime} - \theta^0\right) = 0 \tag{3.10c}$$

Equation (3.10a) expresses the balance of horizontal forces at the leading order, while (3.10b) and (3.10c) come from the balance of both local and global moments at the first two significant orders. Equation (3.10b) also describes the inner equilibrium of the cell and imposes the node rotation θ^0 to be equal to the section rotation α^0. Thus the macroscopic behavior is described by a differential set that governs the mean transverse motion U^0 and the section rotation α^0:

$$\begin{cases} -K_w\left(U^{0\prime\prime}-\alpha^{0\prime}\right)=\Lambda_f\,\omega_0^2\,U^0 \\ -E_w\,I\,\alpha^{0\prime\prime}-K_w\left(U^{0\prime}-\alpha^0\right)=0 \end{cases} \tag{3.11}$$

Eliminating α^0 provides: $$E_w\,I\,U^{0(4)}+\frac{E_w\,I}{K_w}\,\Lambda_f\,\omega^2\,U^{0(2)}-\Lambda_f\,\omega_0^2\,U^0=0$$

which corresponds to (3.7), i.e. a degenerated form of (3.6) with $\gamma\leq O(\tilde{\varepsilon})$.

The similarity with Timoshenko beams is obvious when rewriting (3.11) with the macro shear force $\tilde{T}^0$ and the global bending moment $\tilde{M}^0$ defined in (3.2) (here with ^{0} superscript):

$$\begin{cases} T^{0\prime}=\Lambda_f\,\omega_0^2\,U^0 \\ M^{0\prime}+T^0=0 \end{cases} \tag{3.12}$$

Two features distinguish (3.12) from the usual Timoshenko description of "massive" beams. First, the shear effect (that comes from the bending of the walls in parallel, see (3.1a)) remains at the leading order even if the reticulated structure is slender. Second, while the translation inertia is significant in the force balance (3.12a), the rotation inertia is negligible in the moment balance (3.12b) (where the effective bending results from the opposite extension-compression of the two walls distant of the floor length). In other words, the translation is in dynamic regime but the rotation stays in quasi-static regime for the considered frequency range. This leads to investigate higher frequencies to obtain rotational dynamics.

3.4.3 Atypical Transverse Vibrations: Gyration Modes

This section is devoted to gyration modes, i.e. transverse modes governed by the section rotation α (Fig.3.6). Their existence is first established on a particular case. Then the results are slightly generalized.

Fig. 3.6 Examples of gyration modes

We come back to the structure studied in the previous section and whose geometry and parameters are scaled by (3.8). The frequency range is increased of one order in ε, i.e. $\omega_0=O(\ell_w^{-1}\sqrt{K_w/\Lambda_f})$ which remains sufficiently low to insure that the elements behave quasi-statically at the local scale. Then, the leading order equations

obtained by homogenization become:

$$0 = \Lambda_f\, \omega_0^2\, U^0 \tag{3.13a}$$

$$K_f \left(\alpha^0 - \theta^0\right) = 0 \tag{3.13b}$$

$$-E_w\, I\, \alpha^{0\prime\prime} - K_w \left(U^{0\prime} - \theta^0\right) = \frac{\rho_f\, A_f\, \ell_f^3}{420\, \ell_w}\, \omega_0^2 \left(42\, \alpha^0 - 7\, \theta^0\right) \tag{3.13c}$$

The comparison of (3.10) and (3.13) shows that the higher frequency leaves the inner equilibrium condition of the cell (3.13b) unchanged (thus, here also, the mean rotation of the nodes matches the section rotation, i.e. $\theta^0 = \alpha^0$). Conversely, in (3.13a), the increased order of magnitude of inertia terms makes that $\Lambda_f\, \omega_0^2\, U^0$ cannot be balanced by horizontal elastic forces, thus the section translation vanishes at the leading order, $U^0 = 0$. In parallel, the rotation inertia now appears in the moment of momentum balance (3.13c). After eliminating θ^0, the macroscopic behavior at the leading order is described by the following differential equation of the second degree:

$$-E_w\, I\, \alpha^{0\prime\prime} + K_w\, \alpha^0 = J_f\, \omega_0^2\, \alpha^0 \tag{3.14}$$

$$\theta^0 = \alpha^0; \qquad U^0 = 0; \qquad J_f = \frac{\rho_f\, A_f\, \ell_f^3}{12\, \ell_w}$$

This is an atypical gyration beam model fully driven by the section rotation α^0 without lateral translation (more precisely, one shows that the first non vanishing translation is of the second order $\varepsilon^2 U^2 = \left(K_w/(\Lambda_f\, \omega_0^2)\right)\alpha^{0\prime}$). The gyration dynamics is governed by the mechanism of opposite traction-compression of vertical elements (whose elastic parameter is the global bending stiffness $E_w\, I$), the shear of the cell (stiffness K_w) acting as an inner elastic source of moment, and the rotation inertia of the thick floors (J_f). Solutions of (3.14) (in α^0) have a classical sinusoidal expression but, due to the presence of the source term $K_w\, \alpha^0$, the frequency distribution is atypical.

Note that the thick floors of the specific studied frame lead to neglect the shear stiffness of the floors and the rotation inertia of the walls. The particular description (3.14) can be extended to other types of frames by considering the cell shear stiffness K instead of K_w and rotation inertia J instead of J_f (for structures as in Fig. 3.2, $J = J_f + J_w$ with $J_w = \rho_w\, A_w\, \ell_f^2/2$). Introducing the macroscopic shear force T^0 and the global bending moment M^0 already defined in (3.2) and accounting for $U^0 = 0$ show that (3.14) is nothing but the moment of momentum balance of the usual Timoshenko formulation:

$$T^0 + M^{0\prime} = J_f\, \omega_0^2\, \alpha^0 \tag{3.15}$$

However, in "massive" Timoshenko beams, variables U and α reach the dynamic regime in the same frequency range, hence both are involved in common modes. Conversely, for the reticulated beams studied here, "natural" and gyration modes are uncoupled because the dynamic regimes for U and α occur in different frequency ranges. This specificity implies that in the frequency range of non-homogenizable

"natural" modes, it exists homogenizable gyration modes. For a detailed analysis of the conditions of existence of gyration modes, one may refer to [7].

Because gyration modes appear in a higher frequency domain than "natural" modes, the elements have not necessarily a quasi-static behavior at the local scale and phenomena of local dynamics can also occur. In this case, the bending wavelength in the elements is of the order of their length, whereas the compression wavelength remains much larger. This enables to expand the compression forces and to derive a macroscopic behavior. The governing equation of the second degree presents the same global moment parameter than for local quasi-static state but differs fundamentally by the inertia term and the inner elastic source of moment, both depending on frequency:

$$E_w\, I\, \alpha'' - K(\omega)\, \alpha + J(\omega)\, \omega^2\, \alpha = 0 \tag{3.16}$$

The reason of these modifications lies in the non expanded bending forces that strongly depend on the frequency and that give rise to apparent inertia $J(\omega)$ and moment source. This effect also appears in longitudinal vibrations and is discussed in the next section.

3.5 Longitudinal Vibrations

The longitudinal vibrations, described by (V, Φ, Δ), present a lesser complexity because the main mechanism is the vertical compression. The difference between the identified models only relies in the possible presence of local dynamics.

Local Quasi-Static State: This case leads to the classical description of beam characterized by the compression modulus $2\, E_w\, A_w$ and the linear mass Λ:

$$2\, E_w\, A_w\, V'' + \Lambda \omega^2\, V = 0 \tag{3.17}$$

The domain of validity of this model is derived by expressing that the order of magnitude of the fundamental frequency of the whole structure (described by (3.17)) is much smaller than the one of the elements in bending. For structures whose walls and floors are made of the same material, a sufficient condition is to have a large number of cells: $N \geq (\ell_i / a_i)$.

Local Dynamics: Similarly to gyration modes, the local dynamics introduces a frequency depending apparent mass, that can be expressed analytically [5, 6]:

$$2\, E_w\, A_w\, V'' + \Lambda(\omega)\, \omega^2\, V(x) = 0 \tag{3.18a}$$

$$\Lambda(\omega) = \Lambda_w + \Lambda_f\, \frac{8}{3\pi \sqrt{\frac{\omega}{\omega_{f1}}} \left[\coth\left(\frac{3\pi}{4} \sqrt{\frac{\omega}{\omega_{f1}}} \right) + \cot\left(\frac{3\pi}{4} \sqrt{\frac{\omega}{\omega_{f1}}} \right) \right]} \tag{3.18b}$$

The study of $\Lambda(\omega)$ (cf. Fig. 3.7), shows that (i) $\Lambda(\omega) \to \Lambda$ when $\omega \to 0$, and (ii) $|\Lambda(\omega)| \to \infty$ when $\omega \to \omega_{f(2k+1)}$, where $\omega_{f(2k+1)}$ are the circular frequencies of the odd normal modes of horizontal elements in bending. This induces abnormal response in the vicinity of the $\omega_{f(2k+1)}$ that results in discrete spectrum of frequency band gaps. Other frequency band gaps are generated by the excitation of modes of the walls or of the whole cell which blocks the global kinematics [5]. However this effect is described by higher order equations and, in a damped structure, it has probably less influence than the frequency band gaps of zero order.

3.6 Extension and Application to Buildings

Ordinary concrete buildings (as the one presented in Fig. 3.8) are very frequently made up of identical stories and their structure is periodic in height. Moreover, the experimental modal shapes suggest using continuous beam models to describe their first modes of vibration. For instance, Fig. 3.9 compares experimental data with the normal modes of a Timoshenko beam whose features were chosen in order to fit to the first two experimental frequencies [3, 10]. For these reasons we now propose to adapt the beam models derived in the previous sections to buildings. Such an approach presents two main advantages:

- The upscaling analysis provides a clear understanding of the dynamics of the structure.
- Calculations are greatly reduced since the dynamic analysis is performed on a 1D analytical model instead of the complete 3D numerical model of the building.

Applications concern as well preliminary design of new structures as seismic diagnosis and reinforcement of existing buildings.

As earthquakes principally shake the first "natural" transverse modes of buildings, the study focuses on the models of Sect. 3.4.1. The use of homogenized models requires the structure to respect some conditions. Firstly, the scale separation implies that the building should have at least $N = 5$ stories and that the maximum number of studied modes in a given direction is $n_{max} = N/3$. Secondly, the structure should be symmetric to avoid coupling between the two transverse directions and torsion because the homogenized models describe motion in a plane. Moreover, the models were derived by assuming that elements behave like Euler-Bernoulli beams. This hypothesis is acceptable for structures with columns and beams but not for structures with shear walls. Therefore, we have to add the shear mechanism in the elements. This is the subject of Sect. 3.6.1. Next, the new model is applied to the building of Fig. 3.8 and the calculation of macroscopic parameters is explained (Sect. 3.6.2).

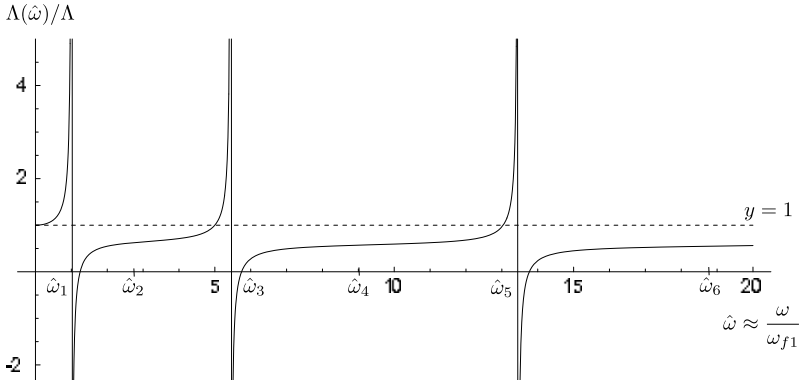

Fig. 3.7 Effect of the local resonance on the apparent dimensionless mass $\Lambda(\hat{\omega})/\Lambda$ for $\Lambda_w = \Lambda_f$

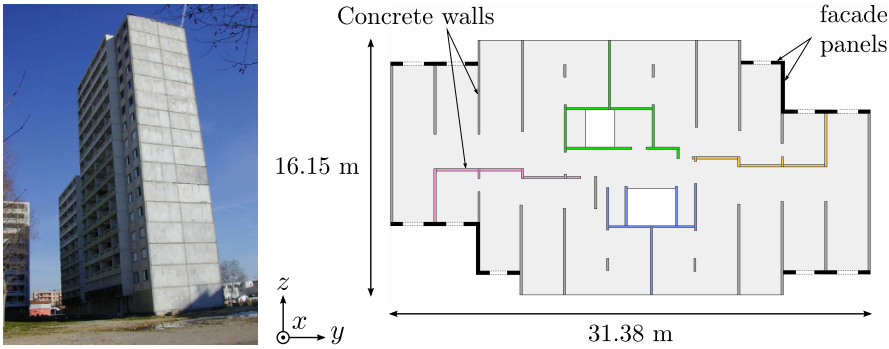

Fig. 3.8 Studied building and its typical floor plan view

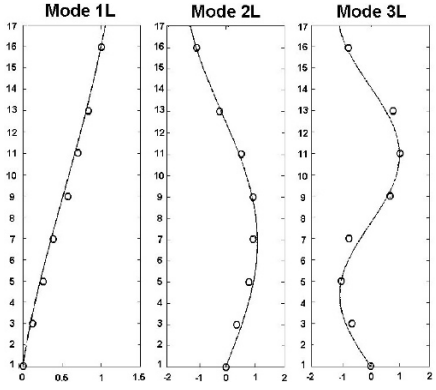

Fig. 3.9 Comparison of experimental (circles) and Timoshenko (continuous lines) mode shapes in direction y. Only two parameters were used for the fitting of the Timoshenko beam: the first two experimental frequencies. (Experimental frequencies in Hz: 2.15 ; 7.24 ; 13.97 ; 20.5 - Timoshenko beam frequencies in Hz: 2.15 ; 7.24 ; 13.96 ; 20.1)

3.6.1 Generic Beam Model for Structures with Shear Walls

For the structures with thin columns studied in Sect. 3.4.1, "natural" transverse modes are governed by three mechanisms: shear, global bending and inner bending (Fig. 3.4). As the global bending results from the opposite extension-compression of the two walls, its physics is unchanged by the increase of the wall thickness. On the contrary, shear and inner bending are generated by the bending of the elements at the local and the global scales respectively. Therefore the shear mechanism in the walls has now to be taken into account. For local bending, this effect is naturally included during the calculation of K the shear stiffness of the cell and it does not modify the beam models. This is not the case for the shear associated to the bending of the walls at the global scale which requires to add a fourth mechanism. Consequently, the generic beam model of Sect. 3.4.1 is valid as long as walls behave like Euler-Bernoulli beams *at the global scale*.

For structures with shear walls which do not respect the previous condition, a new model involving the four mechanisms is derived from the homogenization of the dynamic behavior of structures as in Fig. 3.2 by considering that the elements behave now like Timoshenko beams. To make the shear associated with inner bending emerge at the leading order, the wall geometry should respect: $a_w/\ell_w \geq O(\varepsilon^{-1})$. The new generic beam model is governed by:

- four beam constitutive laws relating the kinematic variables to (i) the shear force associated to the local bending of the floor T, (ii) the shear force associated to the shear in the walls τ, (iii) the global bending moment M and (iv) the inner bending moment $\mathscr{M}$:

$$\begin{aligned} T &= -\mathscr{K}_f\,(\alpha-\theta) & M &= -E_w\,I\,\alpha' \\ \tau &= -\mathscr{K}_w\,\big(U'-\theta\big) & \mathscr{M} &= -E_w\,\mathscr{I}\,\theta' \end{aligned} \tag{3.19}$$

- three balance equations closed to (3.3):

$$\tau' = \Lambda\omega^2\,U; \qquad M'+T=0; \qquad T-\mathscr{M}'=\tau \tag{3.20}$$

Combining (3.19) and (3.20) gives the sixth degree differential equation describing the macroscopic behavior of the structure:

$$\begin{aligned} &\frac{E_w\,\mathscr{I}\,E_w\,I}{\mathscr{K}_f}\,U^{(6)} - \left(E_w\,\mathscr{I}+E_w\,I - \boxed{\Lambda\omega^2\frac{E_w\,\mathscr{I}\,E_w\,I}{\mathscr{K}_w\,\mathscr{K}_f}}\right)U^{(4)} \\ &\quad - \left(\boxed{\frac{E_w\,\mathscr{I}}{\mathscr{K}_w}} + E_w\,I\big(\frac{1}{\mathscr{K}_w}+\frac{1}{\mathscr{K}_f}\big)\right)\Lambda\omega^2\,U'' + \Lambda\omega^2\,U = 0 \end{aligned} \tag{3.21}$$

The main differences with the model presented in Sect. 3.4.1 are listed below:

- The replacement of U'' by θ' in the constitutive law associated to inner bending,
- The distinction between the shear forces in the walls and in the floor,

- An additional balance equation (3.20c) which expresses the inner equilibrium of the cell.

As a result, (3.21) contains two new terms (in frame) which become negligible when the shear of the walls is much more rigid than inner bending ($E_w \mathscr{I} << \mathscr{K}_w L^2$). Moreover, the three variables related to the transverse kinematics, U, α and θ, emerge at the macroscopic scale. Therefore the generalization of this model to more complicated frame-type structures is an open question. However the implementation of the homogenization method on structures with three walls shows that this model is still valid when the three walls are identical. In the following we assume that this model is a good approximation of the behavior of structures with walls mechanical properties of which are not too different.

3.6.2 Calculation of Macroscopic Parameters

This section illustrates the relevance of the previous generalized beam model to describe the dynamic behavior of a 16-story building (Fig. 3.8) on which in situ measurements have been carried out. The structure is in reinforced concrete with precast facade panels. In order to evaluate the accuracy of the beam models, the results are compared with full 3D finite element simulations (and eventually with the experimental data). The COMSOL Multiphysics software is used in the linear range. Floors and shear walls are represented by perfectly connected shells and the influence of facade panels is neglected. We make the number of stories vary between 6 and 30. Reinforced concrete properties are summarized below:

Density	Young's modulus	Poisson's ratio
$\rho = 2300$ kg/m^3	$E = 30000$ MPa	$\nu = 0.2$

(3.22)

The use of the generic beam model of Sect. 3.6.1, which describes shear wall buildings, requires to calculate five macroscopic parameters: the linear mass which is equal to the mass of a story divided by the story height and the rigidities associated to the four mechanisms. The effective inertias of global and inner bending are evaluated with formulas of the beam theory:

$$I = \sum_{\text{walls}} A_j \, d_j^2; \qquad \mathscr{I} = \sum_{\text{walls}} I_j \tag{3.23}$$

where A_j stands for the cross-section area and I_j for the second moment of area of wall j. The parameter d_j is the projection of the distance between the centroid of wall j and the centroid of all the walls onto the axis y or z (Fig 3.8) according to the studied direction.

It remains to estimate the two shear rigidities $\mathscr{K}_f$ and $\mathscr{K}_w$. As the shape of the floor can be very complex, there is no analytical expression of $\mathscr{K}_f$. Thus, we propose to derive it from the shear rigidity of the whole cell K obtained thanks to a finite

element modeling of one story. The boundary conditions are those identified by homogenization and are presented in Fig. 3.10. It consists in:

- preventing the rigid body motion of the cell by blocking both vertical and horizontal translations of a wall and the vertical translation of a second wall at the centroid of their lower cross-sections,
- imposing periodic boundary conditions between bottom and top of each wall,
- applying a distortion $\Delta U/\ell$ where $\ell = 2.70$ m is the story height,
- blocking the vertical translation of all the walls which is consistent with a global shear distortion.

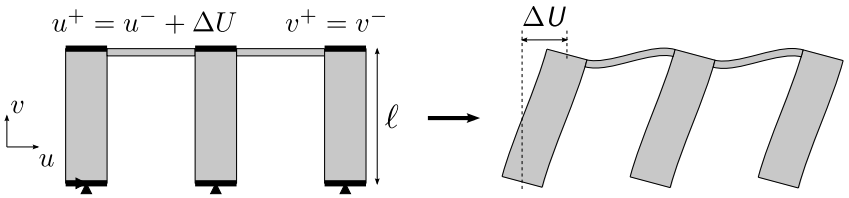

Fig. 3.10 Boundary conditions for the calculation of the shear rigidity of the whole cell K

Note that those boundary conditions allow the rotation of the walls. The shear rigidity of the whole cell K is derived from the calculated shear force in the walls. Then contributions of the floor $\mathscr{K}_f$ and the walls $\mathscr{K}_w$ are separated thanks to the formula obtained by homogenization for structures as in Fig. 3.2 (connection in series):

$$K = \frac{\left|\sum_{\text{walls}} T_j\right|}{\Delta U/\ell}; \qquad \frac{1}{\mathscr{K}_f} = \frac{1}{K} - \frac{1}{\mathscr{K}_w} \tag{3.24}$$

According to the complexity of the walls, the shear rigidity $\mathscr{K}_w$ is evaluated either with analytical expressions of the beam theory or with the finite element modeling of one story. In the latter case, the walls are clamped at their extremities, undergo a distortion (Fig. 3.11) and the shear rigidity is deduced from the calculated shear force.

$$\mathscr{K}_w = \sum_{\text{walls}} \kappa_j A_j G_j \qquad \text{or} \qquad \mathscr{K}_w = \frac{\left|\sum_{\text{walls}} T_j\right|}{\Delta U/\ell} \tag{3.25}$$

(κ_j: Timoshenko shear coefficient, A_j: cross-section area and G_j: shear modulus)

For the studied building, both shear rigidities were estimated with a finite element modeling. Figure 3.12 presents the deformation of one story due to the load applied for the calculation of the shear rigidity of the whole cell K in direction y. Note that the maximum vertical displacement is greater than the imposed horizontal distortion $\Delta U = 1$ mm. The values of all the macroscopic parameters are given in Table 3.1 for direction y. The resonant frequencies calculated with a finite element modeling of the whole structure and with the generic beam models of Sects. 3.4.1 (column structure) and 3.6.1 (shear wall structure) are summarized in Table 3.2.

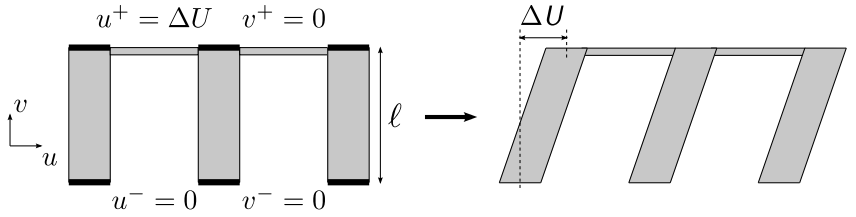

Fig. 3.11 Boundary conditions for the calculation of the shear rigidity of the walls $\mathscr{K}_w$

Table 3.1 Values of macroscopic parameters for the studied building in direction y

Λ (t/m)	I (m^4)	$\mathscr{I}$ (m^4)	K (MN)	$\mathscr{K}_w$ (MN)	$\mathscr{K}_f$ (MN)
100	1648	56	7841	59056	9041

Table 3.2 Resonant frequencies (in Hz) of the studied building in direction y

Mode	Finite Elements		Generic beam of Sect. 3.4.1 (column structure)		Generic beam of Sect. 3.6.1 (shear wall structure)	
			6 stories	$\Rightarrow \quad \varepsilon \approx 0.26$		
1	7.43		10.59	+ 42%	8.10	+ 9.0%
2	23.28		57.48	+ 147%	27.79	+ 19%
			11 stories	$\Rightarrow \quad \varepsilon \approx 0.14$		
1	3.38		4.02	+ 19%	3.54	+ 4.6%
2	11.69		18.50	+ 58%	12.81	+ 9.6%
3	21.00		47.94	+ 128%	25.88	+ 23%
			16 stories	$\Rightarrow \quad \varepsilon \approx 0.098$		
1	2.08	(2.15[a])	2.31	+ 11%	2.13	+ 2.2%
2	7.26	(7.25[a])	9.53	+ 31%	7.63	+ 5.1%
3	14.30	(14.00[a])	23.33	+ 63%	15.61	+ 9.2%
			30 stories	$\Rightarrow \quad \varepsilon \approx 0.052$		
1	0.91		0.96	+ 5.4%	0.92	+ 1.4%
2	3.16		3.52	+ 11%	3.21	+ 1.5%
3	6.36		7.71	+ 21%	6.49	+ 2.0%

[a] Experimental frequencies

The generic beam model of Sect. 3.4.1 gives reasonable results for the first resonant frequencies when the number of stories is sufficiently high and walls behave like Euler-Bernoulli beams at the global scale. But, this model and then all its simplified forms are unsuitable for the higher modes and the structures with few stories. In these cases, the results are significantly improved by the use of the generic beam model of Sect. 3.6.1 which includes the shear in the walls. The estimated frequencies are very closed to the ones calculated by finite elements (and to the experimental

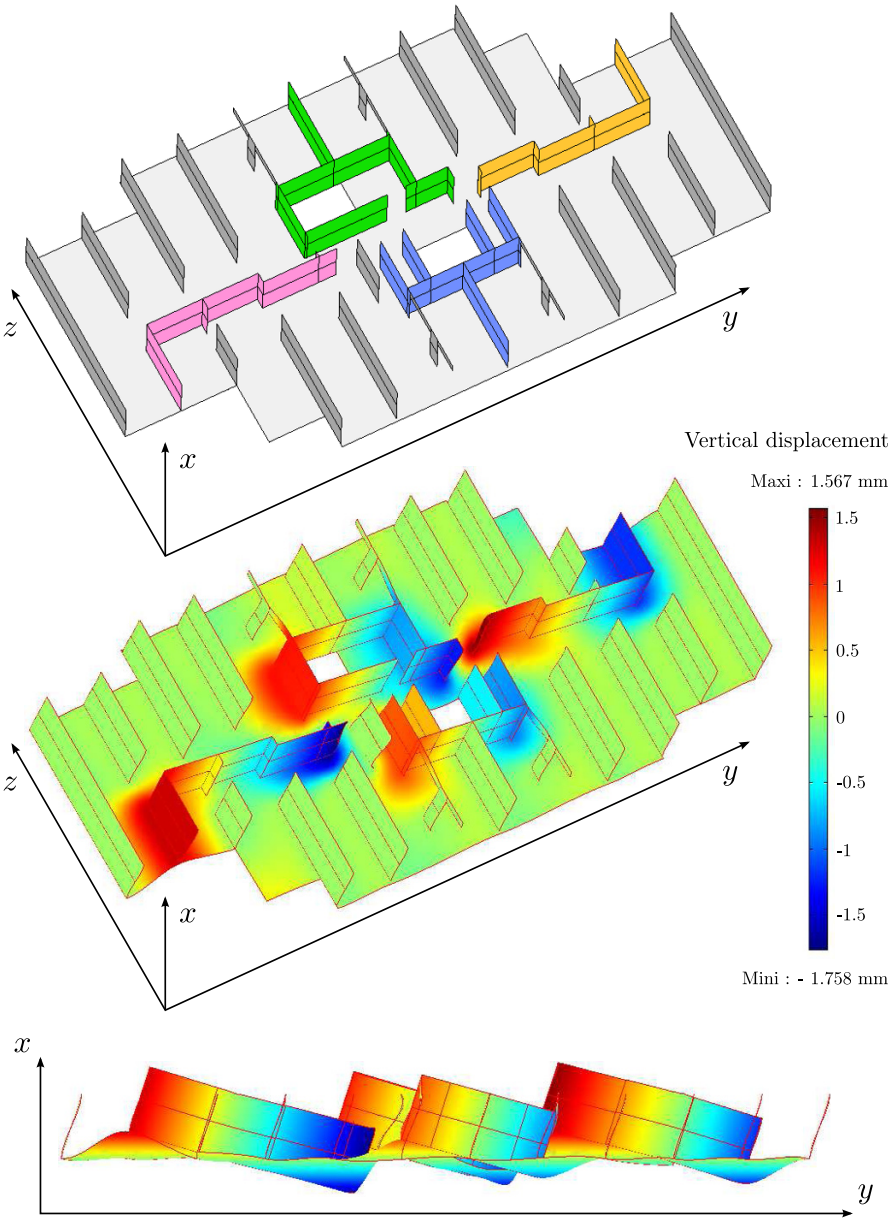

Fig. 3.12 Finite element modeling of one story for the calculation of the shear rigidity of the cell K in direction y. Top: undeformed story, middle and bottom: deformed story.

data), which shows that the physics of the problem has been taken into account with considerably reduced calculations.

3.7 Conclusion

At the macroscopic scale, unbraced (or weakly braced) reticulated structures present a much more complex behavior than usual "massive" media. It comes from the high contrast between shear and compression deformability which enables enriched local kinematics (gyration modes and inner bending mechanism) and phenomena of local resonance in bending. Consequently, there is an analogy between those structures and generalized media. The gyration beam model looks like Cosserat medium, structures where inner bending is not negligible are similar to micromorphic media and local resonance is a way to design metamaterials. Thanks to dimensional analysis, it is possible to extend these results to other types of structures of decametric size such as buildings but also of millimetric size such as foams or of nanometric size such as graphene tubes. Future works can as well deal with the other vibration modes which are governed by the inner deformation of the cell (Fig. 3.1).

Acknowledgements The authors thank Prof. Y. Debard for giving free access to the code RDM6.

References

[1] Basu, A.K., Nagpal, A.K., Bajaj, R.S., Guliani, A.K.: Dynamic characteristics of coupled shear walls. J. Struct. Div. **105**(8), 1637–1652 (1979)
[2] Boutin, C., Hans, S.: Homogenisation of periodic discrete medium: Application to dynamics of framed structures. Comput. Geotech. **30**(4), 303–320 (2003)
[3] Boutin, C., Hans, S., Ibraim, E., Roussillon, P.: In situ experiments and seismic analysis of existing buildings. Part II: Seismic integrity threshold. Earthq. Eng. Struct. Dyn. **34**(12), 1531–1546 (2005)
[4] Caillerie, D., Trompette, P., Verna, P.: Homogenisation of periodic trusses. In: IASS Symposium, 10 Years of Progress in Shell and Spatial Structures. Madrid (1989)
[5] Chesnais, C.: Dynamique de milieux réticulés non contreventés. Application aux bâtiments. PhD thesis, ENTPE, Lyon (2010)
[6] Chesnais, C., Hans, S., Boutin, C.: Wave propagation and diffraction in discrete structures: Effect of anisotropy and internal resonance. PAMM **7**(1), 1090,401–1090,402 (2007)
[7] Chesnais, C., Hans, S., Boutin, C.: Dynamics of reticulated structures. Evidence of atypical gyration modes. Int. J. Multiscale Comput. Eng. (accepted)

[8] Cioranescu, D., Saint Jean Paulin, J.: *Homogenization of Reticulated Structures*, *Applied Mathematical Sciences*, Vol. 136. Springer-Verlag, New York (1999)
[9] Hans, S., Boutin, C.: Dynamics of discrete framed structures: A unified homogenized description. J. Mech. Mater. Struct. **3**(9), 1709–1739 (2008)
[10] Hans, S., Boutin, C., Ibrahim, E., Roussillon, P.: In situ experiments and seismic analysis of existing buildings. Part I: Experimental investigations. Earthq. Eng. Struct. Dyn. **34**(12), 1513–1529 (2005)
[11] Kerr, A.D., Accorsi, M.L.: Generalization of the equations for frame-type structures; a variational approach. Acta Mech. **56**(1-2), 55–73 (1985)
[12] Moreau, G., Caillerie, D.: Continuum modeling of lattice structures in large displacement applications to buckling analysis. Comput. Struct. **68**(1-3), 181–189 (1998)
[13] Ng, S.C., Kuang, J.S.: Triply coupled vibration of asymmetric wall-frame structures. J. Struct. Eng. **126**(8), 982–987 (2000)
[14] Noor, A.K.: Continuum modeling for repetitive lattice structures. Appl. Mech. Rev. **41**(7), 285–296 (1988)
[15] Potzta, G., Kollár, L.P.: Analysis of building structures by replacement sandwich beams. Int. J. Solids Struct. **40**(3), 535–553 (2003)
[16] Sanchez-Palencia, E.: *Non-homogeneous media and vibration theory*, *Lecture notes in physics*, vol. 127. Springer-Verlag, Berlin (1980)
[17] Skattum, K.S.: Dynamic analysis of coupled shear walls and sandwich beams. Rep. EERL 71-06 PhD thesis, California Institute of Technology (1971)
[18] Stafford Smith, B., Kuster, M., Hoenderkamp, J.C.D.: Generalized method for estimating drift in high-rise structures. J. Struct. Eng. **110**(7), 1549–1562 (1984)
[19] Tollenaere, H., Caillerie, D.: Continuous modeling of lattice structures by homogenization. Adv. Eng. Softw. **29**(7-9), 699–705 (1998)

Chapter 4
A Bending-gradient Theory for Thick Laminated Plates Homogenization

Arthur Lebée and Karam Sab

Abstract This work presents a new plate theory for out-of-plane loaded thick plates where the static unknowns are those of the Love-Kirchhoff theory, to which six components are added representing the gradient of the bending moment. The Bending-gradient theory is an extension to arbitrary multilayered plates of the Reissner-Mindlin theory which appears as a special case when the plate is homogeneous. The new theory is applied to multilayered plates and its predictions are compared to full 3D Pagano's exact solutions and other approaches. It gives good predictions of both deflection and shear stress distributions in any material configuration. Moreover, under some symmetry conditions, the Bending-gradient model coincides with the second-order approximation of the exact solution as the slenderness ratio L/h goes to infinity.

Key words: Plate theory. Higher-order models. Laminated plates. Composite plates.

4.1 Introduction

Laminated plates are widely used in engineering applications. For instance angle-ply carbon fiber reinforced laminates are commonly used in aeronautics. However, these materials are strongly anisotropic and the plate overall behavior is difficult to capture. The most common plate theory is the Love-Kirchhoff plate model. However, it is well-known that, when the plate slenderness ratio L/h is not large enough, transverse shear stresses which are not taken into account in the Love-Kirchhoff theory have an increasing influence on the plate deflection.

In recent decades many suggestions have been made to improve the estimation of transverse shear stresses. Two main approaches can be found: asymptotic ap-

Arthur Lebée and Karam Sab
Université Paris-Est, Laboratoire Navier (ENPC/LCPC/CNRS). École des Ponts ParisTech, 6 et 8 avenue Blaise Pascal, 77455 Marne-la-Vallée, France
e-mail: arthur.lebee@enpc.fr, e-mail: karam.sab@enpc.fr

H. Altenbach et al. (eds.), *Mechanics of Generalized Continua,*
Advanced Structured Materials, 7, DOI: 10.1007/978-3-642-19219-7_4,

proaches and axiomatic approaches. The first one is mainly based on asymptotic expansions in the small parameter h/L [2, 3]. However, no distinction between relevant fields and unknowns was made. The second main approach is based on assuming *ad hoc* displacement or stress 3D fields. These models can be "Equivalent Single Layer" or "Layerwise". Equivalent single layer models treat the whole laminate as an equivalent homogeneous plate. However, when dealing with laminated plates, these models lead systematically to discontinuous transverse shear stress distributions through the thickness as indicated by Reddy [4]. In Layerwise models, all plate degrees of freedom are introduced in each layer of the laminate and continuity conditions are enforced between layers. The reader can refer to Reddy [4] and Carrera [5] for detailed reviews of kinematic approaches and to [6, 7, 8] for static approaches. Layerwise models lead to correct estimates of local 3D fields. However, their main drawback is that they involve a number of degrees of freedom proportional to the number of layers. The limitation is immediately pointed out with functionally graded materials, where the plate constituents properties vary continuously through the thickness [9, 10].

Based on Reissner [11] paper, we suggest an Equivalent Single Layer higher-order plate theory which gives an accurate enough estimate of transverse shear stresses in the linear elasticity framework. For this, we are motivated by two observations. The first one is that Love-Kirchhoff strain fields have clearly been identified as good first-order approximation for slender plates thanks to asymptotic expansion approaches. The second one is that the 3D equilibrium plays a critical role in the estimation of transverse shear stress in all the existing approaches. We show in this work that revisiting the use of 3D equilibrium in order to derive transverse shear stress as Reissner [11] did for homogeneous plates leads to a full bending gradient plate theory. The Reissner-Mindlin theory is as a special case of the new Bending-Gradient theory when the plate is homogeneous.

In Sect. 4.2 notations are introduced. In Sect. 4.3.1, we resume Reissner's procedure for deriving transverse shear stress extended to laminated plates. This lead to the Bending-gradient plate theory detailed in Sect. 4.4. Finally, in Sect. 4.5 the Bending-gradient plate theory is applied to fibrous laminates under cylindrical bending and compared to the exact solution and other Single Equivalent Layer approaches.

4.2 Notations

Vectors and higher-order tensors are boldfaced and different typefaces are used for each order: vectors are slanted: $\boldsymbol{T}, \boldsymbol{u}$. Second order tensors are sans serif: M, e. Third order tensors are in typewriter style: $\mathtt{\Phi}, \mathtt{\Gamma}$. Fourth order tensors are in calligraphic style $\mathcal{D}, \mathcal{c}$. Sixth order tensors are double stroked $\mathbb{F}, \mathbb{W}$.

When dealing with plates, both 2-dimensional (2D) and 3D tensors are used. Thus, $\widetilde{\boldsymbol{T}}$ denotes a 3D vector and $\boldsymbol{T}$ denotes a 2D vector or the in-plane part of $\widetilde{\boldsymbol{T}}$. The same notation is used for higher-order tensors: $\widetilde{\boldsymbol{\sigma}}$ is the 3D second-order stress tensor

while $\boldsymbol{\sigma}$ is its in-plane part. When dealing with tensor components, the indexes specify the dimension: a_{ij} denotes the 3D tensor $\widetilde{\mathbf{a}}$ with Latin index $i,j,k.. = 1,2,3$ and $\mathsf{a}_{\alpha\beta}$ denotes the 2D $\mathbf{a}$ tensor with Greek indexes $\alpha,\beta,\gamma,\dots = 1,2$. $\widetilde{\mathcal{C}} = \mathcal{C}_{ijkl}$ is the fourth-order 3D elasticity stiffness tensor. $\widetilde{\mathcal{S}} = \mathcal{S}_{ijkl} = \widetilde{\mathcal{C}}^{-1}$ is the fourth-order 3D elasticity compliance tensor while $\boldsymbol{c} = c_{\alpha\beta\gamma\delta}$ denotes the plane-stress elasticity tensor. $\boldsymbol{c}$ is not the in-plane part of $\widetilde{\mathcal{C}}$ but it is the inverse of the in-plane part of $\widetilde{\mathcal{S}}$: $\boldsymbol{c} = \boldsymbol{\mathcal{S}}^{-1}$. The identity for in-plane elasticity is $\imath_{\alpha\beta\gamma\delta} = \frac{1}{2}\left(\delta_{\alpha\gamma}\delta_{\beta\delta} + \delta_{\alpha\delta}\delta_{\beta\gamma}\right)$, where $\delta_{\alpha\beta}$ is Kronecker symbol ($\delta_{\alpha\beta} = 1$ if $\alpha = \beta$, $\delta_{\alpha\beta} = 0$ otherwise). The transpose operation ${}^t\bullet$ is applied to any order tensors as follows: $({}^tA)_{\alpha\beta\dots\psi\omega} = A_{\omega\psi\dots\beta\alpha}$.

Three contraction products are defined, the usual dot product ($\widetilde{\boldsymbol{a}}\cdot\widetilde{\boldsymbol{b}} = a_i b_i$), the double contraction product ($\widetilde{\mathbf{a}} : \widetilde{\mathbf{b}} = \mathsf{a}_{ij}\mathsf{b}_{ji}$) and a triple contraction product ($\mathbf{A} \therefore \mathbf{B} = \mathtt{A}_{\alpha\beta\gamma}\mathtt{B}_{\gamma\beta\alpha}$). In these definitions Einstein's notation on repeated indexes is used. It should be noticed that closest indexes are summed together in contraction products. Thus, $\boldsymbol{\Phi}\cdot\boldsymbol{n} = \Phi_{\alpha\beta\gamma}n_\gamma$ is different from $\boldsymbol{n}\cdot\boldsymbol{\Phi} = n_\alpha\Phi_{\alpha\beta\gamma}$. The derivation operator $\widetilde{\boldsymbol{\nabla}}$ is also formally represented as a vector: $\widetilde{\mathbf{a}}\cdot\widetilde{\boldsymbol{\nabla}} = \mathsf{a}_{ij}\nabla_j = \mathsf{a}_{ij,j}$ is the divergence and $\widetilde{\mathbf{a}}\otimes\widetilde{\boldsymbol{\nabla}} = \mathsf{a}_{ij}\nabla_k = \mathsf{a}_{ij,k}$ is the gradient. Here $\otimes$ is the dyadic product. Finally, the integration through the thickness is noted $\langle\bullet\rangle$:

$$\int_{-\frac{h}{2}}^{\frac{h}{2}} f(x_3)dx_3 = \langle f\rangle\,.$$

4.3 Revisiting the Reissner-Mindlin Plate Theory

4.3.1 The Three-dimensional Model

We consider a linear elastic plate of thickness h occupying the 3D domain $\Omega = \omega\times]-h/2,h/2[$, where $\omega\subset\mathbb{R}^2$ is the mid-plane of the plate (Figure 4.1). Cartesian

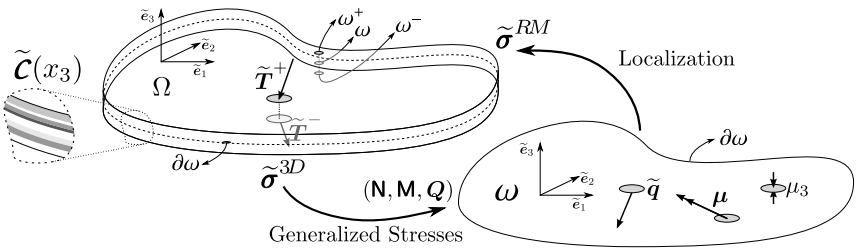

Fig. 4.1 Plate Configuration

coordinates (x_1,x_2,x_3) in the reference frame $(\widetilde{\boldsymbol{e}}_1,\widetilde{\boldsymbol{e}}_2,\widetilde{\boldsymbol{e}}_3)$ are used. The constitutive material is assumed to be invariant with respect to translations in the (x_1,x_2) plane. Hence, the stiffness tensor $\widetilde{\mathcal{C}}$ is a function of x_3 only. The plate is loaded on its upper and lower faces $\omega^{\pm}=\omega\times\{\pm h/2\}$ with the distributed force $\widetilde{\boldsymbol{T}}^{\pm}$. There are no body forces and the plate is clamped on its lateral edge, $\partial\omega\times]-h/2,h/2[$ where $\partial\omega$ is the edge of ω. The 3D problem $\mathscr{P}^{3D}$ is summarized as follows:

$$\mathscr{P}^{3D}\begin{cases}\widetilde{\boldsymbol{\sigma}}\cdot\widetilde{\boldsymbol{\nabla}}=0 \quad \text{on } \Omega. & (4.1a)\\ \widetilde{\boldsymbol{\sigma}}=\widetilde{\mathcal{C}}(x_3):\widetilde{\boldsymbol{\varepsilon}} \quad \text{on } \Omega. & (4.1b)\\ \widetilde{\boldsymbol{\sigma}}\cdot\widetilde{\boldsymbol{e}}_3=\widetilde{\boldsymbol{T}}^{\pm} \quad \text{on } \omega^{\pm}. & (4.1c)\\ \widetilde{\boldsymbol{\varepsilon}}=\dfrac{1}{2}\left(\widetilde{\boldsymbol{\nabla}}\otimes\widetilde{\boldsymbol{u}}+\widetilde{\boldsymbol{u}}\otimes\widetilde{\boldsymbol{\nabla}}\right) \quad \text{on } \Omega. & (4.1d)\\ \widetilde{\boldsymbol{u}}=0 \quad \text{on } \partial\omega\times]-h/2,h/2[. & (4.1e)\end{cases}$$

where $\widetilde{\boldsymbol{u}}$ is the 3D displacement vector field, $\widetilde{\boldsymbol{\varepsilon}}$ is the strain tensor field and $\widetilde{\boldsymbol{\sigma}}$ is the stress tensor field.

4.3.2 Reissner-Mindlin statically compatible fields

We recall here briefly the procedure for the derivation of Reissner-Mindlin equilibrium equations [11, 12, 13]. The generalized Reissner-Mindlin stresses associated to the 3D stress field $\widetilde{\boldsymbol{\sigma}}$ are:

$$\mathsf{N}_{\alpha\beta}(x_1,x_2)=\left\langle\sigma_{\alpha\beta}\right\rangle \tag{4.2}$$

$$\mathsf{M}_{\alpha\beta}(x_1,x_2)=\left\langle x_3\sigma_{\alpha\beta}\right\rangle \tag{4.3}$$

$$Q_{\alpha}(x_1,x_2)=\langle\sigma_{\alpha 3}\rangle \tag{4.4}$$

where $\mathbf{N}$ is the membrane stress, $\mathbf{M}$ the bending moment, and $\boldsymbol{Q}$ the shear forces.

Reissner-Mindlin equilibrium equations are obtained by integrating Eqs (4.1a) and $x_3\times$(4.1a) with respect to x_3. Taking also into account boundary conditions (4.1c) yields:

$$\begin{cases}\mathsf{N}_{\alpha\beta,\beta}+q_{\alpha}=0 & (4.5a)\\ Q_{\alpha,\alpha}+q_3=0 & (4.5b)\\ \mathsf{M}_{\alpha\beta,\beta}-Q_{\alpha}+\mu_{\alpha}=0 & (4.5c)\end{cases}$$

where $q_i=T_i^{+}+T_i^{-}$ are symmetric loadings per unit surface and $\mu_i=\frac{h}{2}(T_i^{+}-T_i^{-})$ are skew-symmetric loadings per unit surface. More precisely, $\boldsymbol{q}=(q_{\alpha})$ are membrane loadings per unit surface, q_3 is the out-of-plane loading per unit surface, $\boldsymbol{\mu}=(\mu_{\alpha})$ are couples per unit surface and μ_3 is the transverse bulk loading.

Since in-plane loadings ($\boldsymbol{q}$, $\boldsymbol{\mu}$) and out-of-plane loadings (q_3, μ_3) are not of the same order in the asymptotic analysis of the plate as h/L goes to 0 (see [3]), and for the sake of simplicity, we focus only on the out-of-plane loading q_3 ($q_\alpha = \mu_i = 0$).

4.3.3 Localization

The second step of Reissner's approach consists in deriving the stress energy per unit surface $w^{*RM}(\mathbf{N},\mathbf{M},\boldsymbol{Q})$ from the 3D model. As in many homogenization procedures, the derivation of w^{*RM} is based on an approximation scheme for the real 3D stress fields in terms of the generalized plate stress fields:

$$\widetilde{\boldsymbol{\sigma}}^{RM}(x_1,x_2,x_3) = \widetilde{\boldsymbol{\sigma}}^{(\mathsf{N})}(x_1,x_2,x_3) + \widetilde{\boldsymbol{\sigma}}^{(\mathsf{M})}(x_1,x_2,x_3) + \widetilde{\boldsymbol{\sigma}}^{(Q)}(x_1,x_2,x_3)$$

where $\widetilde{\boldsymbol{\sigma}}^{(\mathsf{N})}$, $\widetilde{\boldsymbol{\sigma}}^{(\mathsf{M})}$, and $\widetilde{\boldsymbol{\sigma}}^{(Q)}$ are 3D stress fields generated by $\mathbf{N}$, $\mathbf{M}$ and $\boldsymbol{Q}$ as follows:

$$\begin{cases} \sigma_{ij}^{(\mathsf{N})} = s_{ij\alpha\beta}^{(\mathsf{N})}(x_3)\mathsf{N}_{\alpha\beta}(x_1,x_2) & \text{(4.6a)} \\ \sigma_{ij}^{(\mathsf{M})} = s_{ij\alpha\beta}^{(\mathsf{M})}(x_3)\mathsf{M}_{\alpha\beta}(x_1,x_2) & \text{(4.6b)} \\ \sigma_{ij}^{(Q)} = s_{ij\alpha}^{(Q)}(x_3)Q_\alpha(x_1,x_2) & \text{(4.6c)} \end{cases}$$

where $s_{ij\alpha\beta}^{(\mathsf{N})}(x_3)$, $s_{ij\alpha\beta}^{(\mathsf{M})}(x_3)$ and $s_{ij\alpha}^{(Q)}(x_3)$ are localization tensors depending only on the x_3 coordinate. This can be rewritten using contraction products as:

$$\widetilde{\boldsymbol{\sigma}}^{RM} = \widetilde{\boldsymbol{s}}^{(\mathsf{N})} : \mathbf{N} + \widetilde{\boldsymbol{s}}^{(\mathsf{M})} : \mathbf{M} + \widetilde{\boldsymbol{s}}^{(Q)} \cdot \boldsymbol{Q}$$

Once this approximation of stress fields is set, the stress potential energy density $w^{*RM}(\mathbf{N},\mathbf{M},\boldsymbol{Q})$ is defined simply as the quadratic form:

$$w^{*RM}(\mathbf{N}(\boldsymbol{x}),\mathbf{M}(\boldsymbol{x}),\boldsymbol{Q}(\boldsymbol{x})) = \frac{1}{2}\left\langle \widetilde{\boldsymbol{\sigma}}^{RM}(\widetilde{\boldsymbol{x}}) : \widetilde{\boldsymbol{S}}(x_3) : \widetilde{\boldsymbol{\sigma}}^{RM}(\widetilde{\boldsymbol{x}}) \right\rangle \tag{4.7}$$

Hence, a consistent choice for $\widetilde{\boldsymbol{s}}^{(\mathsf{N})}$, $\widetilde{\boldsymbol{s}}^{(\mathsf{M})}$ and $\widetilde{\boldsymbol{s}}^{(Q)}$ is critical.

4.3.4 Love-Kirchhoff Fields

The derivation of $\widetilde{\boldsymbol{s}}^{(\mathsf{N})}$ and $\widetilde{\boldsymbol{s}}^{(\mathsf{M})}$ is based on the Love-Kirchhoff plate theory. According to this theory, plane-stress is assumed and the in-plane part of the strain is linear in x_3:

$$\boldsymbol{\varepsilon}^{LK} = \mathbf{e} + x_3\boldsymbol{\chi} \tag{4.8}$$

where $\mathbf{e}$ is the membrane strain and $\boldsymbol{\chi}$ the curvature. We draw the reader's attention to the fact that strain components ε_{i3} are not null in the general case. Membrane stress $\mathbf{N}$ and bending moments $\mathbf{M}$ are linearly dependent on $\mathbf{e}$ and $\boldsymbol{\chi}$:

$$\begin{cases} \mathbf{N} = \boldsymbol{\mathcal{A}} : \mathbf{e} + \boldsymbol{\mathcal{B}} : \boldsymbol{\chi} & \text{(4.9a)} \\ \mathbf{M} = {}^t\boldsymbol{\mathcal{B}} : \mathbf{e} + \boldsymbol{\mathcal{D}} : \boldsymbol{\chi} & \text{(4.9b)} \end{cases}$$

with:

$$(\boldsymbol{\mathcal{A}}, \boldsymbol{\mathcal{B}}, \boldsymbol{\mathcal{D}}) = \left\langle \left(1, x_3, x_3^2\right) \boldsymbol{c}(x_3) \right\rangle \tag{4.10}$$

Using 3D constitutive equation under plane-stress assumption, Love-Kirchhoff constitutive equation (4.9) and in-plane strains definition (4.8), it is possible to express Love-Kirchhoff stress fields as functions of $\mathbf{N}$ and $\mathbf{M}$:

$$\begin{cases} \boldsymbol{\sigma}^{(\mathsf{N})}(x_1, x_2, x_3) = \boldsymbol{c}(x_3) : \left(\boldsymbol{a} + x_3\, {}^t\boldsymbol{b}\right) : \mathbf{N}(x_1, x_2) \quad \text{and } \sigma_{i3}^{(\mathsf{N})} = 0 & \text{(4.11a)} \\ \boldsymbol{\sigma}^{(\mathsf{M})}(x_1, x_2, x_3) = \boldsymbol{c}(x_3) : (\boldsymbol{b} + x_3\, \boldsymbol{d}) : \mathbf{M}(x_1, x_2) \quad \text{and } \sigma_{i3}^{(\mathsf{M})} = 0 & \text{(4.11b)} \end{cases}$$

where $\boldsymbol{a}$, $\boldsymbol{b}$ and $\boldsymbol{d}$ are the reciprocal compliance tensors of the constitutive equation (4.9).

4.3.5 Stress Field Generated by a Linear Variation of the Bending Moment

The main idea of Reissner's method [11] is to recall that the shear forces are related to the bending moment through the plate equilibrium (4.5). With a homogeneous plate, combining both 3D equilibrium and plate equilibrium enables the derivation of a stress field directly depending on shear forces. However, with laminated plates it is not possible to bring out shear force with this procedure. Here, we suggest considering a more general shear variable for laminates, the full bending gradient: $\mathbf{R} = \mathbf{M} \otimes \boldsymbol{\nabla}$. In the following, we resume the procedure from Reissner [11] for deriving shear fields in the case of laminated plates.

We have $\widetilde{\boldsymbol{\sigma}}^{(\mathsf{M})} \cdot \widetilde{\boldsymbol{\nabla}} = 0$ if $\mathbf{M}$ is (x_1, x_2)-invariant. When $\mathbf{M}$ is function of x_1 and x_2, we have:

$$\widetilde{\boldsymbol{\sigma}}^{(\mathsf{M})} \cdot \widetilde{\boldsymbol{\nabla}} = s_{ij\beta\alpha}^{(\mathsf{M})}(x_3) \mathsf{M}_{\alpha\beta}(x_1, x_2) \nabla_j = s_{ij\beta\alpha}^{(\mathsf{M})} \mathsf{M}_{\alpha\beta,\gamma} \delta_{j\gamma} = s_{i\gamma\beta\alpha}^{(\mathsf{M})} \mathsf{R}_{\alpha\beta\gamma}$$

$f_i^{(\mathsf{R})} = s_{i\gamma\beta\alpha}^{(\mathsf{M})} \mathsf{R}_{\alpha\beta\gamma}$ is the force per unit volume generated by first order variations of the bending moment $\mathbf{R}$. $\mathsf{R}_{\alpha\beta\gamma}$ is a third-order tensor which respects $\mathsf{M}_{\alpha\beta}$ symmetries ($\mathsf{R}_{\alpha\beta\gamma} = \mathsf{R}_{\beta\alpha\gamma}$). Using $\widetilde{\boldsymbol{\sigma}}^{(\mathsf{M})}$ definition (Equation 4.11b) and assuming that each layer follows monoclinic symmetry we identify the force per unit volume as:

$$\boldsymbol{f}^{(\mathsf{R})} = \boldsymbol{c}(x_3) : (\boldsymbol{b} + x_3\, \boldsymbol{d}) \therefore \mathbf{R} \text{ and } f_3^{(\mathsf{R})} = 0 \tag{4.12}$$

Then, we define $\widetilde{\boldsymbol{\sigma}}^{(\mathrm{R})}$ the 3D stress generated by a (x_1,x_2)-invariant bending gradient $\mathbf{R}$ associated to the localization tensor $s^{(\mathrm{R})}_{ij\alpha\beta\gamma}$ such as $\widetilde{\boldsymbol{\sigma}}^{(\mathrm{R})} = \widetilde{\boldsymbol{s}}^{(\mathrm{R})} \therefore \mathbf{R}$. This stress field is derived through the auxiliary problem:

$$\begin{cases} \widetilde{\boldsymbol{\sigma}}^{(\mathrm{R})} \cdot \widetilde{\boldsymbol{\nabla}} + \widetilde{\boldsymbol{f}}^{(\mathrm{R})} = \widetilde{\mathbf{0}} & \text{(4.13a)} \\ \widetilde{\boldsymbol{\sigma}}^{(\mathrm{R})} \cdot \widetilde{\boldsymbol{e}}_3 = \widetilde{\mathbf{0}} \quad \text{for} \quad x_3 = \pm h/2 & \text{(4.13b)} \end{cases}$$

The (x_1,x_2)-invariant solution of this problem is easily found, leading to the explicit determination of $\widetilde{\boldsymbol{s}}^{(\mathrm{R})}$:

$$s^{(\mathrm{R})}_{\alpha 3\eta\zeta\varepsilon}(x_3) = -\int_{-\frac{h}{2}}^{x_3} c_{\alpha\eta\gamma\delta}(z)\left(b_{\delta\gamma\varepsilon\zeta} + z\, d_{\delta\gamma\varepsilon\zeta}\right) dz \;,\; s^{(\mathrm{R})}_{\alpha\beta\eta\zeta\varepsilon} = 0 \text{ and } s^{(\mathrm{R})}_{33\eta\zeta\varepsilon} = 0 \tag{4.14}$$

We have derived a localization tensor $\widetilde{\boldsymbol{s}}^{(\mathrm{R})}$ which depends on all bending gradient components: $\mathrm{R}_{\alpha\beta\gamma} = \mathrm{M}_{\alpha\beta,\gamma}$. Accordingly we define a new approximation of stress fields involving all bending gradient components:

$$\widetilde{\boldsymbol{\sigma}}^{BG} = \widetilde{\boldsymbol{\sigma}}^{(\mathrm{N})} + \widetilde{\boldsymbol{\sigma}}^{(\mathrm{M})} + \widetilde{\boldsymbol{\sigma}}^{(\mathrm{R})}$$

and a new stress energy density identical to Definition 4.7:

$$w^{*BG}(\mathbf{N},\mathbf{M},\mathbf{R})$$

Actually $\widetilde{\boldsymbol{\sigma}}^{BG}$ approximation for 3D stress fields is a higher-order gradient theory, as described in [14] for 3D continuum and [15] for periodic beams. However, to be consistent with higher-order theories, we should have taken into account the gradient of other static unknowns such as the membrane stress gradient for instance. It is the choice of the authors to limit the number of static variables only to those which have a contribution to the macroscopic equilibrium of the plate. Thus the number of unknowns remains limited and adapted to engineering applications, contrary to asymptotic expansions and other rigorous approaches in which no distinction is made between significant static unknowns.

4.3.6 Mechanical Meaning of the Gradient of the Bending Moment

The full bending gradient $\mathbf{R}$ has six components (R_{111}, R_{221}, R_{121}, R_{112}, R_{222}, R_{122}) whereas $\boldsymbol{Q}$ has two components. Thus, using the full bending gradient as static unknown introduces four static unknowns which *a priori* are not related to plate equilibrium (4.5c). Only $(\mathbf{N},\mathbf{M},\boldsymbol{Q})$ appeared while integrating 3D equilibrium equation (4.1a) through the thickness in Section 4.3.2.

Let us derive generalized stresses associated to $\widetilde{\boldsymbol{\sigma}}^{(\mathrm{R})}$. Using Equation 4.14 and integrating by parts when necessary leads to:

$$\left\langle \sigma^{(\mathrm{R})}_{\alpha\beta} \right\rangle = 0, \qquad \left\langle x_3 \sigma^{(\mathrm{R})}_{\alpha\beta} \right\rangle = 0, \qquad \left\langle s^{(\mathrm{R})}_{\alpha 3 \beta \gamma \delta} \right\rangle = i_{\alpha\beta\gamma\delta} \tag{4.15}$$

and we have: $\left\langle \sigma^{(\mathrm{R})}_{\alpha 3} \right\rangle = \boldsymbol{i} \therefore \mathtt{R} = \boldsymbol{Q}$. Only $\boldsymbol{Q}$ remains after integrating $\widetilde{\boldsymbol{\sigma}}^{(\mathrm{R})}$ through the thickness and the four other static unknowns are self-equilibrated stress. More precisely we have:

	$\mathtt{R}_{111}$	$\mathtt{R}_{221}$	$\mathtt{R}_{121}$	$\mathtt{R}_{112}$	$\mathtt{R}_{222}$	$\mathtt{R}_{122}$
σ_{13}	$\left\langle s^{(\mathrm{R})}_{13111} \right\rangle = 1$	$\left\langle s^{(\mathrm{R})}_{13122} \right\rangle = 0$	$\left\langle s^{(\mathrm{R})}_{13121} \right\rangle = 0$	$\left\langle s^{(\mathrm{R})}_{13211} \right\rangle = 0$	$\left\langle s^{(\mathrm{R})}_{13222} \right\rangle = 0$	$\left\langle s^{(\mathrm{R})}_{13221} \right\rangle = 1/2$
σ_{23}	$\left\langle s^{(\mathrm{R})}_{23111} \right\rangle = 0$	$\left\langle s^{(\mathrm{R})}_{23122} \right\rangle = 0$	$\left\langle s^{(\mathrm{R})}_{23121} \right\rangle = 1/2$	$\left\langle s^{(\mathrm{R})}_{23211} \right\rangle = 0$	$\left\langle s^{(\mathrm{R})}_{23222} \right\rangle = 1$	$\left\langle s^{(\mathrm{R})}_{23221} \right\rangle = 0$

$\mathtt{R}_{111}$ and $\mathtt{R}_{222}$ are the cylindrical bending part of shear forces Q_1 and Q_2, $\mathtt{R}_{121}$ and $\mathtt{R}_{122}$ are the torsion part of shear forces and $\mathtt{R}_{112}$ and $\mathtt{R}_{221}$ are linked to strictly self-equilibrated stresses (warping).

4.4 The Bending-gradient Plate Model

Once stress energy density $w^{*BG}(\mathbf{N}, \mathbf{M}, \mathtt{R})$ and plate equilibrium equations 4.5 to which is added $\mathtt{R} = \mathbf{M} \otimes \boldsymbol{\nabla}$ are given it is possible to build a complete plate theory using conventional variational tools. The reader is refered to [16] for details.

4.4.1 Summary of the Plate Model

Equilibrium equations and boundary conditions involving stress fields are gathered in the set of statically compatible fields:

$$\begin{cases} \mathbf{N} \cdot \boldsymbol{\nabla} = \mathbf{0} \text{ on } \omega & \text{(4.16a)} \\ \mathbf{M} \otimes \boldsymbol{\nabla} - \mathtt{R} = 0 \text{ on } \omega & \text{(4.16b)} \\ (\boldsymbol{i} \therefore \mathtt{R}) \cdot \boldsymbol{\nabla} = -q_3 \text{ on } \omega & \text{(4.16c)} \\ \mathbf{N} \cdot \boldsymbol{n} = \boldsymbol{V}^d \text{ on } \partial\omega^s & \text{(4.16d)} \\ \mathbf{M} = \mathbf{M}^d \text{ on } \partial\omega^s & \text{(4.16e)} \\ (\boldsymbol{i} \therefore \mathtt{R}) \cdot \boldsymbol{n} = V_3^d \text{ on } \partial\omega^s & \text{(4.16f)} \end{cases}$$

where $\partial\omega^s$ is the portion of edge on which static boundary conditions apply: $\widetilde{\boldsymbol{V}}^d$ is the force per unit length and $\mathbf{M}^d$ the full bending moment enforced on the edge. This set of equations is almost identical to Reissner-Mindlin equations where shear forces have been replaced by the bending gradient $\mathbf{R}$.

Generalized stresses $\mathbf{N}$, $\mathbf{M}$, and $\mathbf{R}$ work respectively with the associated strain variables: $\mathbf{e}$, the conventional membrane strain, $\boldsymbol{\chi}$ the conventional curvature and $\boldsymbol{\Gamma}$ the generalized shear strain. These strain fields must comply with the following compatibility conditions and boundary conditions:

$$\begin{cases} \mathbf{e} = \boldsymbol{i} : (\boldsymbol{\nabla} \otimes \boldsymbol{U}) \text{ on } \omega & \text{(4.17a)} \\ \boldsymbol{\chi} = \boldsymbol{\Phi} \cdot \boldsymbol{\nabla} \text{ on } \omega & \text{(4.17b)} \\ \boldsymbol{\Gamma} = \boldsymbol{\Phi} + \boldsymbol{i} \cdot \boldsymbol{\nabla} U_3 \text{ on } \omega & \text{(4.17c)} \\ \boldsymbol{\Phi} \cdot \boldsymbol{n} = \mathbf{H}^d \text{ on } \partial\omega^k & \text{(4.17d)} \\ \widetilde{\boldsymbol{U}} = \widetilde{\boldsymbol{U}}^d \text{ on } \partial\omega^k & \text{(4.17e)} \end{cases}$$

where $\widetilde{\boldsymbol{U}}$ is the 3D displacement of the mid-plane of the plate and $\boldsymbol{\Phi}$ is the generalized rotation. $\boldsymbol{\Gamma}$ and $\boldsymbol{\Phi}$ are 2D third-order tensors with the following symmetry: $\Phi_{\alpha\beta\gamma} = \Phi_{\beta\alpha\gamma}$. Moreover, $\partial\omega^k$ is the portion of edge on which kinematic boundary conditions apply: $\widetilde{\boldsymbol{U}}^d$ is a given displacement and $\mathbf{H}^d$ is a symmetric second-order tensor related to a forced rotation on the edge. These fields are almost identical to Reissner-Mindlin kinematically compatible fields where the rotation pseudo-vector is replaced by the generalized rotation $\boldsymbol{\Phi}$.

Finally, for constitutive material following local monoclinic symmetry with respect to (x_1, x_2) plane (uncoupling between $\mathbf{R}$ and $(\mathbf{N}, \mathbf{M})$) the Bending-gradient plate constitutive equations are written as:

$$\begin{cases} \mathbf{N} = \boldsymbol{\mathcal{A}} : \mathbf{e} + \boldsymbol{\mathcal{B}} : \boldsymbol{\chi} & \text{(4.18a)} \\ \mathbf{M} = {}^t\boldsymbol{\mathcal{B}} : \mathbf{e} + \boldsymbol{\mathcal{D}} : \boldsymbol{\chi} & \text{(4.18b)} \\ \boldsymbol{\Gamma} = \mathbb{f} \therefore \mathbf{R}, \quad \text{where} \quad (\mathbb{I} - \mathbb{f} \therefore \mathbb{F}) \therefore \boldsymbol{\Gamma} = 0 & \text{(4.18c)} \end{cases}$$

where conventional Love-Kirchhoff stiffness tensors are defined as:

$$(\boldsymbol{\mathcal{A}}, \boldsymbol{\mathcal{B}}, \boldsymbol{\mathcal{D}}) = \left\langle \left(1, x_3, x_3^2\right) \boldsymbol{c}(x_3) \right\rangle$$

and $\mathbb{f}$ is the generalized shear compliance tensor[1] defined as:

$$\mathbb{f} = \int_{-\frac{h}{2}}^{\frac{h}{2}} \left(\int_{-\frac{h}{2}}^{x_3} \left({}^t\boldsymbol{b} + z\,\boldsymbol{d} \right) : \boldsymbol{c}(z) dz \right) \cdot \mathbf{S}(x_3) \cdot \left(\int_{-\frac{h}{2}}^{x_3} \boldsymbol{c}(z) : (\boldsymbol{b} + z\,\boldsymbol{d})\, dz \right) dx_3 \qquad (4.19)$$

[1] $\mathbb{f}_{\alpha\beta\gamma\delta\varepsilon\zeta}$ follows major symmetry: $\mathbb{f}_{\alpha\beta\gamma\delta\varepsilon\zeta} = \mathbb{f}_{\zeta\varepsilon\delta\gamma\beta\alpha}$ and minor symmetry $\mathbb{f}_{\alpha\beta\gamma\delta\varepsilon\zeta} = \mathbb{f}_{\beta\alpha\gamma\delta\varepsilon\zeta}$. Thus there are only 21 independent components

where $\mathbf{S} = \mathsf{S}_{\alpha\beta} = 4\mathcal{S}_{\alpha 3 \beta 3}$ is the out-of-plane shear compliance tensor. Since $\mathbb{f}$ is not always invertible, we introduced Moore-Penrose pseudo inverse for the shear stiffness tensor $\mathbb{F}$:

$$\mathbb{F} = \lim_{\kappa \to 0} \left(\mathbb{f} \therefore \mathbb{f} + \kappa \mathbb{I} \right)^{-1} \therefore \mathbb{f}$$

where $\mathbb{I}$ is the identity for 2D sixth-order tensors following the generalized shear compliance $\mathbb{f}$ minor and major symmetries ($\mathbb{I}_{\alpha\beta\gamma\delta\varepsilon\zeta} = i_{\alpha\beta\varepsilon\zeta}\,\delta_{\gamma\delta}$). The solution of the plate model must comply with the three sets of equations (4.16, 4.17, 4.18). The compliance $\mathbb{f}$ is positive. However when $\mathbb{f}$ is not definite, there is a set of solutions, up to a self-stress field.

4.4.2 Projection of the Bending-gradient Plate Model

In some cases, the Bending-gradient is turned into a Reissner-Mindlin plate model. This is the case for homogeneous plates. Thus, we need a means to estimate the difference between both plate models. It is possible to define the exact projection of the Bending-gradient model on a Reissner-Mindlin model.

The Reissner-Mindlin part of $\mathbb{f}$ is:

$$\mathbb{f}^{RM} = \left(\frac{2}{3} \boldsymbol{i} \cdot \boldsymbol{i} \right) \therefore \mathbb{f} \therefore \left(\frac{2}{3} \boldsymbol{i} \cdot \boldsymbol{i} \right) \tag{4.20}$$

$\mathbb{f}^{RM}$ can be considered as the restriction of $\mathbb{f}$ when setting warping unknowns to zero. Consequently, we introduce the pure warping part of $\mathbb{f}$ as the orthogonal complement of $\mathbb{f}^{RM}$:

$$\mathbb{f}^{\mathrm{W}} = \mathbb{f} - \mathbb{f}^{RM} \tag{4.21}$$

Finally we suggest the following relative distance between the Bending-gradient plate model and the Reissner-Mindlin one:

$$\Delta^{RM/BG} = \frac{\|\mathbb{f}^{\mathrm{W}}\|}{\|\mathbb{f}\|}, \quad \text{where} \quad \|\mathbb{f}\| = \sqrt{\mathbb{f}_{\alpha\beta\gamma\delta\varepsilon\zeta} \mathbb{f}_{\zeta\varepsilon\delta\gamma\beta\alpha}} \tag{4.22}$$

$\Delta^{RM/BG}$ gives an estimate of the pure warping fraction of the shear stress energy and is a criterion for assessing the need of the Bending-gradient model. When the plate constitutive equation is restricted to a Reissner-Mindlin one, we have exactly $\Delta^{RM/BG} = 0$.

4.5 Application to Laminates

4.5.1 Plate Configuration

We consider angle-ply laminates. Each ply is made of unidirectional fiber-reinforced material oriented at θ relative to the bending direction x_1. All plies have the same thickness and are perfectly bounded. A laminate is denoted between brackets by the successive ply-orientations along thickness. For instance $[0^\circ, 90^\circ]$ denotes a 2-ply laminate where the lower ply fibers are oriented in the bending direction. The constitutive behavior of a ply is assumed to be transversely isotropic along the direction of the fibers and engineering constants are chosen similar to those of [1]:

$$E_L = 25\times 10^6 psi, \quad E_T = 1\times 10^6 psi, \quad G_{LT} = 0.5\times 10^6 psi, \quad G_{TT} = 0.4\times 10^6 psi,$$

$$\nu_{LT} = \nu_{TT} = 0.25$$

where G_{TT} has been changed to preserve transversely isotropic symmetry. L is the longitudinal direction oriented in the (x_1, x_2) plane at θ with respect to $\widetilde{\boldsymbol{e}}_1$, T is the transverse direction.

4.5.2 Distance Between the Reissner-Mindlin and the Bending-gradient Model

In Table 4.1, are given the values of $\Delta^{RM/BG}$ for the laminates considered in this work. For a single ply, the criterion is zero since the Bending-gradient model is exactly a Reissner-Mindlin model in this case. However, when there are several plies, the distance is greater than 10%. Thus with these laminates, the shear constitutive equation cannot be reduced to a Reissner-Mindlin behavior.

Stack	$[0^\circ]$	$[0^\circ, 90^\circ]$	$[30^\circ, -30^\circ]_s$	$[30^\circ, -30^\circ]$
$\Delta^{RM/BG}$	0	16.0%	16.0%	23.9 %

Table 4.1 The criterion $\Delta^{RM/BG}$ for several laminates

4.5.3 Cylindrical Bending

Pagano [1] gives an exact solution for cylindrical bending of simply supported composite laminates. We choose the same configuration for the Bending-gradient model.

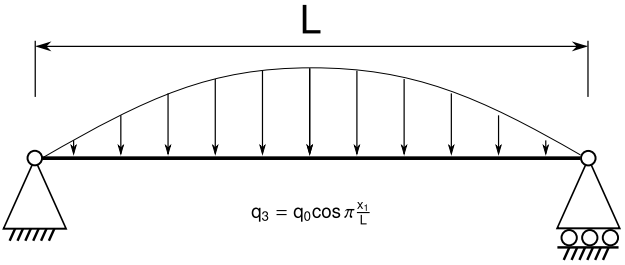

Fig. 4.2 Pagano's cylindrical bending configuration

The plate is invariant and infinite in x_2 direction. It is out-of-plane loaded with $q_3(x_1) = -q_0 \sin \kappa x_1$ where $\lambda = 1/\kappa$ is the wavelength of the loading (Fig. 4.2). The plate is simply supported at $x_1 = 0$ and $x_1 = L$ with traction free edges:

$$U_3(0) = 0,\ U_3(L) = 0,\ \mathbf{M}(0) = 0,\ \mathbf{M}(L) = 0,\ \mathbf{N}(0) \cdot \boldsymbol{e}_1 = \mathbf{0},\ \mathbf{N}(L)\ \boldsymbol{e}_1 = \mathbf{0} \quad (4.23)$$

$\mathsf{M}_{22}(0) = \mathsf{M}_{22}(L) = 0$ is the additional boundary condition compared to the Reissner-Mindlin plate model. This additional boundary condition takes into account free edge effects similar to those described in [17] for periodically layered laminate. The resolution is provided in details in [18].

Closed-form solutions using the Reissner-Mindlin model were also derived in order to compare them with the Bending-gradient. The work of Whitney [19] was used for deriving transverse shear stress distributions and shear correction factors were taken into account into the shear constitutive equation of the Reissner-Mindlin plate model.

A comparison with a finite elements solution was also performed on ABAQUS [20]. Since the Bending-gradient is an Equivalent Single Layer theory, conventional shell elements were chosen (3 displacements and 3 rotations). Transverse shear fields with shell elements in ABAQUS are derived using an approach very similar to [19] where it is furthermore assumed that the plate overall constitutive equation is orthotropic with respect to the main bending direction. *S*4, linear quadrangle with full integration elements, were used. A convergence test was performed. This study enforced the typical size of an element $l_{char} = h/5$ where h is the plate thickness. For instance when the slenderness is $h/L = 1/4$ there are 20 elements. Figure 4.3 shows a typical deformation of this mesh. Periodicity was enforced on lateral edges of the strip in Fig. 4.3 by equating corresponding rotations and displacements. Finally, section integration is performed during the analysis.

Two error estimates are introduced: the first one for the transverse shear part of the stresses for which we introduce the following seminorm:

$$\|\boldsymbol{\sigma}\|^2 = \int_{-\frac{L}{2}}^{\frac{L}{2}} \int_{-\frac{h}{2}}^{\frac{h}{2}} \sigma_{\alpha 3} \mathcal{S}_{\alpha 3 \beta 3} \sigma_{\beta 3} dx_3 dx_1$$

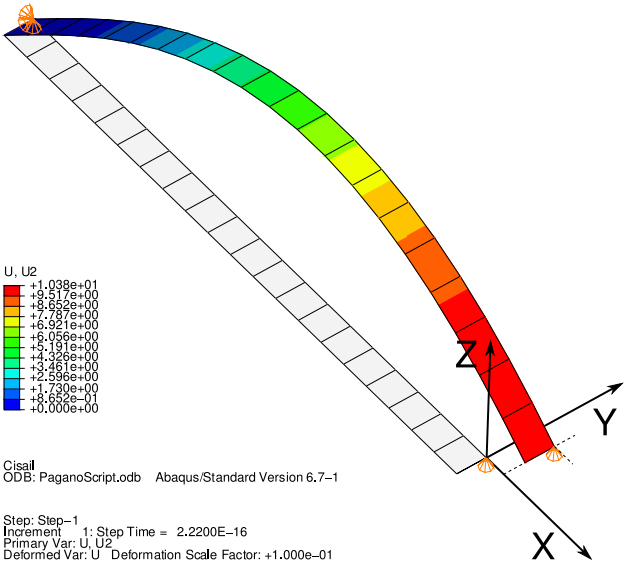

Fig. 4.3 Finite Element undeformed and deformed mesh for an anisotropic laminate

and we define the relative error as: $\Delta(\boldsymbol{\sigma}) = \frac{\|\boldsymbol{\sigma}^{Ex} - \boldsymbol{\sigma}\|}{\|\boldsymbol{\sigma}^{Ex}\|}$, where $\boldsymbol{\sigma}^{Ex}$ is the exact shear stress distribution from Pagano [1, 21, 22]. The second one is the mid-span deflection relative error:

$$\Delta(U_3) = \frac{U_3^{Ex}(L/2) - U_3(L/2)}{U_3^{Ex}(L/2)},$$

where $U_3^{Ex}(x_1)$ is the plate deflection taken for the exact solution.

4.5.4 Results

First, we consider a skew-symmetric cross ply $[0°, 90°]$ laminate. In this case, the plate configuration fulfills the assumptions made for the finite elements approximation (orthotropic laminate). In Fig. 4.4, shear stress distribution in both directions are plotted for the exact solution from Pagano [1] $\boldsymbol{\sigma}^{Ex}$, the Bending-gradient solution $\boldsymbol{\sigma}^{(\mathrm{R})}$, Whitney's shear distribution $\boldsymbol{\sigma}^{(Q),W}$ and the finite elements solution $\boldsymbol{\sigma}^{(Q),FE}$. The slenderness ratio is set to $L/h = 4$ as conventionally done when benchmarking plate models. The three approximate solutions yield the same distribution. The discrepancy with the exact solution is well-known and associated to edge effects. In Fig. 4.5 the transverse shear stress distribution error $\Delta(\boldsymbol{\sigma})$ versus the slenderness ratio L/h is plotted for the Bending-gradient solution (BG), the finite elements solution (RM, FE) and the closed-form Reissner-Mindlin solution (RM, WE). In this case, Whitney's solution converges with L/h whereas finite elements and Bending-

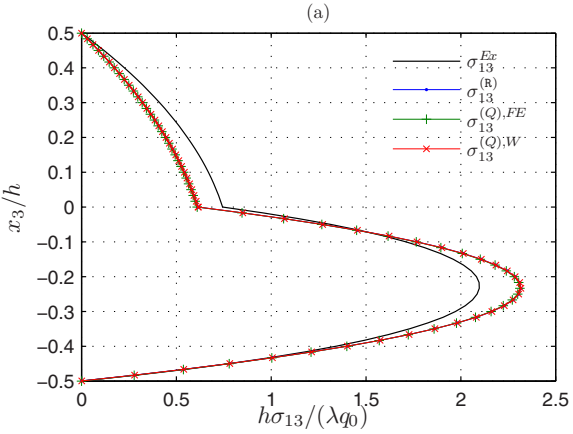

Fig. 4.4 Normalized shear distribution σ_{13} at $x_1 = 0$ for a $[0, 90°]$ laminate, $L/h = 4$

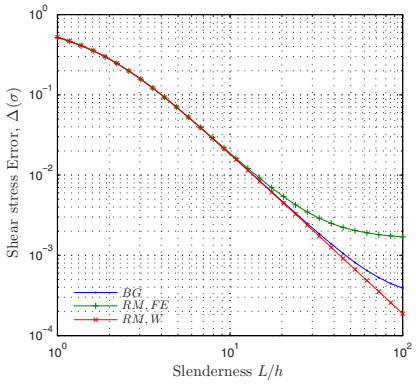

Fig. 4.5 Shear stress distribution error versus slenderness ratio for a $[0°, 90°]$ laminate

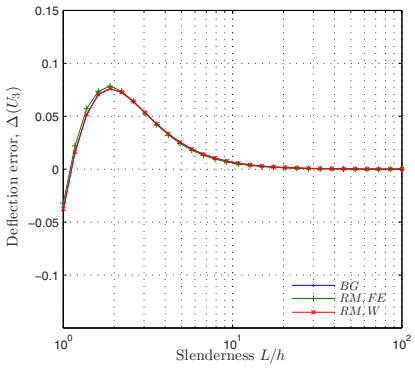

Fig. 4.6 Deflection error versus slenderness ratio for a $[0, 90°]$ laminate

gradient approximations do not converge and lead to rather small errors ($\simeq 10^{-3}$). In Fig. 4.6 the mid-span deflection error is also plotted versus the slenderness ratio. The three approximate solutions yields almost the same error.

We consider now a symmetric and non-orthotropic $[30°, -30°]_s$ laminate. This configuration does not comply with the assumptions made for the finite elements approach. In Fig. 4.7 shear distributions are compared to the exact solution. The Bending-gradient solution remains close to the exact solution. However finite elements and Whitney's solution yield different distributions which are not as accurate as the Bending-gradient. More precisely, in Direction 2, the FE solution does not capture the change of slope associated to the change of ply orientation. In Direction 1 the macroscopic equilibrium is respected for all approximated solutions ($\langle \sigma_{13} \rangle = Q_1$). However in Direction 2 we can see that $\langle \sigma_{23}^{FE} \rangle \neq Q_2$ for both finite

elements and Whitney's solution. In Fig. 4.8 the transverse shear stress distribu-

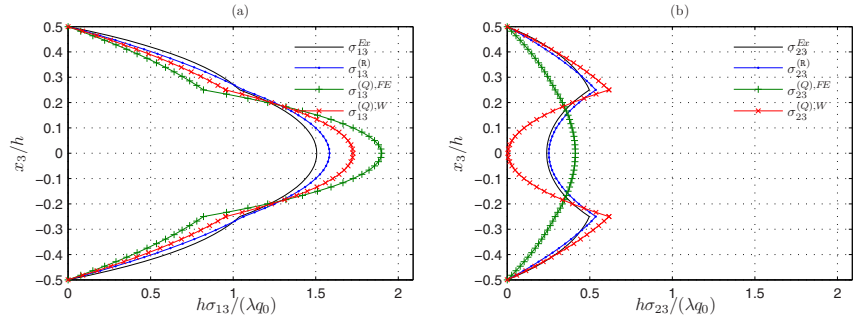

Fig. 4.7 Normalized shear distribution in both directions at $x_1 = 0$ for a $[30°, -30°]_s$ laminate, $L/h = 4$, a) σ_{13} b) σ_{23}.

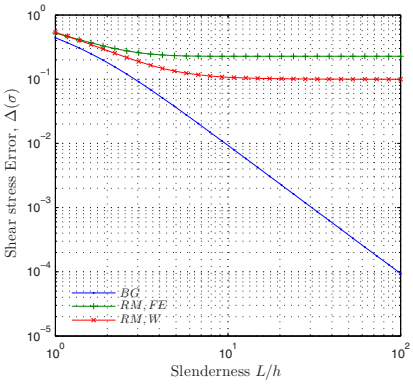

Fig. 4.8 Shear stress distribution error versus slenderness ratio for a $[30°, -30°]_s$ laminate

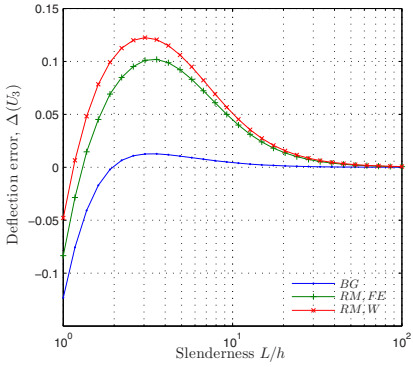

Fig. 4.9 Deflection error versus slenderness ratio for a $[30°, -30°]_s$ laminate

tion error versus the slenderness ratio is plotted. Contrary to the finite elements solution and Whitney's solution, the Bending-gradient solution converges when the plate is slender. More precisely we have: $\Delta(\boldsymbol{\sigma}^{BG}) \propto \left(\frac{h}{L}\right)^2$ in this case. In Fig. 4.9 the mid-span deflection error is also plotted versus the slenderness ratio. The Bending-gradient solution is the most accurate one for conventional slenderness.

Finally, in Fig. 4.10 the comparison is made for a non-symmetric and non-orthotropic ply $[30°, -30°]$. Again, this configuration does not comply with the assumptions made for the finite elements approach. The Bending-gradient solution remains close to the exact solution and Whitney's solution yields acceptable results (except a mismatch for $\sigma_{23}^{(\boldsymbol{Q}),W}$). However in this case, finite elements yields

inappropriate results: in Direction 1 the stress distribution does not respect macroscopic equilibrium $\langle \sigma_{13}^{FE} \rangle \neq Q_1$. We checked nevertheless that FE nodal forces fulfills macroscopic equilibrium. This inaccuracy is also clear in Fig. 4.5 showing the

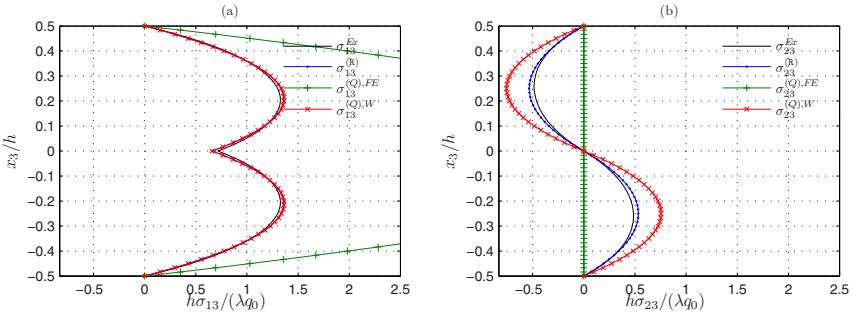

Fig. 4.10 Normalized shear distribution in both directions at $x_1 = 0$ for a $[-30°, 30°]$ laminate, $L/h = 4$, a) σ_{13} b) σ_{23}.

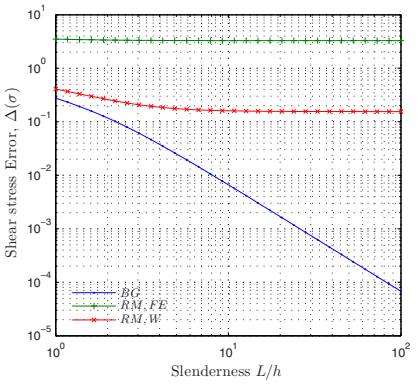

Fig. 4.11 Shear stress distribution error versus slenderness ratio for a $[30°, -30°]$ laminate

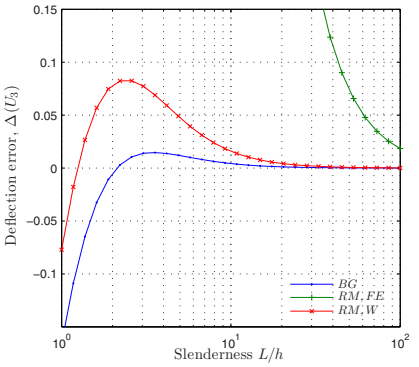

Fig. 4.12 Deflection error versus slenderness ratio for a $[30°, -30°]$ laminate

transverse shear stress distribution error versus the slenderness ratio whereas the Bending-gradient converges as $\Delta(\boldsymbol{\sigma}^{BG}) \propto \left(\frac{h}{L}\right)^2$ and both the Whitney and finite elements solutions lead to non-negligible errors. Again, in Fig. 4.12, the deflection error indicates that FE are too compliant and that the Bending-gradient is more accurate than the Reissner-Mindlin solution.

4.5.5 Discussion

We have compared three approaches for deriving an approximation of the exact solution for cylindrical bending suggested by Pagano [1, 21, 22].

First we derived closed-form solutions for the Reissner-Mindlin model using shear correction factors and shear distributions from [19]. This approach yields a fair estimation of the deflection and shear distributions in cylindrical bending but it is not as accurate as the Bending-gradient approximation in most cases. The main limitation of this approach is the cylindrical bending assumption. It is not sure that shear correction factors and shear distributions will remain valid with more general plate boundary conditions, especially involving torsion, whereas the Bending-gradient theory is not limited to cylindrical bending.

Second, we implemented a finite elements approximation, using conventional shell elements. This approach assumes both cylindrical bending and orthotropy in the same direction. When these assumptions are not valid, the results might be really affected both for deflection and stress distribution as demonstrated for the $[30°, -30°]$ laminate.

Finally, the Bending-gradient solution was presented. This approach enables the derivation of stress distributions and gives good enough deflection and stress distribution estimates whatever the plate configuration and the bending direction are. Moreover, it was numerically demonstrated that in some configurations the Bending-gradient solution converges with the slenderness ratio.

Let us state this convergence condition precisely. We chose to neglect the gradient of membrane stress $\mathbf{N} \otimes \boldsymbol{\nabla}$ since it is not related to macroscopic stress. In the cylindrical bending configuration, the membrane stress is reduced to N_{22}. When $\mathsf{N}_{22} = 0$, the membrane stress gradient vanishes. This is the case for $[30°, -30°]_s$ and $[30°, -30°]$ since they are balanced laminates (as many θ plies as $-\theta$ plies). In these cases, the Bending-gradient solution converges because the stress fields related to the membrane stress gradient do not contribute to the final solution. It is possible to generalize this result to any boundary conditions with mirror symmetric laminates ($\boldsymbol{\mathcal{B}} = 0$) for which the membrane problem is fully uncoupled from the out-of-plane problem. With these laminates, the Bending-gradient solution is the Saint-Venant solution for an out-of-plane loaded plate.

4.6 Conclusion

In the present paper, we derived a new plate theory, the Bending-gradient theory, which is the extension of Reissner-Mindlin theory to laminated plates. Comparison with the exact solution for cylindrical bending of cross ply laminates demonstrates that the Bending-gradient gives good predictions of both deflection and shear stress distributions in any material configuration. It is also the Saint-Venant solution when membrane stresses are fully uncoupled from bending moments and gener-

alized shear stresses. Finally, with usual laminated plates, we pointed out that the Bending-gradient cannot be reduced to a Reissner-Mindlin plate model.

Several outlooks are under consideration. First, this plate theory can be extended to periodic plates such as sandwich panels [23, 24]. Second, the estimation of the influence of the membrane stress gradient on the quality of the shear stress estimation should be studied in detail.

References

[1] N. Pagano, Exact Solutions for Composite Laminates in Cylindrical Bending, Journal of Composite Materials **3** (3) (1969) 398–411

[2] D. Caillerie, Thin elastic and periodic plates., Mathematical Methods in the Applied Sciences **6** (2) (1984) 159 – 191

[3] T. Lewinski, Effective Models Of Composite Periodic Plates . 1. Asymptotic Solution, International Journal of Solids and Structures **27** (9) (1991) 1155–1172

[4] J. N. Reddy, On Refined Computational Models Of Composite Laminates, International Journal for Numerical Methods in Engineering **27** (2) (1989) 361–382

[5] E. Carrera, Theories and finite elements for multilayered, anisotropic, composite plates and shells, Archives of Computational Methods in Engineering 9 (2) (2002) 87–140

[6] A. Diaz Diaz, J.-F. Caron, R. P. Carreira, Model for laminates, Comptes Rendus de l'Académie des Sciences - Series IIB - Mechanics **329** (12) (2001) 873–879

[7] J. F. Caron, A. D. Diaz, R. P. Carreira, A. Chabot, A. Ehrlacher, Multi-particle modelling for the prediction of delamination in multi-layered materials, Composites Science And Technology **66** (6) (2006) 755–765

[8] A. Diaz Diaz, J. F. Caron, A. Ehrlacher, Analytical determination of the modes I, II and III energy release rates in a delaminated laminate and validation of a delamination criterion, Composite Structures **78** (3) (2007) 424–432

[9] T.-K. Nguyen, K. Sab, G. Bonnet, First-order shear deformation plate models for functionally graded materials, Composite Structures **83** (1) (2008) 25–36

[10] T.-K. Nguyen, K. Sab, G. Bonnet, Green's operator for a periodic medium with traction-free boundary conditions and computation of the effective properties of thin plates, International Journal of Solids and Structures **45** (25-26) (2008) 6518–6534

[11] E. Reissner, The effect of transverse shear deformation on the bending of elastic plates, Journal of Applied Mechanics **12** (1945) 68–77

[12] J.-F. Caron, K. Sab, Un nouveau modèle de plaque multicouche épaisse. A new model for thick laminates, Comptes Rendus de l'Académie des Sciences - Series IIB - Mechanics **329** (8) (2001) 595–600

[13] V.-T. Nguyen, J.-F. Caron, K. Sab, A model for thick laminates and sandwich plates, Composites Science and Technology **65** (3-4) (2005) 475 – 489
[14] C. Boutin, Microstructural effects in elastic composites, International Journal of Solids and Structures **33** (7) (1996) 1023–1051
[15] N. Buannic, P. Cartraud, Higher-order effective modeling of periodic heterogeneous beams. I. Asymptotic expansion method, International Journal of Solids and Structures **38** (40-41) (2001) 7139–7161
[16] A. Lebée, K. Sab, A bending gradient model for thick plates, Part I: Theory, *submitted*
[17] A. Lebée, K. Sab, A Cosserat multiparticle model for periodically layered materials, Mechanics Research Communications **37** (3) (2010) 293–297
[18] A. Lebée, K. Sab, A bending gradient model for thick plates, Part II: Closed-form solutions for cylindrical bending, *submitted*
[19] J. Whitney, Stress Analysis of Thick Laminated Composite and Sandwich Plates, Journal of Composite Materials **6** (4) (1972) 426–440
[20] ABAQUS, ABAQUS/Standard user's manual, version 6.7, 2007
[21] N. Pagano, Exact Solutions for Rectangular Bidirectional Composites and Sandwich Plates, Journal of Composite Materials **4** (1) (1970) 20–34
[22] N. Pagano, Influence of Shear Coupling in Cylindrical. Bending of Anisotropic Laminates, Journal of Composite Materials **4** (3) (1970) 330–343
[23] A. Lebée, K. Sab, Reissner-Mindlin Shear Moduli of a Sandwich Panel with Periodic Core Material, in: Mechanics of Generalized Continua, vol. **21** of *Advances in Mechanics and Mathematics*, Springer New York, 169–177, 2010
[24] A. Lebée, K. Sab, Transverse shear stiffness of a chevron folded core used in sandwich construction, International Journal of Solids and Structures **47** (18-19) (2010) 2620–2629

Part III
Advanced Constitutive Models

Chapter 5
Internal Length Scale Effects on the Local and Overall Behavior of Polycrystals

Stéphane Berbenni

Abstract A breakthrough in the general hypothesis of spatially homogeneous intragranular fields accepted in mean field approaches based on the classic Eshelby's inclusion problem (self-consistent schemes, etc.) is proposed. Instead of considering uniform intra-granular plastic strains as usually prescribed in mean field approaches, intragranular slip patterns are modeled in single slip configurations both by distributions of coaxial circular glide loops and by distributions of flat ellipsoids (also called oblate spheroids). Both types of modeling assume slip configurations constrained by spherical grain boundaries, and, mechanical interactions between slip bands are taken into account (for mechanical fields and free energy). It is then found that intra-granular mechanical fields strongly depend on the grain size and the slip band spacing. In addition, in the case of glide loops, the modeling is able to capture different behaviors between near grain boundary regions and grain interiors. In particular, a grain boundary layer with strong gradients of internal stresses (and lattice rotations) is found. These results are confirmed quantitatively by EBSD measurements carried out with orientation imaging mapping (OIM) on deformed Ni polycrystals and on specific grains undergoing quasi single slip. Furthermore, as a result of the computation of the elastic energy, an average back-stress over the grain (in the case of loops) or over slip bands (in the case of oblate spheroids) can be derived so that it is possible to define new interaction laws for polycrystal's behavior which are naturally dependent on grain size and slip band spacing.

Key words: Microstructural internal lengths. Intra-crystalline plasticity. Dislocations. Micro-mechanics.

Stéphane Berbenni
LPMM, CNRS, Arts et Métiers ParisTech, Technopole, 4, rue Augustin Fresnel, 57078 Metz Cedex 03, France
e-mail: stephane.berbenni@ensam.eu

H. Altenbach et al. (eds.), *Mechanics of Generalized Continua,*
Advanced Structured Materials, 7, DOI: 10.1007/978-3-642-19219-7_5,

5.1 Introduction

In the mechanics of materials, the classic scale transition schemes (self-consistent schemes, etc.) were elaborated for efficient and practical reasons from two restrictive hypotheses. The first one is based on a separation of scales between the microscopic and the macroscopic states, and, a macro-homogeneous condition allowing the use of Continuum Mechanics in a simplified local context. The second one is an implicit micro-homogenization of internal inelastic processes like crystallographic slip which are modeled using averaging procedures of discrete slip patterns (Fig. 5.1(a)). The latter reduces the predictive capabilities of homogenization schemes to render microstructural internal length effects on the mechanical fields.

On the experimental point of view, the spatial heterogeneity of plastic flow was first highlighted through the observation of the surface of metals which indicated that slip consists of discrete events localized along slip bands [18, 21, 29, 30, 37]. Deformation patterns emerging at the surface can be observed during tensile or compression tests on single crystals and polycrystals with large grains as well as fine grains for a variety of metals using experimental techniques such as EBSD [1, 2, 20, 23, 40, 45, 47] or AFM [9, 11, 17, 46, 48, 50]. The slip steps observed on the surface of these materials (Fig. 5.1(b)) manifest the cooperative motion of dislocations leading to a highly localized deformation. The collective role of discrete dislocations on the internal mechanical fields is then found to be predominant.

Here, the objective is to describe intra-granular plastic heterogeneities like slip bands from discrete plastic distortions and to study their influences on local elastic fields and global free energies as well as homogenized behavior. These one are not contained in the mean field approaches. More specifically, one describes discrete quantas of plastic slip either by circular glide loops represented by spa-

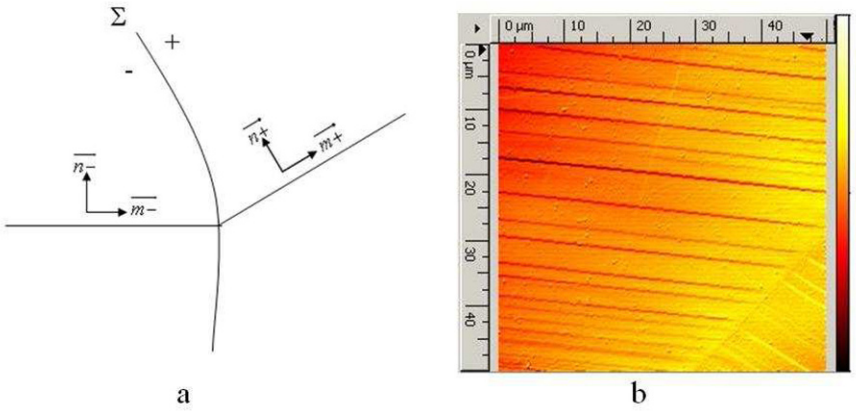

Fig. 5.1 (a) Mean field modeling of the fluctuation of plastic fields at the bi-crystalline interface; (b) Atomic Force Microscopy (AFM) picture of the plastically deformed microstructure close to a grain boundary in Brass (after 1.5% of macroscopic strain).

tial Dirac distribution functions, or, by flat ellipsoidal plastic inclusions (oblate spheroids) inside grains. Thus, intra-granular plastic strains arising from dislocations are no more considered homogeneous and uniform as in classic mean field approaches in continuum mechanics such as the self-consistent model (1st order schemes) [5, 7, 19, 26, 31, 43]. Hence, this work is also a break with the classic Eshelby's framework [14] of the uniform plastic inclusion, considering the case of strongly heterogeneous and discrete plastic events within grains.

In Sect. 5.2, one presents the general theory starting from field equations of the problem. Section 5.3 introduces resolution methods based on Fourier transforms or Green functions. The basics of continuum theory of defects and the mean field approach based on the Eshelby concept are briefly recalled in Sect. 5.4. Section 5.5 considers intra-granular slip bands like super-dislocation loops, theoretical results and experimental comparisons using the EBSD technique. In Sect. 5.6, oblate spheroids are used to describe slip bands and associated numerical results are presented. Section 5.7 proposes a new interaction law in the approximation of diluted plasticity based on an averaged backstress due to plasticization inside super-dislocation loops. Sect. 5.8 concludes.

In the whole paper, the used notations for a given quantity X are the following:

- vector: $\underline{X}$
- 2nd order tensor: $\underset{\sim}{X}$
- 4th order tensor: $\underset{\approx}{X}$

Their index notations are:

- vector: X_i
- 2nd order tensor: X_{ij}
- 4th order tensor: X_{ijkl}

Some symbols are also used. "$\cdot$" represents the simple product between:

- two vectors $\underline{A}$ and $\underline{B}$, $\underline{A} \cdot \underline{B} = A_i B_i$
- one 2nd order tensor and one vector $\underset{\sim}{A}$ and $\underline{B}$, $\underset{\sim}{A} \cdot \underline{B} = A_{ij} B_j$

":" represents the contracted product between:

- two 2nd order tensors $\underset{\sim}{A}$ and $\underset{\sim}{B}$, $\underset{\sim}{A} : \underset{\sim}{B} = A_{ij} B_{ij}$
- one 4th order tensor and one 2nd order tensor $\underset{\approx}{A}$ and $\underset{\sim}{B}$, $\underset{\approx}{A} : \underset{\sim}{B} = A_{ijkl} B_{kl}$

"$\otimes$" represents the dyadic product between:

- two vectors $\underline{A}$ and $\underline{B}$, $\underline{A} \otimes \underline{B} = A_i B_j$

"∇" represents the gradient operator, and, "∇^t" its transpose.

5.2 Field Equations and Thermodynamics

Let us consider an individual spherical inclusion (the considered grain) with volume V_g embedded in an infinite matrix with volume $V \gg V_g$ (i.e. unbounded material). One assumed no volume force and isothermal conditions in the medium. Furthermore, quasi-static loading is assumed.

On the boundary ∂V of V, a prescribed displacement $\underline{u}^d$ (Dirichlet conditions) is considered:

$$\underline{u}^d = \underset{\sim}{\beta}^0 \cdot \underline{x} = \left(\underset{\sim}{E} + \underset{\sim}{\Omega}\right) \cdot \underline{x} \text{ on } \partial V, \tag{5.1}$$

where $\underset{\sim}{\beta}^0$, $\underset{\sim}{E}$, $\underset{\sim}{\Omega}$ are respectively uniform imposed distortion, strain, and rotation on ∂V.

Alternatively, a prescribed traction vector $\underline{t}^d$ on ∂V (Neumann conditions) can also be considered such that:

$$\underline{t}^d = \underset{\sim}{\Sigma} \cdot \underline{n} \text{ on } \partial V, \tag{5.2}$$

where $\underline{n}$ is the outward unit vector to ∂V.

The other field equations are constituted of:

- the stress equilibrium condition for the symmetric Cauchy stress tensor $\underset{\sim}{\sigma}$:

$$\underline{div}\, \underset{\sim}{\sigma} = 0 \text{ in } V, \tag{5.3}$$

- the compatibility relation for total distortion $\underset{\sim}{\beta}$ or total strain $\underset{\sim}{\varepsilon}$ where $\underline{u}$ is the displacement field:

$$\underset{\sim}{\beta} = \nabla \underline{u}, \text{ or }, \underset{\sim}{\varepsilon} = \frac{1}{2}\left(\nabla \underline{u} + \nabla^t \underline{u}\right), \tag{5.4}$$

  so that $\underset{\sim}{\beta}$ splits into two terms:

$$\underset{\sim}{\beta} = \underset{\sim}{\varepsilon} + \underset{\sim}{\omega}, \tag{5.5}$$

  where $\underset{\sim}{\omega}$ is the rotation,

- the total strain (resp. the total distortion) in the small perturbation hypothesis write as the sums of an elastic strain $\underset{\sim}{\varepsilon}^e$ (resp. elastic distortion $\underset{\sim}{\beta}^e$) and a plastic strain $\underset{\sim}{\varepsilon}^p$ (resp. plastic distortion $\underset{\sim}{\beta}^p$) which will be described for various representations, namely discrete vs. mean field approaches:

$$\underset{\sim}{\varepsilon} = \underset{\sim}{\varepsilon}^e + \underset{\sim}{\varepsilon}^p, \quad \underset{\sim}{\beta} = \underset{\sim}{\beta}^e + \underset{\sim}{\beta}^p, \tag{5.6}$$

- the constitutive equation for homogeneous and linear elasticity:

$$\underset{\sim}{\sigma} = \underset{\approx}{C} : \underset{\sim}{\varepsilon}^e = \underset{\approx}{C} : (\underset{\sim}{\varepsilon} - \underset{\sim}{\varepsilon}^p), \tag{5.7}$$

where $\underset{\approx}{C}$ denotes the homogeneous elastic moduli.

Given the symmetries $C_{ijkl} = C_{jikl} = C_{ijlk} = C_{klij}$ and Eqs. (5.3), (5.4) and (5.7), the Navier-type equation is obtained (here written in explicit index notations):

$$C_{ijkl}\left(u_{l,k} - \varepsilon^p_{kl}\right)_{,j} = C_{ijkl}u_{l,kj} - C_{ijkl}\varepsilon^p_{kl,j} = 0. \tag{5.8}$$

The Helmholtz free energy per unit volume ϕ for the whole system V usually depends on the volume density of elastic energy. As it will be further shown due to the singularity of discrete plastic sources (in the case of dislocation loops), the free energy must also include the dislocation core energy owing to elastic but non linear core effects. Other contributions such as the stacking fault energy are neglected. Then:

$$\phi\left(\underset{\sim}{E}, \underset{\sim}{\varepsilon}^p(\underline{x})\right) = \frac{1}{V}\int_V w_{el}(\underline{x})\, dV, \tag{5.9}$$

where $w_{el}(\underline{x}) = \frac{1}{2}\underset{\sim}{\sigma}(\underline{x}) : \underset{\sim}{\varepsilon}^e(\underline{x})$ is the volume density of elastic energy. Equation (5.9) only holds in the case of isothermal and quasi-static conditions. After algebraic manipulations, ϕ takes the form of:

$$\phi\left(\underset{\sim}{E}, \underset{\sim}{\varepsilon}^p(\underline{x})\right) = \frac{1}{2}\left(\underset{\sim}{E} - \underset{\sim}{E}^p\right) : \underset{\approx}{C} : \left(\underset{\sim}{E} - \underset{\sim}{E}^p\right) - \frac{1}{2V}\int_V \underset{\sim}{\tau}(\underline{x}) : \underset{\sim}{\varepsilon}^p(\underline{x})\, dV, \tag{5.10}$$

where $\underset{\sim}{E}^p = \frac{1}{V}\int_V \underset{\sim}{\varepsilon}^p(\underline{x})dV$ denotes the averaged plastic strain over the whole volume V. The last part of ϕ that contains the internal stress field $\underset{\sim}{\tau}(\underline{x})$ will be denoted ϕ_{int} for the internal elastic energy per unit volume. Thus, the internal elastic energy named $\Phi_{int} = V.\phi_{int}$ reads:

$$\Phi_{int} = -\frac{1}{2}\int_V \underset{\sim}{\tau}(\underline{x}) : \underset{\sim}{\varepsilon}^p(\underline{x})\, dV. \tag{5.11}$$

The internal stress $\underset{\sim}{\tau}(\underline{x})$ is defined as follows:

$$\underset{\sim}{\tau}(\underline{x}) = \underset{\sim}{\sigma}(\underline{x}) - \underset{\sim}{\Sigma}, \tag{5.12}$$

where $\underset{\sim}{\Sigma}$ is the macroscopic stress defined by $\underset{\sim}{\Sigma} = \frac{1}{V}\int_V \underset{\sim}{\sigma}(\underline{x})\, dV$ and verifying the macroscopic behavior law:

$$\underset{\sim}{\Sigma} = \underset{\approx}{C} : \left(\underset{\sim}{E} - \underset{\sim}{E}^p\right). \tag{5.13}$$

The Legendre-Fenchel transform [32] of the Helmholtz free energy per unit volume ϕ gives the complementary energy ψ per unit volume:

$$\psi\left(\underset{\sim}{\Sigma}, \underset{\sim}{\varepsilon}^p(\underline{x})\right) = -\phi\left(\underset{\sim}{E}, \underset{\sim}{\varepsilon}^p(\underline{x})\right) + \underset{\sim}{\Sigma} : \underset{\sim}{E}. \tag{5.14}$$

After a few derivations, one finds:

$$\psi\left(\underset{\sim}{\Sigma},\underset{\sim}{\varepsilon}^p(\underline{x})\right)=\frac{1}{2}\underset{\sim}{\Sigma}:\underset{\approx}{S}:\underset{\sim}{\Sigma}+\underset{\sim}{\Sigma}:\underset{\sim}{E}^p+\frac{1}{2V}\int_V\underset{\sim}{\tau}(\underline{x}):\underset{\sim}{\varepsilon}^p(\underline{x})\,dV, \tag{5.15}$$

where $\underset{\approx}{S}=\underset{\approx}{C}^{-1}$.

The unknown fields are the displacements $\underline{u}$, from which the total distortions $\underset{\sim}{\beta}$, and, the stresses $\underset{\sim}{\sigma}$ are derived. The displacement field inside V can be decomposed into the displacements from the remote boundary load $\underline{u}^d$ and internal (or disturbed) displacements $\underline{u}(\underline{x})$. In the following, one only focuses on the internal field $\underline{u}(\underline{x})$ due to the disturbances enhanced by plastic sources in the medium through the resolution of the Navier-type equation (here written in index notation):

$$\begin{aligned}&C_{ijkl}u_{l,kj}(\underline{x})-C_{ijkl}\beta^p_{lk,j}(\underline{x})=0,\\&u_i^d(\underline{x})=0 \text{ on } \partial V.\end{aligned} \tag{5.16}$$

In order to solve Eq. (5.16) for a given plastic field in the grain V_g, two techniques based on the Fourier transforms or the Green functions are adopted in the following.

5.3 Resolution Methods

5.3.1 Fourier Transforms

Following [36] or [34], the problem can be solved using the Fourier transform method, where displacement field $\underline{u}$ or distortion field $\underset{\sim}{\beta}$ are solved in the Fourier space and then in the real space using the inverse Fourier transform theorem. Let $\underline{\xi}$ be the Fourier vector of magnitude $\xi=\sqrt{\underline{\xi}\cdot\underline{\xi}}$ and of components ξ_i in cartesian coordinates. One denotes i as $\mathrm{i}=\sqrt{-1}$.

Let $\widetilde{\underline{u}}(\underline{\xi})$ and $\widetilde{\underset{\sim}{\beta}^p}(\underline{\xi})$ be the Fourier transforms of the displacement and the plastic distortion defined by:

$$\begin{aligned}\widetilde{\underline{u}}(\underline{\xi})&=\int_V\underline{u}(\underline{x})\mathrm{e}^{-\mathrm{i}\underline{\xi}\cdot\underline{x}}dV,\\\widetilde{\underset{\sim}{\beta}^p}(\underline{\xi})&=\int_V\underset{\sim}{\beta}^p(\underline{x})\mathrm{e}^{-\mathrm{i}\underline{\xi}\cdot\underline{x}}dV.\end{aligned} \tag{5.17}$$

Conversely, the inverse Fourier transforms are defined as:

$$\begin{aligned}\underline{u}(\underline{x})&=\frac{1}{8\pi^3}\int_{V_\xi}\widetilde{\underline{u}}(\underline{\xi})\mathrm{e}^{+\mathrm{i}\underline{\xi}\cdot\underline{x}}dV_\xi,\\\underset{\sim}{\beta}^p(\underline{x})&=\frac{1}{8\pi^3}\int_{V_\xi}\widetilde{\underset{\sim}{\beta}^p}(\underline{\xi})\mathrm{e}^{+\mathrm{i}\underline{\xi}\cdot\underline{x}}dV_\xi.\end{aligned} \tag{5.18}$$

Then transforming Eq.(5.16) in the Fourier space gives the following algebraic equation to solve:

$$C_{ijkl}\xi_l\xi_j\widetilde{u_k}(\underline{\xi}) = -\mathrm{i}C_{ijkl}\xi_j\widetilde{\beta^p_{lk}}(\underline{\xi}), \tag{5.19}$$

or in the more compact form:

$$\widetilde{u_k}(\underline{\xi}) = \widetilde{G_{ik}}(\underline{\xi})\widetilde{X}_i(\underline{\xi}), \tag{5.20}$$

where $\widetilde{G_{ik}}(\underline{\xi}) = \left(C_{ijkl}\xi_l\xi_j\right)^{-1}$ and $\widetilde{X}_i(\underline{\xi})$ is defined as:

$$\widetilde{X}_i(\underline{\xi}) = -\mathrm{i}C_{ijmn}\xi_j\widetilde{\beta^p_{nm}}(\underline{\xi}). \tag{5.21}$$

$\widetilde{\underset{\sim}{G}}(\underline{\xi})$ can be identified as the Fourier transform of the elastic Green tensor [36]. Then, the problem solutions in the general case write:

$$\begin{aligned} u_k(\underline{x}) &= \frac{-\mathrm{i}}{8\pi^3}\int_{V_\xi}\xi_j C_{ijmn}\widetilde{G_{ik}}(\underline{\xi})\widetilde{\beta^p_{nm}}(\underline{\xi})\mathrm{e}^{+\mathrm{i}\underline{\xi}\cdot\underline{x}}dV_\xi, \\ \beta_{lk}(\underline{x}) &= \frac{1}{8\pi^3}\int_{V_\xi}\xi_l\xi_j C_{ijmn}\widetilde{G_{ik}}(\underline{\xi})\widetilde{\beta^p_{nm}}(\underline{\xi})\mathrm{e}^{+\mathrm{i}\underline{\xi}\cdot\underline{x}}dV_\xi. \end{aligned} \tag{5.22}$$

Assuming isotropic elasticity defined by shear modulus μ and Poisson's ratio ν, $\widetilde{\underset{\sim}{G}}$ and $\widetilde{\underline{X}}$ read:

$$\widetilde{G_{ik}}(\underline{\xi}) = \frac{1}{\mu}\left(\frac{\delta_{ik}}{\xi^2} - \frac{1}{2(1-\nu)}\frac{\xi_i\xi_k}{\xi^4}\right), \tag{5.23}$$

$$\widetilde{X}_i(\underline{\xi}) = -\mathrm{i}2\mu\underline{\xi}_j\left(\widetilde{\varepsilon^p_{ij}}(\underline{\xi}) + \frac{\nu}{1-2\nu}\delta_{ij}\widetilde{\varepsilon^p_{kk}}(\underline{\xi})\right). \tag{5.24}$$

Then, regarding isotropic elasticity the problem solutions for displacement and distortion fields can be written:

$$\begin{aligned} u_k(\underline{x}) = \frac{-\mathrm{i}}{4\pi^3}\int_{V_\xi}&\left(\frac{\delta_{ik}\xi_j}{\xi^2} - \frac{1}{2(1-\nu)}\frac{\xi_i\xi_j\xi_k}{\xi^4}\right) \\ &\cdot\left(\widetilde{\varepsilon^p_{ij}}(\underline{\xi}) + \frac{\nu}{1-2\nu}\delta_{ij}\widetilde{\varepsilon^p_{qq}}(\underline{\xi})\right)\mathrm{e}^{+\mathrm{i}\underline{\xi}\cdot\underline{x}}dV_\xi, \\ \beta_{lk}(\underline{x}) = \frac{1}{4\pi^3}\int_{V_\xi}&\left(\frac{\delta_{ik}\xi_j\xi_l}{\xi^2} - \frac{1}{2(1-\nu)}\frac{\xi_i\xi_j\xi_k\xi_l}{\xi^4}\right) \\ &\cdot\left(\widetilde{\varepsilon^p_{ij}}(\underline{\xi}) + \frac{\nu}{1-2\nu}\delta_{ij}\widetilde{\varepsilon^p_{qq}}(\underline{\xi})\right)\mathrm{e}^{+\mathrm{i}\underline{\xi}\cdot\underline{x}}dV_\xi. \end{aligned} \tag{5.25}$$

In the peculiar case where $\beta^p_{qq} = 0$ (plastic incompressibility) then Eq.(5.25) reduces to:

$$
\begin{aligned}
u_k(\underline{x}) &= \frac{-\mathrm{i}}{4\pi^3}\int_{V_\xi}\left(\frac{\delta_{ik}\xi_j}{\xi^2}-\frac{1}{2(1-\nu)}\frac{\xi_i\xi_j\xi_k}{\xi^4}\right)\widetilde{\varepsilon^p_{ij}}(\underline{\xi})\mathrm{e}^{+\mathrm{i}\underline{\xi}\cdot\underline{x}}dV_\xi,\\
\beta_{lk}(\underline{x}) &= \frac{1}{4\pi^3}\int_{V_\xi}\left(\frac{\delta_{ik}\xi_j\xi_l}{\xi^2}-\frac{1}{2(1-\nu)}\frac{\xi_i\xi_j\xi_k\xi_l}{\xi^4}\right)\widetilde{\varepsilon^p_{ij}}(\underline{\xi})\mathrm{e}^{+\mathrm{i}\underline{\xi}\underline{x}}dV_\xi.
\end{aligned}
\tag{5.26}
$$

The internal stress field $\underset{\sim}{\tau}(\underline{x})$ is derived from the Hooke's law:

$$
\tau_{ij}(\underline{x}) = 2\mu\left(\varepsilon_{ij}(\underline{x})-\varepsilon^p_{ij}(\underline{x})+\frac{\nu}{1-2\nu}\delta_{ij}\varepsilon_{kk}(\underline{x})\right). \tag{5.27}
$$

Applying Parseval's identity to the last term of Eq.(5.10) containing internal stresses named ϕ_{int} allows us to compute it as:

$$
\phi_{int} = -\frac{1}{2V}\int_V \underset{\sim}{\tau}(\underline{x}):\underset{\sim}{\varepsilon}^p(\underline{x})\,dV = -\frac{1}{8\pi^3}\frac{1}{2V}\int_{V_\xi}\underset{\sim}{\widetilde{\tau}}(\underline{\xi}):\underset{\sim}{\widetilde{\varepsilon^p}\star}(\underline{\xi})\,dV_\xi, \tag{5.28}
$$

where $\underset{\sim}{\widetilde{\varepsilon^p}\star}(\underline{\xi})$ is the complex conjugate of $\underset{\sim}{\widetilde{\varepsilon^p}}(\underline{\xi})$. Furthermore $\underset{\sim}{\widetilde{\tau}}(\underline{\xi})$ writes:

$$
\widetilde{\tau_{ij}}(\underline{\xi}) = 2\mu\left(\widetilde{\varepsilon_{ij}}(\underline{\xi})-\widetilde{\varepsilon^p_{ij}}(\underline{\xi})+\frac{\nu}{1-2\nu}\delta_{ij}\widetilde{\varepsilon_{kk}}(\underline{\xi})\right), \tag{5.29}
$$

with $\widetilde{\varepsilon_{ij}}(\underline{\xi}) = \frac{1}{2}\mathrm{i}\left(\xi_j\widetilde{G_{ki}}(\underline{\xi})+\xi_i\widetilde{G_{kj}}(\underline{\xi})\right)\widetilde{X_k}(\underline{\xi})$.

The methodology to determine the whole mechanical fields and elastic energy is the following. The first step is to compute the Fourier transforms of plastic distortions. Then, in order to calculate the displacement $\underline{u}(\underline{x})$ the integration is performed in the Fourier space. The total strain $\underset{\sim}{\varepsilon}(\underline{x})$ can be computed either from the displacement in the real space or in the Fourier space. Then, the internal stresses $\underset{\sim}{\tau}(\underline{x})$ are computed in the real space using the Hooke's law. $\underset{\sim}{\widetilde{\tau}}(\underline{\xi})$ is also calculated to obtain the internal elastic energy $\Phi_{int} = V.\phi_{int}$ from Parseval's identity (Eq. (5.29)). The main difficulties arise from the calculation of $\underset{\sim}{\widetilde{\beta}^p}(\underline{\xi})$ and from the mathematical integrations linked to inverse Fourier transforms. One gives in the next sections different situations for which the calculations are carried out analytically to derive internal stresses and internal elastic energies in the case of discrete distributions of intra-granular dislocations loops.

5.3.2 Green Functions

The resolution method based on Green functions $\underset{\sim}{G}$ associated to an infinite medium of elastic moduli $\underset{\approx}{C}$ is briefly recalled. From Eq. (5.16) and introducing $\underset{\sim}{G}$, the total distortions $\underset{\sim}{\beta}(\underline{x})$ write in index notations [6]:

$$\beta_{ji}(\underline{x}) = -\int_V G_{ki,lj}\left(\underline{x}-\underline{x}'\right) C_{klmn}\varepsilon^p_{mn}(\underline{x}')dV'. \tag{5.30}$$

Total strains $\underset{\sim}{\varepsilon}(\underline{x})$ and rotations $\underset{\sim}{\omega}(\underline{x})$ are deduced from Eq. (5.30):

$$\begin{aligned}
\underset{\sim}{\varepsilon}(\underline{x}) &= \int_V \underset{\approx}{\Gamma}(\underline{x}-\underline{x}') : \underset{\approx}{C} : \underset{\sim}{\varepsilon}^p(\underline{x}')dV', \\
\underset{\sim}{\omega}(\underline{x}) &= \int_V {}^A\underset{\approx}{\Gamma}(\underline{x}-\underline{x}') : \underset{\approx}{C} : \underset{\sim}{\varepsilon}^p(\underline{x}')dV'
\end{aligned} \tag{5.31}$$

where $\underset{\approx}{\Gamma}$ et ${}^A\underset{\approx}{\Gamma}$ are respectively the so-called symmetric and skew parts of the modified Green tensor as defined by Kröner [28].

$$\begin{aligned}
\Gamma_{ijkl}\left(\underline{x}-\underline{x}'\right) &= -\frac{1}{2}\left(G_{ik,jl}(\underline{x}-\underline{x}') + G_{jk,il}(\underline{x}-\underline{x}')\right), \\
{}^A\Gamma_{ijkl}\left(\underline{x}-\underline{x}'\right) &= -\frac{1}{2}\left(G_{ik,jl}(\underline{x}-\underline{x}') - G_{jk,il}(\underline{x}-\underline{x}')\right).
\end{aligned} \tag{5.32}$$

Using Eq. (5.31) and the Hooke's law gives the internal stresses $\underset{\sim}{\tau}(\underline{x})$ as functions of plastic fields:

$$\underset{\sim}{\tau}(\underline{x}) = \int_V \underset{\approx}{l}(\underline{x}-\underline{x}') : \underset{\sim}{\varepsilon}^p(\underline{x}')dV', \tag{5.33}$$

where $\underset{\approx}{l}(\underline{x}-\underline{x}')$ is given by:

$$\underset{\approx}{l}(\underline{x}-\underline{x}') = -\underset{\approx}{C}\delta(\underline{x}-\underline{x}') + \underset{\approx}{C} : \underset{\approx}{\Gamma}(\underline{x}-\underline{x}') : \underset{\approx}{C}. \tag{5.34}$$

Replacing $\underset{\sim}{\tau}(\underline{x})$ in Eq. (5.10) by Eq. (5.33) gives the expression for the Helmholtz free energy per unit volume as a function of $\underset{\sim}{\Sigma}$ and $\underset{\sim}{\varepsilon}^p(\underline{x})$:

$$\begin{aligned}
\phi\left(\underset{\sim}{E}, \underset{\sim}{\varepsilon}^p(\underline{x})\right) = {} & \frac{1}{2}\left(\underset{\sim}{E}-\underset{\sim}{E}^p\right) : \underset{\approx}{C} : \left(\underset{\sim}{E}-\underset{\sim}{E}^p\right) \\
& - \frac{1}{2V}\int_V \left[\int_V \underset{\approx}{l}(\underline{x}-\underline{x}') : \underset{\sim}{\varepsilon}^p(\underline{x}')dV'\right] : \underset{\sim}{\varepsilon}^p(\underline{x})\, dV.
\end{aligned} \tag{5.35}$$

The complementary energy per unit volume writes according to Eq. (5.15):

$$\psi\left(\underset{\sim}{\Sigma}, \underset{\sim}{\varepsilon}^p(\underline{x})\right) = \frac{1}{2}\underset{\sim}{\Sigma} : \underset{\approx}{S} : \underset{\sim}{\Sigma} + \underset{\sim}{\Sigma} : \underset{\sim}{E}^p + \frac{1}{2V}\int_V \left[\int_V \underset{\approx}{l}(\underline{x}-\underline{x}') : \underset{\sim}{\varepsilon}^p(\underline{x}')dV'\right] : \underset{\sim}{\varepsilon}^p(\underline{x})\, dV. \tag{5.36}$$

Equations (5.33), (5.35) and (5.36) indicate the complexity of interactions between plastic heterogeneities.

5.4 Continuum Theory of Defects and Mean Field Approaches

Several physical mechanisms can be responsible for plastic deformation of metals like creation, motion and annihilation of dislocations. A the level of one grain within the polycrystal (for which the grain size is supposed larger than the induced internal lengths due to plastic deformation mechanisms), plastic flow results from the collective motion of dislocations on well defined crystallographic slip planes [37]. Given the complexity of dislocated crystals (dislocation pile-ups, cells, tangles etc.), piecewise mean plastic fields over the grains lead to strong simplifications.

The kinematics adopted in the framework of crystal plasticity is often limited to mean crystallographic slip which allows to retrieve the overall plastic behavior of polycrystals only [8] but does not capture local effects and size effects. The plastic distortion $\underset{\sim}{\beta}^p(\underline{x})$ induced by one dislocation loop is [24]:

$$\underset{\sim}{\beta}^p(\underline{x}) = \underline{b} \otimes \underline{n} \delta(\underline{S}), \tag{5.37}$$

where $\delta(\underline{S})$ denotes the Dirac delta function in the $\underline{n}$ direction:

$$\delta(\underline{S}) \equiv \int_S \delta(\underline{x} - \underline{x}')\, dS(\underline{x}'). \tag{5.38}$$

Let us consider a crystal (single crystal or grain within a polycrystal) with N slip systems. Each system (s) is characterized by a unit vector normal to the slip plane $\underline{n}^{(s)}$ and a unit vector in the slip direction $\underline{m}^{(s)}$. $\underline{b}^{(s)} = b^{(s)}\underline{m}^{(s)}$ is the Burgers vector associated to (s) where $b^{(s)}$ is its magnitude. From Eq. (5.37), one has for each system (s):

$$\underset{\sim}{\beta}^p(\underline{x}) = \underline{b}^{(s)} \otimes \underline{n}^{(s)} \delta(\underline{S}^{(s)}), \tag{5.39}$$

If several dislocations with same Burgers vector $\underline{b}^{(s)} = \underline{b}$ and unit normal $\underline{n}^{(s)}$ are present in the crystal volume V_c, then the average value of $\underset{\sim}{\beta}^p$ over V_c is:

$$\underset{\sim}{\beta}^p = \gamma^{(s)} \underline{m}^{(s)} \otimes \underline{n}^{(s)}, \tag{5.40}$$

where $\gamma^{(s)}$ is the averaged slip on (s):

$$\gamma^{(s)} = \frac{b}{V_c} \int_{V_c} \delta(\underline{S}^{(s)})\, dV. \tag{5.41}$$

The contributions of the N slip systems in the crystal give:

$$\underset{\sim}{\beta}^p = \sum_{s=1}^{N} \gamma^{(s)} \underline{m}^{(s)} \otimes \underline{n}^{(s)}. \tag{5.42}$$

This averaging scheme leads to a homogeneous plastic deformation inside the crystal volume. A lot of microstructural details are consequently lost, especially the discrete nature of plastic deformation as well as the short range interactions between dislocations. From the continuum mechanics of defects developed by Kröner [25, 27], a dislocation density tensor $\underset{\sim}{\alpha}$ (as first introduced by Nye [38]) can be associated to any $\underset{\sim}{\beta}^p$:

$$\underset{\sim}{\alpha} = -\underset{\sim}{Curl}\ \underset{\sim}{\beta}^p, \text{ or }, \alpha_{ij} = -\in_{ilm} \beta^{\mathrm{p}}_{mj,l}, \tag{5.43}$$

where $\in_{ilm}$ is the permutation operator. Eq. (5.43) is a general definition whatever the physical content of $\underset{\sim}{\beta}^p$. That's the reason why Kröner [25] introduced the notion of "quasidislocation".

The mean field Eshelby-Kröner's plastic inclusion concept [14, 26] considers an isolated grain I with uniform plastic distortion $\underset{\sim}{\beta}^{pI}$. This grain is embedded in a matrix M with uniform plastic distortion $\underset{\sim}{\beta}^{pM}$. Hence, the plastic distortion jump at the interface grain/matrix $[\underset{\sim}{\beta}^p]$ is:

$$[\underset{\sim}{\beta}^p] = \underset{\sim}{\beta}^{pI} - \underset{\sim}{\beta}^{pM}. \tag{5.44}$$

Using Eq. (5.43), this jump leads to a singular distribution of interfacial quasidislocation density:

$$\alpha^S_{ij} = \in_{ilm} [\beta^p_{mj}] n_l, \tag{5.45}$$

where $\underline{n}$ is the unit vector outward normal to the interface in the direction of the matrix.

Let us briefly recall the plastic Eshelby's ellipsoidal inclusion concept [14] as the basic ingredient of the so-called mean field approaches like the Equivalent Inclusion Method [36], the Mori-Tanaka estimate [3, 35, 49], the Self-Consistent scheme [7, 19, 26] etc. Here, only the inclusion I is subjected to a given uniform plastic strain $\underset{\sim}{\varepsilon}^{pI}$, and, $\underset{\sim}{\varepsilon}^I$, $\underset{\sim}{\omega}^I$ are respectively the mean strains and rotations on V^I. From Eqs. (5.31) and from [14]:

$$\begin{aligned} \underset{\sim}{\varepsilon}^I &= \underset{\approx}{T}^{II} : \underset{\approx}{C} : \underset{\sim}{\varepsilon}^{pI}, \\ \underset{\sim}{\omega}^I &= \underset{\approx}{Q}^{II} : \underset{\approx}{C} : \underset{\sim}{\varepsilon}^{pI}, \end{aligned} \tag{5.46}$$

where:

$$\begin{aligned} T^{II}_{ijkl} &= \frac{1}{V^I} \int_{V^I} \left\{ \int_{V^I} \Gamma_{ijkl}(\underline{x} - \underline{x}') dV' \right\} dV, \\ Q^{II}_{ijkl} &= \frac{1}{V^I} \int_{V^I} \left\{ \int_{V^I} {}^A\Gamma_{ijkl}(\underline{x} - \underline{x}') dV' \right\} dV. \end{aligned} \tag{5.47}$$

In Eq. (5.47), $\underset{\approx}{T}^{II} : \underset{\approx}{C}$ is the Eshelby tensor $\underset{\approx}{S}^{Ei}$ associated to $\underset{\approx}{C}$ for interior points to the inclusion. The internal stresses inside the inclusion $\underset{\sim}{\tau}^{I}$ are obtained from the Hooke's law:

$$\underset{\sim}{\tau}^{I} = \underset{\approx}{C} : \left(\underset{\approx}{S}^{Ei} - \underset{\approx}{I} \right) : \underset{\sim}{\varepsilon}^{pI}, \tag{5.48}$$

where $\underset{\approx}{I}$ is the fourth order unit tensor $I_{ijkl} = \frac{1}{2}\left(\delta_{ik}\delta_{jl} + \delta_{il}\delta_{jk}\right)$.

From the previous formulas, one considers now a spherical grain of radius R with volume V_g embedded in an infinite medium V where no macroscopic strain is imposed on its boundary ∂V. Furthermore, only one single slip system is considered and characterized by the unit vector normal to the slip plane $\underline{n} = (0,0,1)$ and the unit vector along the slip direction $\underline{m} = (1,0,0)$. Then, the only non zero plastic strain components are shear components $\varepsilon^p_{13}(\underline{x}) = \varepsilon^p_{31}(\underline{x}) = \frac{1}{2}\beta^p_{31}(\underline{x})$ defined as:

$$\varepsilon^p_{13}(\underline{x}) = \begin{cases} \varepsilon^0_{13} \text{ if } \underline{x} \in V_g \\ 0 \text{ if } \underline{x} \notin V_g, \end{cases} \tag{5.49}$$

where $\varepsilon^0_{13} = 1/2\gamma$. In this mean field representation, γ constitutes a uniform plastic shear produced by glide dislocation loops continuously and uniformly distributed inside the grain. Regarding internal stress for interior points to the grain, the only non zero component τ^0_{13} is then uniform and depends on ε^0_{13} and elastic constants. It comes directly from Eq. (5.48):

$$\tau^0_{13} = -2\mu \frac{7-5\nu}{15(1-\nu)} \varepsilon^0_{13}. \tag{5.50}$$

For exterior points to the grain, the internal stress is no more uniform [15] and for the case of the sphere, its expression is computed using the formulas recently developed in [22]. In this representation, the internal elastic energy named Φ^0_{int} simply yields after Eq.(5.11):

$$\Phi^0_{int} = 8\mu\pi\, R^3 \frac{7-5\nu}{45(1-\nu)} \left(\varepsilon^0_{13}\right)^2. \tag{5.51}$$

The mean field model of plastic source due to dislocation loops consists in a uniform plastic strain inside the grain for which the internal stress field and the internal elastic energy are related to the classic Eshelby tensor for a spherical inclusion. The two following discrete approaches are set up to describe the micro-plastic deformation of metals and the collective formation of slip bands [37] inside grains.

5.5 Modeling Intragranular Slip Bands as Super-dislocation Loops Constrained by Grain Boundaries

The first approach is based on the presence of discrete distributions of circular super-dislocation loops constrained by grain boundaries. Many static configurations are possible like homogeneous and periodic distributions corresponding physically to homogeneous glide (e.g. in the stage I of FCC crystals), or, localized slip (observed during the stage II of FCC metals), or, more general non uniform slip line pattern as observed by Atomic Force Microscopy (AFM). Here, the Fourier transform method is used to calculate the elastic fields.

5.5.1 Elastic Fields

One first considers the case of one circular glide loop of radius a in the local frame $(x_1,x_2,0)$ associated to the slip plane. The loop is characterized by a Burgers vector $\underline{b}=(b,0,0)$ and a unit normal $\underline{n}=(0,0,1)$. The only non zero component of $\underset{\sim}{\beta}^{p}$ is

$$\beta_{31}^{\mathrm{p}}(\underline{x})=bH\left(1-\frac{\rho}{a}\right)\delta(x_3), \tag{5.52}$$

where ρ et x_3 are respectively the radial coordinate and the altitude in cylindrical coordinates (ρ,θ,x_3) defined by $(x_1=\rho\cos\theta,x_2=\rho\sin\theta,x_3)$. $\delta(x_3)$ is the Dirac delta function in the direction (x_3) and H is the Heaviside function:

$$H\left(1-\frac{\rho}{a}\right)=\begin{cases}1 \text{ si } \rho\le a\\ 0 \text{ si } \rho>a.\end{cases} \tag{5.53}$$

The Fourier transform of Eq. (5.52) reads:

$$\widetilde{\beta_{31}^{\mathrm{p}}}(\underline{\xi})=2\pi ba\frac{J_1(aq)}{q}, \tag{5.54}$$

where ξ_1 and ξ_2 are defined by $\xi_1=q\cos\phi$, $\xi_2=q\sin\phi$ with $q=\sqrt{\xi_1^2+\xi_2^2}$, J_1 is the Bessel function of first kind. Using Eq. (5.25), the displacements read:

$$u_k(\underline{x})=\frac{-i}{4\pi^3}\int_{V_\xi}\left(\frac{\delta_{1k}\xi_3+\delta_{3k}\xi_1}{\xi^2}-\frac{1}{1-\nu}\frac{\xi_1\xi_3\xi_k}{\xi^4}\right)\widetilde{\varepsilon_{13}^{\mathrm{p}}}(\underline{\xi})\mathrm{e}^{+\mathrm{i}\underline{\xi}\cdot\underline{x}}dV_\xi, \tag{5.55}$$

In cylindrical coordinates, $dV=\rho d\rho d\theta dx_3$ and (ρ,θ,x_3) are defined by $x_1=\rho\cos\theta$, $x_2=\rho\sin\theta$, $x_3=x_3$, and $\rho=\sqrt{x_1^2+x_2^2}$. The mathematical integrations are performed using the cylindrical coordinates of the Fourier space [4]:

$$
\begin{aligned}
u_\rho &= \frac{b\cos\theta \mathrm{sgn}(x_3)}{4(1-\nu)}\left(2(1-\nu)J(1,0;0)-\frac{|x_3|}{a}J(1,0;1)+\frac{|x_3|}{\rho}J(1,1;0)\right)\\
u_\theta &= \frac{b\sin\theta \mathrm{sgn}(x_3)}{4(1-\nu)}\left(-2(1-\nu)J(1,0;0)+\frac{|x_3|}{\rho}J(1,1;0)\right)\\
u_3 &= \frac{b\cos\theta}{4(1-\nu)}\left((1-2\nu)J(1,1;0)+\frac{|x_3|}{a}J(1,1;1)\right).
\end{aligned}
\tag{5.56}
$$

where $\mathrm{sgn}(x_3)=+1$ for $x_3>0$ and $\mathrm{sgn}(x_3)=-1$ for $x_3<0$. $J(m,n;p)$ are the Lipschitz-Hankel integrals [13, 44] defined by:

$$
J(m,n;p)=\int_0^{+\infty} J_m(Q)J_n(\overline{\rho}Q)e^{-\frac{Q|x_3|}{a}}Q^p\,dQ,
$$

with $\overline{\rho}=\rho/a$, $Q=aq$ and $J_m(Q)$ are Bessel functions of order m (m, n and p are integers). The complete expressions of the elastic fields $\underset{\sim}{\varepsilon}^e(\underline{x})$ and $\underset{\sim}{\omega}^e(\underline{x})$, as well as the internal stresses $\underset{\sim}{\tau}(\underline{x})$ are easily derived from Eq. (5.56) and are given in [4] and [39].

The internal elastic energy of one loop $\Phi_{int}^{1\mathrm{d}}$ is calculated independently using the Parseval's identity:

$$
\Phi_{int}^{1\mathrm{d}}=\frac{\mu b^2}{16\pi^3}\int_{V_\xi}\left(\frac{\xi_2^2}{\xi^2}+\frac{2}{1-\nu}\frac{\xi_1^2\xi_3^2}{\xi^4}\right)|\widetilde{\theta^{1\mathrm{d}}}(\underline{\xi})|^2\,dV_\xi,
\tag{5.57}
$$

with $|\widetilde{\theta^{1\mathrm{d}}}(\underline{\xi})|^2=4\pi^2a^2\left(J_1\left(aq\right)\right)^2/q^2$ (from Eq. (5.54)).
After introducing the dislocation core radius, the mathematical integration gives:

$$
\Phi_{int}^{1\mathrm{d}}=\frac{\mu b^2}{2}a\frac{2-\nu}{1-\nu}\frac{1}{k}\left(\left(1-\frac{k^2}{2}\right)\mathbf{K}(k)-\mathbf{E}(k)\right),
\tag{5.58}
$$

where $k^2=\frac{a^2}{a^2+r_c^2}$, $\mathbf{K}(k)$ and $\mathbf{E}(k)$ are respectively first order and second order elliptic integrals. Here, one follows De Wit [12] by setting r_c to $0.5b$ to take into account the dislocation core energy.

Now, one focuses the study on a distribution of periodic circular glide dislocation loops lying in successive planes parallel to $(x_1,x_2,0)$ along the grain of radius R (Fig. 5.2). Successive loops are spaced by a given distance h. All loops are constrained by the spherical grain boundary (considered as no penetrable to dislocations) and have same Burgers vector $\underline{b}$ defined as $\underline{b}=(b,0,0)$ and same unit normal $\underline{n}=(0,0,1)$. The first objective is to derive the plastic distortion field for this periodic distribution. As shown in Fig. 5.2, an odd number $(2N+1)$ of circular loops is considered so that the only non zero plastic distortion component is:

$$
\beta_{31}^p(\underline{x})=b\sum_{n=-N}^{+N}H\left(1-\frac{\rho}{a^{(n)}}\right)\delta(x_3-nh),
\tag{5.59}
$$

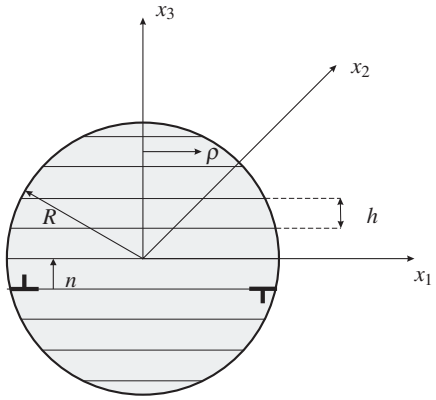

Fig. 5.2 Spherical grain with radius R and periodic dislocation loops spaced by h. The grain is embedded in an infinite elastic medium [4].

where $a^{(n)} = \sqrt{R^2 - (nh)^2}$ is the radius of the loop at altitude $x_3 = nh$. After a few calculations, the Fourier transform reads:

$$\widetilde{\beta_{31}^{\mathrm{p}}}(\underline{\xi}) = b\widetilde{\theta^{\mathrm{d}}}(\underline{\xi}), \tag{5.60}$$

where:

$$\widetilde{\theta^{\mathrm{d}}}(\underline{\xi}) = 2\pi \sum_{n=-N}^{+N} e^{-inh\xi_3} a^{(n)} \frac{J_1\left(a^{(n)}q\right)}{q}. \tag{5.61}$$

The internal stresses and elastic distortions are simply obtained by summing the individual contributions of all concentric circular glide loops of consecutive radii $a^{(n)}$ at altitudes $x_3 = nh$ for n varying from $-N$ to N. The peculiar case of $n = 0$ gives the internal elastic stress field of one loop centered at the origin.

For the distribution depicted in Fig. 5.2, the averaged plastic distortion over the grain volume V_g contains the areas (denoted $S^{(n)}$) formed by the circular loops of radius $a^{(n)}$:

$$\overline{\beta_{31}^{\mathrm{p}}}^{V_g} = b\frac{\sum_{n=-N}^{+N} S^{(n)}}{V_g} = \frac{3}{4}\frac{b}{R}\sum_{n=-N}^{+N}\left(1 - \left(\frac{nh}{R}\right)^2\right), \tag{5.62}$$

One applies the Parseval's identity to find the internal elastic energy due to the distribution of discrete loops denoted Φ_{int}^{d}:

$$\Phi_{int}^{\mathrm{d}} = \frac{\mu b^2}{16\pi^3}\int_{V_\xi}\left(\frac{\xi_2^2}{\xi^2} + \frac{2}{1-\nu}\frac{\xi_1^2\xi_3^2}{\xi^4}\right)|\widetilde{\theta^{\mathrm{d}}}(\underline{\xi})|^2\, dV_\xi, \tag{5.63}$$

with:

$$
\begin{aligned}
|\widetilde{\theta^{\mathrm{d}}}(\underline{\xi})|^2 &= 4\pi^2 \sum_{n=-N}^{+N} a^{(n)^2} \frac{\left(J_1\left(a^{(n)}q\right)\right)^2}{q^2} \\
&+ 8\pi^2 \sum_{n=-N}^{N-1} \sum_{m=n+1}^{+N} \cos\left((m-n)h\xi_3\right) a^{(n)} a^{(m)} \frac{J_1\left(a^{(n)}q\right) J_1\left(a^{(m)}q\right)}{q^2}.
\end{aligned}
\tag{5.64}
$$

Thus, the elastic energy derived in Eq. (5.63) contains two contributions as seen in Eq. (5.64). The first term can be identified as the self energies of the $2N+1$ dislocation loops which are derived from the expression for one loop, and, the second term can be identified as the contribution of interaction energies between the loops. Considering two coaxial circular glide loops of respective radii $a^{(n)}$ and $a^{(m)}$ and separated by a distance d, one has (superscript "$2d$" denotes "2 discrete coaxial dislocation loops"):

$$
\begin{aligned}
|\theta^{2\mathrm{d}}(\underline{\xi})|^2 &= 4\pi^2 \left[a^{(n)^2} \frac{\left(J_1\left(a^{(n)}q\right)\right)^2}{q^2} + a^{(m)^2} \frac{\left(J_1\left(a^{(m)}q\right)\right)^2}{q^2} \right] \\
&+ 8\pi^2 \cos\left(d\xi_3\right) a^{(n)} a^{(m)} \frac{J_1\left(a^{(n)}q\right) J_1\left(a^{(m)}q\right)}{q^2}.
\end{aligned}
\tag{5.65}
$$

The first two terms correspond to the self-energies $\Phi_{self}^{(n)or(m)}$ of the loops with radii $a^{(n)or(m)}$ computed using Eq. (5.58). The last term represents their interaction energy $\Phi_{inter}^{(nm)}$ which writes:

$$
\begin{aligned}
\Phi_{inter}^{(nm)} = \frac{\mu b^2 a^{(n)} a^{(m)}}{2\pi} \int_{V_\xi} &\left(\frac{\xi_2^2}{\xi^2} + \frac{2}{1-\nu} \frac{\xi_1^2 \xi_3^2}{\xi^4} \right) \cos\left(d\xi_3\right) \\
&\frac{J_1\left(a^{(n)}q\right) J_1\left(a^{(m)}q\right)}{q^2} dV_\xi.
\end{aligned}
\tag{5.66}
$$

The mathematical integration of Eq. (5.66) gives [4]:

$$
\begin{aligned}
\Phi_{inter}^{(nm)} &= \mu b^2 \sqrt{a^{(n)} a^{(m)}} \frac{2-\nu}{1-\nu} \frac{1}{k} \left(\left(1 - \frac{k^2}{2}\right) \mathbf{K}(k) - \mathbf{E}(k) \right) \\
&- \frac{\mu b^2}{4} \frac{1}{\sqrt{a^{(n)} a^{(m)}}} \frac{d^2 k}{1-\nu} \left(\left(1 - \frac{k^2}{2}\right) \left(1-k^2\right)^{-1} \mathbf{E}(k) - \mathbf{K}(k) \right),
\end{aligned}
\tag{5.67}
$$

with:

$$
k^2 = \frac{4 a^{(n)} a^{(m)}}{\left(a^{(n)} + a^{(m)}\right)^2 + d^2}. \tag{5.68}
$$

Thus, by carefully summing self- and interaction- energies, one obtains the elastic energy of the discrete distribution Φ_{int}^{d} as:

$$\Phi_{int}^{\mathrm{d}} = \sum_{n=-N}^{+N} \Phi_{self}^{(n)} + \sum_{n=-N}^{N-1} \sum_{m=n+1}^{+N} \Phi_{inter}^{(nm)}. \tag{5.69}$$

In the next section, various distributions corresponding to different values of spatial period h and different grain radii R will be considered.

5.5.2 Theoretical Results

Figure 5.3 displays the internal stress contours in the plane (x_1,x_2) for the shear component τ_{13} at altitude $x_3 = 0.5R$ in case where different numbers of discrete dislocation loops spread in the grain (of volume V_g). By construction, the number of loops is always an odd number. Here, one respectively considers 3 loops (Fig. 5.3(a)), 11 loops (Fig. 5.3(b)) and 101 loops (Fig. 5.3(c)). Now, τ_{13} is normalized with $\mu\varepsilon^{0}_{13}$ to be compared with the Eshelby's solution at same average plastic strain ε^{0}_{13} over the grain. One can show using the equations that the ratio $\tau_{13}/\varepsilon^{0}_{13}$ is independent of the value of the grain radius R. Hence, the result of Fig. 5.3 holds whatever the value of R. For comparison, Fig. 5.3(d) displays the case of the Eshelby's solution of uniform plastic strain ε^{0}_{13} inside the grain. As shown in Fig. 5.3(a,b), it seems that the

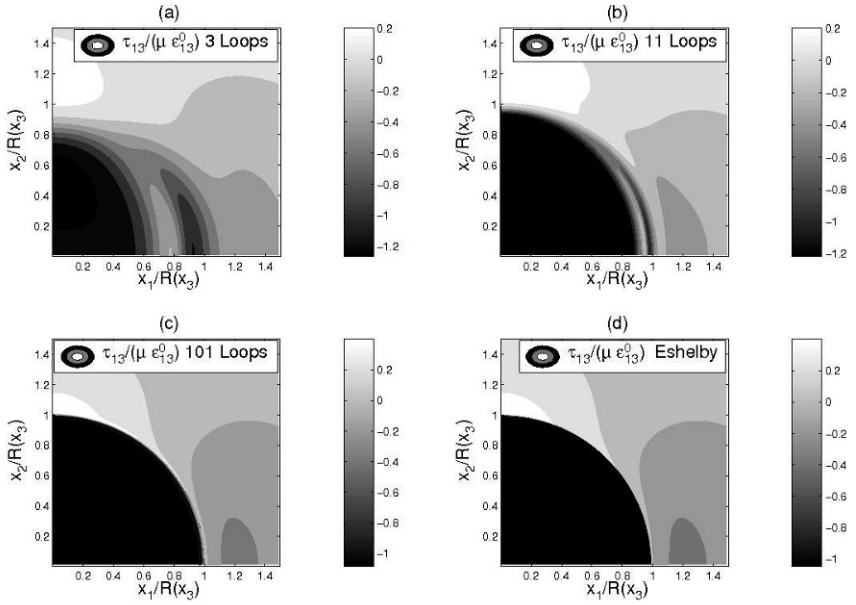

Fig. 5.3 Contours for internal stress component τ_{13} normalized with $\mu\varepsilon^{0}_{13}$ at $x_3 = 0.5R$ for different number of loops. Comparison with the Eshelby's solution at same average plastic strain over the grain. (x_1,x_2) are normalized with $R(x_3) = \sqrt{R^2 + x_3^2}$ [4].

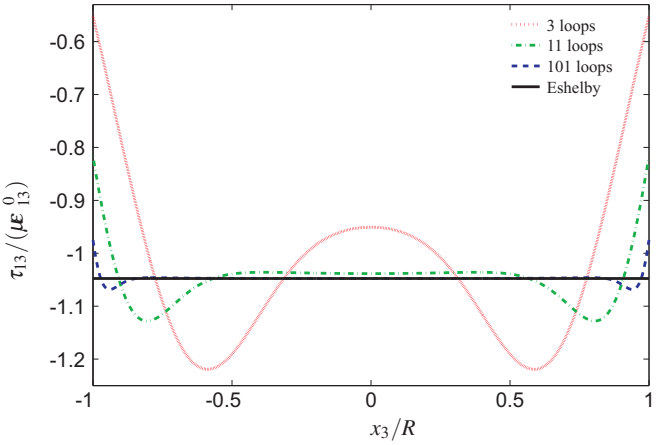

Fig. 5.4 Variation of the internal stress component τ_{13} normalized with $\mu\varepsilon^0_{13}$ along the (x_3) axis at $\rho = 0$ for different number of loops. Comparison with the Eshelby's solution at same average plastic strain over the grain [4].

internal stresses due to a distribution of periodic loops in the (x_3) direction are almost uniform in a region surrounding the center of the sphere (named "grain core") and are highly inhomogeneous in the remaining region close to the grain boundary (named "grain boundary layer"). Figure 5.4 displays the variation of $\tau_{13}/(\mu\varepsilon^0_{13})$ (i.e. the same shear component as on Fig. 5.3) along the (x_3) axis as a function of x_3/R for $\rho = 0$. Fig. 5.3 and Fig. 5.4 clearly show that a gradual increase in the number of loops inside the grain leads to a reduction of the grain boundary layer thickness (in the 3D space). The result given by the analytical Eshelby's solution is retrieved for a very high number of closely separated loops within the physical limit where dislocation cores do not overlap. This tendency which is observed for τ_{13} is also valid for other internal stress components as well as for the volume density of elastic energy defined by $w_{el}(\underline{x}) = \frac{1}{2}\underline{\underline{\sigma}}(\underline{x}) : \underline{\underline{\varepsilon}}^e(\underline{x})$.

Unlike the internal stress fields, the elastic energy, once normalized with

$$8\mu\pi\ R^3(\varepsilon^0_{13})^2$$

to be compared with the grain size independent Eshelby's solution, is not invariant with R (Fig. 5.5). This effect arises from the expression of the self-energy (Eq. (5.58)) which accounts for the dislocation core parameter r_c. As the Burgers vector is the same for each loop whatever the grain size, this variation with R is all the more important as grain size is decreased. For a periodic distribution of loops, it is seen from Fig. 5.5 that the normalized internal elastic energy decreases for an increasing number of loops inside the grain. The convergence towards the Eshelby's solution now depends on R. The Eshelby's solution with a uniform plastic strain ε^0_{13} inside the grain is actually retrieved numerically for the distance $h_{min} \simeq 3.332b$. This value

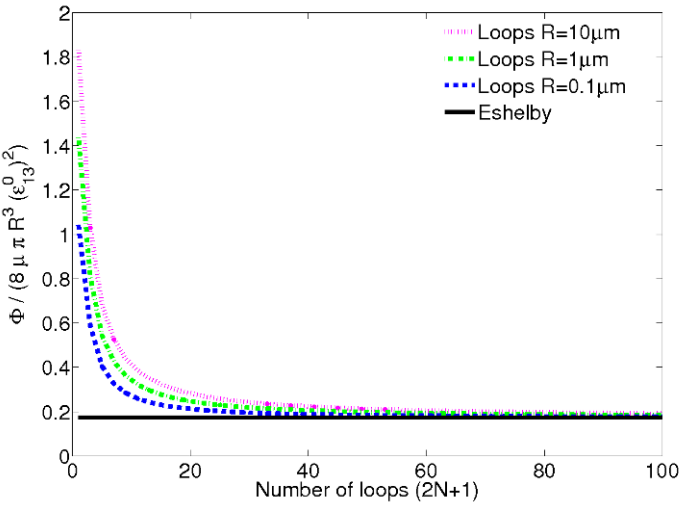

Fig. 5.5 Evolution of the normalized elastic energy for a periodic distribution of single glide dislocation loops as a function of the number of loops inside the grain for various grain sizes. Comparison with the Eshelby's solution at same average plastic strain over the grain [4].

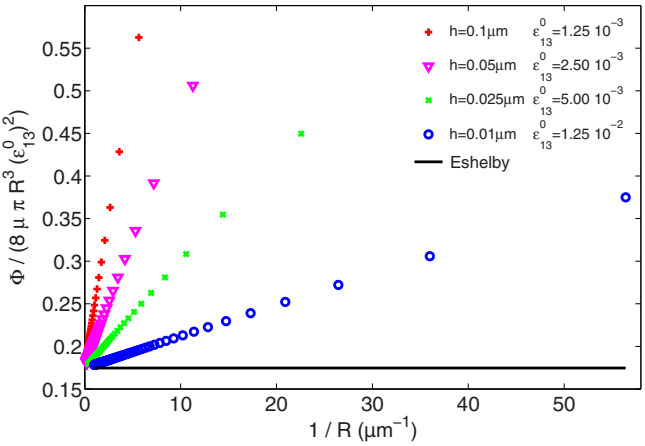

Fig. 5.6 Evolution of the normalized elastic energy for a periodic distribution of single glide dislocation loops as a function of $1/R$ for constant average plastic strain within the grain ε^0_{13} (i.e. different values for h). Comparison with the Eshelby's solution at same average plastic strain over the grain [4].

is only a numerical value which has no physical meaning as the annihilation distance between edge dipoles is found to be on the order of some tens atomic distances [16].

Figure 5.6 shows the evolution of the normalized elastic energy with R for constant values of mean plastic strain ε^0_{13} and distance h between loops. A $1/R$ scaling

law is observed. This grain size effect can be written as follows:

$$\Phi^{(N)} = \alpha \frac{1}{R} + \Phi^{(N)}_{Eshelby}. \tag{5.70}$$

$\Phi^{(N)}$ denotes the "normalized" elastic energy. As observed in Fig. 5.6, the coefficient α depends on ε^0_{13}. Here, ε^0_{13} is fixed by the chosen value for h according to Eq. (5.62). The relation between α and ε^0_{13} (or h) can be easily identified using Fig. 5.6. Here, α decreases with h which means that the grain size effect is even less pronounced that the values of h are low. Thus, Fig. 5.6 demonstrates that a "microstructural error" occurs when the discrete nature of slip is neglected and when plastic slip is assumed homogeneous over the grain. The most important result lies in the grain size dependence of the elastic energy linked to the discrete microstructure.

5.5.3 Experimental Comparisons

The experimental observations of deformed polycrystalline metals show that all grains are quickly plastically deformed through the presence of slip line patterns. In order to evaluate the influence of discrete intra-granular plasticity on the elastic fields like lattice rotations, one has considered particular grains in pure polycrystalline Nickel deforming according to one predominant slip system. Thus, the discrete distribution of intra-granular super-dislocation glide loops can be characterized according to a single slip system by a given discrete distribution for slip band spacing (denoted $h^{(n)}$) depending on the spatial positions of slip bands (n) inside the grain. This distribution have been measured on surface reliefs by Atomic Force Microscopy (AFM) (Fig. 5.7(a)). In the modeling, these particular grains are supposed to be embedded in an infinite elastic matrix representing the surrounding grains. Thus, in spite of the potential presence of inter-granular plasticity effects, these ones are neglected in the present micromechanical model in order to focus only on the effects of the intra-granular discrete microstructure on the rotations inside the grain. In the following, discrete plasticity in the neighboring grains is then disregarded.

Figure 5.8 reports the profile of the surface along a line perpendicular to the slip lines (Fig. 5.7(a)). It is noteworthy that a background correction was performed. Steps due to the emergence of dislocations are observed on the sample surface as peaks labelled "a" to "o". The SEM micrograph reported in Fig. 5.7(b), which corresponds to the peak "g" on Fig. 3a, shows that each peak of the AFM profile corresponds to several discrete slip lines. So, it is important to denote that the resolution does not allow measuring the step produced by a single slip line as observed in Fig. 5.7(b). The steps observed by AFM correspond to slip bands which can be modeled by non uniform description of super-dislocation loops characterized by its "own Burgers vector" with the magnitude $B^{(n)} = k^{(n)}b$, where b is the magnitude of the

Burgers vector $\underline{b}$ for a perfect dislocation. Like in Fig. 5.2, the plastic distortion is defined in the local frame associated with the most active slip system of unit normal $\underline{n} = (0,0,1)$) and with $\underline{B} = (B_1,0,0) = (B,0,0)$ but the distribution in not periodic anymore:

$$\beta_{31}^{p} = \sum_{n} B_1^{(n)} n_3 \delta(S^{(n)}) = \sum_{n} B^{(n)} H\left(1 - \frac{\rho}{a^{(n)}}\right) \delta\left(x_3\left(\left\{h^{(n)}\right\}\right)\right), \tag{5.71}$$

where $a^{(n)} = \left(R^2 - x_3\left(\left\{h^{(n)}\right\}\right)\right)^{0.5}$ is the loop radius at altitude $x_3\left(\left\{h^{(n)}\right\}\right)$ determined by a spatial distribution of non equally spaced slip bands denoted $\left\{h^{(n)}\right\}$. $\delta\left(x_3\left(\left\{h^{(n)}\right\}\right)\right)$ is the Dirac delta function in the (x_3) direction at the altitude $x_3\left(\left\{h^{(n)}\right\}\right)$. The other notations are the same as in Eq. (5.59).

In order to compare experimental data with the results of the presented theory, lattice rotation arising from the presence of dislocations has to be determined in each point of the grain represented in Fig. 5.9. This is performed by making a discrete sum over all the super-dislocation loops present in the grain using of the elastic fields and deriving the misorientation angles in relation to an orientation chosen in the center of the grain. The angles were calculated and compared to EBSD measurements in [39].

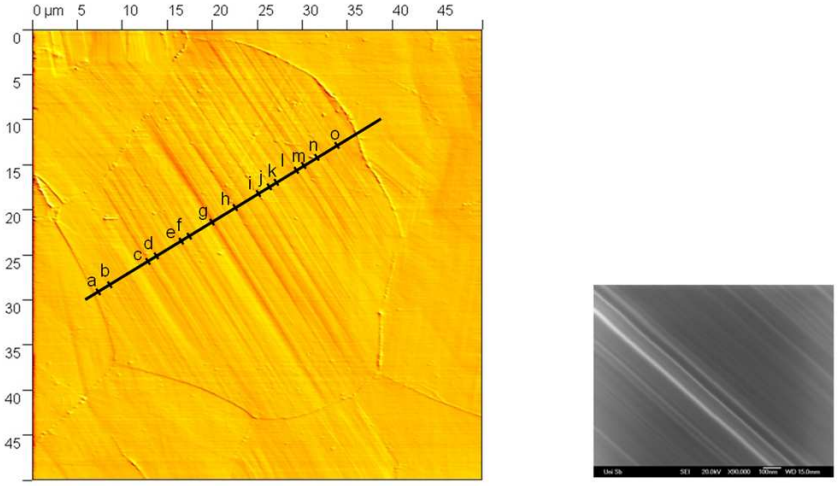

Fig. 5.7 (a) AFM micrograph: Deformation microstructure of a polycrystalline pure nickel sample at 1.5% of macroscopic strain. The slip bands with the highest amplitudes are labeled "a" to "o". (b) SEM micrograph of slip lines constituting the slip band labeled "g" in (a)

To compare the local intra-granular misorientations calculated with the micromechanical model to the EBSD measurements, a line parallel to the slip bands in the observation plane has been selected (Fig. 5.9(b)). The measured variations of these misorientations along this line with respect to a reference point chosen in the grain center are first reported in Fig. 5.10. A strong variation occurs between near grain boundary regions (with a maximal misorientation about 1.6 deg) and grain core (zero misorientation). In Fig. 5.11, the calculated misorientations are reported using the previous assumptions (super-dislocation loops, etc.) in the case of non uniform slip bands spacing distribution as measured on surface relief by AFM. It can be denoted that the model results fit quite well the experimental results. Especially, at grain boundary (left side in Fig. 5.11 from "distance=0 μm"), the perturbed zone size for misorientation and the order of magnitude of the maximal misorientation at grain boundary is consistent with the experimental value. By taking into account the discrete nature of plasticity at the mesoscale, the model is then able to predict the major features of intra-granular elastic fields.

5.6 Modeling Intragranular Slip Bands as Plastic Oblate Spheroids Constrained by Grain Boundaries

The second discrete micromechanical approach treats intra-granular slip bands in single slip configurations as discrete distributions of plastic micro-regions (intra-granular inclusions) of oblate spheroidal shapes. In contrast with super-dislocation loops, the plastic distortion inside each oblate spheroid is considered as uniform (not

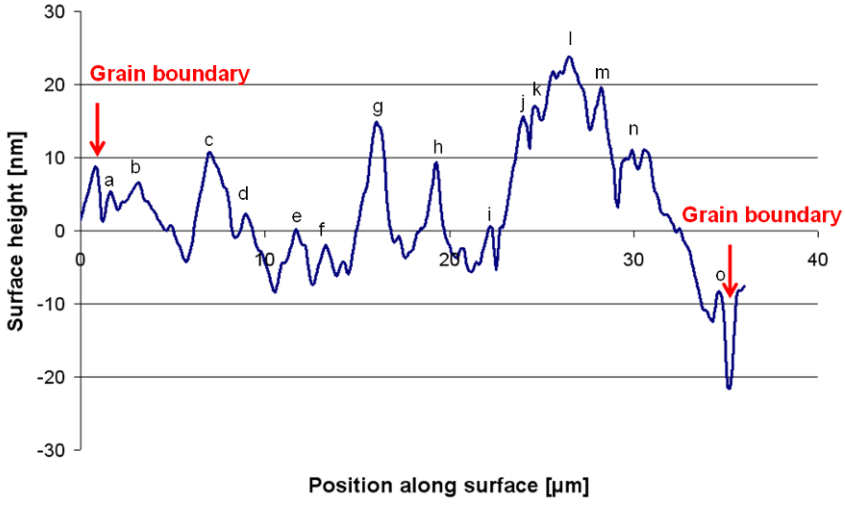

Fig. 5.8 AFM profile of the slip bands inside the grain shown in Fig. 5.7.

singular), i.e. it results from an averaging procedure performed on each slip band. The main advantage is not only to take into account the slip band length effect on mechanical fields but also the one due to their aspect ratios.

5.6.1 Elastic Fields

One considers that plastic deformation is distributed along slip bands inside an individual grain. Due to curved grain boundaries, one assumes that the slip bands are described by oblate spheroids (Fig. 5.12) which are considered periodic, with a characteristic period h, inside a spherical grain of radius R and volume V_g (Fig. 5.13). The use of oblate spheroids allows to take advantage of the Eshelby's properties for ellipsoidal inclusions [14]. One uses the following terminology: the length of the largest half axis of oblate spheroid (denoted by 'a' in Fig. 5.12) is called the oblate radius or the slip band radius, and the length of the smallest half axis of oblate spheroid (denoted by 'c' in Fig.5.12) is called the oblate thickness or the slip band thickness for the sake of simplicity. As for super-dislocation loops, one considers a single slip system with unit vector $\underline{m}$ in the slip direction and unit vector $\underline{n}$ normal to the slip plane. Thus, this static configuration implies that all the slip bands I of volume V_I are coplanar and elongated in the slip plane with the smallest half axis c in the direction of $\underline{n}$.

Hence, two major non-dimensional internal length scale parameters inherent to the microstructure are introduced. The first one is h/R which characterizes the spatial distribution of slip bands. In this study, these ones are considered equally spaced for the sake of simplicity. The second one is c/R which dictates the morphology of

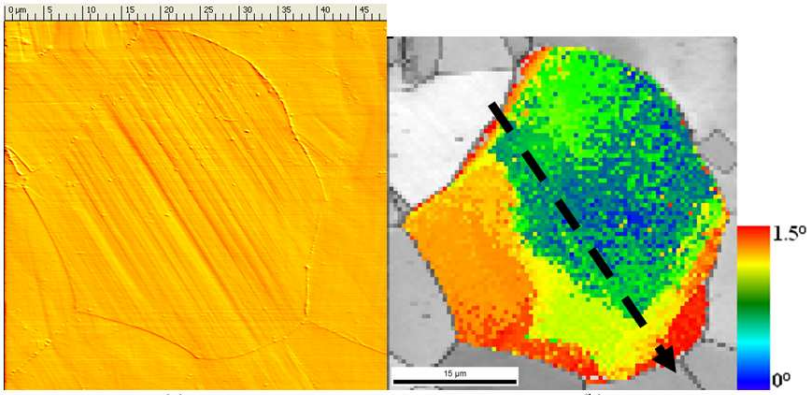

Fig. 5.9 : (a) AFM micrograph: Deformation microstructure of a particular grain in a polycrystalline pure nickel sample with 1.5% plastic strain (b) EBSD measurement of intra-granular misorientations in relation to a reference point in the grain center after 1.5% of global plastic strain. The dotted line serves as reference for the spatial evolution of intra-granular misorientations [39].

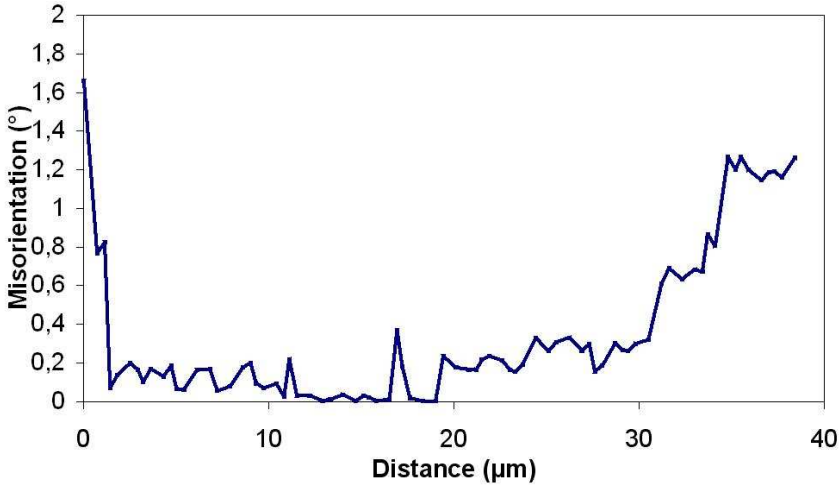

Fig. 5.10 EBSD-OIM measurement: Intra-granular misorientation (in deg) in relation to a reference point in the grain center along a line parallel to the slip lines in the observation plane after 1.5% strain (see Fig. 5.9(b)) [39].

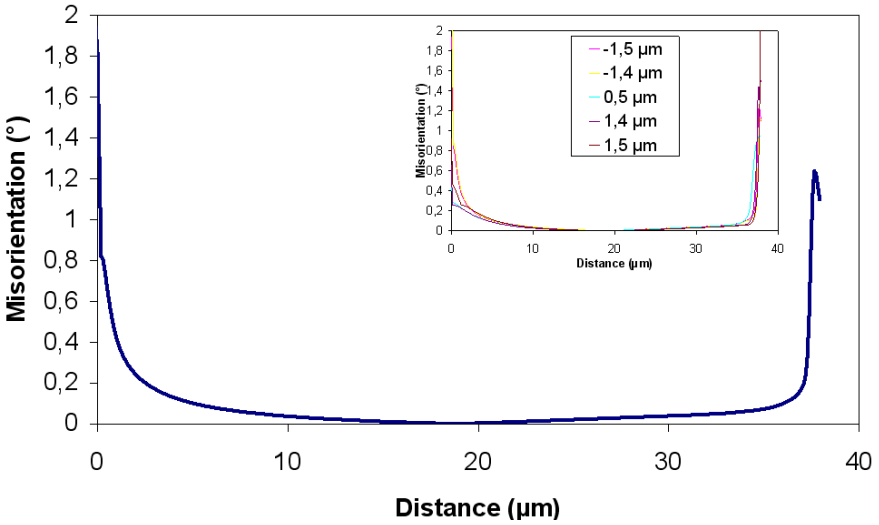

Fig. 5.11 Theoretical intra-granular misorientations (in deg) in the case of a non-uniform distribution of loops at 1.5% of macroscopic strain. The values are given with respect to a reference point in the grain center along a line parallel to the slip lines in the observation plane (Fig. 5.9(b)) and at $1.5\mu m$ from the central super-loop. *Inset:* Effect of the distance from the central loop on the theoretical intra-granular misorientations along the aforementioned line parallel to the slip lines [39].

slip bands, i.e. their aspect ratio. As a consequence, the volume fraction of slip bands inside the grain depends on both parameters.

The associated plastic strain is defined through the Schmid tensor $\underset{\sim}{R} = \frac{1}{2}(\underline{m}\otimes\underline{n}+\underline{n}\otimes\underline{m})$ and the slip $\gamma(\underline{x})$ by:

$$\underset{\sim}{\varepsilon}^p(\underline{x}) = \underset{\sim}{R}\gamma(\underline{x}), \tag{5.72}$$

where:

$$\gamma(\underline{x}) = \sum_I \gamma_I \theta_I(\underline{x}) = \begin{cases} \gamma_I \text{ if } \underline{x} \in V_I, \\ 0 \text{ if } \underline{x} \notin V_I, \end{cases} \tag{5.73}$$

and where $\theta_I(\underline{x})$ is the characteristic function. It depends on the location of the slip band I, on the volume V_I, and, on the fact that the bands are constrained by the grain boundary. Hence, Eq. (5.72) reads:

$$\underset{\sim}{\varepsilon}^p(\underline{x}) = \sum_I \underset{\sim}{\varepsilon}^p_I \theta_I(\underline{x}), \tag{5.74}$$

where $\underset{\sim}{\varepsilon}^p_I = \underset{\sim}{R}\gamma_I$ is the plastic strain in the I^{th} slip band. So, the average plastic strain over the grain is:

$$\underset{\sim}{\overline{\varepsilon^p}}^g = \sum_I f^I \underset{\sim}{\varepsilon}^p_I, \tag{5.75}$$

where $f^I = V_I/V_g$ is the volume fraction of the I^{th} slip band in the grain. The macroscopic strain is deduced from Eq. (5.74) by:

$$\underset{\sim}{E}^p = f^g \underset{\sim}{\overline{\varepsilon^p}}^g, \tag{5.76}$$

where $f^g = V_g/V$ is the grain volume fraction.

Now, if one uses Eq. (5.74) in Eq. (5.33), the average internal stresses over a given slip band N is:

$$\underset{\sim}{\overline{\tau}}^N = \sum_I \underset{\approx}{L}^{NI} : \underset{\sim}{\varepsilon}^p_I, \tag{5.77}$$

where according to Eq. (5.34):

$$\underset{\approx}{L}^{NI} = \frac{1}{V_N}\int_{V_N}\left[-\underset{\approx}{C}\theta_I(\underline{x}) + \underset{\approx}{C} : \int_{V_I}\left(\underset{\approx}{\Gamma}(\underline{x}-\underline{x}')\right) : \underset{\approx}{C}dV'\right]dV. \tag{5.78}$$

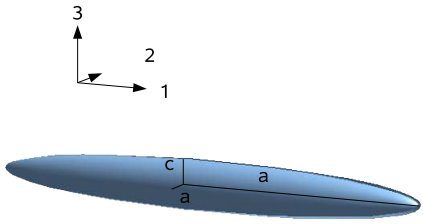

Fig. 5.12 A slip band is represented by an oblate spheroid with half axes (a,a,c) .

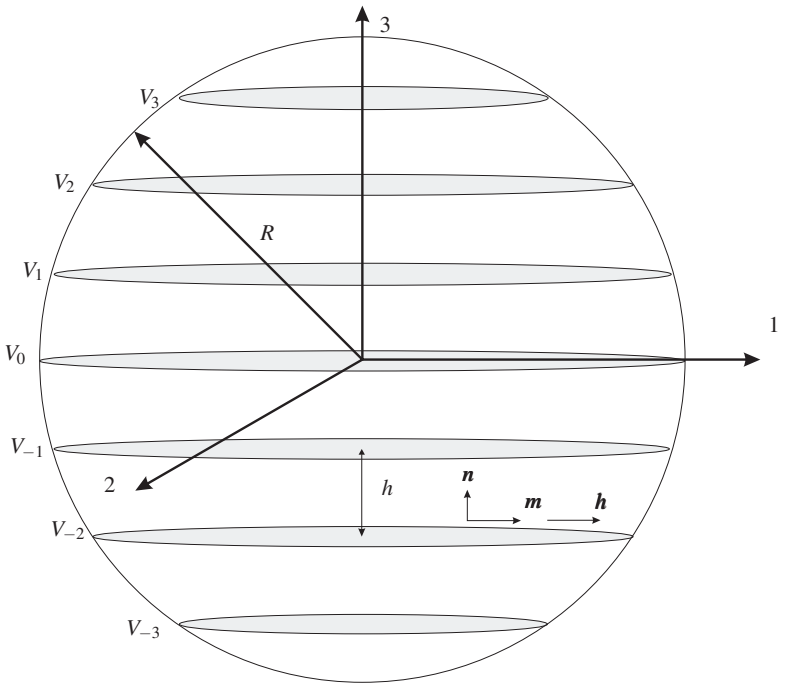

Fig. 5.13 Distribution of slip bands with individual volumes V_I and spatial period h constrained by a spherical grain with radius R. The plastic strain in each band is due to slip in the direction of the perfect Burgers vector $\underline{b}$ in the single slip plane of unit normal $\underline{n}$. The grain is embedded in an infinite elastic matrix.

Finally, the expression for $\overline{\underset{\sim}{\tau}}^N$ is deduced from Eq. (5.78):

$$\overline{\underset{\sim}{\tau}}^N = -\underset{\approx}{C} : \left[\underset{\approx}{I} - \underset{\approx}{S}^{esh,N}\right] : \underset{\sim}{\varepsilon}_N^p + \sum_{\substack{I \\ I \neq N}} \underset{\approx}{C} : \underset{\approx}{T}^{NI} : \underset{\approx}{C} : \underset{\sim}{\varepsilon}_I^p. \tag{5.79}$$

In the last equation, $\underset{\approx}{S}^{esh,N} = \underset{\approx}{T}^{NN} : \underset{\approx}{C}$ is the Eshelby tensor for an oblate spheroid and $\underset{\approx}{T}^{NI}$ is expressed by:

$$\underset{\approx}{T}^{NI} = \frac{1}{V_N} \int_{V_N} \int_{V_I} \underset{\approx}{\Gamma}(\underline{x} - \underline{x}') dV' dV. \tag{5.80}$$

Now, using Eqs. (5.74) and (5.76) in Eq. (5.36) gives:

$$\psi\left(\underset{\sim}{\Sigma}, \underset{\sim}{\varepsilon}^p(\underline{x})\right) = \frac{1}{2} \underset{\sim}{\Sigma} : \underset{\approx}{S} : \underset{\sim}{\Sigma} + f^g \underset{\sim}{\Sigma} : \overline{\underset{\sim}{\varepsilon^p}}^g + \frac{1}{2} f^g \sum_N \sum_I f^N \underset{\sim}{\varepsilon}_N^p : \underset{\approx}{L}^{NI} : \underset{\sim}{\varepsilon}_I^p. \tag{5.81}$$

It is noteworthy that the same expression for $\underset{\sim}{\overline{\tau}}^N$ as Eq. (5.77) can be retrieved directly from Eq. (5.81) by computing the driving force associated with the plasticization process ($\underset{\sim}{\varepsilon}^p_N$) inside the band N denoted $\underset{\sim}{F}^N$ [33, 41]. It writes $\underset{\sim}{F}^N = \frac{\partial \psi}{\partial \underset{\sim}{\varepsilon}^p_N}$ so that $\underset{\sim}{\overline{\tau}}^N = \frac{1}{f^g f^N} \underset{\sim}{F}^N - \underset{\sim}{\Sigma}$.

From the configuration depicted in Fig. 5.13, one considers a spherical grain with a periodic distribution of slip bands characterized in the coordinates of the active slip system by the unit vector in slip direction $\underline{m} = (1,0,0)$ and the unit vector normal to the slip plane $\underline{n} = (0,0,1)$. The plastic strains in the I^{th} slip band ε^{pI} reduces to two non zero components $\varepsilon^{pI}_{13} = \varepsilon^{pI}_{31} = \frac{1}{2}\gamma_I$, so:

$$\varepsilon^p_{13}(\underline{x}) = \sum_I \varepsilon^{pI}_{13} \theta_I(\underline{x}), \tag{5.82}$$

and, from Eq. (5.76):

$$E^p_{13} = f^g \sum_I f^I \varepsilon^{pI}_{13}. \tag{5.83}$$

Again, one considers isotropic elastic properties characterized by Lamé elastic moduli (shear modulus μ and λ). For any $(i,j) = (1,3)$, Eq. (5.77) simplifies to:

$$\overline{\tau}^N_{13} = 2 \sum_I L^{NI}_{1313} \varepsilon^{pI}_{13}. \tag{5.84}$$

where:

$$L^{NN}_{1313} = L^{NN}_{3113} = -2\mu \left(\frac{1}{2} - S^{esh,N}_{1313} \right) \tag{5.85}$$

$$L^{NI}_{1313} = L^{NI}_{3113} = 2\mu^2 \left(T^{NI}_{1313} + T^{NI}_{1331} \right), \text{ if } N \neq I, \tag{5.86}$$

The complementary energy per unit volume reads:

$$\psi \left(\underset{\sim}{\Sigma}, \underset{\sim}{\varepsilon}^p(\underline{x}) \right) = \frac{1}{2} \underset{\sim}{\Sigma} : \underset{\approx}{S} : \underset{\sim}{\Sigma} + 2 f^g \Sigma_{13} \overline{\varepsilon^p_{13}}^g + \psi^{internal}, \tag{5.87}$$

where:

$$\psi^{internal} = 2 f^g \sum_N \sum_I f^N \varepsilon^{pN}_{13} L^{NI}_{1313} \varepsilon^{pI}_{13}. \tag{5.88}$$

The expression of $S^{esh,N}_{1313}$ for oblate spheroids is given in [36], and, the expressions of T^{NI}_{1313} and T^{NI}_{1331} are computed in [10] reducing these interaction terms to single integrals and using a Gauss-Legendre algorithm.

5.6.2 Theoretical Results

In order to exhibit the internal length scale effects of the microstructure at a given macroscopic stress, one compares the results at same $\underset{\sim}{E}^p$, so that the complementary energy per unit volume only depends on the variations of the internal complementary energy per unit volume $\psi^{internal}$ defined in Eq. (5.88). In order to simplify the comparison with the Eshelby's solution, $\psi^{internal}$ is normalized with respect to $(8\pi\mu\ R^3(\overline{\varepsilon_{13}^{p\ g}})^2)/V$. The average plastic strain over the grain $\overline{\varepsilon_{13}^{p\ g}}$ is obtained from Eq. (5.75) and taken equal to the plastic strain ε_{13}^0 introduced in the uniform plastic Eshelby's inclusion (Eq. (5.49)). The normalized internal part of the complementary energy per unit volume for the Eshelby's solution associated with a spherical inclusion gives the constant value $(7-5\nu)/(45(\nu-1))$ [36]. In these simulations, $\nu = 0.3$.

Here, one explores the influence of the spatial period h between slip bands on $\psi_N^{internal}$ for different numbers of bands (from 3 to 99) and for a given grain radius R. Figure 5.14 represents ψ_N^{internal} as a function of the non-dimensional internal length scale parameter h/R when c/R is set to 0.01. One observes that for a given number of slip bands, $\psi_N^{internal}$ reaches a maximum for a critical value of h/R. Furthermore, as the number of bands is increased, this critical value decreases (but does not scale linearly with h/R), and, the corresponding maximum value for ψ_N^{internal} increases without reaching the Eshelby's solution. These simulations show that for a given number of equally-spaced bands in a grain, one can deduce an optimized configuration defined by a critical value of h/R denoted by h_{opt}/R and reported in Table 5.1. The existence of a maximum for ψ_N^{internal} depends on both the spatial distribution and the morphology of slip bands which act simultaneously in a complex way.

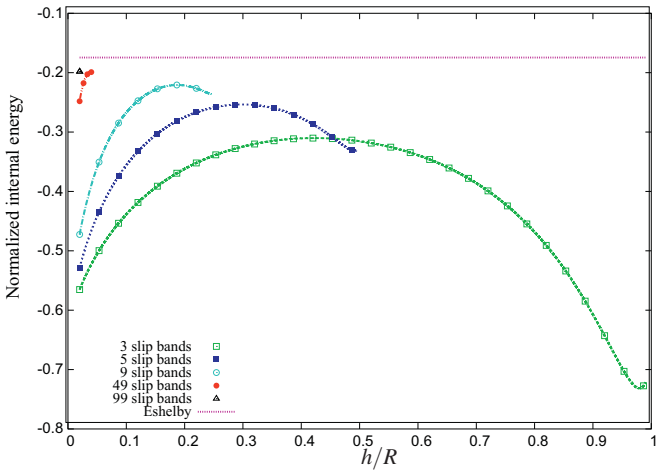

Fig. 5.14 Normalized internal part of the complementary energy per unit volume (denoted $W_N^{internal}$ in the text) as a function of non dimensional internal length parameter h/R for various numbers of slip bands in the grain. Comparison with the Eshelby's solution (*dashed lines*).

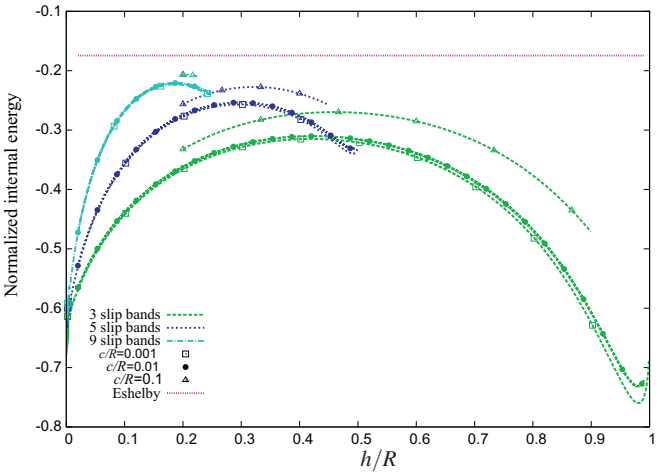

Fig. 5.15 Normalized internal part of the complementary energy per unit volume (denoted $W_N^{internal}$ in the text) as a function of h/R for various numbers of slip bands in the grain and for 3 different values of c/R (*square*: 0.001; *circles*: 0.01; *triangles*: 0.1). Comparison with the Eshelby's solution (*dashed lines*).

For high h/R values with respect to h_{opt}/R and in the case of a few slip bands, these ones are located far from each other, and, their morphologies are much different from the middle to the top of the grain. Thus, the part of ψ_N^{internal} due to self energies is mainly responsible for low levels of ψ_N^{internal}. Conversely, for low h/R values with respect to h_{opt}/R, the slip bands are close to each other and their volume fraction in the grain becomes important which leads to low local slip in each band. In this case, the part of ψ_N^{internal} due to interaction energies is predominant and monitors a decrease of ψ_N^{internal} for low h/R. Finally, between these two states (low and high h/R), the opposite contributions of the two parts due to self- and interaction- energies make occur a configuration of slip bands for which ψ_N^{internal} is maximum. The influence of the second non-dimensional internal length scale parameter c/R is also explored in Fig. 5.15. The number of slip bands is limited to 9 because large values of c/R (up to 0.1) prevent from having more than 9 bands inside the grain. For the same number of slip bands spreading into the grain, one found that the larger c/R, the higher ψ_N^{internal}. In addition, the corresponding values of h_{opt}/R are increased as

c/R	0.001	0.01	0.1
3 bands	0.419	0.422	0.460
5 bands	0.296	0.298	0.322
9 bands	0.186	0.187	0.200
49 bands	0.039	0.039	/
99 bands	0.020	0.020	/

Table 5.1 Numerical values for h_{opt}/R at different c/R for numbers of slip bands inside the grain ranging from 3 to 99.

c/R increases (Table 5.1). Moreover, the effect of c/R becomes less important as the number of slip bands increases. Indeed, in this case, the part of ψ_N^{internal} due to interaction energies also become predominant, and, c/R has less influence on the part due to interaction energies than on the one due to self energies. From Fig. 5.15, the coupled effects of both non-dimensional internal length scale parameters are more pronounced for a small number of slip bands.

5.7 Towards new Interaction Laws Including Discrete Plasticity

From the aforementioned equations for in situ grains with discrete plasticity, it is now possible to define new so-called accommodation laws for polycrystalline metals assuming intra-granular discrete single slip concentrated into slip bands described as periodic distributions of dislocation loops [42] of or oblate spheroids [10]. Let us for illustration focus only on the grain-size dependent accommodation due to intra-granular distributions of dislocation loops. The calculation of an average backstress over the grain due to intra-granular dislocations as the ones described in Fig. 5.2 allows us to define a new interaction law in the case of an approximation of diluted plastic grains. This new law depends on grain size and the spatial distribution of loops inside grains.

Let us now consider the averaged plasticization process of the grain with volume V_g, i.e. the variation of γ considered as the mean plastic slip over V_g (with $\gamma = 2\varepsilon_{13}^0$). As a result of the plasticization process, the Helmholtz free energy per unit volume ϕ (Eq. (5.10)) is modified. Hence, it is possible to define a thermodynamic driving force T [33, 41] accounting for this variation of energy due to the plasticization process such that $T = -\partial\phi / \partial\gamma$. Then, the mean resolved shear backstress denoted τ^* appears in the expression of T as:

$$T = f_g\,(\tau - \tau^*)\,, \tag{5.89}$$

where $f_g = V_g/V$ and τ is the applied resolved shear stress.

In the case of the mean field Eshelby's approach (with isotropic elasticity and plastic incompressibility), one finds from Eq. (5.51):

$$T = f_g\left(\tau - \mu\frac{7-5\nu}{15(1-\nu)}\gamma\right). \tag{5.90}$$

Thus, the mean resolved shear backstress τ^*_{esh} reduces to:

$$\tau^*_{esh} = \mu\frac{7-5\nu}{15(1-\nu)}\gamma. \tag{5.91}$$

This expression shows that τ^*_{esh} scales linearly with γ but is not dependent on the grain radius R.

Let us consider again the discrete distribution of dislocation loops of Fig. 5.2. Besides, loops are assumed to constitute "super-dislocations" with apparent Burgers vector $\underline{B} = k\underline{b}$ where k stands for the number of "real" planar dislocations that have slipped on the glide plane as a result of a Frank-Read process (multiplication of planar dislocation loops on a same glide plane due to a single Frank-Read source). In this case, the mean plastic slip produced by the super-dislocation loops over the grain volume yields:

$$\gamma = B\frac{\sum_{n=-N}^{+N} S^{(n)}}{V_g}. \tag{5.92}$$

where $S^{(n)}$ is the area formed by super-dislocation loop (n) (defined in Eq. (5.62)).

From Eq. (5.92), it can be seen that a variation of γ may be caused either by an increase of the apparent Burgers vector magnitude B or by a modification of the total area formed by the loops. For the sake of simplicity, one assumes no variation of internal length (R and h) during the plastic deformation. Therefore, one neglects the possible multiplication of Frank-Read sources on new glide planes. Besides, one does not take into account the possible formation of dislocation pile-ups, so that the "super-dislocations" remain constrained at the boundary. As a consequence, the plasticization mechanism considered here is restricted to a possible variation of B which is moreover assumed to be continuous in time and identical for all super-dislocation loops in the grain. Such mechanism may be considered as a kind of "continuous Frank-Read source" where dislocation loops multiply on a same glide plane and induce an increasing step at the boundary. It is however a crude description of real complex events as experimental studies reveal strong temporal and spatial heterogeneity of slip lines growth [37]. By using Eqs (5.10, 5.58, 5.69), the expression of τ^* is given by [4, 42] :

$$\tau^* = \tau^*_{esh} + \mu\chi\,(h,R)\,\gamma, \tag{5.93}$$

where χ is a complex function depending on h and R [4, 42].

As a direct application of the previous section, it is possible to model the effect of grain size on the polycrystal's behavior through a simplified description of the intra-granular microstructure and the interaction between grains. In order to better highlight the effects of intra-granular plastic slip heterogeneities on the overall behavior, a very simple transition scheme is used. The objective here is not to develop an accurate homogenization scheme and then to compare the results with existing bounds. The sense of this work is more to shed some light on the differences between a conventional mean-field approach and a discrete, more physically-based one resulting from the previous considerations on the inhomogeneous plastic inclusion problem. For this purpose, a diluted model restricted to small plastic strains is adopted. Plastic grains are supposed to be embedded in a purely elastic homogeneous effective medium (HEM) (Fig. 5.16). Grains of spherical shape and with isotropic orientations are considered. Isotropic and homogeneous elasticity throughout the whole samplematerial is assumed. Plastic deformation is supposed to be

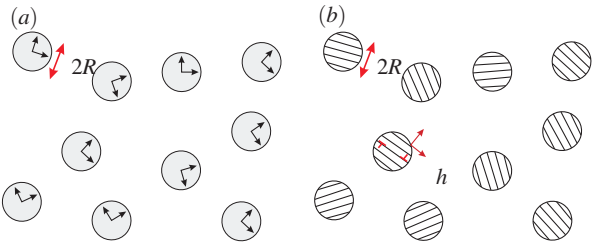

Fig. 5.16 Illustration of the two different situations considered for the HEM. (a) Spherical grains with uniform plastic strain embedded in a purely elastic HEM (diluted Eshelby's model). (b) Spherical grains with a discrete distribution of dislocation loops embedded in a purely elastic HEM. All the loops are constrained by the grain boundary and are spaced by the same distance h [42].

caused by single crystallographic slip only. Consequently, only one slip system can thus be active per grain I, the one giving the highest value of the applied resolved shear stress τ^I_{appl}. For simplicity, the effect of grain rotation is neglected. As in Eshelby-Kröner's model [14, 26], the interaction between grains is supposed to be accommodated in a purely elastic way. Only a small fraction of grains is supposed to become plastic so that the hypothesis of grains embedded in a purely elastic homogeneous equivalent medium holds (Fig. 5.16). These hypotheses can correspond roughly to the early stages of micro-plastic deformation (transient regime). In case of large strains (more than 0.2%), the following simple model would overestimate the values of internal stresses and would give a too stiff estimation of the overall response.

From Eq. (5.93), it is then possible to define a mean "effective" resolved shear stress τ^I_{eff} acting on the single slip system for each grain I:

$$\tau^I_{eff} = \tau^I_{appl} - \mu \left(\frac{7-5\nu}{15(1-\nu)} - \chi(h,R) \right) \gamma^I, \tag{5.94}$$

where $\chi(h,R)$ is given in [42].

A rate-independent crystal plasticity framework is followed. The slip system becomes active (i.e. $\dot{\gamma}^I \neq 0$) if the standard Schmid law with consistency is respected:

$$\begin{cases} \tau^I_{eff} = \underset{\sim}{R} : \underset{\sim}{\sigma}^I = \tau^I_c, \\ \dot{\tau}^I_{eff} = \dot{\tau}^I_c, \end{cases} \tag{5.95}$$

where τ^I_c is the critical resolved shear stress (the same for all grains I). This one is supposed constant during plastic deformation (no additional isotropic hardening is considered). Thus, $\dot{\tau}^I_{eff} = 0$, which is equivalent to:

$$\dot{\gamma}^I = \frac{\dot{\tau}^I_{appl}}{\Theta}, \tag{5.96}$$

where $\Theta = -\mu\left(\frac{7-5\nu}{15(1-\nu)} - \chi(h,R)\right)$ is a constant term during straining.

Uniaxial tensile tests along the (x1) direction in the global frame are simulated from a set of 1000 grains with isotropic orientation distribution. A FCC crystallographic structure is assumed for the grains with 12 slip systems of the type $(111)\langle 110\rangle$. Elastic constants of copper are used ($\mu = 42GPa$ and $\nu = 0.324$). The value of τ_c^I is set to $2MPa$. The proportion of grains that become plastic is fixed to 20%. Accordingly, tests are limited to very small plastic strains and the distance between super-dislocation loops is supposed to be the same for all the simulated tests whatever the grain size. h is set to $0.1\mu m$ which is a value that roughly corresponds to experimental measurements of slip line distance in the stage I of copper single crystals [37].

Figure 5.17 shows a grain-size dependence of the overall tensile behavior of the polycrystals. Contrary to conventional mean-field approaches, the initial strain hardening occurring at very low plastic strains evolves now with the grain size. It should be noted however that, as expected, the pure deviation from elastic response is not grain-size dependent. A grain-size effect on the yield strength, defined for instance as the macroscopic stress at a macroscopic plastic strain of 0.2%, might even so be captured. The simulated size effect arises directly from the internal stresses induced by the considered discrete intra-granular microstructure. The mean resolved shear stress computed for each grain contains indeed the function $\chi(h,R)$. For a constant distance between super-dislocation loops, it was found that this function scales with the inverse of the grain size [4, 42]. Inset of Fig. 5.17 shows that this scaling is retrieved at the macroscopic scale, with an inverse relation between the flow stress Σ_{11} and the grain radius R. From Fig. 5.17, it can be seen that the polycrystal's behavior converges towards the solution given by the traditional diluted plastic Eshelby's homogenization scheme when the grain size increases. Actually, because h is kept

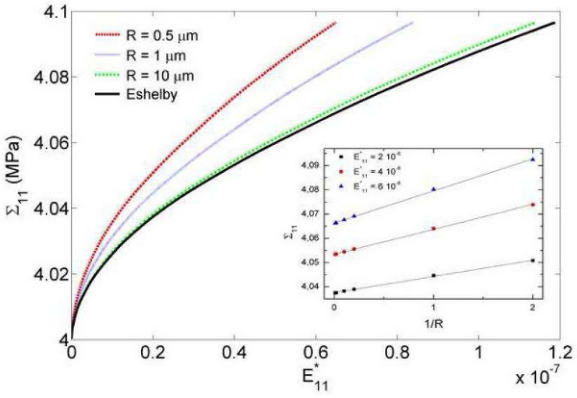

Fig. 5.17 Uniaxial macroscopic tensile stress-plastic strain curves simulated with various grain sizes (the origin of the y-axis starts at $4MPa$). h is set to 0.1 μm for all tests. The curve denoted "Eshelby" represents the response of the diluted Eshelby's model. *Inset*: macroscopic flow stress as a function of $1/R$ for three different plastic strains [42].

constant, the number of dislocation loops per grain increases with the grain size and so plastic distortions inside grains become more and more uniform. This result illustrates the fact that Eq. (5.94) tends to the diluted plastic Eshelby's homogenization scheme (i.e. $\chi(h,R) \to 0$) for a high number of loops inside grains.

5.8 Conclusions

Intragranular plastic slip heterogeneities have been first modeled by discrete distributions of circular glide super-dislocation loops inside a grain embedded in an infinite elastic matrix. Then, field equations and free energy have been solved using the methods of Fourier transforms. The presented results show a strong discrepancy of internal stresses with the Eshelby's solution especially in a grain boundary layer. As the number of loops increases, the thickness of this layer decreases and the classic Eshelby's result is retrieved. These new insights determined through a micromechanics-based approach are consistent with experimental observations (EBSD measurements) reporting different behaviors and dislocation structures between near grain boundary regions and grain interior. On the static viewpoint, the present modeling reports strong stress gradients in the grain boundary layer. Because of such gradients, the relaxation of internal stresses during plasticization will lead to different microstructures between grain boundary region and grain core. From thermodynamic considerations specific to an average plasticization mechanism, a mean back-stress over the inclusion was derived. As a result, it was possible to propose a new interaction law for the polycrystal's behavior which is explicitly dependent on the grain size and on the mean slip line spacing. A diluted model was used to compute the macroscopic deformation of a FCC polycrystal at very low plastic strains.

The second approach described intra-granular slip bands occurring in the microplastic regime of polycrystalline metals by discrete periodic distributions of coplanar flat ellipsoidal plastic inclusions (oblate spheroids). Then, in addition to the grain size, the microstructure is characterized by the spatial period of slip bands and their thickness. One considered the field equations and the thermodynamics framework associated with an isolated in situ plastic grain embedded in an infinite elastic matrix. One investigated the role of both non-dimensional internal length scale parameters of the microstructure on the normalized internal part of the complementary energy per unit volume in the case of an in situ grain. For a given number of slip bands inside the grain, one found there exists a critical value which maximizes this energy. The internal stresses due to the discrete distribution of intra-granular plastic oblate spheroids within the in situ grain can also be used to derive new accommodation laws [10].

Acknowledgements I would like to thank Prof. Marcel Berveiller for initiating me 10 years ago to the research field of micromechanics of materials. I would also like to acknowledge my other colleagues Drs. C. Collard, T. Richeton and V. Favier who contributed to some parts of this work,

as well as a fruitful collaboration with Prof. Horst Vehoff (University of Saarbrücken) through the PhD thesis of Camille Perrin. This research was supported by the ANR and the CNRS.

References

[1] OIM. In: EBSD Lectures: Introduction to OIM analysis. OIM Academy (2007)
[2] Beausir, B., Fressengeas, C., Gurao, N., Toth, L., Suwas, S.: Spacial correlation in grain misorientation distribution. Acta Materialia **57**, 5382–5395 (2009)
[3] Benveniste, Y.: A new approach to the application of Mori-Tanaka's theory in composite materials. Mechanics of Materials **6**(2), 147–157 (1987)
[4] Berbenni, S., Berveiller, M., Richeton, T.: Intra-granular plastic slip heterogeneities: Discrete vs. Mean Field approaches. International Journal of Solids and Structures **45**, 4147–4172 (2008)
[5] Berbenni, S., Favier, V., Lemoine, X., Berveiller, M.: Micromechanical modeling of the elastic-viscoplastic behavior of polycrystalline steels having different microstructures. Materials Science and Engineering **A 372**, 128–136 (2004)
[6] Berveiller, M., Fassi-Fehri, O., Hihi, A.: The problem of two plastic and heterogeneous inclusions in an anisotropic medium. International Journal of Engineering Science **25**(6), 691–709 (1987)
[7] Berveiller, M., Zaoui, A.: An extension of the self-consistent scheme to plastically flowing polycrystals. Journal of the Mechanics and Physics of Solids **26**, 325–344 (1979)
[8] Berveiller, M., Zaoui, A.: Modélisation de la déformation plastique des polycristaux. Techniques Ingénieur **M48**, 1–12 (2000)
[9] Brinck, A., Engelke, C., Kopmann, W., Neuhäuser, H.: Structure and development of slip lines during plastic deformation of the intermetallic phases Fe3Al and CuZn. Materials Science and Engineering **A 239-240**, 180–187 (1997)
[10] Collard, C., Favier, V., Berbenni, S., Berveiller, M.: Role of discrete intragranular slip bands on the strain-hardening of polycrystals. International Journal of Plasticity **26**, 310–328 (2010)
[11] Coupeau, C., Grilhe, J.: Quantitative analysis of surface effects of plastic deformation. Materials Science and Engineering **A271**, 242–250 (1999)
[12] DeWit, R.: The continuum theory of stationary dislocations. Solid State Physics **10**, 269–292 (1960)
[13] Eason, G., Noble, B., Sneddon, I.N.: On certain integrals of Lipschitz-Hankel type involving products of Bessel functions. Philosophical Transactions of the Royal Society of London A. Mathematical and Physical Sciences **247**(935), 529–551 (1955)
[14] Eshelby, J.: The determination of the elastic field of an ellipsoidal inclusion and related problems. Proceedings of the Royal Society London **A241**, 376 (1957)

[15] Eshelby, J.: The elastic field outside an ellipsoidal inclusion. Proceedings of the Royal Society London A **252**, 561–569 (1959)
[16] Essmann, U., Mughrabi, H.: Annihilation of dislocations during tensile tests and cyclic deformation and limit of dislocations densities. Philosophical Magazine **40**, 731,756 (1979)
[17] Fréchard, S., Martin, F., Clément, C., Cousty, J.: Afm and ebsd combined studies of plastic deformation in a duplex stainless steel. Materials Science and Engineering A **418**, 312–319 (2006)
[18] Hansen, N.: Polycrystalline strengthening. Metallurgical Transactions **16A**, 2167 (1985)
[19] Hill, R.: Continuum micro-mechanics of elastoplastic polycrystals. Journal of the Mechanics and Physics of Solids **13**, 89 (1965)
[20] Humphreys, F.J.: Review grain and subgrain characterisation by electron backscatter diffraction. Journal of Materials Science **36**, 3833–3854 (2001)
[21] Jaoul, B.: *Etude de la plasticité et application aux métaux*. Dunod (1965)
[22] Ju, J., Sun, L.: A novel formulation for the exterior point Eshelby's tensor of an ellipsoidal inclusion. ASME Journal of Applied Mechanics **66**, 570–574 (1999)
[23] Kamaya, M., Wilkinson, A., Titchmarsh, J.: Measurement of plastic strain of polycrystalline material by electron backscatter diffraction. Nuclear Engineering and Design **235**, 713–725 (2005)
[24] Kosevich, A.M.: Crystal dislocations and the theory of elasticity (chap. 1). In: Dislocations in Solids (vol 1), pp. 33–141. F.R.N. Nabarro (ed.), Amsterdam, North-Holland (1979)
[25] Kröner, E.: *Kontinuumstheorie der Versetzungen und Eigenspannungen*. Springer Verlag, Berlin (1958)
[26] Kröner, E.: Zur plastischen Verformung des Vielkristalls. Acta Metallurgica **9**, 155 – 161 (1961)
[27] Kröner, E.: Continuum theory of defects. In: Physics of defects, pp. 215–315. R. Balian and al. (Eds.), Les Houches, Session 35, North Holland, New York (1981)
[28] Kröner, E.: Modified Green functions in the theory of heterogeneous and/or anisotropic linearly elastic media. ed. G.J. Weng, M. Taya, M. Abe, Springer Verlag, Berlin Germany (1989)
[29] Margolin, H., Longo, R.: Slip band spacing in alpha titanium. Scripta Metallurgica **13**, 561–564 (1979)
[30] Margolin, H., Stanescu, M.: Polycrystalline strengthening. Acta Metallurgica **23**, 1411–1418 (1975)
[31] Masson, R., Bornert, M., Suquet, P., Zaoui, A.: An affine formulation for the prediction of the effective properties of non linear composites and polycrystals. Journal of the Mechanics and Physics of Solids **48**(6-7), 1203–1227 (2000)
[32] Maugin, G.A.: *The Thermomechanics of Plasticity and Fracture*. Cambridge University Press (1992)

[33] Maugin, G.A., Muschik, W.: Thermodynamics with internal variables: Part I. General concepts. Journal of Non-Equilibrium Thermodynamics **19**, 217–249 (1994)
[34] Meenen, J., Altenbach, H.: Statically equivalent solutions of refined plate theories. Mechanics of Composite Materials **34**(4), 331–342 (1998)
[35] Mori, T., Tanaka, K.: Average stress in matrix and average elastic energy of materials with misfitting inclusions. Acta Metallurgica **21**, 571–574 (1973)
[36] Mura, T.: *Micromechanics of Defects in Solids*. Kluwer Academic Publishers, Dordrecht, The Netherlands (1987)
[37] Neuhäuser, H.: Slip-line formation and collective dislocation motion. 6. ed. F.R.N. Nabarro, Holland Publishing Company (1983)
[38] Nye, J.F.: Some geometrical relations in dislocated crystals. Acta Metallurgica **1**, 153–162 (1953)
[39] Perrin, C., Berbenni, S., Vehoff, H., Berveiller, M.: Role of discrete intragranular slip on lattice rotations in polycrystalline Ni: experimental and micromechanical studies. Acta Materialia **58**, 4639–4649 (2010)
[40] Randle, V., Hansen, N., Jensen, D.J.: The deformation behaviour of grain boundary regions in polycrystalline aluminium. Philosophical Magazine A **73**(2), 265–282 (1996)
[41] Rice, J.R.: Continuum mechanics and thermodynamics plasticity in relation to microscale deformation mechanisms. In: Constitutive equations in plasticity, pp. 23–75. A.S. Argon (ed.), MIT Press, Cambridge (1975)
[42] Richeton, T., Berbenni, S., Berveiller, M.: Grain-size dependent accomodation due to intragranular distribution of dislocation loops. Acta Materialia **57**, 1347–1356 (2009)
[43] Sabar, H., Berveiller, M., Favier, V., Berbenni, S.: A new class of micro-macro models for elastic-viscoplastic heterogeneous materials. International Journal of Solids and Structures **39**, 3257–3276 (2002)
[44] Salamon, N.J., Walter, G.G.: Limits of Lipschitz-Hankel integrals. IMA Journal of Applied Mathematics **24**(3), 237–254 (1979)
[45] Scheriau, S., Pippan, R.: Influence of grain size on orientation changes during plastic deformation. Materials Science and Engineering A **493**, 48–52 (2008)
[46] Serre, I., Salazar, D., Vogt, J.B.: Atomic force microscopy investigation of surface relief in individual phases of deformed duplex stainless steel. Materials Science and Engineering A **492**, 428–433 (2008)
[47] Skjervold, S.R., Ryum, N.: Characterization of local texture in a moderately deformed polycrystalinne AlSi-alloy. Acta Metallurgica **43**, 3159–317 (1995)
[48] Villechaise, P., Sabatier, L., Girard, J.C.: On slip band features and crack initiation in fatigued 316L austenitic stainless steel: Part 1: Analysis by Electron Back-Scattered Diffraction and Atomic Force Microscopy. Materials Science and Engineering **A 323**, 377–385 (2002)
[49] Weng, G.J.: Some elastic properties of reinforced solids with special reference to isotropic ones containing spherical inclusions. International Journal of Engineering Science **22**(7), 845–856 (1984)

[50] Zaiser, M., Madani Grasset, F., Koutsos, V., Aifantis, E.C.: Self-affine surface morphology of plastically deformed metals. Physical Review Letters **93**, 195,507 (2004)

Chapter 6
Formulations of Strain Gradient Plasticity

Samuel Forest and Albrecht Bertram

Abstract In the literature, different proposals for a strain gradient plasticity theory exist. So there is still a debate on the formulation of strain gradient plasticity models used for predicting size effects in the plastic deformation of materials. Three such formulations from the literature are discussed in this work. The pros and the cons are pointed out at the light of the original solution of a boundary value problem that considers the shear deformation of a periodic laminate microstructure.

Key words: Strain gradient plasticity. Continuum thermodynamics. Laminates. Constrained plasticity.

6.1 Introduction

The objective of this work is to present three main formulations of strain gradient plasticity that are available in the literature and to illustrate the pros and the cons of these approaches by means of a specific example for which an analytical solution is derived. The targeted model is one of the most simple strain gradient plasticity model which serves as a paradigm for most available strain gradient theories, namely the well–known Aifantis model [1]. For that purpose we start from an initial plasticity model for which the set of degrees of freedom and of the state variables are defined as follows:

$$DOF0 = \{\underline{u}\} \quad STATE0 = \{\underset{\sim}{\varepsilon}, \quad \alpha\}$$

Samuel Forest
Mines ParisTech CNRS Centre des Matériaux UMR 7633, BP87 91003 Evry, France
e-mail: samuel.forest@ensmp.fr

Albrecht Bertram
Institut für Mechanik, Otto-von-Guericke-Universität, Universitätsplatz 2, 39106 Magdeburg, Germany
e-mail: albrecht.bertram@ovgu.de

H. Altenbach et al. (eds.), *Mechanics of Generalized Continua,*
Advanced Structured Materials, 7, DOI: 10.1007/978-3-642-19219-7_6,

The displacement degrees of freedom are denoted by the vector $\underline{u}$ from which the linear strain tensor $\underset{\sim}{\varepsilon}$ is derived. The hardening/softening properties of materials are accounted for by means of internal variables, α, that can be tensors of any rank[1]. Examples for such internal variables in the context of isotropic plasticity are

$$\alpha = p, \underset{\sim}{\varepsilon}^p, \underset{\sim}{X} ...$$

where $\underset{\sim}{\varepsilon}^p$ is the plastic strain tensor, p is the cumulative plastic strain, that will be used for isotropic hardening, and $\underset{\sim}{X}$, the kinematic hardening variable [2, 3]. The continuum thermomechanics framework with internal variables has been settled in [4, 5, 6]. Internal variables are computed by integrating the evolution equations that are time differential equations. It has already been recognized that these evolution equations may well result from approximations of more general partial differential equations where the spatial derivatives are neglected due to the rapid local variations [7]. The objective of gradient theories is therefore to restore the status of internal degree of freedom to internal variables. Depending on the order of the partial differential equations, additional boundary conditions are usually necessary to solve boundary value problems. In the following, we call

- *internal variables*: state variables, the evolution of which is controlled by time differential equations;
- *internal degrees of freedom*: state variables the evolution of which is controlled by time and space partial differential equations, without need for additional boundary conditions;
- *degrees of freedom*: variables (not necessarily state variables) controlled by a space and time partial differential equations, the resolution of which requires additional boundary conditions to be specified.

The question arises how to enlarge the space of state variables to the gradient of α–variables, so as to introduce characteristic lengths in the continuum modeling:

$$STATE = \{\underset{\sim}{\varepsilon}, \quad \alpha, \quad \nabla\alpha\}$$

Such a gradient term enters in particular Aifantis isotropic model that postulates the following evolution of the equivalent stress measure under plastic loading:

$$\sigma_{eq} = R_0 + Hp - c\nabla^2 p \tag{6.1}$$

where R_0 is the initial yield strength, H is the classical hardening modulus and c denotes the square of a characteristic length. Various attempts have been proposed in order to derive the Laplace term introduced in the yield function from a consistent thermomechanical setting. The first proposal in [8] will be recalled in Sect. 6.2.2. It is based on the introduction of an extra–entropy flux. In contrast, other authors have tried to circumvent the introduction of extra–entropy flux or extra energy terms by setting specific boundary conditions associated to the higher order partial differential equations, as shown in Sect. 6.2.1. An alternative approach is to formulate an

[1] In the present contribution, the variable α is treated as a scalar, for the sake of simplicity.

extended principle of virtual power, as initially proposed by [9] for damage variables. This amounts to raising the status of internal variable to additional degrees of freedom. This is the subject of Sect. 6.3 where the original principle of virtual power [10] is extended to gradient variables in the spirit of [11]. This track has been followed in the last ten years in the following works [12, 13, 14, 15].

Finally, a boundary value problem on a periodic two–phase laminate microstructure under shear loading conditions is solved in order to illustrate the new boundary or interface conditions and determine the variables which are discontinuous across the interface. This example has been originally handled for Cosserat and micromorphic single crystals in [16, 17], but it is solved here for the first time for the Aifantis model, so that comparisons will be drawn with other generalized continuum theories.

Throughout the work, for the sake of conciseness, the temperature θ is assumed to be uniform and constant.

6.2 Derivation Based on the Exploitation of the Entropy Principle

In this section, the energy principle is assumed to hold in its usual local form

$$\dot{e} = \mathscr{P}^{(i)}, \quad \text{with} \quad \mathscr{P}^{(i)} = \underset{\sim}{\sigma} : \dot{\underset{\sim}{\varepsilon}} \tag{6.2}$$

where e is the internal energy density and $\mathscr{P}^{(i)}$ the usual power density of internal forces. The Helmholtz free energy density, $\psi = e - \eta\theta$, is assumed to depend on the already defined set $STATE$ and we give the following names to the partial derivatives with respect to α and its gradient:

$$\psi = e - \theta\eta\,, \quad a = -\frac{\partial \psi}{\partial \alpha}, \quad \underline{b} = -\frac{\partial \psi}{\partial \nabla \alpha} \tag{6.3}$$

where η is the entropy density function.

6.2.1 Vanishing Generalized Tractions

The entropy principle is now postulated first in its global form on the material domain V

$$\int_V \theta \dot{\eta}\, dV \geq 0$$

and converted into the Clausius–Duhem inequality

$$\int_V \left(\mathscr{P}^{(i)} - \dot{\psi} \right) dV \geq 0 \tag{6.4}$$

$$\int_V \left[\left(\underset{\sim}{\sigma} - \frac{\partial \psi}{\partial \underset{\sim}{\varepsilon}} \right) : \dot{\underset{\sim}{\varepsilon}} + a\dot{\alpha} + \underline{b} \cdot \nabla \dot{\alpha} \right] dV \geq 0 \tag{6.5}$$

in the absence of extra–entropy flux. The global Clausius–Duhem inequality is transformed in the following way:

$$\int_V \left[\left(\underset{\sim}{\sigma} - \frac{\partial \psi}{\partial \underset{\sim}{\varepsilon}} \right) : \dot{\underset{\sim}{\varepsilon}} + a\dot{\alpha} - \dot{\alpha} \mathrm{div}\, \underline{b} + \mathrm{div}\,(\dot{\alpha}\underline{b}) \right] dV \geq 0 \tag{6.6}$$

$$\int_V \left[\left(\underset{\sim}{\sigma} - \frac{\partial \psi}{\partial \underset{\sim}{\varepsilon}} \right) : \dot{\underset{\sim}{\varepsilon}} + (a - \mathrm{div}\, \underline{b})\dot{\alpha} \right] dV + \int_{\partial V} \dot{\alpha} \underline{b} \cdot \underline{n}\, dS \geq 0 \tag{6.7}$$

It is temptating to assume at this stage that the flux of $\underline{b}$ vanishes at the boundary of the domain V

$$\underline{b} \cdot \underline{n} = 0, \quad \forall \underline{x} \in \partial V \tag{6.8}$$

This condition corresponds to a Neumann extra–boundary condition for the partial differential equation for α. It follows that the residual dissipation takes the following canonical form involving the rate of the α–variable and the associated thermodynamical force and dissipation potential

$$\int_V \mathscr{A} \dot{\alpha}\, dV \geq 0, \quad \mathscr{A} := a - \mathrm{div}\, \underline{b} \tag{6.9}$$

in addition to the state law $\underset{\sim}{\sigma} = \partial \psi / \partial \underset{\sim}{\varepsilon}$.
Positivity of dissipation can then be ensured by the choice of a convex dissipation potential Ω providing the evolution equation for α:

$$\dot{\alpha} = \frac{\partial \Omega}{\partial \mathscr{A}} \tag{6.10}$$

This condition of vanishing flux at a boundary is discussed in [18] in the context of generalized standard gradient models.

On which domain V of the material body should the previous reasoning be applied? In principle, the thermodynamical statements are to be applied to each subdomain of the body. But it is hard to believe that the condition of vanishing generalized traction will be applied to the boundary of any subdomain. This point will be checked in the analytical example of Sect. 6.4. In the literature, the condition is usually limited to the outer boundary of the considered body (so–called *insulation condition* in [19]), or at the boundary of the part of the body which undergoes plastic loading. The latter applies to the finite element implementation of such gradient models, as proposed in [20].

6.2.2 Extra–entropy Flux

In general, according to the thermodynamics of irreversible processes [6], an extra–entropy flux in the entropy inequality cannot be excluded. It is introduced in the form of the vector field $\underline{k}$ in the local form of the entropy imbalance:

$$\dot{\eta} + \operatorname{div} \underline{k} \geq 0 \tag{6.11}$$

In the isothermal case, the Clausius–Duhem inequality then takes the form:

$$\mathscr{P}^{(i)} - \dot{\psi} + \operatorname{div} \theta \underline{k} \geq 0 \tag{6.12}$$

The exploitation of Clausius–Duhem inequality continues as follows:

$$(\underset{\sim}{\sigma} - \frac{\partial \psi}{\partial \underset{\sim}{\varepsilon}}) : \dot{\underset{\sim}{\varepsilon}} + a\dot{\alpha} + \underline{b} \cdot \nabla \dot{\alpha} + \operatorname{div} \theta \underline{k} \geq 0 \tag{6.13}$$

$$(\underset{\sim}{\sigma} - \frac{\partial \psi}{\partial \underset{\sim}{\varepsilon}}) : \dot{\underset{\sim}{\varepsilon}} + (a - \operatorname{div} \underline{b})\dot{\alpha} + \operatorname{div} (\dot{\alpha} \underline{b} + \theta \underline{k}) \geq 0 \tag{6.14}$$

At this point, the following astute choice of the extra–entropy flux is proposed in [8]

$$\underset{\sim}{\sigma} = \frac{\partial \psi}{\partial \underset{\sim}{\varepsilon}}, \quad \underline{k} := -\frac{\dot{\alpha}}{\theta} \underline{b} \tag{6.15}$$

With this choice, the residual dissipation reduces to the same form as (6.9), so that again a dissipation potential $\Omega(\mathscr{A})$ can be introduced, thus setting the framework of standard generalized gradient models. The difference compared to the previous approach is that no restriction arises in the derivation concerning the additional boundary condition to solve (6.1). As a result, the flux $\underline{b} \cdot \underline{n}$ can take any needed values at boundaries and interfaces. The approach provides no indication nor restrictions on the necessary boundary conditions.

6.3 Derivation Based on the Modification of the Energy Principle

An alternative to the previous approaches is to consider that the introduction of mechanical gradient effects must be accompanied by a modification of the power of internal forces which enters the principle of virtual power. When higher order gradients of the displacement field exist like in Mindlin's second gradient theory [11, 21, 22] or gradients of additional degrees of freedom, like in Eringen's micromorphic model [23], the power of internal variable is extended to include a power induced by the higher order gradients or the gradients of additional degrees of freedom. Let us consider for instance Mindlin's second gradient model which incorporates the effect of the strain gradient $\nabla \underset{\sim}{\varepsilon}$. The stress conjugate of the strain rate

gradient in the power of internal forces is the third rank double stress tensor. If the strain is decomposed into elastic and plastic contributions,

$$\underset{\sim}{\varepsilon} = \underset{\sim}{\varepsilon}^e + \underset{\sim}{\varepsilon}^p, \tag{6.16}$$

one may consider materials for which most of the gradient effects come from $\nabla\underset{\sim}{\varepsilon}^p$, so that the effect of $\nabla\underset{\sim}{\varepsilon}^e$ can be neglected. The latter term disappears but the triple contraction of the double stress and of the gradient of plastic strain remains. This suggests that when the gradient of α–variables is considered, one is entitled to introduce a corresponding internal power. This approach is presented in this section and has been followed in the references [9, 12, 15] for gradient of damage and plasticity models.

We introduce the enriched power density of internal forces and of contact forces

$$\mathscr{P}^{(i)} = \underset{\sim}{\sigma} : \dot{\underset{\sim}{\varepsilon}} + a\dot{p} + \underline{b} \cdot \nabla\dot{p}, \quad \mathscr{P}^{(c)} = \underline{t} \cdot \dot{\underline{u}} + a^c\dot{p} \tag{6.17}$$

where a and $\underline{b}$ are generalized stresses acting on the virtual field α and its gradient, respectively. The usual traction vector is $\underline{t}$ and a^c denotes the generalized traction. Such generalized stresses are called micro–forces in [14]. A generalized principle of virtual power is stated with respect to the virtual fields of displacements and the α–variable. The methodology originates from the works [10, 22] and was extended to generalized continua in [13, 24]. The application of this principle results in an additional balance equation, complementing the usual balance of momentum equation:

$$\operatorname{div}\underset{\sim}{\sigma} = 0, \quad a = \operatorname{div}\underline{b}, \quad \forall \underline{x} \in V \tag{6.18}$$

written here in the static case and in the absence of body forces. The corresponding equilibrium conditions at the boundaries are:

$$\underline{t} = \underset{\sim}{\sigma} \cdot \underline{n}, \quad a^c = \underline{b} \cdot \underline{n}, \quad \forall \underline{x} \in \partial V \tag{6.19}$$

An essential feature of the model is that the extended power of internal forces intervenes in the energy balance equation:

$$\dot{e} = \mathscr{P}^{(i)} \tag{6.20}$$

thus including the additional contributions of generalized stresses. This also holds for the entropy principle in its local form:

$$\mathscr{P}^{(i)} - \dot{\psi} \geq 0 \tag{6.21}$$

The Clausius–Duhem inequality then becomes:

$$(\underset{\sim}{\sigma} - \frac{\partial\psi}{\partial\underset{\sim}{\varepsilon}^e}) : \dot{\underset{\sim}{\varepsilon}}^e + (a - \frac{\partial\psi}{\partial\alpha})\dot{\alpha} + (\underline{b} - \frac{\partial\psi}{\partial\nabla\alpha}) \cdot \nabla\dot{\alpha} + \underset{\sim}{\sigma} : \dot{\underset{\sim}{\varepsilon}}^p \geq 0 \tag{6.22}$$

At this stage, we adopt the following state laws

$$\underset{\sim}{\sigma} = \frac{\partial \psi}{\partial \underset{\sim}{\varepsilon}^e}, \quad a = \frac{\partial \psi}{\partial \alpha} - R, \quad \underline{b} = \frac{\partial \psi}{\partial \nabla \alpha} \tag{6.23}$$

thus assuming that no dissipation is associated with the generalized stress $\underline{b}$. This is the most simple assumption that is sufficient for deriving Aifantis model, in particular. R is the dissipative part of generalized stress a.

At this point it is more convenient to specify the internal variable that is required to derive Aifantis model. We adopt: $\alpha \equiv p$, so that the considered internal variable is the cumulative plastic strain. The residual dissipation is then

$$\underset{\sim}{\sigma} : \dot{\underset{\sim}{\varepsilon}}^p - R\dot{p} \geq 0 \tag{6.24}$$

Let us choose a simple quadratic free energy potential

$$\psi(\underset{\sim}{\varepsilon}^e, p, \nabla p) = \frac{1}{2}\underset{\sim}{\varepsilon}^e : \underset{\approx}{C} : \underset{\sim}{\varepsilon}^e + \frac{1}{2}Hp^2 + \frac{1}{2}c\nabla p \cdot \nabla p \tag{6.25}$$

from which the state laws are derived:

$$\underset{\sim}{\sigma} = \underset{\approx}{C} : \underset{\sim}{\varepsilon}^e, \quad R = Hp - a, \quad \underline{b} = c\nabla p \tag{6.26}$$

where $\underset{\approx}{C}$ is the four–rank tensor of the elastic moduli, H is the usual hardening modulus and c is an additional material parameter (unit MPa.mm^2). The yield function is taken as

$$f(\underset{\sim}{\sigma}, R) = \sigma_{eq} - R_0 - R \tag{6.27}$$

Under plastic loading, this gives

$$\sigma_{eq} = R_0 + R = R_0 + Hp - a = R_0 + Hp - \mathrm{div}\,\underline{b} = R_0 + Hp - c\nabla^2 p \tag{6.28}$$

so that Aifantis equation (6.1) is recovered. The plasticity flow and evolution rules are

$$\dot{\underset{\sim}{\varepsilon}}^p = \dot{\lambda}\frac{\partial f}{\partial \underset{\sim}{\sigma}}, \quad \dot{p} = -\dot{\lambda}\frac{\partial f}{\partial R} = \dot{\lambda} \tag{6.29}$$

with λ being the plastic multiplier. These equations are used in the next section to solve a specific boundary value problem.

6.4 Analysis of a Simple Boundary Value Problem for Laminate Microstructures

Laminate microstructures are prone to size effects especially in the case of metals for which the interfaces act as barriers for the dislocations. The material response then strongly depends on the layer thickness. This situation has been considered for Cosserat and micromorphic single crystals under single and double slip in [16,

17]. The laminate microstructure is considered here in the case of Aifantis isotropic model. It is a periodic arrangement of two phases including a purely elastic material and a plastic strain gradient layer. The unit cell corresponding to this arrangement is shown in Fig. 6.1. It is periodic along all three directions of the space. It must must be replicated in the three directions so as to obtain the complete multilayer material. The thickness of the hard elastic layer is h, whereas the thickness of the soft plastic strain gradient layer is s.

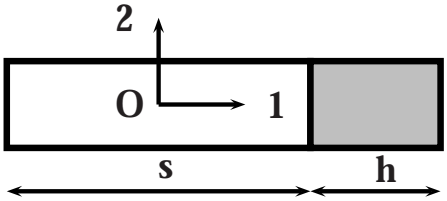

Fig. 6.1 Unit cell of a periodic two–phase laminate.

6.4.1 Position of the Problem

The unit cell of Fig. 6.1 is subjected to a mean simple shear $\bar{\gamma}$ in direction 1. The origin O of the coordinate system is the center of the soft phase. The displacement field is of the form

$$u_1 = \bar{\gamma}\, x_2, \;\; u_2(x_1) = u(x_1), \;\; u_3 = 0 \tag{6.30}$$

where $u(x_1)$ is a periodic function which describes the fluctuation from the homogeneous shear. This fluctuation is the main unknown of the boundary value problem. We compute the gradient of the displacement field and strain tensors:

$$[\nabla \underline{u}] = \begin{bmatrix} 0 & \bar{\gamma} & 0 \\ u_{,1} & 0 & 0 \\ 0 & 0 & 0 \end{bmatrix}, \quad [\underset{\sim}{\varepsilon}] = \begin{bmatrix} 0 & \frac{1}{2}(\bar{\gamma}+u_{,1}) & 0 \\ \frac{1}{2}(\bar{\gamma}+u_{,1}) & 0 & 0 \\ 0 & 0 & 0 \end{bmatrix} \tag{6.31}$$

where $u_{,1}$ denotes the derivative of the displacement u with respect to x_1. After Hooke's law, the only activated simple stress component is σ_{12}. Due to the balance of momentum equation and the continuity of the traction vector, this stress component is homogeneous throughout the laminate.

The elastic law in the elastic phase and the elastic–plastic response of the soft phase are then exploited in the next section to derive the partial differential equations for plastic strain and, finally, for the displacement fluctuation. The explicit solution is found after considering precise interface conditions regarding continuity of various variables.

Note that the solution is known for conventional plasticity, i.e. in the absence of strain gradient effect. The plastic strain is expected to be homogeneous in the soft phase for any loading $\bar{\gamma}$. Plastic strain therefore exhibits the usual jump at the interface. The introduction of higher order interface conditions, associated with strain gradient plasticity, will induce a non–homogeneous plasticity field.

6.4.2 Analytical Solution

Assuming plastic loading in the soft phase, the von Mises criterion is fulfilled:

$$\sqrt{3}|\sigma_{12}| = R_0 + Hp - cp_{,11} \tag{6.32}$$

Since the stress component σ_{12} is uniform, the previous equation can be differentiated with respect to x_1, which gives:

$$p_{,1} - \omega^{-2} p_{,111} = 0, \quad \omega^2 = \frac{H}{c} \tag{6.33}$$

The form of the plastic strain field therefore is

$$p = \alpha \cosh(\omega x_1) + \beta \tag{6.34}$$

where α and β are integration constants. In the elastic zone, the stress is given by

$$\sigma_{12} = \mu(\bar{\gamma} + u^h_{,1}) \quad \Longrightarrow \quad u^h_{,1} = C \tag{6.35}$$

where the uniformity of stress has been used again. An additional integration constant C must be determined. The exponent ^{h} has been added to indicate the displacement fluctuation inside the elastic phase. The arbitrary translation for u^h will be set to zero. The field u^s can be determined from the elasticity law in the soft phase:

$$\sigma_{12} = \mu(\bar{\gamma} u^s_{,1} - \sqrt{3}p) \tag{6.36}$$

An additional constant D arises from the integration of this equation, that remains to be determined.

The four unknown integration constants α, β, C, D will be determined from 4 conditions at the interface between both materials at $x_1 = \pm s/2$:

- Continuity of simple traction:

$$\sqrt{3}\mu(\bar{\gamma} + C) = R_0 + H\beta \tag{6.37}$$

- Continuity of displacement $u(x_1)$ at $s/2$:

$$u^s\left(\frac{s}{2}\right) = u^h\left(\frac{s}{2}\right) \tag{6.38}$$

$$u^h(x_1) = Cx_1, \quad u^s(x_1) = \left[\frac{R_0}{\mu\sqrt{3}} + (\frac{H}{\mu\sqrt{3}} + \sqrt{3})\beta - \bar{\gamma}\right] x_1 + \frac{\sqrt{3}\alpha}{\omega}\sinh(\omega x_1) + D \tag{6.39}$$

- Periodicity of displacement $u(x_1)$:

$$u^s\left(-\frac{s}{2}\right) = u^h\left(\frac{s}{2} + h\right) \tag{6.40}$$

- Continuity of plastic strain p at the interface $x_1 = \frac{s}{2}$

$$p\left(\frac{s}{2}\right) = 0 \tag{6.41}$$

$$\alpha\cosh\left(\omega\frac{s}{2}\right) + \beta = 0 \tag{6.42}$$

The last condition is necessary to close the system. Differentiability and hence continuity of plastic strain p is required in strain gradient plasticity theory. In the elastic phase, $p = 0$ so that p should also vanish at the interface.

The identification of the constants provides:

$$\beta = \frac{\left(\bar{\gamma} - \frac{R_0}{\mu\sqrt{3}}\right)(s+h)}{\frac{H}{\mu\sqrt{3}}(s+h) + \sqrt{3}s - \tanh(\omega\frac{s}{2})\frac{2\sqrt{3}}{\omega}} \tag{6.43}$$

$$\alpha = -\frac{\beta}{\cosh(\omega\frac{s}{2})} \tag{6.44}$$

$$C = \frac{R_0}{\mu\sqrt{3}} - \bar{\gamma} + \frac{H}{\sqrt{3}\mu}\beta \tag{6.45}$$

$$D = C\frac{s}{2} - \left[\frac{R_0}{\mu\sqrt{3}} + (\frac{H}{\mu\sqrt{3}} + \sqrt{3})\beta - \bar{\gamma}\right]\frac{s}{2} - \frac{\sqrt{3}\alpha}{\omega}\sinh\left(\omega\frac{s}{2}\right) \tag{6.46}$$

where homogeneous elasticity has been assumed for simplicity, with μ being the shear modulus of both phases.

As a result, we find that the double traction cannot vanish on the soft side of the interface, $x_1 = s^-/2$.

$$b_1(x_1) = c\alpha\sinh(\omega x_1), \quad b_1(\frac{s^-}{2}) = c\alpha\sinh\left(\omega\frac{s}{2}\right) \neq 0 \tag{6.47}$$

In the elastic phase, the generalized stress identically vanishes since no plastic strain occurs. It follows that the generalized traction b_1 exhibits a jump across the interface.

We illustrate the previous solution for a special choice of material parameters oriented towards plasticity of metals at the micron scale. The parameters used in the simulations are:

$$s = 0.007 \text{ mm}, \; h = 0.003 \text{ mm}, \; \bar{\gamma} = 0.01,$$
$$\mu = 300 \text{ GPa}, \; R_0 = 20 \text{ MPa}, \; H = 10 \text{ GPa}, \; c = 0.005 \text{ MPa.mm}^2.$$

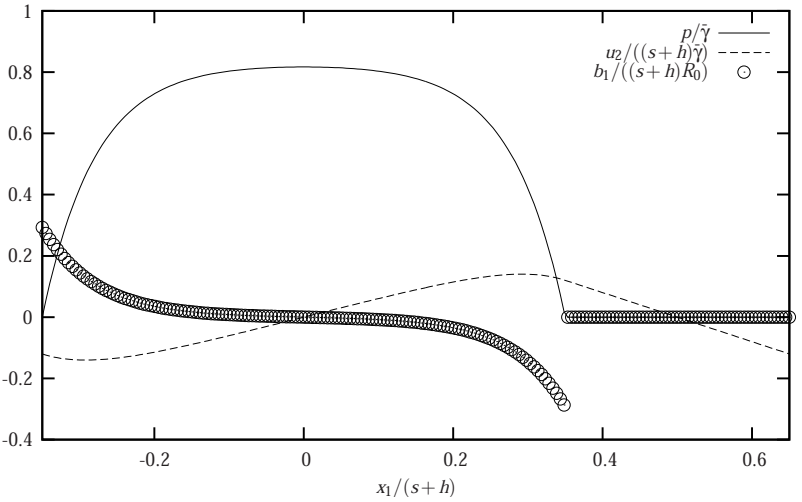

Fig. 6.2 Distributions of plastic strain, normalized displacement fluctuation and normalized generalized stress vector component in the unit cell of the laminate microstructure.

The distribution of plastic slip, of displacement and of generalized stress component b_1 are shown in Fig. 6.2. The plastic strain displays a typical *cosh* profile with boundary layer effects close to the interface, due to the continuity requirement. The displacement fluctuation is clearly periodic. The jump of the generalized traction at the interface is also visible.

6.5 Discussion

Three different formulations of strain gradient plasticity have been reported in this contribution. The first model is based on the assumption of vanishing general traction at the boundary of some domain and in particular, as advocated by several authors, at the interface between the elastic and plastic loading domain. The example of the laminate microstructure considered in Sect. 6.4 clearly shows that this assumption cannot be valid systematically. Indeed, if a condition of vanishing double traction is imposed on the interface $x_1 = s/2$ in the laminate microstructure, this amounts to prescribe vanishing of the plastic strain and its first derivative at the interface. Accordingly, the solution of the equation (6.33) yields $p = Cst$, which is the standard solution in classical plasticity.

The presented analytical example is compatible with the second formulation of strain gradient plasticity based on the introduction of an additional entropy flux.

The third approach based on the introduction of the extended power of internal forces has the advantage that it provides a variational formulation of the strain gradient plasticity boundary value problem in the form of a generalized principle of

virtual power. This has a direct implication on the numerical treatment by means of the finite element method for instance. In the finite element implementation, the plastic strain is handled as an additional degree of freedom. The power of internal forces is discretized in space and the generalized stresses are computed from the constitutive equations (6.26). The plastic multiplier is computed by taking the enhanced hardening rule into account [24]. A Lagrange multiplier is then needed to ensure that the additional degree of freedom coincides with the time integrated cumulative plastic strain. The additional boundary condition arises naturally from the finite element formulation, the reaction to the nodal degrees of freedom being related to the generalized traction.

It seems that there is a real necessity for an energy cost associated with the development of the plastic strain gradient. Finite element simulations are presented in literature that include the plastic strain gradient, computed at the end of the increment, in the hardening rule. They do not consider generalized stresses nor associated additional boundary conditions. Such a procedure is known to lead to mesh–dependent results even in the hardening regime [25]. This pleads for the adoption of the third proposed approach to strain gradient plasticity.

References

[1] E. C. Aifantis: On the microstructural origin of certain inelastic models, Journal of Engineering Materials and Technology **106** (1984) 326–330
[2] A. Bertram: *Elasticity and Plasticity of Large Deformations*, Springer, 2005.
[3] J. Besson, G. Cailletaud, J.-L. Chaboche, S. Forest, M. Blétry: *Non–Linear Mechanics of Materials*, Series: Solid Mechanics and Its Applications , Vol. 167 , Springer (2009)
[4] P. Germain, Q. S. Nguyen, P. Suquet: Continuum thermodynamics, J. of Applied Mechanics **50** (1983) 1010–1020
[5] G. A. Maugin, W. Muschik: Thermodynamics with internal variables, Part I. General concepts, J. Non-Equilib. Thermodyn. **19** (1994) 217–249
[6] G. A. Maugin: *Thermomechanics of nonlinear irreversible behaviors*, World Scientific (1999)
[7] F. Sidoroff: Microstructure and plasticity, Mech. Res. Comm. **2** (1975) 73–77
[8] G. A. Maugin: Internal variables and dissipative structures, J. Non–Equilib. Thermodyn. **15** (1990) 173–192
[9] M. Frémond, B. Nedjar: Damage, gradient of damage and principle of virtual power, Int. J. Solids Structures **33** (1996) 1083–1103
[10] G. A. Maugin: The method of virtual power in continuum mechanics: Application to coupled fields, Acta Mechanica **35** (1980) 1–70
[11] A. Bertram, S. Forest: Mechanics based on an objective power functional, Technische Mechanik **27** (2007) 1–17

[12] S. Forest, R. Sievert, E. C. Aifantis: Strain gradient crystal plasticity: Thermomechanical formulations and applications, Journal of the Mechanical Behavior of Materials **13** (2002) 219–232
[13] S. Forest, R. Sievert: Elastoviscoplastic constitutive frameworks for generalized continua, Acta Mechanica **160** (2003) 71–111
[14] M. E. Gurtin: On a framework for small–deformation viscoplasticity: free energy, microforces, strain gradients, International Journal of Plasticity **19** (2003) 47–90
[15] M. E. Gurtin, L. Anand: Thermodynamics applied to gradient theories involving the accumulated plastic strain: The theories of Aifantis and Fleck & Hutchinson and their generalization, Journal of the Mechanics and Physics of Solids **57** (2009) 405–421
[16] S. Forest: Some links between Cosserat, strain gradient crystal plasticity and the statistical theory of dislocations, Philosophical Magazine **88** (2008) 3549–3563
[17] N. M. Cordero, A. Gaubert, S. Forest, E. Busso, F. Gallerneau, S. Kruch: Size effects in generalised continuum crystal plasticity for two–phase laminates, Journal of the Mechanics and Physics of Solids, in press.
[18] Q. S. Nguyen: On standard dissipative gradient models, to appear in Annals of Solid and Structural Mechanics.
[19] C. Polizzotto, G. Borino: A thermodynamics-based formulation of gradient-dependent plasticity, Eur. J. Mech., A/Solids **17** (1998) 741–761
[20] T. Liebe, A. Menzel, P. Steinmann: Theory and numerics of geometrically non-linear gradient plasticity, International Journal of Engineering Science **41** (2003) 1603–1629
[21] R. D. Mindlin, N. N. Eshel: On first strain gradient theories in linear elasticity, Int. J. Solids Structures **4** (1968) 109–124
[22] P. Germain: La méthode des puissances virtuelles en mécanique des milieux continus, première partie : théorie du second gradient, J. de Mécanique **12** (1973) 235–274
[23] A. C. Eringen: *Microcontinuum Field Theories*, Springer, New York (1999)
[24] S. Forest: The micromorphic approach for gradient elasticity, viscoplasticity and damage, ASCE Journal of Engineering Mechanics **135** (2009) 117–131
[25] C. F. Niordson, J. W. Hutchinson: On lower order strain gradient plasticity theories, European Journal of Mechanics A/Solids **22** (2003) 771–778

Chapter 7
On one Model of Generalized Continuum and its Thermodynamical Interpretation

Elena A. Ivanova

Abstract We consider the mechanical model of a two-component medium whose first component is a classical continuum and the other one is a continuum having only rotational degrees of freedom. We show that the proposed model can be used for the description of thermal and dissipative phenomena. It is the presence of additional rotational degrees of freedom and, accordingly, additional inertia and elastic characteristics which can be interpreted as thermodynamical material parameters that distinguish the proposed model among other continuum models. In special cases the mathematical description of the proposed model is proved to reduce to the well-known equations such as the heat conduction, the self-diffusion and the coupled thermoelastic equations. The mathematical description of the proposed mechanical model includes not only the classical formulation of the coupled problem of thermoelasticity but also the formulation of the coupled problem of thermoelasticity with the hyperbolic type heat conduction equation. In the context of the introduced theory we consider the original model of internal damping.

Key words: Micropolar media. Two-component continuum. Hyperbolic thermoviscoelasticity.

7.1 Introduction

At present thermodynamics covers widespread frame including gas dynamics, thermoelasticity, thermoviscoelasticity, thermoelectric and thermomagnetic phenomena, phase changes and chemical reactions. At the same time it constitutes a set of scientific areas which are not connected to each other and differ by both the inter-

Elena A. Ivanova
Institute for Problems in Mechanical Engineering of the Russian Academy of Sciences, Bolshoy pr. V.O., 61, 199178, Saint Petersburg, Russia
e-mail: elenaivanova239@post.ru

H. Altenbach et al. (eds.), *Mechanics of Generalized Continua,*
Advanced Structured Materials, 7, DOI: 10.1007/978-3-642-19219-7_7,

pretation of the fundamental concepts and the applied mathematical methods. Dealing with the mathematical methods we should refer to the thermodynamic potential theory underlying the chemical and electrochemical thermodynamics, continuum mechanics within the framework of which the models of thermoelastic and thermoviscoelastic media have been developed, the methods of crystal lattice dynamics underlying the description of transport phenomena in solids, and also the classical and quantum statistics [1, 2]. In view of the aforesaid it is important to develop a unified theory for the description of all thermodynamical phenomena which are studied now in different science areas by using various methods. We are firmly convinced that it can be made on the basis of the fundamental laws of mechanics by using the continuum mechanics methods. The idea of the mathematical description of various physical phenomena in microcosm by using the continual models based on rotational degrees of freedom and the moment interactions was repeatedly asserted by P. A. Zhilin [3, 4, 5, 6] and other authors – see e. g. [7, 8, 9]. The model proposed in the present paper is a realization of this idea as applied to the description of thermal and dissipative phenomena.

There exist different macroscopic and microscopic models of internal damping [2, 10, 11, 12, 13]. The point of view that internal damping is concerned with thermal effects is widespread. According to the quantum theory [2], the distribution of phonons is in a local thermodynamical equilibrium and the temperature changes adiabatically, when acoustic wave propagates. Consequently, regions separated by the half-wavelength distance from one another have different temperatures and the irreversible heat flow between these regions arises as a result of the heat conduction phenomena. This process causes transfer of energy of mechanical vibrations into heat energy. We do not call in question the idea about interplay of the internal damping and thermal effects. We emphasize that analysis of the experimental values of the volume (acoustic) viscosity and the shear viscosity of various substances shows that the viscosities are independent substance characteristics which are not related to the heat-conduction coefficient and other thermodynamical parameters [14, 15, 16, 17]. However, we are sure that the internal damping and the heat conduction mechanism have the same physical nature. In our opinion the internal damping and heat conduction should be considered as a result of the interaction of atoms with the infinite surrounding medium which can be called the “thermal field” or the “thermal ether”. We propose the mechanical model “thermal ether” which is a continuum of particles having translational and rotational degrees of freedom and interacting by elastic moments. We consider two problems of elastic interaction of the “thermal ether” with the particle having a special structure. As a result of analysis of the problems we show that the influence of the “thermal ether” on the particle can be modeled by the damping moment proportional to the angular moment of the particle. Using of the damping moment in the model of a two-component medium allows us to describe the internal damping and the heat conduction mechanism.

7.2 The Simplest Model of a Body-point

We consider the material system (see Fig. 7.1) consisting of the frame and N rigid bodies attached to the frame by means of elastic springs. For simplicity we suppose that all bodies can move only in the line of axis x and rotate only on axis x. We introduce following notations: m, J, x, φ are the mass, the moment of inertia, the displacement and the angle of rotation of the frame; m_i, J_i are the mass and the moment of inertia of rigid body number i; x_i, φ_i are the displacement and the angle of rotation of rigid body number i relative to the frame. The springs are considered to be elastic helical lines whose properties consist in the fact that when twisting in one direction they become longer and when twisting in the opposite direction they shorten. Conformably, when stretching and pressing the springs they become twisted in different directions. We suppose that the internal energy U_i of spring number i as well as the force F_i and the twisting moment M_i modeling the influence of spring number i on the frame take the form:

$$U_i = U_i(x_i + \chi\varphi_i), \qquad F_i = \frac{\partial U_i}{\partial x_i}, \qquad M_i = \frac{\partial U_i}{\partial \varphi_i}, \tag{7.1}$$

where χ is the coefficient, characterizing the difference of the elastic spring under consideration from analogous spring possessing axial symmetry. Objects similar to considered spring are usually called chiral objects. Therefore we call χ by coefficient of chirality.

As evident from Eqs (7.1), the force and the twisting moment can be represented by means of the derivative of the internal energy with respect to its argument $x_i + \chi\varphi_i$[1]. As a result the simple relation between M_i and F_i can be brought to light:

$$F_i = U_i', \qquad M_i = \chi U_i' \qquad \Rightarrow \qquad M_i = \chi F_i. \tag{7.2}$$

The equations of motion of the frame have the form:

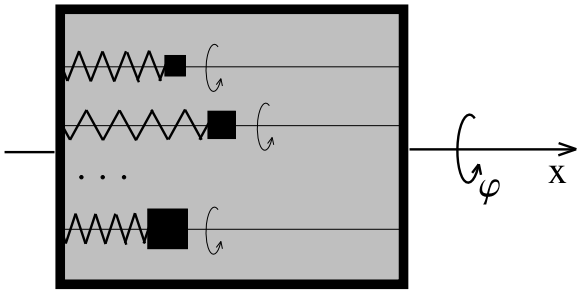

Fig. 7.1 Particle possessing the internal structure

[1] In what follows we denote this derivative by prime.

$$m\ddot{x} = F + \sum_{i=1}^{N} F_i, \qquad J\ddot{\varphi} = M + \sum_{i=1}^{N} M_i, \tag{7.3}$$

where F and M are the external force and the external twisting moment acting on the frame. The equations of motion of the rigid bodies are:

$$m_i(x+x_i)^{\cdot\cdot} = -F_i, \qquad J_i(\varphi+\varphi_i)^{\cdot\cdot} = -M_i, \qquad i = \overline{1,N}. \tag{7.4}$$

The analysis of Eqs (7.3) and (7.4) shows that translational and rotational motion of the frame are interdependent. If there is no external moment acting on the frame and the initial angular velocity is equal to zero, then because of the internal dynamics of the system the frame starts rotating. If there is no external force acting on the frame and the initial velocity is equal to zero, then because of the internal dynamics of the system the frame starts moving.

Example 1. We consider the free motion of the system, represented in Fig. 7.1. Let us introduce notations for total inertia characteristics of the internal bodies of the system:

$$m_* = \sum_{i=1}^{N} m_i, \qquad J_* = \sum_{i=1}^{N} J_i. \tag{7.5}$$

For simplicity we suppose that all rigid bodies have the same masses $m_i = m_*/N$ and the same moments of inertia $J_i = J_*/N$. Moreover, we suppose that the internal energies of the springs U_i are the quadratic forms of deformations and all springs have stiffness equal c. In that case:

$$U_i = c\,(x_i + \chi\varphi_i)^2 \qquad \Rightarrow \qquad F_i = c\,(x_i + \chi\varphi_i), \qquad M_i = \chi c\,(x_i + \chi\varphi_i). \tag{7.6}$$

Taking into account Eqs (7.6) we rewrite the equations of motion of the rigid bodies (7.4) in the form:

$$\frac{m_*}{N}\,(x+x_i)^{\cdot\cdot} = -c\,(x_i+\chi\varphi_i), \qquad \frac{J_*}{N}\,(\varphi+\varphi_i)^{\cdot\cdot} = -\chi c\,(x_i+\chi\varphi_i). \tag{7.7}$$

From Eqs (7.7) we obtain:

$$(x_i+\chi\varphi_i)^{\cdot\cdot} + k_*^2\,(x_i+\chi\varphi_i) = -(x+\chi\varphi)^{\cdot\cdot}, \qquad k_*^2 = Nc\left(\frac{1}{m_*} + \frac{\chi^2}{J_*}\right). \tag{7.8}$$

Provided that $F = 0$, $M = 0$ and F_i, M_i satisfy Eqs (7.6) the equations of the motion of the frame (7.3) take the form:

$$m\ddot{x} = c\sum_{i=1}^{N}(x_i+\chi\varphi_i), \qquad J\ddot{\varphi} = \chi c\sum_{i=1}^{N}(x_i+\chi\varphi_i). \tag{7.9}$$

The system of equations (7.9) can be rewritten in the more convenient form, namely in the form of equation

$$m\ddot{x} = \frac{J}{\chi}\,\ddot{\varphi}, \tag{7.10}$$

and equation

$$(x+\chi\varphi)^{\cdot\cdot} = \frac{\tilde{k}^2}{N}\sum_{i=1}^{N}(x_i+\chi\varphi_i), \qquad \tilde{k}^2 = Nc\left(\frac{1}{m}+\frac{\chi^2}{J}\right). \tag{7.11}$$

From Eqs (7.8) and (7.11) we obtain the equation in $x+\chi\varphi$:

$$(x+\chi\varphi)^{\cdot\cdot\cdot\cdot} + k^2(x+\chi\varphi)^{\cdot\cdot} = 0, \qquad k^2 = k_*^2+\tilde{k}^2. \tag{7.12}$$

Taking into account the initial conditions we get the solution of the system (7.10), (7.12) in the form:

$$\begin{aligned} x(t) &= x|_{t=0} + \dot{x}|_{t=0}\,t \\ &+\frac{c}{mk^2}\sum_{i=1}^{N}\left[(x_i+\chi\varphi_i)\Big|_{t=0}\Big(1-\cos(kt)\Big) + (x_i+\chi\varphi_i)^{\cdot}\Big|_{t=0}\left(t-\frac{\sin(kt)}{k}\right)\right], \end{aligned} \tag{7.13}$$

$$\begin{aligned} \varphi(t) &= \varphi|_{t=0} + \dot{\varphi}|_{t=0}\,t \\ &+\frac{\chi c}{Jk^2}\sum_{i=1}^{N}\left[(x_i+\chi\varphi_i)\Big|_{t=0}\Big(1-\cos(kt)\Big) + (x_i+\chi\varphi_i)^{\cdot}\Big|_{t=0}\left(t-\frac{\sin(kt)}{k}\right)\right]. \end{aligned} \tag{7.14}$$

Now we introduce the quantities averaged over a period:

$$\begin{aligned} \bar{x}(t) &= \frac{k}{2\pi}\int_{t-\pi/k}^{t+\pi/k} x(\tau)d\tau \\ &= x|_{t=0} + \dot{x}|_{t=0}\,t + \frac{c}{mk^2}\left[\sum_{i=1}^{N}(x_i+\chi\varphi_i)\Big|_{t=0} + \sum_{i=1}^{N}(x_i+\chi\varphi_i)^{\cdot}\Big|_{t=0}t\right], \end{aligned} \tag{7.15}$$

$$\begin{aligned} \bar{\varphi}(t) &= \frac{k}{2\pi}\int_{t-\pi/k}^{t+\pi/k} \varphi(\tau)d\tau \\ &= \varphi|_{t=0} + \dot{\varphi}|_{t=0}\,t + \frac{\chi c}{Jk^2}\left[\sum_{i=1}^{N}(x_i+\chi\varphi_i)\Big|_{t=0} + \sum_{i=1}^{N}(x_i+\chi\varphi_i)^{\cdot}\Big|_{t=0}t\right]. \end{aligned} \tag{7.16}$$

Let us assume that we can observe on average values of the displacement and the angle of rotation of the frame. The motion of the rigid bodies inside the frame is not available for observation. In that case we will interpret the system under consideration as a single whole particle ("body-point"). Then quantities $\bar{x}(t)$ and $\bar{\varphi}(t)$ we will consider as characteristics of the position and the orientation of the particle. Now we discuss two variants of the initial conditions.

Variant 1. The stiffness of springs connecting the internal bodies and the frame is very large. In that case impact on the frame setting it in motion in the initial instant of time will set the internal bodies in the same motion. Then it is reasonable to assume that in the initial instant of time the relative displacements and angles of rotation as well as the relative velocities of the internal bodies are equal to zero:

$$x_i\big|_{t=0} = 0, \qquad \varphi_i\big|_{t=0} = 0, \qquad \dot{x}_i\big|_{t=0} = 0, \qquad \dot{\varphi}_i\big|_{t=0} = 0. \tag{7.17}$$

In that case expressions for $\bar{x}(t)$ and $\bar{\varphi}(t)$ are:

$$\bar{x}(t) = x|_{t=0} + \dot{x}|_{t=0}\, t, \qquad \bar{\varphi}(t) = \varphi|_{t=0} + \dot{\varphi}|_{t=0}\, t. \tag{7.18}$$

It is easy to see that the displacements and the angles of rotation determined by Eqs (7.18) are independent.

Variant 2. The stiffness of springs connecting the internal bodies and the frame is very small. Then impact on the frame setting it in motion in the initial instant of time will not be passed to the internal bodies. Therefore we can assume that in the initial instant of time the absolute displacements and angles of rotation as well as the absolute velocities of the internal bodies are equal to zero:

$$(x+x_i)\big|_{t=0} = 0, \quad (\varphi+\varphi_i)\big|_{t=0} = 0, \quad (\dot{x}+\dot{x}_i)\big|_{t=0} = 0, \quad (\dot{\varphi}+\dot{\varphi}_i)\big|_{t=0} = 0. \tag{7.19}$$

In that case expressions for $\bar{x}(t)$ and $\bar{\varphi}(t)$ take the form:

$$\begin{aligned} \bar{x}(t) &= \left[1 - \frac{\mu}{m}\right]\left(x|_{t=0} + \dot{x}|_{t=0}\, t\right) - \frac{\chi\mu}{m}\left(\varphi|_{t=0} + \dot{\varphi}|_{t=0}\, t\right), \\ \bar{\varphi}(t) &= \left[1 - \frac{\chi^2\mu}{J}\right]\left(\varphi|_{t=0} + \dot{\varphi}|_{t=0}\, t\right) - \frac{\chi\mu}{J}\left(x|_{t=0} + \dot{x}|_{t=0}\, t\right), \end{aligned} \tag{7.20}$$

where parameter μ having the dimension of mass calculated by the formula:

$$\mu = \left(\frac{1}{m} + \frac{1}{m_*} + \chi^2\left[\frac{1}{J} + \frac{1}{J_*}\right]\right)^{-1}. \tag{7.21}$$

As evident from Eqs (7.20), the initial displacements and translational velocities of the frame have an influence on its rotational motion, and the initial angles of rotation and angular velocities of the frame influence have action upon its translational motion.

Thus, based on the considered example we conclude that the presence or absence of cross effect of the translational and rotational motions depend on the internal structure and the parameters of the system.

Example 2. We consider the motion of the system represented in Fig. 7.1 under the action of the external force and twisting moment being linear time functions:

$$F = A_F t, \qquad M = A_M t, \qquad A_F = \text{const}, \qquad A_M = \text{const}. \tag{7.22}$$

Taking into account Eqs (7.22) we write the equations of the frame motion (7.3) in the form:

$$m\ddot{x} = A_F t + \sum_{i=1}^{N} F_i, \qquad J\ddot{\varphi} = A_M t + \sum_{i=1}^{N} M_i. \tag{7.23}$$

As in preceding example, we suppose that all rigid bodies have the same masses $m_i = m_*/N$ and the same moments of inertia $J_i = J_*/N$. The elastic forces and moments characterizing the interaction of the rigid bodies and the frame are calculated by Eqs (7.6). The equations of motion of the internal bodies (7.7), as well as their sequent Eqs (7.8), are correct in the problem under discussion.

By using Eqs (7.6) for the forces F_i and the moments M_i the equations of motion of the frame (7.23) can be reduced to the equivalent system including the equation

$$m\ddot{x} - \frac{J}{\chi}\ddot{\varphi} = A_F t - \frac{A_M t}{\chi} \tag{7.24}$$

and equation

$$(x + \chi\varphi)^{\cdot\cdot} = \frac{A_F t}{m} + \frac{\chi A_M t}{J} + \frac{\tilde{k}^2}{N}\sum_{i=1}^{N}(x_i + \chi\varphi_i). \tag{7.25}$$

From Eqs (7.8) and (7.25) we obtain the equation in $x + \chi\varphi$:

$$(x + \chi\varphi)^{\cdot\cdot\cdot\cdot} + k^2(x + \chi\varphi)^{\cdot\cdot} = k_*^2\left(\frac{A_F t}{m} + \frac{\chi A_M t}{J}\right). \tag{7.26}$$

Solving Eq. (7.26) we get the following expression for the variable $(x + \chi\varphi)^{\cdot\cdot}$

$$(x + \chi\varphi)^{\cdot\cdot} = (x + \chi\varphi)\Big|_{t=0}\cos(kt) + \frac{1}{k}(x + \chi\varphi)^{\cdot}\Big|_{t=0}\sin(kt) + \frac{k_*^2}{k^2}\left(\frac{A_F t}{m} + \frac{\chi A_M t}{J}\right). \tag{7.27}$$

Now we suppose that the oscillation period is much smaller than an observing time on the motion process. In that case the characteristics of the motion averaged over a period is of interest for us:

$$\bar{x}(t) = \frac{k}{2\pi}\int_{t-\pi/k}^{t+\pi/k} x(\tau)d\tau, \qquad \bar{\varphi}(t) = \frac{k}{2\pi}\int_{t-\pi/k}^{t+\pi/k} \varphi(\tau)d\tau. \tag{7.28}$$

By averaging over a period Eqs (7.24) and (7.27) we obtain:

$$m\ddot{\bar{x}} - \frac{J}{\chi}\ddot{\bar{\varphi}} = A_F t - \frac{A_M t}{\chi}, \qquad \ddot{\bar{x}} + \chi\ddot{\bar{\varphi}} = \frac{k_*^2}{k^2}\left(\frac{A_F t}{m} + \frac{\chi A_M t}{J}\right). \tag{7.29}$$

Now we transform the system (7.29) to the following form:

$$\begin{aligned} m\left(1+\frac{Jk^2}{\chi^2 mk_*^2}\right)\left(1+\frac{J}{\chi^2 m}\right)^{-1}\ddot{\bar{x}}+\frac{J\tilde{k}^2}{\chi k_*^2}\left(1+\frac{J}{\chi^2 m}\right)^{-1}\ddot{\bar{\varphi}}=A_F t,\\ \frac{\chi m\tilde{k}^2}{k_*^2}\left(1+\frac{J}{\chi^2 m}\right)^{-1}\ddot{\bar{x}}+J\left(1+\frac{Jk^2}{\chi^2 mk_*^2}\right)\left(1+\frac{J}{\chi^2 m}\right)^{-1}\ddot{\bar{\varphi}}=A_M t. \end{aligned} \tag{7.30}$$

Let us suppose that the mass and the moment of inertia of the frame are related by the formula

$$J=\chi^2 m. \tag{7.31}$$

We introduce following notations:

$$\hat{m}=\frac{m}{2}\left(1+\frac{k^2}{k_*^2}\right),\qquad \hat{B}=\frac{\chi m\tilde{k}^2}{2k_*^2},\qquad \hat{J}=\frac{J}{2}\left(1+\frac{k^2}{k_*^2}\right). \tag{7.32}$$

Taking into account Eqs (7.31) and (7.32) we rewrite the system (7.30) in the form:

$$\hat{m}\ddot{\bar{x}}+\hat{B}\ddot{\bar{\varphi}}=A_F t,\qquad \hat{B}\ddot{\bar{x}}+\hat{J}\ddot{\bar{\varphi}}=A_M t. \tag{7.33}$$

By comparison of Eqs (7.33) describing the behavior of the average over a period characteristics of the motion with the starting Eqs (7.23) we see that the influence of the internal structure of the system on the motion of the frame can be taken into account both by means of the internal forces and moments and with the aid of the additional inertial parameters ensuring the interplay of the translational and rotational motions.

Example 3. Now we study the motion of the considered system (see Fig. 7.1) under the action of the external force and twisting moment being periodic time functions:

$$F=F_0\sin(\omega t),\qquad M=M_0\sin(\omega t),\qquad F_0=\text{const},\qquad M_0=\text{const}. \tag{7.34}$$

Taking into account Eqs (7.34) we write down the equations of the motion of the frame (7.3) in the form:

$$m\ddot{x}=F_0\sin(\omega t)+\sum_{i=1}^{N}F_i,\qquad J\ddot{\varphi}=M_0\sin(\omega t)+\sum_{i=1}^{N}M_i. \tag{7.35}$$

After simple transformations similar to those carried out in the preceding example we reduce the equation of the motion of the frame to the system of equations

$$\begin{aligned} m\ddot{x}-\frac{J}{\chi}\ddot{\varphi}&=\left(F_0-\frac{M_0}{\chi}\right)\sin(\omega t),\\ (x+\chi\varphi)^{\cdot\cdot}&=(x+\chi\varphi)\Big|_{t=0}\cos(kt)+\frac{1}{k}(x+\chi\varphi)^{\cdot}\Big|_{t=0}\sin(kt)\\ &\quad+\frac{k_*^2-\omega^2}{k^2-\omega^2}\left(\frac{F_0}{m}+\frac{\chi M_0}{J}\right)\sin(\omega t). \end{aligned} \tag{7.36}$$

Now we suppose that the free period is much smaller than the period of force oscillations. Introducing the average over a period characteristics of the motion (7.28) and averaging Eqs (7.36) over a period we obtain:

$$\begin{gathered} m\ddot{\bar{x}} - \frac{J}{\chi}\ddot{\bar{\varphi}} = \frac{k}{\pi\omega}\sin\left(\frac{\pi\omega}{k}\right)\left(F_0 - \frac{M_0}{\chi}\right)\sin(\omega t), \\ \ddot{\bar{x}} + \chi\ddot{\bar{\varphi}} = \frac{k(k_*^2-\omega^2)}{\pi\omega(k^2-\omega^2)}\sin\left(\frac{\pi\omega}{k}\right)\left(\frac{F_0}{m} + \frac{\chi M_0}{J}\right)\sin(\omega t). \end{gathered} \tag{7.37}$$

We suppose that $\omega \ll k_*$ and, hence, $\omega \ll k$. Moreover, the mass and the moment of inertia of the frame are assumed to be related by Eq. (7.31). Then by using notations (7.32) we can rewrite the system (7.37) in the form:

$$\hat{m}\ddot{\bar{x}} + \hat{B}\ddot{\bar{\varphi}} = F_0\sin(\omega t), \qquad \hat{B}\ddot{\bar{x}} + \hat{J}\ddot{\bar{\varphi}} = M_0\sin(\omega t). \tag{7.38}$$

By comparison of Eqs (7.38) describing the behavior of the average over a period characteristics of the motion with the starting Eqs (7.35) we come to the conclusion that the result is the same to that obtained in the preceding example. Namely, the dynamics of the internal structure of the system has action upon the motion of the frame and the influence in question can be taken into account by means of the additional inertial parameters ensuring the interplay of the translational and rotational motions.

Example 4. Now we study the motion of the considered system (see Fig. 7.1) under the action of conservative load which is modeled by a linear elastic force. In that case the equations of the frame motion (7.3) take the form:

$$m\ddot{x} = -C_F x + \sum_{i=1}^{N} F_i, \qquad J\ddot{\varphi} = \sum_{i=1}^{N} M_i, \tag{7.39}$$

where C_F is the stiffness of the elastic spring. The equations of the frame motion (7.39) by using Eqs (7.6) and (7.8) can be reduced to the following system of equations:

$$m\ddot{x} - \frac{J}{\chi}\ddot{\varphi} = -C_F x, \qquad (x+\chi\varphi)^{\cdot\cdot\cdot\cdot} + k^2(x+\chi\varphi)^{\cdot\cdot} = -\frac{C_F}{m}\left(\ddot{x} + k_*^2 x\right). \tag{7.40}$$

It is easy to see that at the zero initial conditions lead the system (7.40) to the form:

$$m\ddot{x} + \hat{B}\ddot{\varphi} = -C_F x, \qquad \hat{B}\ddot{x} + \hat{J}\ddot{\varphi} = -C_M\varphi, \tag{7.41}$$

where constants $\hat{B}$, $\hat{J}$ and C_M are calculated by the formulae:

$$\hat{B} = -\frac{J}{\chi}, \quad \hat{J} = J\left[\frac{J}{\chi^2 m} + \frac{C_F}{m\tilde{k}^2} + \frac{C_F J}{\chi^2 m^2 \tilde{k}^2}\right], \quad C_M = \frac{C_F J}{m\tilde{k}^2}\left(k^2 + \frac{Jk_*^2}{\chi^2 m}\right). \tag{7.42}$$

As evident from a comparison of Eqs (7.39) and (7.41) in the case of discussion we can take into account the influence of the dynamics of the internal structure by means of of the additional inertial parameters and of an external elastic moment proportional to the angle of rotation of the frame.

Let us consider Eqs (7.33), (7.38) and (7.41). The quantities on the right-hand side of the equations are the forces and the moments. Hence, the left-hand side of Eqs (7.33), (7.38) and (7.41) can be interpreted as the derivatives of the momentum and the angular momentum. Then the foregoing equations should be regarded as the equation of motion of the particle whose momentum K_1, the angular momentum K_2 and kinetic energy K are:

$$K_1 = \hat{m}\dot{x} + \hat{B}\dot{\varphi}, \qquad K_2 = \hat{B}\dot{x} + \hat{J}\dot{\varphi}, \qquad K = \frac{1}{2}\hat{m}\dot{x}^2 + \hat{B}\dot{x}\dot{\varphi} + \frac{1}{2}\hat{J}\dot{\varphi}^2, \qquad (7.43)$$

Consequently, parameter $\hat{B}$ is the moment of inertia. The particle whose dynamic structures are defined by Eqs (7.43) is a special case of the body-point proposed by P. A. Zhilin – see [3].

7.3 Continuum of One-rotor Gyrostats

The material medium (see Fig. 7.2) consisting of one-rotor gyrostats is considered. A one-rotor gyrostat consists of a rotor concealed in a rigid body which is called "carrier body". A rotor can rotate independently of the carrier body rotation, but a rotor can not move independently the carrier body motion. A carrier body of the gyrostat is a classical rigid body, and a rotor is a non-classical particle whose properties will be defined in what follows.

To derive the dynamic equations of the continuum we apply the spatial description. Let vector $\mathbf{r}$ determine the position of some point of space. We introduce following notations: $\rho(\mathbf{r},t)$ is the mass density of the material medium at a given point of space; $\mathbf{v}(\mathbf{r},t)$ is the velocity field; $\mathbf{u}(\mathbf{r},t)$ is the displacement field; $\tilde{\mathbf{P}}(\mathbf{r},t)$, $\tilde{\omega}(\mathbf{r},t)$ are the fields of the rotation tensors and the angular velocity vectors of the carrier bodies; $\mathbf{P}(\mathbf{r},t)$ and $\boldsymbol{\omega}(\mathbf{r},t)$ are fields of the rotation tensors and the angular velocity vectors of the rotors.

The particles of continuum under consideration possess the internal degrees of freedom. Therefore, in order to describe the motion of this continuum it is not sufficient to formulate the balance equations of the momentum and the angular momentum for the control volume of the continuum. It is necessary to add these equations to the balance equation of the angular momentum for the rotors in control volume of the continuum. Therefore below we need the densities of the momentum and the angular momentum of the carrier bodies

$$\rho\mathbf{K}_1^{(\mathrm{cb})} = \rho(1-\zeta)\mathbf{v}, \qquad \rho\mathbf{K}_2^{(\mathrm{cb})} = \rho\left[\mathbf{r}\times(1-\zeta)\mathbf{v} + \mathbf{I}_*\cdot\tilde{\boldsymbol{\omega}}\right], \qquad (7.44)$$

and the momentum and the angular momentum of the rotors

$$\rho \mathbf{K}_1^{(\mathrm{rot})} = \rho(\zeta \mathbf{v} + B\boldsymbol{\omega}), \qquad \rho \mathbf{K}_2^{(\mathrm{rot})} = \rho\left[\mathbf{r} \times (\zeta \mathbf{v} + B\boldsymbol{\omega}) + B\mathbf{v} + J\boldsymbol{\omega}\right]. \quad (7.45)$$

Here $\mathbf{I}_*$ is the inertia tensor of the carrier body of the gyrostat, B and J are the moments of inertia of the rotor. Dimensionless parameter ζ in Eqs (7.44) and (7.45) characterizes the distribution of mass in the gyrostat: if m is the mass of the gyrostat then $(1-\zeta)m$ is the mass of its carrier body and ζm is the mass of its rotor. Below we will see that the value of parameter ζ is not important. The densities of the momentum and the angular momentum of the gyrostats are

$$\rho \mathbf{K}_1 = \rho \mathbf{K}_1^{(\mathrm{cb})} + \rho \mathbf{K}_1^{(\mathrm{rot})}, \qquad \rho \mathbf{K}_2 = \rho \mathbf{K}_2^{(\mathrm{cb})} + \rho \mathbf{K}_2^{(\mathrm{rot})}. \quad (7.46)$$

We assume that in the reference configurations the tensors $\tilde{\mathbf{P}}(\mathbf{r},t)$ and $\mathbf{P}(\mathbf{r},t)$ are equal to the unit tensor. Therefore, upon the linearization near the reference position they take the form

$$\tilde{\mathbf{P}}(\mathbf{r},t) = \mathbf{E} + \boldsymbol{\varphi}(\mathbf{r},t) \times \mathbf{E}, \qquad \mathbf{P}(\mathbf{r},t) = \mathbf{E} + \boldsymbol{\theta}(\mathbf{r},t) \times \mathbf{E}, \quad (7.47)$$

where $\boldsymbol{\varphi}(\mathbf{r},t)$, $\boldsymbol{\theta}(\mathbf{r},t)$ are the rotation vector fields of carrier bodies and rotors, respectively, $\mathbf{E}$ is the unit tensor. Kinematic relations in the linear approximation are

$$\mathbf{v} = \frac{d\mathbf{u}}{dt}, \qquad \tilde{\boldsymbol{\omega}} = \frac{d\boldsymbol{\varphi}}{dt}, \qquad \boldsymbol{\omega} = \frac{d\boldsymbol{\theta}}{dt}. \quad (7.48)$$

The mass balance equation in the linear approximation takes the form

$$\frac{d\rho}{dt} + \rho \nabla \cdot \mathbf{v} = 0 \qquad \Rightarrow \qquad \rho = \rho_* \left(1 - \nabla \cdot \mathbf{u}\right). \quad (7.49)$$

Here ρ_* is the mass density per unit volume in the reference position. Note that mass density at the initial time instant ρ_0 may not coincide with the mass density in the reference position ρ_*. These two quantities are related with each other by the

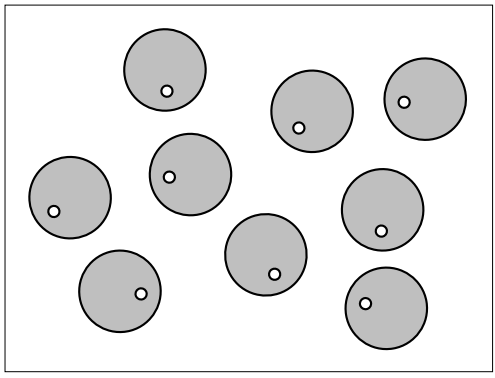

Fig. 7.2 Elementary volume of continuum consisting of one-rotor gyrostats

formula

$$\rho_0 = \rho_* \left(1 - \nabla \cdot \mathbf{u}_0\right), \tag{7.50}$$

and they coincide only if the medium is not deformable at the initial time instant.

The equations of motion of the material continuum can be written in the form

$$\nabla \cdot \boldsymbol{\tau} + \rho_* \mathbf{f} = \rho_* \frac{d}{dt}\left(\mathbf{v} + B\boldsymbol{\omega}\right), \qquad \nabla \cdot \boldsymbol{\mu} + \boldsymbol{\tau}_\times + \rho_* \mathbf{m} = \rho_* \frac{d}{dt}\left(\mathbf{I}_*^{(0)} \cdot \tilde{\boldsymbol{\omega}}\right), \tag{7.51}$$

where inertia tensor $\mathbf{I}_*^{(0)}$ is calculated in the reference configuration. tensor $\boldsymbol{\tau}$ is the stress tensor, and tensor $\boldsymbol{\mu}$ is the moment stress tensor modeling the influence of surrounding medium on the carrier bodies of gyrostats. The second equation in Eqs (7.51) is the equation of the motion of the carrier bodies. That is why the right-hand part of this equation does not depend on the velocity $\mathbf{v}$. The equation of motion of the rotors takes the form

$$\nabla \cdot \mathbf{T} + \rho_* \mathbf{L} = \rho_* \frac{d}{dt}\left(B\mathbf{v} + J\boldsymbol{\omega}\right), \tag{7.52}$$

where $\mathbf{T}$ is the moment stress tensor modeling the influence of surrounding medium on the rotors of gyrostats.

After simple transformations the equation of energy balance is written as follows:

$$\rho_* \frac{dU}{dt} = \boldsymbol{\tau}^T \cdot\cdot \frac{d\boldsymbol{\varepsilon}}{dt} + \boldsymbol{\mu}^T \cdot\cdot \frac{d\boldsymbol{\kappa}}{dt} + \mathbf{T}^T \cdot\cdot \frac{d\boldsymbol{\vartheta}}{dt}, \tag{7.53}$$

where U is the internal energy density per unit mass and the strain tensors $\boldsymbol{\varepsilon}$, $\boldsymbol{\kappa}$, $\boldsymbol{\vartheta}$ are introduced into consideration. These tensors are calculated by the formulas

$$\boldsymbol{\varepsilon} = \nabla \mathbf{u} + \mathbf{E} \times \boldsymbol{\varphi}, \qquad \boldsymbol{\kappa} = \nabla \boldsymbol{\varphi}, \qquad \boldsymbol{\vartheta} = \nabla \boldsymbol{\theta}. \tag{7.54}$$

In what follows we consider the elastic material i. e. a material whose density of internal energy and the tensors of force and moment stresses depend only on the strain tensors and do not depend on the velocities. For the elastic material the Cauchy–Green relations follow from the equation of energy balance (7.53):

$$\boldsymbol{\tau} = \rho_* \frac{\partial U}{\partial \boldsymbol{\varepsilon}}, \qquad \boldsymbol{\mu} = \rho_* \frac{\partial U}{\partial \boldsymbol{\kappa}}, \qquad \mathbf{T} = \rho_* \frac{\partial U}{\partial \boldsymbol{\vartheta}}. \tag{7.55}$$

To close the system of differential equations it is necessary to express the internal energy as a function of the strain tensors

$$\rho_* U = \rho_* U(\boldsymbol{\varepsilon}, \boldsymbol{\kappa}, \boldsymbol{\vartheta}). \tag{7.56}$$

Now we consider the physically linear theory and therefore we represent the density of internal energy in the following form:

$$\rho_* U = \boldsymbol{\tau}_0^T \cdot\cdot \boldsymbol{\varepsilon} + \boldsymbol{\mu}_0^T \cdot\cdot \boldsymbol{\kappa} + \mathbf{T}_*^T \cdot\cdot (\boldsymbol{\vartheta} - \boldsymbol{\vartheta}_*) + \frac{1}{2}\boldsymbol{\varepsilon} \cdot\cdot {}^4\mathbf{C}_1 \cdot\cdot \boldsymbol{\varepsilon} + \boldsymbol{\varepsilon} \cdot\cdot {}^4\mathbf{C}_2 \cdot\cdot \boldsymbol{\kappa} + \\ + \frac{1}{2}\boldsymbol{\kappa} \cdot\cdot {}^4\mathbf{C}_3 \cdot\cdot \boldsymbol{\kappa} + \boldsymbol{\varepsilon} \cdot\cdot {}^4\mathbf{C}_4 \cdot\cdot (\boldsymbol{\vartheta} - \boldsymbol{\vartheta}_*) + \boldsymbol{\kappa} \cdot\cdot {}^4\mathbf{C}_5 \cdot\cdot (\boldsymbol{\vartheta} - \boldsymbol{\vartheta}_*) + \\ + \frac{1}{2}(\boldsymbol{\vartheta} - \boldsymbol{\vartheta}_*) \cdot\cdot {}^4\mathbf{C}_6 \cdot\cdot (\boldsymbol{\vartheta} - \boldsymbol{\vartheta}_*). \tag{7.57}$$

Coefficients $\boldsymbol{\tau}_0$, $\boldsymbol{\mu}_0$ and $\mathbf{T}_*$ are called the initial stresses, $\boldsymbol{\vartheta}_*$ is the reference value of $\boldsymbol{\vartheta}$. Coefficients of the quadratic form ${}^4\mathbf{C}_i$ are called the stiffness tensors. In the linear theory the stiffness tensors do not depend on time. The only restriction imposed on the stiffness tensors is concerned with the requirement of positive definiteness of the quadratic form (7.57). The structure of the stiffness tensors and the values of the coefficients of elasticity are determined by the physical properties of the material medium.

After substituting expression for the density of internal energy (7.57) in the Cauchy–Green relations (7.55) we obtain the following constitutive equations:

$$\begin{aligned} \boldsymbol{\tau}^T &= \boldsymbol{\tau}_0^T + {}^4\mathbf{C}_1 \cdot\cdot \boldsymbol{\varepsilon} + {}^4\mathbf{C}_2 \cdot\cdot \boldsymbol{\kappa} + {}^4\mathbf{C}_4 \cdot\cdot (\boldsymbol{\vartheta} - \boldsymbol{\vartheta}_*), \\ \boldsymbol{\mu}^T &= \boldsymbol{\mu}_0^T + \boldsymbol{\varepsilon} \cdot\cdot {}^4\mathbf{C}_2 + {}^4\mathbf{C}_3 \cdot\cdot \boldsymbol{\kappa} + {}^4\mathbf{C}_5 \cdot\cdot (\boldsymbol{\vartheta} - \boldsymbol{\vartheta}_*), \\ \mathbf{T}^T &= \mathbf{T}_*^T + \boldsymbol{\varepsilon} \cdot\cdot {}^4\mathbf{C}_4 + \boldsymbol{\kappa} \cdot\cdot {}^4\mathbf{C}_5 + {}^4\mathbf{C}_6 \cdot\cdot (\boldsymbol{\vartheta} - \boldsymbol{\vartheta}_*). \end{aligned} \tag{7.58}$$

According to Eqs (7.58) all stress tensors can depend on all strain tensors. It means, in particular, that the moment stress tensor of rotors can depend not only on their relative orientation, but also on the relative orientation and relative position of the carrier bodies.

7.4 The Simplest Theory of One-rotor Gyrostats Continuum

We consider the material continuum (see Fig. 7.3) that consists of one-rotor gyrostats. In limits of linear theory the motion of this continuum is described by Eqs (7.48), (7.49), (7.51), (7.52), (7.54) and (7.58). Free space between the gyrostats is filled up by body-points whose structure coincides with the structure of rotors belonging to the gyroststs. The body-points in the space between the gyrostats are the elementary particles of a continuum which will be called the "thermal ether" in what follows. In fact, the material continuum represented in Fig. 7.3 is a two-component medium. We are not going to study in detail the motion of the body-points continuum ("thermal ether") and the interaction between the gyrostats continuum and the body-points continuum. We consider only the gyrostats continuum as an object under study. The interaction between the carrier bodies of the gyrostats and the interaction between rotors of the gyrostats are characterized by tensors of the force and moment stresses (7.58). The body-points continuum ("thermal ether") positioned in space between gyrostats is considered to be an external factor with respect to the

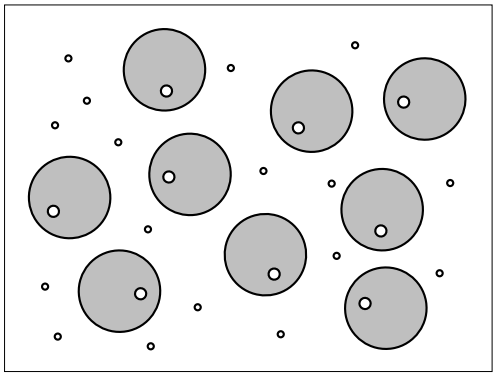

Fig. 7.3 Elementary volume of continuum interacting with environment

continuum under study. That is why we will model the influence of the "thermal ether" on the gyrostats by an external moment in the equation of the rotors motion (7.52).

Accepting two important hypotheses we consider a special case of the linear theory of one-rotor gyrostats continuum.

Hypothesis 1. Vector **L** (the mass density of external actions on the rotors of gyrostats) is a sum of the moment $\mathbf{L}_h$ characterizing external actions of all sorts and the moment of linear viscous damping

$$\mathbf{L}_f = -\beta(B\mathbf{v} + J\boldsymbol{\omega}). \tag{7.59}$$

The moment (7.59) characterizes the influence of the "thermal ether". Structure of the moment is chosen in accordance with the results of solving some model problems. One of these problems is considered in Sect. 7.8. Now we explain the physical meaning of the moment of linear viscous damping (7.59). We suppose that the rotors of the quasi-rigid bodies interact with body-points of the "thermal ether" and this interaction is described by the elastic moments analogous to the moments characterizing the interaction of the rotors with each other. The "thermal ether" having infinite extent eliminates energy of the oscillating rotors. The solution of modeling problems reveals that in the case of an infinite surrounding medium the dissipative moment arising due to the interaction with this medium is proportional to the proper angular momentum vector (dynamic spin).

Hypothesis 2. The moment stress tensor $\mathbf{T}$ characterizing the interactions between rotors is the spherical tensor

$$\mathbf{T} = T\mathbf{E}. \tag{7.60}$$

In view of assumptions (7.59) and (7.60) the equation of the rotors motion (7.52) takes the form

$$\nabla T - \rho_* \beta \left(B\mathbf{v} + J\boldsymbol{\omega}\right) + \rho_* \mathbf{L}_h = \rho_* \frac{d}{dt}\left(B\mathbf{v} + J\boldsymbol{\omega}\right), \tag{7.61}$$

In view of assumption (7.60) the last term on the right-hand side of the energy balance equation (7.53) can be reduced to the more simple form. By using notation $\vartheta = \operatorname{tr}\boldsymbol{\vartheta}$ the energy balance equation (7.53) is written as

$$\rho_* \frac{dU}{dt} = \boldsymbol{\tau}^T \cdot\cdot \frac{d\boldsymbol{\varepsilon}}{dt} + \boldsymbol{\mu}^T \cdot\cdot \frac{d\boldsymbol{\kappa}}{dt} + T\,\frac{d\vartheta}{dt}. \tag{7.62}$$

Since the material medium under consideration is an elastic one, we obtain from Eq. (7.62) the Cauchy–Green relations of which the first and the second ones coincide with the first and the second relations of (7.55) respectively and the third one has a simpler form:

$$\boldsymbol{\tau} = \rho_* \frac{\partial U}{\partial \boldsymbol{\varepsilon}}, \qquad \boldsymbol{\mu} = \rho_* \frac{\partial U}{\partial \boldsymbol{\kappa}}, \qquad T = \rho_* \frac{\partial U}{\partial \vartheta}. \tag{7.63}$$

According to Eq. (7.62) the density of internal energy is a function of arguments $\boldsymbol{\varepsilon}$, $\boldsymbol{\kappa}$ and ϑ. Let us construct the physically linear theory based on representation of the internal energy density in the following form:

$$\rho_* U = \boldsymbol{\tau}_0 \cdot\cdot \boldsymbol{\varepsilon} + T_* (\vartheta - \vartheta_*) + \frac{1}{2}\boldsymbol{\varepsilon} \cdot\cdot {}^4\mathbf{C}_1 \cdot\cdot \boldsymbol{\varepsilon} + \Upsilon \operatorname{tr}\boldsymbol{\varepsilon}\,(\vartheta - \vartheta_*) + \frac{1}{2}K(\vartheta - \vartheta_*)^2. \tag{7.64}$$

Then the constitutive equations (7.58) take the form

$$\boldsymbol{\tau}^T = \boldsymbol{\tau}_0^T + {}^4\mathbf{C}_1 \cdot\cdot \boldsymbol{\varepsilon} + \Upsilon(\vartheta - \vartheta_*)\,\mathbf{E}, \qquad \boldsymbol{\mu} = 0, \qquad T = T_* + \Upsilon \operatorname{tr}\boldsymbol{\varepsilon} + K(\vartheta - \vartheta_*). \tag{7.65}$$

Thus the simplest linear theory of the material continuum consisting of one-rotor gyrostats is described by Eqs (7.48), (7.51), (7.54), (7.61) and (7.65).

7.5 Temperature and Entropy

Let us consider the foregoing mathematical model of elastic continuum of one-rotor gyrostats. Suppose that the model describes the behavior of a classical medium which possesses not only elastic properties but also the viscous and thermic properties. Now we can give a thermodynamic interpretation of the variables describing motion and interaction of the rotors and next we can carry out the identification of the model parameters and well-known thermodynamic constants.

Let us consider the energy balance equation (7.62). Conceive that Eq. (7.62) is the equation of energy balance for a classical moment medium (medium without rotors). Then the last term on the right-hand side of Eq. (7.62) can be treated as a thermodynamical one. The physical quantities T and ϑ acquire the meaning of temperature and volume density of entropy, respectively.

It is evident, that the dimensions of the temperature and the entropy defined by formula (7.62) are different from the dimensions of those in classical thermodynamics of the present simple case. This problem can be solved by introduction of a

normalization factor:

$$T = aT_a, \qquad \vartheta = \frac{1}{a}\,\vartheta_a. \tag{7.66}$$

Here a is the normalization factor; T_a is the absolute temperature measured by a thermometer; ϑ_a is volume density of the absolute entropy. Let us introduce the similar relations for the remaining variables:

$$\boldsymbol{\theta} = \frac{1}{a}\,\boldsymbol{\theta}_a, \qquad \boldsymbol{\omega} = \frac{1}{a}\,\boldsymbol{\omega}_a, \qquad \mathbf{L}_h = a\mathbf{L}_h^a, \qquad \mathbf{L}_f = a\mathbf{L}_f^a. \tag{7.67}$$

Now rewriting all equations for new variables and using new parameters

$$B_a = \frac{B}{a}, \qquad J_a = \frac{J}{a^2}, \qquad \Upsilon_a = \frac{\Upsilon}{a}, \qquad K_a = \frac{K}{a^2}, \tag{7.68}$$

we can eliminate the normalization factor a from these equations at least in the linear formulation of the problem and in some particular cases of physical nonlinearity.

7.6 Linear Theory of Thermoelasticity

Classical theory of thermoelasticity is a momentless one. Therefore considering the problem of thermoelasticity in the context of proposed model we assume only the force interaction between carrier bodies of the gyrostats and only the force action of external factors upon them:

$$\boldsymbol{\mu} = \mathbf{0}, \qquad \mathbf{m} = \mathbf{0}. \tag{7.69}$$

In the static problems from the second equation of (7.51) under the assumption (7.69) it follows that $\boldsymbol{\tau}_\times = \mathbf{0}$. In the dynamic problems the stress tensor can be nonsymmetric in spite of assumption (7.69). In this case it is necessary to take into account the dependence of the strain tensor $\boldsymbol{\varepsilon}$ on the angle of rotation of carrier bodies $\boldsymbol{\varphi}$. Thus, assumption (7.69) does not imply the transition to the momentless theory of elasticity for carrier bodies. In addition let us assume that $\mathbf{I}_*^{(0)} = 0$. In this case tensor $\boldsymbol{\tau}$ will be symmetrically both in the static and dynamic problems and all equations concerned with rotational motions of the carrier bodies of gyrostats can be excluded.

Applying the linear theory it is admissible in certain range of temperatures and entropy densities to change some reference values T_a^* and ϑ_a^*. Let us introduce deviations of the temperature and the density of entropy from their reference values:

$$T_a = T_a^* + \tilde{T}_a, \qquad \vartheta_a = \vartheta_a^* + \tilde{\vartheta}_a. \tag{7.70}$$

Resume of the basic equations of linear theory of the elastic medium consisting of the one-rotor gyrostats includes the dynamic equations (7.51), (7.61) which under notations (7.66) – (7.70) take the form

$$\begin{gathered}\nabla\cdot\boldsymbol{\tau}+\rho_*\mathbf{f}=\rho_*\frac{d}{dt}\left(\mathbf{v}+B_a\boldsymbol{\omega}_a\right),\\ \nabla\tilde{T}_a-\rho_*\beta\left(B_a\mathbf{v}+J_a\boldsymbol{\omega}_a\right)+\rho_*\mathbf{L}_h^a=\rho_*\frac{d}{dt}\left(B_a\mathbf{v}+J_a\boldsymbol{\omega}_a\right),\end{gathered}\tag{7.71}$$

the mass balance equation (7.49), the kinematical and geometrical relations (7.48) and (7.54) which under notations (7.66) and (7.67) and condition of symmetry of the stress tensor are reduced to

$$\begin{gathered}\rho=\rho_*\left(1-\varepsilon\right),\qquad \mathbf{v}=\frac{d\mathbf{u}}{dt},\qquad \boldsymbol{\omega}_a=\frac{d\boldsymbol{\theta}_a}{dt},\\ \boldsymbol{\varepsilon}=\frac{1}{2}\left(\nabla\mathbf{u}+\nabla\mathbf{u}^T\right),\qquad \varepsilon=\operatorname{tr}\boldsymbol{\varepsilon},\qquad \vartheta_a=\operatorname{tr}\boldsymbol{\vartheta}_a=\nabla\cdot\boldsymbol{\theta}_a,\end{gathered}\tag{7.72}$$

and the constitutive equations (7.65) which under notations (7.66) – (7.70) and the condition of symmetry of the stress tensor are written as

$$\boldsymbol{\tau}=\left(K_{\text{ad}}-\frac{2}{3}G\right)\varepsilon\mathbf{E}+G\boldsymbol{\varepsilon}+\Upsilon_a\,\tilde{\vartheta}_a\,\mathbf{E},\qquad \tilde{T}_a=\Upsilon_a\,\varepsilon+K_a\,\tilde{\vartheta}_a,\tag{7.73}$$

where K_{ad} is the adiabatic modulus of compression (the adiabatic bulk modulus), G is the shear modulus.

Let us suppose that $B_a=0$ and other parameters take the values

$$\beta J_a=\frac{T_a^*}{\rho_*\lambda},\qquad K_a=\frac{T_a^*}{\rho_* c_v},\qquad \Upsilon_a=-\frac{\alpha K_{\text{is}}T_a^*}{\rho_* c_v},\tag{7.74}$$

where c_v is the specific heat at constant volume, λ is the heat-conduction coefficient, K_{is} is the isothermal modulus of compression (the isothermal bulk modulus), α is the volume coefficient of thermal expansion,

$$K_{\text{ad}}=K_{\text{is}}\frac{c_p}{c_v},\qquad c_p-c_v=\frac{\alpha^2K_{\text{is}}T_a^*}{\rho_*}\qquad\Rightarrow\qquad K_{\text{ad}}=K_{\text{is}}+\frac{\alpha^2K_{\text{is}}^2T_a^*}{\rho_* c_v},\tag{7.75}$$

where c_p is the specific heat at constant pressure. In this case we can transform the system of equation (7.71) – (7.73) to the following form:

$$\begin{gathered}\nabla\cdot\boldsymbol{\tau}+\rho_*\mathbf{f}=\rho_*\frac{d^2\mathbf{u}}{dt^2},\qquad \boldsymbol{\tau}=\left(K_{\text{is}}-\frac{2}{3}G\right)\varepsilon\mathbf{E}+2G\boldsymbol{\varepsilon}-\alpha K_{\text{is}}\tilde{T}_a\,\mathbf{E},\\ \Delta\tilde{T}_a-\frac{\rho_* c_v}{\lambda}\left(\frac{d\tilde{T}_a}{dt}+\frac{1}{\beta}\frac{d^2\tilde{T}_a}{dt^2}\right)=\frac{\alpha K_{\text{is}}T_a^*}{\lambda}\left(\frac{d\varepsilon}{dt}+\frac{1}{\beta}\frac{d^2\varepsilon}{dt^2}\right)-\rho_*\nabla\cdot\mathbf{L}_h^a,\end{gathered}\tag{7.76}$$

Thus, the mathematical description of the proposed mechanical model includes as a special case the formulation of the coupled problem of thermoelasticity with the hyperbolic type heat conduction equation.

7.7 Model of Internal Damping

There exist different macroscopic and microscopic models of internal damping. At present, however, viscoelasticity is not a well-developed science for the treatment of thermodynamical and dissipative phenomena. The point of view that internal damping is concerned with thermal effects is widespread. The distribution of phonons is in a local thermodynamical equilibrium, i. e. the temperature changes adiabatically, when acoustic wave propagates. Consequently, regions separated by the half-wavelength distance from one another have different temperatures and the irreversible heat flow between these regions arises as a result of the heat conduction phenomena. This process causes transfer of the energy of mechanical vibrations into heat energy. Now we do not call in question the idea about interplay of the internal damping and thermal effects. We emphasize that the analysis of the experimental values of the volume (acoustic) viscosity of various substances shows that the volume viscosity is an independent substance characteristic which is not related to the heat-conduction coefficient and other thermodynamical parameters. This means that we should not consider the nature of the acoustic viscosity to be directly connected with heat conduction mechanisms. Let us emphasize that by discussing the internal damping we mean only the volume (acoustic) viscosity. In our opinion the shear viscosity has an absolutely different nature and it is not discussed here.

Let us consider the energy dissipation caused by heat conduction phenomena. It is well-known that this energy dissipation takes place only in the case when the process is not isothermal and not adiabatic. Now let us consider the energy dissipation caused by the viscosity. This energy dissipation always takes place processes included adiabatic processes. Proceeding from this fact we assume that dissipation is caused only by viscosity and the process is adiabatically, i.e. the volume density of entropy is constant:

$$\vartheta_a = \vartheta_a^* = \text{const} \qquad \Rightarrow \qquad \tilde{\vartheta}_a = 0 \qquad \Rightarrow \qquad \tilde{T}_a = \Upsilon_a \varepsilon. \tag{7.77}$$

By comparison of the equations describing the dynamics of one-rotor gyrostat continuum with the classical equations of thermoelasticity we assumed that $B_a = 0$. Now we reject this restriction. We suppose that the terms containing parameter B_a are concerned with the internal damping mechanism. In order to argue in favor of this hypothesis we consider the heat conduction equation

$$\begin{aligned} &\Delta \tilde{T}_a - \frac{\rho_* \beta J_a}{K_a} \frac{d\tilde{T}_a}{dt} - \frac{\rho_* J_a}{K_a} \frac{d^2 \tilde{T}_a}{dt^2} \\ &\qquad = \beta \rho_* \left(B_a - \frac{\Upsilon_a J_a}{K_a} \right) \frac{d\varepsilon}{dt} + \rho_* \left(B_a - \frac{\Upsilon_a J_a}{K_a} \right) \frac{d^2 \varepsilon}{dt^2} - \rho_* \nabla \cdot \mathbf{L}_h^a. \end{aligned} \tag{7.78}$$

Let us transform this equation by using the adiabatic condition (7.77). As a result we obtain

$$\Upsilon_a \Delta\varepsilon - \rho_* \beta B_a \frac{d\varepsilon}{dt} - \rho_* B_a \frac{d^2 \varepsilon}{dt^2} = -\rho_* \nabla \cdot \mathbf{L}_h^a. \tag{7.79}$$

It is easy to see that Eq. (7.79) contains a dissipative term. This dissipative term is in no way concerned with the heat conduction phenomena.

In order to clarify the physical meaning of the coefficients in Eq. (7.79) we stop the discussion of the proposed model and consider the motion of a viscous fluid in which the pressure obeys the Stokes law. The liquid state (in the case of no external mass forces) is described by the following equations:

$$\nabla p = \rho_* \frac{d\mathbf{v}}{dt}, \qquad p = \eta_v \frac{d\varepsilon}{dt}, \tag{7.80}$$

where η_v is the volume (acoustic) viscosity. From Eqs. (7.80) we obtain the relation between the flow of matter $\rho_* \mathbf{v}$ and the volume strain gradient

$$\eta_v \nabla \varepsilon = \rho_* \mathbf{v}. \tag{7.81}$$

By taking the divergence of both sides of Eqs. (7.81) we obtain the self-diffusion equation which can be generalized by adding the source term $\rho_* \Psi$ to it:

$$\eta_v \Delta \varepsilon - \rho_* \frac{d\varepsilon}{dt} = -\rho_* \Psi. \tag{7.82}$$

Comparing Eq. (7.79) with the self-diffusion equation (7.82) we find these two equations to be equivalent with the only difference that the former contains the inertial term if

$$\frac{\Upsilon_a}{\beta B_a} = \eta_v, \qquad \frac{1}{\beta B_a} \nabla \cdot \mathbf{L}_h^a = \Psi. \tag{7.83}$$

From the first equation of (7.83) by using the third equation of (7.74) we get

$$\beta B_a = -\frac{\alpha K_{\text{is}} T_a^*}{\rho_* c_v \eta_v}. \tag{7.84}$$

As evident from Eq. (7.84), parameter B_a is negative for finite values of the volume viscosity η_v and is equal to zero when $\eta_v \to \infty$.

In order to clarify the physical meaning of the obtained result we now consider the dissipative term in equation (7.71) for the rotor dynamics

$$\rho_* \mathbf{L}_f^a = -\beta \rho_* (B_a \mathbf{v} + J_a \boldsymbol{\omega}_a). \tag{7.85}$$

Upon substituting expressions for parameters (7.74), (7.84) into Eq. (7.85) we get

$$\rho_* \mathbf{L}_f^a = \frac{\alpha K_{\text{is}} T_a^*}{c_v \eta_v} \mathbf{v} - \frac{T_a^*}{\lambda} \boldsymbol{\omega}_a. \tag{7.86}$$

Let us calculate the power of the dissipative moment (7.86):

$$\rho_* \mathbf{L}_f^a \cdot \boldsymbol{\omega}_a = \frac{\alpha K_{\text{is}} T_a^*}{c_v \eta_v} \mathbf{v} \cdot \boldsymbol{\omega}_a - \frac{T_a^*}{\lambda} \boldsymbol{\omega}_a \cdot \boldsymbol{\omega}_a. \tag{7.87}$$

The second term in expression (7.87) is a dissipative one. When the heat-conduction coefficient decreases the dissipation increases. The first term in expression (7.87) determines the process which under the certain conditions can become inverse to the dissipative one. In particular, in the isothermal case the inequality $\mathbf{v} \cdot \boldsymbol{\omega}_a > 0$ is valid and, therefore, the first term in expression (7.87) determines the process of energy supply from the thermal ether. When the volume viscosity decreases the energy supply in the body from the thermal ether increases.

Let us transform Eq. (7.87) by separating the total squares in it:

$$\rho_* \mathbf{L}_f^a \cdot \boldsymbol{\omega}_a = \frac{\lambda \alpha^2 K_{is}^2 T_a^*}{4\eta_v^2 c_v^2} \mathbf{v} \cdot \mathbf{v} - \frac{T_a^*}{\lambda} \left(\boldsymbol{\omega}_a - \frac{\lambda \alpha K_{\text{is}}}{2\eta_v c_v} \mathbf{v} \right)^2 . \tag{7.88}$$

It is easy to see that the second term in expression (7.88) determines the dissipative process and the first term characterizes the process of the energy supply from the thermal ether. The first term is inversely as the square of the viscosity. Therefore, when the volume viscosity decreases the supply of energy of the thermal ether into the body increases. The second term defining the dissipative process also depends on the volume viscosity. As a result the energy interchange between the body and the thermal ether depends on the volume viscosity in a complicated manner. Thus the volume viscosity characterizes the natural ability of a substance to absorb the energy of the thermal ether. Will this ability be realized? It depends on other properties of the substance and external circumstances. The volume viscosity of gases is very small and therefore gases possess a good ability to absorb the energy of the thermal ether. Therefore the gas particles are in a state of intense mgotion in spite of the energy dissipation caused by the heat conduction phenomena. The volume viscosity of fluids (even inviscid fluid) is much larger than the volume viscosity of gases. The volume viscosity of solids is as large as that it can be considered to approach infinity. In this case parameter B_a is negligible. Thus the problem of thermoelasticity is admissible for solids while for fluids and gases it is important to take into account the terms dependint on the volume viscosity.

7.8 Interaction of Body-point and "Thermal Ether"

In what follows we consider a model problem which solution allows us to substantiate the choice of the low of viscous damping (7.59).

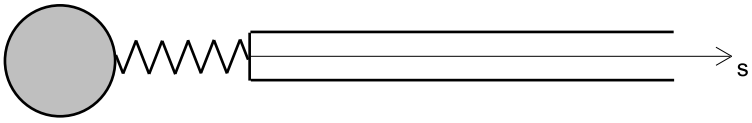

Fig. 7.4 Interaction of the body-point with the semi-infinite continuum

Let us consider a semi-infinite inertial rod (see Fig. 7.4), consisting of the body-points which are similar to the rotors of the one-rotor gyrostats. The rod is connected with the analogous body-point by means of an inertialess spring working in torsion (rotation about the axis of the rod). The inertia of the rod is characterized by the moments of inertia $\hat{B}$, $\hat{J}$ and the linear density $\sigma\tilde{\rho}$, where σ is "the area of rod section" and $\tilde{\rho}$ is the volume density of mass. The elastic properties of the rod are characterized by the torsional stiffness $\sigma\tilde{k}$, where the coefficient σ is introduced in order that stiffness $\tilde{k}$ possesses the dimension in 3D problems. The inertia of the body-point is characterized by the mass m and the moments of inertia B, J. The torsional stiffness of the spring connecting the body-point with the rod is equal to $\sigma k_*/r_0$, where r_0 is "the length" of the spring. The coefficients σ and r_0 are introduced in order that stiffness k_* possesses the dimension like $\tilde{k}$. The motion of the system is described by the following quantities: $u(s,t)$ is the longitudinal displacement of the rod, $\theta(s,t)$ is the rotation angle of the rod particles, $y(t)$ is the displacement of the body-point along the axis of the rod, $\psi(t)$ is the angle of rotation of the body-point about the axis of the rod. We suppose that the particles of the rod interact only by the moment. The force interaction of the rod particles is assumed to be zero. At the initial instant of time the displacements and the rotation angles as well as the translational and angular velocities are equal to zero. The body-point possesses a non-zero initial angular velocity directed along the axis of the rod and a non-zero initial angle of rotation about the axis of the rod. It is evident that under such an initial condition the system will be in motion which are longitudinal–torsional oscillations.

The longitudinal–torsional oscillations of the rod are described by the linear equations:

$$\frac{\partial T}{\partial s} = \sigma\tilde{\rho}\left(\hat{B}\ddot{u} + \hat{J}\ddot{\theta}\right), \qquad T = \sigma\tilde{k}\frac{\partial \theta}{\partial s}, \qquad \sigma\tilde{\rho}\left(\ddot{u} + \hat{B}\ddot{\theta}\right) = 0, \tag{7.89}$$

where s is the space coordinate ($0 \le s < +\infty$). After simple transformation the system (7.89) can be reduced to the wave equation in of the unknown θ:

$$\frac{\partial^2 \theta}{\partial s^2} - \frac{1}{c^2}\ddot{\theta} = 0, \qquad c^2 = \frac{\tilde{k}}{\tilde{\rho}(\hat{J} - \hat{B}^2)}. \tag{7.90}$$

The boundary conditions for the rod take the form:

$$\sigma\tilde{k}\left.\frac{\partial \theta}{\partial s}\right|_{s=0} = -\frac{\sigma k_*}{r_0}\left(\psi - \theta|_{s=0}\right). \tag{7.91}$$

Now we formulate the equations of the body-point motion:

$$m\left(B\ddot{y} + J\ddot{\psi}\right) = -\frac{\sigma k_*}{r_0}\left(\psi - \theta|_{s=0}\right), \qquad m\left(\ddot{y} + B\ddot{\psi}\right) = F. \tag{7.92}$$

Here F is an external force. The initial conditions for the body-point have the form:

$$y(0)=y_0, \qquad \psi(0)=\psi_0, \qquad \dot{y}(0)=v_0, \qquad \dot{\psi}(0)=\omega_0. \tag{7.93}$$

Let us represent the solution of the Eq. (7.90) in the form given by d'Alembert and Euler:

$$\theta(s,t)=f(s-ct)+g(s+ct). \tag{7.94}$$

Since the waves propagate to the right and there are no perturbations at infinity, we can assert that $g(s+ct)=0$. In view of zero initial conditions for the rod we see that the function $f(s-ct)$ is not equal to zero only on the negative semiaxis. Hence

$$\theta(s,t)=\begin{cases} 0, & s>ct, \\ f(s-ct), & s<ct. \end{cases} \tag{7.95}$$

Let us denote:

$$\theta_*(t)=\theta(s,t)\big|_{s=0}=f(s-ct)\big|_{s=0}. \tag{7.96}$$

Then

$$\dot{\theta}_*(t)=-cf'(s-ct)\big|_{s=0}, \tag{7.97}$$

where the derivation with respect to argument $(s-ct)$ is denoted by the stroke. Hence

$$\left.\frac{\partial\theta}{\partial s}\right|_{s=0}=f'(s-ct)\big|_{s=0}=-\frac{1}{c}\,\dot{\theta}_*(t). \tag{7.98}$$

Subject to (7.96), (7.98) the boundary condition for the rod (7.91) takes the form

$$\frac{\sigma\tilde{k}}{c}\,\dot{\theta}_*=\frac{\sigma k_*}{r_0}\big(\psi-\theta_*\big), \tag{7.99}$$

and the equations of the body-point motion (7.92) can be rewritten as follows

$$m(B\ddot{y}+J\ddot{\psi})+\frac{\sigma k_*}{r_0}\big(\psi-\theta_*\big)=0, \qquad m(\ddot{y}+B\ddot{\psi})=F. \tag{7.100}$$

Let us express the difference $(\psi-\theta_*)$ from Eq. (7.99) and put it in the first equation of (7.100). We obtain:

$$B\ddot{y}+J\ddot{\psi}+\frac{\sigma\tilde{k}}{mc}\,\dot{\theta}_*=0. \tag{7.101}$$

Now we integrate Eq. (7.101) taking into account the initial conditions. As a result we obtain:

$$B\dot{y}+J\dot{\psi}+\frac{\sigma\tilde{k}}{mc}\,\theta_*=Bv_0+J\omega_0. \tag{7.102}$$

Let us express θ_* from Eq. (7.102) and substitute it in Eqs (7.100). We obtain the following system of equations:

$$m(B\ddot{y}+J\ddot{\psi})+m\beta(B\dot{y}+J\dot{\psi})+\frac{\sigma k_*}{r_0}\psi=m\beta(Bv_0+J\omega_0), \quad m(\ddot{y}+B\ddot{\psi})=F, \tag{7.103}$$

where coefficient β is calculated by the formula:

$$\beta = \frac{ck_*}{r_0\tilde{k}} = \frac{k_*/r_0}{\sqrt{\tilde{k}\tilde{\rho}(\hat{J}-\hat{B}^2)}}. \tag{7.104}$$

According to Eqs (7.103), the moment of viscous damping characterizing the radiation of energy in the surrounding medium is proportional to the angular momentum of the body-point, i. e. it depends on both the angular velocity and the translational velocity. If $B = 0$ then the dependence on the translational velocity vanishes. In this case the problem under consideration becomes similar to the problem of the motion of an ordinary oscillator on the elastic waveguide. Analysis of formula (7.104) for the coefficient of damping β allows us to conclude that increasing the torsional stiffness of the spring connecting the body-point and the rod causes increasing of the radiation in the surrounding medium.

7.9 Conclusion

A model of a two-component continuum is suggested which takes into account thermomechanical processes. The mathematical description of this model is developed in the framework of physically and geometrically linear theory. In future we intend to carry out further development of the theory in two directions. The first one is concerned with consideration of nonlinear effects in the context of the same mechanical model. This is necessary for describing the behavior of substances in the states near the phase changes and heat-conduction processes under the circumstances of quickly varying and superhigh temperatures. The second direction deals with a modification of the mechanical model by taking into account the additional degrees of freedom for introducing the chemical potential and a number of additional physical characteristics of the medium. This is necessary to describe the phase changes and chemical reactions and also to take into account the interaction of the substance with the electromagnetic field and to describe thermoelectric and thermomagnetic effects.

Acknowledgements

The work was supported by the grant of RFBR N 09-01-00623-a and Sandia National Laboratories under the U.S. DOE/NNSA Advanced Simulation and Computing Program.

References

[1] Tzou, D. Y.: *Macro- and Microscale Heat Transfer: The Lagging Behavior*. Bristol, 1997
[2] Ziman, J. M.: *Electrons and Phonons. The Theory of Transport Phenomena in Solids*. Oxford, 1960
[3] Zhilin, P. A.: *Theoretical Mechanics. Fundamental Laws of Mechanics*. St. Petersburg (2003) (in Russian)
[4] Zhilin, P. A.: *Advanced Problems in Mechanics. Vol.* 1. St. Petersburg (2006) (in Russian)
[5] Zhilin, P. A.: *Advanced Problems in Mechanics. Vol. 2*. St. Petersburg (2006)
[6] Zhilin, P. A.: *Theoretical Mechanics*. St. Petersburg (2001) (in Russian)
[7] Brown, W. F.: *Magnetoelastic Interactions*. Springer, New York, 1966
[8] Eringen, A. C., Maugin, G. A.: *Electrodynamics of Continua*. Springer, New York, 1990
[9] Maugin, G. A.: *Continuum Mechanics of Electromagnetic Solids*. Elsevier Science Publishers, Oxford, 1988
[10] Truesdell, C. *The Elements of Continuum Mechanics*. Springer, New York, 1965
[11] Eringen, A. C.: *Mechanics of Continua*. Huntington - New York, 1980
[12] Christensen, R. M.: *Theory of Viscoelasticity*. Academic Press, New York and London, 1971
[13] Kondepudi, D., Prigogine, I.: *Modern Thermodynamics. From Heat Engines to Dissipative Structures*. Chichester et al. 1998
[14] Koshkin, N. I., Shirkevich, M. G.: *Handbook of Elementary Physics*. Moscow, 1968
[15] Ebert, H.: *Physikalisches Taschenbuch*. Braunschweig, 1957
[16] Handbook of Physical Quantities. Ed. by I.S. Grigoriev and E.Z. Meilikhov. CRC Press, 1997
[17] Physical Acoustics. Principles and Methods. Ed. by W. Mason. Vol. 2, Part A. Properties of Gases, Liquids and Solutions. New York - London, 1965

Chapter 8
Micromechanical Bases of Superelastic Behavior of Certain Biopolymers

Rasa Kazakevičiūtė-Makovska and Holger Steeb

Abstract This work presents a new constitutive theory aiming to describe the truly exceptional, only little known and almost completely uncharacterized thermomechanical properties of the whelk egg capsule biopolymer (WECB) which has been recently reported in the literature. The mechanical model is based on the concept of generalized continua. It includes familiar damage-type models and pseudo-elastic models for stress softening (the Mullins effect) in elastomers (natural and synthetic rubbers) and soft tissues. However, the mechanical behavior of WECB is in many aspects very different from the behavior of other elastomeric materials and these differences have been accounted for in the developed constitutive model.

Key words: Biopolymers. Constitutive models. Superelasticity. Generalized continua.

8.1 Introduction

The macroscopically observed behavior of solid materials is governed by the underlying physical mechanisms which take place at smaller (meso- , micro- and even nano-) scales and which must be accounted for in the relevant continuum models. This multiscale issue is a long standing problem in the field of generalized continua

Rasa Kazakevičiūtė-Makovska
Mechanics-Continuum Mechanics, Ruhr-University Bochum, D-44780 Bochum, Germany
Tel.: +49-(0)234-3228018
Fax: +49-(0)234-3214229
e-mail: Rasa.Kazakeviciute-Makovska@rub.de

Holger Steeb
Mechanics-Continuum Mechanics, Ruhr-University Bochum, D-44780 Bochum, Germany
Tel.: +49-(0)234-3223080
Fax: +49-(0)234-3214229
e-mail: Holger.Steeb@rub.de

H. Altenbach et al. (eds.), *Mechanics of Generalized Continua,*
Advanced Structured Materials, 7, DOI: 10.1007/978-3-642-19219-7_8,

[8]. More recently, there is observed an increasing interest in the molecular basis of mechanical and thermal properties of natural polymers (biopolymers) with the hope to develop biomimetic materials for biomedical applications [3].

This work is concerned with the whelk egg capsule biopolymer (WECB) which is a proteinaceous composite material with truly exceptional thermo-mechanical properties recently reported in the literature [9, 11, 12]. Some of these properties are shortly discussed in Sect. 8.2, where also similarities and dissimilarities with other polymers and elastomers as well as with shape memory alloys are pointed out. In Sect. 8.3, the structure of WECB and the micro-mechanisms underlying the macroscopically observed thermo-mechanical properties of this material are discussed on the bases of results presented in the above cited contributions. This analysis leads to the concept of a scalar micro-structural variable which measures an extent of the α-helix $\leftrightarrow$ β-sheet transition, which has been recognized as the basic mechanism responsible for the behavior of WECB. It is next stipulated, following earlier works [4, 6, 14], that the evolution of this micro-structural variable must be accompanied by microforces and microstresses, which are assumed to satisfy their own balance law. This balance equation, together with the classical balance laws of linear and angular momentum are the only postulates on which the complete purely mechanical theory is developed (Sect. 8.4). This model is phenomenological in nature and it applies to different classes of materials with widely varying mechanical properties. In the following Sect. 8.5, the general theory is reduced to a pseudo-elastic model proposed in [10] and used in the description of the Mullins effect observed in elastomers and soft tissues (see [1, 6] and references cited therein). Then, in Sect. 8.6 we formulate the superelastic model for the whelk egg capsule biopolymer. Subsequently, in Sect. 8.7, we reduce the theory of superelasticity to a one-dimensional setting and develop a methodology to identify the relevant response functions. Finally, an illustrative example of special constitutive model is presented in Sect. 8.8.

8.2 Macroscopic Thermo-mechanical Properties of WECB

In recent experimental studies [9, 11, 12], the qualitative and quantitative thermo-mechanical characterization of the egg capsules produced by Busycon canaliculatum and Busycon carica has been reported with the goal to assess the response of this material to applied stresses and temperature, and to understand how it compares to other structurally important biomaterials.

The results reported in [9, 11, 12] indicate that whelk egg capsule biopolymer (WECB) has a long-range elasticity domain but, additionally, exhibits the interesting feature of a fully recoverable and repeatable order of magnitude decrease in elastic stiffness occurring at approximately 3 % - 5% strain (Fig. 8.1). This drastic reduction in the elastic stiffness appears to be a material failure, yet is fully recoverable as it is clearly observed from cyclic tests (Fig. 8.2). This behavior may be contrasted with the mechanical properties of other polymers and elastomers.

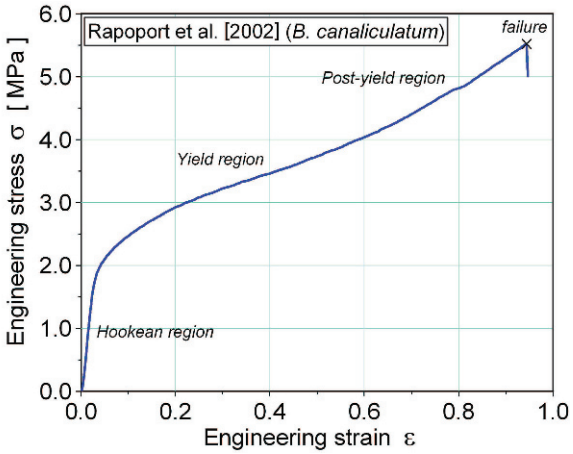

Fig. 8.1 Extension to failure of the WECB specimen

In quasi-static tension tests, typical elastomers such as natural and synthetic rubbers as well as soft tissues show a characteristic stress hardening with increasing strains, *S*-shaped and *J*-shaped stress-strain curves, respectively. This property is a result of the finite chain extensibility which exhibit all elastomeric materials including soft tissues [1, 6, 13]. In contrast, WECB shows a kind of yielding or tensile failure typical for metals rather than for elastomers. An apparent yielding of WECB is transient only and a complete recovery occurs during unloading to zero stress. In contrast, all elastomers show a certain permanent set (plastic strain) upon complete

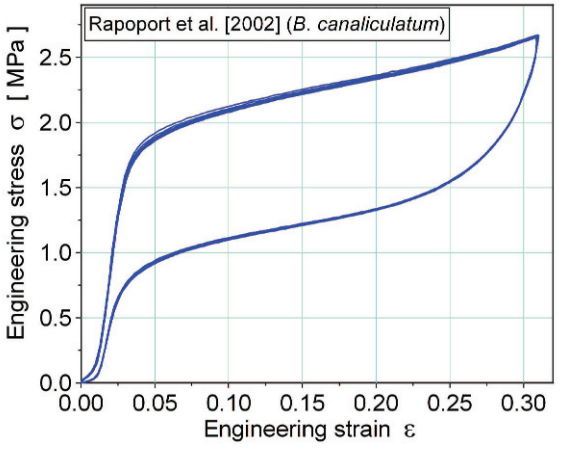

Fig. 8.2 Many cycles of extension of the WECB specimen to a fixed strain level

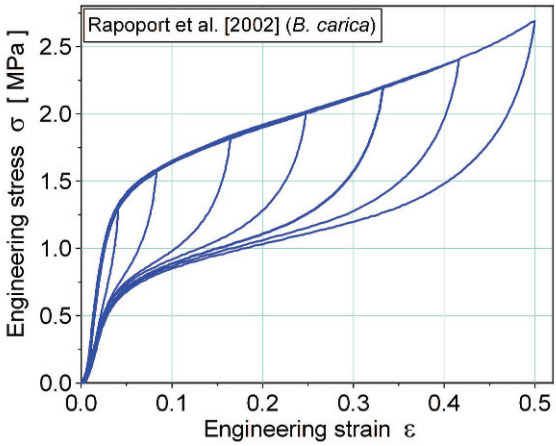

Fig. 8.3 Cycles of extension of the WECB specimen to successively increasing strains

unloading [1, 6, 13]. In this respect, WECB may be considered as a highly elastic protein polymer with self-healing mechanical properties similar to those of the byssal threads, c.f. [9]. However, WECB recovers from stresses much more rapidly, almost instantaneously, a property unknown in any other natural or synthetic material.

Even more striking differences between the behavior of WECB and other elastomeric materials may be observed from cyclic tests to successively increasing strain levels (Fig. 8.3). In the case of WECB, the reloading curves completely coincide with the primary loading curve of the virgin sample. This property is totally absent in all elastomeric materials including soft tissues for which the primary loading, unloading and reloading curves are different [1, 6, 13].

The complete recovery phenomenon of WECB during unloading to a zero stress state is reminiscent of pseudo-elastic effect typical for shape memory alloys (SMA) [7]. This similarity has certain physical bases. However, these two classes of materials are different in their thermal properties. As it could be observed in Fig. 8.4, increasing the temperature of the water bath in which the WECB specimen is being quasi-statically cycled results in a decrease of the yield stress and a recession of the Hookean region. At temperatures approaching $100°C$, the Hookean region appears to be absent (Fig. 8.5). In sharp contrast, for SMA the transition stress has a linear relationship with temperature having the positive slope matching the Clausius-Clapeyron law of thermoelastic martensitic transformations [7]. For WECB, the transition stress is non-linear, in general, with a negative slope (Fig. 8.5). However, the transformation strain in both cases is not influenced by temperature.

The test results of Fig. 8.4 show that the elastic modulus for WECB has an inverse relationship to temperature. Thus, although WECB should be considered as an elastomeric material due to its microstructure and long range elasticity, it behaves

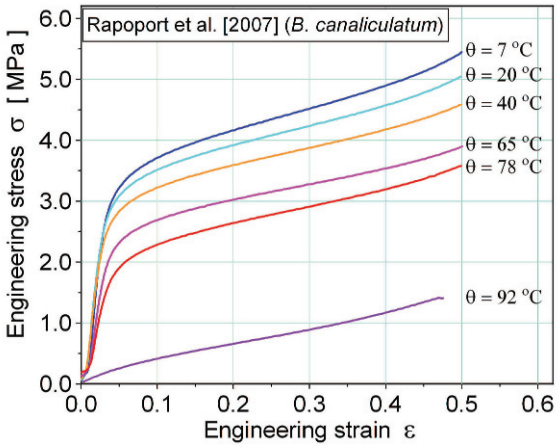

Fig. 8.4 Representative extension curves for the WECB at different temperatures

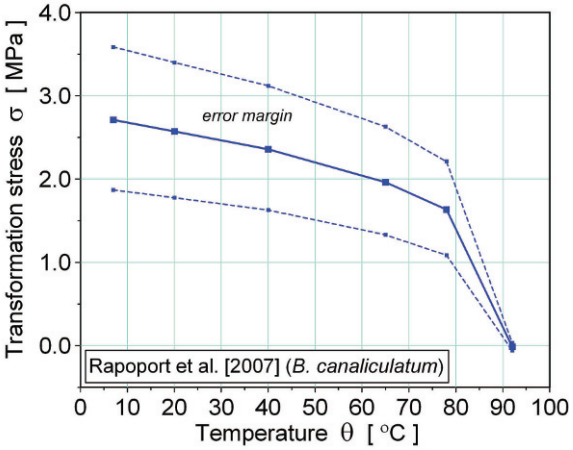

Fig. 8.5 Graph of the WECB yield (transition) stress v.s. temperature exposure

contrary to entropic elasticity, the most characteristic properties of natural and synthetic rubbers as well as of soft tissues [1, 13].

8.3 Structure of WECB and Micro-mechanisms of Straining

The studies [11, 12] show that the whelk egg capsule biopolymer (WECB) is a proteinaceous composite elastomer possessing α-helical structural motifs (determined from X-ray diffraction studies) and hierarchical layers of ordered fibrous

constituents, suggestive of a structure analogous to an intermediate filament (IF)-based material such as that of hard α-keratin [2]. Moreover, the light microscopy studies reported in the same contributions reveal that WECB can be composed of numerous distinct layers of material that possess subtle differences in observable texture, although it is purported that the layers are all composed of the same material.

Furthermore, wide angle X-ray scattering studies reported in [9] show a coiled coil (cc) α-helix $\leftrightarrow$ β-sheet transition when the material is strained past the apparent yield point. This transition is reversed back to the cc α-helix when the material is cycled back to zero strain. The governing physical mechanism is responsible for the macroscopically observed complete recovery of strain upon unloading to the zero stress level, an effect which is know as the superelastic behavior typical for shape memory alloys (SMA) resulting from the austenite-martensite phase transition. The observed analogy in macroscopic behavior and the phase transition mechanisms suggest that the constitutive modeling of WECB may be based on either of the two approaches:

- A quasi-convex relaxation approach used to construct effective models for materials that undergo phase transformations, such as austenite-martensite phase transition in SMA.
- A phase transition variable concept similar to the concept of martensitic volume fraction used in modeling the shape memory alloys. In this concept, the state variables such as stress, strain and temperature are considering as functions of the phase transition variable.

Both approaches are phenomenological, formulated within the well-developed concepts of continuum thermodynamics. Moreover, such models can be built up largely independently of the specific classes of materials. In this paper, we follow another approach which has been earlier applied by the authors to model the basic properties of elastomers [6] and polymers [4, 14].

8.4 Micromechanically Motivated Constitutive Models

Consider a continuous body identified with a fixed uniform reference configuration B in the physical space. A motion of B is the mapping of material points $\boldsymbol{x}$ and time t given by $\boldsymbol{y} = \boldsymbol{y}(\boldsymbol{x},t)$. The deformation gradient is $\boldsymbol{F} = \boldsymbol{\nabla} \boldsymbol{y}$ with $\det \boldsymbol{F} > 0$. Assuming sufficient continuity of the relevant fields, the balance equations of linear and angular momentum take the local form for quasi-static conditions

$$\operatorname{Div} \boldsymbol{P} + \boldsymbol{b} = \boldsymbol{0}, \qquad \boldsymbol{P}\boldsymbol{F}^T - \boldsymbol{F}\boldsymbol{P}^T = \boldsymbol{0}. \tag{8.1}$$

Here $\boldsymbol{P}(\boldsymbol{x},t)$ denotes the first Piola-Kirchhoff stress tensor and $\boldsymbol{b}(\boldsymbol{x},t)$ is the external body force.

Considering α-helix $\leftrightarrow$ β-sheet transition as the physical mechanism underlying the macroscopically observed mechanical properties of WECB, we shall assume

that this process is characterized by a single scalar field variable $\alpha = \alpha(\boldsymbol{x},t)$. This micro-variable serves to measure the amount of phase transition from the α-helix to the β-sheet and hence it varies from 0 to 1 (say), with $\alpha = 0$ and $\alpha = 1$ corresponding to pure α-helix and the β-sheet phases, respectively. Although the mechanism of the α-β transition occurring in WECB due to straining is not completely understood, it is natural to postulate that the evolution of the microvariable α is accompanied by microforces and microstresses satisfy their own law of balance, which in the local form reads [4, 6, 14]

$$\mathrm{Div}\,\boldsymbol{\pi} + \zeta + \beta = 0. \tag{8.2}$$

In this theory, $\boldsymbol{\pi}(\boldsymbol{x},t)$ is a microstress (vector), $\zeta(\boldsymbol{x},t)$ an internal microforce (scalar) and $\beta(\boldsymbol{x},t)$ an external microforce.

The balance laws of macroforces $(8.1)_1$ and microforces (8.2) may be expressed in the weak form

$$W_i(P,t) - W_e(P,t) = 0 \tag{8.3}$$

representing the principle of virtual velocities for any part P of the body B. Here

$$W_i(P,t) = \int_P (\boldsymbol{P}\cdot\boldsymbol{\nabla}\boldsymbol{v} + \zeta v + \boldsymbol{\pi}\cdot\boldsymbol{\nabla}v)\ \mathrm{dV} \tag{8.4}$$

and

$$W_e(P,t) = \int_P (\boldsymbol{b}\cdot\boldsymbol{v} + \beta v)\ \mathrm{dV} - \int_{\partial P} (\boldsymbol{P}\boldsymbol{n}\cdot\boldsymbol{v} + (\boldsymbol{\pi}\cdot\boldsymbol{n})\, v)\ \mathrm{dA} \tag{8.5}$$

are the mechanical power of internal and external macro- and microforces/ stresses acting on any part of the body. In (8.4) and (8.5), $\boldsymbol{v} = \boldsymbol{v}(\boldsymbol{x},t)$ and $v = v(\boldsymbol{x},t)$ are the macroscopic and microscopic velocity fields.

In an isothermal context, the second law of thermodynamics requires that the rate of increase of energy cannot exceed the power expended on any part of the body. Letting Ψ denote the free energy, the second law for the considered purely mechanical theory takes the form of dissipation inequality

$$\delta \equiv \Sigma - \dot{\Psi} \geq 0, \tag{8.6}$$

where the stress power density is given by

$$\Sigma = \boldsymbol{P}\cdot\dot{\boldsymbol{F}} + \zeta\,\dot{\alpha} + \boldsymbol{\pi}\cdot\boldsymbol{\nabla}\dot{\alpha} \tag{8.7}$$

in consistency with the derived form of the internal mechanical power (8.4). Throughout this paper we use a superposed dot to denote the material time derivative with respect to the (macroscopic) motion of the material point.

The constitutive theory requires that Ψ, $\boldsymbol{P}$, ζ and $\boldsymbol{\pi}$ are given as functions of the variables $\boldsymbol{F}$, α, $\boldsymbol{\nabla}\alpha$, $\dot{\boldsymbol{F}}$ and $\dot{\alpha}$. In modern theories of continuum thermodynamics, such response functions must satisfy a priori the dissipation inequality (8.6) for all admissible processes. As a result we obtain:

1) the free energy is independent of $\dot{\boldsymbol{F}}$ and $\dot{\alpha}$,

$$\Psi = \hat{\Psi}(\boldsymbol{z}), \qquad \boldsymbol{z} \equiv (\boldsymbol{F}, \alpha, \boldsymbol{\nabla}\alpha), \tag{8.8}$$

2) the microstress is related to the free energy through the relation

$$\boldsymbol{\pi} = \partial_{\boldsymbol{\nabla}\alpha}\hat{\Psi}(\boldsymbol{z}), \tag{8.9}$$

3) the macrostress and the microforce admit the representations

$$\boldsymbol{P} = \partial_{\boldsymbol{F}}\hat{\Psi}(\boldsymbol{z}) + \hat{\boldsymbol{P}}_v(\boldsymbol{z}, \dot{\boldsymbol{F}}, \dot{\alpha}), \tag{8.10a}$$

$$\zeta = \partial_{\alpha}\hat{\Psi}(\boldsymbol{z}) + \hat{\zeta}_v(\boldsymbol{z}, \dot{\boldsymbol{F}}, \dot{\alpha}), \tag{8.10b}$$

4) the additional response functions $\hat{\boldsymbol{P}}_v(\boldsymbol{z}, \dot{\boldsymbol{F}}, \dot{\alpha})$ and $\hat{\zeta}_v(\boldsymbol{z}, \dot{\boldsymbol{F}}, \dot{\alpha})$ appearing in (8.10a) and (8.10b) must satisfy the reduced dissipation inequality

$$\delta = \hat{\boldsymbol{P}}_v(\boldsymbol{z}, \dot{\boldsymbol{F}}, \dot{\alpha}) \cdot \dot{\boldsymbol{F}} + \hat{\zeta}_v(\boldsymbol{z}, \dot{\boldsymbol{F}}, \dot{\alpha})\dot{\alpha} \geq 0 \tag{8.11}$$

for all admissible values of their arguments.

The microstress $\boldsymbol{\pi}$ drives the changes in the gradient of the microvariable α and thus it will only be a factor in regions where α rapidly varies from point to point in the material. This is the case in problems of strain localizations and size effect observed in many materials [4, 14], but this is not of primary importance in the problem considered in this work.

8.5 Non-gradient Models and Pseudo-elasticity

For homogenous deformation or deformations with only mild changes in α, the influence of the gradient of the microvariable $\boldsymbol{\nabla}\alpha$ on the material behavior may be expected to be small and hence negligible. In this case, the free energy is given by $\Psi = \hat{\Psi}(\boldsymbol{F}, \alpha)$ and the general constitutive equations (8.10a) and (8.10b) are reduced to

$$\boldsymbol{P} = \partial_{\boldsymbol{F}}\hat{\Psi}(\boldsymbol{F}, \alpha) + \hat{\boldsymbol{P}}_v(\boldsymbol{F}, \alpha, \dot{\boldsymbol{F}}, \dot{\alpha}), \tag{8.12a}$$

$$\zeta = \partial_{\alpha}\hat{\Psi}(\boldsymbol{F}, \alpha) + \hat{\zeta}_v(\boldsymbol{F}, \alpha, \dot{\boldsymbol{F}}, \dot{\alpha}) \tag{8.12b}$$

with $\boldsymbol{\pi} = \boldsymbol{0}$ in consistency with the assumption that $\boldsymbol{\nabla}\alpha \cong \boldsymbol{0}$. By implication, the governing macroscopic field equation resulting from the balance of linear momentum takes the form

$$\mathrm{Div}\,(\partial_{\boldsymbol{F}}\hat{\Psi}(\boldsymbol{F}, \alpha) + \hat{\boldsymbol{P}}_v(\boldsymbol{F}, \alpha, \dot{\boldsymbol{F}}, \dot{\alpha})) + \boldsymbol{b} = \boldsymbol{0} \tag{8.13}$$

and the balance law of microforces (8.2) is reduced to an evolution law for the microvariable α in the implicit form

$$\partial_\alpha \hat{\Psi}(\boldsymbol{F}, \alpha) + \hat{\zeta}_v(\boldsymbol{F}, \alpha, \dot{\boldsymbol{F}}, \dot{\alpha}) = 0. \tag{8.14}$$

Here and in the following, we neglect the external microforce β.

If the resulting constitutive relation (8.14) may be solved for the rate of change of the microvariable α, then it assumes the form of an evolution law

$$\dot{\alpha} = \hat{\alpha}(\boldsymbol{F}, \alpha, \dot{\boldsymbol{F}}), \tag{8.15}$$

which in the classical theory of materials with internal variables is postulated as the basic constitutive assumption.

The behavior of all materials, except of truly elastic ones, depends on the history of strain. Creep and stress-relaxation are the most familiar examples of such dependency and the quasilinear viscoelastic model accurately describes these effects. Most of the elastomeric materials, including soft tissues, demonstrate a different strain-history dependence known as stress softening or as the Mullins effect [1, 6, 10]. In such materials, the stress-strain relation depends on the maximum previous strain experienced by the specimen. Moreover, these materials become permanently softened after the strain reaches a new maximum for the first time. It has been also suggested that stress softening may explain preconditioning behavior. Thus, some of the history dependence in elastomeric material that has previously been attributed to viscoelasticity may actually be the result of stress softening, which may be modeled on the basis of the theory presented in the current investigation. Indeed, it has been shown in [6] that under the additional assumption $\hat{\zeta}_v(\boldsymbol{F}, \alpha, \dot{\boldsymbol{F}}, \dot{\alpha}) = 0$, the evolution equation (8.14) representing the balance of microforces reduces to the form postulated in [10] as the basic constitutive equation of a pseudo-elastic model for the Mullins effect.

8.6 Constitutive Model of Superelasticity

Ideal elasticity is the basic model describing the property whereby the energy expended in the deformation of the material recovers completely if the applied forces are entirely removed. In the uni-axial case, the energy expended in deformation is given by the area under the stress-strain curve. Therefore, an ideal elastic material exhibits a perfect reversible stress-strain relation, i.e. the loading and unloading curves coincide.

The whelk egg capsule biopolymer (WECB) is not ideal elastic in that sense. As we can observe in Fig. 8.2, the loading and unloading curves do not coincide. This is also observed for all elastomeric materials. However, WECB exhibits three striking features in its mechanical response totally absent in elastomers and soft tissues:

1. the complete recovery upon reducing the deforming stress to zero (no residual strains or permanent set),
2. the reloading stress-strain path coincide completely with the primary loading curve of the virgin sample,
3. unloading and reloading paths are retraced for any number of cycling loading.

These mechanical properties under the additional assumption of rate independence allow us to formulate the constitutive model for this kind of biopolymers by introducing additional assumptions into the general theory presented in Sect. 8.5.

Keeping in mind the principle of material objectivity, the free energy is assumed to be a function of the Green-Lagrange strain tensor $\boldsymbol{E}$, i.e. $\Psi = \hat{\Psi}(\boldsymbol{E}, \alpha)$, so that the stress-strain relation (8.12a) may be rewritten in terms of the second Piola-Kirchhoff stress tensor $\boldsymbol{S}$ as

$$\boldsymbol{S} = \partial_{\boldsymbol{E}} \tilde{\Psi}(\boldsymbol{E}, \alpha), \tag{8.16}$$

where $\boldsymbol{S}$ and $\boldsymbol{E}$ are defined by

$$\boldsymbol{S} = \boldsymbol{F}^{-1}\boldsymbol{P}, \tag{8.17a}$$

$$\boldsymbol{E} = \frac{1}{2}\left(\boldsymbol{F}^T\boldsymbol{F} - \mathbf{1}\right). \tag{8.17b}$$

In consistency with the assumption of rate independency, the dissipative part of the macroscopic stress tensor has been set to zero in the constitutive relation (8.16). However, this assumption does imply that the dissipative part of the microforce may be neglected. Thus, the constitutive relation (8.14) preserves its general form, which written in terms of $\boldsymbol{E}$ reads

$$\partial_\alpha \tilde{\Psi}(\boldsymbol{E}, \alpha) + \tilde{\zeta}_v(\boldsymbol{E}, \alpha, \dot{\boldsymbol{E}}, \dot{\alpha}) = 0, \tag{8.18}$$

so that the principle of material objectivity is identically satisfied.

For rate independent models, the dependence of the response function $\tilde{\zeta}_v$ on the strain rate is very special, actually it only depends on the distinction between loading and unloading process. In order to quantify loading/unloading process in the general three-dimensional theory, we introduce the scalar measure of deformation extent defined as $\varepsilon = \tilde{\varepsilon}(\boldsymbol{E})$. A simple example of such a measure is given by the Euclidean norm of the strain tensor $\boldsymbol{E}$, but in the present paper we do not specify this measure explicitly. The only general requirement is that ε vanishes in any rigid motion, i.e. $\tilde{\varepsilon}(\mathbf{0}) = 0$. Moreover, we assume that the sign of $\dot{\varepsilon}$ correctly quantifies the loading/unloading process. These requirements combined with the assumption of rate independence allow the constitutive relation (8.18) to be written in the form

$$\partial_\alpha \tilde{\Psi}(\boldsymbol{E}, \alpha) + \tilde{\zeta}_v(\boldsymbol{E}, \alpha, \operatorname{sign}\dot{\varepsilon}, \dot{\alpha}) = 0. \tag{8.19}$$

Thus, the evolution of the microvariable $\alpha(\boldsymbol{x}, t)$ depends on the strain rate only through the sign of the rate of the measure of deformation extent with $\operatorname{sign}\dot{\varepsilon} > 0$ and $\operatorname{sign}\dot{\varepsilon} < 0$ defining the loading and unloading process, respectively.

If in addition the constitutive relation (8.19) may be solved for $\dot{\alpha}$, then the evolution of the microvariable α is determined by two constitutive laws:

$\operatorname{sign}\dot{\varepsilon} > 0$ (loading)

$$\dot{\alpha} = \zeta_L(\boldsymbol{E}, \alpha), \tag{8.20a}$$

$\operatorname{sign}\dot{\varepsilon} < 0$ (unloading)

$$\dot{\alpha} = \zeta_U(\boldsymbol{E}, \alpha; \varepsilon_m), \tag{8.20b}$$

where $\zeta_L(\boldsymbol{E}, \alpha)$ and $\zeta_U(\boldsymbol{E}, \alpha; \varepsilon_m)$ are independent response functions, and ε_m denotes the maximum strain undergone by the material during loading process.

The set of evolution laws (8.20a) and (8.20b) together with the stress-strain relation (8.16) completely describe the behavior of the material for an arbitrary deformation history. Furthermore, the assumptions leading to this constitutive model are consistent with the mechanical properties of whelk egg capsule biopolymer (WECB).

8.7 Identification of Response Functions: 1D Theory

In the one-dimensional case, the general constitutive relations derived in the previous section give the stress-strain relation in the form

$$\sigma = \tilde{\sigma}(\varepsilon, \alpha) = \partial_\varepsilon \tilde{\psi}(\varepsilon, \alpha). \tag{8.21}$$

Here σ and ε are the uni-axial engineering stress and strain, respectively, and $\tilde{\psi}(\varepsilon, \alpha)$ is the corresponding free energy function. Let us recall, that the engineering strain is defined by $\varepsilon = \lambda - 1$, where the stretch $\lambda = dy/dx$ is the ratio of the actual and reference length of a material line element.

In specifying the evolution laws (8.20a) and (8.20b) for the uni-axial case, we make the following assumptions. First, we assume that in the case of uni-axial deformation, the general measure of deformation extent introduced in the previous section coincides with the engineering strain and hence the same symbol is used for both quantities. Second, we assume that the general evolution laws (8.20a) and (8.20b) may be integrated, in order to obtain expressions in an explicit form. By implication of these two assumptions, the evolution laws for the microvariable α are obtained as:

$\operatorname{sign}\dot{\varepsilon} > 0$ (loading)

$$\alpha = \tilde{\alpha}_l(\varepsilon), \tag{8.22a}$$

$\operatorname{sign}\dot{\varepsilon} < 0$ (unloading)

$$\alpha = \tilde{\alpha}_u(\varepsilon; \varepsilon_m). \tag{8.22b}$$

Both assumptions are consistent with the theory of stress softening in elastomeric materials [1, 5, 10]. In effect, the problem of constitutive modeling is reduced to the determination of the response function $\tilde{\sigma}(\varepsilon, \alpha)$ for the stress σ or equivalently to the

determination of the free energy function $\tilde{\psi}(\varepsilon, \alpha)$, and the response functions $\tilde{\alpha}_l(\varepsilon)$ and $\tilde{\alpha}_u(\varepsilon; \varepsilon_m)$ occurring in the evolution laws . The constitutive setting developed below gives the set of evolution laws (8.22a) and (8.22b) for any thermodynamically admissible response function $\tilde{\sigma}(\varepsilon, \alpha)$.

8.7.1 Modeling the Loading Path

In a standard tensile test up to failure (Fig. 8.1), the stress-strain curve exhibits three nearly linear distinct domains with the tangential moduli depending on the strain level in a characteristic way shown in Fig. 8.6. In the presented theory, the

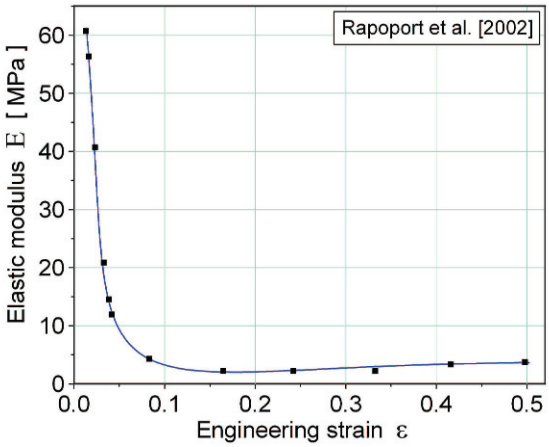

Fig. 8.6 Experimentally determined variation of the tangential modulus of elasticity with strain for the WECB data shown in Fig. 8.1.

tangential modulus is determined by the derivative of the constitutive relation (8.21) with respect to strain:

$$E = \frac{\mathrm{d}\tilde{\sigma}}{\mathrm{d}\varepsilon} = \frac{\partial \tilde{\sigma}}{\partial \varepsilon} + \frac{\partial \tilde{\sigma}}{\partial \alpha}\frac{\partial \tilde{\alpha}}{\partial \varepsilon}. \tag{8.23}$$

Setting

$$A(\varepsilon, \alpha) \equiv \frac{\partial \tilde{\sigma}(\varepsilon, \alpha)}{\partial \alpha}, \qquad B(\varepsilon, \alpha) \equiv \frac{\partial \tilde{\sigma}(\varepsilon, \alpha)}{\partial \varepsilon} \tag{8.24}$$

for notational simplicity, the relation (8.23) takes the form of the first order differential equation of the form

$$A(\varepsilon, \alpha)\frac{\partial \tilde{\alpha}(\varepsilon)}{\partial \varepsilon} + B(\varepsilon, \alpha) - E(\varepsilon) = 0. \tag{8.25}$$

Both $A(\varepsilon,\alpha)$ and $B(\varepsilon,\alpha)$ are uniquely determined functions whenever any particular form of the response function $\tilde{\sigma}(\varepsilon,\alpha)$ is assumed. Moreover, the tangential elastic modulus as function of strain, $E(\varepsilon)$, may be determined from the data of standard tensile test (see Fig. 8.6). As a result, the general solution of the differential equation (8.25) with the initial condition $\tilde{\alpha}(0)=0$ yields the evolution law (8.22a) in the most general form. This methodology makes it possible to determine the evolution law (8.22a) directly from the experimental data for any particular form of the response function $\tilde{\sigma}(\varepsilon,\alpha)$, equivalently for the assumed free energy function $\tilde{\psi}(\varepsilon,\alpha)$.

8.7.2 Modeling the Unloading Paths

In order to determine the evolution law (22b) for the unloading process, we first need an appropriate method to characterize the unloading curves from any predefined strain ε_m. For the complete loading-unloading cycle with given ε_m, the most important property is the hysteretic effect. It was shown in [11] that the hysteresis sharply increases for pre-strains up to abound 5 % and only small changes are observed for higher pre-strains. This observation is in close relation with the variation in the tangent elastic modulus shown in Fig. 8.6.

Besides the hysteresis for the complete loading-unloading cycle, we need to characterize the unloading curves within each cycle. There are two basic quantities which serve this purpose, the stress ratio defined as $\rho_\sigma \equiv \sigma_u/\sigma_l$ at any value of strain ε and the strain ratio $\rho_\varepsilon \equiv \varepsilon_u/\varepsilon_l$ or strain difference $\delta_\varepsilon = \varepsilon_l - \varepsilon_u$ defined at any value of stress σ (Fig. 8.7).

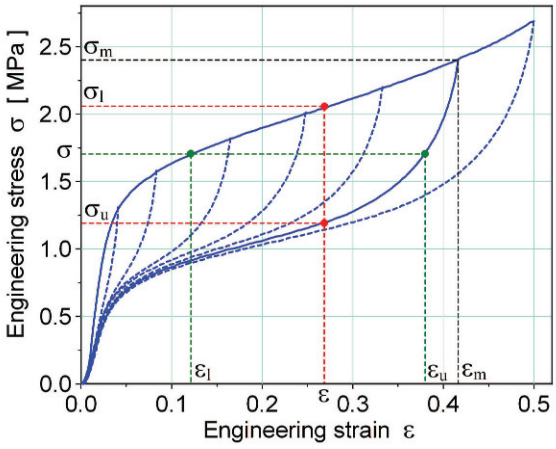

Fig. 8.7 Cyclic tension test: Definition of stress and strain ratio

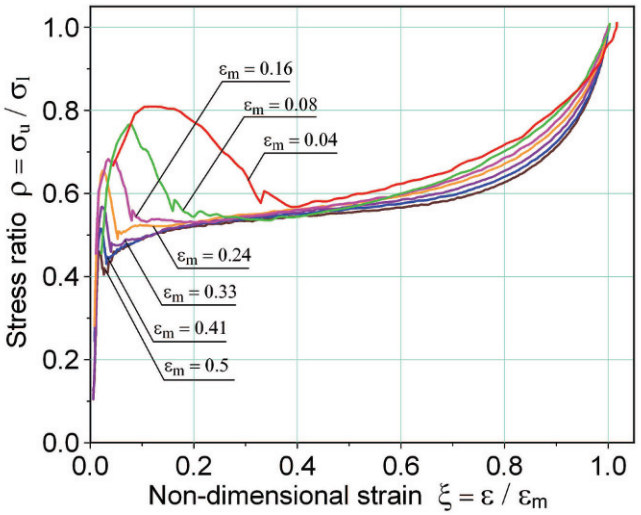

Fig. 8.8 Stress ratio vs. normalized strain for the data of Fig. 8.3.

Figure 8.8 shows the stress ratio computed for the data shown in Fig. 8.3. Here the normalized strain is defined by $\xi \equiv \varepsilon/\varepsilon_m$ for any pre-strain ε_m. Using the concept of the stress ratio ρ_σ and the strain ratio ρ_ε, the response function in the evolution law for the unloading process can be determined as follows. Taking into account the constitutive law (8.21) together with the evolution laws (8.22a) and (8.22b), we obtain

$$\rho_\sigma = \tilde{\rho}_\sigma(\varepsilon;\varepsilon_m) \equiv \frac{\sigma_u}{\sigma_l} = \frac{\tilde{\sigma}(\varepsilon,\tilde{\alpha}_u(\varepsilon,\varepsilon_m))}{\tilde{\sigma}(\varepsilon,\tilde{\alpha}_l(\varepsilon))}. \tag{8.26}$$

Furthermore, it follows that the stress-strain relation for the unloading from any value of pre-strain ε_m is given by the relation

$$\tilde{\sigma}_u(\varepsilon;\varepsilon_m) = \tilde{\rho}_\sigma(\varepsilon;\varepsilon_m)\tilde{\sigma}_l(\varepsilon), \tag{8.27}$$

where

$$\tilde{\sigma}_u(\varepsilon;\varepsilon_m) \equiv \tilde{\sigma}(\varepsilon,\tilde{\alpha}_u(\varepsilon;\varepsilon_m)), \quad \tilde{\sigma}_l(\varepsilon) \equiv \tilde{\sigma}(\varepsilon,\tilde{\alpha}_l(\varepsilon)). \tag{8.28}$$

Note that the stress ratio $\tilde{\rho}_\sigma(\varepsilon;\varepsilon_m)$ may be determined directly from cyclic tension tests. Moreover, the response function $\tilde{\sigma}_l(\varepsilon)$ for the loading process is determined by the method described in the previous section. Thus, the relation (8.27) serves to determine the response function $\tilde{\sigma}_u(\varepsilon;\varepsilon_m)$ for the unloading process and implicitly it determines the response function for evolution law (8.22b). It could be observed in Fig. 8.8, that the stress ratio curves determined for different pre-strains collapse to a single curve for a normalized strain ξ higher than 0.4. Thus, within this range the mechanical behavior of WECB during unloading is essentially independent of

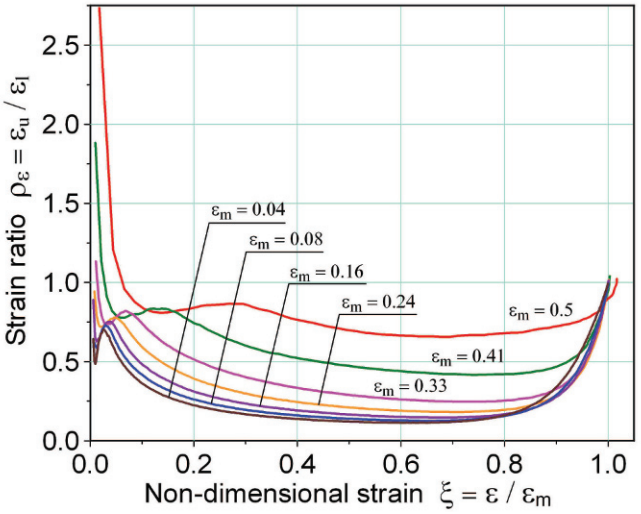

Fig. 8.9 Plots of strain ratio vs normalized strain for the data of Fig. 8.3.

the pre-strain ε_m. In view of the relations derived above, we conclude that the extent of the α-helix $\leftrightarrow$ β-sheet transition in that range of deformation is actually independent of the pre-strain. However, for lower values of ξ , the sharp differences are observed between the stress ratio computed for different unloading curves. It is interesting to note that the highest value of stress ratio is obtained at the smallest pre-strain. This observation may be used to characterize quantitatively the extent of the α-helix $\leftrightarrow$ β-sheet transition. However, in that range of deformation, the computation of the stress ratio is very sensitive to measurement errors. For this reason, the strain ratio may be considered as a more appropriate quantity for the characterization of the unloading curves (see Fig. 8.9) and for the development of the corresponding evolution law.

8.8 Special Models

As an illustrative example of the general constitutive relations for the superelastic behavior of WECB in uni-axial cyclic tension tests, let us consider a very simple stress-strain law in the form

$$\sigma = \tilde{\sigma}(\varepsilon, \alpha) = H(\alpha)\varepsilon \tag{8.29}$$

with the (effective) elastic modulus $H(\alpha)$ given by

$$H(\alpha) = (1 - \alpha)E_A + \alpha E_B. \tag{8.30}$$

Here, E_A and E_B are the elastic moduli in the Hookean and yield regime indicated in Fig. 8.1. Under the assumptions (8.29) and (8.30), Eq. (8.25) reads

$$\varepsilon \frac{\partial \tilde{\alpha}(\varepsilon)}{\partial \varepsilon} + \tilde{\alpha}(\varepsilon) + \tilde{E}(\varepsilon) = 0, \tag{8.31}$$

where $\tilde{E}(\varepsilon)$ is defined by

$$\tilde{E}(\varepsilon) = \frac{1}{E_A - E_B}(E(\varepsilon) - E_A). \tag{8.32}$$

The general solution of differential equation (8.31) has the form

$$\tilde{\alpha}(\varepsilon) = \frac{1}{\varepsilon}(-\int \tilde{E}(\varepsilon) d\varepsilon + C) \tag{8.33}$$

with the constant C to be determined from the initial condition $\tilde{\alpha}(0) = 0$. The constants E_A and E_B as well as the function $E(\varepsilon)$ may be determined from the data (see e.g. Fig. 8.6). Then, the integral in (8.33) may easily be computed yielding the evolution law (8.22a) for α in the loading process. For the unloading process, the substitution of the assumptions (8.29) and (8.30) into the relation (8.27) gives

$$E_A - (E_A - E_B)\tilde{\alpha}_u(\varepsilon; \varepsilon_m) = \tilde{\rho}_\sigma(\varepsilon; \varepsilon_m) H(\tilde{\alpha}_l(\varepsilon)), \tag{8.34}$$

where $H(\tilde{\alpha}(\varepsilon))$ is defined by (8.33) and (8.30). As a result, the evolution law (8.22b) is obtained in the form

$$\tilde{\alpha}_u(\varepsilon; \varepsilon_m) = \frac{1}{E_A - E_B}(E_A - \tilde{\rho}_\sigma(\varepsilon; \varepsilon_m) H(\tilde{\alpha}_l(\varepsilon))). \tag{8.35}$$

The same approach may be applied to more general assumptions than (8.29) and (8.30).

8.9 Discussion

The present contribution provides a basis for the constitutive modeling of biopolymers having the thermo-mechanical properties observed for the whelk egg capsule. This biomaterial displays true superelasticity in the sense that it fully recovers its shape after the deforming force is removed. However, the loading and unloading paths do not coincide. Therefore, this material is not elastic in the sense of classical theories of continuum mechanics. Moreover, the behavior of the whelk egg capsule biopolymers (WECB) is totally different from the behavior of known elastomeric materials including soft tissues and some other biomaterials. In particular, for WECB the reloading curve completely coincides with the loading curve of the virgin sample, the property totally absent in other materials. Hence, we introduced a novel modeling framework for such a material behavior which is denoted as su-

perelasticity. This theory is distinct from superelastic models for the shape memory alloys as well as from pseudo-elastic models for the stress softening behavior of elastomers. The proposed extended continuum theory is based on micromechanisms which are built into the macroscopic theory through a scalar phase field measuring the extent of the α - β transition. In a general setting, the evolution of this microvariable is accompanied by microforces and microstresses satisfying their own balance equation. Thus, it fits in the context of extended continuum theories. When restricted to smooth deformations, the balance of microforces could be reduced to a (local) evolution law for the extent of the α-helix $\leftrightarrow$ β-sheet transition.

References

[1] Diani, J., Fayolle, B., Gilormini, P.: A review on the Mullins effect. Eur. Polym. Journal **45**, 601–612 (2009)

[2] Feughelman, M.: Natural protein fibers. J. Appl. Polymer Sci. **83**, 489–507 (2002)

[3] Fratzl, P.: Biomimetic materials research: what can we really learn from nature's structural materials? J. R. Soc. Interface **4**, 637–642 (2007)

[4] Johlitz, M., Steeb, H., Jänicke, R., Diebels, S.: Effective properties and size effects in filled polymers. GAMM-Mitteilungen **31**, 210–224 (2008)

[5] Kazakevičiūtė-Makovska, R.: Experimentally determined properties of softening functions in pseudo-elastic models of Mullins effect. Int. J. Solids Struct. **44**, 4145–4157 (2007)

[6] Kazakevičiūtė-Makovska, R., Kačianauskas, R.: Modelling of stress softening in elastomeric materials: foundations of simple theories. Mech. Res. Comm. **31**, 395–403 (2004)

[7] Liu, Y., Yang, H.: Strain dependence of the Clausius-Clapeyron relation for thermoelastic martensitic transformations in NiTi. Smart Mat. Struct. **16**, 22–27 (2007)

[8] Maugin, G.: Generalized continuum mechanics: What do we mean by that? In: *Mechanics of Generalized Continua: One hundred years after the Cosserats*. Eds. Maugin, G.A., Metrikine, A.V., 3–13 (2010)

[9] Miserez, A., Wasko, S., Carpenter, C., Waite, J.: Non-entropic and reversible long-range deformation of an encapsulating bioelastomer. Nature Materials **8**, 910–916 (2009)

[10] Ogden, R., Roxburgh, D.: A pseudo-elastic model for the Mullins effect in filled rubber. Proc. R. Soc. Lond. A **455**, 2861–2877 (1999)

[11] Rapoport, H., Shadwick, R.: Mechanical characterization of an unusual elastic biomaterial from the egg capsules of marine snails (Busycon spp.). Biomacromolecules **3**, 42–50 (2002)

[12] Rapoport, H., Shadwick, R.: Reversibly labile, sclerotization-induced elastic properties in a keratin analog from marine snails: whelk egg capsule biopolymer (WECB). J. Exp. Biology **210**, 12–26 (2007)

[13] Sacks, M., Sun, W.: Multiaxial mechanical behavior of biological materials. Annual Rev. Biomed. Eng. **5**, 251–284 (2003)
[14] Steeb, H., Diebels, S.: Modeling thin films applying an extended continuum theory based on a scalar-valued order parameter. Part I: Isothermal case. Int. J. Solids Struct. **41**, 5071–5085 (2004)

Chapter 9
Construction of Micropolar Continua from the Homogenization of Repetitive Planar Lattices

Francisco Dos Reis and Jean-François Ganghoffer

Abstract The derivation of the effective mechanical properties of planar lattices made of articulated bars is herewith investigated, relying on the asymptotic homogenization technique to get closed form expressions of the equivalent properties versus the geometrical and mechanical microparameters. Considering lattice microrotations as additional degrees of freedom at both scales, micropolar equivalent continua are constructed from discrete lattices made of a repetitive unit cell, from an extension of the asymptotic homogenization technique. We will show that it is necessary to solve on two different orders a linear system of equations giving the kinematic variables, at both the first and second order. The effective strain and effective curvature appear respectively as the first and second order strain variables. In the case of a centrosymmetric unit cell, there is no coupling between couple stresses and strains nor between stress and curvature. The unknown kinematic variables are determined by solving the translational and rotational equilibrium for the whole lattice. This in turn leads to the expression of the stress vector and couple stress vector, allowing to construct the Cauchy stress and couple stress tensors. The homogenized behavior of the tetragonal and hexagonal lattices is determined in terms of homogenized micropolar moduli.

Key words: Lattice homogenization. Micropolar continuum. Effective properties. Negative Poisson's ratio. Hexagonal lattice. Centrosymmetric solid.

9.1 Introduction

The derivation of the mechanical properties of foams with a regular architecture (in the sense of endowed with a quasi periodic network) in relation to the topology of

Francisco Dos Reis and Jean-François Ganghoffer
LEMTA, ENSEM, 2, Avenue de la Forêt de Haye, BP 160, 54504 Vandoeuvre Cedex, France
e-mail: jean-francois.ganghoffer@ensem.inpl-nancy.fr
e-mail: francisco.dos-reis@ac-strasbourg.fr

H. Altenbach et al. (eds.), *Mechanics of Generalized Continua,*
Advanced Structured Materials, 7, DOI: 10.1007/978-3-642-19219-7_9,

the cellular material and the material mechanical properties is especially interesting and important, in order to understand the observed behavior and to possibly tune the foam architecture to achieve certain properties at the structural level. The interest of the extension of the equivalent medium representative of the initial discrete lattice at the macroscopic scale to a micropolar medium is particularly visible in the understanding of the behavior of those lattices under certain loading conditions (concentrated forces, damage tolerance, holes) and/or geometry (stress concentration in a perforated plate). For example, in a biomechanical context, the micropolar theory applied to bone (Fatemi et al. [3], Rosenberg and Cimrman [13], Yoo and Jasiuk [17]). Fatemi et al. [3] shows that stress concentrations at the bone-prosthesis interface are significantly smaller, when compared to a classical elasticity theory. In another context, Liu and Su [8] show an increase of the microbending stiffness of multilayered beams.

Some authors have used methods based on strain energy to homogenize: in [6] the strain energy density is expressed as a function of the kinematic parameters; a continuum results when using a Taylor series expansion of those parameters, which limits the method to cells with a single node. The energy is the equivalent continuum is then expressed versus the strain tensor and microbending. A similar energy approach is involved in Florence and Sab [4], Pradel and Sab [10], but in situations with more than one node per unit cell. It is nevertheless necessary to obtain the kinematic parameters giving the minimum of the energy functional via Lagrange multipliers. Another approach is given in Warren and Byskov [16], basing on the writing of the equilibrium equations at the truss nodes and the homogenization by averaging the forces acting on a RVE. The resolution of the derived equations is done in the specific case of lattice symmetry with a mesh endowed with 120 degrees rotational symmetry ("three-fold symmetry"). In conclusion, we note that the micropolar homogenization methods being developed present limitations related to the type of mesh treaties or to a rather cumbersome mathematical method. There is accordingly a need to develop a general and versatile tool able to calculate the effective behavior of taylored materials endowed with a discrete topology up to polar continua.

In the present contribution, we extend the discrete homogenization technique recently developed by (Caillerie et al. [1], Mourad [9], Raoult et al. [11], Tollenaere and Caillerie [14]) to calculate the effective behavior of periodic lattices endowed with local rotational degrees of freedom; the geometrically linear framework is considered in the present contribution. Contrary to literature works, the method is not limited to a single node per cell. Its originality lies in that it reflects the mechanical equilibrium at each node and its resolution leads to a system of linear equations sufficiently simple and general to be easily programmable. We shall restrict our study to the 2D case, small elastic deformations and unit cells exhibiting a central symmetry.

The outline of the paper is as follows: we briefly recapitulate the constitutive equations of micropolar continua and the central problem of the asymptotic expansion of the parameters. We next discuss the main steps of the micropolar asymptotic method. The classical examples of the tetragonal and hexagonal lattices are treated to illustrate the method, and the effective elastic micropolar properties of those lat-

tices are calculated versus the lattice geometrical and mechanical parameters. We conclude with a few perspectives this work opens up.

9.2 Micropolar Constitutive Equations

The micropolar theory and its variant the so-called 'couple stress theory' is a generalization of classical elasticity based on a single variable kinematic displacement. A micropolar theory assumes the existence of an additional kinematic local rotation variable, called microrotation, associated with pairs of stress components. In a 2D plane stress situation, the stress tensor has four components $\sigma_x, \sigma_y, \sigma_{xy}, \sigma_{yx}$ and the couple stress (or moment per unit area) has two components m_{xz}, m_{yz} in 2D (Fig. 9.1). In the same way as for the stress field, the components of microbending $\varkappa_{xz}$

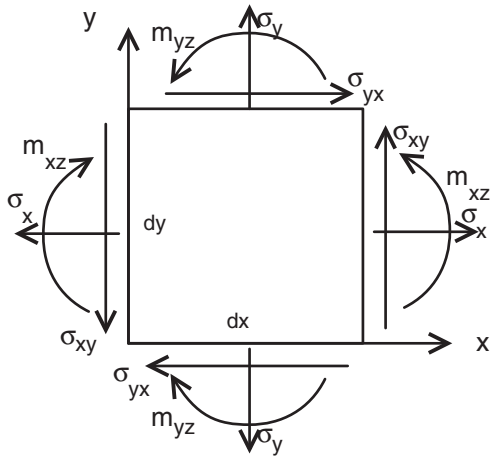

Fig. 9.1 Components of stress and couple stress problem in a plane micropolar

and $\varkappa_{yz}$ induced by the couple stress enter as additional kinematic variables. The components of the unsymmetrical strain and curvature tensors are then defined by (following Eringen, see [2])

$$\varepsilon_x = \frac{\partial u}{\partial x}, \varepsilon_y = \frac{\partial v}{\partial y}, \varepsilon_{xy} = \frac{\partial v}{\partial x} - \phi, \varepsilon_{yx} = \frac{\partial u}{\partial y} + \phi, \varkappa_{xz} = \frac{\partial \phi}{\partial x}, \varkappa_{yz} = \frac{\partial \phi}{\partial y}.$$

The constitutive equations of a general linear anisotropic micropolar elastic medium write

$$\begin{aligned} \sigma_{kl} &= A_{klmn}\varepsilon_{mn} + B_{klmn}\varkappa_{mn} \\ m_{kl} &= C_{klmn}\varepsilon_{mn} + D_{klmn}\varkappa_{mn} \end{aligned} \tag{9.1}$$

For periodic and centro-symmetric structures (the stiffness coefficients of the medium are invariant under coordinates inversion), the two pseudo tensors $B_{klmn} =$

C_{klmn} therein are nil [6, 7, 15]. The constitutive equations in the more specific case of an isotropic planar Cosserat medium then reduce to the relations

$$\begin{aligned} \sigma_{kl} &= \lambda\varepsilon_{rr}\delta_{kl} + (\mu^* + \varkappa)\,\varepsilon_{kl} + \mu^*\varepsilon_{lk} \\ m_{kl} &= \alpha\phi_{r,r}\delta_{kl} + \beta\phi_{k,l} + \gamma\phi_{l,k} \end{aligned} \tag{9.2}$$

For a 2D problem, the constants α and β therein are zero. An equivalent form of the constitutive law is $\{\sigma\} = [K]\{\varepsilon\}$, with the stiffness matrix

$$[K] = \begin{bmatrix} K_{11} & K_{12} & K_{13} & K_{14} & 0 & 0 \\ K_{21} & K_{22} & K_{23} & K_{24} & 0 & 0 \\ K_{31} & K_{32} & K_{33} & K_{34} & 0 & 0 \\ K_{31} & K_{42} & K_{43} & K_{44} & 0 & 0 \\ 0 & 0 & 0 & 0 & K_{55} & 0 \\ 0 & 0 & 0 & 0 & 0 & K_{66} \end{bmatrix}$$

As there are no normal efforts (to the considered plane) in the considered plane stress situation, we deduce the compliance $[S] = [K]^{-1}$. The micropolar moduli are then expressed from the relations

$$\mu^* + \varkappa = K_{33} = K_{44}; \quad \mu^* = K_{34} = K_{43}\gamma = K_{55} = K_{66}.$$

As for nonpolar media, one derives the homogenized traction modulus

$$E_1^* = \frac{1}{S_{11}},$$

the Poisson's ratio $\nu_{12} = -S_{21}E_1^*$, and the effective shear modulus

$$G = \mu^* + \frac{\varkappa}{2}.$$

Additional quantities typical of the micropolar theory are the characteristic length

$$l_{\text{chara}} = \sqrt{\frac{\gamma}{2\,(2\mu^* + \varkappa)}}$$

and the coupling factor

$$N^2 = \frac{\varkappa}{2\,(\mu^* + \varkappa)}.$$

N ranges from 0 (the classical elastic theory) to 1 (for the "couple stress theory").

9.3 Asymptotic Parameters

The discrete homogenization techniques requires a development of the beam length $l^{\varepsilon b}$, width $t^{\varepsilon b}$ and thickness $e^{\varepsilon b}$, and the two kinematic variables, viz the displacement $\mathbf{u}^{\varepsilon n}$, and the rotation at the lattices nodes $\phi^{\varepsilon n}$, versus the small parameter ε, ratio of the beam length to a characteristic length of the lattice at the macro scale. Regarding the beam length $l^{\varepsilon b}$, we rely on the results of Mourad [9], hence write $l^{\varepsilon b} = \varepsilon l^{b0} + \varepsilon^2 l^{b1} + ...$ As to the width of the beam t^b, we can simplify the expressions of the bending and stretching stiffness by defining the parameter

$$\eta = \frac{t^b}{l^b}.$$

The thickness can be considered as a constant $e = \text{const} = 1$. Observe that other models identify the beam width to its thickness. Hence, the stretch behavior is quantified by the extensional stiffness

$$k_l = \frac{E_s S}{l^b} = \frac{E_s t^b e}{l^b} = E_s \eta,$$

whereas a bending stiffness is elaborated as

$$k_f = \frac{12 E_s I}{\left(l^b\right)^3} = E_s \eta^3,$$

with the quadratic moment given by

$$I = \frac{e\left(t^b\right)^3}{12}.$$

This yields the following expressions for the asymptotic expansions of the tensions and moments adopting a Bernoulli beam model

$$N^{b\varepsilon} = E_s \eta \left(\mathbf{e}^b \cdot \Delta \mathbf{U}^{b\varepsilon}\right) \tag{9.3}$$

$$T_t^{b\varepsilon} = E_s \eta^3 \mathbf{e}^{b\perp} \cdot \Delta \mathbf{U}^{b\varepsilon} - \frac{1}{2} E_s \eta^3 \varepsilon L^{b0} \left(\phi^{O(b)\varepsilon} + \phi^{E(b)\varepsilon}\right) \tag{9.4}$$

$$M^{O(b)\varepsilon} = E_s \eta^3 \varepsilon^2 \frac{\left(L^b\right)^2}{6} \left(2\phi^{O(b)\varepsilon} + \phi^{E(b)\varepsilon}\right) - \frac{1}{2} E_s \eta^3 \varepsilon L^b \mathbf{e}^{b\perp} \cdot \Delta \mathbf{U}^{b\varepsilon} \tag{9.5}$$

$$M^{E(b)\varepsilon} = E_s \eta^3 \varepsilon^2 \frac{\left(L^b\right)^2}{6} \left(\phi^{O(b)\varepsilon} + 2\phi^{E(b)\varepsilon}\right) - \frac{1}{2} E_s \eta^3 \varepsilon L^b \mathbf{e}^{b\perp} \cdot \Delta \mathbf{U}^{b\varepsilon} \tag{9.6}$$

Other frameworks may be considered, as one may keep only one of the two parameters ε, η in the expression of resultants and moments; we presently keep both parameters, which avoids oversimplifications of the expression of the transverse effort, which depends on parameter η.

We notice a difference with the method developed in Mourad [9] and Caillerie et al. [1]: those authors use the moment equilibrium to replace the expression of the transverse forces $\mathbf{T}_t^b$ in the Eq. (9.4) by the couple M generated by the angular variation between two consecutive beams. This modeling approach is customary in the field of applications considered by the authors, namely molecular dynamics or interatomic physics, with an application to carbon nanotubes. The authors adopt the mechanics of interacting bars, whereas we choose beam mechanics for the description of the lattice behavior. In our treatment, the expression of the couple stresses and thereby of the transverse forces is linked to the difference of displacements between the extremity nodes of a given beam. Figure (9.3) shows the difference between both methods (considering the linearized method adopted in Caillerie et al. [1]). In present approach, the couple is a function of the displacement difference between the end nodes of a given beam; contrary to this, the angular variation between two beams is used in Caillerie et al. [1]. Moreover, in order to be able to

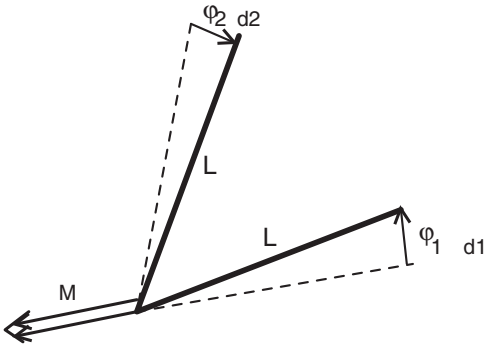

Fig. 9.2 Differences between the couples in the present method and in Caillerie et al. [1]: Couple due to the angular variation between two bars

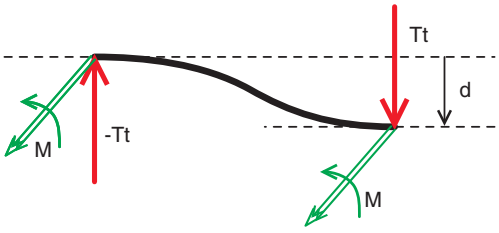

Fig. 9.3 Differences between the couples in the present method and in Caillerie et al. [1]: Couple generated by the displacement difference between the end nodes of the same beam (present work)

use the rotational equilibrium equations, the previous authors identify the rotation of the beam to a rigid body motion, implying the assumption of beams without internal transverse force. We adopt, to the contrary, the beam theory, with the couple considered as an internal moment.

As to the kinematic variables, we consider that the two terms in the expression of the shear forces and moments are of identical order to formulate the following development of the displacement

$$\mathbf{u}^{\varepsilon}(\lambda^{\varepsilon}) = \mathbf{u}_0(\lambda^{\varepsilon}) + \varepsilon \mathbf{u}_1(\lambda^{\varepsilon}) + \varepsilon^2 \mathbf{u}_2(\lambda^{\varepsilon}) + \ldots \tag{9.7}$$

which in turn gives the displacement difference between the end nodes of a beam

$$\begin{aligned} \Delta \mathbf{U}^{b\varepsilon} &= \mathbf{u}^{\varepsilon}(E(b)) - \mathbf{u}^{\varepsilon}(O(b)) \\ &= \underbrace{\varepsilon\left(\mathbf{u}_1^{E_R(b)} - \mathbf{u}_1^{O_R(b)} + \frac{\partial \mathbf{u_0}}{\partial \lambda^i}\delta^{ib}\right)}_{\Delta \mathbf{U}_1^b} + \varepsilon^2 \underbrace{\left(\mathbf{u}_2^{E_R(b)} - \mathbf{u}_2^{O_R(b)}\right)}_{\Delta \mathbf{U}_2^b} \end{aligned} \tag{9.8}$$

For the rotation variable, we separate the terms function of the symmetric and antisymmetric strain tensors (respectively denoted by the symmetrical and antisymmetrical brackets)

$$\phi^{n\varepsilon}(\lambda^{\varepsilon}) = \phi_{0][}(\lambda^{\varepsilon}) + \phi^n_{0[]}(\lambda^{\varepsilon}) + \varepsilon \phi^n_{1][}(\lambda^{\varepsilon}) + \ldots \tag{9.9}$$

The first order antisymmetrical part of the microrotation, term

$$\phi_{0][}(\lambda^{\varepsilon})$$

is independent of the node, hence it represents the equivalent (homogenized) microrotation of the unit cell. Reporting previous expansions of the microrotation gives the following expression of the rotation variable at the origin and end nodes (Fig. 9.4)

$$\phi^{O(b)\varepsilon} = \phi_{0][} + \phi_{0[]}^{O_R(b)} + \varepsilon \phi_{1][}^{O_R(b)} + \ldots \tag{9.10}$$

$$\phi^{E(b)\varepsilon} = \phi_{0][} + \phi_{0[]}^{E_R(b)} + \varepsilon\left(\frac{\partial \phi_{0][}}{\partial \lambda^i}\delta^{ib} + \phi_{1][}^{E_R(b)}\right) + \ldots \tag{9.11}$$

9.4 Asymptotic Homogenization of Polar Lattices: Description of the Main Steps

The general principle of the micropolar asymptotic method (this denomination is relevant for polar lattices, and will be used here and in the sequel) consists in writing

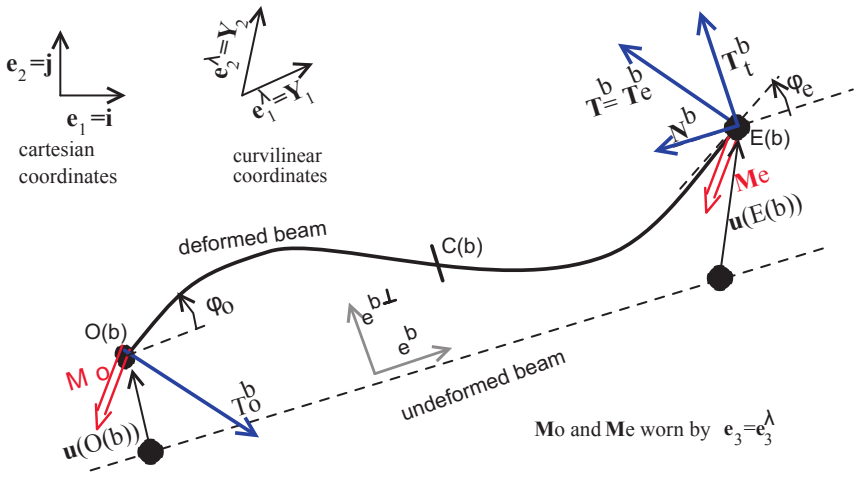

Fig. 9.4 Deformation parameters of the beam

the equilibrium equations of the equivalent micropolar continuum in virtual power form to evidence the stress tensor and σ and the micromoment tensor m as internal dyadic products (in the space of tensors) with the base vectors of a curvilinear coordinate system, viz

$$\int_{\Omega} \underbrace{(g\boldsymbol{\sigma}\cdot\mathbf{e}_{\lambda}^{\mathbf{i}})}_{\mathbf{S^i}}.\frac{\partial \mathbf{v}}{\partial \lambda_i}d\lambda + \int_{\Omega} \underbrace{(g\mathbf{m}\cdot\mathbf{e}_{\lambda}^{\mathbf{i}})}_{\mu^{\mathbf{i}}}.\frac{\partial \mathbf{w}}{\partial \lambda_i}d\lambda = 0$$

In a second step and anticipating forthcoming developments, one shall show that the equilibrium equations of the discrete medium take the same form after homogenization, viz

$$\sum_b \mathbf{T^b}.\mathbf{v} + \sum_b \mathbf{M^b}.\mathbf{w} = 0 \overset{\text{homogenization}}{\rightarrow} \int_{\Omega} \mathbf{S}^i.\frac{\partial \mathbf{v}}{\partial \lambda_i}d\lambda + \int_{\Omega} \boldsymbol{\mu}^i.\frac{\partial \mathbf{w}}{\partial \lambda_i}d\lambda = 0$$

The comparison of the homogenized formulation with the previous continuum micropolar equilibrium allows then to identify the stress vector $\mathbf{S}^i$ and the couple stress vector $\boldsymbol{\mu}^i$, leading thereafter to the elaboration of the associated stress and couple stress. The underlying steps of the asymptotic method are next detailed.

9.4.1 First Step: Formulation of the Equilibrium Equations Highlighting the Stress Vector $\mathbf{S}^i$ and the Couple Vector $\boldsymbol{\mu}^i$

In order to set the stage, let write the equilibrium equations of a micropolar medium in a quasi static context Forest [5], adopting a weak formulation:

$$\begin{aligned}&\int_{\Omega}(\boldsymbol{\sigma}.\nabla_x).\mathbf{v}dx+\int_{\Omega}(\mathbf{m}.\nabla_x-\in:\boldsymbol{\sigma}).\mathbf{w}dx\\&=-\int_{\Omega}\mathbf{f}^{\mathrm{vol}}.\mathbf{v}dx-\int_{\Omega}\mathbf{c}^{\mathrm{vol}}.\mathbf{w}dx\\&-\int_{\partial\Omega}(\boldsymbol{\sigma}.\mathbf{n}-\mathbf{t}^{\mathrm{edge}}).\mathbf{v}ds-\int_{\partial\Omega}(\mathbf{m}.\mathbf{n}-\mathbf{M}^{\mathrm{edge}}).\mathbf{w}ds\end{aligned}\tag{9.12}$$

considering a domain Ω submitted to edge traction $\mathbf{t}^{\mathrm{edge}}$ and surface couples $\mathbf{M}^{\mathrm{edge}}$. The weak form of those equilibrium equations involve virtual velocities$\{\mathbf{v},\mathbf{w}\}$, respectively equivalent to the rates $\{\dot{\mathbf{u}},\dot{\boldsymbol{\phi}}\}$. The components of the two tensors $\mathbf{m}$ and $\boldsymbol{\sigma}$ are decoupled in the case of a centro-symmetric medium, which implies that the terms of the couple stress tensor are self-balanced in the absence of distributed couples. According to Riahi and Curran [12], in the absence of torque density and if the terms of the couple stress tensor are self-balanced, then the term $\in:\boldsymbol{\sigma}=\mathbf{0}$, which means that Cauchy stress remains symmetrical. Choosing the virtual fields $\mathbf{v}$, $\mathbf{w}$ nil outside the considered domain Ω , previous equations resume to the sole volume integrals; in the absence of body forces and body couples, previous general equilibrium equations then entail the following quasi static equilibrium equations:

$$\int_{\Omega}(\boldsymbol{\sigma}.\nabla_x).\mathbf{v}dx=0\tag{9.13}$$

$$\int_{\Omega}(\mathbf{m}.\nabla_x).\mathbf{w}dx=0\tag{9.14}$$

The stress and couple stress tensors shall be evidenced thanks to a change of variables, following the method developed in Mourad [9]. Let x_i denote the cartesian coordinates of a material point P, such that $\mathbf{x}=x_i\mathbf{e}_i$ in a fixed cartesian basis $\mathbf{e}_i$, and let define the generalized curvilinear coordinates $\lambda=(\lambda^1,\lambda^2,\lambda^3)$, inducing the change of variables $\mathbf{x}=\boldsymbol{\psi}(\lambda^1,\lambda^2,\lambda^3)$, assumed to be one-to-one. Observe that the parameterization of material points with a curvilinear Lagrangian variable allows the treatment of lattices having the geometry of 2D shells. The following covariant vectors are defined

$$\mathbf{e}_k^{\lambda}=\frac{\partial x^i}{\partial\lambda^i}\mathbf{e}_i\tag{9.15}$$

dual to the contravariant vectors $\mathbf{e}_{\lambda}^i$, in the sense of the inner products $\mathbf{e}_{\lambda}^i.\mathbf{e}_j^{\lambda}=\delta_j^i$ (the Kronecker symbol). The change of variable $x=x(\lambda)$ is next done in Eqs (9.13) and (9.14): this induces the transformation $dx=gd\lambda$. The gradients of the virtual

velocities are next expressed in the curvilinear coordinate system, viz

$$\nabla_x \mathbf{v} = \frac{\partial \mathbf{v}}{\partial \lambda^i} \otimes \mathbf{e}_\lambda^i; \quad \nabla_x \mathbf{w} = \frac{\partial \mathbf{w}}{\partial \lambda^i} \otimes \mathbf{e}_\lambda^i.$$

The Eqs (9.13) and (9.14) can be expressed under the form:

$$\begin{aligned} &\int_\Omega (\boldsymbol{\sigma}.\nabla_x).\mathbf{v} dx = \int_\Omega \boldsymbol{\sigma} : (\nabla_x \mathbf{v}) dx \\ &= \int_\Omega \boldsymbol{\sigma} : (\frac{\partial \mathbf{v}}{\partial \lambda^i} \otimes \mathbf{e}_\lambda^\mathbf{i}) g d\lambda = \int_\Omega (\boldsymbol{\sigma} \mathbf{e}_\lambda^\mathbf{i}).\frac{\partial \mathbf{v}}{\partial \lambda^i} g d\lambda = 0 \end{aligned} \tag{9.16}$$

$$\begin{aligned} &\int_\Omega (\mathbf{m}.\nabla_x).\mathbf{w} dx = \int_\Omega \mathbf{m} : (\nabla_x \mathbf{w}) dx \\ &= \int_\Omega \mathbf{m} : (\frac{\partial \mathbf{w}}{\partial \lambda^i} \otimes \mathbf{e}_\lambda^\mathbf{i}) g d\lambda = \int_\Omega (\mathbf{m} \mathbf{e}_\lambda^\mathbf{i}).\frac{\partial \mathbf{w}}{\partial \lambda^i} g d\lambda = 0 \end{aligned} \tag{9.17}$$

One adopts the following definition of the stress and couple stress vectors:

$$\mathbf{S}^i = g \sigma \mathbf{e}_\lambda^i \tag{9.18}$$

$$\boldsymbol{\mu}^i = g \mathbf{m} \mathbf{e}_\lambda^i \tag{9.19}$$

From the Eqs (9.16) and (9.18), one can write the translational equilibrium:

$$\int_\Omega \mathbf{S}^\mathbf{i}.\frac{\partial \mathbf{v}}{\partial \lambda^i} d\lambda = 0 \tag{9.20}$$

Similarly, from Eqs (9.17) and (9.19), the moment equilibrium writes:

$$\int_\Omega \boldsymbol{\mu}^\mathbf{i}.\frac{\partial \mathbf{w}}{\partial \lambda^i} d\lambda = 0 \tag{9.21}$$

One then expresses the curvilinear gradients of the virtual velocities versus those of the nodal positions,

$$\frac{\partial \mathbf{v}}{\partial \lambda^i} = \nabla_x \mathbf{v}.\frac{\partial \mathbf{R}}{\partial \lambda^i}; \frac{\partial \mathbf{w}}{\partial \lambda^i} = \nabla_x \mathbf{w}.\frac{\partial \mathbf{R}}{\partial \lambda^i},$$

with $\mathbf{R}$ the position vector of a lattice node. The two previous discrete equilibrium equations can then be transformed into continuous formulations after homogenization. Pursing further, one can write the Eqs (9.20) and (9.21) under the form

$$\int_\Omega \mathbf{S}^\mathbf{i}.\frac{\partial \mathbf{v}}{\partial \lambda^i} d\lambda = \int_\Omega \mathbf{S}^\mathbf{i}.(\nabla_x \mathbf{v}.\frac{\partial \mathbf{R}}{\partial \lambda^i}) d\lambda = \int_\Omega \left(\mathbf{S}^\mathbf{i} \otimes \frac{\partial \mathbf{R}}{\partial \lambda^i} \right) : (\nabla_x \mathbf{v}) \frac{1}{g} dx = 0 \tag{9.22}$$

$$\int_{\Omega} \boldsymbol{\mu}^{\mathbf{i}}.\frac{\partial \mathbf{w}}{\partial \lambda^i}d\lambda = \int_{\Omega} \mu^{\mathbf{i}}.\left(\nabla_x \mathbf{w}.\frac{\partial \mathbf{R}}{\partial \lambda^i}\right)d\lambda = \int_{\Omega}\left(\boldsymbol{\mu}^{\mathbf{i}} \otimes \frac{\partial \mathbf{R}}{\partial \lambda^i}\right) : (\nabla_x \mathbf{w})\,\frac{1}{g}dx = 0 \tag{9.23}$$

Those equations highlight the stress and couple stress tensors as the following dyadic products of the stress and couple stress vectors with the curvilinear gradient of the position vector:

$$\boldsymbol{\sigma} = \frac{1}{g}\mathbf{S}^{\mathbf{i}} \otimes \frac{\partial \mathbf{R}}{\partial \lambda^i} \tag{9.24}$$

$$\mathbf{m} = \frac{1}{g}\boldsymbol{\mu}^{\mathbf{i}} \otimes \frac{\partial \mathbf{R}}{\partial \lambda^{\mathbf{i}}} \tag{9.25}$$

The next step consists in expressing both vectors $\mathbf{S}^i$ and $\boldsymbol{\mu}^i$ according to the topology of the unit cell and the mechanical properties of the constitutive beams.

9.4.2 Second Step: Homogenization of the Discrete Equilibrium Equations

The vectors of effort $\mathbf{T}^b$ decomposes into a normal and a transverse contribution

$$\mathbf{T}^b = N^b\mathbf{e}^b + T_t^b\mathbf{e}^{b\perp} \tag{9.26}$$

The equilibrium of forces for the whole lattice expresses in virtual power form and after asymptotic development as

$$\sum_{v^i \in \mathbb{Z}^2} \sum_{b \in \mathscr{B}_{\mathscr{R}}} \mathbf{T}^{\varepsilon b}.\left(\mathbf{v}^{\varepsilon}\left(O\left(b\right)\right) - \mathbf{v}^{\varepsilon}\left(E\left(b\right)\right)\right) = 0 \tag{9.27}$$

with $\mathbf{v}\left(.\right)$ a virtual velocity field choosing to vanish on the edges. The description of the kinematic and static variables for a bar within the lattice is exposed on the Fig. 9.4. The moment equilibrium can be written in two different ways, as the virtual power for all lattice nodes

$$\sum_{v^i \in \mathbb{Z}^2} \sum_{b \in \mathscr{B}_{\mathscr{R}}} \left(\mathbf{M}^{O(b)}.\mathbf{w}\left(O\left(b\right)\right) + \mathbf{M}^{E(b)}.\mathbf{w}\left(E\left(b\right)\right)\right) = \mathbf{0} \tag{9.28}$$

or as the sum of the equilibrium balances of the individual beams

$$\begin{aligned}\sum_{v^i \in \mathbb{Z}^2} \sum_{b \in \mathscr{B}_{\mathscr{R}}} \Big(&\mathbf{M}^{O(b)}.\mathbf{w}\left(O\left(b\right)\right) + \mathbf{M}^{E(b)}.\mathbf{w}\left(E\left(b\right)\right) \\ &+ \frac{L^b}{2}(\mathbf{e}^b \wedge \mathbf{T}^{E(b)}).\mathbf{w}\left(C\left(b\right)\right) - \frac{L^b}{2}(\mathbf{e}^b \wedge \mathbf{T}^{O(b)}).\mathbf{w}\left(C\left(b\right)\right)\Big) = \mathbf{0}\end{aligned} \tag{9.29}$$

with $\mathbf{e}^b$the director for each bar, and L^b the bar length; those two elements remain fixed under the presently adopted small strains formalism. $\mathbf{M}^{O(b)}$ and $\mathbf{M}^{E(b)}$are the moments in the origins and ends of a generic beam respectively, and $\mathbf{w}(.)$ the virtual rotation rate.

9.4.2.1 Description and Parametrization of the Lattice Geometry

We denote by $\mathscr{N}_{\mathscr{R}}$ and $\mathscr{B}_{\mathscr{R}}$ respectively, the set of node and beam indices belonging to the reference cell. Thus, to each pair $v^i = (v^1, v^2) \in \mathbb{Z}^2$, we associate a reference cell. The nodes of the whole lattice can then be defined by the triplet $\tilde{n} = \left(n, v^1, v^2\right) \in \mathscr{N}_{\mathscr{R}} \times \mathbb{Z}^2$. Similarly, the beams of the lattice can be described by the triplet $\tilde{b} = \left(b, v^1, v^2\right) \in \mathscr{B}_{\mathscr{R}} \times \mathbb{Z}^2$.

In the reference cell, each beam is oriented so that it has an origin node $O\left(\tilde{b}\right)$ and an end node $E\left(\tilde{b}\right)$. Although we can choose the origin node as part of the reference cell, this is not necessarily the case for the end node; the end node belongs nevertheless to a cell that is close. If the original node $O\left(\tilde{b}\right)$ is associated with a triplet $\tilde{n} = \left(n, v^1, v^2\right)$, the end node $E\left(\tilde{b}\right)$ is necessarily associated with a node numbered $\left(m, v^1 + \delta^1, v^2 + \delta^2\right)$. In most cases, the end node belongs to an adjacent cell, which means that the shift variables δ^i belong to the set $\delta^i \in \{-1, 0, 1\}$. We further associate to each beam a node at its center, denoted $C(b)$.

9.4.2.2 Asymptotic Development of the Virtual Velocity and Rotation Rate

For any virtual velocity field $\mathbf{v}^\varepsilon(\lambda)$, a Taylor series development leads to

$$\mathbf{v}^\varepsilon\left(E\left(b\right)\right) - \mathbf{v}^\varepsilon\left(O\left(b\right)\right) = \mathbf{v}^\varepsilon(\lambda^\varepsilon + \varepsilon\delta^{ib}) - \mathbf{v}^\varepsilon(\lambda^\varepsilon) = \varepsilon\frac{\partial \mathbf{v}(\lambda^\varepsilon)}{\partial \lambda^i}\delta^{ib} \tag{9.30}$$

Similarly, the previous expansion of the rotation rate leads to

$$\begin{aligned} \mathbf{w}^{C(b)\varepsilon} &= \frac{1}{2}\left(\mathbf{w}^{E(b)\varepsilon} + \mathbf{w}^{O(b)\varepsilon}\right) \\ \mathbf{w}^{O(b)\varepsilon}(\lambda) &= \mathbf{w}(\lambda) \\ \mathbf{w}^{E(b)\varepsilon}(\lambda + \varepsilon\delta^i) &= \mathbf{w}\left(\lambda\right) + \varepsilon\frac{\partial \mathbf{w}\left(\lambda\right)}{\partial \lambda^i}\delta^{ib} \end{aligned} \tag{9.31}$$

9.4.2.3 Final Balance Equations

Inserting Eqs (9.30), (9.4) and (9.3) in (9.27) leads after development and ordering following the successive powers of ε to

$$\begin{aligned}
&\sum_{v^i\in\mathbb{Z}^2}\sum_{b\in\mathscr{B}_{\mathscr{R}}}\Big[\varepsilon^2\left(E_s\eta\left(\mathbf{e}^b\cdot\Delta\mathbf{U_1}\right)\mathbf{e}^b\right.\\
&+\left.\left(E_s\eta^3\mathbf{e}^{b\perp}\cdot\Delta\mathbf{U}_1-\frac{1}{2}E_s\eta^3L^{b0}\left(2\phi_{0][}+\phi_{0[]}^{O_R(b)}+\phi_{0[]}^{E_R(b)}\right)\right)\mathbf{e}^{b\perp}\right)\cdot\frac{\partial\mathbf{v}(\lambda^\varepsilon)}{\partial\lambda^i}\delta^{ib}\\
&+\varepsilon^3\left(E_s\eta\left(\mathbf{e}^b\cdot\Delta\mathbf{U_2}\right)\mathbf{e}^b+\left(E_s\eta^3\mathbf{e}^{b\perp}\cdot\Delta\mathbf{U}_2\right.\right.\\
&-\left.\left.\frac{1}{2}E_s\eta^3L^{b0}\left(\phi_{1][}^{O_R(b)}+\phi_{1][}^{E_R(b)}+\frac{\partial\phi_{0][}}{\partial\lambda^i}\delta^{ib}\right)\right)\mathbf{e}^{b\perp}\right)\cdot\frac{\partial\mathbf{v}(\lambda^\varepsilon)}{\partial\lambda^i}\delta^{ib}\Big]
\end{aligned}\tag{9.32}$$

This discrete equation is transformed into a continuous Riemann integral on the domain Ω when the family of lattices parameterized by ε tends to a continuum (we envisage a fixed reference domain, and increase the density of belas within this domain). For any enough regular function g, the quantity

$$\varepsilon^2\sum_{v^i\in\mathbb{Z}^2}g(\varepsilon v^i)$$

can be interpreted as the Riemann sum of an integral over Ω, viz

$$\int_\Omega g(\lambda)d\lambda$$

when $\varepsilon\to 0$. The Eq. (9.32) becomes after homogenization :

$$\int_\Omega \mathbf{S}^i.\frac{\partial\mathbf{v}(\lambda)}{\partial\lambda^i}d\lambda=0\tag{9.33}$$

with the stress vector $\mathbf{S}^i=\mathbf{S}_1^i+\varepsilon\mathbf{S}_2^i$ decomposing into a first and second order contribution, respectively vectors $\mathbf{S}_1^i$, $\mathbf{S}_2^i$, as

$$\begin{aligned}
\mathbf{S}_1^i=&\sum_{b\in\mathscr{B}_{\mathscr{R}}}\left(E_s\eta\left(\mathbf{e}^b\cdot\Delta\mathbf{U_1}\right)\mathbf{e}^b\right.\\
&+\left.\left(E_s\eta^3\mathbf{e}^{b\perp}\cdot\Delta\mathbf{U}_1-\frac{1}{2}E_s\eta^3L^{b0}\left(2\phi_{0][}+\phi_{0[]}^{O_R(b)}+\phi_{0[]}^{E_R(b)}\right)\right)\mathbf{e}^{b\perp}\right)\delta^{ib}
\end{aligned}$$

and

$$\begin{aligned}
\mathbf{S}_2^i=&\sum_{b\in\mathscr{B}_{\mathscr{R}}}\left(E_s\eta\left(\mathbf{e}^b\cdot\Delta\mathbf{U_2}\right)\mathbf{e}^b\right.\\
&+\left.\left(E_s\eta^3\mathbf{e}^{b\perp}\cdot\Delta\mathbf{U}_2-\frac{1}{2}E_s\eta^3L^{b0}\left(\phi_{1][}^{O_R(b)}+\phi_{1][}^{E_R(b)}+\frac{\partial\phi_{0][}}{\partial\lambda^i}\delta^{ib}\right)\right)\mathbf{e}^{b\perp}\right)\delta^{ib}.
\end{aligned}$$

The stress tensor $\boldsymbol{\sigma}$ is then reconstructed from $\mathbf{S^i}$ as Eq. (9.24)

$$\boldsymbol{\sigma}=\frac{1}{g}\mathbf{S}^i\otimes\frac{\partial\mathbf{R}}{\partial\lambda^i}\tag{9.34}$$

The moment equilibrium, Eq. (9.29) is further homogenized inserting the asymptotic expansions of the virtual rotation rate, Eq. (9.31), the parameters and moments, Eqs (9.6) and (9.5). We obtain after simplification the following expression (supported by the normal vector to the lattice plane)

$$\begin{aligned}\sum_{v^i\in\mathbb{Z}^2}\sum_{b\in\mathscr{B}_{\mathscr{R}}}&\left(\varepsilon^3\left(E_s\eta^3\frac{\left(L^b\right)^2}{12}\left(\phi_{0[]}^{E_R(b)}-\phi_{0[]}^{O_R(b)}\right)\right)\right.\\&\left.+\ \varepsilon^4\left(E_s\eta^3\frac{\left(L^b\right)^2}{12}\left(-\phi_{1][}^{O_R(b)}+\frac{\partial\phi_{0][}}{\partial\lambda^i}\delta^{ib}+\phi_{1][}^{E_R(b)}\right)\right)\right)\delta^{ib}.\frac{\partial w^0}{\partial\lambda^i}=0\end{aligned}\tag{9.35}$$

The homogenization of this equation is done similarly as for the efforts: it becomes after passage to the limit $\varepsilon\to 0$

$$\int_{\Omega}\boldsymbol{\mu}^{\mathbf{i}}\frac{\partial\mathbf{w^0}(\lambda)}{\partial\lambda^i}d\lambda=0\tag{9.36}$$

with the couple vector identified to

$$\mu^i=\mu_1^i+\varepsilon\mu_2^i,$$

incorporating the first order micropolar stress vector

$$\boldsymbol{\mu}_1^i=\sum_{b\in\mathscr{B}_{\mathscr{R}}}\left(E_s\eta^3\frac{\left(L^b\right)^2}{12}\left(\phi_{0[]}^{E_R(b)}-\phi_{0[]}^{O_R(b)}\right)\right)\delta^{ib}$$

and the second order micropolar vector

$$\boldsymbol{\mu}_2^i=\sum_{b\in\mathscr{B}_{\mathscr{R}}}\left(E_s\eta^3\frac{\left(L^b\right)^2}{12}\left(-\phi_{1][}^{O_R(b)}+\frac{\partial\phi_{0][}}{\partial\lambda^i}\delta^{ib}+\phi_{1][}^{E_R(b)}\right)\right)\delta^{ib}.$$

This allows finding the couple stress tensor $\mathbf{m}$ from the vectors μ^i as described in Sect. 9.4.1

$$\mathbf{m}=\frac{1}{g}\mu^{\mathbf{i}}\otimes\frac{\partial\mathbf{R}}{\partial\lambda^i}\tag{9.37}$$

9.4.2.4 Simplification of the Expressions of $\mathbf{S}^i$ and $\boldsymbol{\mu}^i$

We can simplify the expressions of the vectors of effort $\mathbf{S}^i$ and couple stress $\boldsymbol{\mu}^i$ using a result on the symmetry properties of the lattice. It was recalled in the introductory paragraph (Sect. 9.2) the general form of the constitutive equations of linear micropolar elasticity

$$\sigma_{kl}=A_{klmn}\varepsilon_{mn}+B_{klmn}\varkappa_{mn}$$

$$m_{kl}=C_{klmn}\varepsilon_{mn}+D_{klmn}\varkappa_{mn}$$

Relying on the obtained expression of the homogenized constitutive law, we can identify this form from the expressions of the homogenized stress and couple stress tensors:

$$\boldsymbol{\sigma} = \frac{1}{g}\left(\mathbf{S}_1^i + \varepsilon \mathbf{S}_2^i\right) \otimes \frac{\partial \mathbf{R}}{\partial \lambda^i}$$
$$\boldsymbol{\sigma} = \underbrace{\frac{1}{g}\mathbf{S}_1^i \otimes \frac{\partial \mathbf{R}}{\partial \lambda^i}}_{[A]\{\varepsilon\}} + \underbrace{\frac{1}{g}\varepsilon \mathbf{S}_2^i \otimes \frac{\partial \mathbf{R}}{\partial \lambda^i}}_{[B]\{\varkappa\}} \tag{9.38}$$

$$\mathbf{m} = \frac{1}{g}\left(\mu_{\mathbf{1}}^{\mathbf{i}} + \varepsilon \mu_{\mathbf{2}}^{\mathbf{i}}\right) \otimes \frac{\partial \mathbf{R}}{\partial \lambda^i}$$
$$\mathbf{m} = \underbrace{\frac{1}{g}\mu_1^i \otimes \frac{\partial \mathbf{R}}{\partial \lambda^i}}_{[C]\{\varepsilon\}} + \underbrace{\frac{1}{g}\varepsilon \mu_2^i \otimes \frac{\partial \mathbf{R}}{\partial \lambda^i}}_{[D]\{\varkappa\}} \tag{9.39}$$

It has been shown that for centro-symmetric medium Trovalusci and Masiani [15], the coupling matrices $[B]$ and $[C]$ vanish; we limit our study to this type of lattice. This means that the previously defined vectors $\boldsymbol{\mu}_1^i$ and $\mathbf{S}_2^i$ vanish. This in turn leads to a substantial simplification of the expression of the stress and couple stress vectors:

$$\mathbf{S}^i = \mathbf{S}_1^i = \sum_{b \in \mathscr{B}_{\mathscr{R}}} \left(E_s \eta \left(\mathbf{e}^b \cdot \Delta \mathbf{U}_\mathbf{1} \right) \mathbf{e}^b \right.$$
$$\left. + \left(E_s \eta^3 \mathbf{e}^{b\perp} \cdot \Delta \mathbf{U}_1 - \frac{1}{2} E_s \eta^3 L^{b0} \left(2\phi_{0][} + \phi_{0[]}^{O_R(b)} + \phi_{0[]}^{E_R(b)} \right) \right) \mathbf{e}^{b\perp} \right) \delta^{ib}$$
$$= \sum_{b \in \mathscr{B}_{\mathscr{R}}} \left(N_1^b \mathbf{e}^b + T_{1t}^b \mathbf{e}^{b\perp} \right) \delta^{ib} \tag{9.40}$$

$$\boldsymbol{\mu}^i = \boldsymbol{\mu}_2^i = \underbrace{\sum_{b \in \mathscr{B}_{\mathscr{R}}} \left(\left(E_s \eta^3 \frac{\left(L^b\right)^2}{12} \left(-\phi_{1][}^{O_R(b)} + \frac{\partial \phi_{0][}}{\partial \lambda^i} \delta^{ib} + \phi_{1][}^{E_R(b)} \right) \right) \right) \delta^{ib}}_{\sum_{b \in \mathscr{B}_{\mathscr{R}}} \frac{1}{2}\left(M_2^{E(b)} - M_2^{O(b)} \right) \delta^{ib} = \sum_{b \in \mathscr{B}_{\mathscr{R}}} \left(\mathbf{M}_2^{E(b)} + \varepsilon \frac{L^b}{2} (\mathbf{e}^b \wedge \mathbf{T}_2^b) \right) . \mathbf{e}_3 \delta^{ib}} \tag{9.41}$$

There are still unknown displacements and rotations in the vectors $\mathbf{S}^i$ and $\boldsymbol{\mu}^i$, namely the functions of displacement $\mathbf{u}_1^n$, $\mathbf{u}_2^n$ (first order kinematic variables) and the functions of rotation $\phi_{0[]}^n$ and $\phi_{1][}^n$, which intervene at the second order. The resolution of these unknowns is the goal of the next section.

9.4.3 Determination of the Unknown Displacements $\mathbf{u}_1^n$, $\mathbf{u}_2^n$ and Unknown Rotations $\boldsymbol{\phi}_{0[]}^n$ and $\boldsymbol{\phi}_{1][}^n$

As the lattice is in equilibrium, the unit cell is too, so we can write from Eq. (9.27) the lattice translational equilibrium

$$\sum_{b\in\mathscr{B}_{\mathscr{R}}}\left(N\mathbf{e}^{\mathbf{b}}+T_t\mathbf{e}^{b\perp}\right)\cdot\left(\mathbf{v}\left(E\left(b\right)\right)-\mathbf{v}\left(O\left(b\right)\right)\right)=0 \tag{9.42}$$

As this equation is about two orders, we will resolve it on each order

$$\begin{cases}\sum\limits_{b\in\mathscr{B}_{\mathscr{R}}}\left(E_s\eta\left(\mathbf{e}^b\cdot\Delta\mathbf{U_1}\right)\mathbf{e}^{\mathbf{b}}+\left(E_s\eta^3\mathbf{e}^{b\perp}\cdot\Delta\mathbf{U}_1\right.\right.\\ \left.-\dfrac{1}{2}E_s\eta^3L^{b0}\left(2\phi_{0][}+\phi_{0[]}^{O_R(b)}+\phi_{0[]}^{E_R(b)}\right)\right)\mathbf{e}^{b\perp}\Big)\cdot\left(\mathbf{v}\left(E\left(b\right)\right)-\mathbf{v}\left(O\left(b\right)\right)\right)=0\\ \sum\limits_{b\in\mathscr{B}_{\mathscr{R}}}\left(E_s\eta\left(\mathbf{e}^b\cdot\Delta\mathbf{U_2}\right)\mathbf{e}^{\mathbf{b}}+\left(E_s\eta^3\mathbf{e}^{b\perp}\cdot\Delta\mathbf{U}_2\right.\right.\\ \left.\left.-\dfrac{1}{2}E_s\eta^3L^{b0}\left(\phi_{1][}^{O_R(b)}+\phi_{1][}^{E_R(b)}+\dfrac{\partial\phi_{0][}}{\partial\lambda^i}\delta^{ib}\right)\right)\mathbf{e}^{b\perp}\right)\cdot\left(\mathbf{v}\left(E\left(b\right)\right)-\mathbf{v}\left(O\left(b\right)\right)\right)=0\end{cases} \tag{9.43}$$

Since the virtual velocity field is a priori arbitrary, one can develop each of the two previous equations in as many independent equations as the number of nodes in the elementary cell. Reasoning in the same way for the moments from the Eq. (9.28), the rotational balance of the mesh nodes must be ensured, hence

$$\sum_{b\in\mathscr{B}_{\mathscr{R}}}\left(\mathbf{M}^{O(b)}.\mathbf{w}\left(O\left(b\right)\right)+\mathbf{M}^{E(b)}.\mathbf{w}\left(E\left(b\right)\right)\right)=\mathbf{0} \tag{9.44}$$

This general equation writes more specifically

$$\begin{cases}\sum\limits_{b\in\mathscr{B}_{\mathscr{R}}}\left(\left(k_f^b\dfrac{L^b}{6}\left(L^b\left(3\phi_{0][}+2\phi_{0[]}^{O_R(b)}+\phi_{0[]}^{E_R(b)}\right)\right.\right.\right.\\ \left.\left.\left.-3\mathbf{e}^{b\perp}\cdot\left(\Delta\mathbf{U}_1^b\right)\right)\right)\mathbf{e}_3\Big).\mathbf{w}\left(O\left(b\right)\right)\\ +\left(\left(k_f^b\dfrac{L^b}{6}\left(L^b\left(3\phi_{0][}+\phi_{0[]}^{O_R(b)}+2\phi_{0[]}^{E_R(b)}\right)\right.\right.\right.\\ \left.\left.\left.-3\mathbf{e}^{b\perp}\cdot\left(\Delta\mathbf{U}_1^b\right)\right)\right)\mathbf{e}_3\Big).\mathbf{w}\left(E\left(b\right)\right)=\mathbf{0}\\ \sum\limits_{b\in\mathscr{B}_{\mathscr{R}}}\left(\left(k_f^b\dfrac{L^b}{6}\left(L^b\left(2\phi_{1][}^{O_R(b)}+\phi_{1][}^{E_R(b)}+\dfrac{\partial\phi_{0][}(\lambda^\varepsilon)}{\partial\lambda^i}\delta^{ib}\right)\right.\right.\right.\\ \left.\left.\left.-3\mathbf{e}^{b\perp}\cdot\left(\Delta\mathbf{U}_2^b\right)\right)\right)\mathbf{e}_3\Big).\mathbf{w}\left(O\left(b\right)\right)\\ +\left(\left(k_f^b\dfrac{L^b}{6}\left(L^b\left(\phi_{1][}^{O_R(b)}+2\left(\phi_{1][}^{E_R(b)}+\dfrac{\partial\phi_{0][}(\lambda^\varepsilon)}{\partial\lambda^i}\delta^{ib}\right)\right)\right.\right.\right.\\ \left.\left.\left.-3\mathbf{e}^{b\perp}\cdot\left(\Delta\mathbf{U}_2^b\right)\right)\right)\mathbf{e}_3\Big).\mathbf{w}\left(E\left(b\right)\right)=\mathbf{0}\end{cases} \tag{9.45}$$

In the same way as for the equilibrium of forces, and since the virtual rotation rate $\mathbf{w}(.)$ is a priori arbitrary, those equations expand in as many independent equations as nodes in the elementary cell: totally, $6n$ scalar equations are written, with n the number of elementary cell nodes, to solve for the $6n$ unknowns (for each node, on two orders, one has two vectorial displacement, $\mathbf{u}_1^n$, $\mathbf{u}_2^n$, and two scalar rotations, $\phi_{0[]}$ and $\phi_{1][}$). The first order rotation $\phi_{0][}$, linked to the anti-symmetric part of tensor strain, is obtained by identifying afterwards the variable micropolar rotation

$$\phi_{0][} = \frac{1}{2}\left(\frac{\partial v}{\partial x} - \frac{\partial u}{\partial y}\right) = \phi$$

in the first order solution for the micropolar rotation variables. The present homogenization scheme has been automatized and implemented into a dedicated code, allowing to treat any lattice, with the topology of the unit cell together with the beam mechanical properties given as input; the homogenized properties (and the effective constitutive law) are given as output. Finite element simulations for a complete lattice may be performed in parallel to assess the computed effective behavior. Two examples are chosen in the sequel to illustrate the presented methodology.

9.5 Examples

9.5.1 Square Lattice

Despite its simplicity, the square lattice shown in Fig. 9.5 is an interesting application, since literature works report various homogenized micropolar behaviors, with sometimes even contradictory results. The unit cell consists of two orthogonal bars

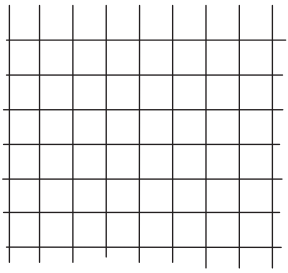

Fig. 9.5 Square lattice: Macroscopic lattice

of identical length L, with associated directors $\mathbf{e}^1 = (1,0)^T$; $\mathbf{e}^2 = (0,1)^T$. The previous formula for the normal and transverse efforts Eqs (9.45) and (9.43) give for this lattice at first order the resultants (normal and transverse effort) and moment as

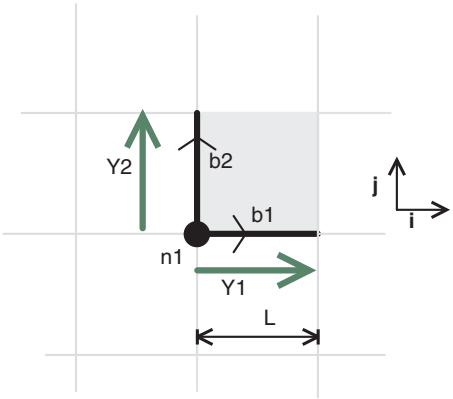

Fig. 9.6 Square lattice: Unit cell of the square lattice

$$N_1^1 = k_l \frac{\partial u}{\partial x}; \quad N_1^2 = k_l \frac{\partial v}{\partial y};$$

$$T_{1t}^1 = k_f \left(L\frac{\partial v}{\partial x} - L\phi_1^1 \right); \quad T_{1t}^2 = k_f \left(-L\frac{\partial u}{\partial x} - L\phi_1^1 \right);$$

$$M_1^{E(1)} = \frac{k_f L^2}{2}\left(\phi_1^1 - \frac{\partial v}{\partial x}\right); M_1^{O(1)} = \frac{k_f L^2}{2}\left(\phi_1^1 - \frac{\partial v}{\partial x}\right); M_1^{E(2)} = \frac{k_f L^2}{2}\left(\phi_1^1 + \frac{\partial u}{\partial y}\right);$$

$$M_O^{b2} = \frac{k_f L^2}{2}\left(\phi_1^1 + \frac{\partial u}{\partial y}\right)$$

There is a single unknown in these equations, the first order rotation ϕ_1^1, that after resolution becomes

$$\phi_1^1 = \frac{1}{2}\left(\frac{\partial v}{\partial x} - \frac{\partial u}{\partial y}\right).$$

Identifying $\phi_{0][} = \phi$, gives immediately,

$$\phi_1^1 = \frac{1}{2}\left(\frac{\partial v}{\partial x} - \frac{\partial u}{\partial y}\right) = \phi.$$

At the second order, one has the following expression of the resultant and moment:

$$N_2^1 = 0; \quad N_2^2 = 0;$$

$$T_{2t}^1 = -\frac{k_f L}{2}\left(2\phi_2^1 + L\frac{\partial \phi_{0][}}{\partial x}\right); \quad T_{2t}^2 = -\frac{k_f L}{2}\left(2\phi_2^1 + L\frac{\partial \phi_{0][}}{\partial y}\right);$$

$$M_2^{E(1)} = \frac{k_f L^2}{6}\left(3\phi_2^1 + 2L\frac{\partial \phi_{0][}}{\partial x}\right); \quad M_2^{O(1)} = \frac{k_f L^2}{6}\left(3\phi_2^1 + L\frac{\partial \phi_{0][}}{\partial x}\right);$$

$$M_2^{E(2)} = \frac{k_f L^2}{6}\left(3\phi_2^1 + 2L\frac{\partial \phi_{0][}}{\partial y}\right); \quad M_2^{O(2)} = \frac{k_f L^2}{6}\left(3\phi_2^1 + L\frac{\partial \phi_{0][}}{\partial y}\right).$$

To second order, there is also a single rotation variable ϕ_2^1, that after resolution expresses as

$$\phi_2^1 = -\frac{L}{4}\left(\frac{\partial \phi_{0][}}{\partial x} + \frac{\partial \phi_{0][}}{\partial y}\right) = \phi_{1][}^1.$$

We can now express the vectors $\mathbf{S}^i$et μ^i, from the Eqs (9.40) and (9.41)

$$\mathbf{S^1} = \begin{bmatrix} k_l L\dfrac{\partial u}{\partial x} \\ k_f L\left(\dfrac{\partial v}{x} - \phi\right) \end{bmatrix}; \quad \mathbf{S^2} = \begin{bmatrix} k_f L\left(\dfrac{\partial u}{y} - \phi\right) \\ k_l L\dfrac{\partial v}{\partial y} \end{bmatrix};$$

$$\boldsymbol{\mu}^1 = \begin{bmatrix} 0 \\ 0 \\ \dfrac{k_f L^3}{12}\dfrac{\partial \phi}{\partial x} \end{bmatrix}; \quad \boldsymbol{\mu^2} = \begin{bmatrix} 0 \\ 0 \\ \dfrac{k_f L^3}{12}\dfrac{\partial \phi}{\partial y} \end{bmatrix}$$

The stress and couple stress tensors are successively obtained from the Eqs (9.24) and (9.25), viz

$$\sigma = \frac{1}{g}\mathbf{S^i} \otimes \frac{\partial \mathbf{R}}{\partial \lambda^i}; \mathbf{m} = \frac{1}{g}\mu^{\mathbf{i}} \otimes \frac{\partial \mathbf{R}}{\partial \lambda^{\mathbf{i}}},$$

with $g = L^2$ the determinant of the Jacobean and the position vector R being extended to account for the third dimension, with derivatives

$$\frac{\partial \mathbf{R}}{\partial \lambda^1} = \begin{bmatrix} L \\ 0 \end{bmatrix}, \quad \frac{\partial \mathbf{R}}{\partial \lambda^2} = \begin{bmatrix} 0 \\ L \end{bmatrix}.$$

The 2D micropolar constitutive law is best formulated in matrix form, using the vector representation of the kinematic and static variables:

$$\{\boldsymbol{\sigma}\} = \begin{Bmatrix} \sigma_{xx} \\ \sigma_{yy} \\ \sigma_{xy} \\ \sigma_{yx} \\ m_{zx} \\ m_{zy} \end{Bmatrix} = [K] \begin{Bmatrix} \varepsilon_{xx} \\ \varepsilon_{yy} \\ \varepsilon_{xy} \\ \varepsilon_{yx} \\ \varkappa_{zx} \\ \varkappa_{zy} \end{Bmatrix} = [K] \begin{Bmatrix} \dfrac{\partial u}{\partial x} \\ \dfrac{\partial v}{\partial y} \\ \dfrac{\partial u}{\partial y} + \phi \\ \dfrac{\partial v}{\partial x} - \phi \\ \dfrac{\partial \phi}{\partial x} \\ \dfrac{\partial \phi}{\partial y} \end{Bmatrix}$$

The stiffness $[K]$ diagonal matrix has here a simple diagonal form

$$[K] = \begin{bmatrix} k_l & & & & & & \\ & k_l & & & & & \\ & & k_f & & & & \\ & & & k_f & & & \\ & & & & \frac{k_f L^2}{12} & & \\ & & & & & \frac{k_f L^2}{12} & \end{bmatrix} = \begin{bmatrix} E_s\eta & 0 & 0 & 0 & 0 & 0 \\ 0 & E_s\eta & 0 & 0 & 0 & 0 \\ 0 & 0 & E_s\eta^3 & 0 & 0 & 0 \\ 0 & 0 & 0 & E_s\eta^3 & 0 & 0 \\ 0 & 0 & 0 & 0 & \frac{L^2 E_s\eta^3}{12} & 0 \\ 0 & 0 & 0 & 0 & 0 & \frac{L^2 E_s\eta^3}{12} \end{bmatrix}$$

$$= \begin{bmatrix} \frac{E_s t}{L} & & & & & \\ & \frac{E_s t}{L} & & & & \\ & & \frac{12E_s I_z}{L^3} & & & \\ & & & \frac{12E_s I_z}{L^3} & & \\ & & & & \frac{E_s I_z}{L} & \\ & & & & & \frac{E_s I_z}{L} \end{bmatrix} \tag{9.46}$$

The Young's modulus is trivial, since this lattice is ortho-tetragonal, only the beams in the direction of loading therefore appears:

$$E_1^* = E_2^* = k_l = E_s\,\eta = \frac{E_s t}{L}.$$

The Poisson's modulus is zero $\nu_{12} = \nu_{21} = 0$, hence this lattice shows no contraction. The micropolar moduli $\varkappa$ and μ^* are:

$$\varkappa = k_f = E_s\,\eta^3 = 12\,\frac{E_s I_z}{L^3}; \quad \mu^* = 0.$$

The shear modulus is:

$$G = \frac{k_f}{2} = \frac{E_s\,\eta^3}{2} = 6\,\frac{E_s I_z}{L^3}.$$

The modulus of microbending stiffness is identical for both axes:

$$\gamma = \frac{k_f L^2}{12} = \frac{L^2 E_s \eta^3}{12} = \frac{E_s I_z}{L},$$

and has the units of Newton, contrary to the other micropolar modulus $\varkappa$, expressing in N/m. One may add the following constants related to the micropolar theory, namely the characteristic length $L^2_{\text{chara}} = \frac{L^2}{24}$ and the coupling coefficient $N^2_{\text{coupl}} = \frac{1}{2}$. Note that this coupling coefficient is not equal to 1, thereby proving that we are not in the case of a theory "couple stress" but rather a micropolar theory.

9.5.2 Hexagonal Lattice

The hexagonal lattice defined by Fig. 9.7 allows to validate the homogenization method in the case of a non-orthogonal set of unit cell vectors; furthermore, the unit cell includes internal nodes, which illustrate the powerfulness of the discrete homogenization technique (most literature works restrict to unit cells including a single node).

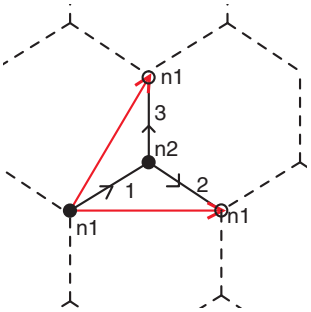

Fig. 9.7 Unit cell of the hexagonal lattice

Each beam has a length L; the lengths of the periodicity vectors $\mathbf{Y}_1$ and $\mathbf{Y}_2$ in the Cartesian basis are $L_1 = L_2 = \sqrt{3}L$. The other features of the lattice are synthesized in the connectivity Table 9.1.

Table 9.1 Connectivity array for the hexagonal lattice

beam	1	2	3
O(b)	1	2	2
E(b)	2	1	1
δ_1	0	1	0
δ_2	0	0	1

We obtain after calculations the homogenized stress tensor

$$\boldsymbol{\sigma} = \begin{bmatrix} \sigma_{11} & \sigma_{12} \\ \sigma_{21} & \sigma_{22} \end{bmatrix}$$

with

$$\sigma_{11} = \frac{k_l\sqrt{3}(k_l\,\frac{\partial u}{\partial x} + 3\,k_f\,\frac{\partial u}{\partial x} + k_l\,\frac{\partial v}{\partial y} - \left(\frac{\partial v}{\partial y}\right)k_f)}{6(k_l+k_f)},$$
$$\sigma_{12} = \frac{k_f\sqrt{3}\left(k_l\,\frac{\partial v}{\partial x} - k_f\,\frac{\partial v}{\partial x} + k_f\,\frac{\partial u}{\partial y} + 3\left(\frac{\partial u}{\partial y}\right)k_l + 2\,\phi\,k_l + 2k_f\,\phi\right)}{6(kl+kt)},$$
$$\sigma_{21} = \frac{k_f\sqrt{3}(3\,k_l\,\frac{\partial v}{\partial x} + \left(\frac{\partial u}{\partial y}\right)k_l + k_f\,\frac{\partial v}{\partial x} - k_f\,\frac{\partial u}{\partial y} - 2\,\phi k_l - 2k_f\,\phi)}{6(k_l+k_f)},$$
$$\sigma_{11} = \frac{k_l\sqrt{3}\left(k_l\,\frac{\partial u}{\partial x} - k_f\,\frac{\partial u}{\partial x} + k_l\,\frac{\partial v}{\partial y} + 3\left(\frac{\partial v}{\partial y}\right)k_f\right)}{6(k_l+kf)}$$

and the homogenized couple stress tensor

$$\boldsymbol{m} = \begin{bmatrix} 0 & 0 & 0 \\ 0 & 0 & 0 \\ \frac{\sqrt{3}L^2k_f}{36}\frac{\partial\phi}{\partial x} & \frac{\sqrt{3}L^2k_f}{36}\left(\frac{\partial\phi}{\partial y}\right) & 0 \end{bmatrix}$$

Using the condensed vector notation, we obtain the stiffness matrix

$$[K] = \begin{bmatrix} \frac{\sqrt{3}k_l\left(k_l+3k_f\right)}{6(k_l+k_f)} & \frac{\sqrt{3}k_l\left(k_l-k_f\right)}{6(k_l+k_f)} & 0 & 0 & 0 & 0 \\ \frac{\sqrt{3}k_l\left(k_l-k_f\right)}{6(k_l+k_f)} & \frac{\sqrt{3}k_l\left(k_l+3k_f\right)}{6(k_l+k_f)} & 0 & 0 & 0 & 0 \\ 0 & 0 & \frac{\sqrt{3}k_f\left(k_f+3k_l\right)}{6(k_l+k_f)} & \frac{\sqrt{3}k_f\left(k_l-k_f\right)}{6(k_f+k_f)} & 0 & 0 \\ 0 & 0 & \frac{\sqrt{3}k_f\left(k_l-k_f\right)}{6(k_f+k_f)} & \frac{\sqrt{3}k_f\left(k_f+3k_l\right)}{6(k_l+k_f)} & 0 & 0 \\ 0 & 0 & 0 & 0 & \frac{\sqrt{3}k_f.L^2}{36} & 0 \\ 0 & 0 & 0 & 0 & 0 & \frac{\sqrt{3}k_f.L^2}{36} \end{bmatrix}$$

$$= \begin{bmatrix} K_{11} & K_{12} & 0 & 0 & 0 & 0 \\ K_{21} & K_{22} & 0 & 0 & 0 & 0 \\ 0 & 0 & K_{33} & K_{34} & 0 & 0 \\ 0 & 0 & K_{43} & K_{44} & 0 & 0 \\ 0 & 0 & 0 & 0 & K_{55} & 0 \\ 0 & 0 & 0 & 0 & 0 & K_{66} \end{bmatrix}$$

with

$$K_{11} = K_{22} = \frac{1}{6}\frac{\sqrt{3}E_s\,\eta\,\left(1+3\,\eta^2\right)}{1+\eta^2}$$
$$K_{12} = K_{12} = -\frac{1}{6}\frac{\sqrt{3}E_s\,\eta\,\left(-1+\eta^2\right)}{1+\eta^2}$$
$$K_{33} = K_{44} = \frac{1}{6}\frac{\sqrt{3}E_s\,\eta^3\left(3+\eta^2\right)}{1+\eta^2}$$
$$K_{34} = K_{43} = -\frac{1}{6}\frac{\sqrt{3}E_s\,\eta^3\left(-1+\eta^2\right)}{1+\eta^2}$$
$$K_{55} = K_{66} = \frac{E_s\eta^3\sqrt{3}L^2}{36}$$

We extract from the previous matrix the homogenized moduli, which express versus the geometrical and mechanical lattice parameters:

$$\mu^* = \frac{1}{6}\frac{\sqrt{3}k_f\left(k_l-k_f\right)}{k_l+k_f} = -\frac{\sqrt{3}Es\,\eta^3\left(-1+\eta^2\right)}{6\left(1+\eta^2\right)} = -2\frac{I_z E_s\left(-tL^2+12I_z\right)\sqrt{3}}{L^3\left(tL^2+12I_z\right)};$$

$$\varkappa = \frac{k_f\sqrt{3}}{3} = \frac{Es\,\eta^3\sqrt{3}}{3} = 4\frac{\sqrt{3}I_z E_s}{L^3}; \quad \gamma = \frac{\sqrt{3}k_f.L^2}{36} = \frac{E_s\eta^3\sqrt{3}L^2}{36} = \frac{\sqrt{3}I_z E_s}{3L}$$

$$E^* = \frac{4\left(k_f k_l\sqrt{3}\right)}{3\left(k_l+3k_f\right)} = 4/3\,\frac{Es\,\eta^3\sqrt{3}}{1+3\,\eta^2} = 16\frac{\sqrt{3}E_s I_z t}{L\left(tL^2+36I_z\right)};$$

$$\nu = \frac{k_l-k_f}{k_l+3k_f} = -\frac{-1+\eta^2}{1+3\,\eta^2} = -\frac{-tL^2+12I_z}{tL^2+36I_z};$$

$$G^* = \frac{1}{3}\frac{k_l k_f\sqrt{3}}{k_l+k_f} = \frac{Es\,\eta^3\sqrt{3}}{3\left(1+\eta^2\right)} = 4\frac{\sqrt{3}E_s I_z t}{L\left(tL^2+12I_z\right)}$$

$$l^2_{\text{chara}} = \frac{L^2\left(k_l+k_f\right)}{48k_l} = \frac{L^2\left(1+\eta^2\right)}{48}; \quad N^2 = \frac{k_l+k_f}{3k_l+k_f} = \frac{1+\eta^2}{3+\eta^2}$$

We find the same results as other authors such as Pradel and Sab [10] and Kumar and McDowell [7], but with a different method. From a mathematical point of view, other methods search the minimum of an energy functional by means of gradients or Lagrange multipliers. We have to solve a linear system, which seems to be the simplest resolution method.

9.6 Conclusions and Perspectives

The discrete homogenization method based on asymptotic expansions of the fields (nodal position, forces and moments) proves a systematic method to calculate the equivalent - in an homogenized sense - properties of lattices with a general periodic architecture, characterized by the topology of bars within a repetitive unit cell. The construction of micropolar continua from elastic lattices endowed with translational

and rotational degrees of freedom has been undertaken in the present contribution, whereby the asymptotic homogenization method has been extended to polar lattices. From a technical viewpoint, the novelty of the present approach lies in the calculation of the transverse forces, which does not require the moment equilibrium, since the expression of the transverse forces is linked to the relative displacements of the extremities of a given bar, in the spirit of beam theory. The extension of the asymptotic homogenization to micropolar continua has been presently exemplified by the treatment of the tetragonal and hexagonal lattices in the micropolar framework. The advantage of this method is its simplicity of implementation, and generality. It boils down to a final matrix system to solve analytically, that lends itself readily to programming and automatic processing of any centro-symmetric lattice.

The micropolar continuum is in fact not the more general effective model one can obtain from the present two scale homogenization procedure: since the kinematics is developed up to second order of the small parameter ε, one shall expect to formulate a second order gradient (in the displacement) micropolar continuum. Due to truncation in the asymptotic expansions of the kinematic variables (hence also in the static variables) and the restriction to centro-symmetrical unit cells, the second order gradients of the displacements have been presently discarded.

The asymptotic homogenization scheme opens the way for the study of a multitude of different lattices (auxetic, chiral, non centrosymmetric), the automatized calculation of their effective mechanical behavior and the understanding of the underlying deformation mechanisms at the cell scale. From a general point of view, it opens the perspective of optimizing the topology and the mechanical properties of materials having a discrete structure such as foams, but also textiles or more generally any repetitive structure made of discrete elements akin to 1D structural elements like bars or beams. Globally speaking, the discrete homogenization provides an explicit link between the micro and macroscale behaviors, hence increasing our understanding of the microstructural origin of the deformation mechanisms of the taylored materials widely used nowadays.

References

[1] D. Caillerie, A. Mourad, and A. Raoult. Discrete homogenization in graphene sheet modeling. *Journal of Elasticity*, 84:33–68, 2006.

[2] A. C. Eringen Theory of micropolar fluids. *Journal of Mathematics and Mechanics*, 16:1–18, 1966.

[3] J. Fatemi, F. Van Keulen, and P.R. Onck. Generalized continuum theories: Application to stress analysis in bone. *Meccanica*, 37:385–396, 2002.

[4] C. Florence and K. Sab. A rigorous homogenization method for the determination of the overall ultimate strength of periodic discrete media and an application to general hexagonal lattices of beams. *European Journal of Mechanics A/Solids*, 25:72–97, 2006.

[5] S. Forest. Mechanics of Cosserat Media – an Introduction. 2005.

[6] R. S. Kumar and D. L. McDowell. Generalized continuum modeling of 2-d periodic cellular solids. *International Journal of Solids and Structures*, 41: 7399–7422, 2004.

[7] R. S. Kumar and D. L. McDowell. Multifunctional design of two-dimensional cellular materials with tailored mesostructure. *International Journal of Solids and Structures*, 46:2871–2885, 2009.

[8] S. Liu and W. Su. Effective couple-stress continuum model of cellular solids and size effects analysis. *International Journal of Solids and Structures*, 46: 2887–2899, 2009.

[9] A. Mourad. *Description topologique de l'architecture fibreuse et modelisation mecanique du myocarde*. PhD thesis, Institut National Polytechnique de Grenoble, 2003.

[10] F. Pradel and K. Sab. Cosserat modelling of elastic periodic lattice structures. *C. R. Acad. Sci. Paris,*, t. 326, Serie II b: 699–704, 1998.

[11] A. Raoult, D. Caillerie, and A. Mourad. Elastic lattices: equilibrium, invariant laws and homogenization. *Ann Univ Ferrara*, 54:297–318, 2008.

[12] A. Riahi and J. H. Curran. Full 3d finite element cosserat formulation with application in layered structures. *Applied Mathematical Modelling*, 33:3450–3464, 2009.

[13] J. Rosenberg and R. Cimrman. Microcontinuum approach in biomechanical modeling. *Mathematics and Computers in Simulation*, 61:249–260, 2003.

[14] H. Tollenaere and D. Caillerie. Continuous modeling of lattice structures by homogenization. *Advances in Engineering Software*, 29:699–705, 1998.

[15] P. Trovalusci and R. Masiani. Material symmetries of micropolar continua equivalent to lattices. *International Journal of Solids and Structures*, 36:2091–2108, 1999.

[16] W. E. Warren and E. Byskov. Three-fold symmetry restrictions on two-dimensional micropolar materials. *European Journal of Mechanics A/Solids*, 21:779–792, 2002.

[17] A. Yoo and I. Jasiuk. Couple-stress moduli of a trabecular bone idealized as a 3d periodic cellular network. *Journal of Biomechanics*, 39:2241–2252, 2006.

Part IV
Dynamics and Stability

Chapter 10
Nonlinear Waves in the Cosserat Continuum with Constrained Rotation

Vladimir I. Erofeev, Aleksandr I. Zemlyanukhin, Vladimir M. Catson, and Sergey F. Sheshenin

Abstract The nonlinear viscoelastic micropolar medium with constrained rotation (the Cosserat pseudo-continuum) is considered. Using the method of bound normal waves, the original nonlinear system describing the dynamics of the medium is transferred to a system of evolutionary equations. It is shown that these evolutionary equations are four nonlinear partial differential equations two of which are the Burgers equations and the other two are the modified Korteweg-de Vries (mKdV) equations. The paper presents the results of the numerical study of nonlinear viscoelastic wave evolution.

10.1 Basic Hypotheses and Dynamic Equations

It is known that one of assumptions of the classical mechanics of continuous media is the supposition about the equivalence of action of all internal forces applied to an area, to the action of their resultant applied to the gravity center of the area. However it is fulfilled not always, and generally action of the system of forces applied to the area, is equivalent to the action of the main vector and the main moment of these forces. The natural moments of momentum of material points of the medium and the presence of the distributed bulk and surface couples, which are usually assumed to be negligible in the classical mechanics of continuous media, will be taken into account in this paper.

Vladimir I. Erofeev and Sergey F. Sheshenin
Nizhny Novgorod Branch of Blagonravov Mechanical Engineering Research Institute RAS, Belinskogo St. 85, 603024 Nizhny Novgorod , Russia
e-mail: erf04@sinn.ru, e-mail: shesheninsf@nnov.transneft.ru
Aleksandr I. Zemlyanukhin and Vladimir M. Catson
Saratov State Technical University, Politekhnicheskaja St. 77, 410054 Saratov, Russia
e-mail: zemlyanukhinai@sstu.ru, e-mail: bobah311@yandex.ru

H. Altenbach et al. (eds.), *Mechanics of Generalized Continua,*
Advanced Structured Materials, 7, DOI: 10.1007/978-3-642-19219-7_10,

Under such assumptions, there arise in the solid body both stresses σ_{ji} and couple stresses m_{ji}, which are described by the asymmetrical tensors. The motion of such a medium is characterized by two field variables: the displacement vector $\bar{u}$ and the vector of rotations $\bar{\Psi}$. It is generally considered that the components of the vectors of displacements and rotations are kinematically independent (Cosserat continuum) [1], and the vector equations for the momentum and the moment of momentum play the role of the basic governing equations.

Besides the general case, the simplified alternative of the micropolar medium (the pseudo-Cosserat continuum) is considered, in which the strong dependence of the vector of rotations on the rotor of displacements ($\bar{\Psi} = \left(1/2\right) \operatorname{rot} \bar{u}$ is the constrained rotation) is supposed that coincides with the relations of the classical theory of elasticity, but couple stresses and the asymmetry of the stress tensor are maintained. In such a medium, the symmetric part of the stress tensor depends on the symmetric tensor of the strains in the same way as in classical theory of elasticity.

The dynamic equations of the pseudo-Cosserat continuum have the form [2]:

$$\rho \ddot{\bar{u}} - (\lambda + \mu) \operatorname{grad} \operatorname{div} \bar{u} - \mu \Delta \bar{u} - \frac{1}{4}(\gamma + \varepsilon) \operatorname{rot} \operatorname{rot} \Delta \bar{u} + \frac{I}{4} \operatorname{rot} \operatorname{rot} \ddot{\bar{u}} = \bar{F}_1 + \bar{F}_2. \quad (10.1)$$

Here λ and μ are the Lamé constants; α, γ, and ε are additional elastic constants of the micropolar material, satisfying the restrictions $\alpha \geq 0$, $\gamma + \varepsilon \geq 0$, $-(\gamma + \varepsilon) \leq \gamma - \varepsilon \leq (\gamma + \varepsilon)$; ρ is the density of the medium; I is a constant describing the inertia properties of the macrovolume. This constant is equal to the product of the moment of inertia of a particle of the substance around of any axis passing through its gravity center and the number of particles in the unit volume.

Vector $\bar{F}_1$ includes the viscoelastic components, and vector $\bar{F}_2$ comprises the nonlinear elastic components. The explicit view of the nonlinear terms is given for some cases in [2], the viscoelastic components – in [3].

System (10.1) enables one to describe both the longitudinal elastic waves (dilatation waves) and the shear waves. Thus, waves of a dilatation in the Cosserat medium are identical to the properties of the corresponding waves in the classical medium. These waves propagate with the velocity

$$c_l = \sqrt{(\lambda + 2\mu)/\rho},$$

while the shear waves are dispersive in such a medium and distinct from the classical shear waves. In the low-frequency range ($\omega \to 0$) these waves travel with the velocity close to

$$c_\tau = \sqrt{\mu/\rho},$$

and in a high-frequency field ($\omega \to \infty$) – with the velocity close to

$$c_2 = \sqrt{(\gamma + \varepsilon)/I}.$$

Let us consider the propagation of plane waves along the x_1-axis: longitudinal waves $u_1 = u(x,t)$ and shear waves $u_3 = w(x,t)$. In this case the vector equation (10.1) will be rewritten as a system of two one-dimensional scalar equations:

$$\begin{cases} \dfrac{\partial^2 u}{\partial t^2} - c_l^2 \dfrac{\partial^2 u}{\partial x^2} = \dfrac{1}{\rho}\dfrac{\partial}{\partial x}\left\{ \dfrac{g_1}{2}\left(\dfrac{\partial u}{\partial x}\right)^2 + \dfrac{g_2}{2}\left(\dfrac{\partial w}{\partial x}\right)^2 \right\} + \gamma_1 \dfrac{\partial^3 u}{\partial x^2 \partial t}, \\ \dfrac{\partial^2 w}{\partial t^2} - c_\tau^2 \dfrac{\partial^2 w}{\partial x^2} + \dfrac{(\gamma+\varepsilon)}{4\rho}\dfrac{\partial^4 w}{\partial x^4} - \dfrac{I}{4\rho}\dfrac{\partial^4 w}{\partial x^2 \partial t^2} \\ \qquad = \dfrac{1}{\rho}\dfrac{\partial}{\partial x}\left\{ g_2 \dfrac{\partial u}{\partial x}\dfrac{\partial w}{\partial x} + g_5 \left(\dfrac{\partial w}{\partial x}\right)^3 \right\} + \gamma_2 \dfrac{\partial^3 w}{\partial x^2 \partial t} - \gamma_3 \dfrac{\partial^3 w}{\partial t^3}. \end{cases} \tag{10.2}$$

Here

$$\begin{aligned} g_1 &= 3\lambda + 6\mu + 2A + 6B + 2C, \\ g_2 &= \frac{\lambda}{2} + \mu + \frac{A}{4} + \frac{B}{2}, \\ g_5 &= 3\left(\frac{\lambda}{2} + \mu + \frac{A}{2} + B + J\right) \end{aligned}$$

are coefficients characterizing the nonlinearity of the material; γ_1, γ_2, and γ_3 are factors describing its viscosity; A, B, C, D, G, J, H are the Landau elasticity moduli [2].

10.2 Derivation of Evolution Equations

The investigation of the wave propagation of waves with finite amplitudes in the Cosserat continuum considering the constrained rotation is rather complicated even in the case of the one-dimensional processes (10.2). It is much easier to deal with evolutionary equations, which are approximate and maintain in itself the major factors influencing the wave processes. There exist physically and mathematically enough correct methods of transition from the initial equations to the evolutionary ones [4]. We shall use the method of the bound normal waves, developed in [4]. For this purpose, we rewrite the system (10.2) in the form

$$\frac{\partial \mathbf{u}}{\partial t} + \mathbf{B}(q)\,\mathbf{u} = \mathbf{F}(u,q) \tag{10.3}$$

with $\mathbf{u}^T = (V, u, w, Q)$ as a four-dimensional vector of physical variables; $V = \partial u/\partial t$; $Q = \partial w/\partial t$;

$$\mathbf{B}(q)=\begin{pmatrix} 0 & -c_l^2q^2 & 0 & 0 \\ -1 & 0 & 0 & 0 \\ 0 & 0 & 0 & -1 \\ 0 & 0 & -c_\tau^2q^2+\dfrac{\gamma+\varepsilon-Jc_\tau^2}{4\rho}q^4 & 0 \end{pmatrix}$$

is a linear operator matrix;

$$\mathbf{F}=\begin{pmatrix} \left\{\dfrac{g_1}{\rho}u^2+\dfrac{g_2}{\rho}w^2+\gamma_1c_lu\right\}q^3 \\ 0 \\ 0 \\ \left\{\dfrac{2g_2}{\rho}uw+\left(\gamma_2c_\tau-\gamma_3c_\tau^3\right)w\right\}q^3+\dfrac{3g_5}{\rho}w^3q^4 \end{pmatrix}$$

is a vector of nonlinear quantities; $q=\partial/\partial x$ is a differential operator.

The conversion from the system (10.2) to the equations of the bound normal waves consists in a diagonalization of the operator matrix $\mathbf{B}(q)$ by transition into its natural basis using the change of variables

$$u(x,t)=\sum_{k=1}^{4}r_k(q)U_k(x,t), \tag{10.4}$$

where $U_k(x,\,t)$ are new variables; $\mathbf{r}_k$ are the right eigenvectors of matrix $\mathbf{B}$

$$\mathbf{B}\cdot\mathbf{r}_k=p_k\mathbf{r}_k;$$

$p_k(q)$ are its eigenvalues.

Substitution of Eq. (10.4) into the vector equation (10.3) and multiplication of its left-hand and right-hand sides by the left-hand eigenvectors $\mathbf{l}_j(q)$ lead, if one takes into account the orthogonality condition $\mathbf{l}_j\mathbf{r}_k=0$ at $j\neq k$, to equations of the bound normal waves $(\partial U_k/\partial\,t)+p_k(q)U_k=(\mathbf{l}_j\mathbf{r}_k)^{-1}\left[\mathbf{l}_k\mathbf{F}(r_kU_k,q)\right]$, where p_k determines different branches of the dispersion equation of the linearized system. Arbitrariness in a choice of eigenvectors can be used for the reduction of the right-hand side to the simplest form. Using this fact, let us decompose the eigenvalues p_k into Taylor series on q. If only the first two terms in this expansion are preserved, we shall obtain the following evolutionary equations:

$$\begin{aligned}
&\frac{\partial U_{1,2}}{\partial\,t}\pm c_l\frac{\partial U_{1,2}}{\partial x}\pm\frac{\gamma_1}{2}\frac{\partial^2U_{1,2}}{\partial x^2}=\mp\frac{g_1}{c_l\rho}U_{1,2}\frac{\partial U_{1,2}}{\partial x}\mp\frac{g_2}{c_l\rho}U_{3,4}\frac{\partial U_{3,4}}{\partial x},\\
&\frac{\partial U_{3,4}}{\partial t}\pm c_\tau\frac{\partial U_{3,4}}{\partial x}\pm\frac{\left(\gamma_2c_\tau-\gamma_3c_\tau^3\right)}{2c_\tau}\frac{\partial^2U_{3,4}}{\partial x^2}\pm\frac{\left(Jc_\tau^2-\gamma-\varepsilon\right)}{8c_\tau\rho}\frac{\partial^3U_{3,4}}{\partial x^3}\\
&\qquad=\mp\frac{9g_5}{2c_\tau\rho}U_{3,4}^2\frac{\partial U_{3,4}}{\partial x}\mp\frac{g_2}{c_\tau\rho}U_{1,2}\frac{\partial U_{3,4}}{\partial x}\,.
\end{aligned}\tag{10.5}$$

The relations between the new variables (U_i) with the original ones (u,w) are defined by the following expressions:

$$\begin{aligned}\frac{\partial u}{\partial x} &= U_1 + U_2,\\ \frac{\partial w}{\partial x} &= U_3 + U_4\,.\end{aligned} \tag{10.6}$$

The first two equations of the set $(U_{1,2})$ represent Burgers' equation known in the theory of nonlinear waves, whereas the second two equations $(U_{3,4})$ are the not less known modified Korteweg-de Vries equations (mKdV) [5]. Here the equations are interrelated with each other.

10.3 Numerical Simulation

In the numerical experiment we consider the waves running in one direction, in other words, we analyze the set of equations for U_1 and U_3:

$$\begin{aligned}&\frac{\partial U_1}{\partial\, t} + c_l\frac{\partial U_1}{\partial x} + \frac{\gamma_1}{2}\frac{\partial^2 U_1}{\partial x^2} = -\frac{g_1}{c_l\rho}U_1\frac{\partial U_1}{\partial x} - \frac{g_2}{c_l\rho}U_3\frac{\partial U_3}{\partial x},\\ &\frac{\partial U_3}{\partial t} + c_\tau\frac{\partial U_3}{\partial x} + \frac{\left(\gamma_2 c_\tau - \gamma_3 c_\tau^3\right)}{2c_\tau}\frac{\partial^2 U_3}{\partial x^2} + \frac{\left(Jc_\tau^2 - \gamma - \varepsilon\right)}{8c_\tau\rho}\frac{\partial^3 U_3}{\partial x^3}\\ &\qquad = -\frac{9g_5}{2c_\tau\rho}U_3^2\frac{\partial U_3}{\partial x} - \frac{g_2}{c_\tau\rho}U_1\frac{\partial U_3}{\partial x}\,.\end{aligned} \tag{10.7}$$

As a matter of convenience of simulation, we introduce the dimensionless variables (x',t'), pass into the moving reference frame and use the classical designations for the longitudinal and the shear wave modes:

$$x' = \frac{x}{\Lambda}, \qquad t' = \frac{t\cdot c_l}{\Lambda},$$

$$\begin{aligned}x^* &= x' - t', \quad t^* = t',\\ U_1 &= U, \quad U_3 = W.\end{aligned}$$

where Λ is a characteristic wavelength. Then, Eqs (10.7) take the form (a "sprocket wheel" index is hereinafter dropped):

$$\begin{aligned}&\frac{\partial U}{\partial\, t} + a_1\frac{\partial^2 U}{\partial x^2} + a_2 U\frac{\partial U}{\partial x} + a_3 W\frac{\partial W}{\partial x} = 0,\\ &\frac{\partial W}{\partial t} + C\frac{\partial W}{\partial x} + a_4\frac{\partial^2 W}{\partial x^2} + a_5\frac{\partial^3 W}{\partial x^3} + a_6 W^2\frac{\partial W}{\partial x} + a_7 U\frac{\partial W}{\partial x} = 0\,.\end{aligned} \tag{10.8}$$

Here

$$a_1 = \frac{\gamma_1}{2c_l\Lambda}, \quad a_2 = \frac{g_1}{c_l^2\rho}, \quad a_3 = \frac{g_2}{c_l^2\rho}, \quad C = \left(\frac{c_\tau}{c_l} - 1\right), \quad a_4 = \frac{\left(\gamma_2 c_\tau - \gamma_3 c_\tau^3\right)}{2c_\tau c_l \Lambda},$$

$$a_5 = \frac{\left(Jc_\tau^2 - \gamma - \varepsilon\right)}{8c_\tau c_l \rho \Lambda^2}, \quad a_6 = \frac{9g_5}{2c_\tau c_l \rho}, \quad a_7 = \frac{g_2}{c_\tau c_l \rho}.$$

For computing the Eqs (10.8), the semi-implicit spectral scheme [6] is used with the following parameters of the grid: step $\Delta x = 0,25$; length L = 128; number of nodes N = 512; time step $\Delta t = 0,1$. The requirement of periodicity is supposed for x-coordinate.

With the initial conditions in the form

$$u_0(x) = w_0(x) = 2\exp\left\{-\left(\frac{1}{1000\Delta x}\left[x - \frac{L}{4}\right]\right)^2\right\},$$

shown in Fig. 10.1 and the following values of the coefficients $a_1 = 2$, $a_2 = 1$, $a_3 = 0,5$, $a_4 = 0,01$, $a_5 = 2$, $a_6 = 2$, $a_7 = 0,1$, $C = -0,5$, the wave behavior will be rather stable. The choice of small a_4 applies particular restrictions on the coefficients γ_2 and γ_3 of the original set (10.7).

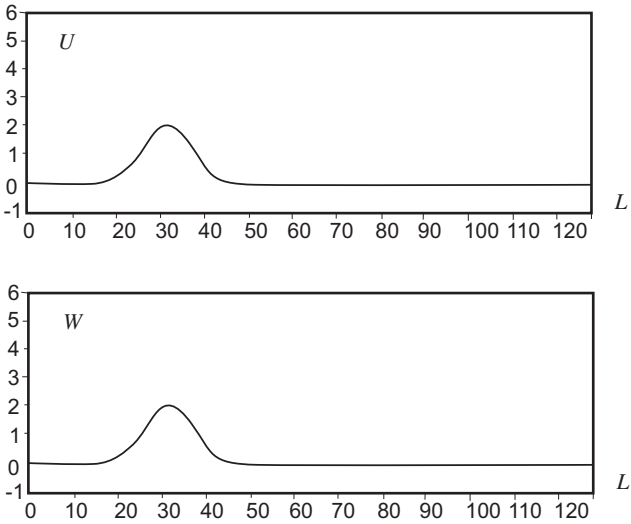

Fig. 10.1 Initial conditions (t = 0) for the longitudinal (U) and shear (W) waves in the form of Gauss pulse

Such a choice is also made because the great value of the viscosity coefficient leads to too fast attenuation of perturbations that prevents from formation of solitary waves. The Gauss pulse of the function W exhibits the classical behavior that is typical for the mKdV equation: it breaks up on some soliton-like perturbations (Fig. 10.3). However, in contrast to the classical mKdV solitons, the amplitude of

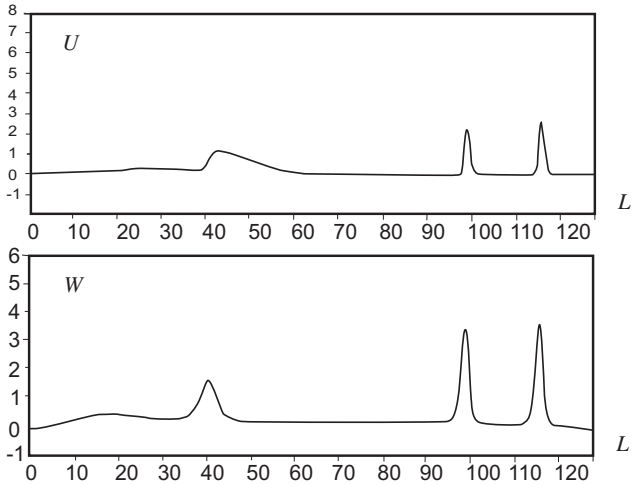

Fig. 10.2 Longitudinal (U) and shear (W) solitons at time $t = 20$

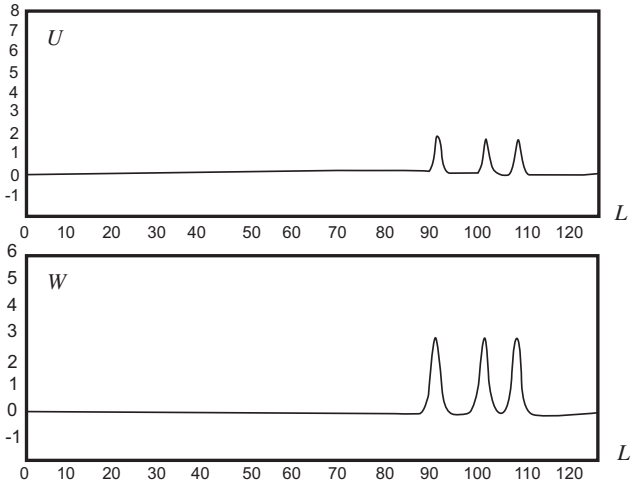

Fig. 10.3 Longitudinal (U) and shear (W) solitons at time $t = 80$

solitons of function W prolongs to grow up to some limiting value constrained by attenuation factors (a_1,$a_4 = 0,01$). After some time, the three first solitons are leveled on amplitudes, and the wave tail damps (Fig. 10.3). Perturbations of the function U behave a little differently. Here, the major source of soliton-like waves is not the initial perturbation, but the nonlinear coupling with the equation for W. Solitons U are induced by soliton-like pulses W, due to that their amplitude depends on the quantity of the coupling coefficient a_3. In this system such behavior is natural, as the equation for U does not contain dispersion terms and cannot have natural solitary-wave solutions. The increase of coupling coefficients a_3 and a_7 leads to the increase

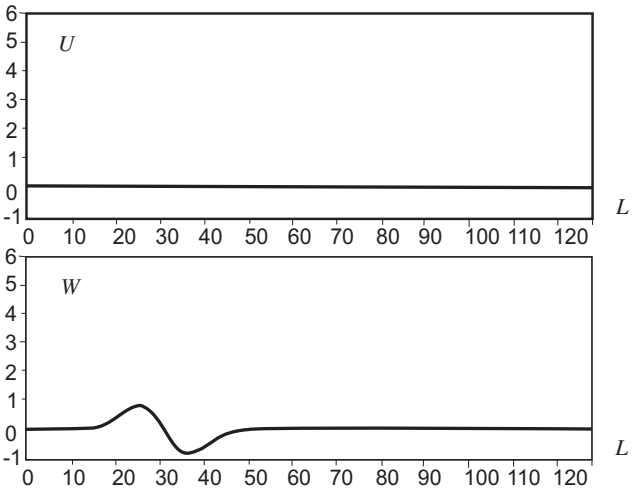

Fig. 10.4 Initial conditions (t = 0) for the longitudinal (U) and shear (W) waves in the form of Gauss pulse

of the limiting amplitude of solitons and to the decrease of their width. Thus, in the Cosserat medium with the constrained rotation, solitons of the longitudinal strain are generated only on account of shear solitons.

The choice of initial conditions in the form of a pulse with zero initial energy for the shear wave W and in the case of absence of the longitudinal wave $U = 0$

$$w_0(x) = -\frac{0,06}{\Delta \mathrm{x}} \left(x - \frac{L}{4}\right) \exp\left\{-\left(\frac{1}{1000\Delta x}\left[x - \frac{L}{4}\right]\right)^2\right\}$$

gives the following evolutionary pattern for the values of the coefficients $a_1 = 2$, $a_2 = 1$, $a_3 = 1$, $a_4 = 0,01$, $a_5 = 2$, $a_6 = 2$, $a_7 = 0,2$, $C = -0,5$ (Fig. 10.4). The positive part of the perturbation W grows and, at the particular moment, absorbs the negative part, being transformed into a solitary wave. The solitary wave W, like in the above considered case, induces soliton-like perturbation of function U (Fig. 10.5).

It is interesting to note that the wave a behavior drastically changes if the correlation between the nonlinearity coefficients in the equation for U varies, namely, if a_2 increases and a_3 decreases. We shall keep former initial conditions for U and W (Fig. 10.4), but we shall increase a_2 up to 4,5 and simultaneously decrease a_3 twice. Thus, we have: $a_1 = 2$; $a_2 = 4,5$; $a_3 = 0,5$; $a_4 = 0,01$; $a_5 = 2$; $a_6 = 2$; $a_7 = 0,2$; $C = -0,5$.

The evolution of perturbation W qualitatively differs a little from the previous case unless the height of a solitary wave pulse is not so great. At the same time, before formation of a soliton, perturbation U passes through a certain transition process. The competition of effects of nonlinearity of the second (in the equation for U) and the third (in the equation for W) orders leads to that the forward front

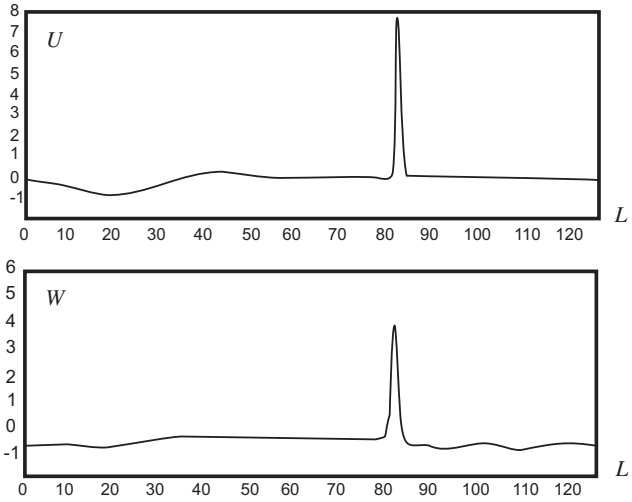

Fig. 10.5 Longitudinal (U) and shear (W) solitons at time $t = 34$

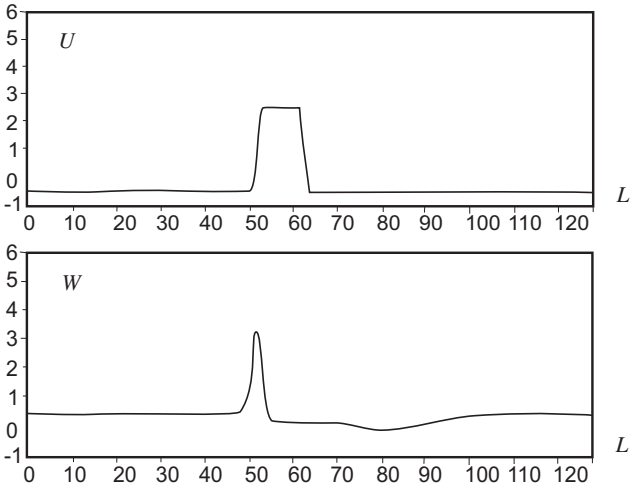

Fig. 10.6 The Π-shaped pulse of longitudinal wave (U) and the shear (W) soliton

of perturbation moves a little bit faster than a back one. As a result, the Π-shaped pulse generates, which moves with the velocity of the soliton function W (Fig. 10.3). However, after a time, the back front starts to overtake the forward one, and the Π-shaped pulse is transformed into a usual solitary wave (Fig. 10.3).

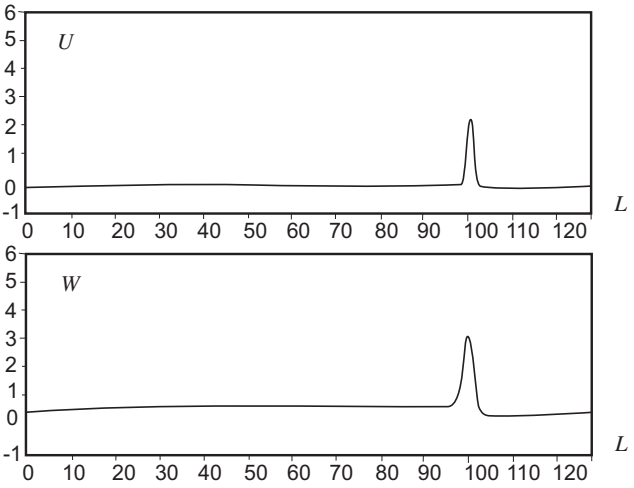

Fig. 10.7 Longitudinal (U) and shear (W) solitons

References

[1] Cosserat, E., Cosserat, F.: *Théorie des Corps Déformables*. Hermann Editeurs, Paris (1909) (Reprint, Gabay, Paris, 2008)

[2] Erofeyev, V.I.: *Wave Processes in Solids with Microstructure*. World Scientific. New Jersey–London–Singapore–Hong Kong (2003)

[3] Erofeev V.I., Kazhaev V.V., Semerikova N.P.: Macromechanical Modelling of Cosserat Elastic and Visco-Elastic Media. Computational Continuum Mechanics. **2**(2) 40-47 (2009)

[4] Engelbrecht, J.K., Fridman, V.E., Pelinovsky, E.N.: *Nonlinear Evolution Equations*. Pitman. London (1988)

[5] Dodd, R.K., Eilbeck, J.C., Gibbon, J.D., Morris, H.C.: *Solitons and Nonlinear Wave Equations*. Academic Press. London–Orlando–San Diego–New York–Toronto–Montreal–Sydney–Tokyo (1984)

[6] Press, W.H., Teukolsky, S.L., Vetterling, W.T., Flannery, B.P.: *Numerical Recipes in C. The Art of Scientific Computing*. Cambrige University Press. Cambridge (1992)

Chapter 11
Wave Propagation in Quasi-continuous Linear Chains with Self-similar Harmonic Interactions - Towards a Fractal Mechanics

Thomas M. Michelitsch, Gérard A. Maugin, Franck C. G. A. Nicolleau, Andrzej F. Nowakowski and Shahram Derogar

Abstract Many systems in nature have arborescent and bifurcated structures such as trees, fern, snails, lungs, the blood vessel system, but also porous materials etc. look self-similar over a wide range of scales. Which are the mechanical and dynamic properties that evolution has optimized by choosing *self-similarity* so often as an inherent material symmetry? How can we describe the mechanics of self-similar structures in the static and dynamic framework? In order to analyze such material systems we construct self-similar functions and linear operators such as a self-similar variant of the Laplacian and of the D'Alembertian wave operator. The obtained self-similar linear wave equation describes the dynamics of a quasi-continuous linear chain of infinite length with a spatially self-similar distribution of nonlocal inter-particle springs. The dispersion relation of this system is obtained by the negative eigenvalues of the self-similar Laplacian and has the form of a Weierstrass-Mandelbrot function which exhibits self-similar and fractal features. We deduce a continuum approximation that links the self-similar Laplacian to fractional integrals which also yields in the low-frequency regime a power law scaling for the oscillator density with strictly positive exponent leading to a vanishing oscillator density at frequency zero. We suggest that this power law scaling is a characteristic and universal feature of self-similar systems with complexity well beyond of our present model. For more details we refer to our recent paper [7].

Thomas M. Michelitsch and Gérard A. Maugin
Institut Jean le Rond d'Alembert, CNRS UMR 7190, Université Pierre et Marie Curie, Paris 6, France
e-mail: michel@lmm.jussieu.fr
e-mail: gerard.maugin@upmc.fr

Franck C.G.A. Nicolleau and Andrzej F. Nowakowski
Department of Mechanical Engineering, University of Sheffield, United Kingdom
e-mail: f.nicolleau@shefield.ac.uk
e-mail: a.f.nowakowski@shefield.ac.uk

Shahram Derogar
Department of Civil and Structural Engineering, University of Sheffield, United Kingdom
e-mail: derogar2002@yahoo.com

H. Altenbach et al. (eds.), *Mechanics of Generalized Continua,*
Advanced Structured Materials, 7, DOI: 10.1007/978-3-642-19219-7_11,

Key words: Fractal Mechanics. Wave-propagation. Dynamics: Self-similarity. Self-similar functions. Affine transforms. Fractal functions. Fractals. Power laws.

11.1 Introduction

So far there is no generally accepted theory which is able to describe material systems with fractal micro-structures possessing self-similarity as a material symmetry. Nevertheless, some important initial steps have been performed (see papers [1, 2, 3, 4, 5, 6] and the references therein). One direction is to model fractal materials by using fractional calculus as suggested recently by Ostoja-Starzewski [3]. This theory aims to construct a homogenized continuum theory of fractal materials.

In the meantime simple models are desirable of physical systems with fractal and self-similar features where "simple" means here simple enough to be accessible for an analysis. The hope is to gain in this way some general insight in the physics and the mechanics of fractal media by capturing some essential physical properties due to self-similarity and fractality. The goal of this paper is to introduce such a simple model. This paper is organized as follows: First we derive the mathematical framework which allows us to tackle material systems with self-similar features. To establish the physical model we introduce the notion of self-similar functions and *self-similar linear operators* such as the Laplacian and deduce the conditions of their existence. By utilizing this machinery we analyze the wave propagation properties of a one-dimensional linear chain having self-similar harmonic interactions. This model system is probably one of the most simple one featuring self-similar physical properties. It turns out that physical systems with self-similarity as a symmetry property require non-local particle-particle interactions and a (quasi-) continuous distribution of mass. We define this model system by its Hamiltonian functional which yields an equation of motion which can be conceived as a fractal, self-similar wave equation containing the self-similar Laplacian introduced in the mathematical framework. The (negative) eigenvalue spectra of this self-similar Laplacian is obtained in the form of Weierstrass-Mandelbrot functions which are exactly self-similar and in certain cases fractal functions. Moreover, we consider a continuum limit where the Laplacian takes the form of fractional integrals giving a link to the approach proposed by Ostoja-Starzewski [3]. In this continuum approach the vibrational spectra takes the form of power functions yielding a density of normal oscillators in form of a characteristic power law for low frequencies with positive exponents giving a vanishing oscillator density at frequency $\omega = 0$. We believe that this feature is universal for self-similar material systems.

11.2 The Mathematical Framework

11.2.1 The Self-similar Problem - Self-similar Functions

Before we consider a physical problem we need to define the notion "self-similar". We call a function $\phi(h)$ self-similar with respect to variable h if it fulfills [7]

$$\phi(Nh) = N^{\delta}\phi(h) \tag{11.1}$$

$\forall h > 0$, but only for a given value $N > 1 \in \mathbb{R}^1$ and as a consequence for all of its integer powers N^s, $s \in \mathbb{Z}_0$). We call (11.1) the affine problem where ϕ constitutes a (non-unique) solution to be found. A such solution of (11.1) can be represented in the form

$$\phi(h) = \sum_{s=-\infty}^{\infty} N^{-\delta s} f(N^s h) \tag{11.2}$$

where f can be any function for which the series (11.2) converges. We can write (11.2) more conveniently in operator form

$$\phi(h) = \hat{T}_N(h) f(h) \tag{11.3}$$

where $\hat{T}_N(h)$ is a self-similar operator defined by

$$\hat{T}_N = \sum_{s=-\infty}^{\infty} N^{-\delta s} \hat{A}_N^s \tag{11.4}$$

where the operator $\hat{A}_N$ is defined by

$$\hat{A}_N f(h) =: f(Nh) \tag{11.5}$$

The operator (11.4) fulfills also the condition of self-similarity $\hat{A}_N \hat{T}_N = N^{\delta} \hat{T}_N$. We emphasize that we can restrict ourselves on $N > 1$ ($N \in \mathbb{R}$) and exclude the pathological case $N = 1$.

It is important to consider for which class of functions $f(t)$ the series (11.2) converges absolutely. One shows that $f(t)$ is admissible if they are restraint by power functions ($t > 0$)

$$\lim_{t \to 0} |f(t)| \leq a_0 t^{\alpha} \tag{11.6}$$

and

$$\lim_{t \to \infty} |f(t)| \leq c_{\infty} t^{\beta} \tag{11.7}$$

where $a_0, c_{\infty} > 0$ are positive nonzero constants. The exponents $\alpha, \beta \in \mathbb{R}$ are allowed to take values $\beta < \alpha$ only. From this follows that neither power functions $f = t^{\gamma}$

[1] We can restrict ourselves on $N > 1$ since exchange $N \to N^{-1}$ in (11.1) represents the identical problem.

nor self-similar functions themselves are admissible in (11.2). A function $f(t)$ is admissible if the series $\phi(h)$ of (11.2) converges absolutely, i.e. δ is within the interval

$$\beta < \delta < \alpha \tag{11.8}$$

The case $\beta = 0$ is met if $|f(t)| \leq const$ which includes all periodic functions, however only some of them are admissible. As we introduced the affine problem (11.1) it does not have a unique solution. The self-similarity condition (11.1) defines only the function space of possible solutions. The following brief consideration shows which condition is to be added in order to make its solution unique. To this end we put

$$h = N^u = N^{n+\chi} \tag{11.9}$$

where $n = \text{floor}(u) \in \mathbb{Z}_0$ denoting the largest integer inferior to u where $u = \frac{\ln h}{\ln N}$. That is we can put

$$u = \text{floor}(u) + \chi(u) \tag{11.10}$$

where $0 \leq \chi(u) < 1$ denotes the non-integer rest which is zero when u itself is integer. We hence can write for the self-similar function

$$\phi(h) = \phi(N^n N^\chi) = N^{\delta n}\phi(N^\chi),\ 0 \leq \chi < 1 \tag{11.11}$$

which can be rewritten by using $N^n = hN^{-\chi}$ in the form

$$\phi(h) = h^\delta N^{-\delta\chi}\phi(N^\chi),\ 0 \leq \chi < 1 \tag{11.12}$$

From this relation follows that any value of $\phi(h)$ is uniquely determined by its values $\phi(N^\chi)$ in the interval $1 \leq h = N^\chi < N$ (since $0 \leq \chi < 1$) and can be constructed from these by (11.12). From these observations we can now formulate the *self-similar* problem having a unique solution:

It exists a unique function $\phi(h)$ which fulfills (11.1) $\forall h > 0$ for prescribed $N > 1$ and δ which takes in the interval $1 \leq \tau < N$ the values

$$\phi(\tau) = v(\tau),\ 1 \leq \tau < N \tag{11.13}$$

where $v(\tau)$ can be any arbitrary function defined over $[1,N)$ and its solution has the representation

$$\phi(\tau) = h^\delta N^{-\delta\chi} v(\tau),\ 1 \leq \tau = N^\chi < N \tag{11.14}$$

Hence by adding (11.13) to the condition of self-similarity (11.1) makes its solution unique. (11.14) is in accordance with (11.2) when we introduce $v(\tau)$ nonzero uniquely in the interval $1 \leq \tau < N$ and zero elsewhere. Then the series

$$\phi(h = N^n\tau) = \sum_{s=-\infty}^{\infty} N^{-\delta s} v(N^{s+n}\tau) \tag{11.15}$$

has the only non-vanishing term for $s = -n$ and converges for all $\delta \in \mathbb{R}$ and yields

$$\phi(h) = N^{\delta n} v(\tau) = h^{\delta} N^{-\delta\chi} v(\tau) \tag{11.16}$$

in accordance with (11.14).

Before we pass to the physical model another observation on self-similar functions might be useful: In many physical problems an expansion of solutions into ortho-normal modes reflecting the symmetry of the physical system and being eigenmodes of the physical problem are highly desirable. As starting point to construct a complete set of ortho-normal self-similar eigenmodes we make use of (11.12) which we can rewrite in the form

$$\phi(h) = h^{\delta} g(\ln h) \tag{11.17}$$

where $g(\ln h) = N^{-\delta\chi}\phi(N^{\chi})$ is invariant when we replace h by Nh (since $\chi(u+n) = \chi(u)$). It is for our convenience that we write g as a function of $\ln(h)$. That is

$$g(\ln(Nh)) = g(\ln h + \ln N) = g(\ln h) \tag{11.18}$$

is a periodic function with periodicity length $\ln N$. It follows that $g(\ln h)$ can be represented in terms of a Fourier series

$$g(\ln h) = \sum_{m=-\infty}^{\infty} a_m \, \mathrm{e}^{\frac{2\pi i m}{\ln N} \ln h} \tag{11.19}$$

where each of the functions

$$\mathrm{e}^{\frac{2\pi i m}{\ln N} \ln h} = h^{\frac{2\pi i m}{\ln N}}$$

fulfills this symmetry. We hence can write for $\phi(h)$ with (11.17)

$$\phi(h) = \sum_{m=-\infty}^{\infty} a_m h^{\delta + \frac{2\pi i m}{\ln N}} \tag{11.20}$$

where the ensemble of functions

$$\phi_m(h) = h^{\delta + \frac{2\pi i m}{\ln N}}$$

constitute a set of eigenfunctions with self-similar symmetry, each obeying the relation of self similarity

$$\phi_m(Nh) = N^{\delta} \phi_m(h) \tag{11.21}$$

and with the orthogonality condition ($\phi_n^+(h) = h^{-\delta - \frac{2\pi i n}{\ln N}}$)

$$\int_1^N \phi_n^+(h) \phi_m(h) \frac{\mathrm{d}h}{h} = \int_1^N h^{\frac{2\pi i (m-n)}{\ln N} - 1} \mathrm{d}h = \delta_{nm} \ln N \tag{11.22}$$

where δ_{mn} denotes the Kronecker-symbol. The a_m are uniquely determined by the values of in the interval $v(\tau)$ $1 \le \tau < N$, namely

$$a_m = \frac{1}{\ln N} \int_1^N v(\tau) \tau^{-(\delta + 1 + \frac{2\pi i m}{\ln N})} \mathrm{d}\tau \tag{11.23}$$

from which follows ($1 \leq h < N$)

$$v(h) = \sum_{m=-\infty}^{\infty} \frac{1}{\ln N} \int_1^N \frac{h^{\delta+\frac{2\pi i m}{\ln N}}}{\tau^{(\delta+1+\frac{2\pi i m}{\ln N})}} v(\tau) \mathrm{d}\tau = \int_1^N \delta(h-\tau) v(\tau) \mathrm{d}\tau \tag{11.24}$$

from which follows

$$\frac{1}{\ln N} \sum_{m=-\infty}^{\infty} \frac{1}{\tau} \left(\frac{t}{\tau}\right)^{\delta+\frac{2\pi i m}{\ln N}} = \delta(t-\tau), \tag{11.25}$$

where $\delta(\xi)$ denotes Dirac's δ-function.

11.2.2 A Self-similar Analogue to the Laplace Operator

We construct an exactly self similar function from the second difference according to

$$\phi(x,h) = \hat{T}_N(h)\left(u(x+h) + u(x-h) - 2u(x)\right) \tag{11.26}$$

which assumes the form

$$\phi(x,h) = \sum_{s=-\infty}^{\infty} N^{-\delta s} \left\{u(x+N^s h) + u(x-N^s h) - 2u(x)\right\} \tag{11.27}$$

which is a self-similar function with respect to its dependence on h with

$$\hat{A}_N(h)\phi(x,h) = \phi(x,Nh) = N^{\delta}\phi(x,h)$$

but a regular function with respect to x. Function $\phi(x,h)$ exists if the series (11.27) is convergent. Let us assume that $u(x)$ is a smooth function with a convergent Taylor series for any h. Then we have with

$$u(x \pm h) = \mathrm{e}^{\pm h\frac{d}{dx}} u(x)$$

and

$$u(x+h) + u(x-h) - 2u(x) = \left(\mathrm{e}^{h\frac{d}{dx}} + \mathrm{e}^{-h\frac{d}{dx}} - 2\right) u(x)$$

which can be written as

$$u(x+h) + u(x-h) - 2u(x) = 4\sinh^2\left(\frac{h}{2}\frac{d}{dx}\right) u(x) = h^2 \frac{d^2}{dx^2} u(x) + orders\ h^{\geq 4} \tag{11.28}$$

thus $\alpha = 2$ in criteria (11.6) is met. If we demand $u(x)$ being Fourier transformable we have as necessary condition that

$$\int_{-\infty}^{\infty} |u(x)| \mathrm{d}x \tag{11.29}$$

exists. From this we have with $\lim_{t\to\infty}|u(t)|=0$ the behavior

$$\lim_{t\to\infty}|u(x+t)+u(x-t)-2u(x)|=|-2u(x)|=2|u(x)|t^0 \tag{11.30}$$

from which follows $\beta=0$ in criteria (11.7). Hence (11.27) is convergent in the range

$$0<\delta<2 \tag{11.31}$$

The 1D Laplacian Δ_1 is defined by

$$\Delta_1 u(x)=\frac{d^2}{dx^2}u(x)=\lim_{\tau\to 0}\frac{(u(x+\tau)+u(x-\tau)-2u(x))}{\tau^2} \tag{11.32}$$

where the limiting case $\tau\to 0$ is well defined. In the following we will see that this is not so in the case of its self-similar counterpart. Let us define a self-similar analogue to the 1D Laplacian. We emphasize that also other definitions could be imagined. However, the definition to follow has a certain "physical" justification as we will see in the next section. We put

$$\begin{aligned}\Delta_{(\delta,N,\tau)}u(x) &=: const\lim_{\tau\to 0}\tau^{-\lambda}\phi(x,\tau) \\ &= const\lim_{\tau\to 0}\tau^{-\lambda}\sum_{s=-\infty}^{\infty}N^{-\delta s}\left(u(x+N^s\tau)+u(x-N^s\tau)-2u(x)\right)\end{aligned} \tag{11.33}$$

where we have introduced a renormalisation-multiplier $\tau^{-\lambda}$ with the power λ to be determined to keep the limiting case finite. The constant factor *const* indicates that there is a certain arbitrariness in this definition.

Let us now consider the limit $\tau\to 0$ by the sequence $\tau_n=N^{-n+\chi}$ with $n\to\infty$ and $0\le\chi<1$ kept constant during the limiting process. Then we have

$$\Delta_{(\xi,N,h)}u(x)=\lim_{n\to\infty}N^{\lambda(n-\chi)}N^{-\delta n}\sum_{s=-\infty}^{\infty}\xi^{s-n}\left[u(x+N^{s-n}N^{\chi})+u(x-N^{s-n}N^{\chi})-2u(x)\right] \tag{11.34}$$

which assumes by replacing $s\to s-n$ the form

$$\Delta_{(\delta,N,h=N^{\chi})}u(x)=N^{-\lambda\chi}\phi(x,N^{\chi})\lim_{n\to\infty}N^{-(\delta-\lambda)n} \tag{11.35}$$

which is only finite and nonzero if $\lambda=\delta$. We see that the limiting case $h(\chi)\to 0$ is non-unique as it depends on χ. The "Laplacian" can then be defined by for any h by

$$\Delta_{(\delta,N,h)}u(x)=:\lim_{n\to\infty}N^{\delta n}\phi(x,N^{-n}h)=\phi(x,h) \tag{11.36}$$

which simply recovers expression (11.27). By using (11.28) we can write for (11.27)

$$\Delta_{(\delta,N,h)}=4\hat{T}_N(h)\sinh^2\left(\frac{h}{2}\frac{\partial}{\partial x}\right)=4\sum_{s=-\infty}^{\infty}N^{-\delta s}\sinh^2\left(\frac{N^s h}{2}\frac{\partial}{\partial x}\right) \tag{11.37}$$

where $\hat{T}_N(h)$ is the self-similar operator defined in (11.4). The self-similar analogue of Laplace operator defined by (11.37) depends actually on the constants δ, N,

$$\chi = \frac{\ln h}{\ln N} - floor\left(\frac{\ln h}{\ln N}\right) \quad \text{with} \quad 0 \le \chi < 1.$$

We furthermore observe the self-similarity of Laplacian (11.37), namely

$$\Delta_{(\delta,N,Nh)} = N^{\delta}\Delta_{(\delta,N,h)} \tag{11.38}$$

11.2.3 Continuum Approximation - Link with Fractional Derivatives

It will be illuminative to consider in brief the link of the self-similar Laplacian defined by (11.27) and fractional derivatives. To this end we consider the limiting case $N = 1+\varepsilon$ and $s\varepsilon = v$ where $0 < \varepsilon << 1$ is assumed to be "small" so that $\mathrm{d}v \approx \varepsilon$ and $N^s = (1+\varepsilon)^{\frac{v}{\varepsilon}} \approx e^v$. Then we can write (11.2) in the form

$$\phi(h) = \sum_{s=-\infty}^{\infty} N^{-s\delta} f(N^s h) \approx \frac{1}{\varepsilon}\int_{-\infty}^{\infty} \mathrm{e}^{-\delta v} f(h e^v)\mathrm{d}v \tag{11.39}$$

which can be further written with $h\mathrm{e}^v = \tau$ and $\frac{\mathrm{d}\tau}{\tau} = \mathrm{d}v$ and $\tau(v \to -\infty) = 0$ and $\tau(v \to \infty) = \infty$ as

$$\phi(h) \approx \frac{h^{\delta}}{\varepsilon}\int_0^{\infty} \frac{f(\tau)}{\tau^{1+\delta}}\,\mathrm{d}\tau \tag{11.40}$$

which has the same conditions of existence as the discrete sum, i.e. it is required that $\beta < \delta < \alpha$ where f has to be a function fulfilling (11.6) and (11.7). Application of (11.40) on Laplacian (11.37) yields

$$\Delta_{(\delta,N,h)}u(x) \approx \frac{h^{\delta}}{\varepsilon}\int_0^{\infty} \frac{(u(x-\tau)+u(x+\tau)-2u(x))}{\tau^{1+\delta}}\,\mathrm{d}\tau \tag{11.41}$$

where $0 < \delta < 2$ as in the discrete case. After some simple manipulations integral (11.41) can be further expressed as a convolution in the form

$$\Delta_{(\delta,\varepsilon,h)}u(x) \approx \int_{-\infty}^{\infty} g(|x-\tau|)\frac{d^2u}{d\tau^2}(\tau)\mathrm{d}\tau \tag{11.42}$$

with the kernel

$$g(|x-\tau|) = \frac{h^{\delta}}{\delta(\delta-1)\varepsilon}\,|x-\tau|^{1-\delta}, \qquad 0 < \delta < 2\,, \delta \neq 1 \tag{11.43}$$

and $g(|x|) = -\frac{h}{\varepsilon}\ln|x|$ for $\delta = 1$. After some manipulations we can further write for $\delta \neq 1$ (11.42) in terms of *fractional integrals* [7]

$$\Delta_{(\delta=2-D,\varepsilon,h)}u(x) \approx \frac{h^{2-D}}{\varepsilon}\frac{\Gamma(D)}{(D-1)(D-2)}\left(\mathscr{D}^{-D}_{-\infty,x} + (-1)^D\mathscr{D}^{-D}_{\infty,x}\right)\Delta_1 u(x) \quad (11.44)$$

where $\Delta_1 u(x) = \frac{d^2}{dx^2}u(x)$ denotes the conventional 1D-Laplacian and $D = 2-\delta > 0$ which is positive in the admissible range of $0 < \delta < 2$. For $0 < \delta < 1$ the quantity D can be identified with the (estimated) fractal dimension of the fractal dispersion relation of the Laplacian [8]. In (11.44) we have introduced the Riemann-Liouville fractional integral $\mathscr{D}^{-D}_{a,x}$ which is defined by (e.g. [9, 10])

$$\mathscr{D}^{-D}_{a,x}v(x) = \frac{1}{\Gamma(D)}\int_a^x (x-\tau)^{D-1}v(\tau)\mathrm{d}\tau \quad (11.45)$$

where $\Gamma(D)$ denotes the Γ-function which represents the generalization of the factorial function to non-integer $D > 0$. The Γ-function is defined as

$$\Gamma(D) = \int_0^\infty \tau^{D-1}\mathrm{e}^{-\tau}\mathrm{d}\tau, \qquad D > 0 \quad (11.46)$$

For positive integers $D > 0$ the Γ-function reproduces the factorial-function $\Gamma(D) = (D-1)!$ with $D = 1, 2, ..\infty$.

11.3 The Physical Model

In this section we utilize parts of the above developed machinery to analyze a simple self-similar model system. A physical system which exhibits self-similarity (scaling invariance) as a symmetry property is distinguished by certain characteristic functions such as their Hamiltonian reflecting this symmetry which we introduce in the form [7]

$$H = \frac{1}{2}\int_{-\infty}^{\infty}\left(\dot{u}^2(x,t) + \mathscr{V}(x,t,h)\right)\mathrm{d}x \quad (11.47)$$

where the elastic energy density $\mathscr{V}(x,t,h)$ is a self-similar function with respect to h is given by[2]

$$\begin{aligned}\mathscr{V}(x,t,h) = \frac{1}{2}\sum_{s=-\infty}^{\infty} N^{-\delta s}\big[&(u(x,t) - u(x+N^s h,t))^2 \\ &+ (u(x,t) - u(x-N^s h,t))^2\big]\end{aligned} \quad (11.48)$$

Each mass point represented by x is connected by springs of spring constants $N^{-\delta s}$ to mass points $x \pm hN^s$ ($N > 1 \in \mathbb{R}$, $s = -\infty, .. + \infty$) distant from x by hN^s. The

[2] The additional multiplier $1/2$ avoids double counting.

range of these distances is from infinitely close ($s=-\infty$) to infinitely far ($s=+\infty$). The elastic energy density (11.48) fulfills the condition of self-similarity

$$\mathscr{V}(x,t,Nh)=N^{\delta}\mathscr{V}(x,t,h) \tag{11.49}$$

for all $h>0$ and where $N>1\in\mathbb{R}$ is given fix. It follows that (11.49) also holds when we replace N by any of its integer powers including zero N^s ($s\in\mathbb{Z}_0$). The exigence of convergence of the elastic energy (11.48) defines the range of admissible exponents δ, namely

$$0<\delta<2 \tag{11.50}$$

The equation of motion of this system is obtained by

$$\frac{\partial^2 u}{\partial t^2}=-\frac{\delta H}{\delta u} \tag{11.51}$$

(where $\delta/\delta u$ denotes a functional derivative) and can be written as

$$\begin{aligned}\frac{\partial^2 u}{\partial t^2}&=-\sum_{s=-\infty}^{\infty}N^{-\delta s}\Big\{2u(x,t)\\&\qquad-u(x+hN^s,t)-u(x-hN^s,t)\Big\}\\\frac{\partial^2 u}{\partial t^2}&=\Delta_{(\delta,N,h)}u(x,t)\end{aligned}$$

where $\Delta_{(\delta,N,h)}$ is the self-similar variant of the Laplacian operator introduced in (11.27). Equation (11.52) can be conceived as wave equation in a medium of self-similar symmetry. The series (11.52) converges only in the range (11.50), i.e. only for δ being in this interval the elastic energy density is finite and our physical problem is well-posed.

By exploiting that the displacement field $u(x,t)$ is Fourier transformable

$$u(x,t)=\frac{1}{2\pi}\int_{-\infty}^{\infty}\tilde{u}(k,t)\mathrm{e}^{ikx}\mathrm{d}k \tag{11.52}$$

and with e^{ikx} being an eigenfunction of our Laplacian defined in (11.52), we find its eigenvalue-spectra by

$$\frac{\partial^2\tilde{u}}{\partial t^2}(k,t)=-\bar{\omega}^2(k)\,\tilde{u}(k,t) \tag{11.53}$$

and obtain the dispersion relation $\bar{\omega}^2(k)=\omega^2(kh)$ in the form

$$\omega^2(kh)=4\sum_{s=-\infty}^{\infty}N^{-\delta s}\sin^2\left(\frac{khN^s}{2}\right) \tag{11.54}$$

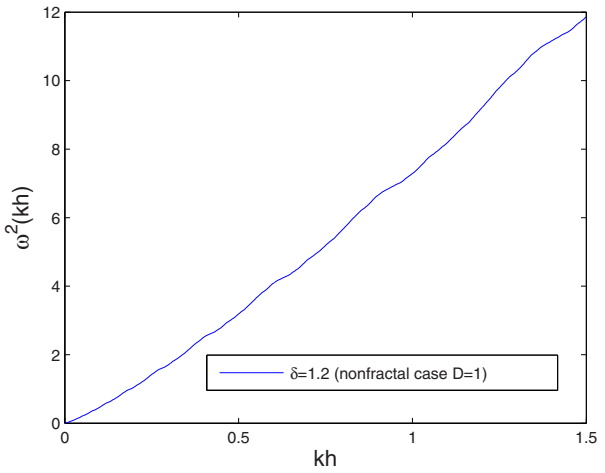

Fig. 11.1 Dispersion relation $\omega^2(k)$ in arbitrary units (non-fractal case)

representing a *Weierstrass-Mandelbrot* type function which converges only in the interval (11.50). The dispersion relation (11.54) is in the subinterval $0 < \delta < 1$ a non-differentiable and fractal function having the fractal (Hausdorff) dimension $D = 2 - \delta$ $(1 < D < 2)$ [8] whereas in the interval $1 < \delta < 2$ a smooth and once continuously differentiable function of $D = 1$. Relation (11.54) fulfills in its entire range of convergence (11.50) the condition of self-similarity

$$\omega^2(Nkh) = N^{\delta}\,\omega^2(kh) \tag{11.55}$$

reflecting nothing else but the self-similarity of the Laplacian of equation (11.52). Figures 1-4 are representations of the self-similar dispersion relation (11.54) in the admissible range $0 < \delta < 2$: Fig.1 represents a non-fractal case, i.e. the dispersion relation is here a non-fractal smooth curve of $D = 1$. Figures 2-4 represent fractal cases where $0 < \delta < 1$ has been decreased, i.e. the fractal dimension $1 < D < 2$ is increasing from figure 2 to figure 4. The increase of the fractal dimension causes an increasingly erratic behavior of the curves where fig. 4 is already close to the plane-filling dimension 2.

11.4 Density of Normal Modes

We consider now again the limiting case as in Sec. 11.2.3 which allows a continuum approximation, i.e. for $N = 1 + \varepsilon$, $0 < \varepsilon << 1$. For sufficiently "small" $|k|h$ $(h > 0)$, we arrive by replacing the sum (11.54) by the corresponding integral at [7]

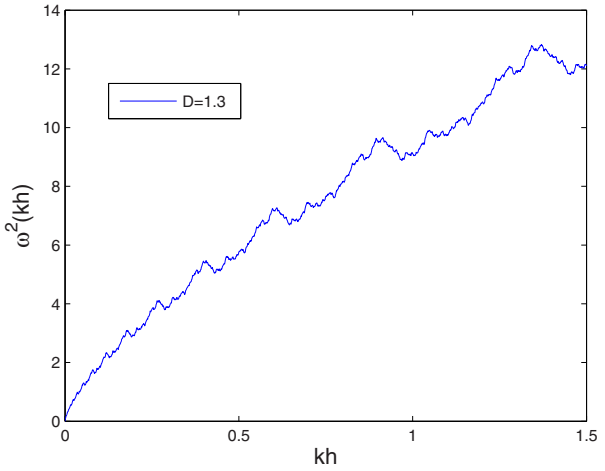

Fig. 11.2 Dispersion relation $\omega^2(k)$ in arbitrary units of fractal dimension D

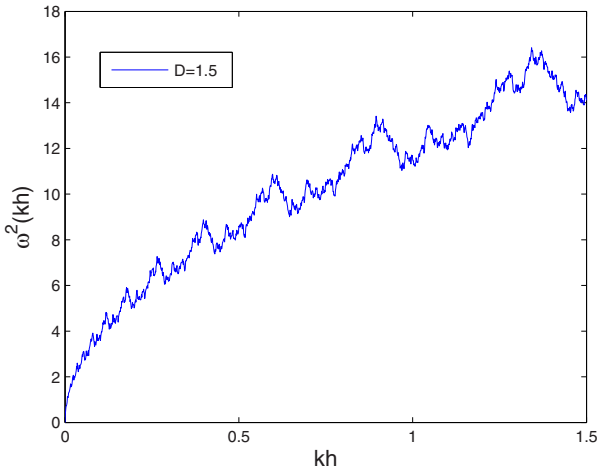

Fig. 11.3 Dispersion relation $\omega^2(k)$ in arbitrary units of fractal dimension D

$$\omega^2(kh) \approx \frac{(h|k|)^\delta}{\varepsilon} C \tag{11.56}$$

which is only finite if $(|k|h)^\delta$ is in the order of magnitude of ε or smaller. In this way we smoothen the dispersion curve, i.e. in this operation we loose its fractal character. This regime which includes the long-wave limit $k \to 0$ is hence characterized by a power law behavior $\bar{\omega}(k) \approx \text{const}|k|^{\delta/2}$ of the dispersion relation. The constant C introduced in (11.56) is given by the integral

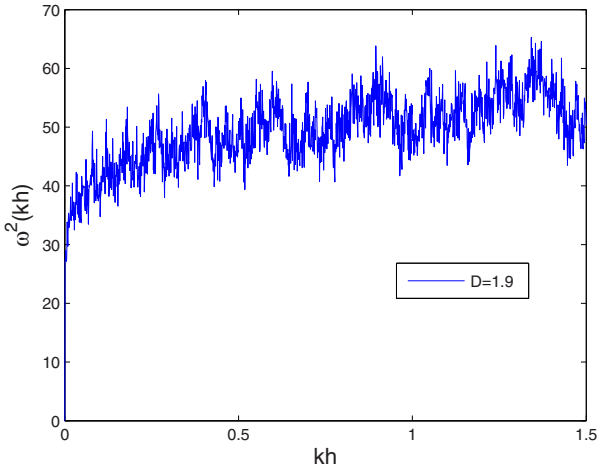

Fig. 11.4 Dispersion relation $\omega^2(k)$ in arbitrary units of fractal dimension D

$$C = 2\int_0^\infty \frac{(1-\cos\tau)}{\tau^{1+\delta}}\mathrm{d}\tau \tag{11.57}$$

which exists for δ being within interval $0 < \delta < 2$.

We again emphasize that this approximation holds only for "small" $\varepsilon \approx \ln N \neq 0$ $(0 < \varepsilon \ll 1)$[3]. In this limiting case we obtain the oscillator density [7][4]

$$\rho(\omega) = 2\frac{1}{2\pi}\frac{d|k|}{d\omega} \tag{11.58}$$

which is normalized such that $\rho(\omega)\mathrm{d}\omega$ counts the number (per unit length) of normal oscillators having frequencies within the interval $[\omega, \omega + \mathrm{d}\omega]$. We obtain then asymptotically for sufficiently small ω a power law of the form

$$\rho(\omega) = \frac{2}{\pi\delta h}\left(\frac{\varepsilon}{C}\right)^{\frac{1}{\delta}}\omega^{\frac{2}{\delta}-1} \tag{11.59}$$

where δ is restricted within interval $0 < \delta < 2$. We observe that in this δ-interval the power $\frac{2}{\delta} - 1$ is restricted within the range $0 < \frac{2}{\delta} - 1 < \infty$, especially with always vanishing oscillator density $\rho(\omega \to 0) = 0$. We conjecture that a power law scaling in the vicinity of $\omega = 0$ of the oscillator density of the form (11.59) with always positive exponent and vanishing oscillator density at $\omega = 0$ is an universal footprint of self-similar and fractal material systems.

[3] $\varepsilon = 0$ has to be excluded since it corresponds to $N = 1$.

[4] The additional multiplier "2" takes into account the two branches of the dispersion relation (11.54) (one for $k < 0$ and one for $k > 0$).

11.5 Conclusions

We have developed a mathematical framework which enables us to construct in a simple manner self-similar functions and linear operators. In this way we are able to tackle a wide range of physical problems with inherent self-similar symmetry. We also demonstrated existing links to the fractional calculus. The present framework could be a useful point of departure versus a "fractal mechanics" which is presently a widely open but more than ever exciting new field.

References

[1] A.N. Bondarenko, V.A. Levin: Science and Technology (2005) KORUS Proceedings. The 9th Russian-Korean Int. Symposium, 33-35.
[2] V.E. Tarasov, J. Phys. A: Math. Theor. **41**, 035101 (2008).
[3] M. Ostoja-Starzewski, *ZAMP* **58**, 1085 (2007).
[4] J. Kigami, Japan J. Appl. Math. **8**, 259 (1989).
[5] J.C. Claussen, J. Nagler, H.G. Schuster, Phys. Rev. E **70**, 032101 (2004).
[6] M. Epstein, S.M. Adeeb, Int. J. Solids Struct. **45**(11-12), 3238 (2008).
[7] T.M. Michelitsch, G.A. Maugin, F.C.G.A. Nicolleau, A.F. Nowakowski, S. Derogar, Dispersion relations and wave operators in self-similar quasicontinuous linear chains, *Phys. Rev. E* **80**, 011135 (2009), e-prints: hal-00371945 and arXiv:0904.0780, french version: arXiv: 0910.0728 .
[8] G.H. Hardy, Trans - Amer. Math. Soc., 1**7**, 301 (1916).
[9] K.S. Miller, An Introduction to the Fractional Calculus and Fractional Differential Equations, by Kenneth S. Miller, Bertram Ross (Editor), John Wiley & Sons, Chichester, 1993.
[10] A.A. Kilbas, H.M. Srivastava, J.J. Trujillo, Theory and Application of Fractional Differential Equations, Mathematical Studies 204, Jan von Mill (Editor) (Elsevier, Amsterdam, 2006).

Chapter 12
Nonlinear Dynamic Processes in Media with Internal Structure

Alexey V. Porubov, Boris R. Andrievsky and Eron L. Aero

Abstract The generation of the bell-shaped localized defects in the lattice is studied numerically using essentially nonlinear proper structural model that describes coupling with macro-strains. It is macro-strain localized wave that provides defects generation, the parameters of this wave are very important for localization or delocalization of the variations in the structure of the lattice.

Key words: Microstructure. Localized defect. Nonlinear wave.

12.1 Governing Equations

Generally nonlinear model of the crystalline lattice taking into account deep variations in the structure of solid, allows description of the cardinal, qualitative variations of the cell properties, lowering of potential barriers, switching of interatomic connections, arising from singular defects and other damages, phase transitions.

Here we consider an essentially proper structural nonlinear model that treats a continuum approach and a crystal translational symmetry without making a continuum limit of a discrete model [1, 2]. The equations are derived for the vectors of macro-displacement U and relative micro-displacement u for the pair of atoms with masses m_1, m_2,

$$\mathbf{U} = \frac{m_1\mathbf{U_1} + m_2\mathbf{U_2}}{m_1 + m_2}, \; \mathbf{u} = \frac{\mathbf{U_1} - \mathbf{U_2}}{a},$$

where a is a period of sub-lattice. The first variable allows us to describe macro-strains, while the second variable accounts for the reference displacement of the

Alexey V. Porubov, Boris R. Andrievsky, and Eron L. Aero
Institute of Problems in Mechanical Engineering, Bolshoy av. 61, V.O., 199178 Saint-Petersburg, Russia
e-mail: porubov.math@mail.ioffe.ru, e-mail: bandri@yandex.ru,
e-mail: 16aero@mail.ru

H. Altenbach et al. (eds.), *Mechanics of Generalized Continua,*
Advanced Structured Materials, 7, DOI: 10.1007/978-3-642-19219-7_12,

internal or the lattice structure. The following coupled governing equations are obtained in [1, 2] in the 1D case,

$$\rho U_{tt} - E\, U_{xx} \;=\; S(\cos(u) - 1)_x, \tag{12.1}$$

$$\mu u_{tt} - \kappa u_{xx} \;=\; (SU_x - p)\sin(u). \tag{12.2}$$

Choice of the trigonometric function allows us to describe translational symmetry of the crystal lattice. It accounts for a strong nonlinearity allowing transition of atoms in neighboring cells to realize the micro-mechanism of the cardinal re-arrangement of the structure.

12.2 Localized Macro-strain Waves and Corresponding Deviations in Crystalline Lattice

Exact localized traveling wave solutions to Eqs (12.1) and (12.2) may be obtained by direct integration [3]. Assume that solution depends only on the phase variable $\theta \;=\; x - V\,t$. Then Eq. (12.1) is resolved for the micro-field by

$$\cos(u) \;=\; 1 - \frac{(E - \rho V^2)U_\theta - \sigma}{S}, \tag{12.3}$$

where σ is a constant of integration. Equation (12.2) is integrated once, multiplied by u_θ and integrated again. Then Eq. (12.3) is substituted in this equation finally giving an ordinary differential equation for the macro-strain $v \;= U_\theta$

$$v_\theta^2 \;=\; a_0 + a_1\, v + a_2\, v^2 + a_3\, v^3 + a_4\, v^4, \tag{12.4}$$

these coefficients may be found in [3]. When $a_0 \;= 0$, $a_1 \;=\; 0$, the ODE (12.4) possesses known exact localized bell-shaped traveling wave solutions of two kinds

$$v_1 \;=\; \frac{A}{Q\cosh(k\,\theta) + 1}, \tag{12.5}$$

$$v_2 \;=\; -\frac{A}{Q\cosh(k\,\theta) - 1}. \tag{12.6}$$

these parameters are defined for two values of σ, $\sigma \;=\; 0$ and $\sigma \;=\; -2S$ [3]. Thus, for are $\sigma \;=\; 0$ we obtain

$$A \;=\; \frac{4\,S}{\rho(c_0^2 + c_L^2 - V^2)}, Q_\pm \;=\; \pm\frac{c_L^2 - V^2 - c_0^2}{c_L^2 - V^2 + c_0^2}, k \;=\; 2\sqrt{\frac{p}{\mu(c_l^2 - V^2)}}, \tag{12.7}$$

where $c_L^2 \;=\; E/\rho, c_l^2 \;=\; \kappa/\mu, c_0^2 \;=\; S^2/(p\,\rho)$.

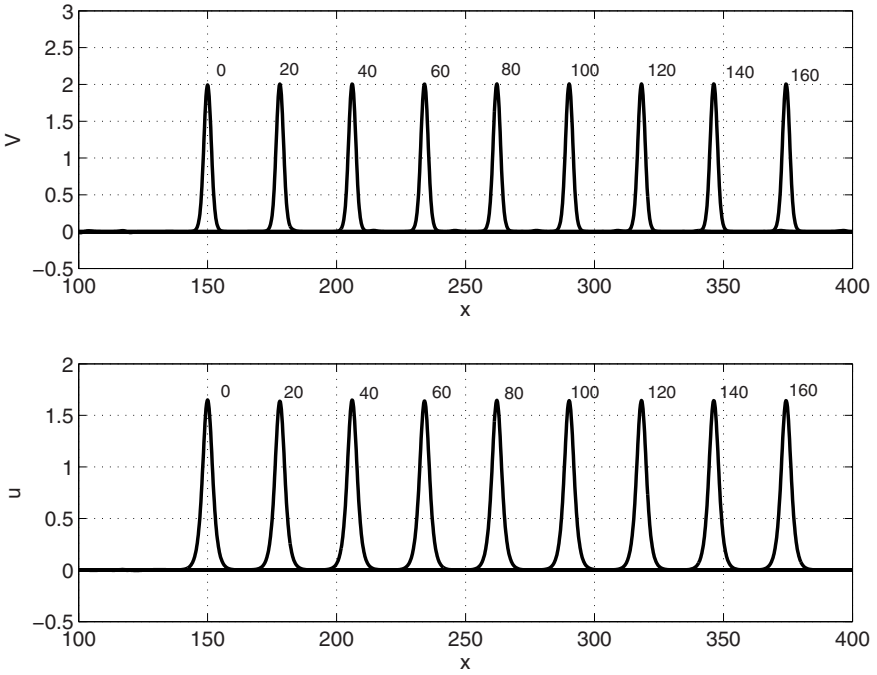

Fig. 12.1 Simultaneous propagation of macro- and micro- bell-shaped strain waves according to the exact solutions. Points of time correspond to the neighboring peaks.

Table 12.1 Wave shapes for $\sigma = 0$

V^2	$(0; c_L^2 - c_0^2)$	$(c_L^2 - c_0^2; c_L^2)$	$(c_L^2; c_L^2 + c_0^2)$	$> c_L^2 + c_0^2$
Shape of v	Tensile (12.5)	Tensile (12.5)	Compression (12.6)	Compression (12.5)
Shape of u	Kink	Bell-shaped	Kink	Kink
Choice of $Q_\pm$	Q_+	Q_-	Q_+	Q_+

The shape of u depends upon the value of the first derivative at $\theta = 0$ in the r.h.s. of Eq. (12.3). Reversing the cos- function for derivation of the expression for u, one has to avoid the points where the first derivative does not exist. This breaking happens for $\theta = 0$ at $\sigma = 0$ and for $Q = Q_+$. Therefore, the solution for u obtained using both (12.5) and (12.6) should be written as

$$u = \pm \arccos\left(\frac{(\rho V^2 - E)U_x}{S} + 1\right) \text{ for } \theta \leq 0, \tag{12.8}$$

$$u = \pm\pi \mp \arccos\left(\frac{(\rho V^2 - E)U_x}{S} + 1\right) \text{ for } \theta > 0. \tag{12.9}$$

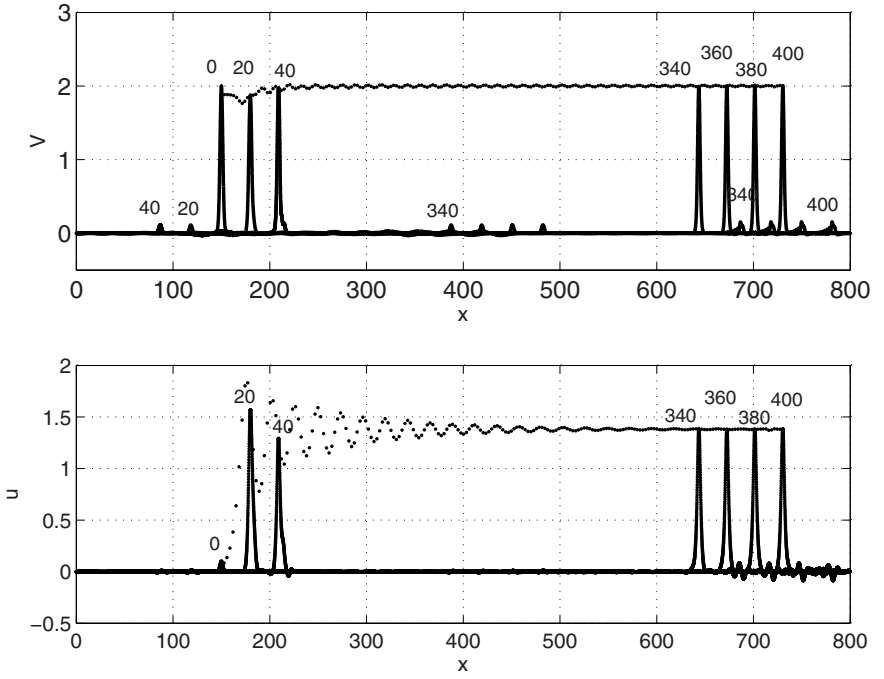

Fig. 12.2 Generation of moving tensile localized bell-shaped defect in a lattice from initial motionless Gaussian input for u. Points of time correspond to the neighboring peaks. Dotted oscillating lines account for the amplitude variations.

However, the first derivative is zero for $Q = Q_-$ at $\theta = 0$, and the expression for u reads

$$u = \pm \arccos\left(\frac{(\rho V^2 - E)U_x}{S} + 1\right). \tag{12.10}$$

The solution (12.8), (12.9) accounts for the kink-shaped profile of the wave, while solution (12.10) describes the bell-shaped localized wave. The velocity intervals when one or another profile exists are shown in Table 12.1. Similar analysis for $\sigma = -2S$ may be found in [3, 4].

It is known [3] that simultaneous existence of macro-strain waves v of tensile and compression is impossible. This is not true for the waves u describing structural deviations or defects in the lattice, due to the signs $\pm$ in Eqs (12.8), (12.9) or (12.10). Shown in Fig. 12.1 is the propagation of macro-strain tensile wave and the tensile wave of u in the interval $(c_L^2 - c_0^2; c_L^2)$ for $\sigma = 0$. However, the same tensile macro-strain wave v may be accompanied by the micro-strain compression wave, u, this is governed by the initial condition for u. An important problem is to know which wave is generated when an initial condition for u differs from the exact solutions (12.5), (12.10) at $t = 0$. What happens when an initial profile contains both the tensile and compression parts, and how its initial position relative to the initial position of the

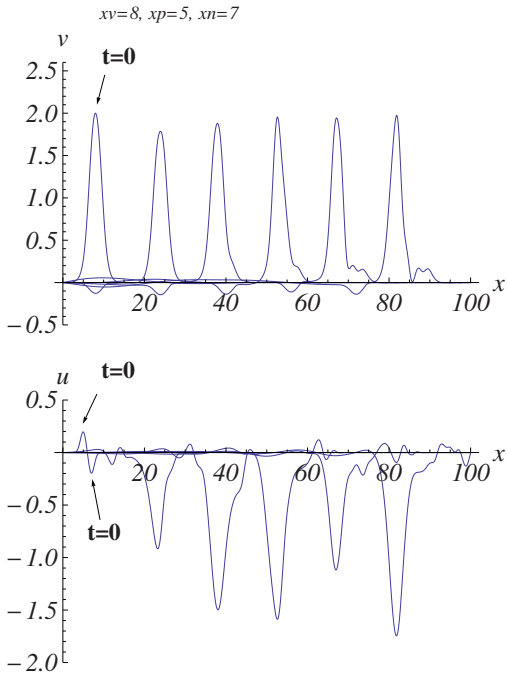

Fig. 12.3 Generation of moving compression localized bell-shaped defect in a lattice from the input for u containing both positive and negative amplitude parts. The initial positions of the peak of v maximum and minimum of u are noted by xv, xp and xn respectively. They are also marked by arrows.

macro-strain wave v affect generation and propagation of the localized bell-shaped waves for u and v? These questions will be studied numerically in the next Section.

12.3 Generation of Localized Defects in Crystalline Lattice

To solve Eqs (12.1) and (12.2) numerically the standard MATLAB routine *ode45* is used [5]. For this purpose the equations are transformed to a finite-dimensional approximation, substituting finite difference relations for corresponding space derivatives. To check numerical results parallel computing using numerical tools of the Mathematica 7 is performed.

We consider only the interval $(c_L^2 - c_0^2; c_L^2)$ for $\sigma = 0$. According to the exact solution here only bell-shaped localized waves may propagate. Numerical simulations with initial conditions coinciding with exact solutions (12.5), (12.10) at $t = 0$ confirm propagation of the bells-shaped waves of permanent shape and velocity according to the exact solutions, see Fig. 12.1.

The single equation with ODE of the form (12.4) has been studied numerically in [6, 7, 8]. It was found that rather arbitrary initial pulse splits into a sequence of localized waves, and each of them is described by the exact solitary wave solutions. Localization or delocalization of the input took place according to the conditions od the existence of the traveling wave solutions. Now we are going to see whether

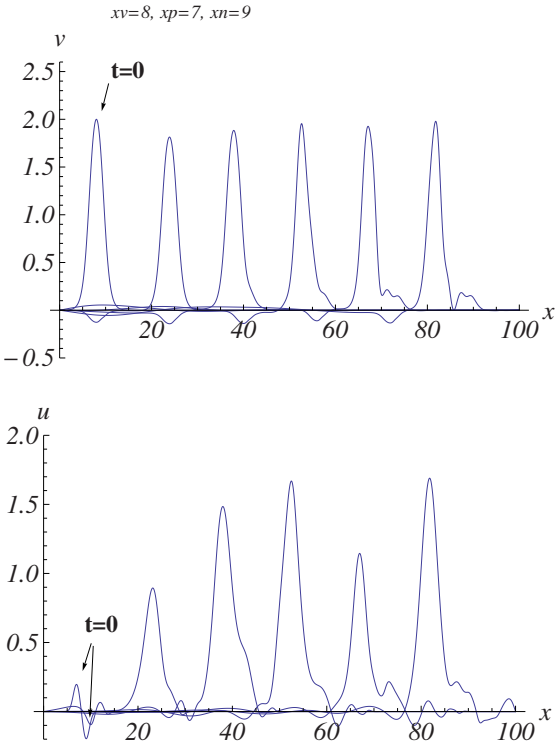

Fig. 12.4 Generation of moving tensile localized bell-shaped defect in a lattice from the input for u containing positive and negative amplitude parts. The initial positions of the peak of v maximum and minimum of u are noted by xv, xp and xn respectively. They are also marked by arrows.

the same predictions of the solutions (12.5), (12.10) are realized for the coupled equations (12.1) and (12.2).

First the initial condition for u is chosen in the form of the motionless Gaussian distribution while the input for v has the form of the exact solution (12.5) at $t = 0$, and its initial velocity is chosen equal to that of the exact solution. Shown in Fig. 12.2 is a generation of the tensile localized wave u with the amplitude finally propagating according to the exact solution (12.10) shown in Fig. 12.1. During this process the wave for v suffers variations in the amplitude. The formation of the wave happens with oscillating variations in the amplitude which are shown by dotted line in the figure. Finally the amplitudes and velocities of the bell-shaped waves for u and v do not vary anymore, and traveling bell-shaped tensile waves with constant velocity propagate according to the exact solution (12.5), (12.10). Similarly a compression bell-shaped wave for u arises when an initial profile for u is chosen with negative amplitude.

One has to note that the positions of the maxima/minima for the inputs for v and u coincide in Figs 12.1 and 12.2. Next series of calculations demonstrates strong affect of their relative positions on the wave localization. Now the motionless input for u contains both positive and negative parts, each having the form of the Gaussian distribution, while the input for v remains in the form of the exact solution (12.5)

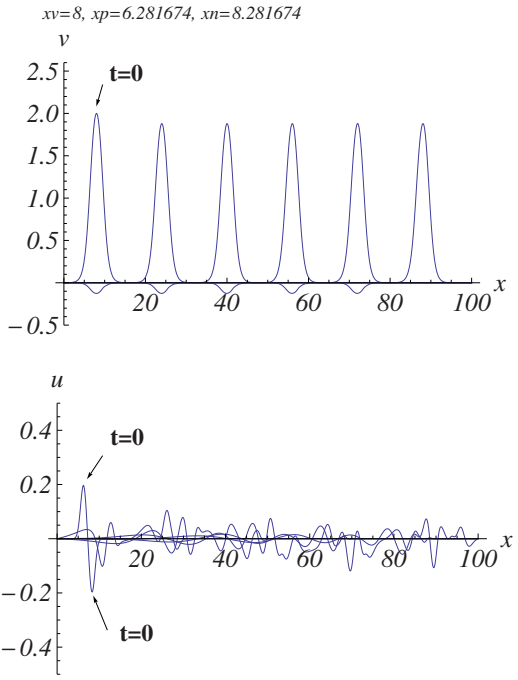

Fig. 12.5 Delocalization of the input for u containing positive and negative amplitude parts. The initial positions of the peak of v maximum and minimum of u are noted by xv, xp and xn respectively. They are also marked by arrows.

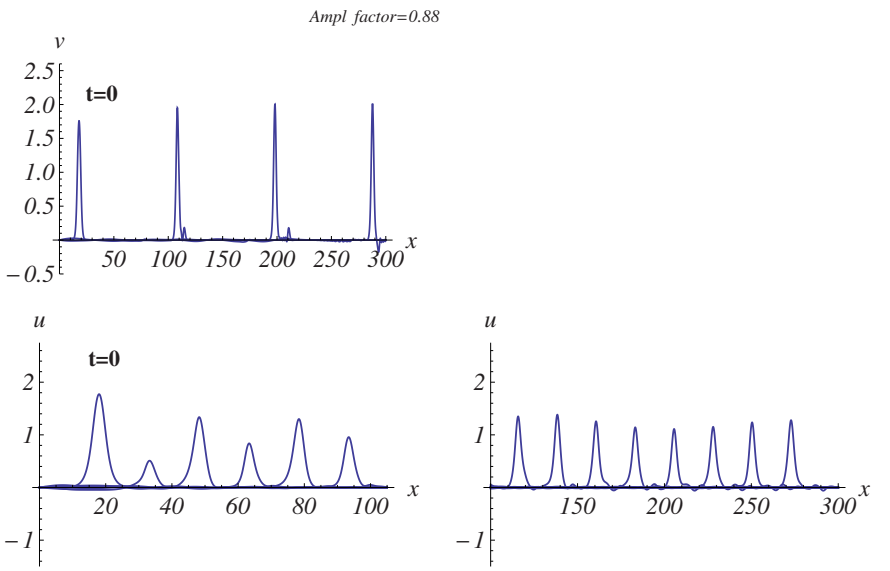

Fig. 12.6 Variations in the tensile wave for u due to decrease in the initial amplitude by factor noted in figure.

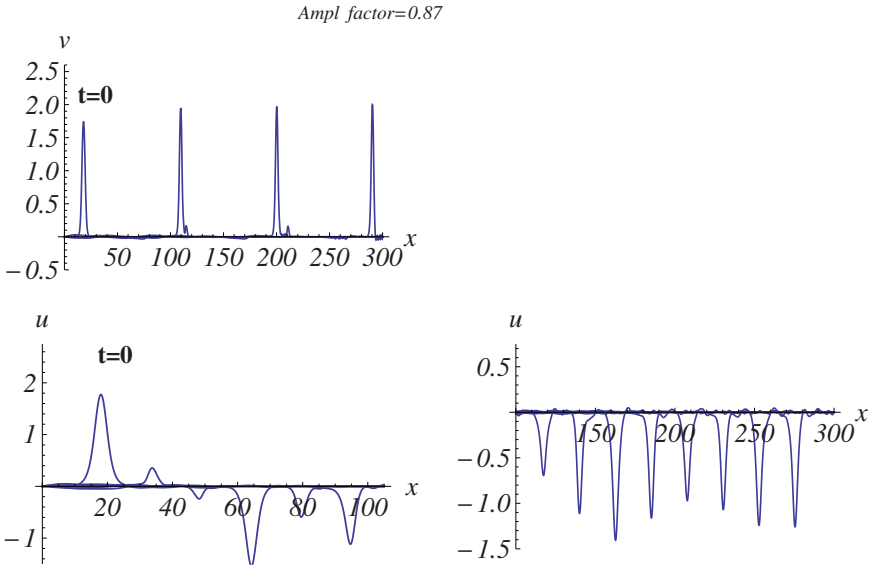

Fig. 12.7 Changing of the initial tensile wave for u to the compression one due to decrease in the initial amplitude of u by factor noted in figure.

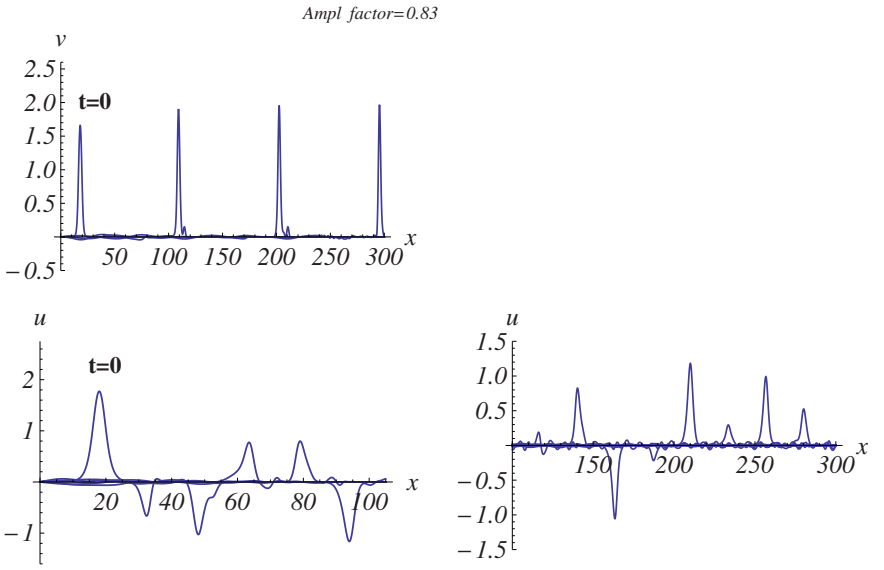

Fig. 12.8 Changing of the sign of localized wave for u due to decrease in the initial amplitude of u by factor noted in figure.

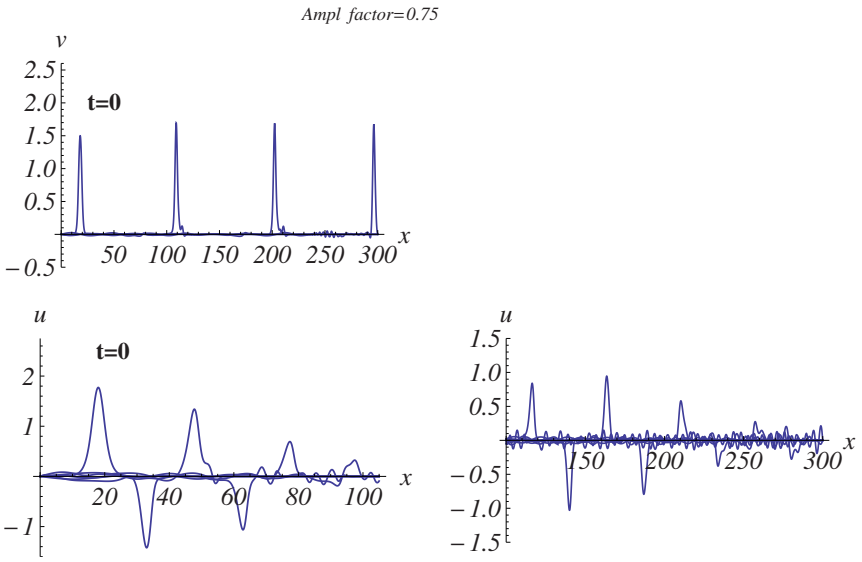

Fig. 12.9 Delocalization of the wave for u due to decrease in the initial amplitude of u by factor noted in figure.

at $t = 0$. The position of the maximum of the input for v is denoted by xv in Figs 12.3,12.4 and 12.5, while the positions of the maximum and the minimum of the input for u are denoted by xp and xn respectively. No simultaneous generation of tensile and compression waves of u is seen in figures, either compression wave arises in Fig. 12.3 or tensile one in Fig. 12.4 depending on the values of xv and xp and xn. Certainly there exist the values of the initial positions when no localized wave for u arises, see Fig. 12.5.

Similar changing of the kind of localized wave for u is observed when initial conditions in the form of the exact solutions are chosen for both functions v and u but the first one is multiplied by an amplitude factor. One can see in Fig. 12.6 that decrease in the initial amplitude of v gives rise to oscillating variations of the amplitude of moving localized defect u. Further decrease in amplitude yields change of the sign of the amplitude of u shown in Fig. 12.7 but the resulting wave evolves to the wave of permanent shape similar to the case shown in Fig. 12.2. At smaller initial amplitude of v a more complicated evolution of u is shown in Fig. 12.8 where changing of the sign of the amplitude of the wave for u is seen. Decreasing the initial amplitude for v we finally obtain a delocalization of the initial profile of u in Fig. 12.9.

No localized wave formation is observed from motionless inputs for v and u that might be an evidence of the dependence of existence of the bell-shaped waves on their velocity, see Table 1. Also no multiple solitary wave formation is found contrary to the results for a single equation in [6, 7, 8].

12.4 Conclusions

It is shown how localized moving defects may arise in a lattice due to the propagation of a macro-strain wave. The role of the sign of the input for u as well as the relative position of the inputs and the amplitude and velocity of the input for v are found to affect generation of tensile or compression localized bell-shaped dynamic internal deviations, u. An analysis based on the traveling wave exact solution may explain some features of generation of localized strain waves in the general case.

Acknowledgements The work has been supported by the Russian Foundation for Basic Researches, grants No 09-01-00469a and 10-01-00243-a.

References

[1] Aero, E.L.: Micromechanics of a double continuum in a model of a medium with variable periodic structure. J. Eng. Math. **55**, 81–95 (2002)
[2] Aero, E.L., Bulygin, A. N. : Strongly Nonlinear Theory of Nanostructure Formation Owing to Elastic and Nonelastic Strains in Crystalline Solids. Mechanics of Solids. **42**, 807–822 (2007)
[3] Porubov, A.V., Aero, E.L., Maugin, G.A.: Two approaches to study essentially nonlinear and dispersive properties of the internal structure of materials. Phys. Rev. E. **79**, 046608 (2009)
[4] Porubov, A.V., Aero, E.L., Andrievsky, B.R.: Dynamical properties of essentially nonlinear generalized continua. In: G.A. Maugin. A.V. Metrikin (eds), Mechanics of Generalized Continua,p. 161–168, Springer, Berlin (2009)
[5] Shampine, L. F. and Reichelt, M. W.: SIAM Journal on Scientific Computing, **18-1** (1997)
[6] Porubov, A.V., Maugin, G.A. : Longitudinal strain solitary waves in presence of cubic nonlinearity. Intern. J. Nonl. Mech. **40**, 1041–1048 (2005)
[7] Porubov, A.V., Maugin, G.A.: Improved description of longitudinal strain solitary waves. Journal of Sound and Vibration. **310**, 694–701 (2008)
[8] Porubov, A.V., Maugin, G.A. : Cubic nonlinearity and longitudinal surface solitary waves. Intern. J. Nonl. Mech. **44**, 552-559 (2009)

Chapter 13
Buckling of Elastic Composite Rods made of Micropolar Material Subjected to Combined Loads

Denis Sheydakov

Abstract In the present paper, the stability of a nonlinearly elastic rod with a composite structure is analyzed. It is assumed that the interior (core) of the rod is made of micropolar material, while the behavior of the exterior (coating) is investigated in the framework of a classic non-polar continuum model. The problem is studied for a case of axial compression of a rod under external hydrostatic pressure. Using the linearization method in a vicinity of the basic state, the neutral equilibrium equations have been derived, which describe the perturbed state of a composite rod. By solving these equations numerically for some specific materials, the critical curves and corresponding buckling modes have been found, and the stability regions have been constructed in the planes of loading parameters (relative compression and external pressure). An extensive analysis has been carried out for the influence of a size effect and coating properties on the buckling of elastic composite rod made of micropolar material subject to combined loads.

Key words: Buckling. Nonlinear elasticity. Micropolar rod. Coating influence. Combined loads.

13.1 Introduction

The problem of equilibrium stability for deformable bodies is of major importance both from theoretical and practical point of view, because the exhaustion of load-carrying capability and collapse of buildings and engineering structures quite often occurs due to buckling under external loads. In the case of elastic medium, the stability theory is extensively developed for classic non-polar materials. There is large number of papers on stability both for thin and thin-walled bodies in the form of

Denis Sheydakov
South Scientific Center of Russian Academy of Sciences, Chekhova Ave. 41, 344006 Rostov on Don, Russia
e-mail: sheidakov@mail.ru

H. Altenbach et al. (eds.), *Mechanics of Generalized Continua,*
Advanced Structured Materials, 7, DOI: 10.1007/978-3-642-19219-7_13,

rods, plates and shells, and for massive (three-dimensional) bodies. However, due to the increasing number of new constructional materials, the problem of stability analysis for bodies with a complex structure becomes relevant. One example of a prospective class of new materials is foams, which are used in the modern automotive and airspace industries. The constructions made of metallic or polymeric foams combine low weight, high specific strength, and excellent possibilities to absorb energy. As a rule, they have a composite structure (porous core covered by hard and stiff shell), which is necessary for corrosion protection and optimization of mechanical properties during loading. Due to a microstructure influence, the behavior of foams cannot be adequately described within the framework of classic non-polar continuum model. To create a mathematical model of the porous elastic body, it seems reasonable to use the model of micropolar continuum, or Cosserat continuum [1, 3, 4, 7, 10], i.e. medium with couple stresses and rotational degrees of freedom. Given the above, in the present paper we have carried out the stability analysis for a quite common element of constructions – a composite cylindrical rod with a porous core.

13.2 Equilibrium of the Compressed Composite Cylinder under External Pressure

Consider the composite cylindrical rod of length l and radius r_2. The behavior of the inner part of the rod $(0 \le r \le r_1)$ is described by the model of micropolar elastic body. The outer part $(r_1 \le r \le r_2)$ is made of classic non-polar material. Then, in the case of axial compression of the rod under external hydrostatic pressure, the position of a particle in the strained state is given by the radius vectors $\mathbf{R}$ and $\mathbf{R}_*$ (here and below by '$*$' we denote the quantities related to the coating, without '$*$' – related to the inner part of the rod) [6, 11]:

$$R = \begin{cases} f(r), & 0 \le r \le r_1 \\ f_*(r), & r_1 \le r \le r_2 \end{cases}, \qquad \Phi = \varphi, \qquad Z = \alpha z \tag{13.1}$$

$$\begin{aligned} \mathbf{R} &= f(r)\,\mathbf{e}_R + \alpha z\,\mathbf{e}_Z, \quad 0 \le r \le r_1 \\ \mathbf{R}_* &= f_*(r)\,\mathbf{e}_R + \alpha z\,\mathbf{e}_Z, \quad r_1 \le r \le r_2 \end{aligned} \tag{13.2}$$

Here r, φ, z are cylindrical coordinates in the reference configuration (Lagrangian coordinates), R, Φ, Z are Eulerian cylindrical coordinates, $\{\mathbf{e}_r, \mathbf{e}_\varphi, \mathbf{e}_z\}$ and $\{\mathbf{e}_R, \mathbf{e}_\Phi, \mathbf{e}_Z\}$ are orthonormal vector bases of Lagrangian and Eulerian coordinates, respectively, α is compression ratio along the axis of the cylinder, $f(r)$ and $f_*(r)$ are some functions characterizing the radial deformation of the composite rod and determined from the equilibrium equations and boundary conditions.

In addition, for $r \le r_1$ a proper orthogonal tensor of microrotation $\mathbf{H}$ is given, which represents the rotation of the particle for micropolar medium and at the considered strain has the form

$$\mathbf{H} = \mathbf{e}_r \otimes \mathbf{e}_R + \mathbf{e}_\varphi \otimes \mathbf{e}_\Phi + \mathbf{e}_z \otimes \mathbf{e}_Z \tag{13.3}$$

According to expressions (13.1), (13.2), the deformation gradients $\mathbf{C}$ and $\mathbf{C}_*$ are (hereinafter $'$ denotes the derivative with respect to r):

$$\begin{aligned} \mathbf{C} &= \operatorname{grad} \mathbf{R} = f' \mathbf{e}_r \otimes \mathbf{e}_R + \frac{f}{r} \mathbf{e}_\varphi \otimes \mathbf{e}_\Phi + \alpha \mathbf{e}_z \otimes \mathbf{e}_Z, \qquad 0 \le r \le r_1 \\ \mathbf{C}_* &= \operatorname{grad} \mathbf{R}_* = f_*' \mathbf{e}_r \otimes \mathbf{e}_R + \frac{f_*}{r} \mathbf{e}_\varphi \otimes \mathbf{e}_\Phi + \alpha \mathbf{e}_z \otimes \mathbf{e}_Z, \qquad r_1 \le r \le r_2 \end{aligned} \tag{13.4}$$

where grad is gradient in the Lagrangian coordinates.

It follows from relations (13.3), (13.4) that for the micropolar part $(0 \le r \le r_1)$ of the rod the wryness tensor $\mathbf{L}$ is equal to zero [8, 9]

$$\mathbf{L} \times \mathbf{E} = -(\operatorname{grad} \mathbf{H}) \cdot \mathbf{H}^{\mathrm{T}} = 0$$

and stretch tensor $\mathbf{Y}$ is expressed as follows

$$\mathbf{Y} = \mathbf{C} \cdot \mathbf{H}^{\mathrm{T}} = f' \mathbf{e}_r \otimes \mathbf{e}_r + \frac{f}{r} \mathbf{e}_\varphi \otimes \mathbf{e}_\varphi + \alpha \mathbf{e}_z \otimes \mathbf{e}_z \tag{13.5}$$

According to (13.4), for the coating $(r_1 \le r \le r_2)$ the expressions for stretch tensor $\mathbf{U}_*$ and macrorotation tensor $\mathbf{A}_*$ have the form [6]:

$$\begin{aligned} \mathbf{U}_* &= \left(\mathbf{C}_* \cdot \mathbf{C}_*^{\mathrm{T}} \right)^{\frac{1}{2}} = f_*' \mathbf{e}_r \otimes \mathbf{e}_r + \frac{f_*}{r} \mathbf{e}_\varphi \otimes \mathbf{e}_\varphi + \alpha \mathbf{e}_z \otimes \mathbf{e}_z \\ \mathbf{A}_* &= \mathbf{U}_*^{-1} \cdot \mathbf{C}_* = \mathbf{e}_r \otimes \mathbf{e}_R + \mathbf{e}_\varphi \otimes \mathbf{e}_\Phi + \mathbf{e}_z \otimes \mathbf{e}_Z \end{aligned} \tag{13.6}$$

We assume that the elastic properties of the rod are described by the physically linear material, whose specific strain energy in the case of micropolar body is a quadratic form of the tensors $\mathbf{Y} - \mathbf{E}$ and $\mathbf{L}$ [2, 5]:

$$\begin{aligned} W(\mathbf{Y}, \mathbf{L}) = \frac{1}{2} \lambda \operatorname{tr}^2 (\mathbf{Y} - \mathbf{E}) + \frac{1}{2} (\mu + \kappa) \operatorname{tr} \left((\mathbf{Y} - \mathbf{E}) \cdot (\mathbf{Y} - \mathbf{E})^{\mathrm{T}} \right) + \\ + \frac{1}{2} \mu \operatorname{tr} (\mathbf{Y} - \mathbf{E})^2 + \frac{1}{2} \gamma_1 \operatorname{tr}^2 \mathbf{L} + \frac{1}{2} \gamma_2 \operatorname{tr} \left(\mathbf{L} \cdot \mathbf{L}^{\mathrm{T}} \right) + \frac{1}{2} \gamma_3 \operatorname{tr} \mathbf{L}^2 \end{aligned} \tag{13.7}$$

$$\mu + \kappa > 0, \qquad \lambda + 2\mu + \kappa > 0, \qquad \gamma_2 \ge 0, \qquad \gamma_1 + \gamma_2 + \gamma_3 > 0$$

and in the case of classic non-polar medium – quadratic form of the tensor $\mathbf{U}_* - \mathbf{E}$ [6]:

$$W_*(\mathbf{U}_*) = \frac{1}{2} \lambda_* \operatorname{tr}^2 (\mathbf{U}_* - \mathbf{E}) + \mu_* \operatorname{tr} (\mathbf{U}_* - \mathbf{E})^2, \qquad \mu_* > 0, \quad \lambda_* + 2\mu_* > 0 \tag{13.8}$$

Here λ, μ and λ_*, μ_* are Lame coefficients for the rod core and coating, respectively, $\kappa, \gamma_1, \gamma_2, \gamma_3$ are micropolar elastic coefficients, $\mathbf{E}$ is the unit tensor.

It follows from expressions (13.3), (13.5), and (13.7) that for the inner part of the rod the Piola-type couple stress tensor is equal to zero in the case of axial compression of the rod under external hydrostatic pressure

$$\mathbf{G} = \frac{\partial W}{\partial \mathbf{L}} \cdot \mathbf{H} = \left(\gamma_1 \left(\mathrm{tr} \mathbf{L} \right) \mathbf{E} + \gamma_2 \mathbf{L} + \gamma_3 \mathbf{L}^{\mathrm{T}} \right) \cdot \mathbf{H} = 0$$

and Piola-type stress tensor $\mathbf{D}$ is

$$\begin{gathered} \mathbf{D} = \frac{\partial W}{\partial \mathbf{Y}} \cdot \mathbf{H} = \left(\lambda \mathrm{tr} \left(\mathbf{Y} - \mathbf{E} \right) \mathbf{E} + \mu \left(\mathbf{Y}^{\mathrm{T}} - \mathbf{E} \right) + \left(\mu + \kappa \right) \left(\mathbf{Y} - \mathbf{E} \right) \right) \cdot \mathbf{H} = \\ = \left(\lambda s + \chi \left(f' - 1 \right) \right) \mathbf{e}_r \otimes \mathbf{e}_R + \left(\lambda s + \chi \left(\frac{f}{r} - 1 \right) \right) \mathbf{e}_\varphi \otimes \mathbf{e}_\Phi + \\ + \left(\lambda s + \chi \left(\alpha - 1 \right) \right) \mathbf{e}_z \otimes \mathbf{e}_Z; \qquad s = f' + \frac{f}{r} + \alpha - 3, \qquad \chi = 2\mu + \kappa \end{gathered} \tag{13.9}$$

According to (13.6), (13.8), the expression of Piola stress tensor $\mathbf{D}_*$ for coating has the form:

$$\begin{gathered} \mathbf{D}_* = \frac{\partial W_*}{\partial \mathbf{U}_*} \cdot \mathbf{A}_* = \left(\lambda_* \mathrm{tr} \left(\mathbf{U}_* - \mathbf{E} \right) \mathbf{E} + 2\mu_* \left(\mathbf{U}_* - \mathbf{E} \right) \right) \cdot \mathbf{A}_* = \\ = \left(\lambda_* s_* + 2\mu_* \left(f_*' - 1 \right) \right) \mathbf{e}_r \otimes \mathbf{e}_R + \left(\lambda_* s_* + 2\mu_* \left(\frac{f_*}{r} - 1 \right) \right) \mathbf{e}_\varphi \otimes \mathbf{e}_\Phi + \\ + \left(\lambda_* s_* + 2\mu_* \left(\alpha - 1 \right) \right) \mathbf{e}_z \otimes \mathbf{e}_Z; \qquad s_* = f_*' + \tfrac{f_*}{r} + \alpha - 3 \end{gathered} \tag{13.10}$$

The equilibrium equations of nonlinear micropolar elasticity in the absence of mass forces and moments are written as follows [2, 11]

$$\mathrm{div} \mathbf{D} = 0, \qquad \mathrm{div} \mathbf{G} + \left(\mathbf{C}^{\mathrm{T}} \cdot \mathbf{D} \right)_\times = 0 \tag{13.11}$$

where div is the divergence in the Lagrangian coordinates. The symbol $_\times$ represents the vector invariant of a second-order tensor:

$$\mathbf{K}_\times = \left(K_{mn} \mathbf{e}_m \otimes \mathbf{e}_n \right)_\times = K_{mn} \mathbf{e}_m \times \mathbf{e}_n$$

The equilibrium equations for classic non-polar continuum in the absence of mass forces have the form [6]:

$$\mathrm{div} \mathbf{D}_* = 0 \tag{13.12}$$

Boundary conditions

$$D_r^*|_{r=r_2} = -\frac{\alpha p f_* \left(r_2 \right)}{r_2}, \quad D_r^*|_{r=r_1} = D_r|_{r=r_1}, \quad f_* \left(r_1 \right) = f \left(r_1 \right), f \left(0 \right) = 0 \tag{13.13}$$

express the effect of hydrostatic pressure p (calculated per unit area of the deformed configuration) on the lateral surface of the rod $(r = r_2)$, rigid coupling of coating

with micropolar part ($r = r_1$) and the absence of radial displacement on the axis of the rod ($r = 0$).

By solving the boundary problem (13.11) – (13.13) while taking into account the relations (13.9), (13.10), we find the unknown functions $f(r)$ and $f_*(r)$

$$f(r) = c_1 r, \qquad f_*(r) = c_1^* r + \frac{c_2^*}{r}$$

$$c_1 = \frac{(2\mu_* - \alpha p)(k - k_*)\left(r_1^2 - r_2^2\right) + 2(\lambda_* + 2\mu_*) k r_2^2}{(2(\lambda - \lambda_* - \mu_*) + \chi)(2\mu_* - \alpha p) r_1^2 + (2\lambda + \chi + 2\mu_*)(2\lambda_* + 2\mu_* + \alpha p) r_2^2}$$

$$c_1^* = \frac{(2\mu_* - \alpha p)(k - k_*) r_1^2 + (2(\lambda + \mu_*) + \chi) k_* r_2^2}{(2(\lambda - \lambda_* - \mu_*) + \chi)(2\mu_* - \alpha p) r_1^2 + (2\lambda + \chi + 2\mu_*)(2\lambda_* + 2\mu_* + \alpha p) r_2^2}$$

$$c_2^* = \frac{([1 - \alpha](2\lambda\mu_* - \lambda_*\chi) + \alpha p(k - k_*)) r_1^2 r_2^2}{(2(\lambda - \lambda_* - \mu_*) + \chi)(2\mu_* - \alpha p) r_1^2 + (2\lambda + \chi + 2\mu_*)(2\lambda_* + 2\mu_* + \alpha p) r_2^2}$$

$$k = (3 - \alpha)\lambda + \chi, \qquad k_* = (3 - \alpha)\lambda_* + 2\mu_*$$

13.3 Equations of Neutral Equilibrium

Suppose that in addition to the above-described state of equilibrium for the composite rod, there is infinitely close equilibrium state under the same external loads, which is determined by:

1. for the micropolar part – the radius vector $\mathbf{R} + \eta\mathbf{v}$, and microrotation tensor $\mathbf{H} - \eta\mathbf{H} \times \omega$,
2. for the coating – the radius vector $\mathbf{R}_* + \eta\mathbf{v}_*$.

Here η is a small parameter, $\mathbf{v}$ and $\mathbf{v}_*$ are vectors of additional displacements, ω is a linear incremental rotation vector, which characterizes the small rotation of the particles for micropolar medium, measured from the initial strain state.

The perturbed state of equilibrium for the micropolar medium is described by the equations [2]:

$$\mathrm{div}\mathbf{D}^\bullet = 0, \qquad \mathrm{div}\mathbf{G}^\bullet + \left[\mathrm{grad}\mathbf{v}^{\mathrm{T}} \cdot \mathbf{D} + \mathbf{C}^{\mathrm{T}} \cdot \mathbf{D}^\bullet\right]_\times = 0 \tag{13.14}$$

$$\mathbf{D}^\bullet = \frac{d}{d\eta}\mathbf{D}(\mathbf{R} + \eta\mathbf{v}, \mathbf{H} - \eta\mathbf{H} \times \omega)\Big|_{\eta=0}$$

$$\mathbf{G}^\bullet = \frac{d}{d\eta}\mathbf{G}(\mathbf{R} + \eta\mathbf{v}, \mathbf{H} - \eta\mathbf{H} \times \omega)\Big|_{\eta=0}$$

where $\mathbf{D}^\bullet$ and $\mathbf{G}^\bullet$ are the linearized Piola-type stress tensor and couple stress tensor. In the case of physically linear micropolar material (13.7) for these tensors the following relations are valid:

$$\mathbf{D}^\bullet = \left(\frac{\partial W}{\partial \mathbf{Y}}\right)^\bullet \cdot \mathbf{H} + \frac{\partial W}{\partial \mathbf{Y}} \cdot \mathbf{H}^\bullet = \left(\lambda\,(\mathrm{tr}\,\mathbf{Y}^\bullet)\,\mathbf{E} + (\mu+\kappa)\,\mathbf{Y}^\bullet + \mu\,\mathbf{Y}^{\bullet\mathrm{T}}\right)\cdot\mathbf{H} - \\ - \left(\lambda\,\mathrm{tr}\,(\mathbf{Y}-\mathbf{E})\,\mathbf{E} + \mu\left(\mathbf{Y}^\mathrm{T}-\mathbf{E}\right) + (\mu+\kappa)\,(\mathbf{Y}-\mathbf{E})\right)\cdot\mathbf{H}\times\boldsymbol{\omega} \tag{13.15}$$

$$\mathbf{G}^\bullet = \left(\frac{\partial W}{\partial \mathbf{L}}\right)^\bullet \cdot \mathbf{H} + \frac{\partial W}{\partial \mathbf{L}} \cdot \mathbf{H}^\bullet = \left(\gamma_1\,(\mathrm{tr}\,\mathbf{L}^\bullet)\,\mathbf{E} + \gamma_2\mathbf{L}^\bullet + \gamma_3\mathbf{L}^{\bullet\mathrm{T}}\right)\cdot\mathbf{H} - \\ - \left(\gamma_1\,(\mathrm{tr}\,\mathbf{L})\,\mathbf{E} + \gamma_2\mathbf{L} + \gamma_3\mathbf{L}^\mathrm{T}\right)\cdot\mathbf{H}\times\boldsymbol{\omega} \tag{13.16}$$

$$\mathbf{Y}^\bullet = (\mathrm{grad}\mathbf{v} + \mathbf{C}\times\boldsymbol{\omega})\cdot\mathbf{H}^\mathrm{T}, \qquad \mathbf{L}^\bullet = \mathrm{grad}\,\boldsymbol{\omega}\cdot\mathbf{H}^\mathrm{T}$$

Here $\mathbf{Y}^\bullet$ is the linearized stretch tensor, $\mathbf{L}^\bullet$ is the linearized wryness tensor.

The equations of neutral equilibrium in the framework of non-polar nonlinear theory of elasticity have the form [6]:

$$\mathrm{div}\,\mathbf{D}_*^\bullet = 0, \qquad \mathbf{D}_*^\bullet = \frac{d}{d\eta}\mathbf{D}_*\left(\mathbf{R}_* + \eta\,\mathbf{v}_*\right)\Big|_{\eta=0} \tag{13.17}$$

Representation of the linearized Piola stress tensor $\mathbf{D}_*^\bullet$ for physically linear material (13.8) is obtained by linearization of constitutive relations (13.10) with regard to (13.6):

$$\mathbf{D}_*^\bullet = \left(\frac{\partial W_*}{\partial \mathbf{U}_*}\right)^\bullet \cdot \mathbf{A}_* + \left(\frac{\partial W_*}{\partial \mathbf{U}_*}\right)\cdot\mathbf{A}_*^\bullet = (\lambda_*\,(\mathrm{tr}\mathbf{U}_*^\bullet)\,\mathbf{E} + 2\mu_*\mathbf{U}_*^\bullet)\cdot\mathbf{A}_* + \\ + (\lambda_*\mathrm{tr}\,(\mathbf{U}_*-\mathbf{E})\,\mathbf{E} + 2\mu_*\,(\mathbf{U}_*-\mathbf{E}))\cdot\mathbf{U}_*^{-1}\cdot(\mathrm{grad}\,\mathbf{v}_* - \mathbf{U}_*^\bullet\cdot\mathbf{A}_*) \tag{13.18}$$

Here $\mathbf{U}_*^\bullet$ is the linearized stretch tensor, which can be expressed in terms of the linearized Cauchy-Green deformation tensor:

$$(\mathbf{U}_*\cdot\mathbf{U}_*)^\bullet = \left(\mathbf{C}_*\cdot\mathbf{C}_*^\mathrm{T}\right)^\bullet \quad\Longrightarrow\quad \mathbf{U}_*^\bullet\cdot\mathbf{U}_* + \mathbf{U}_*\cdot\mathbf{U}_*^\bullet = \mathrm{grad}\mathbf{v}_*\cdot\mathbf{C}_*^\mathrm{T} + \mathbf{C}_*\cdot(\mathrm{grad}\mathbf{v}_*)^\mathrm{T}$$

Linearized boundary conditions on the lateral surface of the composite rod $(r=r_2)$ and on the interface $(r=r_1)$ are written as follows:

$$\mathbf{e}_r\cdot\mathbf{D}_*^\bullet|_{r=r_2} = -pJ_*\mathbf{e}_r\cdot\mathbf{C}_*^{-\mathrm{T}}\cdot\left((\mathrm{Div}\,\mathbf{v}_*)\mathbf{E} - \mathrm{Grad}\,\mathbf{v}_*^\mathrm{T}\right), \qquad J_* = \det\mathbf{C}_* \\ \mathbf{e}_r\cdot\mathbf{D}_*^\bullet|_{r=r_1} = \mathbf{e}_r\cdot\mathbf{D}^\bullet|_{r=r_1}, \qquad \mathbf{v}_*|_{r=r_1} = \mathbf{v}|_{r=r_1}, \qquad \mathbf{e}_r\cdot\mathbf{G}^\bullet|_{r=r_1} = 0 \tag{13.19}$$

where Div and Grad are the divergence and gradient in the Eulerian coordinates.

We assume that at the ends of the rod $(z = 0, l)$ there is no friction and constant normal displacement is given. This leads to the following linearized boundary conditions:

1) for the micropolar part of the rod $(0 \le r \le r_1)$:

$$\begin{aligned} \mathbf{e}_z \cdot \mathbf{D}^\bullet \cdot \mathbf{e}_R|_{z=0,l} = \mathbf{e}_z \cdot \mathbf{D}^\bullet \cdot \mathbf{e}_\Phi|_{z=0,l} = \mathbf{e}_z \cdot \mathbf{v}|_{z=0,l} = 0 \\ \mathbf{e}_z \cdot \mathbf{G}^\bullet \cdot \mathbf{e}_Z|_{z=0,l} = \mathbf{e}_r \cdot \omega|_{z=0,l} = \mathbf{e}_\varphi \cdot \omega|_{z=0,l} = 0 \end{aligned} \tag{13.20}$$

2) for the coating $(r_1 \le r \le r_2)$:

$$\mathbf{e}_z \cdot \mathbf{D}_*^\bullet \cdot \mathbf{e}_R|_{z=0,l} = \mathbf{e}_z \cdot \mathbf{D}_*^\bullet \cdot \mathbf{e}_\Phi|_{z=0,l} = \mathbf{e}_z \cdot \mathbf{v}_*|_{z=0,l} = 0 \tag{13.21}$$

We write the vectors of additional displacements $\mathbf{v}$ and $\mathbf{v}_*$, and incremental rotation ω in the basis of Eulerian cylindrical coordinates:

$$\begin{aligned} \mathbf{v} &= v_R \mathbf{e}_R + v_\Phi \mathbf{e}_\Phi + v_Z \mathbf{e}_Z \\ \mathbf{v}_* &= v_R^* \mathbf{e}_R + v_\Phi^* \mathbf{e}_\Phi + v_Z^* \mathbf{e}_Z \\ \omega &= \omega_R \mathbf{e}_R + \omega_\Phi \mathbf{e}_\Phi + \omega_Z \mathbf{e}_Z \end{aligned} \tag{13.22}$$

With respect to representation (13.22), the expressions for the linearized stretch tensors $\mathbf{Y}^\bullet$ and $\mathbf{U}_*^\bullet$, and wryness tensor $\mathbf{L}^\bullet$ have the form:

$$\begin{aligned} \mathbf{Y}^\bullet = &\left(\frac{\partial v_\Phi}{\partial r} - f' \omega_Z \right) \mathbf{e}_r \otimes \mathbf{e}_\varphi + \frac{1}{r} \left(\frac{\partial v_R}{\partial \varphi} - v_\Phi + f \omega_Z \right) \mathbf{e}_\varphi \otimes \mathbf{e}_r + \\ &+ \left(\frac{\partial v_Z}{\partial r} + f' \omega_\Phi \right) \mathbf{e}_r \otimes \mathbf{e}_z + \left(\frac{\partial v_R}{\partial z} - \alpha \omega_\Phi \right) \mathbf{e}_z \otimes \mathbf{e}_r + \\ &+ \frac{1}{r} \left(\frac{\partial v_Z}{\partial \varphi} - f \omega_R \right) \mathbf{e}_\varphi \otimes \mathbf{e}_z + \left(\frac{\partial v_\Phi}{\partial z} + \alpha \omega_R \right) \mathbf{e}_z \otimes \mathbf{e}_\varphi + \\ &+ \frac{\partial v_R}{\partial r} \mathbf{e}_r \otimes \mathbf{e}_r + \frac{1}{r} \left(\frac{\partial v_\Phi}{\partial \varphi} + v_R \right) \mathbf{e}_\varphi \otimes \mathbf{e}_\varphi + \frac{\partial v_Z}{\partial z} \mathbf{e}_z \otimes \mathbf{e}_z \end{aligned} \tag{13.23}$$

$$\begin{aligned} \mathbf{U}_*^\bullet = &\frac{\partial v_R^*}{\partial r} \mathbf{e}_r \otimes \mathbf{e}_r + \frac{1}{r} \left(\frac{\partial v_\Phi^*}{\partial \varphi} + v_R^* \right) \mathbf{e}_\varphi \otimes \mathbf{e}_\varphi + \frac{\partial v_Z^*}{\partial z} \mathbf{e}_z \otimes \mathbf{e}_z + \\ &+ \frac{1}{r f_*' + f_*} \left(f_*' \left(\frac{\partial v_R^*}{\partial \varphi} - v_\Phi^* \right) + f_* \frac{\partial v_\Phi^*}{\partial r} \right) \left(\mathbf{e}_r \otimes \mathbf{e}_\varphi + \mathbf{e}_\varphi \otimes \mathbf{e}_r \right) \\ &+ \frac{1}{f_*' + \alpha} \left(f_*' \frac{\partial v_R^*}{\partial z} + \alpha \frac{\partial v_Z^*}{\partial r} \right) \left(\mathbf{e}_r \otimes \mathbf{e}_z + \mathbf{e}_z \otimes \mathbf{e}_r \right) + \\ &+ \frac{1}{f_* + \alpha r} \left(f_* \frac{\partial v_\Phi^*}{\partial z} + \alpha \frac{\partial v_Z^*}{\partial \varphi} \right) \left(\mathbf{e}_z \otimes \mathbf{e}_\varphi + \mathbf{e}_\varphi \otimes \mathbf{e}_z \right) \end{aligned} \tag{13.24}$$

$$\begin{aligned}\mathbf{L}^{\bullet} = &\frac{\partial \omega_R}{\partial r}\mathbf{e}_r \otimes \mathbf{e}_r + \frac{1}{r}\left(\frac{\partial \omega_\Phi}{\partial \varphi} + \omega_R\right)\mathbf{e}_\varphi \otimes \mathbf{e}_\varphi + \frac{\partial \omega_Z}{\partial z}\mathbf{e}_z \otimes \mathbf{e}_z + \\ &+ \frac{\partial \omega_\Phi}{\partial r}\mathbf{e}_r \otimes \mathbf{e}_\varphi + \frac{1}{r}\left(\frac{\partial \omega_R}{\partial \varphi} - \omega_\Phi\right)\mathbf{e}_\varphi \otimes \mathbf{e}_r + \frac{\partial \omega_Z}{\partial r}\mathbf{e}_r \otimes \mathbf{e}_z + \\ &+ \frac{\partial \omega_R}{\partial z}\mathbf{e}_z \otimes \mathbf{e}_r + \frac{1}{r}\frac{\partial \omega_Z}{\partial \varphi}\mathbf{e}_\varphi \otimes \mathbf{e}_z + \frac{\partial \omega_\Phi}{\partial z}\mathbf{e}_z \otimes \mathbf{e}_\varphi\end{aligned} \tag{13.25}$$

According to relations (13.3) – (13.6), (13.15), (13.16), (13.18), (13.22) – (13.24), the components of the linearized Piola-type stress tensor $\mathbf{D}^{\bullet}$ and couple stress tensor $\mathbf{G}^{\bullet}$, and Piola stress tensor $\mathbf{D}^{\bullet}_{*}$ are written as follows:

$$\begin{aligned}
\mathbf{e}_r \cdot \mathbf{D}^{\bullet} \cdot \mathbf{e}_R &= (\lambda + \chi)\frac{\partial v_R}{\partial r} + \frac{\lambda}{r}\left(\frac{\partial v_\Phi}{\partial \varphi} + v_R\right) + \lambda \frac{\partial v_Z}{\partial z} \\
\mathbf{e}_r \cdot \mathbf{D}^{\bullet} \cdot \mathbf{e}_\Phi &= (\mu + \kappa)\frac{\partial v_\Phi}{\partial r} + \frac{\mu}{r}\left(\frac{\partial v_R}{\partial \varphi} - v_\Phi\right) + \left(\lambda s + \mu\left(f' + \frac{f}{r}\right) - \chi\right)\omega_Z \\
\mathbf{e}_r \cdot \mathbf{D}^{\bullet} \cdot \mathbf{e}_Z &= (\mu + \kappa)\frac{\partial v_Z}{\partial r} + \mu \frac{\partial v_R}{\partial z} - \left(\lambda s + \mu\left(f' + \alpha\right) - \chi\right)\omega_\Phi \\
\mathbf{e}_\varphi \cdot \mathbf{D}^{\bullet} \cdot \mathbf{e}_R &= \frac{\mu + \kappa}{r}\left(\frac{\partial v_R}{\partial \varphi} - v_\Phi\right) + \mu \frac{\partial v_\Phi}{\partial r} - \left(\lambda s + \mu\left(f' + \frac{f}{r}\right) - \chi\right)\omega_Z \\
\mathbf{e}_\varphi \cdot \mathbf{D}^{\bullet} \cdot \mathbf{e}_\Phi &= \lambda \frac{\partial v_R}{\partial r} + \frac{\lambda + \chi}{r}\left(\frac{\partial v_\Phi}{\partial \varphi} + v_R\right) + \lambda \frac{\partial v_Z}{\partial z} \\
\mathbf{e}_\varphi \cdot \mathbf{D}^{\bullet} \cdot \mathbf{e}_Z &= \frac{\mu + \kappa}{r}\frac{\partial v_Z}{\partial \varphi} + \mu \frac{\partial v_\Phi}{\partial z} + \left(\lambda s + \mu\left(\frac{f}{r} + \alpha\right) - \chi\right)\omega_R \\
\mathbf{e}_z \cdot \mathbf{D}^{\bullet} \cdot \mathbf{e}_R &= (\mu + \kappa)\frac{\partial v_R}{\partial z} + \mu \frac{\partial v_Z}{\partial r} + \left(\lambda s + \mu\left(f' + \alpha\right) - \chi\right)\omega_\Phi \\
\mathbf{e}_z \cdot \mathbf{D}^{\bullet} \cdot \mathbf{e}_\Phi &= (\mu + \kappa)\frac{\partial v_\Phi}{\partial z} + \frac{\mu}{r}\frac{\partial v_Z}{\partial \varphi} - \left(\lambda s + \mu\left(\frac{f}{r} + \alpha\right) - \chi\right)\omega_R \\
\mathbf{e}_z \cdot \mathbf{D}^{\bullet} \cdot \mathbf{e}_Z &= \lambda \frac{\partial v_R}{\partial r} + \frac{\lambda}{r}\left(\frac{\partial v_\Phi}{\partial \varphi} + v_R\right) + (\lambda + \chi)\frac{\partial v_Z}{\partial z}
\end{aligned} \tag{13.26}$$

$$
\begin{aligned}
\mathbf{e}_r\cdot\mathbf{G}^{\bullet}\cdot\mathbf{e}_R &= (\gamma_1+\gamma_2+\gamma_3)\frac{\partial\omega_R}{\partial r}+\frac{\gamma_1}{r}\left(\frac{\partial\omega_\Phi}{\partial\varphi}+\omega_R\right)+\gamma_1\frac{\partial\omega_Z}{\partial z}\\
\mathbf{e}_r\cdot\mathbf{G}^{\bullet}\cdot\mathbf{e}_\Phi &= \gamma_2\frac{\partial\omega_\Phi}{\partial r}+\frac{\gamma_3}{r}\left(\frac{\partial\omega_R}{\partial\varphi}-\omega_\Phi\right)\\
\mathbf{e}_\varphi\cdot\mathbf{G}^{\bullet}\cdot\mathbf{e}_R &= \frac{\gamma_2}{r}\left(\frac{\partial\omega_R}{\partial\varphi}-\omega_\Phi\right)+\gamma_3\frac{\partial\omega_\Phi}{\partial r}\\
\mathbf{e}_r\cdot\mathbf{G}^{\bullet}\cdot\mathbf{e}_Z &= \gamma_2\frac{\partial\omega_Z}{\partial r}+\gamma_3\frac{\partial\omega_R}{\partial z},\\
\mathbf{e}_z\cdot\mathbf{G}^{\bullet}\cdot\mathbf{e}_R &= \gamma_2\frac{\partial\omega_R}{\partial z}+\gamma_3\frac{\partial\omega_Z}{\partial r}\\
\mathbf{e}_\varphi\cdot\mathbf{G}^{\bullet}\cdot\mathbf{e}_\Phi &= \gamma_1\frac{\partial\omega_R}{\partial r}+\frac{\gamma_1+\gamma_2+\gamma_3}{r}\left(\frac{\partial\omega_\Phi}{\partial\varphi}+\omega_R\right)+\gamma_1\frac{\partial\omega_Z}{\partial z}\\
\mathbf{e}_\varphi\cdot\mathbf{G}^{\bullet}\cdot\mathbf{e}_Z &= \frac{\gamma_2}{r}\frac{\partial\omega_Z}{\partial\varphi}+\gamma_3\frac{\partial\omega_\Phi}{\partial z},\\
\mathbf{e}_z\cdot\mathbf{G}^{\bullet}\cdot\mathbf{e}_\Phi &= \gamma_2\frac{\partial\omega_\Phi}{\partial z}+\frac{\gamma_3}{r}\frac{\partial\omega_Z}{\partial\varphi}\\
\mathbf{e}_z\cdot\mathbf{G}^{\bullet}\cdot\mathbf{e}_Z &= \gamma_1\frac{\partial\omega_R}{\partial r}+\frac{\gamma_1}{r}\left(\frac{\partial\omega_\Phi}{\partial\varphi}+\omega_R\right)+(\gamma_1+\gamma_2+\gamma_3)\frac{\partial\omega_Z}{\partial z}
\end{aligned}
\tag{13.27}
$$

$$
\begin{aligned}
\mathbf{e}_r\cdot\mathbf{D}^{\bullet}_{*}\cdot\mathbf{e}_R &= (\lambda_*+2\mu_*)\frac{\partial v^*_R}{\partial r}+\frac{\lambda_*}{r}\left(\frac{\partial v^*_\Phi}{\partial\varphi}+v^*_R\right)+\lambda_*\frac{\partial v^*_Z}{\partial z}\\
\mathbf{e}_r\cdot\mathbf{D}^{\bullet}_{*}\cdot\mathbf{e}_\Phi &= \left(2\mu_*+\frac{(\lambda_*s_*-2\mu_*)r}{rf'_*+f_*}\right)\frac{\partial v^*_\Phi}{\partial r}-\frac{\lambda_*s_*-2\mu_*}{rf'_*+f_*}\left(\frac{\partial v^*_R}{\partial\varphi}-v^*_\Phi\right)\\
\mathbf{e}_r\cdot\mathbf{D}^{\bullet}_{*}\cdot\mathbf{e}_Z &= \left(2\mu_*+\frac{\lambda_*s_*-2\mu_*}{f'_*+\alpha}\right)\frac{\partial v^*_Z}{\partial r}-\frac{\lambda_*s_*-2\mu_*}{f'_*+\alpha}\frac{\partial v^*_R}{\partial z}\\
\mathbf{e}_\varphi\cdot\mathbf{D}^{\bullet}_{*}\cdot\mathbf{e}_R &= \left(\frac{2\mu_*}{r}+\frac{\lambda_*s_*-2\mu_*}{rf'_*+f_*}\right)\left(\frac{\partial v^*_R}{\partial\varphi}-v^*_\Phi\right)-\frac{(\lambda_*s_*-2\mu_*)r}{rf'_*+f_*}\frac{\partial v^*_\Phi}{\partial r}\\
\mathbf{e}_\varphi\cdot\mathbf{D}^{\bullet}_{*}\cdot\mathbf{e}_\Phi &= \lambda_*\frac{\partial v^*_R}{\partial r}+\frac{\lambda_*+2\mu_*}{r}\left(\frac{\partial v^*_\Phi}{\partial\varphi}+v^*_R\right)+\lambda_*\frac{\partial v^*_Z}{\partial z}\\
\mathbf{e}_\varphi\cdot\mathbf{D}^{\bullet}_{*}\cdot\mathbf{e}_Z &= \left(\frac{2\mu_*}{r}+\frac{\lambda_*s_*-2\mu_*}{f_*+\alpha r}\right)\frac{\partial v^*_Z}{\partial\varphi}-\frac{(\lambda_*s_*-2\mu_*)r}{f_*+\alpha r}\frac{\partial v^*_\Phi}{\partial z}\\
\mathbf{e}_z\cdot\mathbf{D}^{\bullet}_{*}\cdot\mathbf{e}_R &= \left(2\mu_*+\frac{\lambda_*s_*-2\mu_*}{f'_*+\alpha}\right)\frac{\partial v^*_R}{\partial z}-\frac{\lambda_*s_*-2\mu_*}{f'_*+\alpha}\frac{\partial v^*_Z}{\partial r}\\
\mathbf{e}_z\cdot\mathbf{D}^{\bullet}_{*}\cdot\mathbf{e}_\Phi &= \left(2\mu_*+\frac{(\lambda_*s_*-2\mu_*)r}{f_*+\alpha r}\right)\frac{\partial v^*_\Phi}{\partial z}-\frac{\lambda_*s_*-2\mu_*}{f_*+\alpha r}\frac{\partial v^*_Z}{\partial\varphi}\\
\mathbf{e}_z\cdot\mathbf{D}^{\bullet}_{*}\cdot\mathbf{e}_Z &= \lambda_*\frac{\partial v^*_R}{\partial r}+\frac{\lambda_*}{r}\left(\frac{\partial v^*_\Phi}{\partial\varphi}+v^*_R\right)+(\lambda_*+2\mu_*)\frac{\partial v^*_Z}{\partial z}
\end{aligned}
\tag{13.28}
$$

Expressions (13.14), (13.17), describing the perturbed state of equilibrium for micropolar rod with a solid coating, constitute a system of nine partial differential equations with nine unknown functions $v_R, v_\Phi, v_Z, v^*_R, v^*_\Phi, v^*_Z, \omega_R, \omega_\Phi, \omega_Z$ in it. Substitute into

$$
\begin{aligned}
v_R &= V_R(r)\cos n\varphi\cos\beta z, & v_\Phi &= V_\Phi(r)\sin n\varphi\cos\beta z\\
v_Z &= V_Z(r)\cos n\varphi\sin\beta z, & v_R^* &= V_R^*(r)\cos n\varphi\cos\beta z\\
v_\Phi^* &= V_\Phi^*(r)\sin n\varphi\cos\beta z, & v_Z^* &= V_Z^*(r)\cos n\varphi\sin\beta z\\
\omega_R &= \Omega_R(r)\sin n\varphi\sin\beta z, & \omega_\Phi &= \Omega_\Phi(r)\cos n\varphi\sin\beta z\\
& & \omega_Z &= \Omega_Z(r)\sin n\varphi\cos\beta z
\end{aligned}
\tag{13.29}
$$

$$
\beta = \pi m/l, \qquad m = 1,2,..., \qquad n = 0,1,...
$$

leads to the separation of variables φ, z in these equations and allows to satisfy the linearized boundary conditions (13.20), (13.21) at the ends of the rod.

By taking into account the relations (13.4), (13.9), (13.22), (13.26) – (13.29), equations of neutral equilibrium (13.14), (13.17) are written as follows:

$$
\begin{aligned}
&(\lambda+\chi)V_R'' + \frac{\lambda+\chi}{r}V_R' - \frac{\lambda+(\mu+\kappa)\xi+\mu}{r^2}V_R + \frac{n(\lambda+\mu)}{r}V_\Phi' -\\
&-\frac{n(\lambda+3\mu+2\kappa)}{r^2}V_\Phi + \beta(\lambda+\mu)V_Z' + \beta B_2\Omega_\Phi - \frac{nB_1}{r}\Omega_Z = 0
\end{aligned}
$$

$$
\begin{aligned}
&(\mu+\kappa)V_\Phi'' - \frac{n(\lambda+\mu)}{r}V_R' - \frac{n(\lambda+3\mu+2\kappa)}{r^2}V_R + \frac{\mu+\kappa}{r}V_\Phi' -\\
&-\frac{(\lambda+\mu)n^2+(\mu+\kappa)\xi}{r^2}V_\Phi - \frac{n\beta(\lambda+\mu)}{r}V_Z - \beta B_3\Omega_R + B_1\Omega_Z' = 0
\end{aligned}
$$

$$
\begin{aligned}
&(\mu+\kappa)V_Z'' - \beta(\lambda+\mu)V_R' - \frac{\beta(\lambda+\mu)}{r}V_R - \frac{n\beta(\lambda+\mu)}{r}V_\Phi + \frac{\mu+\kappa}{r}V_Z' -\\
&-\left((\lambda+\mu)\beta^2 + \frac{\xi-1}{r^2}(\mu+\kappa)\right)V_Z + \frac{nB_3}{r}\Omega_R - B_2\Omega_\Phi' - \frac{B_3}{r}\Omega_\Phi = 0
\end{aligned}
$$

$$
\begin{aligned}
&\gamma\Omega_R'' - \beta B_3 V_\Phi + \frac{nB_3}{r}V_Z + \frac{\gamma}{r}\Omega_R' - \left[\frac{\gamma+\gamma_2(\xi-1)}{r^2} - \left(\frac{f}{r}+\alpha\right)B_3\right]\Omega_R -\\
&-\frac{n(\gamma-\gamma_2)}{r}\Omega_\Phi' + \frac{n(\gamma+\gamma_2)}{r^2}\Omega_\Phi - \beta(\gamma-\gamma_2)\Omega_Z' = 0
\end{aligned}
$$

$$
\begin{aligned}
&\gamma_2\Omega_\Phi'' + \beta B_2 V_R + B_2 V_Z' + \frac{n(\gamma-\gamma_2)}{r}\Omega_R' + \frac{n(\gamma+\gamma_2)}{r^2}\Omega_R + \frac{\gamma_2}{r}\Omega_\Phi' -\\
&-\left[\frac{(\gamma-\gamma_2)n^2+\gamma_2\xi}{r^2} - (f'+\alpha)B_2\right]\Omega_\Phi - \frac{n\beta(\gamma-\gamma_2)}{r}\Omega_Z = 0
\end{aligned}
$$

$$
\begin{aligned}
&\gamma_2\Omega_Z'' - \frac{nB_1}{r}V_R - B_1 V_\Phi' - \frac{B_1}{r}V_\Phi + \beta(\gamma-\gamma_2)\Omega_R' + \frac{\beta(\gamma-\gamma_2)}{r}\Omega_R -\\
&-\frac{n\beta(\gamma-\gamma_2)}{r}\Omega_\Phi + \frac{\gamma_2}{r}\Omega_Z' - \left[\gamma\beta^2 + \frac{n^2}{r^2}\gamma_2 - B_1\left(f'+\frac{f}{r}\right)\right]\Omega_Z = 0
\end{aligned}
\tag{13.30}
$$

$$(\lambda_*+2\mu_*)(V_R^*)''+\frac{\lambda_*+2\mu_*}{r}(V_R^*)'+\frac{n}{r}\left(\lambda_*+\mu_*-\frac{rB_1^*}{rf_*'+f_*}\right)(V_\Phi^*)'-$$
$$-\frac{n}{r^2}\left(\lambda_*+3\mu_*+\frac{rB_1^*}{rf_*'+f_*}\right)V_\Phi^*+\beta\left(\lambda_*+\mu_*-\frac{B_2^*}{f_*'+\alpha}\right)(V_Z^*)'-$$
$$-\frac{1}{r^2}\left(\lambda_*+(\xi+1)\mu_*+\frac{\beta^2r^2B_2^*}{f_*'+\alpha}+\frac{n^2rB_1^*}{rf_*'+f_*}\right)V_R^*=0$$

$$\left(\mu_*+\frac{rB_1^*}{rf_*'+f_*}\right)(V_\Phi^*)''-\frac{1}{r^2}\left((\lambda_*+\mu_*)n^2+\mu_*\xi+\frac{rB_1^*}{rf_*'+f_*}+\frac{\beta^2r^3B_3^*}{f_*+\alpha r}\right)V_\Phi^*-$$
$$-\frac{n}{r}\left(\lambda_*+\mu_*-\frac{rB_1^*}{rf_*'+f_*}\right)(V_R^*)'-\frac{n}{r^2}\left(\lambda_*+3\mu_*+\frac{rB_1^*}{rf_*'+f_*}\right)V_R^*+$$
$$+\frac{1}{r}\left(\mu_*+\frac{rB_1^*}{rf_*'+f_*}\right)(V_\Phi^*)'-\frac{n\beta}{r}\left(\lambda_*+\mu_*-\frac{rB_3^*}{f_*+\alpha r}\right)V_Z^*=0$$

$$\left(\mu_*+\frac{B_2^*}{f_*'+\alpha}\right)(V_Z^*)''-\left((\lambda_*+2\mu_*)\beta^2+\frac{n^2}{r^2}\left[\mu_*+\frac{rB_3^*}{f_*+\alpha r}\right]\right)V_Z^*-$$
$$-\beta\left(\lambda_*+\mu_*-\frac{B_2^*}{f_*'+\alpha}\right)(V_R^*)'-\frac{\beta}{r}\left(\lambda_*+\mu_*-\frac{B_3^*}{f_*'+\alpha}+\frac{f_*''rB_2^*}{(f_*'+\alpha)^2}\right)V_R^*-$$
$$-\frac{n\beta}{r}\left(\lambda_*+\mu_*-\frac{rB_3^*}{f_*+\alpha r}\right)V_\Phi^*+\frac{1}{r}\left(\mu_*+\frac{B_3^*}{f_*'+\alpha}-\frac{rf_*''B_2^*}{(f_*'+\alpha)^2}\right)(V_Z^*)'=0$$

$$B_1=\mu\left(f'+\frac{f}{r}\right)+\lambda s-\chi,\qquad B_2=\mu\left(f'+\alpha\right)+\lambda s-\chi$$
$$B_3=\mu\left(\frac{f}{r}+\alpha\right)+\lambda s-\chi,\qquad B_1^*=\mu_*\left(f_*'+\frac{f_*}{r}-2\right)+\lambda_*s_*$$
$$B_2^*=\mu_*\left(f_*'+\alpha-2\right)+\lambda_*s_*,\qquad B_3^*=\mu_*\left(\frac{f_*}{r}+\alpha-2\right)+\lambda_*s_*$$

$$\xi=n^2+r^2\beta^2+1,\qquad \gamma=\gamma_1+\gamma_2+\gamma_3$$

The expressions for the linearized boundary conditions (13.19) take the form:

1) for $r=r_2$:

$$(\lambda_*+2\mu_*)(V_R^*)'+\frac{\lambda_*+\alpha p}{r_2}(V_R^*+nV_\Phi^*)+\beta\left(\lambda_*+\frac{f_*}{r_2}p\right)V_Z^*=0$$

$$\left(\frac{\alpha p-\mu_*}{r_2}+\frac{B_1^*}{r_2f_*'+f_*}\right)(nV_R^*+V_\Phi^*)+\left(\mu_*+\frac{r_2B_1^*}{r_2f_*'+f_*}\right)(V_\Phi^*)'=0 \quad (13.31)$$

$$\beta\left(\frac{f_*}{r_2}p-\mu_*+\frac{B_2^*}{f_*'+\alpha}\right)V_R^*+\left(\mu_*+\frac{B_2^*}{f_*'+\alpha}\right)(V_Z^*)'=0$$

2) for $r=r_1$:

$$(\lambda_*+2\mu_*)(V_R^*)'+\frac{\lambda_*}{r_1}(V_R^*+nV_\Phi^*)+\beta\lambda_*V_Z^*-(\lambda+\chi)V_R'-$$
$$-\frac{\lambda}{r_1}(V_R+nV_\Phi)-\beta\lambda V_Z=0$$

$$\left(\frac{B_1^*}{r_1f_*'+f_*}-\frac{\mu_*}{r_1}\right)(nV_R^*+V_\Phi^*)+\left(\mu_*+\frac{r_1B_1^*}{r_1f_*'+f_*}\right)(V_\Phi^*)'+$$
$$+\frac{\mu}{r_1}(nV_R+V_\Phi)-(\mu+\kappa)V_\Phi'-B_1^*\Omega_Z=0 \quad (13.32)$$

$$\beta\left(\frac{B_2^*}{f_*'+\alpha}-\mu_*\right)V_R^*+\left(\mu_*+\frac{B_2^*}{f_*'+\alpha}\right)(V_Z^*)'+\mu\beta V_R-$$
$$-(\mu+\kappa)V_Z'+B_2^*\Omega_\Phi=0$$

$$\gamma\Omega_R'+\frac{\gamma_1}{r_1}(\Omega_R-n\Omega_\Phi)-\gamma_1\beta\Omega_Z=0,\qquad \frac{\gamma_3}{r_1}(n\Omega_R-\Omega_\Phi)+\gamma_2\Omega_\Phi'=0$$

$$\gamma_3\beta\Omega_R+\gamma_2\Omega_Z'=0,\qquad V_R-V_R^*=0,\qquad V_\Phi-V_\Phi^*=0,\qquad V_Z-V_Z^*=0$$

Thus, the stability analysis of the composite rod is reduced to solving a linear homogeneous boundary problem (13.30) – (13.32) for a system of ordinary differential equations. For its solvability, it is necessary to formulate an additional six conditions at $r=0$, which can be obtained by requiring boundedness of unknown functions and their derivatives with respect to r [12]:

$$\begin{aligned} &n=0: V_R(0)=V_\Phi(0)=V_Z'(0)=0,\quad \Omega_R(0)=\Omega_\Phi(0)=\Omega_Z'(0)=0\\ &n=1: V_R'(0)=V_\Phi'(0)=V_Z(0)=0,\quad \Omega_R'(0)=\Omega_\Phi'(0)=\Omega_Z(0)=0 \end{aligned} \quad (13.33)$$

13.4 Numerical Results

In the present paper, we have carried out the stability analysis for the composite cylindrical rod, the inner part of which is made of dense polyurethane foam [5]

$$\lambda = 797.3 \text{ MPa}, \qquad \mu = 99.67 \text{ MPa}, \qquad \kappa = 8.67 \text{ MPa}$$
$$\gamma_1 = -26.65 \text{ Pa}\cdot\text{m}^2, \quad \gamma_2 = 45.3 \text{ Pa}\cdot\text{m}^2, \quad \gamma_3 = 34.65 \text{ Pa}\cdot\text{m}^2$$

As the coating material, we have considered aluminum

$$\lambda_* = 61.9 \cdot 10^3 \text{ MPa}, \quad \mu_* = 26.2 \cdot 10^3 \text{ MPa}$$

and polycarbonate

$$\lambda_* = 2.3 \cdot 10^3 \text{ MPa}, \quad \mu_* = 0.8 \cdot 10^3 \text{ MPa}$$

By numerical solution [13] of the linear homogeneous boundary value problem (13.30) – (13.33) on the buckling of an elastic micropolar rod with a solid coating subject to axial compression and external pressure, in the plane of the loading parameters the critical curves corresponding to different buckling modes are found for these materials. As a result of analysis of these curves, the stability regions are constructed for rods of various sizes and with different coating thickness.

For convenience, we introduce the following dimensionless parameters:

$$\delta = 1 - \alpha, \qquad \tilde{p} = p/\mu, \qquad \tilde{l} = l/l_b, \qquad h = 1 - r_1/r_2$$

where $l_b = \sqrt{\gamma_2/2\,(2\mu + \kappa)}$ is characteristic length for bending [5]. The ratio of the length of the undeformed rod to its diameter is 20 ($l = 40r_2$) for all the presented results. Stability analysis was carried out for the rods, whose coating thickness does not exceed 5% of the diameter ($h \le 0.1$).

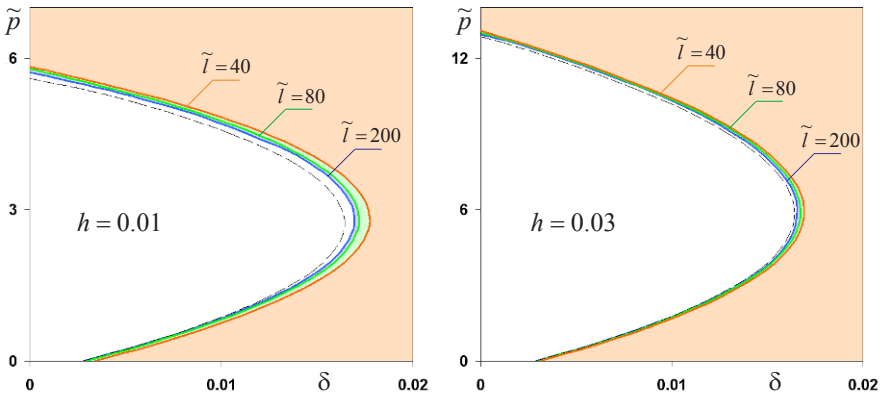

Fig. 13.1 Stability regions in the case of a thin aluminum coating

In Fig. 13.1, the stability regions are constructed in the plane of the loading parameters (relative axial compression δ and external pressure $\tilde{p}$) for a rod with a thin aluminum coating. Instability regions are shaded. The relative thickness of the coating is 0.5% ($h = 0.01$, left graph) and 1.5% ($h = 0.03$, right graph) of the di-

ameter for the undeformed rod. The stability boundaries for rods of different size are presented – $\tilde{l} = 40$, $\tilde{l} = 80$ and $\tilde{l} = 200$. Also on the graphs are the stability boundary (dotted line), obtained in the buckling analysis of composite rod without the influence of couple stresses, i.e. when the behavior of the inner part of the rod is described by the physically linear material (13.8) with the Lame coefficients λ, μ.

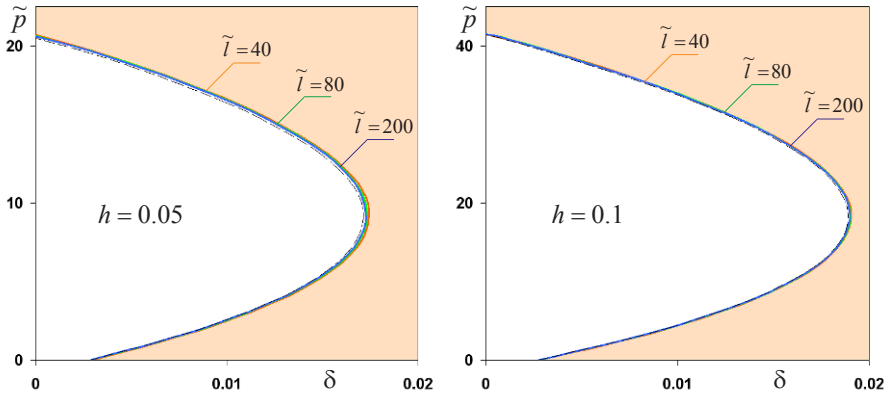

Fig. 13.2 Stability regions in the case of an aluminum coating of average thickness

The results obtained for a rod with an aluminum coating of average thickness are shown in Fig. 13.2. The relative thickness of the coating is 2.5% ($h = 0.05$, left graph) and 5% ($h = 0.1$, right graph) of the diameter. All notations are the same as the one used in Fig. 13.1.

It follows from graphs in Fig. 13.1 and Fig. 13.2 that in the case of the aluminum coating at $h \leq 0.1$ the stability of the rod with respect to the external pressure very much depends on the thickness of the coating. It is established that the rods with a thicker coating are generally more stable, except in the case of low pressure, when the rods with a thinner coating are more stable. In addition, from Fig. 13.1 shows that the stability of a rod with a thin aluminum coating noticeably depends on its size – for $\tilde{l} < 500$ rod having a small size is more stable than a large rod (for $\tilde{l} > 500$ the size effect was not detected). However, in the case of coating of average thickness $(0.04 < h \leq 0.1)$, the influence of size on the loss of stability is very small (see Fig. 13.2). Therefore, for this case the couple stresses can be neglected in the stability analysis.

In Fig. 13.3 and Fig. 13.4, the stability regions are constructed for a rod with a softer (in comparison with aluminum) polycarbonate coating. The relative thickness of the coating is 0.5% (Fig. 13.3, left graph), 1.5% (Fig. 13.3, right graph), 2.5% (Fig. 13.4, left graph) and 5% (Fig. 13.4, right graph) of the diameter for the undeformed rod.

It follows from graphs that in the case of the polycarbonate coating at $h \leq 0.1$ the stability of the rod with respect to the external pressure do not depends very much on the thickness of the coating. In connection with this, the rods with a thinner coating

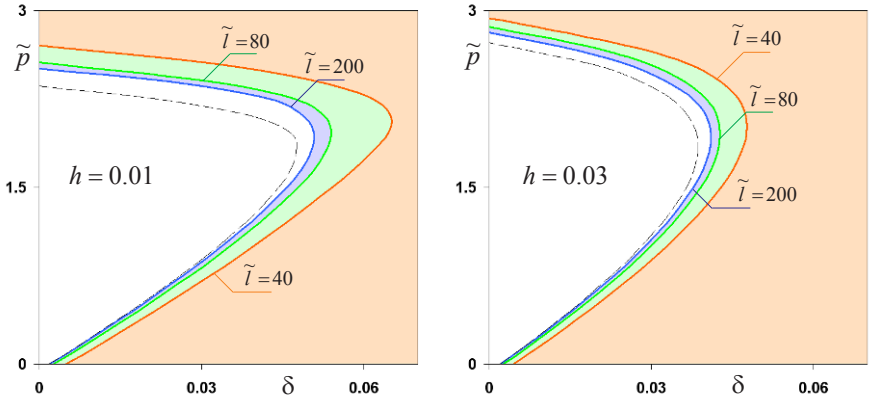

Fig. 13.3 Stability regions in the case of a thin polycarbonate coating

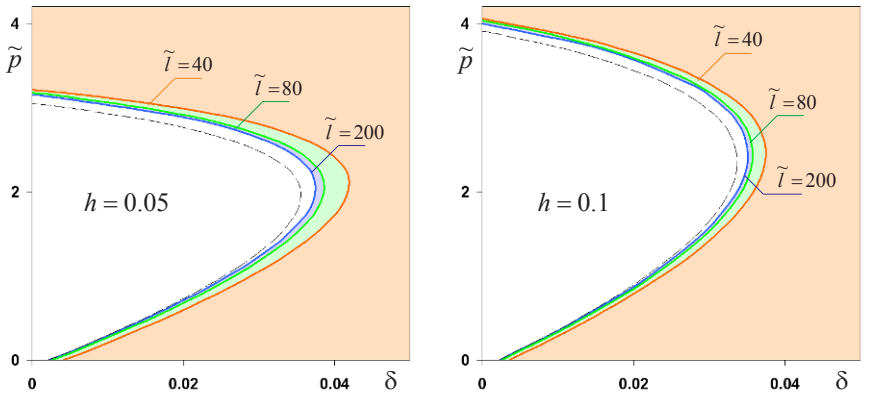

Fig. 13.4 Stability regions in the case of a polycarbonate coating of average thickness

are generally more stable, except in the case of high pressure, when the rods with a thicker coating are more stable. At the same time, according to the obtained results the stability of a rod with a polycarbonate coating considerably depends on its size (the size effect was detected for $\tilde{l} < 1000$). Moreover, unlike the case of aluminum coating, the influence of size on the stability of the rod is rather significant not only for a thin polycarbonate coating ($h \leq 0.04$), but also for a coating of average thickness ($0.04 < h \leq 0.1$), as shown in Fig. 13.3 and Fig. 13.4. This confirms the expediency of taking into account the couple stresses in this case.

13.5 Conclusion

In the framework of bifurcation approach, the stability analysis was carried out for an elastic micropolar rod with a solid coating subject to axial compression and ex-

ternal pressure. For the physically linear material, a system of linearized equilibrium equations was derived, which describes the behavior of the composite rod in a perturbed state. Using a special substitution the stability analysis was reduced to solving a linear homogeneous boundary problem (13.30) – (13.33) for a system of ordinary differential equations. In the case of a cylindrical rod of dense polyurethane foam with aluminum or polycarbonate coating the stability regions were found in the plane of loading parameters. It was established that for $h \leq 0.1$ in the case of an aluminum coating usually the rods with a thicker coating are more stable, but in case of polycarbonate coating on the contrary – with a thinner coating. In addition, it was revealed that for a rod with a polycarbonate coating the size effect on the rod stability is quite considerable, in contrast to the rod with an aluminum coating, for which this effect is apparent only in the case of a thin coating $(h \leq 0.04)$.

Acknowledgements This work was supported by the President of Russian Federation (grant MK-6315.2010.1) and by the Russian Foundation for Basic Research (grant 09-01-00459-a).

References

[1] Cosserat, E., Cosserat, F.: *Théorie des Corps Déformables*. Hermann Editeurs, Paris (1909) (Reprint, Gabay, Paris, 2008)
[2] Eremeyev, V.A., Zubov, L.M.: On stability of elastic bodies with couple-stresses. Mekhanika Tverdovo Tela (3), 181–190 (1994) (in Russ.)
[3] Eringen, A.C.: *Microcontinuum Field Theory. I. Foundations and Solids*. Springer, New York (1999)
[4] Kafadar, C.B., Eringen, A.C.: Micropolar media - I. The classical theory. International Journal of Engineering Science **9**, 271–305 (1971)
[5] Lakes, R.: Experimental methods for study of Cosserat elastic solids and other generalized elastic continua. In: Muhlhaus, H. (ed.) Continuum Models for Materials with Micro-structure, pp. 1–22. Wiley, New York (1995)
[6] Lurie, A.I.: Non-linear Theory of Elasticity. North-Holland, Amsterdam (1990)
[7] Maugin, G.A.: On the structure of the theory of polar elasticity. Philosophical Transactions of Royal Society London A **356**, 1367–1395 (1998)
[8] Nikitin, E., Zubov, L.M.: Conservation laws and conjugate solutions in the elasticity of simple materials and materials with couple stress. Journal of Elasticity **51**, 1–22 (1998)
[9] Pietraszkiewicz, W., Eremeyev, V.A.: On natural strain measures of the non-linear micropolar continuum. International Journal of Solids and Structures **46**, 774–787 (2009)
[10] Toupin, R.A.: Theories of elasticity with couple-stress. Archives for Rational Mechanics and Analysis **17**, 85–112 (1964)

[11] Zubov, L.M.: *Nonlinear Theory of Dislocations and Disclinations in Elastic Bodies*. Springer, Berlin (1997)

[12] Zubov, L.M., Sheidakov, D.N.: The effect of torsion on the stability of an elastic cylinder under tension. PMM Journal of Applied Mathematics and Mechanics **69**(1), 49–56 (2005)

[13] Zubov, L.M., Sheidakov, D.N.: Instability of a hollow elastic cylinder under tension, torsion, and inflation. Transactions of ASME. Journal of Applied Mechanics **75**(1) (2008)

Part V
Geometry and Defects

Chapter 14
Theory of Isolated and Continuously Distributed Disclinations and Dislocations in Micropolar Media

Mikhail I. Karyakin and Leonid M. Zubov

Abstract The paper deals with nonlinear theory of defects like dislocations and disclinations either isolated or distributed with a certain density in an elastic medium with internal rotational degrees of freedom and couple stresses. The general theory is illustrated by finding the solution of problems of internal stresses induced in an elastic disc with an isolated wedge disclination as well as the distribution of such disclinations. Some results concerning the influence of the microstructure on the possibility of the hole formation along the dislocation line are presented.

Key words: Dislocations. Disclinations. Cosserat continuum. Micropolar media. Couple stresses. Cavitation.

14.1 Introduction

Classical continuum mechanics, in particular, classical elasticity, is based on the model of simple material [6]; the free energy density and stresses at a particle of simple material are completely determined by the values of deformation gradient and temperature in the particle; besides, the Cauchy stress tensor is symmetric. The model of simple material perfectly describes behavior of medium in many cases however there are situations when we have to consider micro-inhomogeneous structure of the material; to these, polycrystalline grained materials, polymers, composites, suspensions, liquid crystals, geophysical structures, etc. assume to attract ideas of micro-non-homogeneity [5]. To describe mathematically the physical and mechanical properties of above medium, continuum theories dealing with couple stresses and rotational interaction of particles are used.

The most essential distinction between the results of couple stress elasticity and those of classical theory occurs when the stressed state of the body changes drasti-

Mikhail I. Karyakin and Leonid M. Zubov
Southern Federal University, Milchakova 8a, 344090 Rostov on Don, Russia
e-mail: karyakin@math.sfedu.ru, e-mail: zubov@math.sfedu.ru

H. Altenbach et al. (eds.), *Mechanics of Generalized Continua,*
Advanced Structured Materials, 7, DOI: 10.1007/978-3-642-19219-7_14,

cally, that is in some vicinity of stress concentrators such as corners, crack edges, dislocation and disclination lines and other defects. Thus the study of nonlinear effects of couple stresses in the theory of dislocations and disclinations is of interest.

The paper presents main relations of the nonlinear theory of isolated dislocations in micropolar media. Some examples of the influence of the couple stresses accounting upon the mechanical fields generated by dislocations and disclinations in the nonlinear elastic media and upon the cavitation near the crystal structure defects are given. It is established that this influence is qualitatively different for the dislocations and disclinations.

The resolving equations of the continual theory of defects are obtained by the limiting transition from the discrete set of isolated dislocations and disclinations to their continuous distribution. It is particularly shown that such transition in the general three-dimensional case can be performed for continuous distribution of dislocations only when disclinations are absent or isolated. The transition is possible in the plane problem for the micropolar elastic medium. The general theory is illustrated by solving a problem of internal stresses induced in an elastic disc by a given distribution of wedge disclinations.

14.2 Isolated Defects in Nonlinearly Elastic Bodies with Couple Stresses

14.2.1 Nonlinear Cosserat Continuum

The model of nonlinearly elastic Cosserat continuum suggests that any continuum particle has all the rigid body degrees of freedom. A position of particle in the deformed state is specified by the radius-vector $\mathbf{R}$, while the particle orientation is determined by a proper orthogonal tensor $\mathbf{H}$ called the microrotation tensor. Following the principle of local action in continuum mechanics, we suggest the function of specific (per reference configuration unit volume) potential strain energy of elastic continuum of the form

$$\begin{gathered} W = W(\mathbf{R}, \operatorname{grad}\mathbf{R}, \mathbf{H}, \operatorname{grad}\mathbf{H}), \quad \operatorname{grad} = \mathbf{r}^s \frac{\partial}{\partial q^s}, \\ \mathbf{r}_k = \frac{\partial \mathbf{r}}{\partial q^k}, \quad \mathbf{r}^s \cdot \mathbf{r}_k = \delta^s_k, \quad s,k = 1,2,3, \end{gathered} \tag{14.1}$$

where q^s are Lagrangian coordinates, $\mathbf{r}$ is the particle radius-vector in the reference (undeformed) configuration. By the principle of material frame indifference [6], the strain energy density of elastic body, W, is invariant under rigid body motions of medium. The invariance of W under translations results in the independence of W (in Eq. (14.1)) of the argument $\mathbf{R}$. The invariance under observer frame rotations implies that

$$W((\operatorname{grad}\mathbf{R})\cdot\mathbf{O},\mathbf{H}\cdot\mathbf{O},(\operatorname{grad}\mathbf{H})\cdot\mathbf{O}) = W(\operatorname{grad}\mathbf{R},\mathbf{H},\operatorname{grad}\mathbf{H}) \tag{14.2}$$

for any orthogonal (that is $\mathbf{O}^{\mathrm{T}} = \mathbf{O}^{-1}$) tensor $\mathbf{O}$. Setting $\mathbf{O} = \mathbf{H}^{\mathrm{T}}$ in Eq. (14.2), we obtain

$$W = W\left((\operatorname{grad}\mathbf{R})\cdot\mathbf{H}^{\mathrm{T}},(\operatorname{grad}\mathbf{H})\cdot\mathbf{H}^{\mathrm{T}}\right). \tag{14.3}$$

In Eq. (14.3), it was taken into account that $\mathbf{H}\cdot\mathbf{H}^{\mathrm{T}} = \mathbf{E}$, where $\mathbf{E}$ is the identity tensor. The relation (14.3) is a necessary consequence of the equality (14.2); it is easy to verify that it is sufficient for the invariance of the energy under rigid body motions. Taking into account the skew symmetry of tensors $(\partial\mathbf{H}/\partial q^k)\cdot\mathbf{H}^{\mathrm{T}}$ $(k = 1,2,3)$ we can represent the third order tensor $\operatorname{grad}\mathbf{H}\cdot\mathbf{H}^{\mathrm{T}}$ in terms of the second order tensor L as follows

$$\operatorname{grad}\mathbf{H}\cdot\mathbf{H}^{\mathrm{T}} = -\mathbf{L}\times\mathbf{E},\quad \mathbf{L} = \frac{1}{2}\mathbf{r}^k\left(\frac{\partial\mathbf{H}}{\partial q^k}\cdot\mathbf{H}^{\mathrm{T}}\right)_{\times}. \tag{14.4}$$

Here $\mathbf{T}_{\times}$ denotes the vector invariant of a 2nd order tensor $\mathbf{T}$, $\mathbf{T}_{\times} = (T_{sk}\mathbf{r}^s\otimes\mathbf{r}^k)_{\times} = T_{sk}\mathbf{r}^s\times\mathbf{r}^k$. By Eqs (14.3), (14.4), the elastic potential, W, at a given material particle, relates with the deformation of a neighborhood of the particle by two 2nd order tensors: the strain measure,

$$\mathbf{Y} = (\operatorname{grad}\mathbf{R})\cdot\mathbf{H}^{\mathrm{T}}, \tag{14.5}$$

and the bending strain tensor, $\mathbf{L}$.

For simplicity we assume that both mass external loads, and forces and couples distributed over the body surface are absent. Then from the variation principle $\delta\int_v W\,dv = 0$ we obtain an equilibrium equations

$$\operatorname{div}(\mathbf{P}\cdot\mathbf{H}) = 0,\qquad \operatorname{div}(\mathbf{K}\cdot\mathbf{H}) + (\mathbf{C}^{\mathrm{T}}\cdot\mathbf{P}\cdot\mathbf{H})_{\times} = 0, \tag{14.6}$$

boundary conditions for ∂v

$$\mathbf{n}\cdot\mathbf{P}\cdot\mathbf{H} = 0,\quad \mathbf{n}\cdot\mathbf{K}\cdot\mathbf{H} = 0, \tag{14.7}$$

and the equations of state

$$\mathbf{P} = \frac{\partial W}{\partial\mathbf{Y}},\quad \mathbf{K} = \frac{\partial W}{\partial\mathbf{L}},\quad W = W(\mathbf{Y},\mathbf{L}). \tag{14.8}$$

Here, $\mathbf{P}$ and $\mathbf{K}$ are the stress tensor and couple stress tensor, respectively, both of the Kirchhoff type; div is the divergence operator in the reference configuration of the material body (i.e., in the Lagrangian coordinates); v is the volume occupied by the elastic Cosserat medium in reference configuration; $\mathbf{n}$ is normal to the boundary of the body ∂v.

14.2.2 Weingarten's Theorem for the Finite Plane Deformation of Couple Stress Medium

Consider the problem of determining the displacement and microrotation fields of the Cosserat continuum when the fields of tensors **Y** and **L** are given as twice differentiable functions of Lagrangian coordinates.

Restricting ourselves to the case of plane strain described by the relations

$$X_l = X_1(x_1, x_2), \quad X_2 = X_2(x_1, x_2), \quad X_3 = x_3, \tag{14.9}$$

where x_k, X_k are the coordinates of medium points in the Cartesian basis $\mathbf{i}_k$ before and after the deformation, respectively, we can simplify the problem on the stresses due to isolated defect, in particular, we can obtain expressions for its characteristics in terms of ordinary contour integrals. Let us introduce the complex coordinates

$$\zeta = x_1 + ix_2, \quad \bar{\zeta} = x_1 - ix_2, \quad z = X_1 + iX_2, \quad \bar{z} = X_1 - iX_2.$$

The plane deformation (14.9) is described by a complex-valued function

$$z = z(\zeta, \bar{\zeta}), \quad X_3 = x_3. \tag{14.10}$$

In the multiply connected domain occupied by the body in undeformed state, the tensors **Y** and **L** are given by

$$\mathbf{L} = L_1(\zeta, \bar{\zeta})\mathbf{f}^1\mathbf{f}_3 + L_2(\zeta, \bar{\zeta})\mathbf{f}^2\mathbf{f}_3, \tag{14.11}$$

$$\mathbf{Y} = Y_\alpha^\beta(\zeta, \bar{\zeta})\mathbf{f}^\alpha\mathbf{f}_\beta + \mathbf{f}^3\mathbf{f}_3, \tag{14.12}$$

where $\mathbf{f}^\alpha$, $\mathbf{f}_\beta$ are the complex bases associated with the complex coordinates ζ, $\bar{\zeta}$ [9], $\mathbf{f}^3 = \mathbf{f}_3 = \mathbf{i}_3$.

We shall seek **H** in the form

$$\mathbf{H} = e^{i\chi}\mathbf{f}^1\mathbf{f}_1 + e^{-i\chi}\mathbf{f}^2\mathbf{f}_2 + \mathbf{f}^3\mathbf{f}_3. \tag{14.13}$$

In this general representation of rotation tensor under plane strain, χ is the particle finite rotation angle to be determined. Substituting Eqs (14.11), (14.13) into Eq. (14.4), we get

$$\frac{\partial\chi}{\partial\zeta} = L_1, \quad \frac{\partial\chi}{\partial\bar{\zeta}} = L_2. \tag{14.14}$$

We can write the solvability condition for Eqs (14.14) with respect to χ as

$$\frac{\partial L_1}{\partial\bar{\zeta}} = \frac{\partial L_2}{\partial\zeta}. \tag{14.15}$$

Comparing the expression for the deformation gradient, $\operatorname{grad}\mathbf{R}$, answering the transformation (14.10), with $\operatorname{grad}\mathbf{R} = \mathbf{Y}\cdot\mathbf{H}$, derived from the definition of **Y**, with

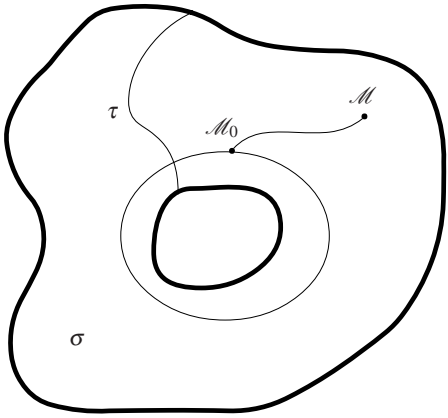

Fig. 14.1 Integration contour from $\mathscr{M}_0$ to $\mathscr{M}$ in the doubly connected domain σ.

regard for Eqs (14.12), (14.13), we find

$$\frac{\partial z}{\partial \zeta} = Y_1^1 e^{i\chi}, \quad \frac{\partial z}{\partial \bar{\zeta}} = Y_2^1 e^{i\chi}. \tag{14.16}$$

In view of Eq. (14.14), the solvability condition for these equations takes the form

$$\frac{dY_2^1}{d\zeta} - \frac{dY_1^1}{d\bar{\zeta}} + iL_1 Y_2^1 - iL_2 Y_1^1 = 0. \tag{14.17}$$

Thus the Eqs (14.15), (14.17) are the compatibility equations under plane medium deformation which are equivalent to three real-valued equations.

If a value of the rotation angle, $\chi_0 = \chi(\zeta_0, \bar{\zeta}_0)$ is given at a point $\mathscr{M}_0$ with complex coordinates ζ_0, $\bar{\zeta}_0$, then the rotation field in a simply connected domain is uniquely determined by the system (14.14). Having found $\chi(\zeta, \bar{\zeta})$, we can uniquely evaluate the function $z(\zeta, \bar{\zeta})$ by integrating the system (14.16) with a given value $z_0 = z(\zeta_0, \bar{\zeta}_0)$.

Let us now consider the case of doubly connected domain (Fig. 14.1). Suppose that the integration contour consists of a curve connecting points $\mathscr{M}_0$, $\mathscr{M}$ and non-intersecting the partition τ, and a closed, non-contractible-into-point contour which revolves n times (n full turns) in positive direction. In a doubly connected domain the solution of Eqs (14.14) is multi-valued and takes the form

$$\begin{gathered} \chi = \chi_* + nK, \quad \chi_* = \chi_0 + \int_{\mathscr{M}_0}^{\mathscr{M}} \left(L_1\, d\zeta + L_2\, d\bar{\zeta}\right), \\ K = \oint L_1\, d\zeta + L_2\, d\bar{\zeta}. \end{gathered} \tag{14.18}$$

From Eqs (14.16), (14.18), it follows a multi-valued expression for the quantity z which describes the location of continuum particles in the deformed state

$$z = z_0 + e^{inK} \int_{\mathscr{M}_0}^{\mathscr{M}} e^{i\chi_*} \left(Y_1^1 \, d\zeta + Y_2^1 \, d\bar{\zeta} \right) + \\ + \left(1 + e^{iK} + \ldots + e^{i(n-1)K} \right) \oint e^{i\chi_*} \left(Y_1^1 \, d\zeta + Y_2^1 \, d\bar{\zeta} \right), \tag{14.19}$$

where n is a constant for multi-valuedness of the problem. The integrals with variable upper limit are evaluated over the curves which do not enclose the domain hole; the closed contour is through $\mathscr{M}_0$ and passes around the hole one time.

On the cut converting the domain into a simply connected one, the limiting values of functions χ and z are related by

$$\chi_+ - \chi_- = K, \quad z_+ = z_- e^{iK} + \beta, \tag{14.20}$$

$$\beta = z_0 \left(1 - e^{iK} \right) + \oint e^{i\chi_*} \left(Y_1^1 \, d\zeta + Y_2^1 \, d\bar{\zeta} \right). \tag{14.21}$$

The relation (14.20) represents the statement of Weingarten's theorem in the case of nonlinear couple-stress theory of plane elasticity; it can be rewritten in the real-valued form

$$\mathbf{u}_+ - \mathbf{u}_- = \frac{4}{4+\omega^2} \omega \times \left(\mathbf{R}_- + \frac{1}{2} \omega \times \mathbf{R}_- \right) + \mathbf{b}, \\ \mathbf{b} = \Re(\beta)\mathbf{i}_1 + \Im(\beta)\mathbf{i}_2, \quad \omega = 2 \tan \frac{K}{2} \mathbf{i}_3 \tag{14.22}$$

14.2.3 Wedge Disclination

The problem to find out the stressed state of couple-stress body with Volterra dislocation can be solved by the following approach: the problem states in a multiply connected domain, the strain tensors $\mathbf{Y}$ and $\mathbf{L}$, as unknowns, must satisfy the equilibrium equations, the compatibility equations, and the integral relations specifying the dislocation and disclination parameters. As an example of application of this approach, let us consider the plane problem of defect in an elastic ring.

We shall seek tensors $\mathbf{Y}$ and $\mathbf{L}$ in the form

$$\mathbf{Y} = Y_r(r)\mathbf{e}_r \otimes \mathbf{e}_r + Y_\varphi(r)\mathbf{e}_\varphi \otimes \mathbf{e}_\varphi + \mathbf{e}_z \otimes \mathbf{e}_z, \\ \mathbf{L} = L_r(r)\mathbf{e}_r \otimes \mathbf{e}_z + L_\varphi(r)\mathbf{e}_\varphi \otimes \mathbf{e}_z, \tag{14.23}$$

where r, φ, z are cylindrical coordinates in the reference configuration, $\mathbf{e}_r$, $\mathbf{e}_\varphi$, $\mathbf{e}_z$ are the unit basis vectors related to the coordinates. The compatibility equation (14.15) now becomes

$$\frac{dL_\varphi}{dr} + \frac{1}{r} L_\varphi = 0,$$

whence $L_\varphi = C/r$. To define the constant C, we invoke the relation (14.18) with a given constant K,

$$L_\varphi = \frac{K}{2\pi r}. \tag{14.24}$$

In view of Eqs (14.23), (14.24), the complex-valued compatibility equation (14.17) is equivalent to the following real relations

$$L_r(r) = 0, \quad \frac{dY_\varphi}{dr} + \frac{1}{r}Y_\varphi - \frac{\kappa}{r}Y_r = 0, \quad \kappa = 1 + \frac{K}{2\pi}. \tag{14.25}$$

Using Eq. (14.14), we find the rotation field of medium $\chi_* = (\kappa - 1)\varphi$. Thus by Eq. (14.13), the microrotation tensor is defined.

Calculating the parameter β from Eq. (14.21), we obtain the relation

$$\beta = \left(1 - e^{iK}\right)\left(z_0 - \frac{1}{\kappa}Y_\varphi(r_0)\right),$$

which demonstrates that the representation (14.23) enables us to solve the problem on the wedge disclination in the ring whereas this representation is not sufficient to solve the translational dislocation problem. Indeed if $\kappa \neq 0$, setting $K = 0$ we obtain that $\beta = 0$ also, that means that there is no defect in the body.

Let us now study the stressed state of a body with disclination for physically linear micropolar material [9] with the specific potential energy of the form

$$\begin{aligned} 2W = \lambda\,\mathrm{tr}^2\,\mathbf{U} + (\mu + \psi)\,\mathrm{tr}\,(\mathbf{U}\cdot\mathbf{U}^{\mathrm{T}}) + (\mu - \psi)\,\mathrm{tr}\,\mathbf{U}^2 + \\ + \delta\,\mathrm{tr}^2\,\mathbf{L} + (\gamma + \eta)\,\mathrm{tr}\,(\mathbf{L}\cdot\mathbf{L}^{\mathrm{T}} + (\gamma - \eta)\,\mathrm{tr}\,\mathbf{L}^2, \quad \mathbf{U} = \mathbf{Y} - \mathbf{E}, \end{aligned} \tag{14.26}$$

where λ, μ, δ, γ, ψ, and η are elastic moduli. Using Eqs (14.8), (14.23) and (14.26), one can verify that the couple equilibrium equation in (14.6) is satisfied identically, and the force equilibrium equation for unloaded body takes the form

$$\begin{aligned} (\lambda + 2\mu)\frac{dY_r}{dr} + \lambda\frac{dY_\varphi}{dr} + \frac{\lambda(1-\kappa) + 2\mu}{r}Y_r + \\ + \frac{\lambda(1-\kappa) - 2\mu\kappa}{r}Y_\varphi = 2(\lambda + \mu)\frac{1-\kappa}{r}. \end{aligned} \tag{14.27}$$

We assume that the ring boundaries, $r = r_l$ and $r = r_0$ are free of load. This implies the following boundary conditions:

$$(\lambda + 2\mu)Y_r + \lambda Y_\varphi = 2(\lambda + \mu) \text{ at } r = r_1, r_0 \tag{14.28}$$

The case of solid disk ($r_1 = 0$) is of most interest. Solving the boundary problem (14.25), (14.27) and (14.28) and then passing to the limit as $r_1 \to 0$, we obtain

$$Y_r = \frac{\kappa(1-2\nu)}{(1+\kappa)(1-\nu)}\rho^{\kappa-1} + \frac{1}{(1+\kappa)(1-\nu)},$$
$$Y_\varphi = \frac{\kappa(1-2\nu)}{(1+\kappa)(1-\nu)}\rho^{\kappa-1} + \frac{\kappa}{(1+\kappa)(1-\nu)}, \tag{14.29}$$
$$\nu = \frac{\lambda}{2(\lambda+\mu)}, \quad \rho = \frac{r}{r_0}.$$

Introducing the tensors of stresses $\mathbf{T}$ and couple stresses $\mathbf{M}$, which are similar to the Cauchy stress tensor in the elasticity theory of simple materials by relations

$$\mathbf{T} = J^{-1}(\operatorname{grad}\mathbf{R})^{\mathrm{T}} \cdot \mathbf{P}, \quad \mathbf{M} = J^{-1}(\operatorname{grad}\mathbf{R})^{\mathrm{T}} \cdot \mathbf{K},$$

$$J = \det(\operatorname{grad}\mathbf{R}),$$

on the basis of Eqs (14.26) and (14.29) we find the components of Cauchy stress tensor

$$T_{RR} = 2\mu\frac{\rho^{\kappa-1}-1}{(1-2\nu)\rho^{\kappa-1}+1},$$
$$T_{\Phi\Phi} = 2\mu\frac{\kappa\rho^{\kappa-1}-1}{(1-2\nu)\kappa\rho^{\kappa-1}+1}.$$

These expressions have no singularity at the disclination axis and coincide with principal stresses in elastic medium without couple stresses [8].

The non-vanishing components of the couple-stress tensor $\mathbf{M}$ take the form

$$M_{\Phi Z} = (\gamma+\eta)\frac{\kappa-1}{rY_r},$$
$$M_{Z\Phi} = (\gamma-\eta)\frac{\kappa-1}{rY_rY_\varphi}. \tag{14.30}$$

Relations (14.29), (14.30) show that, as $\rho \to 0$, the couple stress $M_{\Phi Z}$ has a singularity of the order ρ^{-1} if $\kappa > 1$ and of the order $\rho^{-\kappa}$ if $\kappa < 1$, whereas the singularity of $M_{Z\Phi}$ is of the order ρ^{-1} if $\kappa > 1$ and of the order $\rho^{1-2\kappa}$ if $\kappa < 1$. The linearization of Eqs (14.30) with respect to parameter $(\kappa-1)$, when $\rho > 0$, results in some formulas, known from linear couple-stress theory [4], according to which the singularity of couple stresses is of the order ρ^{-1} as $\rho \to 0$ for all $\kappa \neq 0$.

14.3 Continuously Distributed Dislocations and Disclinations in Nonlinearly Elastic Micropolar Media

14.3.1 Density of Dislocations

To introduce the density of dislocations in a micropolar medium, let us consider the problem of determining the field of displacements in the medium $\mathbf{u} = (X_k - x_k)\mathbf{i}_k$ by using the tensor fields of deformation measure $\mathbf{Y}(x_s)$ and microrotations $\mathbf{H}(x_s)$ that are assumed to be continuously differentiable and single-valued in the multiply connected domain σ. Taking into account that $\operatorname{grad}\mathbf{u} = \mathbf{Y}\cdot\mathbf{H} - \mathbf{E}$ and following [1], we arrive at the expression

$$\mathbf{b}_N = \oint_{\gamma_N} \mathbf{i}_k \cdot \mathbf{Y}\cdot\mathbf{H}\, dx_k \tag{14.31}$$

for the Burgers vectors of dislocations that are responsible for the lack of uniqueness of the displacement field in the multiply connected domain. Here, γ_N is a simple closed contour enveloping the line of only the Nth dislocation. Taking (14.31) into account, we apply the method proposed in [1] to move from the discrete set of translational defects, or dislocations, to their continuous distribution. Using the known definition of the density of dislocations as the tensor $\mathbf{d}_0$ [7] whose flux through any surface is equal to the total Burgers vector of dislocations crossing this surface, we arrive at the equation

$$\operatorname{curl}(\mathbf{Y}\cdot\mathbf{H}) = \mathbf{d}_0, \tag{14.32}$$

where curl is the curl operator in the Lagrangian coordinates. For a given dislocation density tensor $\mathbf{d}_0$, which must satisfy the condition $\operatorname{div}\mathbf{d}_0 = 0$, Eqs. (14.4), (14.6), (14.8), and (14.32) form a complete system of equations with unknowns $\mathbf{Y}$ and $\mathbf{H}$.

Under certain assumptions about the dislocation density, the system of Eqs (14.4), (14.6), (14.8) and (14.32) can be transformed by excluding the microrotation tensor $\mathbf{H}$ from the unknown functions and taking the tensor fields $\mathbf{Y}$ and $\mathbf{L}$ as unknowns. Multiplying Eqs (14.6) and (14.32) by the tensor $\mathbf{H}^{\mathrm{T}}$ from the right and taking representation (14.4) into account, we obtain the system of equations

$$\begin{gathered}\operatorname{div}\mathbf{P} - (\mathbf{P}^{\mathrm{T}}\cdot\mathbf{L})_{\times} = 0,\\ \operatorname{div}\mathbf{K} - (\mathbf{K}^{\mathrm{T}}\cdot\mathbf{L} + \mathbf{P}^{\mathrm{T}}\cdot\mathbf{Y})_{\times} = 0,\end{gathered} \tag{14.33}$$

$$\operatorname{curl}\mathbf{Y} + \mathbf{Y}\times\times\mathbf{L} = \mathbf{d}, \quad \mathbf{d} \equiv \mathbf{d}_0\cdot\mathbf{H}^{\mathrm{T}}. \tag{14.34}$$

Here, the invariant fiber bundle of second-rank tensors is defined in terms of the vector products of the basis vectors $\mathbf{r}_s$ as follows:

$$\mathbf{Y}\times\times\mathbf{L} = (Y_{mn}\mathbf{i}_m\otimes\mathbf{i}_n)\times\times(L_{ks}\mathbf{i}_k\otimes\mathbf{i}_s) = Y_{mn}L_{ks}(\mathbf{i}_m\times\mathbf{i}_k)\otimes(\mathbf{i}_n\times\mathbf{i}_s).$$

Below, the modified dislocation density tensor $\mathbf{d}$ will be treated as given.

The microrotation tensor must also be excluded from relation (14.4), specifying the bending strain tensor of the micropolar medium. To this end, we consider the problem of determining the microrotation tensor field $\mathbf{H}$ in the micropolar medium with continuously distributed dislocations in terms of a given bending strain tensor field $\mathbf{L}$. We now remove the requirement of the uniqueness of the tensor field $\mathbf{H}$ in the multiply connected domain σ and use the condition of uniqueness and differentiability of the tensor $\mathbf{L}$ in this domain. Using Eq. (14.4), we compose the following system of equations for the tensor $\mathbf{H}$:

$$\frac{\partial \mathbf{H}}{\partial x_s} = -\mathbf{L}_s \times \mathbf{H}, \quad \mathbf{L}_s = \mathbf{i}_s \cdot \mathbf{L}. \tag{14.35}$$

Excluding the unknown orthogonal tensor $\mathbf{H}$ from system (14.35), we arrive at the tensor solvability condition

$$\operatorname{curl} \mathbf{L} + \frac{1}{2}\mathbf{L} \times\times \mathbf{L} = 0. \tag{14.36}$$

This condition is a necessary and sufficient condition for the existence of the unique microrotation field in the simply connected domain σ when the tensor $\mathbf{H}$ is given in a certain point of the domain. If the σ domain is multiply connected, the solution of the Cauchy problem for system (14.35) is generally multi-valued. The possible multiple-valuedness of the solution is removed after the transformation of the multiply connected domain to simply connected one by introducing the necessary number of cuts τ_M, $M = 1, 2, \ldots$. The microrotation tensor takes different values $\mathbf{H}_+$ and $\mathbf{H}_-$ at the different edges of the cut. The relation $\mathbf{H}_+ = \mathbf{H}_- \cdot \boldsymbol{\Phi}_M$, where $\boldsymbol{\Phi}_M$ is the properly orthogonal tensor that is constant for a given cut τ_M, is proved by using the continuity and uniqueness of the bending strain tensor $\mathbf{L}$ in the domain σ and applying the method proposed in [9]. The existence of the above jump of the microrotation tensor at the cut τ_M means the existence of isolated rotational defects, or disclinations, in an elastic micropolar body with distributed dislocations. As well as in the Cosserat continuum without dislocations [9], the Frank vector of each isolated disclination is expressed in terms of the bending strain tensor field through the multiplicative contour integral. These integral relations, together with Eqs. (14.33), (14.34), and (14.36) and the boundary conditions on the body surface, provide the formulation of the boundary value problem concerning the equilibrium of the micropolar medium with continuously distributed dislocations and isolated disclinations. Since the properties of multiplicative line integrals are complicated [9], the limiting transition from a discrete set of isolated disclinations to their continuous distribution is generally impossible. Nevertheless, as will be shown below, this transition is possible in the plane problem for the micropolar elastic medium.

14.3.2 Plane Deformation

We consider plane deformation in the (x_1,x_2) plane. In this case, the dislocation density tensor has the form $\mathbf{d}_0 = \mathbf{i}_3 \otimes \mathbf{a}_0$ $(\mathbf{a}_0 \cdot \mathbf{i}_3 = 0)$ [1], where $\mathbf{a}_0$ is the edge dislocation density vector, and the distortion tensor $\mathbf{C}$ satisfies the incompatibility equation

$$\nabla \cdot (\mathbf{e} \cdot \mathbf{C}) = \mathbf{a}_0, \quad \mathbf{e} = -\mathbf{i}_3 \times \mathbf{E}, \quad \nabla = \mathbf{i}_1 \frac{\partial}{\partial x_1} + \mathbf{i}_2 \frac{\partial}{\partial x_2}. \tag{14.37}$$

Here, ∇ is the two-dimensional gradient operator and $\mathbf{e}$ is the discriminant tensor. The $\mathbf{H}$ tensor for plane deformation is expressed in terms of the angle χ of microrotation about the x_3 axis through the formula

$$\mathbf{H} = \mathbf{g}\cos\chi + \mathbf{e}\sin\chi + \mathbf{i}_3 \otimes \mathbf{i}_3, \quad \mathbf{g} = \mathbf{E} - \mathbf{i}_3 \otimes \mathbf{i}_3. \tag{14.38}$$

Using Eqs (14.4) and (14.38), we obtain

$$\mathbf{L} = \mathbf{l} \otimes \mathbf{i}_3, \quad \mathbf{l} = \nabla\chi. \tag{14.39}$$

In view of Eqs (14.5) and (14.38), Eq. (14.39) is transformed as

$$\nabla \cdot (\mathbf{e} \cdot \mathbf{Y} \cdot \mathbf{g}) + \mathbf{l} \cdot (\mathbf{e} \cdot \mathbf{Y} \cdot \mathbf{e}) = \mathbf{a}, \tag{14.40}$$

where $\mathbf{a} = \mathbf{a}_0 \cdot \mathbf{H}^{\mathrm{T}}$.

According to Eq. (14.39), the microrotation field is determined in terms of the bending strain field through the quadratures

$$\chi = \int_{\mathbf{r}_0}^{\mathbf{r}} \mathbf{l} \cdot d\mathbf{r} + \chi(\mathbf{r}_0), \quad \mathbf{r} = x_1\mathbf{i}_1 + x_2\mathbf{i}_2. \tag{14.41}$$

When the condition $\nabla \cdot \mathbf{e} \cdot \mathbf{l} = 0$ is valid, the line integral in Eq. (14.41) is independent of the integration path if the σ domain is simply connected. For the multiply connected plane domain homeomorphic to the circle with circular holes, expression (14.41) generally specifies a multi-valued function. Transforming the multiply connected domain to the simply connected one by means of cuts, we find that the values $\chi_\pm$ at the opposite edges of each cut may differ by a constant:

$$\chi_+ - \chi_- = \theta_S, \quad S = 1,2,\ldots.$$

Constants θ_S are independent of the choice of the system of cuts and are expressed in terms of the bending strain field through an ordinary (not multiplicative) contour integral. The existence of nonzero constants θ_S means that isolated wedge disclinations exist in a multiply connected micropolar body. Using the method described in [1] for the transformation of a discrete set of disclinations to their continuous distribution, we arrive at the following incompatibility equation for bending strains of

the plane medium:

$$\nabla \cdot \mathbf{e} \cdot \mathbf{l} = \beta, \tag{14.42}$$

where β is the scalar density of wedge disclinations. For the plane case, equilibrium equations (14.33) take the form

$$\nabla \cdot \mathbf{P} + \mathbf{l} \cdot \mathbf{P} \cdot \mathbf{e} = 0, \quad \nabla \cdot \mathbf{K} \cdot \mathbf{i}_3 = \mathrm{tr}\,(\mathbf{P} \cdot \mathbf{e} \cdot \mathbf{Y}^{\mathrm{T}} \cdot \mathbf{g}) \tag{14.43}$$

and, together with incompatibility equations (14.40) and (14.42), form the complete system of nonlinear equations determining the internal stresses in the plane medium with distributed dislocations and disclinations. When $\alpha = \beta = 0$ relations (14.40), (14.42) constitute another form of the compatibility equations (14.15), (14.17).

14.3.3 Sample Problem

We illustrate the above theory by solving the problem of determining internal stresses induced in an elastic disc by the axisymmetrically distributed wedge disclinations. Let us use the model of the physically linear micropolar medium (14.26) and let $\mathbf{a} = 0$ and $\beta = \beta(r)$. We seek the strain field in the form

$$\begin{gathered} \mathbf{Y} = Y_1(r)\mathbf{e}_r \otimes \mathbf{e}_r + \frac{h(r)}{r}\mathbf{e}_\varphi \otimes \mathbf{e}_\varphi + \mathbf{i}_3 \otimes \mathbf{i}_3, \\ \mathbf{l} = l_1(r)\mathbf{e}_r + l_2(r)\mathbf{e}_\varphi, \\ \mathbf{e}_r = \mathbf{i}_1 \cos\varphi + \mathbf{i}_2 \sin\varphi, \quad \mathbf{e}_\varphi = -\mathbf{i}_1 \sin\varphi + \mathbf{i}_2 \cos\varphi, \end{gathered} \tag{14.44}$$

where the polar coordinates r and φ on the disc plane vary in the intervals $r_1 \le r \le r_0$ and $0 \le \varphi \le 2\pi$. In view of Eqs (14.8), (14.26) and (14.44), the system of Eqs (14.40), (14.42) and (14.43) is reduced to the equation

$$h'' - \frac{g'}{g}h' - g^2 h = \frac{(1 - rg)g}{1 - \nu}, \tag{14.45}$$

$$\nu = \frac{\lambda}{2(\lambda + \mu)}, \quad rg(r) = \int_{r_1}^{r} \beta(\rho)\rho\, d\rho + 1.$$

The strain components and couple stresses are expressed in terms of the functions $h(r)$ and $g(r)$ as

$$\begin{gathered} Y_1 = \frac{h'(r)}{rg(r)}, \quad l_1 = 0, \quad l_2 = g(r) - \frac{1}{r}, \\ \mathbf{K} = [g(r) - r^{-1}][(\gamma + \eta)\mathbf{e}_\varphi \otimes \mathbf{i}_3 + (\gamma - \eta)\mathbf{i}_3 \otimes \mathbf{e}_\varphi]. \end{gathered} \tag{14.46}$$

Equation (14.45) has the general solution

$$h(r) = C_1 e^{t(r)} + C_2 e^{-t(r)} + \frac{1}{1-\nu}\left[r - e^{-t(r)} \int e^{t(r)}\, dr\right],$$

$$t(r) = \int g(r)\, dr.$$

The constants C_1 and C_2 are found from the condition that the disc edges $r = r_1$ and r_0 are unloaded.

14.4 Singular Solutions of the Problems of the Nonlinear Theory of Elastic Dislocations

It is known [2, 3] that problems on the equilibrium of nonlinear elastic bodies containing dislocations or disclinations might have so called singular solutions describing the holes formation along the line of the defects. The integral relation was presented [3] that could be used to determine the radius of the forming hole depending on the model of elastic media and parameters of defect. For incompressible elastic cylinder this relation could be obtained by means of calculation the variation of the specific (per unit length) strain energy of the deformed cylinder Π with respect to virtual hole radius A:

$$\frac{\mathrm{d}\Pi}{\mathrm{d}A} = 2\pi \int_0^{r_0} r \frac{\partial W}{\partial \mathbf{C}} \odot \frac{\partial \mathbf{C}}{\partial A}\, dr = 0, \tag{14.47}$$

where $\mathbf{C}$ — deformation gradient tensor, $W(\mathbf{C})$ — strain-energy function, r_0 — radius of the cylinder in the undeformed state, $\odot$ denotes the inner product in the space of second-order tensors. Parameter A is the constant of integration when solving incompressibility condition $\det\mathbf{C} = 1$ to find the radius of the point of the cylinder in the deformed state $R = \sqrt{r^2 + A^2}$. It is obvious that for solid cylinder A has the sense of the hole radius; if $A = 0$ then no hole arises.

Since the vicinity of dislocation line (so called "dislocation core") is obviously the region of the high stress concentration the account of microstructure effects on its study within the framework of continuum mechanics seems to be quite actual. The simplest way of such microstructure accounting is the usage of Cosserat model of elastic media.

For the problem of the screw dislocation the deformed state of the cylinder with dislocation can be expressed by means of following semi-inverse representation

$$R = R(r), \quad \Phi = \varphi, \quad Z = a\varphi + z, \tag{14.48}$$

and

$$\mathbf{H} = \mathbf{e}_r\mathbf{e}_r + \cos\chi(r)(\mathbf{e}_\varphi\mathbf{e}_\varphi + \mathbf{e}_z\mathbf{e}_z) + \sin\chi(r)(\mathbf{e}_\varphi\mathbf{e}_z - \mathbf{e}_z\mathbf{e}_\varphi), \tag{14.49}$$

where $a = b/2\pi$, b — Burgers vector length.

Strain tensors $\mathbf{Y}$ and $\mathbf{L}$ relevant to (14.48), (14.49) have the form

$$\mathbf{Y} = R'(r)\mathbf{e}_r\mathbf{e}_r + \frac{1}{r}\left[R(r)\cos\chi(r) + a\sin\chi(r)\right]\mathbf{e}_\varphi\mathbf{e}_\varphi + \frac{1}{r}(a\cos\chi(r) -$$

$$-R(r)\sin\chi(r))\mathbf{e}_\varphi\mathbf{e}_z + \sin\chi(r)\mathbf{e}_z\mathbf{e}_\varphi + \cos\chi(r)\mathbf{e}_z\mathbf{e}_z, \quad (14.50)$$

$$\mathbf{L} = \chi'(r)\mathbf{e}_r\mathbf{e}_r + \frac{\sin\chi(r)}{r}\mathbf{e}_\varphi\mathbf{e}_\varphi + \frac{\cos\chi(r)-1}{r}\mathbf{e}_\varphi\mathbf{e}_z. \quad (14.51)$$

For the case of pseudo-Cosserat continuum function $\chi(r)$ is obtained from the conditions of constrained rotation $\mathbf{Y}_\times = 0$:

$$\chi(r) = \operatorname{arctg}\frac{a}{r+R}. \quad (14.52)$$

From all has been said it follows the relation for determination of the arising hole radius that replaces (14.47) in the case of incompressible Cosserat media

$$\frac{\mathrm{d}\Pi}{\mathrm{d}A} = 2\pi\int_0^{r_0} r\frac{\partial W}{\partial\mathbf{Y}}\odot\frac{\partial\mathbf{Y}}{\partial A}\,dr + 2\pi\int_0^{r_0} r\frac{\partial W}{\partial\mathbf{L}}\odot\frac{\partial\mathbf{L}}{\partial A}\,dr = 0. \quad (14.53)$$

The necessary condition of the hole formation can be written as some asymptotic condition for the function of specific potential energy. It follows from the condition of the convergence of integrals in (14.53) at the $R = 0$. For the most typical case of additive structure of the strain-energy function

$$W = W_{\mathrm{Y}}(\mathbf{Y}) + W_{\mathrm{L}}(\mathbf{L}),$$

we obtained two independent conditions for each integral. In particular for strain-energy function containing terms $\mathrm{tr}^\alpha\mathbf{L}$ the hole formation is possible only if $\alpha < 2$; if this function contains term $\mathrm{tr}(\mathbf{Y}-\mathbf{I})^n$ then cavitation can exist only for $n = 1$; for materials with strain-energy functions with terms $\mathrm{tr}^\alpha(\mathbf{L}\cdot\mathbf{L}^{\mathrm{T}})$, $\mathrm{tr}^\alpha(\mathbf{L}^2)$ the non-regular solution can exist only for $\alpha < 1$.

Some results of numerical investigation of the hole formation in the incompressible cylinder for pseudo-Cosserat continuum with the strain-energy function

$$W = 2\mu\,\mathrm{tr}\mathbf{U} + \eta\,|\mathrm{tr}\mathbf{L}|, \quad \mathbf{U} = \mathbf{Y} - \mathbf{E}, \quad (14.54)$$

are presented at the Fig. 14.2.

The solid line at the figure corresponds to the case of vanishing couple stresses when (14.54) reduces to the Bartenev-Hazanovich model. One can see that in this case the account of microstructure in the problem of screw dislocation leads to the decreasing of the formed hole radius in contrast with classical elastic media up to the total disappearance of the hole. It should be noted that in this case as well as in the case of momentless nonlinear elasticity the total energy of the cylinder with a hole is less than that of solid cylinder.

For more complex constitutive equation with energy

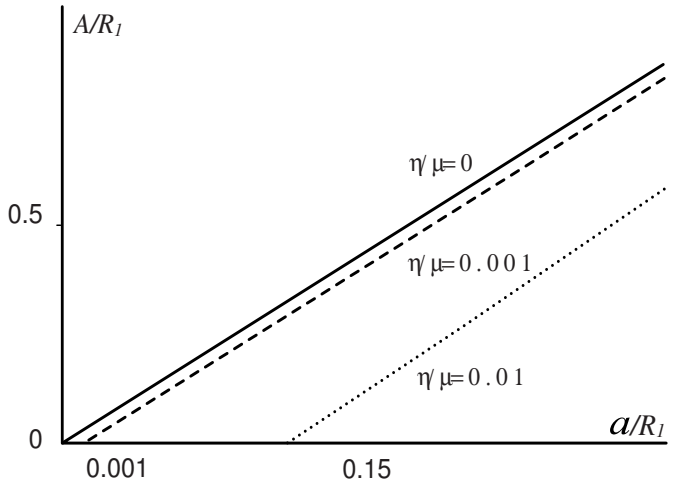

Fig. 14.2 The dependence of the hole radius on the dislocation parameter $a = b/2\pi$. Material (14.54).

$$W = 2\mu \operatorname{tr}\mathbf{U} + \frac{\eta}{\alpha} |\operatorname{tr}\mathbf{L}|^{\alpha} \tag{14.55}$$

the influence of couple stress upon the hole formation is not such unambiguous: the account of couple stresses might lead both to increasing and decreasing of the hole radius. There exists a region of material parameters of elastic potential (14.55) where the singular solution does not exist for some areas of the Burgers vector. It was shown numerically that it was the couple stresses component of elastic potential that influenced upon the disappearance of the singular solution.

It should be noted that the same analysis performed for the problem of wedge disclination showed that conversely to the case of screw dislocation the account for microstructure by means of Cosserats model doesn't lead to any changes in the ability of the hole formation as well as its size in comparison with classical nonlinear elasticity theory. All types of the considered Cosserat models (both compressible and incompressible, pseudo-continuum and true continuum) exhibit the same behavior in this sense.

Acknowledgements This work was supported by Russian Foundation for Basic Research (Project 09-01-00459) and by Federal Program "Scientific and pedagogical cadre of innovative Russia for 2009–2013 years".

References

[1] Derezin, S.V., Zubov L.M.: Equations of nonlinearly elastic media with continuously distributed dislocations and disclinations. Dokl. Phys. **44**, 391–394

(1999)
[2] Eremeev, V.A., Zubov, L.M., Karyakin, M.I., Chernega, N.Ya.: Formation of cavities in nonlinearly elastic bodies with dislocations and disclinations. Dokl. Ross. Akad. Nauk, **326**, 968–971 (1992)
[3] Karyakin, M.I., Pustovalova, O.G.: Singular solutions of the problems of the non-linear theory of elastic dislocations. Journal of Applied Mechanics and Technical Physics, **36**, 789–795 (1995)
[4] Nowacki, W.: On discrete dislocations in micropolar elasticity. Arch. Mech., **26**, No. 1, 3–11 (1974)
[5] Panin, V.E., Likhachev, V.A., Grinyaev, Yu.V.: *Structural Levels of Deformation of Solids*. Nauka, Novosibirsk (1985)
[6] Truesdell, C.: *A First Course in Rational Continuum Mechanics*. Academic Press, New York (1977)
[7] Vakulenko, A.A. Itogi Nauki Tekh., Ser.: Mekh. Deform. Tverd. Tela. **22**, 3 (1991)
[8] Zubov, L.M.: Isolated disclination in a nonlinearly elastic compressible body. Izv. Akad. Nauk SSSR, Mekh. Tverd. Tela. 1, 69–73 (1986)
[9] Zubov, L.M.: *Nonlinear Theory of Dislocations and Disclinations in Elastic Bodies*. Springer, Berlin (1997)

Chapter 15
On the Form-Invariance of Lagrangian Function for Higher Gradient Continuum

Nirmal Antonio Tamarasselvame and Lalaonirina R. Rakotomanana

Abstract In this work, we consider an elastic continuum of third grade. For the sake of simplicity, we do not consider kinetic energy in the Lagrangian function. In this work, we reformulate the problem by considering Lagrangian function depending on the metric tensor $\mathbf{g}$ and on the affine connection ∇ assumed to be compatible with the metric $\mathbf{g}$, and rewrite the Lagrangian function as $\mathscr{L}(\mathbf{g}, \nabla, \nabla^2)$. Following the method of Lovelock and Rund, we apply the form-invariance requirement to the Lagrangian $\mathscr{L}$. It is shown that the arguments of the function $\mathscr{L}$ are necessarily the torsion $\aleph$ and/or the curvature $\Re$ associated with the connection, in addition to the metric $\mathbf{g}$. The following results are obtained: (1) $\mathscr{L}(\mathbf{g}, \nabla)$ is form-invariant if and only if $\mathscr{L}(\mathbf{g}, \aleph)$; (2) $\mathscr{L}(\mathbf{g}, \nabla^2)$ is form-invariant if and only if $\mathscr{L}(\mathbf{g}, \Re)$; and (3) $\mathscr{L}(\mathbf{g}, \nabla, \nabla^2)$ is form-invariant if and only if $\mathscr{L}(\mathbf{g}, \aleph, \Re)$.

Key words: Strain gradient continuum. Form-invariance. Nonholonomic deformation. Quotient law.

15.1 Introduction

For analyzing the deformation of the elastic continuous media, the strain tensor and the stress are related by the constitutive laws. It is then convenient to introduce a potential energy function here denoted $\mathscr{W}$ and also called the strain energy function because of its dependence with respect to the strain. For extended model including couple-stress, the same kinematics as classical elasticity is used but the strain energy density is assumed to be a function of both the strain and the curl of strain e.g. [32]. Another extension of the model was the elastic continuum with micro-structure e.g.

Nirmal Antonio Tamarasselvame and Lalaonirina R. Rakotomanana
IRMAR - UMR 6625 CNRS, Université de Rennes 1, 35042 Rennes Cedex, France
e-mail: nirmal.antonio-tamarasselvame@univ-rennes1.fr,
e-mail: lalaonirina.rakotomanana-ravelonarivo@univ-rennes1.fr

H. Altenbach et al. (eds.), *Mechanics of Generalized Continua,*
Advanced Structured Materials, 7, DOI: 10.1007/978-3-642-19219-7_15,

[21] where the strain energy density is function of the strain, the first gradient of the strain and the second gradient of the strain.

15.1.1 Lagrangian Function

In continuum mechanics, the deformation is classically defined by means of the field of displacement vector $\mathbf{u}(\mathbf{x},t) \in \mathbb{R}^3$ defined on a manifold, where $\mathbf{x} \in \mathbb{R}^3$ and $t \in \mathbb{R}_+$ defines a material point position within the space and the time respectively e.g. [19]. In theory of elasticity, one uses the strain energy function $\mathscr{W} = \mathscr{W}(\mathbf{E})$ which depends only on strain tensor $\mathbf{E}$ (Green-Lagrange strain tensor). The strain tensor $\mathbf{E} = (1/2)(\nabla\mathbf{u} + \nabla^T\mathbf{u} + \nabla^T\mathbf{u}\nabla\mathbf{u})$ is formulated by means of covariant derivatives of displacement field $\mathbf{u}$. The symbol ∇ represents more generally an affine connection introduced for the derivation of tensor fields defined on a Riemannian manifold e.g. [19]. The (material) metric tensor $\mathbf{g} = \mathbf{I} + 2\mathbf{E}$ is related to strain, and consequently to derivatives of displacement. In elasticity, the Lagrangian scalar density $\mathscr{L}(\mathbf{u}_t, \nabla\mathbf{u}) = (\rho/2)\|\mathbf{u}_t\|^2 - \mathscr{W}(\nabla\mathbf{u})$ is used in dynamic problems to obtain the equations of motion [19]. The first term is the kinetic energy and the second term one the strain energy density (per volume unit). For the sake of simplicity in this paper, we do not consider kinetic energy in the Lagrangian density. Consequently we limit ourself to the strain energy density $\mathscr{L} \equiv \mathscr{W}$, third grade model accounting for the inertial terms may be found in e.g. [1] where they applied Noether's theorem for establishing conservation and balance laws. From another point of view, it may be observed that the introduction of the method of path-integration, or Cartan circuit method, allowed to point out the influence of the torsion tensor in the formulation of linear momentum conservation for discrete points e.g. [12] or continuous medium e.g. [13], [26].

In early 1960s, Toupin developed elastic continuum models with couple-stress [32] and observed that some components of the gradient of strain were not accounted for. Later he pointed out the correspondence of strain gradient elastic models and discrete lattice models of solids with nevertheless some flaws when considering centro-symmetric materials. To overcome this problem, Mindlin [21] have proposed a strain gradient theory, adapted for elastic material, in which the strain energy function is assumed to depend on both the strain, strain gradient, and second gradient of the strain. More recently, the correspondence of the second gradient strain continuum with fluid like material with heterogeneous density including capillarity effects was analyzed by Forest et al. [9]. It should be also noticed that the second gradient of strain theory may find its roots in the domain of solids with Volterra's dislocations where torsion and curvature tensors are involved e.g. [27]. More precisely, last 1999s and early 2000s, the strain gradient theory have been used notably in the works of Hutchinson and Fleck [7], [8], Nix, Gao and al. [10], [11], Cermelli and Gurtin [5]. The theories of elastic or elastic plastic continuous media were developed by accounting for the presence of dislocations and disclinations into the material (heterogeneous body), either with a strain gradient density e.g. [15], [16],

or in the context of affinely connected manifold with torsion e.g. [14], [24], [27], [33]. Constitutive laws of heterogeneous solids are obtained by choosing free energy functions depending on higher order of displacement and rotation gradient e.g. [18], or on density dislocation tensor e.g. [25]. Most of them were derived from original potential proposed by Mindlin e.g. [21].

All of these previous results suggested us to consider, in the present work, higher gradient continuum elastic properties which are often resumed by a potential energy function $\mathscr{W}(E_{ij}, E_{ij,k}, E_{ij,kl})$ depending on higher derivatives of the components of the strain tensor $\mathbf{E}$. In this work, we slightly modify the dependence and thus consider a strain gradient elastic continuum defined by a Lagrangian function of the type $\mathscr{L}(g_{\alpha\beta}, g_{\alpha\beta\,|\lambda}, g_{\alpha\beta\,|\lambda|\mu})$ where the (material) metric tensor $g_{\alpha\beta} := \delta_{\alpha\beta} + \nabla_\alpha u_\beta + \nabla_\beta u_\alpha + \nabla_\alpha u^\gamma \nabla_\beta u_\gamma$ is formulated by means of derivatives of displacement field $\mathbf{u}$ ($g_{\alpha\beta}$ is usually called Cauchy-Green strain tensor). We notice that quantities $g_{\alpha\beta}$ are the components of the metric tensor onto a material base which deforms with the continuum. A generic function of the type $\mathscr{L}(\nabla_\alpha u_\beta, \nabla_\lambda \nabla_\alpha u_\beta, \nabla_\mu \nabla_\lambda \nabla_\alpha u_\beta)$ can be considered for elastic material of grade three e.g. [1], such a model is included in the class of materials we are studying in the present paper. The symbol $|$ denotes the covariant derivative with respect to an affine connection ∇. It is reminded that the affine connection is not a tensor. Such a Lagrangian function defines second / third grade continuum models e.g. [21]. As we previously mention, we do not consider kinetic energy in the Lagrangian function.

15.1.2 Invariance Principles

Our investigations in the present work are focused on the invariance properties of the Lagrangian function, defined on a Riemannian manifold with an affine connection. It is necessary to define the notion of invariance of such function. We introduce three following notions of invariance: Euclidean-Frame-Indifference (EFI), Form-Invariance (FI) and Rigid-Motion-Indifference (RMI). These notions are more precisely defined in e.g. [30]:

- Euclidean-Frame-Indifference (EFI): Invariance with respect to Euclidean observers.
- Form-Invariance (FI): The Lagrangian function has the same mathematical shape in any coordinate system.
- Rigid-Motion-Indifference (RMI): Invariance with respect to superimposed rigid body motions.

The term ”invariance” is related to a mathematical function, it is then used for FI. Whereas the term ”indifference” is related to the visions of Euclidean observers (see [30]), it is then used for EFI and RMI. In the present paper, a method is given to select the invariant variables under the action of the homeomorphism, upon which this model must depend. Actually it will be the action of the diffeomorphism, since we work with a differential manifold and we will introduce some higher gradient

variables. In physics, form-invariance is also known as diffeomorphism-invariance meaning that the expression of physical quantities (for instance the energy) have the same form under the arbitrary coordinate transformation. It is merely a kind of change of variable with a diffeomorphism. The term "Form-invariance" is used instead of "diffeomorphism-invariance", but both of them may be used hereafter. Since we are dealing with continuum evolving in an Euclidean ambient space, the condition EFI is required for any constitutive laws. And it is also proved in [30] that any two of previous notions automatically imply the third. Consequently, the additional condition of FI allows to ensure the indifference of the constitutive laws with respect to the superimposed rigid body motion (RMI). In the following, central focus is the FI (under the action of the homeomorphisms, and more exactly of the diffeomorphisms in such a case) that appears like a mathematical condition for ensuring the principle of objectivity of constitutive laws of continuous medium. Principle based on homeomorphisms is unambiguously developed in lieu of the usual material frame-indifference.

15.1.3 Objectives

Many strain gradient models use an Euclidean connection which derives from the metric, e.g. [34] for which the connection is that of Levi-Civita. Any affine connection defines the tensor of torsion $\aleph$ and the tensor of curvature $\Re$ and according to the Fundamental theorem in Riemannian geometry, the torsion associated with the connection of Levi-Civita is null e.g. [4]. There exist some approaches based on Cartan geometry [3] with a connection which does not derive from the metric and for which the associated torsion and curvature do not necessarily vanish e.g [27]. The functions defined on Riemannian manifold should be tensors, which are used to represent physical fields. We aim to extend the form of the strain density $\mathscr{L}$, more precisely by analyzing the arguments of $\mathscr{L}$. For more generality we will consider a scalar field, also noted $\mathscr{L}$, rather than a density field. To obtain the corresponding density field, it is sufficient to multiply the scalar field by the volume-form, uniform and constant e.g. [28]. We will shed light on the invariance principle of the scalar field, or more precisely the Form-Invariance of the Lagrangian function. In a first part we consider a strain gradient elastic continuum defined by a Lagrangian function of the type $\mathscr{L}(\mathbf{g}, \nabla\mathbf{g}, \nabla^2\mathbf{g})$ which may be formulated $\mathscr{L}(g_{\alpha\beta}, g_{\alpha\beta\,|\gamma}, g_{\alpha\beta\,|\gamma|\lambda})$, in an arbitrary coordinate system (x^α). The symbol $|$ denotes the covariant derivative with respect to an affine connection ∇ (we call bi-connection the operator second covariant derivative $\nabla^2 = \nabla \circ \nabla$). Lovelock and Rund have shown that if one assumes a dependence as $\mathscr{L}(g_{\alpha\beta}, g_{\alpha\beta\,,\gamma})$ (comma denotes a partial derivative), then by applying the form-invariance requirement, the scalar function takes necessarily the form of $\mathscr{L}(g_{\alpha\beta})$. The first part of the present work was inspired in part of results in Lovelock and Rund, [17] (1975). In their work, Lovelock and Rund have implicitly used the Levi-Civita affine connection. By applying the Lemma of Ricci,

the covariant derivative of the metric tensor with respect to this connection is equal to zero e.g. [4].

Remark 15.1. It should be stressed that our purpose in this paper is not particularly to consider the formulation of constitutive laws satisfying the Euclidean Frame-Indifference and / or the Indifference with respect to Superimposed Rigid Body Motions such as rotations and translations. The term invariance is taken in the sense of Form-Invariance [30]. It is not limited to the so-called Euclidean objectivity. Indeed, by assuming that the potential energy density admits the metric tensor components as arguments, the Euclidean-Frame Indifference is *a priori* satisfied. We would like to go one step further for strain gradient continuum as in e.g. [31].

In a second part we consider both independent arguments metric and affine connection which is compatible with the metric (meaning that $\nabla \mathbf{g} \equiv 0$). To obviate the problem of metric compatibility, we slightly extend the dependence of the Lagrangian function by proposing the form of $\mathscr{L}(\mathbf{g}, \nabla, \nabla^2)$. Applying the form-invariance principle, it is shown that the arguments of the function $\mathscr{L}$ are necessarily the torsion $\mathfrak{K}$ and/or the curvature $\mathfrak{R}$ associated with the connection, in addition to the metric. Finally, the strain energy density of a continuous medium depends on tensorial arguments, which is expected to describe some physical phenomenons. To start with, we recall some mathematical preliminaries in differential geometry, necessary for our work.

15.2 Mathematical Preliminaries and Framework

15.2.1 Coordinate Systems

We fixe once and for all the n-dimensional vector space E (referential rigid body). An n-dimensional manifold X, embedded onto E, is a point set which is covered completely by a countable set of neighborhoods $U_1, U_2, ...$, such that each point $P \in X$ belongs to at least one of these neighborhoods. A coordinate system is defined on each U_k such that one may assign in a unique manner n real numbers $x^1, ..., x^n$ to each point $P \in U_k$. As P ranges over U_k, the corresponding numbers $x^1, ..., x^n$ range over an open domain D_k of E. Thus it exists a one-to-one mapping of each U_k onto D_k, this mapping will be assumed continuous. The numbers $x^1, ..., x^n$ are called the coordinates of P. In the case where $U_1 \cap U_2 \neq \emptyset$ there are two sets of coordinates associated to a same point $P \in U_1 \cap U_2$. Let (y^i) *(Latin indices)* and (x^α) *(Greek indices)* corresponding coordinate systems respectively in U_1 and U_2, Latin indices and Greek indices will be used to distinguish two different coordinate systems. The transformation between coordinates (y^i) and (x^α) is diffeomorphic:

$$y^i = y^i(x^\alpha), \quad x^\alpha = x^\alpha(y^i) \tag{15.1}$$

$$J_i^\alpha = \frac{\partial x^\alpha}{\partial y^i}, \quad J_{ij}^\alpha = \frac{\partial J_i^\alpha}{\partial y^j} = \frac{\partial^2 x^\alpha}{\partial y^i \partial y^j}, \quad J_{ijk}^\alpha = \frac{\partial J_{ij}^\alpha}{\partial y^k} = \frac{\partial^3 x^\alpha}{\partial y^i \partial y^j \partial y^k} \tag{15.2}$$

We also have that for any coordinate system (y^i), and for any permutation $\sigma \in \Im_n$

$$\frac{\partial^n}{\partial y^1 ... \partial y^n} = \frac{\partial^n}{\partial y^{\sigma(1)} ... \partial y^{\sigma(n)}} \tag{15.3}$$

When a lowercase index such as j, k, l,... appears twice in a term then summation over that index is implied. The range of summation is 1,..., n, the letter n is exceptionnaly exclued from the summation. We have

$$\frac{\partial x^\alpha}{\partial y^i}\frac{\partial y^i}{\partial x^\beta} = J_i^\alpha A_\beta^i = \delta_\beta^\alpha, \quad \frac{\partial y^i}{\partial x^\alpha}\frac{\partial x^\alpha}{\partial y^j} = A_\alpha^i J_j^\alpha = \delta_j^i \tag{15.4}$$

with respectively summation (Einstein's convention) over i and α from 1 to n.

15.2.2 Components of Tensor

We notice $T_P X$ the tangent space of X at point P and $T_P X^*$ its dual space. Let $\{\mathbf{e}_1, ..., \mathbf{e}_n\}$ a base of $T_P X$ (contravariant vectors with the lower index) and the reciprocal base $\{\mathbf{f}^1, ..., \mathbf{f}^n\}$ in $T_P X^*$ (covariant vectors with upper index) such that $\langle \mathbf{f}^i, \mathbf{e}_j \rangle = \delta_j^i$ (symbol of Kronecker).

Definition 15.1. (Tensor) Let $\{\mathbf{u}_1, ..., \mathbf{u}_q\} \in T_P X$ and $\{\mathbf{v}^1, ..., \mathbf{v}^p\} \in T_P X^*$ some arbitrary vectors. A p-contravariant and q-covariant tensor field $\mathscr{T}$ on X is a multilinear form defined at each point $P \in X$ by

$$\mathscr{T} : (\mathbf{v}^1, ..., \mathbf{v}^p, \mathbf{u}_1, ..., \mathbf{u}_q) \in (T_P X^*)^p \times (T_P X)^q \longrightarrow \mathscr{T}(\mathbf{v}^1, ..., \mathbf{v}^p, \mathbf{u}_1, ..., \mathbf{u}_q) \in \mathbb{R}$$

The sum $(p+q)$ is called the rank of the tensor field. The couple (p,q) is called its type.

Definition 15.2. (Components of tensor) If $\mathscr{T}$ is a tensor field of type (p,q) then the scalars $\mathscr{T}_{l_1 ... l_p}^{j_1 ... j_q}$ are the components of $\mathscr{T}$ with respect to the base formed by $\{\mathbf{e}_{j_1}, ..., \mathbf{e}_{j_q}\}$ and $\{\mathbf{f}^{l_1}, ..., \mathbf{f}^{l_p}\}$, defined by

$$\mathscr{T}_{j_1 ... j_q}^{l_1 ... l_p} = \mathscr{T}(\mathbf{f}^{l_1}, ..., \mathbf{f}^{l_p}, \mathbf{e}_{j_1}, ..., \mathbf{e}_{j_q})$$

In the present study, a tensor will be assimilated to its components, as soon as the vector bases are defined.

Definition 15.3. If $\mathscr{T}_{k_1 ... k_s}^{h_1 ... h_r}$ constitutes the components of a tensor type (r,s) then, under the transformation (15.1)

$$\mathscr{T}_{l_1 ... l_s}^{j_1 ... j_r} = A_{\alpha_1}^{j_1} ... A_{\alpha_r}^{j_r} J_{l_1}^{\beta_1} ... J_{l_s}^{\beta_s} \mathscr{T}_{\beta_1 ... \beta_s}^{\alpha_1 ... \alpha_r} \tag{15.5}$$

and the corresponding inverse formulation

$$\mathscr{T}^{\alpha_1\ldots\alpha_r}_{\beta_1\ldots\beta_s} = J^{\alpha_1}_{j_1}\ldots J^{\alpha_r}_{j_r} A^{l_1}_{\beta_1}\ldots A^{l_s}_{\beta_s}\mathscr{T}^{j_1\ldots j_r}_{l_1\ldots l_s} \tag{15.6}$$

Properties 15.2.1 *According to the previous results:*

- *A scalar ψ is a tensor type $(0,0)$ which has the same form in any coordinate system : ψ in (y^i), $\overline{\psi}$ in (x^α) and $\psi = \overline{\psi}$.*
- *If all the components of a tensor vanish in an arbitrary coordinate system then they vanish in any other coordinate system.*

Definition 15.4. (Metric) A metric tensor, noted $\mathbf{g}$, is a tensor type $(0,2)$, symmetric and inversible. In base $\{\mathbf{e}_1,...,\mathbf{e}_n\}$, the components of $\mathbf{g}$ are g_{ij}, the components of the inverse of $\mathbf{g}$ are g^{ij} and $g^{ik}g_{kj} = \delta^i_j$.

Definition 15.5. (Riemannian manifold) A differential manifold X endowed with a metric $(X,\mathbf{g})$ is a Riemannian manifold.

In the present paper, the choice of a metric tensor components $g_{\alpha\beta}$ may be explained as follows. Locally, at any point $P \in X$ of the Riemannian manifold, it should be mentioned that in any coordinate basis, the tangent space T_PX is spanned by $\{\mathbf{e}_1,\cdots,\mathbf{e}_n\}$, and the dual space T_PX^* by $\{\mathbf{f}^1,\cdots,\mathbf{f}^n\}$. There is an alternative choice by taking the base defined as $\hat{\mathbf{e}}_a := \mathbf{F}^{-1}(\mathbf{e}_a)$, where $\det\mathbf{F} > 0$, and in such a way that $\mathbf{g}(\hat{\mathbf{e}}_b,\hat{\mathbf{e}}_b) := \delta_{ab}$. The quantity $\mathbf{F}$ is related to the so-called gradient of transformation in continuum mechanics e.g. [19], or also "vielbeins" in differential geometry e.g. [23]. In the present paper, $\mathbf{F}$ is not necessarily a gradient of a mapping. In continuum mechanics, it is thus possible to define the Green-Lagrange strain tensor $\mathbf{E}$ as follows:

$$E_{\alpha\beta} := (1/2)\left[\mathbf{g}\left(\mathbf{e}_\alpha,\mathbf{e}_\beta\right) - \mathbf{g}\left(\hat{\mathbf{e}}_\alpha,\hat{\mathbf{e}}_\beta\right)\right]$$

Conceptually, it is not necessary to introduce the tensor $\mathbf{E}$ as a basic strain variable, $\mathbf{g}$ being sufficient. We just remind that the arguments of any scalar field $\mathscr{L}$ may be chosen as the components of the metric $g_{\alpha\beta}$ onto a "deformed base" $\{\mathbf{e}_1,\cdots,\mathbf{e}_n\}$, according to a linear tangent transformation $\mathbf{F}$, instead of $E_{\alpha\beta}$.

Remark 15.2. The definition of strain $\mathbf{E}$ do not require *a priori* the explicit introduction of displacement field and its gradient. It merely expresses the difference of shape between two configurations of a continuum. This aspect will be detailed in the following.

15.2.3 Affine Connection

A connection is an extra structure which specifies how vectors and more generally tensors are transported along a curve on the manifold. An infinite number of connections exist on a manifold X, such as affine connection, geodesic connection and crystal connection. A local tangent base is associated to a coordinate system: the contravariant base $\{\mathbf{e}_\alpha\}$ is associated to the system $\{y^\alpha\}$.

Definition 15.6. (Affine connection) An affine connection ∇ on X is a map defined by

$$\nabla : (\mathbf{u}, \mathbf{v}) \in T_P(X) \times T_P(X) \longrightarrow \nabla_{\mathbf{u}}\mathbf{v} \in T_P(X) \tag{15.7}$$

wich satifies the following conditions (λ and μ are scalars, ϕ is scalar field)

- $\nabla_{\lambda\mathbf{u}_1+\mu\mathbf{u}_2}\mathbf{v} = \lambda\nabla_{\mathbf{u}_1}\mathbf{v} + \mu\nabla_{\mathbf{u}_2}\mathbf{v}$
- $\nabla_{\mathbf{u}}(\lambda\mathbf{v}_1 + \mu\mathbf{v}_2) = \lambda\nabla_{\mathbf{u}}\mathbf{v}_1 + \mu\nabla_{\mathbf{u}}\mathbf{v}_2$
- $\nabla_{\phi\mathbf{u}}\mathbf{v} = \phi\nabla_{\mathbf{u}}\mathbf{v}$
- $\nabla_{\mathbf{u}}(\phi\mathbf{v}) = \phi\nabla_{\mathbf{u}}\mathbf{v} + \mathbf{u}(\phi)\mathbf{v}$

The coefficients of the affine connection are Γ^c_{ab} such that $\nabla_{\mathbf{e}_a}\mathbf{e}_b := \Gamma^c_{ab}\mathbf{e}_c$. The quantity $\nabla_{\mathbf{u}}$ represents a derivative along the direction $\mathbf{u}$. It is usual to define the covariant derivative, which generalizes the derivative of tensor fields defined on manifold, in the sense of the affine connection ∇. The covariant derivative of a tensor type (p,q) is a tensor type $(p,q+1)$. For example, the covariant derivative of a scalar field ϕ and a vector field $\mathbf{w}$ along the vector $\mathbf{e}_k$ (one of the vectors of the base) may be expressed in terms of their components on the local base $\{\mathbf{e}_a\}$ associated to the coordinate system (y^a)

$$\nabla_{\mathbf{e}_k}\phi = \frac{\partial\phi}{\partial y^k}, \qquad \nabla_{\mathbf{e}_k}\mathbf{w} = \left(\frac{\partial w^a}{\partial y^k} + \Gamma^a_{kc}w^c\right)\mathbf{e}_a.$$

For tensor components, we adopt the notations $\dfrac{\partial(..)}{\partial y^k} = (..)_{,k}$ and $\nabla_{\mathbf{e}_k}(..) = (..)_{|k}$.

15.2.3.1 Torsion and Curvature

We now consider a manifold endowed with an affine connection ∇.

Definition 15.7. (Torsion) The torsion tensor $\aleph$ is a tensor type $(1,2)$

$$\begin{cases} \aleph\left(\mathbf{f}^k, \mathbf{e}_i, \mathbf{e}_j\right) = \mathbf{f}^k\left(\nabla_{\mathbf{e}_i}\mathbf{e}_j - \nabla_{\mathbf{e}_j}\mathbf{e}_i\right) \\ \aleph^k_{ij} = \Gamma^k_{ij} - \Gamma^k_{ji} \end{cases} \tag{15.8}$$

Definition 15.8. (Curvature) The curvature tensor $\mathfrak{R}$ is a tensor type $(1,3)$

$$\begin{cases} \mathfrak{R}\left(\mathbf{f}^k, \mathbf{e}_i, \mathbf{e}_j, \mathbf{e}_l\right) = \mathbf{f}^k\left(\nabla_{\mathbf{e}_i}\nabla_{\mathbf{e}_j}\mathbf{e}_l - \nabla_{\mathbf{e}_j}\nabla_{\mathbf{e}_i}\mathbf{e}_l\right) \\ \mathfrak{R}^k_{ijl} = (\Gamma^k_{jl,i} + \Gamma^m_{jl}\Gamma^k_{im}) - (\Gamma^k_{il,j} + \Gamma^m_{il}\Gamma^k_{jm}) \end{cases} \tag{15.9}$$

Remark 15.3. First, the definition of the torsion and the curvature tensors do not require the existence of a metric tensor on the manifold. Second, there exist general definitions of the torsion and the curvature, which used the Lie-Jacobi bracket e.g. [4]. The theorem of Frobenius, e.g. [23], allows to simplify the expression of the torsion and the curvature projected onto the vector base associated to a coordinate system.

15.2.3.2 Levi-Civita Connection

The connection of Levi-Civita is an example of Euclidean connection (derived from the metric) and introduced by the following fundamental theorem, see proof in e.g. [23]:

Theorem 15.1. *(Fundamental theorem of Riemannian geometry) On any Riemannian manifold $(X,\mathbf{g})$, there exists a unique connection compatible with the metric and free-torsion ($\aleph = 0$). This connection is called the Levi-Civita connection and usually denoted $\overline{\nabla}$.*

The coefficients of $\overline{\nabla}$ reduce to the symbols of Christoffel $\dfrac{\partial \mathbf{e}_b}{\partial y^a} = \overline{\Gamma}^c_{ba}\mathbf{e}_c$, calculated in terms of the metric $\mathbf{g}$ e.g. [23]

$$\overline{\Gamma}^c_{ab} = (1/2)g^{cd}(g_{ad,b} + g_{db,a} - g_{ab,d}) \tag{15.10}$$

For example, if $\mathbf{h}$ is a tensor type $(0,2)$ then the covariant derivative (in the sense of Levi-Civita) with respect to $\mathbf{e}_k$ (a vector of the base) is a tensor type $(0,2+1)$ for which the coordinates are noticed

$$\overline{\nabla}_{\mathbf{e}_k} h_{ij} = h_{ij|k} = \left(h_{ij,k} - \Gamma^a_{ik}h_{aj} - \Gamma^a_{jk}h_{ia}\right) \tag{15.11}$$

and then with respect to $\mathbf{e}_l$ (vector of the base), the second covariant derivative (in the sense of Levi-Civita) is $\overline{\nabla}_{\mathbf{e}_l}\left[\overline{\nabla}_{\mathbf{e}_k} h_{ij}\right] = h_{ij|k|l}$ with

$$\begin{aligned} h_{ij|k|l} = {} & h_{ij,kl} - \Gamma^a_{ik}h_{aj,l} - \Gamma^a_{jk}h_{ia,l} - \Gamma^a_{ik,l}h_{aj} - \Gamma^a_{jk,l}h_{ia} - \Gamma^b_{il}h_{bj,k} \\ & + \Gamma^b_{il}(\Gamma^c_{bk}h_{cj} + \Gamma^c_{jk}h_{bc}) - \Gamma^b_{jl}h_{ib,k} + \Gamma^b_{jl}(\Gamma^c_{ik}h_{cb} + \Gamma^c_{bk}h_{ic}) \\ & - \Gamma^b_{kl}h_{ij,b} + \Gamma^b_{kl}(\Gamma^c_{ib}h_{cj} + \Gamma^c_{jb}h_{ic}) \end{aligned} \tag{15.12}$$

where we have considered $\overline{\Gamma} = \Gamma$ for the sake of the simplicity.

Properties 15.2.2 *Let X a Riemannian manifold and $P \in X$ any point. In orthonormal base (associated to a normal coordinate system) centered on P, the symbols of Christoffel vanish: $\overline{\Gamma}^k_{ij}(P) = 0$ for $i,j,k = 1,...,n$.*

Remark 15.4. A normal coordinate system on a Riemannian manifold centered at P may be also defined by local relations:

$$g_{\alpha\beta}(P) := \delta_{\alpha\beta}\,, \qquad \overline{\Gamma}^{\gamma}_{\alpha\beta}(\xi)\,\xi^{\alpha}\xi^{\beta} \equiv 0$$

where $(\xi^1,\cdots,\xi^n)$ are local coordinates of points $P' := P + \xi$ about the center P. Riemannian normal coordinates are a standard tool of various differential geometry theorems, their choice to derive equations allow to simplify most problems.

No confusion will be done between the differentiation of any tensor field with respect to y^k (in the sense of Levi-Civita) and the differentiation with respect to the affine connection $\nabla_{\mathbf{e}_k}$.

15.2.4 Holonomic and Nonholonomic Transformations

Consider a Riemannian manifold $(X, \mathbf{g})$ embedded in a n-dimensional Euclidean space E. Let $\mathbf{X} \in X$ a point of the manifold, and let consider a mapping φ which associates $\mathbf{X}$ to a point of the Euclidean space $\mathbf{x} \in E$. We denote the mapping $\mathbf{x}(\mathbf{X})$ for simplifying. For the sake of the simplicity, we assume that the coordinates $\mathbf{X} = (X^1, \cdots, X^n)$ are Cartesian.

15.2.4.1 Holonomic Mapping

Let consider a smooth and single valued mapping (it is a homeomorphism and we call it holonomic mapping e.g. [27]). It is usual to define the deformation gradient also called basis triads (rigorously it is not a gradient) in components form, together with its reciprocal basis triads:

$$F_\alpha^i(\mathbf{X}) := \frac{\partial x^i}{\partial X^\alpha}(\mathbf{X}), \qquad F_j^\beta(\mathbf{x}) := \frac{\partial X^\beta}{\partial x^j}(\mathbf{x})$$

The triads satisfy the orthogonality and the completeness relationships:

$$F_\alpha^i(\mathbf{X})\ F_i^\beta[\mathbf{x}(\mathbf{X})] = \delta_\alpha^\beta, \qquad F_\alpha^i(\mathbf{X})\ F_j^\alpha[\mathbf{x}(\mathbf{X})] = \delta_j^i$$

We may write the vector transformation and the components of the metric tensor, where $\hat{\mathbf{e}}_i$ is a vector rigidly attached to the Euclidean space E:

$$\mathbf{e}_\alpha = F_\alpha^i\ \hat{\mathbf{e}}_i, \qquad g_{\alpha\beta} = \mathbf{g}\left(\mathbf{e}_\alpha, \mathbf{e}_\beta\right)$$

On the one hand, since the transformation $\mathbf{x}(\mathbf{X})$ is smooth and single valued, it is integrable, i.e. its derivative commute, by using the classic Schwarz's integrability conditions:

$$\frac{\partial F_\alpha^i}{\partial X^\beta} - \frac{\partial F_\beta^i}{\partial X^\alpha} = \frac{\partial^2 x^i}{\partial X^\beta \partial X^\alpha} - \frac{\partial^2 x^i}{\partial X^\alpha \partial X^\beta} = 0$$

On the other hand, we can differentiate the vector base, :

$$\frac{\partial \mathbf{e}_\alpha}{\partial X^\beta} := \Gamma_{\alpha\beta}^\gamma\ \mathbf{e}_\gamma = \frac{\partial F_\alpha^i}{\partial X^\beta}\ \hat{\mathbf{e}}_i = \frac{\partial F_\alpha^i}{\partial X^\beta}\ F_i^\gamma\ \mathbf{e}_\gamma \quad \Longrightarrow \quad \Gamma_{\alpha\beta}^\gamma = \frac{\partial F_\alpha^i}{\partial X^\beta}\ F_i^\gamma$$

Then it is straightforward to check that the torsion tensor is equal to zero during an holonomic transformation:

$$\aleph_{\alpha\beta}^\gamma := \left(\frac{\partial F_\alpha^i}{\partial X^\beta} - \frac{\partial F_\beta^i}{\partial X^\alpha}\right) F_i^\gamma = 0$$

15.2.4.2 Nonholonomic Mapping and Torsion

Let consider mapping that is not smooth and/or not single valued. In such a case, the basis triads are not integrable. However, it is possible to map the points surrounding $\mathbf{X}$ defined by the tangent vector $d\mathbf{X}$ to the vector $d\mathbf{x}$ via an infinitesimal transformation defined by the triads:

$$\mathbf{e}_\alpha = F^i_\alpha \, \hat{\mathbf{e}}_i, \qquad dx^i = F^i_\alpha \, dX^\alpha$$

in which the coefficients functions $F^i_\alpha(\mathbf{X})$ are not integrable in the sense of

$$\frac{\partial F^i_\alpha}{\partial X^\beta} - \frac{\partial F^i_\beta}{\partial X^\alpha} = \frac{\partial^2 x^i}{\partial X^\beta \partial X^\alpha} - \frac{\partial^2 x^i}{\partial X^\alpha \partial X^\beta} \neq 0$$

In such a case, the mapping is called nonholonomic. It is necessary to modify slightly the previous development to give (the base $\{\hat{\mathbf{e}}_1, \cdots, \hat{\mathbf{e}}_n\}$ is assumed rigidly attached to the Euclidean space):

$$\frac{\partial \mathbf{e}_\alpha}{\partial X^\beta} - \frac{\partial \mathbf{e}_\beta}{\partial X^\alpha} = \left(\frac{\partial F^i_\alpha}{\partial X^\beta} - \frac{\partial F^i_\beta}{\partial X^\alpha} \right) F^\gamma_i \mathbf{e}_\gamma \neq 0$$

showing that the torsion tensor $\aleph^\gamma_{\beta\alpha} \, \mathbf{e}_\gamma$ is not equal to zero for such a nonholonomic mapping. It does not lead to a single valued mapping $\mathbf{x}(\mathbf{X})$. Such a transformation may capture the translational dislocations of Volterra e.g. [20].

15.2.4.3 Nonholonomic Transformation and Curvature

As third example, consider a transformation for which $\mathbf{x}(\mathbf{X})$ may be or not itself integrable, while the first derivatives of the vectors $\{\mathbf{e}_1, \cdots, \mathbf{e}_n\}$, where $\mathbf{e}_\alpha := F^i_\alpha \, \hat{\mathbf{e}}_i$, are not integrable. Such non integrability is captured by the non commutativity of the second-order derivatives:

$$\frac{\partial}{\partial X^\alpha} \left(\frac{\partial \mathbf{e}_\lambda}{\partial X^\beta} \right) - \frac{\partial}{\partial X^\beta} \left(\frac{\partial \mathbf{e}_\lambda}{\partial X^\alpha} \right) = \frac{\partial}{\partial X^\alpha} \left(\Gamma^\kappa_{\lambda\beta} \mathbf{e}_\kappa \right) - \frac{\partial}{\partial X^\beta} \left(\Gamma^\kappa_{\lambda\alpha} \mathbf{e}_\kappa \right)$$

From this relation, we easily deduce that the Cartan curvature is not equal to zero:

$$\mathfrak{R}^\kappa_{\alpha\beta\lambda} = \left(\Gamma^\kappa_{\beta\lambda\,,\alpha} + \Gamma^\xi_{\beta\lambda} \Gamma^\kappa_{\alpha\xi} \right) - \left(\Gamma^\kappa_{\alpha\lambda\,,\beta} + \Gamma^\xi_{\alpha\lambda} \, \Gamma^\kappa_{\beta\xi} \right) \neq 0$$

We can also calculate the non-commutativity by directly introducing the basis triads to give

$$\mathfrak{R}^\kappa_{\alpha\beta\lambda} = F^\kappa_i \left(\frac{\partial^2 F^i_\lambda}{\partial X^\alpha \partial X^\beta} - \frac{\partial^2 F^i_\lambda}{\partial X^\beta \partial X^\alpha} \right) \neq 0$$

Such a transformation may be related to the process of rotational dislocations e.g. [20], or some plastic deformation. This short section permits us to highlight the role of torsion and curvature tensors on the classification of continuum transformations. More general proof may be found in a previous work, devoted to the class of "weakly continuous medium" [26].

Remark 15.5. Torsion tensor is associated to translational dislocations or also to the local discontinuity of any scalar field on the continuum, while curvature tensor is associated to the rotational dislocations or also to the local discontinuity of vector field on the continuum [26] .

15.3 Quotient Law

Now we remind some technical theorems in tensorial analysis [17].

Lemma 15.1. *Locally at point P, let the both* $(n \times n)$ *quantities* Σ^{ij} *and* $\overline{\Sigma}^{ij}$ *then the both* $(n \times n \times n)$ *quantities* $\Sigma^{ij,k}$ *and* $\overline{\Sigma}^{ij,k}$ *(the comma "," doesn't represent partial derivative). If, for any symmetric tensor type (0,2) h,*

$$\Sigma^{ij} h_{ij} + \Sigma^{ij,k} h_{ij|k} = \overline{\Sigma}^{ij} h_{ij} + \overline{\Sigma}^{ij,k} h_{ij|k} \tag{15.13}$$

then

$$(\Sigma^{ij} + \Sigma^{ji}) = (\overline{\Sigma}^{ij} + \overline{\Sigma}^{ji}) \tag{15.14}$$

and

$$(\Sigma^{ij,k} + \Sigma^{ji,k}) = (\overline{\Sigma}^{ij,k} + \overline{\Sigma}^{ji,k}) \tag{15.15}$$

for i, j, k = $1, ..., n$

Proof. The equality (15.13) being valid for any symmetric tensor h, it is thus valid for a non null constant tensor (locally). The covariant derivative vanishes and from (15.13) we have the following equality $(\Sigma^{ij})h_{ij} = (\overline{\Sigma}^{ij})h_{ij}$. The term h_{ij} cannot simplify because of the summation in i and j. For i and j fixed, we choose $h_{ij} = h_{ji} = 1$ and the other components null. For i and j range over $\{1, ..., n\}$, we obtain

$$\begin{cases} \Sigma^{11} = \overline{\Sigma}^{11} \\ \Sigma^{12} + \Sigma^{21} = \overline{\Sigma}^{12} + \overline{\Sigma}^{21} \\ \Sigma^{13} + \Sigma^{31} = \overline{\Sigma}^{13} + \overline{\Sigma}^{31} \\ \quad \ldots \end{cases} \tag{15.16}$$

thus we obtain (15.14). In the same way, locally at point P, a null tensor h with a non null constant covariant derivative can be chosen too. In this case from (15.13) $(\Sigma^{ij,k})h_{ij|k} = (\overline{\Sigma}^{ij,k})h_{ij|k}$. The term $h_{ij|k}$ cannot simplified because of the summation in i, j and k. For i, j and k fixed, we choose $h_{ij|k} = h_{ji|k} = 1$ and the other components null. For i, j and k range over $\{1, ..., n\}$, we obtain

$$\begin{cases} \Sigma^{11,1} = \overline{\Sigma}^{11,1} \\ \Sigma^{11,2} = \overline{\Sigma}^{11,2} \\ \Sigma^{12,1} + \Sigma^{21,1} = \overline{\Sigma}^{12,1} + \overline{\Sigma}^{21,1} \\ \Sigma^{12,2} + \Sigma^{21,2} = \overline{\Sigma}^{12,2} + \overline{\Sigma}^{21,2} \\ \Sigma^{13,1} + \Sigma^{31,1} = \overline{\Sigma}^{13,1} + \overline{\Sigma}^{31,1} \\ \Sigma^{13,2} + \Sigma^{31,2} = \overline{\Sigma}^{31,2} + \overline{\Sigma}^{31,2} \\ \quad \ldots \end{cases} \tag{15.17}$$

thus we obtain (15.15).

□

We have also the version with the partial derivative:

Lemma 15.2. *Locally at point P, let the both $(n \times n)$ quantities Σ^{ij} and $\overline{\Sigma}^{ij}$ then the both $(n \times n \times n)$ quantities $\Sigma^{ij,k}$ and $\overline{\Sigma}^{ij,k}$ (the comma "," doesn't represent partial derivative). If, for any symmetric tensor type (0,2) h,*

$$\Sigma^{ij} h_{ij} + \Sigma^{ij,k} h_{ij,k} = \overline{\Sigma}^{ij} h_{ij} + \overline{\Sigma}^{ij,k} h_{ij,k} \tag{15.18}$$

then

$$(\Sigma^{ij} + \Sigma^{ji}) = (\overline{\Sigma}^{ij} + \overline{\Sigma}^{ji}) \tag{15.19}$$

and

$$(\Sigma^{ij,k} + \Sigma^{ji,k}) = (\overline{\Sigma}^{ij,k} + \overline{\Sigma}^{ji,k}) \tag{15.20}$$

for i, j, k = 1,...,n

Now the following quotient theorem holds e.g. [17]

Theorem 15.2. *(Quotient law) Locally at point P, if the $(n \times n)$ quantities Σ^{ij} and the $(n \times n \times n)$ quantities $\Sigma^{ij,k}$ (the comma "," doesn't represent the partial derivative) are such that the quantities $\Sigma^{ij} h_{ij} + \Sigma^{ij,k} h_{ij|k}$ represent a scalar field for any symmetric tensor type (0,2) h, then the quantities $(\Sigma^{ij} + \Sigma^{ji})$ and $(\Sigma^{ij,k} + \Sigma^{ji,k})$ represent respectively the components of a tensor type (2,0) and the components of a tensor type (3,0).*

Proof. Let define the scalar $\psi = \Sigma^{ij} h_{ij} + \Sigma^{ij,k} h_{ij|k}$ and $\overline{\psi} = \Sigma^{\alpha\beta} h_{\alpha\beta} + \Sigma^{\alpha\beta,\gamma} h_{\alpha\beta|\gamma}$ in the system (y^i) and (x^α) respectively for any symmetric tensor type (0,2) h. The equality $\psi = \overline{\psi}$ becomes

$$\Sigma^{ij} h_{ij} + \Sigma^{ij,k} h_{ij|k} = \Sigma^{\alpha\beta} \frac{\partial y^i}{\partial x^\alpha} \frac{\partial y^j}{\partial x^\beta} h_{ij} + \Sigma^{\alpha\beta,\gamma} \frac{\partial y^i}{\partial x^\alpha} \frac{\partial y^j}{\partial x^\beta} \frac{\partial y^k}{\partial x^\gamma} h_{ij|k} \tag{15.21}$$

According to the lemma 15.1

$$\Sigma^{ij} + \Sigma^{ji} = \Sigma^{\alpha\beta} \frac{\partial y^i}{\partial x^\alpha} \frac{\partial y^j}{\partial x^\beta} + \Sigma^{\alpha\beta} \frac{\partial y^j}{\partial x^\alpha} \frac{\partial y^i}{\partial x^\beta} \tag{15.22}$$

and

$$\Sigma^{ij,k} + \Sigma^{ji,k} = \Sigma^{\alpha\beta\,,\gamma} \frac{\partial y^i}{\partial x^\alpha} \frac{\partial y^j}{\partial x^\beta} \frac{\partial y^k}{\partial x^\gamma} + \Sigma^{\alpha\beta\,,\gamma} \frac{\partial y^j}{\partial x^\alpha} \frac{\partial y^i}{\partial x^\beta} \frac{\partial y^k}{\partial x^\gamma} \tag{15.23}$$

then a permutation between i and j gives

$$\begin{cases} \Sigma^{ij} + \Sigma^{ji} = (\Sigma^{\alpha\beta} + \Sigma^{\beta\alpha}) \dfrac{\partial y^i}{\partial x^\alpha} \dfrac{\partial y^j}{\partial x^\beta} \\ \Sigma^{ij,k} + \Sigma^{ji,k} = (\Sigma^{\alpha\beta\,,\gamma} + \Sigma^{\beta\alpha,\gamma}) \dfrac{\partial y^i}{\partial x^\alpha} \dfrac{\partial y^j}{\partial x^\beta} \dfrac{\partial y^k}{\partial x^\gamma} \end{cases} \tag{15.24}$$

Therefore $(\Sigma^{ij} + \Sigma^{ji})$ and $(\Sigma^{ij,k} + \Sigma^{ji,k})$ are respectively components of tensor type (2,0) and (3,0) according to the definitions (15.5) and (15.6).

□

15.4 Dependence with Respect to the Metric

In this section, we consider a scalar field $\mathscr{L}$ depending on the metric tensor and its partial derivatives $\mathscr{L} = \mathscr{L}(g_{ij}, g_{ij,k}, g_{ij,kl})$ and $\mathscr{L} = \mathscr{L}(g_{\alpha\beta}, g_{\alpha\beta\,,\gamma}, g_{\alpha\beta\,,\gamma\lambda})$ respectively in system (y^i) and (x^α). The corresponding partial derivatives are noticed

$$\Lambda^{ij} = \frac{\partial \mathscr{L}}{\partial g_{ij}}, \quad \Lambda^{ij,k} = \frac{\partial \mathscr{L}}{\partial g_{ij,k}}, \quad \Lambda^{ij,kl} = \frac{\partial \mathscr{L}}{\partial g_{ij,kl}}. \tag{15.25}$$

According to the symmetry of $\mathbf{g}$, we have the major properties of symmetry

$$\Lambda^{ij} = \Lambda^{ji}, \quad \Lambda^{ij,k} = \Lambda^{ji,k}, \quad \Lambda^{ij,kl} = \Lambda^{ji,kl} = \Lambda^{ij,lk}. \tag{15.26}$$

Minor symmetry property $\Lambda^{ij,kl} = \Lambda^{kl,ij}$ is also satisfied but they are not necessary here. The form-invariance of the Lagrangian function $\mathscr{L}$ (which could be considered as a necessary part of the Indifference of the constitutive laws with respect to Superimposed Rigid Body Motions e.g. [2]) takes the form of

$$\mathscr{L}(g_{\alpha\beta}, g_{\alpha\beta\,,\gamma}, g_{\alpha\beta\,,\gamma\lambda}) = \mathscr{L}(g_{ij}, g_{ij,k}, g_{ij,kl}). \tag{15.27}$$

Remark 15.6. For recall, because no observer is distinguished, laws in physics have to be observer-invariant. For our particular case about the Lagrangian function formulation, this means that the functions $\mathscr{L}$ should have the same shape for arbitrary coordinate systems: they are called form-invariant.

15.4.1 Metric Tensor

According to the definitions (15.5) and (15.6), the components of the metric and its derivatives satisfy the following transformations

$$\left\{\begin{array}{l} g_{ij} = J_i^\alpha J_j^\beta g_{\alpha\beta} \\ g_{ij,k} = (J_{ik}^\alpha J_j^\beta + J_i^\alpha J_{jk}^\beta) g_{\alpha\beta} + J_i^\alpha J_j^\beta J_k^\gamma g_{\alpha\beta,\gamma} \\ g_{ij,kl} = (J_{ikl}^\alpha J_j^\beta + J_{ik}^\alpha J_{jl}^\beta + J_{il}^\alpha J_{jk}^\beta + J_i^\alpha J_{jkl}^\beta) g_{\alpha\beta} \\ \qquad + \ (J_{ik}^\alpha J_j^\beta J_h^\gamma + J_i^\alpha J_{jk}^\beta J_l^\gamma + J_{il}^\alpha J_j^\beta J_k^\gamma + J_i^\alpha J_{jl}^\beta J_k^\gamma + J_i^\alpha J_j^\beta J_{kl}^\gamma) g_{\alpha\beta,\gamma} \\ \qquad + \ (J_i^\alpha J_j^\beta J_k^\gamma J_l^\lambda) g_{\alpha\beta,\gamma\lambda} \end{array}\right. \tag{15.28}$$

According to the symmetry $J_{pq}^\mu = J_{qp}^\mu$ (the transformation is assumed of class C^2), one can write $J_{pq}^\mu = (1/2)(J_{pq}^\mu + J_{qp}^\mu)$, that induces [1] $(\partial J_{ij}^\alpha / \partial J_{pq}^\mu) = (1/2)\delta_\mu^\alpha(\delta_i^q \delta_j^p + \delta_j^q \delta_i^p)$, $(\partial J_{ijk}^\alpha / \partial J_{pq}^\mu) = 0$ and $(\partial J_i^\alpha / \partial J_{pq}^\mu) = 0$. Now, introducing the expressions (15.28) into the equality (15.27), and differentiating with respect to J_{pq}^μ give

$$\begin{aligned} 0 = {} & \Lambda^{ij,k}\left[\delta_\mu^\alpha(\delta_k^q\delta_i^p + \delta_i^q\delta_k^p)J_j^\beta + \delta_\mu^\beta(\delta_k^q\delta_j^p + \delta_j^q\delta_k^p)J_i^\alpha\right] g_{\alpha\beta} \\ & + \Lambda^{ij,kl}\left[J_i^\alpha J_j^\beta \delta_\mu^\gamma(\delta_k^q\delta_l^p + \delta_l^q\delta_k^p) + J_i^\alpha J_k^\gamma \delta_\mu^\beta(\delta_j^q\delta_l^p + \delta_l^q\delta_j^p)\right] g_{\alpha\beta,\gamma} \\ & + \Lambda^{ij,kl}\left[J_j^\beta J_k^\gamma \delta_\mu^\alpha(\delta_i^q\delta_l^p + \delta_l^q\delta_i^p) + J_i^\alpha J_l^\gamma \delta_\mu^\beta(\delta_j^q\delta_k^p + \delta_k^q\delta_j^p)\right] g_{\alpha\beta,\gamma} \\ & + \Lambda^{ij,kl}\left[J_j^\beta J_l^\gamma \delta_\mu^\alpha(\delta_i^q\delta_k^p + \delta_k^q\delta_i^p)\right] g_{\alpha\beta,\gamma} \\ & + \Lambda^{ij,kl}\left[J_{jk}^\beta \delta_\mu^\alpha(\delta_i^q\delta_l^p + \delta_l^q\delta_i^p) + J_{il}^\alpha \delta_\mu^\beta(\delta_j^q\delta_k^p + \delta_k^q\delta_j^p)\right] g_{\alpha\beta} \\ & + \Lambda^{ij,kl}\left[J_{jl}^\beta \delta_\mu^\alpha(\delta_i^q\delta_k^p + \delta_k^q\delta_i^p) + J_{ik}^\alpha \delta_\mu^\beta(\delta_j^q\delta_l^p + \delta_l^q\delta_j^p)\right] g_{\alpha\beta} \end{aligned}$$

The previous equation is valid for an arbitrary coordinate transformation, in particular for the identity transformation: $x^\alpha = y^i$, $J_i^\alpha = \delta_i^\alpha$, $J_{ij}^\alpha = 0$. In such a case, we simplify

$$\begin{aligned} 0 = {} & \Lambda^{ij,k}\left[\delta_\mu^\alpha(\delta_k^q\delta_i^p + \delta_i^q\delta_k^p)\delta_j^\beta + \delta_\mu^\beta(\delta_k^q\delta_j^p + \delta_j^q\delta_k^p)\delta_i^\alpha\right] g_{\alpha\beta} \\ & + \Lambda^{ij,kl}\left[\delta_i^\alpha \delta_j^\beta \delta_\mu^\gamma(\delta_k^q\delta_l^p + \delta_h^t\delta_k^p) + \delta_i^\alpha \delta_k^\gamma \delta_\mu^\beta(\delta_j^q\delta_l^p + \delta_l^q\delta_j^p)\right] g_{\alpha\beta,\gamma} \\ & + \Lambda^{ij,kl}\left[\delta_j^\beta \delta_k^\gamma \delta_\mu^\alpha(\delta_i^q\delta_l^p + \delta_l^q\delta_i^p) + \delta_i^\alpha \delta_l^\gamma \delta_\mu^\beta(\delta_j^q\delta_k^p + \delta_k^q\delta_j^p)\right] g_{\alpha\beta,\gamma} \\ & + \Lambda^{ij,kl}\left[\delta_j^\beta \delta_l^\gamma \delta_\mu^\alpha(\delta_i^q\delta_k^p + \delta_k^q\delta_i^p)\right] g_{\alpha\beta,\gamma} \end{aligned}$$

Further simplifications and symmetry of Λ induce [2]

[1] If one does not consider the symmetric part then there is a loss of some terms in the derivation.

[2] The Latin indices and Greek indices mix since the transformation is the identity.

$$2\Lambda^{q\beta,\gamma p}g_{\mu\beta,\gamma}+2\Lambda^{p\beta,\gamma q}g_{\mu\beta,\gamma}+\Lambda^{\alpha\beta,pq}g_{\alpha\beta,\mu}+\Lambda^{p\beta,q}g_{\mu\beta}+\Lambda^{q\beta,p}g_{\mu\beta}=0. \quad (15.29)$$

In the particular case of a normal coordinate system, these reduce to $\Lambda^{p\mu,q}+\Lambda^{q\mu,p}=0$. According to the symmetry of $\Lambda^{ij,k}$, for arbitrary indices i,j,k, we have

$$\begin{aligned}
&\Lambda^{ji,k}+\Lambda^{ki,j}=0\\
&\Lambda^{kj,i}+\Lambda^{ki,j}=0 \quad (i\longleftrightarrow k)\\
&\Lambda^{ji,k}+\Lambda^{kj,i}=0 \quad (i\longleftrightarrow j)
\end{aligned}$$

then

$$\Lambda^{ji,k}=-\Lambda^{ki,j}=\Lambda^{kj,i}=-\Lambda^{ji,k},$$

and finally

$$\Lambda^{ji,k}=\Lambda^{ij,k}=0. \quad (15.30)$$

Nevertheless equations (15.30) are only valid in normal coordinate system.

15.4.2 Introduction of Tensors

Introducing the expressions (15.28) into (15.27) and differentiating respectively with respect to $g_{\alpha\beta,\gamma\lambda}$, $g_{\alpha\beta,\gamma}$, $g_{\alpha\beta}$, allows to write

$$\left\{\begin{aligned}
\Lambda^{\alpha\beta,\gamma\lambda}&=\Lambda^{ij,kl}J_i^\alpha J_j^\beta J_k^\gamma J_l^\lambda\\
\Lambda^{\alpha\beta,\gamma}&=\Lambda^{ij,kl}\frac{\partial g_{ij,kl}}{\partial g_{\alpha\beta,\gamma}}+\Lambda^{ij,k}\frac{\partial g_{ij,k}}{\partial g_{\alpha\beta,\gamma}}\\
\Lambda^{\alpha\beta}&=\Lambda^{ij,kl}\frac{\partial g_{ij,kl}}{\partial g_{\alpha\beta}}+\Lambda^{ij,k}\frac{\partial g_{ij,k}}{\partial g_{\alpha\beta}}+\Lambda^{ij}\frac{\partial g_{ij}}{\partial g_{\alpha\beta}}
\end{aligned}\right. \quad (15.31)$$

The first equation shows that $\Lambda^{ij,kl}$ are components of a tensor type $(4,0)$. Conversely the two others equations show that $\Lambda^{ij,k}$ and Λ^{ij} are not components of tensor. Thus we should introduce two tensorial quantities instead of $\Lambda^{ij,k}$ and Λ^{ij} respectively. Let **h** an arbitrary symmetric tensor type $(0,2)$ (i.e. **h** follows the same rule of transformation (15.28) as **g**), and Π^{ij} and $\Pi^{ij,k}$ (the comma "," doesn't represent partial derivative) two unknown quantities that verify the following equation

$$\Lambda^{ij,kl}h_{ij,kl}+\Lambda^{ij,k}h_{ij,k}+\Lambda^{ij}h_{ij}=\Lambda^{ij,kl}h_{ij|k|l}+\Pi^{ij,k}h_{ij|k}+\Pi^{ij}h_{ij} \quad (15.32)$$

The formulations of the covariant derivative (15.11) and (15.12) are introduced into (15.32), that reduces to an equality without covariant derivative terms. It depends on $\{\Gamma^k_{ij},\Gamma^k_{ij,l}\}$, $\{h_{ij},h_{ij,k},h_{ij,kl}\}$, $\{\Lambda^{ij},\Lambda^{ij,k},\Lambda^{ij,kl}\}$ and $\{\Pi^{ij},\Pi^{ij,k}\}$. Then, the lemma 15.2 is applied to the equation (15.32) in order to identify the coefficients of $h_{ij,k}$ and h_{ij} (the coefficients of $h_{ij,kl}$ are the same in both hand sides of equation). Some adequate permutations between the indices are necessary. For the sake of the clarity, details of calculus are reported in annex. Let us recall that Λ^{ij} , $\Lambda^{ij,k}$ and $\Lambda^{ij,kl}$ have

properties of symmetry but it is not necessary the case for Π^{ij} and $\Pi^{ij,k}$. Thus we obtain the following equations

$$\left\{\begin{array}{l}\Pi^{ij,k}_{(S)} = \Lambda^{ij,k} + 2\Gamma^i_{al}\Lambda^{aj,kl} + 2\Gamma^j_{al}\Lambda^{ia,kl} + \Gamma^k_{bl}\Lambda^{ij,bl} \\ \Pi^{ij}_{(S)} = \Lambda^{ij} + \Gamma^i_{ak,l}\Lambda^{aj,kl} + \Gamma^j_{ak,l}\Lambda^{ia,kl} \\ \qquad - \ \Gamma^b_{al}\Gamma^i_{bk}\Lambda^{aj,kl} - \Gamma^b_{cl}\Gamma^j_{bk}\Lambda^{ic,kl} \\ \qquad - \ \Gamma^i_{bl}\Gamma^j_{ck}\Lambda^{bc,kl} - \Gamma^j_{bl}\Gamma^i_{ck}\Lambda^{bc,kl} \\ \qquad - \ \Gamma^b_{kl}\Gamma^i_{cb}\Lambda^{cj,kl} - \Gamma^b_{kl}\Gamma^j_{cb}\Lambda^{ci,kl} \\ \qquad + \ (1/2)\Gamma^i_{ak}(\Pi^{aj,k} + \Pi^{ja,k}) + (1/2)\Gamma^j_{ak}(\Pi^{ia,k} + \Pi^{ai,k})\end{array}\right. \tag{15.33}$$

where $\Pi^{ij,k}_{(S)} = (1/2)(\Pi^{ij,k} + \Pi^{ji,k})$ and $\Pi^{ij}_{(S)} = (1/2)(\Pi^{ij} + \Pi^{ji})$.

Lemma 15.3. *$F := \Lambda^{ij,kl}h_{ij,kl} + \Lambda^{ij,k}h_{ij,k} + \Lambda^{ij}h_{ij}$ is a scalar field.*

Proof. Let us notice $F = \Lambda^{ij,kl}h_{ij,kl} + \Lambda^{ij,k}h_{ij,k} + \Lambda^{ij}h_{ij}$ and $\overline{F} = \Lambda^{\alpha\beta\,,\gamma\lambda}h_{\alpha\beta\,,\gamma\lambda} + \Lambda^{\alpha\beta\,,\gamma}h_{\alpha\beta\,,\gamma} + \Lambda^{\alpha\beta}h_{\alpha\beta}$ respectively in system (y^i) and (x^α). According to (15.31),

$$\begin{aligned}\Lambda^{\alpha\beta\,,\gamma\lambda}h_{\alpha\beta\,,\gamma\lambda} &= \left[\Lambda^{ij,kl}J^\alpha_i J^\beta_j J^\gamma_k J^\lambda_l\right]h_{\alpha\beta\,,\gamma\lambda} \\ \Lambda^{\alpha\beta\,,\gamma}h_{\alpha\beta\,,\gamma} &= \left[\Lambda^{ij,kl}\frac{\partial g_{ij,kl}}{\partial g_{\alpha\beta\,,\gamma}} + \Lambda^{ij,k}\frac{\partial g_{ij,k}}{\partial g_{\alpha\beta\,,\gamma}}\right]h_{\alpha\beta\,,\gamma} \\ \Lambda^{\alpha\beta}h_{\alpha\beta} &= \left[\Lambda^{ij,kl}\frac{\partial g_{ij,kl}}{\partial g_{\alpha\beta}} + \Lambda^{ij,k}\frac{\partial g_{ij,k}}{\partial g_{\alpha\beta}} + \Lambda^{ij}\frac{\partial g_{ij}}{\partial g_{\alpha\beta}}\right]h_{\alpha\beta}\end{aligned}$$

By factorization of the coefficients of $\Lambda^{ij,kl}$, $\Lambda^{ij,k}$ and Λ^{ij} we obtain $\overline{F} = (a) + (b) + (c)$ with

$$\begin{aligned}(a) &= \Lambda^{ij,kl}\left[\frac{\partial g_{ij,kl}}{\partial g_{\alpha\beta\,,\gamma\lambda}}h_{\alpha\beta\,,\gamma\lambda} + \frac{\partial g_{ij,kl}}{\partial g_{\alpha\beta\,,\gamma}}h_{\alpha\beta\,,\gamma} + \frac{\partial g_{ij,kl}}{\partial g_{\alpha\beta}}h_{\alpha\beta}\right] \\ (b) &= \Lambda^{ij,k}\left[\frac{\partial g_{ij,k}}{\partial g_{\alpha\beta\,,\gamma}}h_{\alpha\beta\,,\gamma} + \frac{\partial g_{ij,k}}{\partial g_{\alpha\beta}}h_{\alpha\beta}\right] \\ (c) &= \Lambda^{ij}\left[\frac{\partial g_{ij}}{\partial g_{\alpha\beta}}h_{\alpha\beta}\right]\end{aligned}$$

According to the relations (15.28), the quantities in square brackets are simplified, (a) $= \Lambda^{ij,kl}\left[h_{ij,kl}\right]$, (b) $= \Lambda^{ij,k}\left[h_{ij,k}\right]$, (c) $= \Lambda^{ij}\left[h_{ij}\right]$ and thus $\overline{F} = F$.

□

Lemma 15.4. *(F - $\Lambda^{ij,kl}h_{ij|k|l}$) is a scalar.*

Proof. Let us notice $G := \Lambda^{ij,kl}h_{ij|k|l}$ and $\overline{G} := \Lambda^{\alpha\beta\,,\gamma\lambda}h_{\alpha\beta\,|\gamma|\lambda}$. By (15.31) we have

$$\Lambda^{\alpha\beta\,,\gamma\lambda}h_{\alpha\beta\,|\gamma|\lambda} = \Lambda^{ij,kl}J^\alpha_i J^\beta_j J^\gamma_k J^\lambda_l h_{\alpha\beta\,|\gamma|\lambda} \tag{15.34}$$

h being a tensor type (0,2), the second covariant derivative $h_{\alpha\beta\,|\gamma|\lambda}$ form the components of a tensor type (0,4). Consequently $J_i^\alpha J_j^\beta J_k^\gamma J_l^\lambda h_{\alpha\beta\,|\gamma|\lambda} = h_{ij|k|l}$, thus $\overline{G} = G$. By previous lemma, we have $\overline{F} - \overline{G} = F - G$.

□

Remark 15.7. A direct and simple proof may be obtained by observing that Λ^{ijkl} is in fact a tensor type $(4,0)$ and $h_{ij|k|l}$ is a tensor type $(0,4)$, then their contraction is a scalar.

Consequently, $\Pi^{ij,k}h_{ij|k} + \Pi^{ij}h_{ij}$ is a scalar for an arbitrary tensor type (0,2) **h**. Using the quotient theorem 15.2, $\Pi^{ij,k}_{(S)}$ and $\Pi^{ij}_{(S)}$ are the components of tensor type (3,0) and (2,0) respectively, these tensors are also symmetric.

15.4.3 Theorem

The expressions of $\Pi^{ij,k}_{(S)}$ in (15.33) holds in an arbitrary coordinate system. In normal coordinate system, the Christoffel symbols vanish, e.g. [23] and we have, from (15.33), $\Pi^{ij,k}_{(S)} = \Lambda^{ij,k}$. However, from (15.30) $\Lambda^{ij,k} = 0$ in normal coordinate system, thus $\Pi^{ij,k}_{(S)} = 0$ in normal coordinate system and too for any other coordinate system, because $\Pi^{ij,k}_{(S)}$ are components of tensor. The first equation in (15.33) is simplified in any coordinate system

$$0 = \Lambda^{ij,k} + 2\Gamma^i_{al}\Lambda^{aj,kl} + 2\Gamma^j_{al}\Lambda^{ia,kl} + \Gamma^k_{bl}\Lambda^{ij,bl}. \tag{15.35}$$

We can establish the following theorem:

Theorem 15.3. *Let a scalar field* $\mathscr{L} = \mathscr{L}\left(g_{ij}, g_{ij,k}, g_{ij,kl}\right)$ *defined on a Riemannian manifold. If* $\dfrac{\partial \mathscr{L}}{\partial g_{ij,kl}} = 0$ *then* $\dfrac{\partial \mathscr{L}}{\partial g_{ij,k}} = 0$.

Proof. $\forall\, i,j,k,l$, the condition $\Lambda^{ij,kl} = 0$ is introduced into (15.35).

□

Consequently, from the second equality of (15.33), we deduce $\dfrac{\partial \mathscr{L}}{\partial g_{ij}} = \Pi^{ij}_{(S)}$. An equivalent formulation of theorem 15.3 may be found in [Lovelock and Rund, [17]].

Theorem 15.4. *On a Riemannian manifold, there does not exist a scalar density such* $\mathscr{L} = \mathscr{L}(g_{ij}, g_{ij,k})$ *that only depends on the metric* g_{ij} *and their first partial derivatives* $g_{ij,k}$.

15.4.4 Discussion

In any coordinate system, we have the following decomposition

$$\begin{cases} \Pi^{ij} = (1/2)(\Pi^{ij} + \Pi^{ji}) + (1/2)(\Pi^{ij} - \Pi^{ji}) \\ \Pi^{ij,k} = (1/2)(\Pi^{ij,k} + \Pi^{ji,k}) + (1/2)(\Pi^{ij,k} - \Pi^{ji,k}) \end{cases} \tag{15.36}$$

In [17], the quantities Π^{ij} and $\Pi^{ij,k}$ are assumed to be symmetric with respect to the indices i and j: $\Pi^{ij} = \Pi^{ji}$, $\Pi^{ij,k} = \Pi^{ji,k}$ and it is proven that the quantities $\Pi^{ij,k}$ are always null. In the present study it has been proven that only the symmetric part $\Pi^{ij,k}_{(S)}$ is null: the quantities $\Pi^{ij,k}$ are skew-symmetric $\Pi^{ij,k} = -\Pi^{ji,k}$. The present study is slightly more general than the result presented in [17].

To study the fields in physics, the arguments must be tensors. The metric is a tensor and consequently the Lagrangian $\mathscr{L}(\mathbf{g})$ depends on a tensor. To extend the arguments of $\mathscr{L}$, defined on Riemannian manifold endowed with an affine connection ∇, the new form is then $\mathscr{L}(\mathbf{g}, \nabla\mathbf{g}, \nabla^2\mathbf{g})$ where all the arguments are tensors. The corresponding form in the coordinate system (x^α) is $\mathscr{L}(g_{\alpha\beta}, g_{\alpha\beta\,|\gamma}, g_{\alpha\beta\,|\gamma|\lambda})$. If the connection is Euclidean (derived from the metric) then we have $g_{\alpha\beta\,|\gamma} \equiv g_{\alpha\beta\,,\gamma}$ since $\Gamma^\gamma_{\alpha\beta} \sim g_{\alpha\beta\,,\gamma}$. In [17], the used connection is implicitly that of Levi-Civita, thus we have studied the form with partial derivatives $\mathscr{L}(g_{\alpha\beta}, g_{\alpha\beta\,,\gamma}, g_{\alpha\beta\,,\gamma\lambda})$. Another motivation is that, according to the Lemma of Ricci e.g. [4], the covariant derivative of the metric tensor $\mathbf{g}$, in the sense of Levi-Civita connection, is identically equal to zero.

15.5 Invariance with Respect to the Connection

The metric is imposed by the ambiant space (Euclidean space) and there exist many possibilities for the affine connection. It is possible to put restrictions on the possible form of connections. We demand that the metric be covariantly constant: $\nabla\mathbf{g} \equiv 0$. In such a case the connection is said to be compatible with the metric. The choice of the connection is free but it is worth to use a connection compatible with the metric. This involves that $\nabla\mathbf{g}$ cannot be an explicit argument of the Lagrangian $\mathscr{L}$. This is the reason why we consider an argument ∇ rather than $\nabla\mathbf{g}$. We labeled the biconnection $\nabla^2 = \nabla \circ \nabla$. In order to extend the list of arguments of $\mathscr{L}$, we will consider the following forms: $\mathscr{L}(\mathbf{g}, \nabla)$, $\mathscr{L}(\mathbf{g}, \nabla^2)$ and $\mathscr{L}(\mathbf{g}, \nabla, \nabla^2)$. However it should be stressed that the connection is not tensor conversely to the metric, thus we aim to obtain tensorial arguments instead of the connection and/or the bi-connection.

15.5.1 Preliminary

We define the invariance of any scalar field (more precisely the form-invariance): $\mathscr{L}(X,Y) = \mathscr{L}(X',Y')$ with both formal arguments X and Y defined in any two coordinate systems (with and without ').

Lemma 15.5. *Let us consider arbitrary constants K_1, K_2, C_1, C_2, C_3 and the variables x, x′, y, y′, p, p′, q, q′ which follow the transformations*

$$\begin{cases} x' = K_1\, x + K_2 \\ y' = K_1\, y \\ p' = C_1\, p + C_2\, (x+y) + C_3 \\ q' = C_1\, q \end{cases} \tag{15.37}$$

Now let us consider a scalar function $\mathscr{L}$ which satisfies the equations (form-invariance)

1. $\mathscr{L}(x,y) = \mathscr{L}(x',y')$
2. $\mathscr{L}(p,q) = \mathscr{L}(p',q')$
3. $\mathscr{L}(x,y,p,q) = \mathscr{L}(x',y',p',q')$.

If $(\partial K_1/\partial K_2) = 0$, $(\partial K_1/\partial C_3) = 0$, $(\partial K_2/\partial C_3) = 0$, $(\partial C_1/\partial C_3) = 0$ then, from equation (1.) we have $\mathscr{L}(y) = \mathscr{L}(y')$, from equation (2.) we have $\mathscr{L}(q) = \mathscr{L}(q')$, from equation (3.) we have $\mathscr{L}(y,q) = \mathscr{L}(y',q')$.

Proof.
Equation 1
According to (15.37) we have $\mathscr{L}(x,y) = \mathscr{L}(K_1\, x + K_2, K_1\, y)$. We differentiate this equation with respect to K_2, to find

$$\begin{aligned} 0 &= \frac{\partial \mathscr{L}}{\partial x'}\frac{\partial x'}{\partial K_2} + \frac{\partial \mathscr{L}}{\partial y'}\frac{\partial y'}{\partial K_2} \\ 0 &= \frac{\partial \mathscr{L}}{\partial x'}\left[\frac{\partial K_1}{\partial K_2}\, x + 1\right] + \frac{\partial \mathscr{L}}{\partial y'}\frac{\partial K_1}{\partial K_2}\, y \end{aligned}$$

which involves that $\partial \mathscr{L}/\partial x' = 0$ if $\partial K_1/\partial K_2 = 0$. Then, according to $(\partial \mathscr{L}/\partial x) = (\partial \mathscr{L}/\partial x')(\partial x'/\partial x)$, we prove that $\partial \mathscr{L}/\partial x = 0$.
Equation 2
According to (15.37) we have $\mathscr{L}(p,q) = \mathscr{L}(C_1\ p + C_2\ (x+y) + C_3, C_1\ q)$. We differentiate this equation with respect to C_3, to find

$$\begin{aligned} 0 &= \frac{\partial \mathscr{L}}{\partial p'}\frac{\partial p'}{\partial C_3} + \frac{\partial \mathscr{L}}{\partial q'}\frac{\partial q'}{\partial C_3} \\ 0 &= \frac{\partial \mathscr{L}}{\partial p'}\left[\frac{\partial C_1}{\partial C_3}\, p + \frac{\partial C_2}{\partial C_3}\, (x+y) + 1\right] + \frac{\partial \mathscr{L}}{\partial q'}\frac{\partial C_1}{\partial C_3}\, q \end{aligned}$$

which involves that $\partial \mathscr{L}/\partial p' = 0$ if $\partial C_1/\partial C_3 = 0$, the term in square brackets not vanishing. Then, according to $(\partial \mathscr{L}/\partial p) = (\partial \mathscr{L}/\partial p')(\partial p'/\partial p)$, we prove that

$\partial\mathscr{L}/\partial p = 0$. Finally we obtain $\mathscr{L}(q) = \mathscr{L}(q')$.
Equation 3
According to (15.37) we have $\mathscr{L}(x,y,p,q) = \mathscr{L}(K_1\,x+K_2, K_1\,y, C_1\,p+C_2\,(x+y)+C_3, C_1\,q)$. We differentiate this equation with respect to C_3, to find

$$\begin{aligned} 0 &= \frac{\partial\mathscr{L}}{\partial x'}\frac{\partial x'}{\partial C_3} + \frac{\partial\mathscr{L}}{\partial y'}\frac{\partial y'}{\partial C_3} + \frac{\partial\mathscr{L}}{\partial p'}\frac{\partial p'}{\partial C_3} + \frac{\partial\mathscr{L}}{\partial q'}\frac{\partial q'}{\partial C_3} \\ 0 &= \frac{\partial\mathscr{L}}{\partial x'}\left[\frac{\partial K_1}{\partial C_3}\,x + \frac{\partial K_2}{\partial C_3}\right] + \frac{\partial\mathscr{L}}{\partial y'}\frac{\partial K_1}{\partial C_3}\,y + \frac{\partial\mathscr{L}}{\partial p'}\left[\frac{\partial C_1}{\partial C_3}\,p + \frac{\partial C_2}{\partial C_3}\,(x+y) + 1\right] \\ &\quad + \frac{\partial\mathscr{L}}{\partial q'}\frac{\partial C_1}{\partial C_3}\,q \end{aligned}$$

which involves that $\partial\mathscr{L}/\partial p' = 0$ if $\partial K_1/\partial C_3 = 0$, $\partial K_2/\partial C_3 = 0$, $\partial C_1/\partial C_3 = 0$. Then we have $\partial\mathscr{L}/\partial p = 0$. According to $(\partial\mathscr{L}/\partial x) = (\partial\mathscr{L}/\partial p')(\partial p'/\partial x)$, we prove that $\partial\mathscr{L}/\partial x = 0$. To finish, according to $(\partial\mathscr{L}/\partial x) = (\partial\mathscr{L}/\partial x')(\partial x'/\partial x) = (\partial\mathscr{L}/\partial x')\,K_1$, we prove that $\partial\mathscr{L}/\partial x' = 0$. Finally we obtain $\mathscr{L}(y,q) = \mathscr{L}(y',q')$.

□

Remark 15.8. The previous proof is based on the principle of fields invariance introduced by Lovelock and Rund [17]. It is equivalent to the form-invariance, a term borrowed from [30].

In an arbitrary coordinate system (y^i), the components of the metric, the connection and the bi-connection are respectively g_{ij}, Γ^k_{ij} and $\Gamma^k_{ij,l} + \Gamma^m_{ij}\Gamma^k_{lm}$. The forms $\mathscr{L}(g,\nabla)$, $\mathscr{L}(g,\nabla^2)$ and $\mathscr{L}(g,\nabla,\nabla^2)$ are then explicitly written as $\mathscr{L}(g_{ij},\Gamma^k_{ij})$, $\mathscr{L}\left(g_{ij},\Gamma^k_{ij,l}+\Gamma^m_{ij}\Gamma^k_{lm}\right)$ and $\mathscr{L}\left(g_{ij},\Gamma^k_{ij},\Gamma^k_{ij,l}+\Gamma^m_{ij}\Gamma^k_{lm}\right)$, respectively. Let (x^α) an other coordinate system, let us assume the form-invariance of the scalar field $\mathscr{L}$ (three cases):

$$\left\{\begin{array}{c} \mathscr{L}(\Gamma^k_{ij}) = \mathscr{L}(\Gamma^\gamma_{\alpha\beta}) \\ \mathscr{L}(\Gamma^k_{ij,l}+\Gamma^m_{ij}\Gamma^k_{lm}) = \mathscr{L}(\Gamma^\gamma_{\alpha\beta\,,\lambda}+\Gamma^\mu_{\alpha\beta}\Gamma^\gamma_{\lambda\mu}) \\ \mathscr{L}(\Gamma^k_{ij},\Gamma^k_{ij,l}+\Gamma^m_{ij}\Gamma^k_{lm}) = \mathscr{L}(\Gamma^\gamma_{\alpha\beta},\Gamma^\gamma_{\alpha\beta\,,\lambda}+\Gamma^\mu_{\alpha\beta}\Gamma^\gamma_{\lambda\mu}) \end{array}\right. \tag{15.38}$$

where the components of the metric will be omitted for the sake of simplicity. For further applications, let us introduce the following components

$$\left\{\begin{array}{l} \mathbb{T}^k_{ij} = (1/2)\left(\Gamma^k_{ij}-\Gamma^k_{ji}\right) \\ \mathbb{S}^k_{ij} = (1/2)\left(\Gamma^k_{ij}+\Gamma^k_{ji}\right) \\ \mathbb{B}^k_{lij} = (1/2)\left(\Gamma^k_{ij,l}+\Gamma^m_{ij}\Gamma^k_{lm}-\Gamma^k_{lj,i}-\Gamma^m_{lj}\Gamma^k_{im}\right) \\ \mathbb{A}^k_{lij} = (1/2)\left(\Gamma^k_{ij,l}+\Gamma^m_{ij}\Gamma^k_{lm}+\Gamma^k_{lj,i}+\Gamma^m_{lj}\Gamma^k_{im}\right) \end{array}\right. \tag{15.39}$$

According to (15.39), one permutation between i and j allows the decomposition $\Gamma^k_{ij} = \mathbb{S}^k_{ij} + \mathbb{T}^k_{ij}$. One permutation between i and l allows the decomposition $\Gamma^k_{ij,l} +$

$\Gamma^m_{ij}\Gamma^k_{lm} = \mathbb{A}^k_{lij} + \mathbb{B}^k_{lij}$. One first permutation between i and j then one other successive permutation between i and l allow the simultaneous decompositions $\Gamma^k_{ij} = \mathbb{S}^k_{ij} + \mathbb{T}^k_{ij}$ and $\Gamma^k_{ij,l} + \Gamma^m_{ij}\Gamma^k_{lm} = \mathbb{A}^k_{lij} + \mathbb{B}^k_{lij}$. The details of calculus are given in annex. Thanks to these decompositions, the form-invariance of $\mathscr{L}$ (15.38) becomes

$$\begin{cases} \mathscr{L}(\mathbb{S}^k_{ij}, \mathbb{T}^k_{ij}) = \mathscr{L}(\mathbb{S}^\gamma_{\alpha\beta}, \mathbb{T}^\gamma_{\alpha\beta}) \\ \mathscr{L}(\mathbb{A}^k_{lij}, \mathbb{B}^k_{lij}) = \mathscr{L}(\mathbb{A}^\gamma_{\lambda\alpha\beta}, \mathbb{B}^\gamma_{\lambda\alpha\beta}) \\ \mathscr{L}(\mathbb{S}^k_{ij}, \mathbb{T}^k_{ij}, \mathbb{A}^k_{lij}, \mathbb{B}^k_{lij}) = \mathscr{L}(\mathbb{S}^\gamma_{\alpha\beta}, \mathbb{T}^\gamma_{\alpha\beta}, \mathbb{A}^\gamma_{\lambda\alpha\beta}, \mathbb{B}^\gamma_{\lambda\alpha\beta}) \end{cases} \tag{15.40}$$

15.5.2 Application

Let us consider the following identification of variables x, x', y, y', p, p', q, q':

$$x = \mathbb{S}^k_{ij}, \;\; y = \mathbb{T}^k_{ij}, \;\; p = \mathbb{A}^k_{lij}, \;\; q = \mathbb{B}^k_{lij}, \tag{15.41}$$

$$x' = \mathbb{S}^\gamma_{\alpha\beta}, \;\; y' = \mathbb{T}^\gamma_{\alpha\beta}, \;\; p' = \mathbb{A}^\gamma_{\lambda\alpha\beta}, \;\; q' = \mathbb{B}^\gamma_{\lambda\alpha\beta}. \tag{15.42}$$

The transformation laws between the above variables take the form of (15.37) with (see annex)

$$\begin{cases} K_1 = J^i_\alpha J^j_\beta A^\gamma_k \\ K_2 = J^j_{\alpha\beta} A^\gamma_j \\ C_1 = J^i_\alpha J^j_\beta J^l_\lambda A^\gamma_k \\ C_2 = J^i_{\alpha\lambda} J^j_\beta A^\gamma_k + J^i_\lambda J^j_{\alpha\beta} A^\gamma_k + J^i_\alpha J^j_{\beta\lambda} A^\gamma_k \\ C_3 = J^i_\mu J^l_\lambda J^j_{\alpha\beta} A^\gamma_j A^\mu_{il} + J^i_{\mu\lambda} J^j_{\alpha\beta} A^\mu_i A^\gamma_j \end{cases} \tag{15.43}$$

We have $\partial K_1/\partial K_2 = 0$, $\partial K_1/\partial C_3 = 0$, $\partial K_2/\partial C_3 = 0$, $\partial C_1/\partial C_3 = 0$. According to lemma 15.5, the invariance of $\mathscr{L}$ (15.40) means

$$\begin{cases} \mathscr{L}(\mathbb{T}^k_{ij}) = \mathscr{L}(\mathbb{T}^\gamma_{\alpha\beta}) \\ \mathscr{L}(\mathbb{B}^k_{lij}) = \mathscr{L}(\mathbb{B}^\gamma_{\lambda\alpha\beta}) \\ \mathscr{L}(\mathbb{T}^k_{ij}, \mathbb{B}^k_{lij}) = \mathscr{L}(\mathbb{T}^\gamma_{\alpha\beta}, \mathbb{B}^\gamma_{\lambda\alpha\beta}) \end{cases} \tag{15.44}$$

We now identify the components of torsion tensor by $\aleph^k_{ij} = 2\mathbb{T}^k_{ij}$ and the components of curvature tensor by $\Re^k_{lij} = 2\mathbb{B}^k_{lij}$. From (15.44) we have

$$\begin{cases} \mathscr{L}(\aleph^k_{ij}) = \mathscr{L}(\aleph^\gamma_{\alpha\beta}) \\ \mathscr{L}(\Re^k_{lij}) = \mathscr{L}(\Re^\gamma_{\lambda\alpha\beta}) \\ \mathscr{L}(\aleph^k_{ij}, \Re^k_{lij}) = \mathscr{L}(\aleph^\gamma_{\alpha\beta}, \Re^\gamma_{\lambda\alpha\beta}) \end{cases} \tag{15.45}$$

15.5.3 Synthesis

For the sake of the simplicity we have previously omitted the argument g_{ij}. Adding this argument does not change the proof. The overall result then includes the metric, the connection, and the bi-connection as arguments of the Lagrangian function $\mathscr{L}$. We also have the following Form-Invariance:

$$\begin{cases} \mathscr{L}(g_{ij}, \aleph^k_{ij}) = \mathscr{L}(g_{\alpha\beta}, \aleph^\gamma_{\alpha\beta}) \\ \mathscr{L}(g_{ij}, \Re^k_{lij}) = \mathscr{L}(g_{\alpha\beta}, \Re^\gamma_{\lambda\alpha\beta}) \\ \mathscr{L}(g_{ij}, \aleph^k_{ij}, \Re^k_{lij}) = \mathscr{L}(g_{\alpha\beta}, \aleph^\gamma_{\alpha\beta}, \Re^\gamma_{\lambda\alpha\beta}) \end{cases} \tag{15.46}$$

All the arguments of $\mathscr{L}$ are components of tensors, they are invariant under the action of the diffeomorphism (in the sense that they transform covariantly according to usual tensor transformations depending on their type). Therefore, the Lagrangian function is form-invariant. The components of torsion are explicitly defined according to the coefficients of connection and the components of curvature are explicitly defined according to the coefficients of biconnection. From (15.46) we have

$$\begin{cases} \mathscr{L}(g_{ij}, \Gamma^k_{ij}) = \mathscr{L}(g_{\alpha\beta}, \Gamma^\gamma_{\alpha\beta}) \\ \mathscr{L}(g_{ij}, \Gamma^k_{ij} + \Gamma^m_{ij}\Gamma^k_{lm}) = \mathscr{L}(g_{\alpha\beta}, \Gamma^\gamma_{\alpha\beta,\lambda} + \Gamma^\mu_{\alpha\beta}\Gamma^\gamma_{\lambda\mu}) \\ \mathscr{L}(g_{ij}, \Gamma^k_{ij}, \Gamma^k_{ij,l} + \Gamma^m_{ij}\Gamma^k_{lm}) = \mathscr{L}(g_{\alpha\beta}, \Gamma^\gamma_{\alpha\beta}, \Gamma^\gamma_{\alpha\beta,\lambda} + \Gamma^\mu_{\alpha\beta}\Gamma^\gamma_{\lambda\mu}) \end{cases} \tag{15.47}$$

The results are summarized in the following theorem:

Theorem 15.5. *Let a Riemannian manifold $(X, \mathbf{g})$ embedded into an Euclidean space and endowed with an affine connection ∇ compatible with the metric $(\nabla \mathbf{g} = 0)$. To the connection are associated the torsion tensor $\aleph$ and the curvature tensor $\Re$. For any scalar field $\mathscr{L}$ defined on X, the form-invariance induces*

$$\mathscr{L}(\mathbf{g}, \nabla) = \mathscr{L}(\mathbf{g}, \aleph), \quad \mathscr{L}(\mathbf{g}, \nabla^2) = \mathscr{L}(\mathbf{g}, \Re), \quad \mathscr{L}(\mathbf{g}, \nabla, \nabla^2) = \mathscr{L}(\mathbf{g}, \aleph, \Re) \tag{15.48}$$

The equations (15.48) can be read in the two directions:

- $\mathscr{L} = \mathscr{L}(\mathbf{g}, \nabla)$ *is form-invariant if and only if* $\mathscr{L} = \mathscr{L}(\mathbf{g}, \aleph)$
- $\mathscr{L} = \mathscr{L}(\mathbf{g}, \nabla^2)$ *is form-invariant if and only if* $\mathscr{L} = \mathscr{L}(\mathbf{g}, \Re)$
- $\mathscr{L} = \mathscr{L}(\mathbf{g}, \nabla, \nabla^2)$ *is form-invariant if and only if* $\mathscr{L} = \mathscr{L}(\mathbf{g}, \aleph, \Re)$

Under the same hypothesis as for the theorem 15.5, we have the corollary:

Corollary 15.1. *On Riemannian manifold, there does not exist a scalar field $\mathscr{L}$ (form-invariant) which depends on the metric $\mathbf{g}$ and the Levi-Civita connection $\overline{\nabla}$.*

Proof. According to the theorem 15.1 and theorem 15.5: $\mathscr{L}(\mathbf{g}, \overline{\nabla}) = \mathscr{L}(\mathbf{g}, \aleph = 0) = \mathscr{L}(\mathbf{g})$.

□

Remark 15.9. The corollary 15.1 can be proven by using the components formulation. Indeed, the coefficients of the connection of Levi-Civita are the Christoffel

symbols labeled $\overline{\Gamma}^{k}_{ij}$ (15.10) which depend on the components of the metric and its first partial derivatives e.g. [23]. According to the theorem 15.4: $\mathscr{L}(g_{ij},\overline{\Gamma}^{k}_{ij}) = \mathscr{L}(g_{ij},g_{ij,k}) = \mathscr{L}(g_{ij})$.

Remark 15.10. Our extension consists in using an affine connection which does not derive from a metric but however compatible with the metric, and thus to introduce the torsion and/or the curvature to describe the dislocations and the disclinations field e.g. [20], [27]. However the connection of Levi-Civita is compatible, is derived from the metric and especially the associated torsion necessary vanishes (theorem 15.1). Although essential and used for models of continuous medium, the application of Levi-Civita connection seems limited and is not adapted in this framework.

15.6 Strain Gradient Continuum

According to the form of the strain energy potential (part of the Lagrangian function), the potential energy of a system depends on the strain tensor $\mathbf{E}$ and possibly on other arguments. In Riemannian geometry, the metric $\mathbf{g}$ and the affine connection ∇ are fundamental tools to describe the tensor fields and their derivatives defined on manifold. The torsion $\aleph$ and the curvature $\Re$ are tensors which are associated to the affine connection. This geometrical approach is applied in the study of defects through continuous media e.g. [13], [20], [27], [33] and more generally in physics, e.g. [4], [12]. For continuum mechanics, the metric tensor $\mathbf{g}$ is related with the strain tensor $\mathbf{E}$, by the following relation [29]:

$$\mathbf{g} = \mathbf{I} + 2\mathbf{E}, \qquad g_{ij} = \delta_{ij} + 2E_{ij} \tag{15.49}$$

where $\mathbf{I}$ is the identity tensor type $(0,2)$. It should be also stressed that the relation (15.49) implicitly assumes that material coordinates within the continuum are used for describing the continuum transformation (i.e. we use Lagrangian description with convected vector base e.g. [27]). Consequently the first type of the scalar field (Lagrangian) $\mathscr{L}$ we would like to analyze, takes the form of (by abuse of notation)

$$\mathscr{L}(g_{ij},g_{ij,k},g_{ij,kl}) \equiv \mathscr{L}(E_{ij},E_{ij,k},E_{ij,kl}). \tag{15.50}$$

In the framework of strain gradient continuum, the forms of Lagrangian functions are $\mathscr{L}(E_{ij},E_{ij|k})$ for first or $\mathscr{L}(E_{ij},E_{ij|k},E_{ij|k|l})$ for second strain gradient model. Many strain gradient models use an affine connection which derives from the metric. Consequently, the Lagrangian is respectively reformulated by $\mathscr{L}(E_{ij},E_{ij,k})$ and $\mathscr{L}(E_{ij},E_{ij,k},E_{ij,kl})$. According to the theorem 15.4 [17], the form $\mathscr{L}(E_{ij},E_{ij,k})$ does not exist. Consequently the possible forms are e.g. [1]:

- $\mathscr{L}(E_{ij})$ which is used in classical elasticity theory.
- $\mathscr{L}(E_{ij},E_{ij,kl})$ and $\mathscr{L}(E_{ij},E_{ij,k},E_{ij,kl})$ which are used in strain gradient theory.

In the case where the affine connection is Euclidean[3], among the Lagrangian arguments we find necessarily the second order of the derivative of the strain. Thus the strain gradient theory is more precisely named the second strain gradient theory, also called continuum of grade three e.g. [1]. But the partial derivatives of tensor components are not necessary the components of tensor, therefore the quantities $E_{ij,k}$ and $E_{ij,kl}$ may not represent physical quantities, in general. Indeed, according to the equation between the strain and the metric (15.49), we observe that the components $g_{ij,k}$ and $g_{ij,kl}$ are not components of tensor by (15.28). We choose then a non Euclidean connection but compatible with the metric. The affine connection is not a tensor however, the studied forms $\mathscr{L}(\mathbf{g},\nabla)$, $\mathscr{L}(\mathbf{g},\nabla^2)$ and $\mathscr{L}(\mathbf{g},\nabla,\nabla^2)$ are respectively equivalent to $\mathscr{L}(\mathbf{g},\aleph)$, $\mathscr{L}(\mathbf{g},\Re)$ and $\mathscr{L}(\mathbf{g},\aleph,\Re)$. All the arguments are tensors and can represent physical quantities. The proof is based on the invariance principle, essential criterium in study of fields in physics.

Let us consider a continuous medium (continuum) modeled by a Riemannian manifold endowed with an affine connection (compatible with the metric). The choice of the continuum comes owing to the fact that torsion is null (Riemannian approach) or not (Cartan approach). By the way, the introduction of torsion and curvature was done in previous works as tensorial measures of Volterra dislocations and disclinations e.g. [20], [27].

- $\mathscr{L}(\mathbf{g},\aleph=0,\Re=0)$ corresponds to an elastic energy strain function.
- $\mathscr{L}(\mathbf{g},\aleph)$ is associated to an elastic continuum with dislocation.
- $\mathscr{L}(\mathbf{g},\aleph,\Re)$ is associated to an elastic continuum with dislocation and disclination.

The elasticity of the continuum refers to the metric as argument of the Lagrangian whereas the dislocations and disclinations are described by the torsion and the curvature tensors associated to the affine connection ∇ e.g. [20], [26].

Remark 15.11. For establishing the form-invariance requirement we are searching for constitutive laws of higher gradient continuum mechanics, we do not take all applicable arbitrary coordinate systems. We limit to coordinate systems x^α and y^i that are all diffeomorphically equivalent to each other. This is obviously a larger class than the orthogonal transformations (rotation and translation of coordinates) and even much larger than the class of coordinate systems related by linear transformations, but it should be again recalled that still just an small fraction of all possible coordinate systems e.g. [27]. Further studies in this direction still hold as great challenge, by considering the concept of path-dependent integration method e.g. [12].

15.7 Concluding Remarks

Most of the materials may be regarded as Noll's simple materials [24]. Reduced form of their constitutive laws are therefore determined through both the Euclidean-

[3] The Euclidean connection derived from the metric tensor of a referential body was mostly the connection used in mechanics for over two centuries, e.g. [27].

Frame Indifference and the Form-Indifference that ensure the Indifference with respect to Superimposed Rigid Body Motions (rigid translation and rigid rotation) [30]. Elastic simple material is therefore well defined by a strain energy density function depending on the metric tensor components as arguments. Strain Gradient continuum does not belong to the Noll's simple materials class, strain energy density also depend on higher space derivatives of the metric tensor. The goal of the present paper was to analyze the form-invariance of second strain gradient, or also named third grade continuum. The ratio supporting the interest of such a third grade continuum may be found initially in [22] and recently in e.g. [9], [15]. In a previous work, we were also leaded to third grade models however from a differential geometry point of view, when accounting for discontinuity of scalar and vector fields within the continuum [26]. We do not pay attention to the inertial terms in the present paper, reducing the Lagrangian function to the strain energy density function.

According to a method borrowed from [17], the present investigations has shown, on the one hand, the necessary dependence of the Lagrangian function on the second order derivative of the metric, or the strain (main argument). On the other hand, the form-invariance method applied to a Lagrangian function that depends on both the metric and the (compatible) connection involves the necessary dependence of the Lagrangian with respect to the torsion and/or the curvature associated to the connection. It is observed that the introduction of the affine connection as arguments of any physical quantity, such as the Lagrangian function, has its roots in basic physics of spacetime. Connection was already introduced in the earlier works of Einstein, Weyl, and Cartan to describe the concept of gravity e.g. [6], in which the both metric and connection are considered as two of the fundamentals tools for mechanics and physics. The Lagrangian function is reduced to an elastic potential energy function and the dimension of its arguments inform on the character of higher order of gradient. The form $\mathscr{L}(\mathbf{g}, \mathfrak{K})$ is associated to a second strain gradient elastic continuum with the argument torsion, whereas the form $\mathscr{L}(\mathbf{g}, \mathfrak{K}, \mathfrak{R})$ is associated to an elastic continuum of third grade with the curvature also as additional argument.

Acknowledgements N. Antonio Tamarasselvame has been supported by an ARED grant of the "Région de Bretagne".

Appendix 1

Let (y^i) and (x^α) two coordinate systems associated to respectively the tangent bases $\{\mathbf{e}_i\}$ and $\{\mathbf{e}_\alpha\}$. Let ∇ the affine connection and its coefficients

$$\nabla_{\mathbf{e}_i}\mathbf{e}_j = \Gamma_{ij}^k \mathbf{e}_k$$
$$\nabla_{\mathbf{e}_\alpha}\mathbf{e}_\beta = \Gamma_{\alpha\beta}^\gamma \mathbf{e}_\gamma$$

The coordinate transformation of ∇ is

$$\begin{aligned}\Gamma^{\gamma}_{\alpha\beta}\mathbf{e}_{\gamma} &= \nabla_{\mathbf{e}_{\alpha}}\mathbf{e}_{\beta}\\ &= \nabla_{J^{i}_{\alpha}\mathbf{e}_{i}}\left(J^{j}_{\beta}\mathbf{e}_{j}\right)\\ &= J^{i}_{\alpha}\left[\nabla_{\mathbf{e}_{i}}\left(J^{j}_{\beta}\right)\mathbf{e}_{j}+J^{j}_{\beta}\nabla_{\mathbf{e}_{i}}\mathbf{e}_{j}\right]\\ &= J^{i}_{\alpha}\left[\nabla_{A^{\alpha}_{i}\mathbf{e}_{\alpha}}\left(J^{j}_{\beta}\right)\mathbf{e}_{j}+J^{j}_{\beta}\Gamma^{k}_{ij}\mathbf{e}_{k}\right]\\ &= J^{i}_{\alpha}\left[A^{\alpha}_{i}J^{j}_{\alpha\beta}\,\mathbf{e}_{j}+J^{j}_{\beta}\Gamma^{k}_{ij}\mathbf{e}_{k}\right],\end{aligned}$$

say

$$\left[\Gamma^{\gamma}_{\alpha\beta}\right]=\left[\left(J^{i}_{\alpha}J^{j}_{\beta}A^{\gamma}_{k}\right)\Gamma^{k}_{ij}\right]+J^{j}_{\alpha\beta}A^{\gamma}_{j}. \tag{15.51}$$

Let the "double connection" $\nabla^2=\nabla\circ\nabla$

$$\begin{aligned}\nabla_{\mathbf{e}_{\lambda}}\left[\nabla_{\mathbf{e}_{\alpha}}\mathbf{e}_{\beta}\right] &= \nabla_{\mathbf{e}_{\lambda}}\left[\Gamma^{\mu}_{\alpha\beta}\,\mathbf{e}_{\mu}\right]\\ &= \nabla_{\mathbf{e}_{\lambda}}\left[\Gamma^{\mu}_{\alpha\beta}\right]\mathbf{e}_{\mu}+\Gamma^{\mu}_{\alpha\beta}\left[\nabla_{\mathbf{e}_{\lambda}}\mathbf{e}_{\mu}\right]\\ &= \Gamma^{\mu}_{\alpha\beta\,,\lambda}\mathbf{e}_{\mu}+\Gamma^{\mu}_{\alpha\beta}\Gamma^{\gamma}_{\lambda\mu}\mathbf{e}_{\gamma}\\ &= \left[\Gamma^{\gamma}_{\alpha\beta\,,\lambda}+\Gamma^{\mu}_{\alpha\beta}\Gamma^{\gamma}_{\lambda\mu}\right]\mathbf{e}_{\gamma}.\end{aligned}$$

Without going into details, the coordinate transformation of ∇^2 is

$$\begin{aligned}\left[\Gamma^{\gamma}_{\alpha\beta\,,\lambda}+\Gamma^{\mu}_{\alpha\beta}\Gamma^{\gamma}_{\lambda\mu}\right] &= \left[J^{i}_{\alpha}J^{j}_{\beta}J^{l}_{\lambda}A^{\gamma}_{k}\left(\Gamma^{k}_{ij,l}+\Gamma^{d}_{ij}\Gamma^{k}_{ld}\right)\right]\\ &+\left(J^{i}_{\alpha\lambda}J^{j}_{\beta}A^{\gamma}_{k}+J^{i}_{\lambda}J^{j}_{\alpha\beta}A^{\gamma}_{k}+J^{i}_{\alpha}J^{j}_{\beta\lambda}A^{\gamma}_{k}\right)\Gamma^{k}_{ij}\\ &+J^{i}_{\mu}J^{l}_{\lambda}J^{j}_{\alpha\beta}A^{\gamma}_{j}A^{\mu}_{il}+J^{i}_{\mu\lambda}J^{j}_{\alpha\beta}A^{\mu}_{i}A^{\gamma}_{j}\end{aligned} \tag{15.52}$$

The equalities (15.51) and (15.52) show that the connection ∇ and the biconnection ∇^2 are not tensors, according to (15.6). However, in the both equalities, if the terms out of the square brackets vanish then the components are components of tensor. These quantities are symmetric with respect to α and β for (15.51) and with respect to α and λ for (15.52). Then the torsion (15.7) and the curvature (15.8) are defined, with respect to the affine connection ∇, on the base $\{\mathbf{e}_a\}$ associated to coordinate system (y^a).

Appendix 2

Identification of Coefficients

Let us apply the Lemma 15.2 to the equation

$$\Lambda^{ij,kl}h_{ij,kl}+\Lambda^{ij,k}h_{ij,k}+\Lambda^{ij}h_{ij}=\Lambda^{ij,kl}h_{ij|k|l}+\Pi^{ij,k}h_{ij|k}+\Pi^{ij}h_{ij},$$

for the identification of the coefficients of $h_{ij,k}$ and h_{ij}. Let us recall that

$$\begin{aligned}\Lambda^{ij,kl}h_{ij|k|l}=\Lambda^{ij,kl}[&h_{ij,kl}-\Gamma^a_{ik}h_{aj,l}-\Gamma^a_{jk}h_{ia,l}-\Gamma^a_{ik,l}h_{aj}-\Gamma a_{jk,l}h_{ia}\\&-\Gamma^b_{il}h_{bj,k}+\Gamma^b_{il}(\Gamma^c_{bk}h_{cj}+\Gamma^{jk}_{c}h_{bc})-\Gamma^b_{jl}h_{ib,k}\\&+\Gamma^b_{jl}(\Gamma^c_{ik}h_{cb}+\Gamma^c_{bk}h_{ic})-\Gamma^b_{kl}h_{ij,b}+\Gamma^b_{kl}(\Gamma^c_{ib}h_{cj}+\Gamma^c_{jb}h_{ic})]\end{aligned}$$

and

$$\Pi^{ij,k}h_{ij|k}=\Pi^{ij,k}[h_{ij,k}-\Gamma^a_{ik}h_{aj}-\Gamma^a_{jk}h_{ia}].$$

The equation of the coefficients of "$h_{ij,k}$" is

$$\Lambda^{ij,k}h_{ij,k}=-\Lambda^{ij,kl}[\Gamma^a_{ik}h_{aj,l}+\Gamma^a_{jk}h_{ia,l}+\Gamma^b_{il}h_{bj,k}+\Gamma^b_{jl}h_{ib,k}+\Gamma^b_{kl}h_{ij,b}]+\Pi^{ij,k}h_{ij,k}.$$

The following permutations are necessary to write explicitly the common factor $h_{ij,k}$ in all the terms in right hand side (above):

- $a\longleftrightarrow i$ and $l\longleftrightarrow k$ for $\Lambda^{ij,kl}\Gamma^a_{ik}h_{aj,l}$
- $a\longleftrightarrow j$ and $l\longleftrightarrow k$ for $\Lambda^{ij,kl}\Gamma^a_{jk}h_{ia,l}$
- $b\longleftrightarrow i$ then $b\to a$ for $\Lambda^{ij,kl}\Gamma^b_{il}h_{bj,k}$
- $b\longleftrightarrow j$ then $b\to a$ for $\Lambda^{ij,kl}\Gamma^b_{jl}h_{ib,k}$
- $k\longleftrightarrow b$ for $\Lambda^{ij,kl}\Gamma^b_{kl}h_{ij,b}$.

Then, the symmetry of Λ and h reduces the identification of coefficients of $h_{ij,k}$

$$(1/2)(\Pi^{ij,k}+\Pi^{ji,k})=\Lambda^{ij,k}+2\Gamma^i_{al}\Lambda^{aj,kl}+2\Gamma^j_{al}\Lambda^{ia,kl}+\Gamma^k_{bl}\Lambda^{ij,bl}.$$

In the same way, the equation of the coefficients of "h_{ij}" is

$$\begin{aligned}\Lambda^{ij}h_{ij}=\Lambda^{ij,kl}[&-\Gamma^a_{ik,l}h_{aj}-\Gamma^a_{jk,l}h_{ia}+\Gamma^b_{il}(\Gamma^c_{bk}h_{cj}+\Gamma^c_{jk}h_{bc})+\Gamma^b_{jl}(\Gamma^c_{ik}h_{cb}+\Gamma^c_{bk}h_{ic})\\&+\Gamma^b_{kl}(\Gamma^c_{ib}h_{cj}+\Gamma^c_{jb}h_{ic})]-\Pi^{ij,k}\Gamma^a_{ik}h_{aj}-\Pi^{ij,k}\Gamma^a_{jk}h_{ia}+\Pi^{ij}h_{ij}.\end{aligned}$$

The following permutations are necessary to refind the common factor h_{ij} in all the terms in right hand side (above):

- $a\longleftrightarrow i$ for $\Lambda^{ij,kl}\Gamma^a_{ik,l}h_{aj}$ and $\Pi^{ij,k}\Gamma^a_{ik}h_{aj}$
- $a\longleftrightarrow j$ for $\Lambda^{ij,kl}\Gamma^a_{jk,l}h_{ia}$ and $\Pi^{ij,k}\Gamma^a_{jk}h_{ia}$
- $c\longleftrightarrow i$ for $\Lambda^{ij,kl}\Gamma^b_{il}\Gamma^c_{bk}h_{cj}$ and $\Lambda^{ij,kl}\Gamma^b_{kl}\Gamma^c_{ib}h_{cj}$
- $c\longleftrightarrow j$ for $\Lambda^{ij,kl}\Gamma^b_{jl}\Gamma^c_{bk}h_{ic}$ and $\Lambda^{ij,kl}\Gamma^b_{kl}\Gamma^c_{jb}h_{ic}$
- $c\longleftrightarrow i$ and $b\longleftrightarrow j$ for $\Lambda^{ij,kl}\Gamma^b_{il}\Gamma^c_{jk}h_{bc}$ and $\Lambda^{ij,kl}\Gamma^b_{jl}\Gamma^c_{ik}h_{cb}$.

Then, the symmetry of Λ and h reduces the identification of coefficients of h_{ij}

$$
\begin{aligned}
(1/2)(\Pi^{ij}+\Pi^{ji}) = \Lambda^{ij} &+ \Gamma^{i}_{ak,l}\Lambda^{aj,kl} + \Gamma^{j}_{ak,l}\Lambda^{ia,kl} \\
&- \Gamma^{b}_{al}\Gamma^{i}_{bk}\Lambda^{aj,kl} - \Gamma^{b}_{cl}\Gamma^{j}_{bk}\Lambda^{ic,kl} \\
&- \Gamma^{i}_{bl}\Gamma^{j}_{ck}\Lambda^{bc,kl} - \Gamma^{j}_{bl}\Gamma^{i}_{ck}\Lambda^{bc,kl} \\
&- \Gamma^{b}_{kl}\Gamma^{i}_{cb}\Lambda^{cj,kl} - \Gamma^{b}_{kl}\Gamma^{j}_{cb}\Lambda^{ci,kl} \\
&+ (1/2)\Gamma^{i}_{ak}(\Pi^{aj,k}+\Pi^{ja,k}) + (1/2)\Gamma^{j}_{ak}(\Pi^{ia,k}+\Pi^{ai,k}).
\end{aligned}
$$

Coefficients of Biconnection

We apply the permutation between i and l, like this

$$
\begin{aligned}
&\mathbb{S}^{k}_{ij,l} + \mathbb{T}^{k}_{ij,l} + \mathbb{S}^{m}_{ij}\mathbb{S}^{k}_{lm} + \mathbb{S}^{m}_{ij}\mathbb{T}^{k}_{lm} + \mathbb{T}^{m}_{ij}\mathbb{S}^{k}_{lm} + \mathbb{T}^{m}_{ij}\mathbb{T}^{k}_{lm} \\
&= (1/2)\left[\mathbb{S}^{k}_{ij,l} + \mathbb{S}^{m}_{ij}\mathbb{S}^{k}_{lm} + \mathbb{S}^{m}_{ij}\mathbb{T}^{k}_{lm} + \mathbb{S}^{k}_{lj,i} + \mathbb{S}^{m}_{lj}\mathbb{S}^{k}_{im} + \mathbb{S}^{m}_{lj}\mathbb{T}^{k}_{im}\right] \\
&+(1/2)\left[\mathbb{S}^{k}_{ij,l} + \mathbb{S}^{m}_{ij}\mathbb{S}^{k}_{lm} + \mathbb{S}^{m}_{ij}\mathbb{T}^{k}_{lm} - \mathbb{S}^{k}_{lj,i} - \mathbb{S}^{m}_{lj}\mathbb{S}^{k}_{im} - \mathbb{S}^{m}_{lj}\mathbb{T}^{k}_{im}\right] \\
&+(1/2)\left[\mathbb{T}^{k}_{ij,l} + \mathbb{T}^{m}_{ij}\mathbb{T}^{k}_{lm} + \mathbb{T}^{m}_{ij}\mathbb{S}^{k}_{lm} + \mathbb{T}^{k}_{lj,i} + \mathbb{T}^{m}_{lj}\mathbb{T}^{k}_{im} + \mathbb{T}^{m}_{lj}\mathbb{S}^{k}_{im}\right] \\
&+(1/2)\left[\mathbb{T}^{k}_{ij,l} + \mathbb{T}^{m}_{ij}\mathbb{T}^{k}_{lm} + \mathbb{T}^{m}_{ij}\mathbb{S}^{k}_{lm} - \mathbb{T}^{k}_{lj,i} - \mathbb{T}^{m}_{lj}\mathbb{T}^{k}_{im} - \mathbb{T}^{m}_{lj}\mathbb{S}^{k}_{im}\right].
\end{aligned}
$$

Then we develop the expression in the right hand side. We have

$$
\mathbb{S}^{k}_{ij,l} - \mathbb{S}^{k}_{lj,i} + \mathbb{T}^{k}_{ij,l} - \mathbb{T}^{k}_{lj,i} = \Gamma^{k}_{ij,l} - \Gamma^{k}_{lj,i},
$$

and

- $$
\begin{aligned}
\mathbb{S}^{m}_{ij}\mathbb{S}^{k}_{lm} - \mathbb{S}^{m}_{lj}\mathbb{S}^{k}_{im} &= (1/4)\left(\Gamma^{m}_{ij}\Gamma^{k}_{lm} - \Gamma^{m}_{lj}\Gamma^{k}_{im}\right) + (1/4)\left(\Gamma^{m}_{ij}\Gamma^{k}_{ml} - \Gamma^{m}_{lj}\Gamma^{k}_{mi}\right) \\
&+ (1/4)\left(\Gamma^{m}_{ji}\Gamma^{k}_{lm} - \Gamma^{m}_{jl}\Gamma^{k}_{im}\right) + (1/4)\left(\Gamma^{m}_{ji}\Gamma^{k}_{ml} - \Gamma^{m}_{jl}\Gamma^{k}_{mi}\right)
\end{aligned}
$$
- $$
\begin{aligned}
\mathbb{S}^{m}_{ij}\mathbb{T}^{k}_{lm} - \mathbb{S}^{m}_{lj}\mathbb{T}^{k}_{im} &= (1/4)\left(\Gamma^{m}_{ij}\Gamma^{k}_{lm} - \Gamma^{m}_{lj}\Gamma^{k}_{im}\right) - (1/4)\left(\Gamma^{m}_{ij}\Gamma^{k}_{ml} - \Gamma^{m}_{lj}\Gamma^{k}_{mi}\right) \\
&+ (1/4)\left(\Gamma^{m}_{ji}\Gamma^{k}_{lm} - \Gamma^{m}_{jl}\Gamma^{k}_{im}\right) - (1/4)\left(\Gamma^{m}_{ji}\Gamma^{k}_{ml} - \Gamma^{m}_{jl}\Gamma^{k}_{mi}\right)
\end{aligned}
$$
- $$
\begin{aligned}
\mathbb{T}^{m}_{ij}\mathbb{T}^{k}_{lm} - \mathbb{T}^{m}_{lj}\mathbb{T}^{k}_{im} &= (1/4)\left(\Gamma^{m}_{ij}\Gamma^{k}_{lm} - \Gamma^{m}_{lj}\Gamma^{k}_{im}\right) - (1/4)\left(\Gamma^{m}_{ij}\Gamma^{k}_{ml} - \Gamma^{m}_{lj}\Gamma^{k}_{mi}\right) \\
&- (1/4)\left(\Gamma^{m}_{ji}\Gamma^{k}_{lm} - \Gamma^{m}_{jl}\Gamma^{k}_{im}\right) + (1/4)\left(\Gamma^{m}_{ji}\Gamma^{k}_{ml} - \Gamma^{m}_{jl}\Gamma^{k}_{mi}\right)
\end{aligned}
$$
-

$$\mathbb{T}^m_{ij}\mathbb{S}^k_{lm} - \mathbb{T}^m_{lj}\mathbb{S}^k_{im} = (1/4)\left(\Gamma^m_{ij}\Gamma^k_{lm} - \Gamma^m_{lj}\Gamma^k_{im}\right) + (1/4)\left(\Gamma^m_{ij}\Gamma^k_{ml} - \Gamma^m_{lj}\Gamma^k_{mi}\right) - (1/4)\left(\Gamma^m_{ji}\Gamma^k_{lm} - \Gamma^m_{jl}\Gamma^k_{im}\right) - (1/4)\left(\Gamma^m_{ji}\Gamma^k_{ml} - \Gamma^m_{jl}\Gamma^k_{mi}\right).$$

The sum of the four previous equalities is equal to $\Gamma^m_{ij}\Gamma^k_{lm} - \Gamma^m_{lj}\Gamma^k_{im}$. Then we have

$$\mathbb{S}^k_{ij,l} + \mathbb{S}^k_{lj,i} + \mathbb{T}^k_{ij,l} + \mathbb{T}^k_{lj,i} = \Gamma^k_{ij,l} + \Gamma^k_{lj,i},$$

and

- $$\mathbb{S}^m_{ij}\mathbb{S}^k_{lm} + \mathbb{S}^m_{lj}\mathbb{S}^k_{im} = (1/4)\left(\Gamma^m_{ij}\Gamma^k_{lm} + \Gamma^m_{lj}\Gamma^k_{im}\right) + (1/4)\left(\Gamma^m_{ij}\Gamma^k_{ml} + \Gamma^m_{lj}\Gamma^k_{mi}\right) + (1/4)\left(\Gamma^m_{ji}\Gamma^k_{lm} + \Gamma^m_{jl}\Gamma^k_{im}\right) + (1/4)\left(\Gamma^m_{ji}\Gamma^k_{ml} + \Gamma^m_{jl}\Gamma^k_{mi}\right)$$
- $$\mathbb{S}^m_{ij}\mathbb{T}^k_{lm} + \mathbb{S}^m_{lj}\mathbb{T}^k_{im} = (1/4)\left(\Gamma^m_{ij}\Gamma^k_{lm} + \Gamma^m_{lj}\Gamma^k_{im}\right) - (1/4)\left(\Gamma^m_{ij}\Gamma^k_{ml} + \Gamma^m_{lj}\Gamma^k_{mi}\right) + (1/4)\left(\Gamma^m_{ji}\Gamma^k_{lm} + \Gamma^m_{jl}\Gamma^k_{im}\right) - (1/4)\left(\Gamma^m_{ji}\Gamma^k_{ml} + \Gamma^m_{jl}\Gamma^k_{mi}\right)$$
- $$\mathbb{T}^m_{ij}\mathbb{T}^k_{lm} + \mathbb{T}^m_{lj}\mathbb{T}^k_{im} = (1/4)\left(\Gamma^m_{ij}\Gamma^k_{lm} + \Gamma^m_{lj}\Gamma^k_{im}\right) - (1/4)\left(\Gamma^m_{ij}\Gamma^k_{ml} + \Gamma^m_{lj}\Gamma^k_{mi}\right) - (1/4)\left(\Gamma^m_{ji}\Gamma^k_{lm} + \Gamma^m_{jl}\Gamma^k_{im}\right) + (1/4)\left(\Gamma^m_{ji}\Gamma^k_{ml} + \Gamma^m_{jl}\Gamma^k_{mi}\right)$$
- $$\mathbb{T}^m_{ij}\mathbb{S}^k_{lm} + \mathbb{T}^m_{lj}\mathbb{S}^k_{im} = (1/4)\left(\Gamma^m_{ij}\Gamma^k_{lm} + \Gamma^m_{lj}\Gamma^k_{im}\right) + (1/4)\left(\Gamma^m_{ij}\Gamma^k_{ml} + \Gamma^m_{lj}\Gamma^k_{mi}\right) - (1/4)\left(\Gamma^m_{ji}\Gamma^k_{lm} + \Gamma^m_{jl}\Gamma^k_{im}\right) - (1/4)\left(\Gamma^m_{ji}\Gamma^k_{ml} + \Gamma^m_{jl}\Gamma^k_{mi}\right).$$

The sum of the four previous equalities is equal to $\Gamma^m_{ij}\Gamma^k_{lm} + \Gamma^m_{lj}\Gamma^k_{im}$. Consequently,

$$\mathbb{S}^k_{ij,l} + \mathbb{T}^k_{ij,l} + \mathbb{S}^m_{ij}\mathbb{S}^k_{lm} + \mathbb{S}^m_{ij}\mathbb{T}^k_{lm} + \mathbb{T}^m_{ij}\mathbb{S}^k_{lm} + \mathbb{T}^m_{ij}\mathbb{T}^k_{lm}$$

$$= (1/2)\left(\Gamma^k_{ij,l} + \Gamma^m_{ij}\Gamma^k_{lm} - \Gamma^k_{lj,i} - \Gamma^m_{lj}\Gamma^k_{im}\right) + (1/2)\left(\Gamma^k_{ij,l} + \Gamma^m_{ij}\Gamma^k_{lm} + \Gamma^k_{lj,i} + \Gamma^m_{lj}\Gamma^k_{im}\right).$$

References

[1] Agiasofitou EK, Lazar M. Conservation and balance laws in linear elasticity, *Journal of Elasticity* 94, 2099, pp 69-85.

[2] Betram A, Svendsen B. On Material Objectivity and Reduced Constitutive Equations, *Archive of Mechanics* 53 (6), 2001, pp 653-675.
[3] Cartan E. *On manifolds with an affine connection and the theory of general relativity*, English translation of the French original by A. Magnon and A. Ashtekar, Bibliopolis, Napoli, 1986.
[4] Choquet-Bruhat Y, De Witt-Morette C, Dillard-Bleick M. *Analysis manifolds and physics*, North-Holland, New-York, 1977, part 3 and 5.
[5] Cermelli P , Gurtin ME. Geometrically necessary dislocations in viscoplastic single crystals and bicrystals undergoing small deformations, *Int J of Solids and Struct* 39, 2002, pp 6281-6309.
[6] Ehlers J. The nature and concept of spacetime, *The Physicist's concept of nature*, Edited by J. Mehra, Reidel Publishing Compagny, Dordrecht-Holland, 1973, pp 71-91.
[7] Fleck NA, Hutchinson JW. Strain gradient plasticity, *Adv in Appl Mech* 33, 1997, pp 295-361.
[8] Fleck NA, Hutchinson JW. A reformulation of strain gradient plasticity, *J Mech Phys Solids* 49, 2001, pp 2245-2271.
[9] Forest S, Cordero NM, Busso EP. First vs. second gradient of strain theory for capillarity effects in an elastic fluid at small length scales, *Computational Material Sciences*, 2010 (to appear).
[10] Gao H, Huang Y, Nix WD, Hutchinson JH. Mechanim-based strain gradient plasticity I : Theory, *J Mech Phys Solids* 47, 1999, pp 1239-1263.
[11] Huang Y, Gao H, Nix WD, Hutchinson JH. Mechanism-based strain gradient plasticity II. Analysis, *J Mech Phys Solids* 48, 2000, pp 99-128.
[12] Kleinert H. *Multivalued Fields: in Condensed matter, Electromagnetism, and Gravitation*, World Scientific, Singapore, 2008.
[13] Kroener E. Continuum theory of defects, *Physique des défauts*, Les Houches July 28 - August 29, North-Holland Publishing, Edited by Balian et al, 1981, pp 219-315.
[14] Lazar M. An elastoplastic theory of dislocations as a physical field with torsion, *Journal Phys A : Math Gen* 35, 2002, pp 1983-2004.
[15] Lazar M, Maugin G, Aifantis E. Dislocations in second strain gradient elasticity, *Int J of Solids and Struct* 43, 2006, pp 1787-1817.
[16] Le KC, Stumpf H. On the determination of the crystal reference in nonlinear continuum theory of dislocations, *Proc R Soc Lond A* 452, 1996, pp 359-371.
[17] Lovelock D, Rund H. *Tensors, Differential Forms, and Variational Principles*, Wiley, New-York, 1975, chap 8.
[18] Lubarda VA. The effect of couple stresses on dislocations strain energy, *Int J of Solids and Struct* 40, 2003, pp 3807-3826.
[19] Marsden JE, Hughes TJR. *Mathematical foundations of elasticity*, Prentice-Hall, 1983.
[20] Maugin G. *Material Inhomogeneities in Elasticity*. Chapman and Hall, 1993.
[21] Mindlin RD. Micro-structure in linear elasticity, *Arch Rat Mech Analysis* 16, 1964, pp 51-78.

[22] Mindlin RD. Second gradient of strain and surface-tension in linear elasticity, *Int J of Solids and Struct* 1, 1965, pp 417-438.
[23] Nakahara M. Geometry, Topology and Physics, *Graduate Student Series in Physics*, edited by D.F. Brewer, Institute of Physics Publishing, Bristol, 1996.
[24] Noll W. Materially uniform simple bodies with inhomogeneities, *Arch Rat Mech Analysis* 27, 1967, pp 1-32.
[25] Popov VL, Kröner E. Theory of elastopolastic media with mesostructures, *Theoritical and Applied Fracture Mechanics* 37, 2001, pp 299-310.
[26] Rakotomanana RL. Contribution à la modélisation géométrique et thermodynamique d'une classe de milieux faiblement continus, *Arch Rat Mech Analysis* 141, 1997, pp 199-236.
[27] Rakotomanana RL. *A geometric approach to thermomechanics of dissipating continua*, Birkauser, Boston, 2003.
[28] Rakotomanana RL. Some class of SG continuum models to connect various length scales in plastic deformation, *Mechanics of material forces* chap 32, edited by P. Steimann and G. A. Maugin, Springer, 2005.
[29] Rakotomanana RL. *Élements de dynamiques des structures et solides déformables*, Presses Polytechniques et Universitaires Romandes, Lausanne, 2009.
[30] Svendsen B, Betram A. On frame-indifference and form-invariance in constitutive theory, *Acta Mechanica* 132, 1999, pp 195-207.
[31] Svendsen B, Neff P, Menzel A. On Constitutive and configurational aspects of models for gradient continua with microstructure, *Z Angew Math Mech* 89(8), 2009, pp 687-697.
[32] Toupin RA. Elastic materials with couple stresses, *Arch Rat Mech Analysis* 11, 1962, pp 385-414.
[33] Wang CC. Geometric structure of simple bodies, or mathematical foundation for the theory of continuous distributions of dislocations, *Arch Rat Mech Analysis* 27, 1967, pp 33-94.
[34] Zhao J, Pedroso D. Strain gradient theory in orthogonal curvilinear coordinates, *Int J of Solids and Struct* 45, 2008, pp 3507-3520.

Part VI
Further Applications

Chapter 16
Cahn-Hilliard Generalized Diffusion Modeling Using the Natural Element Method

Paul Fischer, Amirtham Rajagopal, Ellen Kuhl, and Paul Steinmann

Abstract In this work, we present an application of two versions of the natural element method (NEM) to the Cahn-Hilliard equation. The Cahn-Hilliard equation is a nonlinear fourth order partial differential equation, describing phase separation of binary mixtures. Numerical solutions requires either a two field formulation with C^0 continuous shape functions or a higher order C^1 continuous approximations to solve the fourth order equation directly. Here, the C^1 NEM, based on Farin's interpolant is used for the direct treatment of the second order derivatives, occurring in the weak form of the partial differential equation. Additionally, the classical C^0 continuous Sibson interpolant is applied to a reformulation of the equation in terms of two coupled second order equations. It is demonstrated that both methods provide similar results, however the C^1 continuous version needs fewer degrees of freedom to capture the contour of the phase boundaries.

16.1 Introduction

The Cahn-Hilliard equation is a mathematical description of the kinematics and morphology evolution of phase separation. Typical examples of phase separation include multiphase fluid flow [1, 2], image processing [3], mineral exsolution and growth [4], biological applications [5] and polymer science [6], just to mention a few.

In phase separation or spinodal decomposition, a binary mixture of two components moves against the concentration gradients and forms components pure in each

Paul Fischer, Amirtham Rajagopal and Paul Steinmann
Chair of Applied Mechanics, University of Erlangen-Nuremberg, Egerlandstrasse 5, 91058 Erlangen, e-mail: paul.fischer@ltm.uni-erlangen.de

Ellen Kuhl
Departments of Mechanical Engineering, Bioengineering and Cardiothoracic Surgery, Stanford, CA 94305, USA e-mail: ekuhl@stanford.edu

H. Altenbach et al. (eds.), *Mechanics of Generalized Continua,*
Advanced Structured Materials, 7, DOI: 10.1007/978-3-642-19219-7_16,

phase. This effect is driven by the gradients of the chemical potential. The whole process is governed by two energies, a local configurational energy and a nonlocal surface energy. The local configurational energy is a function of the concentrations, whereas the surface energy is dependent on the concentration gradients.
Starting with a homogeneous mixture, the spinodal decomposition can be classified into two stages. The initial stage of the phase separation minimizes the configurational energy by driving the local concentration into the two valleys of the energy potential that are associated with the pure phases. The second stage, which could be identified to be equivalent to Ostwald ripening [7], minimizes the surface energy by reducing the number of pure phase regions.
The numerical solution of the Cahn-Hilliard equation is extremely challenging. This is because of multiple reasons. Firstly, the initial phase separation and the minimization of the surface energy takes place at different time scales. Secondly, the configurational energy is a highly nonlinear function of the concentration. And third, maybe the most critical, the Cahn-Hilliard equation is a fourth order partial differential equation. These three difficulties result in the necessity of adaptive time stepping schemes and the requirement of iterative solutions within the application of implicit time stepping schemes. The treatment of the fourth order gradients of the concentration is requiring either higher-order approximation schemes or the decomposition of the partial differential equation into two equations, requiring a lower continuity.
Both methods have shown to be applicable for the solution of the Cahn-Hilliard equation, i.e. see [8, 9, 10] for C^1 continuous approximation schemes, [11] for the application to the discontinuous Galerkin method or [4, 12, 13] for application of the operator decomposition.
In this paper, we present a comparison of the direct solution based on the C^1 natural element method and an equation decomposition, treated with the C^0 NEM based on Sibson's interpolant.
We start with a review of the Cahn-Hilliard equation in section 16.2, the decomposition of the Cahn-Hilliard equation into two second order equations is revisited in section 16.3. This is followed by section 16.4, introducing the weak forms of the equations. The natural element method, used for the discretization of the concentration field is explained in section 16.5. The special treatment of periodic boundary conditions is mentioned as well. For temporal discretization, a generalized trapezoidal method is discussed in section 16.6. This is followed by the introduction of the discrete residuals and stiffness matrices in section 16.7. The contribution closes with a numerical example and discussion of the results in section 16.8 and section 16.9.

16.2 Governing equations

Considering a binary mixture of two constituents with c and $1-c$ as their respective concentrations. The concentration c satisfies $0 \leq c \leq 1$. Pure phases are obtained for $c = 0$ and $c = 1$. Let $\mathscr{B} \subset \mathbb{R}^d$, $d = 1$, 2 or 3 be and open, simply connected domain.

The Cahn-Hilliard equation describes the evolution of the concentration $\dot{c}$ by the following diffusion equation,

$$\dot{c} = -\nabla \cdot \mathbf{j} \text{ with } \mathbf{j} = -M\nabla\mu. \tag{16.1}$$

Here, the flux of the concentration $\mathbf{j}$ is driven by the gradients of the chemical potential $\nabla\mu$ weighted by the mobility $M > 0$.
The chemical potential μ is the variational derivative of the free energy density Ψ^c, $\mu = \delta_c(\Psi^c)$. For the Cahn-Hilliard equation, the free energy density

$$\Psi^c = \Psi^{con}(c) + \Psi^{sur}(\nabla c), \tag{16.2}$$

is decomposed into the configurational energy, parameterized in terms of the local concentration c and the surface term $\Psi^{sur}(\nabla c)$, parameterized in the concentration gradient.
The configurational energy is assumed to have the symmetric form

$$\Psi^{con} = RT\,[c\log(c) + [1-c]\log(1-c) + 2\theta c[1-c]]. \tag{16.3}$$

In the previous equation (16.3) R is the gas constant, T_c the critical temperature, i.e. the lowest temperature at which the two phases attain the same composition, T the absolute temperature in Kelvin and $\theta = T_c/T$ is the dimensionless ratio between the critical and the absolute temperature. The contribution of the configurational energy to the chemical potential will be denoted as

$$\mu_c = \delta_c \Psi^{con}. \tag{16.4}$$

$\Psi^{sur}(\nabla c)$, denotes the surface energy parameterized in terms of the concentration gradient ∇c. Here a quadratic function is used for the interface energy expression

$$\Psi^{sur} = \frac{1}{2}\lambda ||\nabla c||^2, \tag{16.5}$$

where the parameter λ is related to an internal length scale l as $\lambda = l^2 RT$. Its contributions to the chemical potential takes the following explicit representation

$$-\nabla \cdot (\delta_{\nabla c}\Psi^{sur}) = -\lambda \Delta\, c. \tag{16.6}$$

By inserting (16.4) and (16.6) in (16.1), we obtain the typical fourth order Cahn-Hilliard equation

$$\dot{c} = \nabla \cdot (M\nabla(\mu_c - \lambda\Delta\, c)). \tag{16.7}$$

To achieve the initial boundary value problem, the boundary $\Gamma = \partial\mathscr{B}$ of the domain with an outward unit normal $\mathbf{n}$ is considered. Here, it is assumed that the boundary is sufficiently smooth. The boundary is composed of two complementary parts $\Gamma = \Gamma_c \cup \Gamma_t = \Gamma_g \cup \Gamma_q$ on which either Dirichlet or Neumann boundary conditions are prescribed. The strong form of the problem is stated as follows:
Find $c : \mathscr{B} \times (0, \mathscr{T}) \to \mathbb{R}$ such that

$$\dot{c} = \nabla \cdot (M \nabla(\mu_c - \lambda \Delta c)) \text{ in } \mathscr{B} \times (0, \mathscr{T}) \tag{16.8}$$

satisfying the initial value

$$c(x,0) = c_0(x) \text{ in } \mathscr{B} \tag{16.9}$$

subject to the following boundary conditions

$$\begin{array}{rrr} c = \bar{c} & \text{on } \Gamma_c \times (0,\mathscr{T}) & \text{or } M\nabla(\mu_c - \lambda\Delta c)\cdot \mathbf{n} = \bar{t} \text{ on } \Gamma_t \times (0,\mathscr{T}) \\ \nabla c \cdot \mathbf{n} = \bar{g} & \text{on } \Gamma_g \times (0,\mathscr{T}) & \text{or } M\lambda\Delta c = \bar{q} \text{ on } \Gamma_q \times (0,\mathscr{T}). \end{array} \tag{16.10}$$

In the above equation (16.10), the boundary conditions are represented in a general form. The upper row constitute the Dirichlet boundary conditions on the concentration and the first order Neumann boundary conditions. The second row of (16.10) represent the remaining set of boundary conditions. In this contribution, periodic Dirichlet boundary conditions are used.

Mobility:

In most physical applications, the mobility M is assumed as $M = Dc[1-c]/[RT]$, where D is the diffusivity which has units of $length^2/time$. The above relationship for the mobility restricts the diffusion process primarily to the interfacial zones and is commonly referred to as degenerate mobility. To simplify the equations, the mobility is often approximated to be constant $M = D/[RT]$.

16.3 Decomposition of the diffusion equation

To avoid the difficulty of the fourth order diffusion equation, the additional non-local concentration field

$$\bar{c} = c + \kappa \Delta c \tag{16.11}$$

is introduced. Accordingly the surface part of the chemical potential

$$-\nabla \lambda \Delta c = -\gamma \nabla(\bar{c} - c) \tag{16.12}$$

can be expressed in terms of the local concentration field c and the nonlocal concentration field $\bar{c}$. The new parameters κ and γ are introduced as decomposition of the parameter λ by $\gamma = \lambda/\kappa$. In principle, this decomposition can be chosen arbitrarily. Here the concrete value is used for scaling of the numerical equations.

By inserting (16.12) into the original form of the Cahn-Hilliard equation (16.7), the single fourth order partial differential equation is thus replaced by the two sets of second order equations

$$\begin{aligned} \dot{c} &= \nabla \cdot (M \nabla(\mu_c + \gamma[c - \bar{c}])) \\ \bar{c} &= c + \kappa \Delta c. \end{aligned} \tag{16.13}$$

16.4 Weak form of the Cahn-Hilliard equation

The weak form of equation (16.7) and (16.13) is achieved by multiplication with the test functions w and $\bar{w}$ and integrating over the domain $\mathscr{B}$. By application of integration by parts, symmetric equations are derived. The result of the fourth order equation (16.7) is given by

$$\begin{aligned}&\int_{\mathscr{B}} w\dot{c} + \Delta w M\lambda\Delta\, c + \nabla w\cdot[M\nabla\mu_c + \nabla M\lambda\Delta\, c]\ \mathrm{dV}\\ &-\int_{\Gamma} wM\nabla(\mu_c - \lambda\Delta\, c)\cdot\mathbf{n} - M\lambda\Delta_c\nabla w\cdot\mathbf{n}\ \mathrm{dA}\doteq 0.\end{aligned} \tag{16.14}$$

Whereas the weak form of (16.13) results in

$$\begin{aligned}\int_{\mathscr{B}} \dot{c}w + \nabla w\cdot[M\nabla\cdot[\mu_c + \gamma[c-\bar{c}]]]\ \mathrm{dV} - \int_{\Gamma} wM\nabla\mu\cdot\mathbf{n}\ \mathrm{dA}\doteq 0\\ \int_{\mathscr{B}} w[\bar{c}-c] + \nabla\bar{w}\cdot\kappa\nabla c\ \mathrm{dV} - \int_{\Gamma}\bar{w}\lambda^2\nabla c\cdot\mathbf{n}\ \mathrm{dA}\doteq 0.\end{aligned} \tag{16.15}$$

In contrast to (16.14), where second order derivatives are occurring, (16.15) only contains first derivatives in the resulting expressions.

16.5 The natural element method

For the approximation of the concentration field c, we make use of the natural element method. In the C^0 continuous case, the shape functions are the Sibson's interpolant [17]. Here, the definition of these functions is shortly revisited.
Considering a set of nodes $\mathscr{N} = \{\mathbf{p}_1, \mathbf{p}_2, ..., \mathbf{p}_n\} \in \mathbb{R}^d$, the first-order Voronoi diagram $\mathscr{V}(\mathscr{N})$ is the subdivision of the Euclidian space $\mathbb{R}^d$ into convex regions

$$V(\mathbf{p}_I) = \{c \in \mathbb{R}^d : ||\mathbf{x} - \mathbf{p}_I|| < ||\mathbf{x} - \mathbf{p}_J|| \forall J \neq I\}, \tag{16.16}$$

the Voronoi cells. The Voronoi cell is the set of points being closer the point $\mathbf{p}_I$ than to any other point $\mathbf{p}_J \in \mathscr{N}$. By the introduction of a new nodal point $\mathbf{x}$, in the set $\mathscr{N}$, the new set $\tilde{\mathscr{N}} := \mathscr{N} \cup \mathbf{x}$ is introduced. The corresponding Voronoi cells are denoted as $\tilde{V}(\mathbf{p}_i)$. The Sibson's interpolant is thus defined as

$$N_I^0(\mathbf{x}) := \frac{A(V(\mathbf{p}_I) \cap \tilde{V}(\mathbf{x}))}{A(\tilde{V}(\mathbf{x}))}, \tag{16.17}$$

where $A(\circ)$ denotes the d-dimensional volume measure. The overlap of the sets $V(\mathbf{p}_I)$ and $\tilde{V}(\mathbf{x})$ is demonstrated in Fig. 1(a). The Sibson interpolant posseses the properties non-negativity, $0 \leq N_I^0 \leq 1$, partition of unity $\sum_I N_I^0 = 1$, interpolation at the nodes $N_I(\mathbf{p}_J) = \delta_{IJ}$, linear completeness $\sum_I \mathbf{p}_I N_I^0(\mathbf{x}) = \mathbf{x}$ and linear behavior along the boundary, thus allowing the exact imposition of essential boundary

conditions. The functions are C^{∞} everywhere apart from the boundary of the shape function supports and the nodes, where they are C^1 and C^0, respectively. The Sibson interpolant, related to the point $\mathbf{p}_5$ is presented in Fig. 1(b).

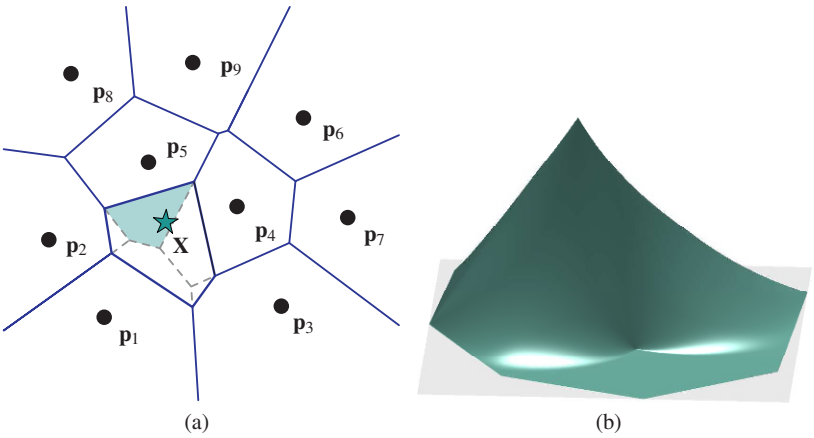

Fig. 16.1 (a) Overlap of the original Voronoi cell $\mathcal{V}_5$ and $\tilde{\mathcal{V}}_{\mathbf{x}}$. (b) Sibson interpolant N_5^0.

Farin's C^1 interpolant is making use of the fact that the Sibson natural neighbor interpolants can be considered as generalized barycentric coordinates. The C^1 continuity at the nodal points is then introduced by the embedding of the Sibson interpolant into a cubic Bernstein-Bézier patch. For a point $\mathbf{x}$, the shape functions, interpolating the concentration are given by

$$N^1_{3I-2}(\mathbf{x}) = (N^0_I(\mathbf{x}))^3 + \sum_{J\neq I} 3(N^0_I(\mathbf{x}))^2 N^0_J(\mathbf{x}) + \sum_{J\neq I\neq K\neq J} 2N^0_I(\mathbf{x})N^0_J(\mathbf{x})N^0_K(\mathbf{x}). \tag{16.18}$$

and the additional functions for the interpolation of the gradients

$$\begin{pmatrix} N^I_{3I-1}(\mathbf{x}) \\ N^I_{3I}(\mathbf{x}) \end{pmatrix} = \sum_{I\neq J} [\mathbf{p}_J - \mathbf{p}_I] N^0_I(\mathbf{x})^2 N^0_J(\mathbf{x}) + \frac{1}{4} \sum_{J\neq I\neq K\neq J} [\mathbf{p}_J + \mathbf{p}_K - 2\mathbf{p}_I] N^0_I(\mathbf{x})N^0_J(\mathbf{x})N^0_K(\mathbf{x}). \tag{16.19}$$

For the detailed description, the interested reader is referred to [16] or [15]. The C^1 continuous natural element shape functions have the following desirable properties:

- quadratic completeness
- behavior like cubic Hermit shape functions along the boundary of the geometry

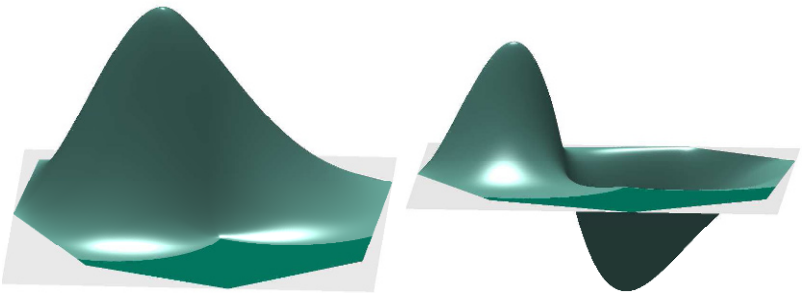

Fig. 16.2 C^1 Natural element shape functions, related to the nodal concentration value and the nodal gradient. (a) N^1_{13} and (b) N^1_{15}

- interpolation of the nodal function values and nodal derivatives
$$N^1_{3I-2}(\mathbf{x}_J) = \delta_{IJ},\ N^1_{3I-1}(\mathbf{x}_J) = 0,\quad N^1_{3I}(\mathbf{x}_J) = 0$$
$$N^1_{3I-2,x}(\mathbf{x}_J) = 0,\quad N^1_{3I-1,x}(\mathbf{x}_J) = \delta_{IJ},\ N^1_{3I,x}(\mathbf{x}_J) = 0$$
$$N^1_{3I-2,y}(\mathbf{x}_J) = 0,\quad N^1_{3I-1},y(\mathbf{x}_J) = 0,\quad N^1_{3I,y}(\mathbf{x}_J) = \delta_{IJ}.$$

Those properties and the ability to model highly complex geometries makes them extremely suitable for numerical treatment of the Cahn-Hilliard equation. In contrast to different C^1 continuous methods, the NEM has the advantage, that it is interpolationary at the boundary of the domain and it can easily handle complex topologies of the domain. However its major advantage is that its complexity does not increase when extending to three dimensions.

16.5.1 Periodic boundary conditions

The behavior of the C^1 interpolants along the boundary of the domain is identical to cubic Hermite interpolation. Unfortunately, this statement is not true for the normal derivatives of the function. Due to this reason, for exact application of C^1 continuous boundary conditions either the bubble functions $b = N^0_I N^0_J N^0_K$ have to be rearranged at the boundary, such that the normal derivative is linear between two boundary nodes or the Voronoi cells have to be computed directly on the periodic topology. In this contribution, the latter has been chosen.
Considering a periodic box with width l_1 and height l_2, the distance on the modulo space $\mathbb{R}/l_1\mathbb{R} \times \mathbb{R}/l_2\mathbb{R}$ is given by

$$d(\mathbf{x},\mathbf{y}) := \left[\sum_i \left[\min\left\{|x_i - y_i|, l_1 - |x_i - y_i|\right\}\right]^2\right]^{\frac{1}{2}} \tag{16.20}$$

and the periodicity is a simple consequence of the definition of the Sibon interpolant.

16.6 Time integration

To discretize the residual equation in time, the generalized trapezoidal method is used. To this end, the time interval $(0,\tau)$ is partitioned into discrete strictly positive subintervals $[t_n, t_{n+1}]$ with current increment $\Delta t = t_{n+1} - t_n$. From here on, the index $\circ_{n+1}$ is omitted for sake of transparency.
The starting point is the known concentration c_n, at the beginning of the current time step Δt. The generalized trapezoidal method is used for the update of the concentration in time, according to the concentration functional

$$\begin{aligned}\Pi_{\mathscr{B}}(c,w) = &\int_{\mathscr{B}} \Delta w M \lambda \Delta c + \nabla w \cdot [M \nabla \mu_c + \nabla M \lambda \Delta c] \ \mathrm{dV} \\ &- \int_{\Gamma} w M \nabla(\mu_c - \lambda \Delta c) \cdot \mathbf{n} + M \lambda \Delta c \nabla w \cdot \mathbf{n} \ \mathrm{dA}\end{aligned} \tag{16.21}$$

or the corresponding expression for the two field problem

$$\begin{aligned}\Pi^c_{\mathscr{B}}(c,w) = &\int_{\mathscr{B}} \nabla w \cdot [M \nabla \cdot [\mu_c + \gamma[c - \bar{c}]]] \ \mathrm{dV} \\ &- \int_{\Gamma} M \nabla \mu \cdot \mathbf{n} \ \mathrm{dA}\end{aligned} \tag{16.22}$$

In a semi-discretized form, using the generalized trapezoidal method, we write

$$R_{n,\alpha}(c,w) = \int_{\mathscr{B}} \frac{1}{\Delta t} w[c - c_n] \ \mathrm{dV} + \alpha \Delta t \Pi_{\mathscr{B}}(c,w) + [1-\alpha]\Delta t \Pi_{\mathscr{B}}(c_n,w) \doteq 0. \tag{16.23}$$

16.7 Stiffness matrices

By introducing the C^1 continuous interpolation functions in the semi-discretized form (16.23), the discrete residuals are

$$R_{n,\alpha}(c,N^1_I) = \int_{\mathscr{B}} N^1_I \frac{1}{\Delta t}[c - c_n] \ \mathrm{dV} + \alpha \Pi_{\mathscr{B}}(c,N^1_I) + [1-\alpha]\Pi_{\mathscr{B}}(c_n,N^1_I) \doteq 0. \tag{16.24}$$

For the solution of the highly-nonlinear discrete residual equations (16.24), the Newton-Raphson method is used,

$$R_{n,\alpha}^{k+1} = R_{n,\alpha}^{k} + dR_{n,\alpha} \doteq 0 \;\text{ with }\; dR_I = \sum_{J=1}^{3m} K_{IJ} dc_J. \tag{16.25}$$

The corresponding iteration matrix takes the following explicit representation:

$$\begin{aligned} K_{IJ} = & \int_{\mathscr{B}} N_I^1 \frac{1}{\Delta t} N_J^1 \\ & + \alpha \Big[\int_{\mathscr{B}} \Delta N_I^1 \lambda \left[M \Delta \partial_c M N_j^1 \right] \, \mathrm{dV} \\ & + \int_{\mathscr{B}} \nabla N_I^1 \cdot \left[\nabla \mu_c \partial_c M N_J^1 + M \partial_c \mu_c \nabla N_J^1 + \lambda \left[\Delta c \partial_c M \nabla N_J^1 + \nabla M \Delta N_J^1 \right] \right] \, \mathrm{dV} \\ & + \int_{\mathscr{B}} \nabla N_I^1 \cdot \left[\lambda \Delta \, c \partial_c^2 M \nabla c N_J^1 + M \partial_c^2 \mu_c \nabla c N_J^1 \right] \, \mathrm{dV} \Big]. \end{aligned} \tag{16.26}$$

For the mixed form, the two sets of residual equations are identified as follows:

$$\begin{aligned} R_{n,\alpha}^{c} &= N_I^0 \frac{c - c^n}{\Delta t} + \alpha \Pi_{\mathscr{B}}(c, N_I^0) + [1-\alpha] \Pi_{\mathscr{B}}(c_n, N_I^0) \doteq 0 \\ R^{\bar{c}} &= N_J^0 \left[\bar{c} - c \right] + \nabla N_J^0 \kappa \nabla c \end{aligned} \tag{16.27}$$

with the following iteration matrices

$$\begin{aligned} K_{IK}^{cc} = & \int_{\mathscr{B}} N_I^0 \frac{1}{\Delta t} N_K^0 \\ & + \nabla N_I^0 \cdot \left[M \partial_c \mu_c + \gamma \right] \nabla N_K^0 \\ & + \nabla N_I^0 \cdot \left[\partial_c M \nabla \left[\mu_c + \gamma [c - \bar{c}] \right] \right] N_K^0 \\ & + \nabla N_I^0 \cdot \left[M \partial_c \nabla c \mu_c \right] N_K^0 \, \mathrm{dV} \\ K_{IL}^{c\bar{c}} = & - \int_{\mathscr{B}} \nabla N_I^0 \cdot M \gamma \nabla N_L^0 \, \mathrm{dV} \\ K_{JK}^{\bar{c}c} = & - \int_{\mathscr{B}} N_J^0 N_K^0 + \nabla N_J \cdot \kappa \nabla N_K^0 \, \mathrm{dV} \\ K_{IL}^{\bar{c}\bar{c}} = & \int_{\mathscr{B}} N_J^0 N_L^0 \, \mathrm{dV}. \end{aligned} \tag{16.28}$$

16.8 Computational results

Here, the solution for the C^0 and C^1 NEM are compared. A periodic unit square domain with length $l_1 = 20$ and $l_2 = 20$ is used. For the comparison of the results, the initial concentration is given by

$$c_0(\mathbf{x}) = \begin{cases} 0.45 & \text{for } \min_i(x_i) \leq 2.34 \\ 0.45 & \text{for } \min_i(x_i) > 2.34. \end{cases} \tag{16.29}$$

The computations are performed with degenerate mobility and the following dimensionless material parameters: $D = 2$, $RT = 2000$, $\theta = 1.1$ and $\lambda = 500$. An initial time step of $\Delta t = 10 \times 10^{-3}$ is considered. Fig. 16.3 illustrates the behavior of the internal energies for different discretizations. The fine discretizations have 200, 1250 and 5000 degrees of freedom in case of the C^0 continuous discretization and 192, 1200 and 7500 in case of the C^1 continuous results. To be able to see any differences

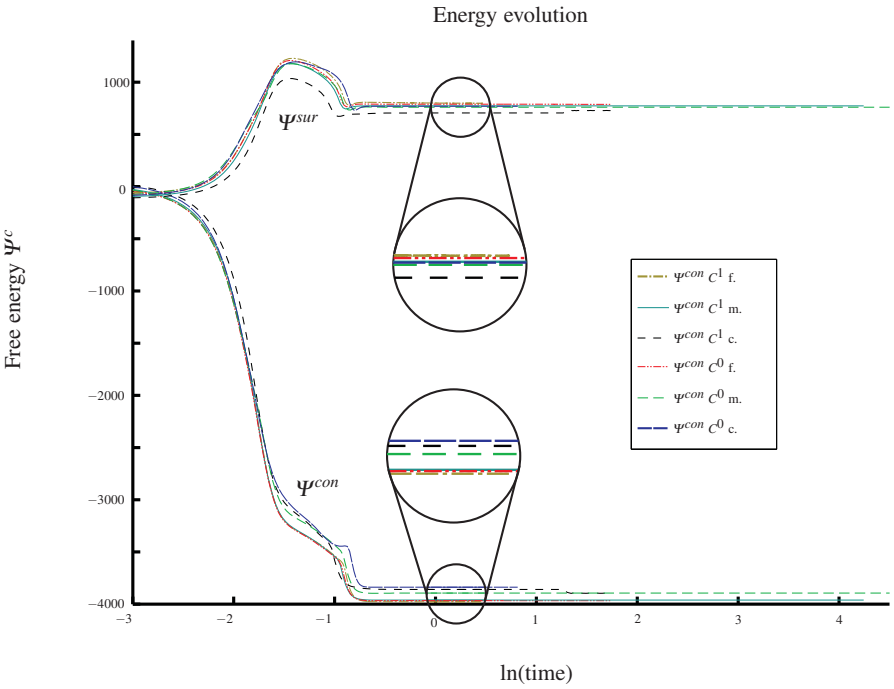

Fig. 16.3 Energy evolution whithin the phase separation processes.

the coarsest meshes with 64 points in case of the C^1 solution and 100 points for the C^0 continuous solution is used for the contour plots in Fig. 16.4.

16.9 Conclusions

In case of the natural element method, we have shown that both, the C^1 as well as the C^0 continuous discretization methods lead to similar results. For the coarse solution, the C^1 continuous discretization delivers smoother pictures, compare Fig. 16.4. However, even more important, the C^1 continuous discretization demonstrates faster convergence in the energy plot, see Fig. 16.3. Especially to reach the energy level of the semi-stable solution after phase separation, the C^0 continuous discretization

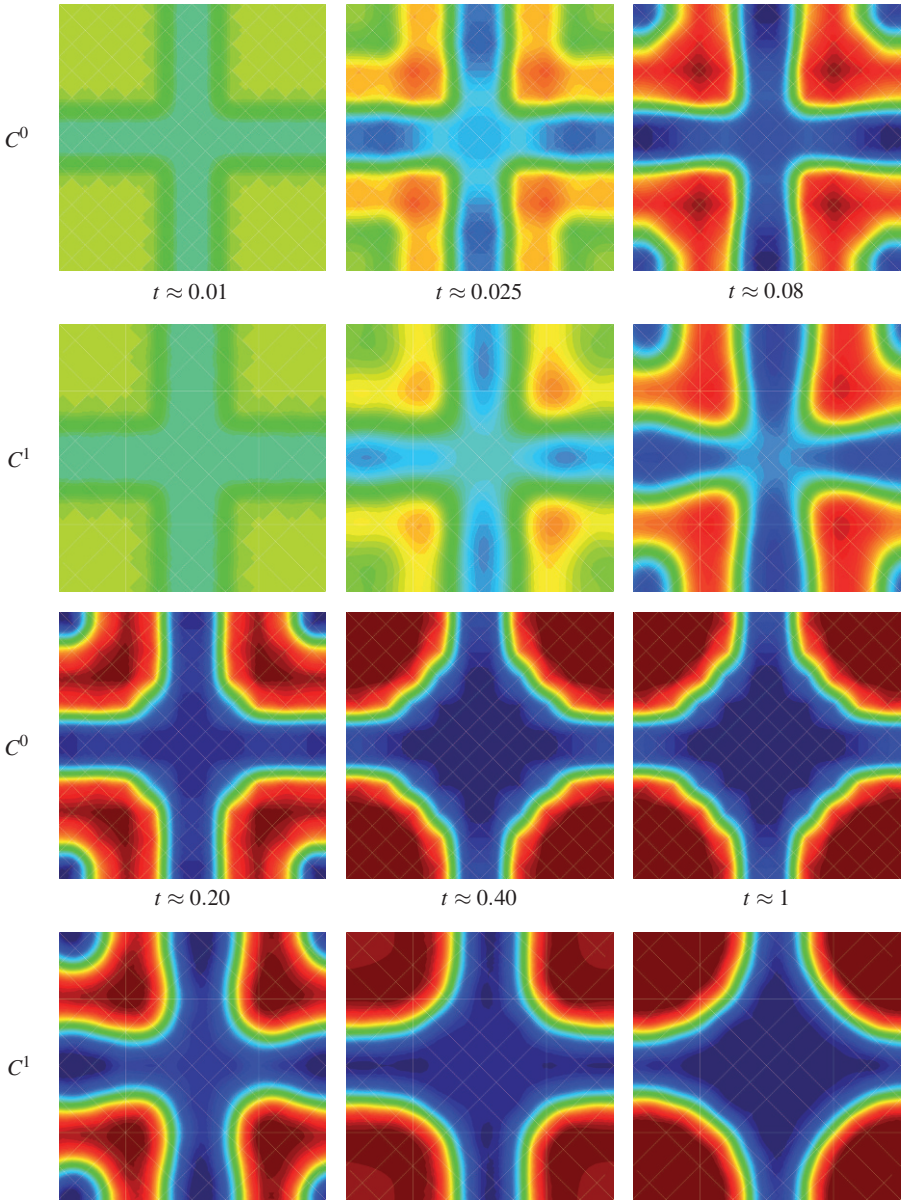

Fig. 16.4 Evolution of concentration for a coarse mesh. Comparison of C^1 and C^0 NEM.

method needs a much higher total number of degrees of freedom. Additionally, the initial behavior for the C^1 NEM is similar for the medium and fine concentrations, whereas it is still varying a lot in case of the C^0 NEM. Therefore, we propose to chose the C^1 continuous discretization whenever possible.

References

[1] Cahn J. W. Free energy of a non uniform system ii: thermodynamic basis. *J. Chem. Phys.*, 30:1121–1124, 1959.

[2] Falk F. Cahn-Hilliard theory and irreversible thermodynamics. *J. Non-Equilib. Thermodyn.*, 17(1):53–65, 1992.

[3] Dolcetta I. C., Vita S. F., March R. Area preserving curve shortening flows: from phase transitions to image processing. *Interfaces Free Boundaries*, 4(4):325–343, 2002.

[4] Kuhl E., Schmid D. W. Computational modeling of mineral unmixing and growth- an application of the Cahn-Hilliard equation. *Comput. Mech.*, 39:439–451, 2007.

[5] Khain E., Sander L. W. Generalized Cahn-Hilliard equation for biological applications. *Phys. Rev. Lett. E*, 77(5):1–7, 2008.

[6] Wu X. F., Dzenis W. A. Phase-field modeling of the formation of lamellar nanostructures in diblock copolymer thin film under inplanar electric field. *Phys. Rev. Lett. E*, 77(3,4):1–10, 2008.

[7] Ostwald W. ber die vermeintliche Isometrie des roten und gelben Queck-silberoxyds und die Oberflächenspannung fester Körper. *Z. Phys. Chem.*, 6A:495–503, 1900.

[8] Rajagopal A., Fischer P., Kuhl E., P. Steinmann P. Natural element analysis of the Cahn-Hilliard phase-field model *Comput. Mech.*, 46:471–493, 2010.

[9] Stogner, R. H., Carey, G. F., B. T. Murray. Approximation of Cahn-Hilliard diffuse interface models using parallel adaptive mesh refinement and coarsening with C^1 elements. *Int. J. Numer. Methods Eng.*, 76:636–661, 2008.

[10] Gomez, H., Calo, V. M., Bazilevs, Y., Hughes, T. J. R. Isogeometric analysis of the Cahn-Hilliard phase-field model. *Comput. Meth. Appl. Mech. Eng.*, 197:4333–4352, 2008.

[11] Wells, G.N., Kuhl, E., Garikipati, K. A discontinuous galerkin method for Cahn-Hilliard equation. *J. Comput. Phys*, 218:860–877, 2006.

[12] Elliott, C. M. and French, D. A. A non-conforming finite element method for the two-dimensional Cahn-Hilliard equation. *SIAM J. Numer. Anal.*, 26(4):884–903, 1989.

[13] Ubachs, R. L. J. M., Schreurs, R. J. G., and Geers, M. G. D. A nonlocal diffuse interface model for microstructure evolution in tin-lead solder. *J. Mech. Phys. Solids*, 52(8):1763–1792, 2004.

[14] Farin, G. Surfaces over Dirichlet tessellations. *Comp. Aided Geom. D.*, 7:281–292, 1990.

[15] Fischer, P., Mergheim, J., Steinmann, P. On the C^1 continuous discretization of nonlinear gradient elasticity: a comparison of NEM and FEM based on Bernstein-Bezier patches. *Int. J. Numer. Methods Eng.*, 82(10):1282–1307, 2010.

[16] Sukumar, N., Moran, B. C^1 natural neighbor interpolant for partial differential equations. *Numer. Meth. Part. D. E.* , 15:417–447, 1999.

[17] Sibson, R. A vector identity for the Dirichlet tessellation. *Math. Proc. Cambridge*, 87:151–153, 1980.

Chapter 17
Constitutive Models of Mechanical Behavior of Media with Stress State Dependent Material Properties

Evgeny V. Lomakin

Abstract The behavior of heterogeneous materials is studied. The dependence of the effective elastic properties of micro-heterogeneous materials on the loading conditions are analyzed and corresponding mathematical methods for the description of the observed effects are proposed. The constitutive relations of the theory of elasticity for isotropic solids with stress state dependent deformation properties are considered. The possible approach to the formulation of the constitutive relations for the elastic anisotropic solids that elastic properties depend on the stress state type is considered, and the corresponding constitutive relations are proposed. The method for the determination of material's functions on the base of experimental data is proposed. The quite satisfactory correspondence between the theoretical results and experimental data is shown.

Key words: Micro-heterogeneous materials. Phenomenological approach. Elastic properties. Isotropic materials. Anisotropic materials. Stress state dependent properties.

17.1 Introduction

The experimental studies of deformation properties of many heterogeneous and composite materials display the dependence of their properties on the conditions of loading. There are different mechanisms related to this phenomenon. In the case of granular porous materials, the area of contact between the particles increases under compressive loads. Then one would expect that the elastic characteristics would increase under compression in comparison with values corresponding to the action

Evgeny V. Lomakin
Faculty of Mechanics and Mathematics, Moscow State Lomonosov University, 119992 Moscow, Russia
e-mail: lomakin@mech.math.msu.su

H. Altenbach et al. (eds.), *Mechanics of Generalized Continua,*
Advanced Structured Materials, 7, DOI: 10.1007/978-3-642-19219-7_17,

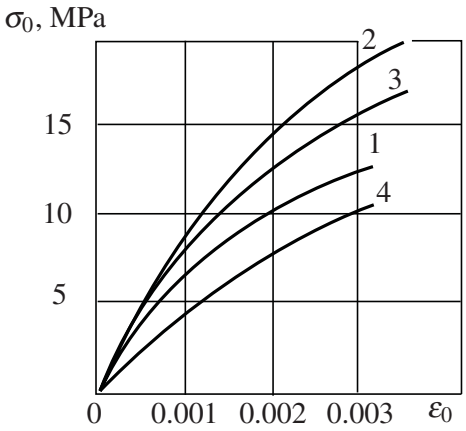

Fig. 17.1 Effective stress-strain diagrams of ARV graphite.

of tensile loads. In the case of cracked materials, the crack opening occurs under tensile load and the effective cross section carrying the load is less than in a solid material. Therefore the effective deformation properties depend on the concentration of microcracks. Under the conditions of compressive loads, it is possible that the closure of microcracks and the contact of crack faces would happen. The mechanical properties in this case depend on the conditions of interactions on the crack faces that are determined in one's turn by the ratios between different components of the stress tensor. This applies equally to an arbitrary type of loading. It means that the material properties are not invariant to the type of external forces but depend on the stress state type. For example, the initial slope of the stress-strain curve under conditions of compression is from 1.3 to 2 times the initial slope of the curve for tension [8].

Similar results have been obtained for structural graphite [1]. The effective stress-strain curves of ARV graphite are shown in the Fig. 17.1, which were obtained by a proportional loading of tubular specimens under plane stress conditions. The effective stress is $\sigma_0 = \sqrt{\frac{3}{2} S_{ij} S_{ij}}$, where $S_{ij} = \sigma_{ij} - \sigma\delta_{ij}$ is the stress deviator and $\sigma = \frac{1}{3}\sigma_{ii}$ is the hydrostatic component of the stress. The effective strain is $\varepsilon_0 = \sqrt{\frac{2}{3} e_{ij} e_{ij}}$, where $e_{ij} = \varepsilon_{ij} - \frac{1}{3}\varepsilon\delta_{ij}$ is the strain deviator and $\varepsilon = \varepsilon_{ii}$ is the bulk strain. Curves 1, 2, 3 and 4 correspond to uniaxial tension, uniaxial compression, shear and uniform biaxial tension, respectively. Instead of the single curve, as usually supposed in different theories of deformation, there is a fan of effective stress-strain curves and their deviation is noticeable. The curves have a weak non-linearity and a linear approximation of them is possible in a certain deformation range. Similar effects can be demonstrated for rocks, concrete, cast-iron and other materials [4].

The opposite effect sometimes can be observed in the case of composites. The fabric based carbon-carbon composites or composites with triaxial weave usually have considerable porosity. The fibers are tightened up under tension but they can buckle into the pores space under compression. The mechanisms of deformation are quite different for these loading conditions. The bending stiffness of fibers is much

lower in comparison with the tensile one. Thus the elastic modulus of the composite under tension can be greater by a factor of 4 or 5 then the elastic modulus under compression [2].

17.2 Constitutive Relations for Isotropic Materials

The deformation properties of materials under consideration are the stress-state-dependent ones. In the general case, the stress state type can be characterized by two parameters $\xi = \sigma/\sigma_0$ and $S_{\mathrm{III}}/\sigma_0^3$, where $S_{\mathrm{III}} = S_{ij}S_{jk}S_{kj}$ is the third invariant of the deviator of the stress tensor. The hydrostatic component of the stress σ characterizes the mean value of normal stresses at arbitrary point of a continuum and the effective stress or the stress intensity σ_0 defines the mean value of shear stress at the same point of a continuum. The parameter ξ characterizes the stress state type on the average but the parameter $S_{\mathrm{III}}/\sigma_0^3$ specifies the deviation from this average value. For the formulation of the constitutive relations the parameter ξ is used. The potential for the elastic solids with stress state dependent properties can be represented in the form

$$\Phi = \frac{1}{2}\left[1+\zeta(\xi)\right]\left(\mathrm{A}+\mathrm{B}\xi^2\right)\sigma_0^2 \tag{17.1}$$

Differentiating Eq. (17.1) with respect to the stresses σ_{ij}, the strain-stress relations can be obtained

$$\begin{aligned}
\varepsilon_{ij} &= \frac{3}{2}\left[\mathrm{A}+\omega(\xi)\right]S_{ij}+\frac{1}{3}\left[\mathrm{B}+\Omega(\xi)\right]\sigma\delta_{ij},\\
\omega(\xi) &= -\frac{1}{2}\left(\mathrm{A}+\mathrm{B}\xi^2\right)\zeta'(\xi)\xi+\mathrm{A}\zeta(\xi),\\
\Omega(\xi) &= \frac{1}{2}\left(\mathrm{A}+\mathrm{B}\xi^2\right)\zeta'(\xi)/\xi+\mathrm{B}\zeta(\xi).
\end{aligned} \tag{17.2}$$

The prime denotes the derivative of function with respect to ξ. The functions $\omega(\xi)$ and $\Omega(\xi)$ and their derivatives are related

$$\begin{aligned}
&\omega+\xi^2\Omega = \left(\mathrm{A}+\mathrm{B}\xi^2\right)(1+\zeta),\\
&\omega'+\xi^2\Omega' = 0.
\end{aligned} \tag{17.3}$$

From Eqs (17.2) and (17.3), it is possible to obtain the following expressions for the bulk strain ε end the effective strain ε_0:

$$\varepsilon = \left[\mathrm{B}+\Omega(\xi)\right]\sigma, \qquad \varepsilon_0 = \left[\mathrm{A}+\omega(\xi)\right]\sigma_0 \tag{17.4}$$

The Eqs (17.4) determine the relation between the bulk strain and the effective strain

$$\varepsilon = \frac{\mathrm{B} + \Omega(\xi)}{\mathrm{A} + \omega(\xi)} \xi \varepsilon_0 \tag{17.5}$$

Equation (17.5) signifies that the shear strains can cause the volume alteration of a material. The bulk strain ε is proportional to the strain intensity ε_0, but the proportionality factor is not constant but it depends on the stress state type parameter ξ. This factor is the variable quantity according to the type of loading and it has different values for uniaxial tension, uniaxial compression, shear, different types of biaxial and triaxial stress states.

Without loss of generality, we can assume that in the case of pure shear ($\xi = 0$) the function $\omega(\xi)$ has value $\omega(0) = 0$. Then the constant A in Eqs (17.2) is determined by the slope of effective stress-strain curve in the case of pure shear and $\zeta(0) = 0$. The functions $\omega(\xi)$, $\zeta(\xi)$ and $\Omega(\xi)$ can be determined on the base of a series of diagrams of the dependence between the effective strain ε_0 and the effective stress σ_0. According to the Eq. (17.4), the function $\omega(\xi) = -\mathrm{A} + \varepsilon_0/\sigma_0$. The second expression of Eq. (17.2) can be integrated, and it is possible to obtain the following expression for the function $\zeta(\xi)$:

$$1 + \zeta(\xi) = \left(\mathrm{A} + \omega + \mathrm{B}\xi^2 - \xi^2 \int \frac{\omega' \mathrm{d}\xi}{\xi^2} \right) (\mathrm{A} + \mathrm{B}\xi^2)^{-1}$$

As an example of experimental determination of all the parameters in the constitutive relations (17.2), the data obtained for graphite and represented in Fig. 17.1 can be used.

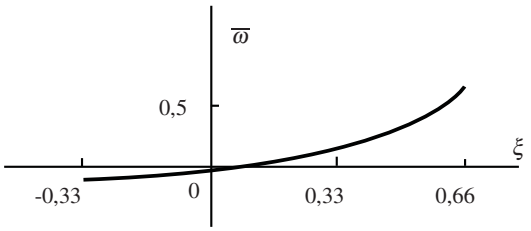

Fig. 17.2 The graph of function $\overline{\omega}(\xi)$ for ARV graphite.

In consequence of the weak non-linearity of effective stress-strain curves in Fig. 17.1, it is possible to approximate them by linear functions in the range of deformation 0.001. For this approximation the following values of elastic modulus and Poisson's ratio are obtained: $E^+ = 5.1 \cdot 10^3$ MPa, $\nu^+ = 0.2$ for uniaxial tension and $E^- = 7.83 \cdot 10^3$ MPa, $\nu^- = 0.3$ for uniaxial compression, respectively. The constant A can be obtained on the base of the curve 3 in Fig. 17.1 corresponding pure shear, and it has the value $\mathrm{A} = 1.35 \cdot 10^{-4}\,\mathrm{MPa}^{-1}$. The graph of function $\overline{\omega} = \omega(\xi)/\mathrm{A}$ is shown in Fig. 17.2. The piecewise linear approximation $\overline{\omega} = C\xi$ can be used for this function with $C = 0.45$ for $\xi > 0$ and $C = 0.3$ for $\xi < 0$, respectively. The constant B can be determined on the base of the value of elastic modulus for tension E^+, and this value is $\mathrm{B} = 1.76 \cdot 10^{-4}\,\mathrm{MPa}^{-1}$. The calculated value of elastic modulus under compression is $E^- = 7.81 \cdot 10^3$ MPa. The calculated values of Poisson's ratio under

tension and compression are $\nu^+ = 0.195$ and $\nu^- = 0.42$, respectively. The correspondence between the experimental and calculated values of graphite deformation properties is quite satisfactory.

The Eqs (17.2) can be solved for the stresses by introducing the parameter $\gamma = \varepsilon/\varepsilon_0$. The Eq. (17.5) gives the possibility to express the parameter ξ as a function of parameter γ, The potential can be represented in the form

$$\mathrm{U} = \frac{1}{2}[1+\eta(\gamma)]\left(\frac{1}{\mathrm{A}}+\frac{\gamma^2}{\mathrm{B}}\right)\varepsilon_0^2 \tag{17.6}$$

The stress-strain relations can be obtained by differentiating Eq. (17.6) with respect to the strains ε_{ij}

$$\begin{aligned}
\sigma_{ij} &= \frac{2}{3}\psi(\gamma)e_{ij} + \Psi(\gamma)\varepsilon\delta_{ij}, \\
\psi(\gamma) &= -\frac{1}{2}\left(\frac{1}{A}+\frac{\gamma^2}{\mathrm{B}}\right)\eta(\gamma)\gamma + \frac{1}{A}[1+\eta'(\gamma)], \\
\Psi(\gamma) &= \frac{1}{2}\left(\frac{1}{A}+\frac{\gamma^2}{\mathrm{B}}\right)\eta(\gamma)\gamma^{-1} + \frac{1}{B}[1+\eta'(\gamma)].
\end{aligned} \tag{17.7}$$

Some properties of the constitutive relations (17.2) and (17.7) are analyzed in [4, 5, 6]. It is shown that some traditional approaches to the solution of boundary value problems can not be accepted and new methods are proposed [7].

17.3 Constitutive Relations for Anisotropic Materials

The formulation of the constitutive relations for the anisotropic materials is much more complex in comparison with the isotropic ones. In general, it is necessary to suppose that all the anisotropy coefficients are the functions of the stress state parameter ξ. The potential for an anisotropic solid with stress state dependent deformation properties can be represented in the following form:

$$\Phi = \frac{1}{2}\mathrm{A}_{ijkl}(\xi)\sigma_{ij}\sigma_{kl} \tag{17.8}$$

Equation (17.8) represents some generalization of classic elastic potential. Differentiating Eq. (17.8) with respect to the stresses and taking into account that

$$\frac{\partial\sigma_0}{\partial\sigma_{ij}} = \frac{3}{2}\frac{S_{ij}}{\sigma_0}$$

and

$$\frac{\partial\sigma}{\partial\sigma_{ij}} = \frac{1}{3}\delta_{ij},$$

we obtain the dependence of the strains on the stresses:

$$\varepsilon_{ij} = \mathrm{A}_{ijkl}(\xi)\sigma_{kl} + \frac{1}{2}\mathrm{A}'_{mnpq}(\xi)\sigma_{mn}\sigma_{pq}\left[\left(\frac{1}{3}+\frac{3}{2}\xi^2\right)\delta_{ij} - \frac{3}{2}\xi\sigma_{ij}\sigma_0^{-1}\right]\sigma_0^{-1} \tag{17.9}$$

From Eq. (17.9) it follows that the strains consist of two parts, one corresponds to deformations of an anisotropic solid, the second one represents the deformations of some isotropic solid because this part has isotropic nature. The strain potential represents the homogeneous function of second order of the components of stress tensor and according to the Euler theorem one can obtain

$$2\Phi = \sigma_{ij}\varepsilon_{ij} \tag{17.10}$$

From Eq. (17.10) it follows that the Clapeyron theorem is valid for materials under consideration, namely the work of external forces

$$\mathrm{A} = \frac{1}{2}\int\limits_V \sigma_{ij}\varepsilon_{ij}\mathrm{d}V. \tag{17.11}$$

As distinct from classic anisotropic solid, the problem of determination an anisotropy coefficients as the functions of the stress state parameter ξ arises. Thus, in general for each stress state type, it is necessary to determine the set of coefficients $\mathrm{A}_{ijkl}(\xi)$. The constitutive relations (17.9) seem to be very complex but their nature is clear and simple and the procedure for the determination of the anisotropy functions can be proposed. Analyzing these constitutive relations one can discover that the complex expression in the square brackets reduces to zero in the case of uniaxial tension and uniaxial compression when the parameter ξ is equal $1/3$ and $-1/3$, respectively. Let us consider plane stress conditions of an anisotropic solid. Then relations (17.9) reduce to the following:

$$\begin{aligned}
\varepsilon_x &= \mathrm{a}_{11}(\xi)\sigma_x + \mathrm{a}_{12}(\xi)\sigma_y + \left[\left(\frac{1}{3\xi}+\frac{3}{2}\xi\right)\sigma - \frac{3}{2}\xi\sigma_x\right]\Phi_1\sigma_0^{-2},\\
\varepsilon_y &= \mathrm{a}_{12}(\xi)\sigma_x + \mathrm{a}_{22}(\xi)\sigma_y + \left[\left(\frac{1}{3\xi}+\frac{3}{2}\xi\right)\sigma - \frac{3}{2}\xi\sigma_y\right]\Phi_1\sigma_0^{-2},\\
\gamma_{xy} &= \left[\mathrm{a}_{66}(\xi) - \frac{3}{2}\xi\Phi_1\sigma_0^{-2}\right]\tau_{xy},\\
\Phi_1 &= \frac{1}{2}\left[\mathrm{a}'_{11}(\xi)\sigma_x^2 + \mathrm{a}'_{22}(\xi)\sigma_y^2 + 2\mathrm{a}'_{12}(\xi)\sigma_x\sigma_y + \mathrm{a}'_{66}(\xi)\tau_{xy}^2\right].
\end{aligned} \tag{17.12}$$

In the case of potential (17.8), it is necessary to determine the character of dependence of coefficients A_{ijkl} on the parameter ξ on the base of the experimental data. The most simple and useful one is a piecewise approximation. In the case of linear dependence of the coefficients A_{ijkl} on the parameter ξ, it is possible to write

$$\mathrm{A}_{ijkl} = \mathrm{A}^0_{ijkl} + C_{ijkl}(\xi - 1/3), \tag{17.13}$$

where A^0_{ijkl} are the values of anisotropy coefficients under uniaxial tension ($\xi = 1/3$). Then the coefficients $\mathrm{a}_{ij}(\xi)$ and the function Φ_1 can be represented in the form of

$$\begin{aligned} &\mathrm{a}_{ij}(\xi) = \mathrm{a}^0_{ij} + c_{ij}(\xi - 1/3), \qquad \mathrm{a}^0_{ij} = \mathrm{a}_{ij}(1/3), \\ &\Phi_1 = \frac{1}{2}(c_{11}\sigma_x^2 + c_{22}\sigma_y^2 + 2c_{12}\sigma_x\sigma_y + \sigma_{66}\tau_{xy}^2). \end{aligned} \tag{17.14}$$

Rotating the coordinate system the coefficients of anisotropy a_{ij} are transformed according to the usual equations for the transformation of components of a fourth rank tensor [3]. In principal stress axes p and q, Eq. (17.12) can be represented in the form

$$\begin{aligned} \varepsilon_p &= \mathrm{b}_{11}(\xi)\sigma_p + \mathrm{b}_{12}\sigma_q + \left[\left(\frac{1}{9\xi} - \xi\right)\sigma_p + \left(\frac{1}{9\xi} + \frac{1}{2}\xi\right)\sigma_q\right]\Phi_1\sigma_0^{-2}, \\ \varepsilon_q &= \mathrm{b}_{21}(\xi)\sigma_p + \mathrm{b}_{22}\sigma_q + \left[\left(\frac{1}{9\xi} - \xi\right)\sigma_q + \left(\frac{1}{9\xi} + \frac{1}{2}\xi\right)\sigma_p\right]\Phi_1\sigma_0^{-2}, \\ \gamma_{pq} &= \mathrm{b}_{61}(\xi)\sigma_p + \mathrm{b}_{62}(\xi)\sigma_q, \\ \sigma_0^2 &= \sigma_p^2 + \sigma_q^2 - \sigma_p\sigma_q, \end{aligned} \tag{17.15}$$

where b_{ij} are the coefficients of anisotropy in the principal stress axes. Coefficients a_{ij} and b_{ij} are related by the following formulae:

$$\begin{aligned} \mathrm{b}_{11} &= \mathrm{a}_{11}\cos^4\varphi + (2\mathrm{a}_{12} + \mathrm{a}_{66})\sin^2\varphi\cos^2\varphi + \mathrm{a}_{22}\sin^4\varphi, \\ \mathrm{b}_{22} &= \mathrm{a}_{11}\sin^4\varphi + (2\mathrm{a}_{12} + \mathrm{a}_{66})\sin^2\varphi\cos^2\varphi + \mathrm{a}_{22}\cos^4\varphi, \\ \mathrm{b}_{12} &= (\mathrm{a}_{11} + \mathrm{a}_{22} - 2\mathrm{a}_{12} - \mathrm{a}_{66})\sin^2\varphi\cos^2\varphi + \mathrm{a}_{12}. \end{aligned} \tag{17.16}$$

Similar equations can be written for the coefficients b_{61}, b_{62} and b_{66}, too. The coefficients a^0_{ij} and c_{ij} can be determined on the base of experimental data for the conditions of uniaxial tension and uniaxial compression along the principal axes of orthotropy and along the directions at some angles with them. Under conditions of uniaxial tension, $\sigma = \frac{1}{3}\sigma_p$, $\sigma_0 = \sigma_p$, $\xi = \frac{1}{3}$ and for the strains along the x and y axes from Eqs (17.12) we obtain

$$\begin{aligned} \varepsilon_x &= \mathrm{a}^0_{11}\sigma_x, \qquad \varepsilon_y = \left(\mathrm{a}^0_{12} + \frac{1}{4}c_{11}\right)\sigma_x \\ \varepsilon_y &= \mathrm{a}^0_{22}\sigma_y, \qquad \varepsilon_x = \left(\mathrm{a}^0_{12} + \frac{1}{4}c_{22}\right)\sigma_y \end{aligned} \tag{17.17}$$

Under conditions of uniaxial compression ($\xi = -1/3$) along the same axes, it can be obtained

$$\begin{aligned}
\varepsilon_x &= \left(\mathrm{a}_{11}^0 - \frac{2}{3}c_{11}\right)\sigma_x, \qquad \varepsilon_y = \left(\mathrm{a}_{12}^0 - \frac{2}{3}c_{12} - \frac{1}{4}c_{11}\right)\sigma_x \\
\varepsilon_y &= \left(\mathrm{a}_{22}^0 - \frac{2}{3}c_{22}\right)\sigma_y, \qquad \varepsilon_x = \left(\mathrm{a}_{12}^0 - \frac{2}{3}c_{12} - \frac{1}{4}c_{22}\right)\sigma_y
\end{aligned} \tag{17.18}$$

The coefficients a_{11}^0 and a_{22}^0 are determined as ratio of the axial strain to the axial stress according to Eqs (17.17). The coefficients c_{11} and c_{22} can be determined from Eq. (17.18). The coefficients a_{12}^0, a_{66}^0 c_{12} and c_{66} can be determined on the base of the results of experiments under conditions of uniaxial tension and uniaxial compression at some angle to the principal axes using Eqs (17.13)–(17.18).

In the case of similar dependence of anisotropy coefficients on the stress state type parameter ξ, it could be considered a simplified potential

$$\Phi = \frac{1}{2}[1 + \zeta(\xi)]\mathrm{A}_{ijkl}\sigma_{ij}\sigma_{kl} \tag{17.19}$$

In this case, the strain-stress relations (17.12) reduce to the following ones:

$$\begin{aligned}
\varepsilon_x &= [1 + \zeta(\xi)](\mathrm{a}_{11}\sigma_x + \mathrm{a}_{12}\sigma_y) + \left[\left(\frac{1}{3\xi} + \frac{3}{2}\xi\right)\sigma - \frac{3}{2}\xi\sigma_x\right]\zeta'(\xi)\Phi_0\sigma_0^{-2}, \\
\varepsilon_y &= [1 + \zeta(\xi)](\mathrm{a}_{12}\sigma_x + \mathrm{a}_{22}\sigma_y) + \left[\left(\frac{1}{3\xi} + \frac{3}{2}\xi\right)\sigma - \frac{3}{2}\xi\sigma_y\right]\zeta'(\xi)\Phi_0\sigma_0^{-2}, \\
\gamma_{xy} &= \left\{[1 + \zeta(\xi)]\mathrm{a}_{66} - \frac{3}{2}\xi\zeta'(\xi)\Phi_0\sigma_0^{-2}\right\}\tau_{xy}, \\
\Phi_0 &= \frac{1}{2}\left[\mathrm{a}_{11}\sigma_x^2 + \mathrm{a}_{22}\sigma_y^2 + 2\mathrm{a}_{12}\sigma_x\sigma_y + \mathrm{a}_{66}\tau_{xy}^2\right], \\
\sigma_0 &= (\sigma_x^2 + \sigma_y^2 - \sigma_x\sigma_y + 3\tau_{xy})^{1/2}
\end{aligned} \tag{17.20}$$

Here the x and y directions coincide with the warp and woof directions of the cloth, respectively. Coefficients b_{ij} in Eqs (17.15) can be represented in the form $\mathrm{b}_{ij}(\xi) = [1 + \zeta(\xi)]\mathrm{b}_{ij}$. Coefficients a_{ij} and b_{ij} are related by the conversion of formulae (17.16). We can denote the coefficients of the transverse deformation for the principal and rotated coordinate systems as $k_{12} = \varepsilon_y/\sigma_x$ and $k'_{12} = \varepsilon_q/\sigma_p$, respectively. Then from Eqs (17.16) it can be found

$$\begin{aligned}
\mathrm{a}_{12} &= \left[\mathrm{b}_{11}k_{12} - \mathrm{a}_{11}(\mathrm{b}_{11} - k'_{12} - \mathrm{a}_{11}\cos^2\varphi - \mathrm{a}_{22}\sin^2\varphi)\right](\mathrm{b}_{11} - \mathrm{a}_{11})^{-1}, \\
\mathrm{a}_{66} &= \mathrm{b}_{11}(\cos^2\varphi\sin^2\varphi)^{-1} - \mathrm{a}_{11}\cot^2\varphi - \mathrm{a}_{22}\tan^2\varphi - 2\mathrm{a}_{12}
\end{aligned} \tag{17.21}$$

For uniaxial test conditions the coefficients $\mathrm{a}_{11} = \varepsilon_x/\sigma_x$, $\mathrm{a}_{22} = \varepsilon_y/\sigma_y$, $\mathrm{b}_{11} = \varepsilon_p/\sigma_p$.

For the potential (17.19), the only function of the stress state type $\zeta(\xi)$ has to be determined and all the coefficients of anisotropy can be determined on the base of experiments under conditions of uniaxial tension. The function $\zeta(\xi)$ can be determined on the base of Eqs (17.10) and (17.19), from which it follows:

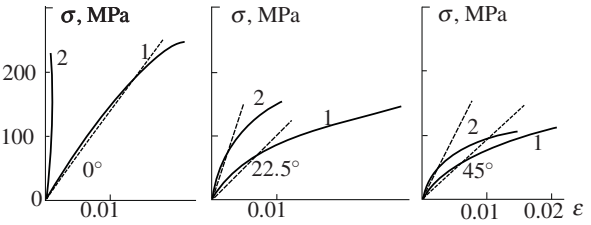

Fig. 17.3 The stress-strain diagrams for the composite fiberglass cloth/polyether resin under conditions of tension at the angles 0°, 22.5° and 45° to the direction of the warp of the cloth.

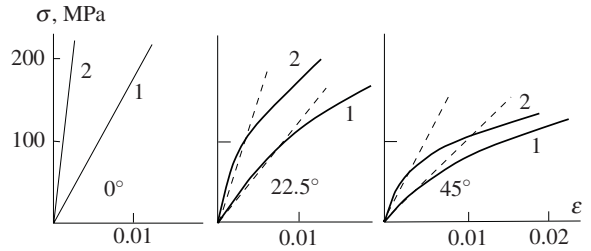

Fig. 17.4 The stress-strain diagrams under conditions of compression of the composite at the angles 0°, 22.5° and 45° to the direction of the warp of the cloth.

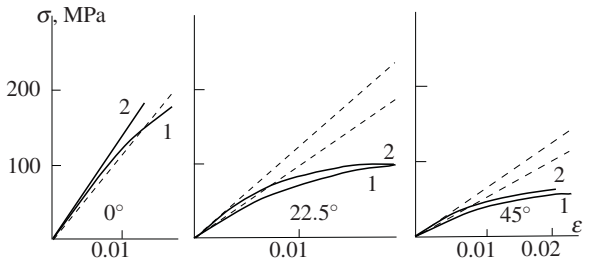

Fig. 17.5 The stress-strain diagrams for the conditions of shear with tension-compression directions $0° - 90°$, $22.5° - 112.5°$ and $45° - 135°$.

$$1 + \zeta = \sigma_{ij}\varepsilon_{ij}\left(a_{ijkl}\sigma_{ij}\sigma_{kl}\right)^{-1} \tag{17.22}$$

For each stress state type or the type of loading, it is possible to define the values of function ζ using the known values of strains and stresses. Without the loss of the generality, one can suppose that $\zeta(1/3) = 0$.

The possibilities of the constitutive relations (17.20) in the description of the mechanical behavior of composite materials can be demonstrated on the base of the comparison of theoretical prediction and experimental data for the composite on the base of glass cloth and polyether matrix [9]. The plain specimens were used in the experiments. Therefore the Eqs (17.15), (17.16) and (17.20) can be used for the analysis of the results of experimental studies of the deformation properties of the composite. The stress-strain diagrams under tension of the composite in the direction of the warp of the cloth and at the angles 22.5° and 45°to this direction are shown in Fig. 17.3. The stress-strain diagrams under conditions of uniaxial compression of the composite are shown in the Figs 17.4 for the same directions. Curves 1 and 2 refer to longitudinal and transverse deformation, respectively. The diagram for compression along the fibers is linear up to failure. The diagram for tension displays some nonlinearity. With a certain degree of accuracy, the diagram for ten-

Direction of loading		0°		22.5°		45°	
	ξ	$\frac{\varepsilon_x}{\sigma_x}$	$\frac{\varepsilon_y}{\sigma_x}$	$\frac{\varepsilon_p}{\sigma_p}$	$\frac{\varepsilon_q}{\sigma_p}$	$\frac{\varepsilon_p}{\sigma_p}$	$\frac{\varepsilon_q}{\sigma_p}$
Experimental	$1/3$	7.0	-0.64	9.9	-3.14	–	–
Theoretical	$1/3$	–	–	–	–	13	-5.7
Experimental	$-1/3$	5.34	-0.97	7.8	-3.23	10.2	-5.4
Theoretical	$-1/3$	–	-0.94	7.5	-3.04	9.9	-5.2
Experimental	0	8.39	-7.04	14.7	-12.15	20.3	-16.9
Theoretical	0	8.17	-6.08	13.7	-11.37	19.7	-16.2

Table 17.1 Experimental and theoretical values of the deformation coefficients of the composite in $10^{-5}\,\mathrm{MPa}^{-1}$

sion can also be approximated by a linear one. It is possible to accept a measure of deviation from the initial slope of the diagram corresponding to the nonlinear deformation of 0.002. This linear diagram for the tension in the warp direction is shown in the Figs 17.3 by the dotted line. Under this approximation, the elastic modulus of the composite under tension along the fibers is $E^+ = 1.428 \cdot 10^4\,\mathrm{MPa}$. The elastic modulus under the compression in the same direction is $E^- = 1.873 \cdot 10^4\,\mathrm{MPa}$.

The analysis of the results of experiments under uniform biaxial loading indicates that the compliances of the composite in the directions of warp and woof of the cloth are almost equal within the frame of the adopted approximation. Thus it can be assumed that $\mathrm{a}_{11} = \mathrm{a}_{22} = 1/E^+ = 7 \cdot 10^{-5}\,\mathrm{MPa}^{-1}$. On the base of Eq. (17.21) using the values of compliances given in the first line of Table 17.1 we can determine the values of other two elastic constants $\mathrm{a}_{12} = -1.6 \cdot 10^{-5}\,\mathrm{MPa}^{-1}$ and $\mathrm{a}_{66} = 41.2 \cdot 10^{-5}\,\mathrm{MPa}^{-1}$. When all the anisotropy coefficients for plane stress conditions are determined, it is possible to calculate the value of function $\zeta(\xi)$ for the conditions of uniaxial compression ($\xi = -1/3$). In accordance with Eq. (17.22) and the value of compliance ε_x/σ_x under compression we obtain $\zeta = -0.24$.

The stress-strain diagrams for the conditions of shear ($\xi = 0$) in the plane of composite layers are shown in Figs 17.5. The experiments were carried out for three directions of tension-compression with respect to the warp of the cloth, that is $0^\circ - 90^\circ$, $22.5^\circ - 112.5^\circ$ and $45^\circ - 135^\circ$. Indexes 1 and 2 refer to the tensile strain and the compressive strain, respectively. Using the values of the strains and the stresses for the $0^\circ - 90^\circ$ conditions, we can determine the value of function $\zeta(\xi)$ for shear, $\zeta(0) = -0.13$. The graph of the function $\zeta(\xi)$ for the range of variation of parameter ξ, $-1/3 \leqslant \xi \leqslant 1/3$, is shown in Fig. 17.6.

Since all the parameters of the constitutive relations represented by Eq. (17.20) are determined, it is possible to compare the theoretical and experimental data obtained for plane stress conditions. In the case of shear,

$$\sigma_y = -\sigma_x, \quad \sigma_0 = \sqrt{3}\sigma_x, \quad \Phi_0 = (\mathrm{a}_{11} - \mathrm{a}_{22})\sigma_x^2, \quad \xi = 0$$

and according to Eq. (17.20) we have

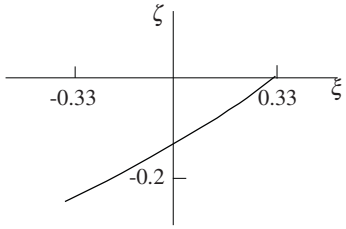

Fig. 17.6 The graph of function $\zeta(\xi)$ for the composite.

$$\begin{aligned}\varepsilon_x/\sigma_x &= (a_{11} - a_{12})[1 + \zeta(0) + \zeta'(0)(3\sqrt{3})^{-1}],\\ \varepsilon_y/\sigma_x &= -(a_{11} - a_{12})[1 + \zeta(0) - \zeta'(0)(3\sqrt{3})^{-1}]\end{aligned} \tag{17.23}$$

For the case when the stresses are applied at some angle to the fiber direction, the coefficients a_{11} and a_{12} in Eq. (17.23) should be replaced by the coefficients b_{11} and b_{12} in accordance with Eq. (17.16). The theoretical and experimental values of compliances for different types of loading and various loading directions are given in Table 17.1. The correspondence between the theoretical values and experimental data is quite satisfactory. The calculated initial slope of the stress-strain diagrams are shown in Fig. 17.3–Fig. 17.5 by the dotted lines, and the trend of the variation of initial elastic deformation properties of the composite under various external forces is described by the considered constitutive equations satisfactorily.

17.4 Conclusions

The dependence of the effective elastic properties of micro-heterogeneous materials on the conditions of loading or the conditions of deformation is studied. The phenomenological approach to the description of the behavior of the heterogeneous materials under different types of external forces is considered. The constitutive equations of the theory of elasticity for isotropic solids with stress state dependent deformation properties are analyzed. Some properties of constitutive equations are studied. The method for experimental determination of material functions is proposed.

A possible approach to the formulation of the constitutive equations of the theory of elasticity for the anisotropic solids, which deformation properties depend on the stress state type is considered. The mechanical properties of these materials are characterized by a set of the anisotropy functions instead of a set of elastic constants in the case of the classic linear elastic solid. The method for the determination of anisotropy functions on the base of experimental data is described. The results of experimental studies of properties of composite materials on the base of fiberglass cloth and polyether resin obtained under different loading conditions are analyzed. The satisfying correspondence between the calculated values of deformation coefficients and experimental data is demonstrated.

Acknowledgements The work was supported by the Russian Foundation for Basic Research (grant 11-01-00168).

References

[1] Berezin, A.V., Lomakin, E.V., Strokov, V.I., Barabanov, V.N.: Resistance to deformation and fracture of isotropic graphite materials in complex stress state conditions. Problemy Prochnosti. (2),60–65 (1979).
[2] Kratsch, K.M., Schutzler, J.C., Eitman, D.A.: Carbon-carbon 3-D ortohogonal material behavior. AIAA Paper, 365 (1972)
[3] Lekhnitskii, S.G.: *Theory of the Elasticity of an Anisotropic Elastic Body*. New York Holden-Day, (1963)
[4] Lomakin, E.V.: Mechanics of media with stress-state dependent properties. Physical Mesomechanics. **10**(5), 41-52 (2007)
[5] Lomakin, E.V., Rabotnov, Yu.N.: A theory of elasticity for an isotropic body with different moduli in tension and compression. Mechanics of Solids **13**(6), 25–30, (1978).
[6] Lomakin, E.V.: Uniqueness of solutions of problems in the theory of elasticity in the case of an isotropic polymodular body. Mechanics of Solids **14**(2), 42–45, (1979)
[7] Lomakin, E.V.: Torsion of cylindrical bodies with varying strain properties. Mechanics of Solids. **43**(3), 502–511, (2008).
[8] Panferov, V.M.: Theory of elasticity and deformation theory of plasticity for solids with different properties under compression, tension and torsion. Doklady AN SSSR. **180**(1), 41–44 (1968).
[9] Smith, E.W., Pascoe, K.J.: The role of shear deformation in the fatigue failure of a glass fiber-reinforced composite. Composites **8**(4), 237–243, (1977)